High Resolution NMR Based Approaches for Facilitating Chromatography Method Development

by

Azzedine Abdelah Dabo

Thesis

Submitted to the University of Warwick

For the degree of

Doctor of Philosophy

Supervised by Józef R. Lewandowski and Prof. Melissa Hanna-Brown

Department of Chemistry

April 2019

WARWICK
THE UNIVERSITY OF WARWICK

CONTENTS

List of Tables

List of Appendices Tables

List of Figures

List of Appendices Figures

List of Statistical Script

Acknowledgements

The work presented in this study was performed at the Department of Chemistry, University of Warwick, from September 2013 to August 2017. During this period, several people have contributed towards completing this project.

First, I want to say a big thank you to my supervisor, Dr Józef R. Lewandowski who provided me with endless amounts of help and his expertise in this area. He guided and motivated me during both difficult and enjoyable times. Without his support, passion and drive for NMR I wouldn't have been able to complete this project and for this I will forever be grateful. Gratitude also goes to my second supervisor, Melissa Hannah Brown for her insightful discussions about HPLC chromatography. To Jonathan Lamley who kindly helped me throughout this project especially by showing me how to use the 500 MHz NMR spectrometer and deepening my understanding of Solid State NMR.

My Gratitude goes to James Hogbin, Sam Louis Young and Joshua Bucceri for their help and expertise in running the HPLC experiments in Pfizer. Special thanks to the Warwick University NMR group with whom I have made unforgettable memories throughout my time at Warwick, including the cake club. A big thank you to both Pfizer and EPSRC for funding this exciting project.

Many thanks to my brothers who supported and motivated me throughout this project. A very special thanks to my wife to be Amy Donegan and the one and only sister Saphora Dabo for helping me with my grammar and spelling. Finally, I am extremely grateful to my parents for their love and words of wisdom throughout my life.

Azzedine A. Dabo

Declaration

I hereby declare that this thesis High Resolution NMR Based Approaches for Facilitating Chromatography Method Development is an original work and has not been submitted for a diploma or degree at another university. This thesis has been composed by myself unless specifically acknowledged or referenced.

The research was conducted under the supervision of Dr Józef R. Lewandowski and Prof. Melissa Hanna-Brown at the University of Warwick and Pfizer between September 2013 to April 2017.

All the NMR results were obtained at the University of Warwick. The ^{13}C and ^{29}Si were obtained with the help of Angelo Gallo. The AFM images were acquired at Warwick University by Faduma Maddar. The HPLC results presented in this thesis were all obtained at Pfizer Ltd, Analytical Research & Development Laboratories, Small Molecule Pharmaceutical Sciences Sandwich, Canterbury, Kent, CT13 9ND, United Kingdom.

Abstract

Reversed-Phase High Performance Liquid Chromatography (RP-HPLC) is one of the most widely used techniques for provision of analytical measurement information in the pharmaceutical industry from discovery through to development, clinical and manufacturing analytical laboratories. The pharma industry has been for many years attempting to transform the efficiency of method development and increasingly attention has turned to using in silico methodologies. Pfizer have been at the forefront of developing streamlined workflows and more recently, models for retention time prediction so as to reduce the amount of experimental effort in method development. Many of the in-silico strategies used rely on calculated parameters of the molecules under investigation and to some extent the characteristics of the RP-HPLC stationary phases, but no models yet have captured any measures that capture any description of the multiple and complex analyte – stationary phase-mobile phase interactions within any one RP-HPLC method condition.

To accomplish this, ^{1}H high resolution magic angle spinning (HR-MAS) nuclear magnetic resonance (NMR) spin-lattice (T_1) and spin-spin (T_2) relaxation measurements were carried out to probe site-specific molecular motion of a series of aromatic compounds and reversed phase HPLC stationary phases in two different mobile phases. The NMR relaxation measurements provided insight about the nature of the site-specific interaction between the compounds with different stationary phases.

Keywords: method development, reversed phase high pressure liquid chromatography; atomic resolution; spin-lattice relaxation; spin-spin relaxation; site-specific interaction; aromatic compounds; high resolution magic angle spinning NMR; Predictive modelling programs.

List of Abbreviations and Acronyms

HPLC	High Pressure Liquid Chromatography
RP-HPLC	Reversed Phase High Pressure Liquid Chromatography
NP-HPLC	Normal Phase HPLC
NMR	Nuclear Magnetic Resonance
FT	Fourier Transformed
MAS	Magic Angle Spinning
CP	Cross Polarization
HR	High-Resolution
DOSY	Diffusion-Ordered Spectroscopy
BEH	Ethylene Bridged Hybrid
CSH	Charged Surface Hybrid
HSS	High Strength Silica
GC	Gas Chromatography
MS	Mass Spectrometer
t_R	Retention time
MP	Mobile Phase
SP	Stationary Phase
RF	Radio Frequency
TMS	Tetramethylsilane
DSS	4,4-Dimethyl-4-Silapentane-1-Sulfonic acid
CSA	Chemical Shift Anisotropy
FID	Free Induction Decay
2D	Two Dimensional
HMBC	Heteronuclear Multiple Bond Correlation
NOESY	Nuclear Overhauser Effect Spectroscopy
EXSY	Exchange Spectroscopy
CPMG	Carr-Purcell Meiboom-Gill
AFM	Atomic Force Microscopy
MeCN	Acetonitrile
MeOH	Methanol

1 INTRODUCTION

High pressure liquid chromatography (HPLC) is an analytical technique used to identify, quantify and separate compounds in a mixture. Over the years, HPLC has been developed to cover a broad range of applications it has today. In the pharmaceutical industry, reversed phase high pressure liquid chromatography (RP-HPLC) is heavily relied upon from discovery through development and clinical to manufacturing laboratories. RP-HPLC method development strategies have over the years gained significant attention across the industry and in the scientific literature and regardless of the strategy it is common to see several steps [1, 2] being required before optimal starting conditions for method development and validation can be selected (see Figure 1.1.). The most important information required at the start of the activity are the physical and chemical properties of analytes in the samples requiring separation. These commonly include molecular chemical structure, molecular weight, pK_a, log$D$, Log$P$, solubility and UV spectra. Such characteristics enable the chromatographer to narrow down the selection of detector as well as mobile and stationary phases for the development activities.

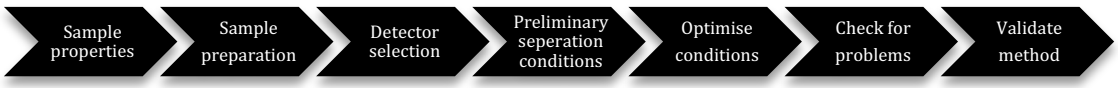

Figure 1.1. Steps followed in HPLC method development

It is important to gather as much detail as possible about the sample matrix, sampling procedure and sample source prior to any sample manipulation in readiness for the RP-HPLC analysis. In pharmaceutical development laboratories, its generally true that

sample preparation is avoided whenever possible (to ensure as far as possible that samples are unchanged before analysis) and so most samples for RP-HPLC are only diluted into the relevant mobile phase used in the separation method ready for injection (this ensures any solvent miss-matches between sample matrix and mobile phase are avoided which can be evident in chromatograms exhibiting peak asymmetry/split peaks etc). A variety of detectors are used with HPLC systems including: UV/Visible, mass spectrometry, NMR spectrometry [3-5], fluorescence , electrochemical , refractive-index and many more [6]. The detector used depends on the separation goals and the physico-chemical properties of the analyte of interest. For instance, neutral compounds cannot be detected via mass spectrometry but can be visible under UV/Vis (often used in combination with MS for HPLC).

Once the sample properties and goals for the analysis have been considered, some preliminary separation conditions for the method can be applied. Table 1.1 summarises fundamental experimental conditions that need to be considered for the initial method. In some cases, previously successful validated methods with similar goals can be used. The initial conditions might not be optimal but will be sufficient for a starting point for the method development. As shown in Table 1.1, a large number of parameters can be altered with different conditions to achieve the best separating conditions. For instance, the column dimensions, particle size and stationary phase material can each be changed. The mobile phase organic solvent, mobile phase ratio, isocratic or gradient elution mode, use of buffers and additives can also be altered depending on the goals of the method and samples investigated. Selecting the best optimal separating condition in HPLC method development can be both time and money consuming [7, 8]. For instance, Pfizer uses a series of screening experiments to identify the most suitable column (typically three to five phases) and approximate composition of the mobile which can subsequently be optimized to provide the best selectivity [9, 10].

An alternative approach of predicting optimal separation conditions is through predictive modelling programmes. There are several commercially available software packages for chromatography method development, optimisation and validation including: DryLab and ChromSword [11-15].

Table 1.1. Experimental conditions that affect HPLC separation.

Separation Variable	**Initial Conditions**
Column	
Dimensions (inner diameter and length)	2.1 mm x 50 mm or 4.6 mm x 250 mm
Particle size	1.7 µm or 5 µm (depending on system)
Stationary phase	C18 or Phenyl or RP18 or HSS T_3
Mobile Phase	
Solvent A/B	Water/acetonitrile
%-B	Isocratic or Gradient
Buffer (compound, pH and concentration)	Depending on samples properties
Additives (e.g. ion-pair reagents, amines)	Depending on samples properties (and not usually used for initial starting conditions)
Flow rate	Variable (mL/min)
Temperature	40°C
Sample Size	
Injection volume	5 µL
Stock concentration	~0.5 mg/mL (variable)

Drylab software is an example programme which can perform simple calculations (e.g. linear solvent strength predictions) based on experimental RP-HPLC data [16]. ChromSword is another commercially available software which combines both molecular structures and collected retention times to model retention [17]. Both programmes can be used to predict retention times of analytes under isocratic or linear gradient RP-HPLC methods [11, 12]. ChromGenius, an alternative predictive modelling software program has been used for a more efficient selection of the most optimal starting conditions for method development[18]. ChromGenius software similarly uses molecular structures and large databases of RP-HPLC retention times as the basis to predict, using built-in physicochemical prediction algorithms, retention time and chromatograms for new compounds [2].

Pfizer recently have been developing new quantitative structure retention time relationship models (QSRR) which currently outperform any commercial software available [19-27]. The predictive algorithms have been used even whilst still being refined and their application to support both selection of suitable starting conditions for RP-HPLC method development but also for troubleshooting purposes have been clear. Specific examples of troubleshooting include the efficient proposal of the most likely structure responsible for new peaks arising during commercial manufacturing or on stability studies allowing rapid structural confirmation. This has been a significant efficiency saving as the usual process for identification of likely structures often involves synthetic chemist brainstorming followed by synthesis of structures posed and the final confirmation by a structural elucidation team.

QSRR models are however not new. Introduced in the 1970s [28], QSRRS have gained significant attention for retention time prediction in various modes of HPLC. In QSRR studies, retention time observed in any HPLC experiment is related to molecular structure and the relationship is defined by numerical descriptions of the molecular structure. There are thousands of molecular descriptors available – many of which can be calculated (Dragon is a typically referred to calculation engine – [29]). To harness the most appropriate descriptors suitable for retention time prediction of any specific molecular structures, generally QSRR models are developed using a representative set of compounds (typically referred to as a training set of compounds) for which the retention times will be gathered experimentally. The most informative molecular descriptors (independent variables) can then be correlated with the retention times (dependent variables) using statistical significance as the selection strategy. This then produces a mathematical model which can be tested with new molecular structures which have experimentally measured retention times (but which are not in the training set) to check the accuracy of the model.

The thesis of this whole project was to test whether a new measure might bring some future way of providing additional molecular descriptors for improved insight into the interactions between molecule and stationary phase in HPLC. Most molecular descriptors used in chromatographic QSRR studies are related to the molecules themselves and chromatography is a complex dynamic situation wherein any one molecule in the column will have interactions with the stationary phase and mobile phase. The relative strength of each interaction determines the residence time of the analyte in the column and thus

being able to provide some insight on the molecule-stationary phase interactions might serve to enhance the prediction of the QSRR model in development.

The history and evolution of NMR spectroscopy is remarkably fascinating [30]. In 1942, Cornelis Jacobus Gorter published an article [31] describing his attempt to obtain ^{7}Li NMR spectra of LiCl, LiF and other analytes. The reasons for the failure to this original experiments were that LiF had long longitudinal (T_1) relaxation and low signal-to-noise ratio available, which was confirmed by successful NMR experiments that were obtained 10 years later with one of Gorter's original crystals [32]. Shortly after Gorter's discovery, Isidor Isaac Rabi (Columbia University) described how to detect and measure magnetic moments of nuclei. He discovered that applying an oscillating magnetic field could perturb and flip the magnetic moment of a nuclei away from its principal axis [33]. This is when NMR spectroscopy was born. He was awarded the Nobel Prize in Physics in 1944 [34].

Towards the end of Second World War in 1945, Felix Bloch began experimental work on radar scattering and the theory of magnetrons. Expecting that their water samples have long T_1 relaxation, Bloch went off to a ski trip to enable the system to return to equilibrium [35-37]. He later discovered that, in fact, the relaxation rate of water samples was only on the order of a few seconds or even shorter [32]. Soon after their successful experiments at Stanford, a very similar discovery was made at Harvard by Edward Mills Purcell and his co-workers [38, 39]. The work of both Bloch and Purcell was published in January 1946 and, 6 years later, they were both awarded the Nobel Prize for physics. This positive achievement in NMR experimental method development generated excitement for scientists and, as such, NMR now has a multitude of evolving applications in chemistry, biology, physics, geology and even medical diagnosis [40].

The fundamental theory of chemical shift [41-45] and indirect spin-spin coupling, or J coupling [46], was primarily developed in the early 1950s. Fourier transformed NMR (FT-NMR) spectroscopy was first introduced in 1966 [47]. This enabled the NMR spectrometers to compile the signals in the time domain. This discovery in NMR experimental methodology improved the signal-to-noise ratio of NMR spectroscopy. FT-NMR spectroscopy opened new paths for exciting, novel techniques such as two- and three-dimension NMR experiments for molecular characterisation [48]. Consequently, Richard R. Ernst was awarded with a Nobel Prize for his remarkable contribution to FT-NMR spectroscopy [49] in 1992.

Yet one challenge that remained a mystery involved observing broad NMR lines for solid samples due to magnetic dipolar interactions and non-averaged anisotropic interactions. Brownian motion of liquid enables the anisotropic interactions to be averaged hence sharp lines are observed. Raymond Andrews and his colleagues developed a method which involved rotating the sample at a fixed angle (54.44°) about the applied magnetic field [50]. This technique drastically removed the anisotropic interactions in solid samples and was referred as "magic" by Gorter in the early 1960s [30]. Similarly, Irving Lowe also came up with the idea of spinning solids which led to the concept of magic angle spinning (MAS) [50-52]. MAS NMR spectroscopy is widely used in solid-state NMR with spinning speeds up to 150 kHz has been achieved and proven very informative in recent years [53, 54]. Although MAS was a huge breakthrough in solid state NMR, the low signal sensitivity of low abundance nuclei (e.g. ^{13}C or ^{15}N) remained a challenge. The combination of a concept developed by Hartmann Hahn [55] in 1962 and MAS created the heavily used technique known as cross polarization [56] (CP-MAS) method [56]. The CP-MAS technique was and is effective for observing high resolution solid-state spectra of low sensitivity and abundance nuclei.

MAS NMR spectroscopy applications are not only limited to solid samples but also benefit solution and heterogeneous samples. In the mid-90's it was discovered that MAS NMR technique improved the resolution of solution and heterogeneous samples [57-60] by averaging the dipolar coupling and magnetic susceptibility in the samples [61]. This novel technique is known as High-Resolution Magic Angle Spinning NMR (HR-MAS NMR). Over the years, the principal application to date for ^{1}H HR-MAS technique has largely been used for the profiling of biological tissues [62, 63] and inorganic solids [64, 65]. Importantly, in the context of the current work, (^{1}H) HR-MAS NMR has previously been used to investigate and characterise the separation behaviour in RP-HPLC. Similar experimental conditions of RP-HPLC can be achieved using ^{1}H HR-MAS NMR. An advantage of ^{1}H HR-MAS is that well resolved spectra of heterogenous samples consisting of RP-HPLC stationary phase, mobile and analytes can be obtained.

In the mid-90's, a ^{1}H HR-MAS spectra of an attached organic solvent to a solid-phase synthesis beads was published by Fitch *et al.* [66] followed by several articles on the topic in the subsequent years [57, 67, 68]. Combined ^{13}C and ^{29}Si CP/MAS NMR experiments were very successful for detailed characterisation of silica surfaces and bonded phase [69, 70]. One of the first solid-state NMR spectra of reversed phase materials was published in the early 1980s by Maciel *et al.* [71]. ^{29}Si CP/MAS NMR was used to characterise

silica surfaces by examining the surface chemistry of various reversed phase materials [70, 72-75].

Alongside ^{19}Si CP/MAS NMR investigations, ^{13}C CP/MAS NMR was also used to gain further information of the structural and conformational order of immobilised monofunctional C8, C18 and C30 ligands [72, 76, 77]. The signal assignment was achieved by similar NMR studies of polyethylene [78] and nonporous silica materials [79]. Additionally, temperature [77, 80, 81] and solvent influence [70, 82-88] on RP materials was also reported using ^{13}C and ^{29}Si CP/MAS. Despite the success of CP/MAS NMR for characterising silica surface, the information obtained using this technique is often not quantitative [69].

In the 1980s, the molecular mobility of the RP materials via the determination of spin-lattice relaxation T_1 was achieved [87, 89, 90]. The idea of using ^{1}H HR-MAS NMR T_1 relaxation measurements for obtaining a quantitative measure to characterise the interaction behaviour of silica materials was explored by Klaus Albert [91-93]. Coen *et al.* similarly probed the molecular dynamics of RP materials by using ^{1}H HR-MAS NMR T_1 and T_2 relaxation measurements [94, 95]. They first investigated the water environments with a C18 bounded silica phase using ^{1}H HR-MAS NMR. Due to the impressive well-resolved spectra obtained in the ^{1}H HR-MAS NMR spectra, two sets of peaks were observed. Sharp peaks of water (free) and corresponding broad peaks (bound) were also observed. The broad peaks represent the water molecules in a more motionally restricted environment than the sharp resonances. This suggests the water molecules are bound to the silica surface (e.g. free silanols) [94]. Thanks to the high resolution obtained using this technique, site specific ^{1}H HR-MAS NMR relaxation can be obtained as proposed by Coen *et al.* [95]. As an alternative approach diffusion-ordered spectroscopy (DOSY) was also used to stimulate the HPLC retention behaviour. Caldarelli *et al*. [96-100] and others [97, 101-103] demonstrated a huge success using DOSY experiments for NMR chromatography. Even though DOSY experiments are successful in recent years, this technique does not provide site specific contribution to the retention mechanism and requires some specialised instrumentation and expertise.

Even though several very specific studies has been accomplished in this area, a systematic study of multiple samples with various experimental conditions still remains a mystery.

The thesis of this body of work was to test whether ^{1}H HR-MAS NMR spin-lattice (T_1) and spin-spin (T_2) relaxation measurements would bring some improved insight into the

interactions between molecule and stationary phase in RP-HPLC. To do this, a carefully selected series of molecules, mobile phases and five different RP-HPLC stationary phases (BEH-C18, BEH-phenyl, BEH-RP18, CSH-phenyl and HSS T_3) were investigated. NMR relaxation measurements provide vital information about the molecular dynamics and therefore the strength of interaction.

This thesis is divided into several Chapters: the history and theory of RP-HPLC method development is covered in Chapter 2. The fundamental theory of NMR spectroscopy and NMR relaxation is shortly outlined in Chapter 3 and 4. Chapters 5-9 summarize the results acquired in this study. Chapter 5 proposes a systematic ^{1}H HR-MAS NMR method development, (6) NMR spectroscopy, Raman spectroscopy and atomic force microscopy is used to characterise and probe the morphology of five RP stationary phases (7) approaches of expressing T_1 and T_2 relaxation, (8) illustrates the elaborated ^{1}H HR-MAS relaxation measurements in comparison to acquired HPLC retention times and (9) a comparison between NMR relaxation, experimental and predicted RP-HPLC retention behaviour of a series of compounds, mobile phases and stationary phases.

2 REVERSED PHASE HPLC

In this chapter, the origin, retention mechanism, intermolecular interactions, resolution and method development of reversed phase (RP) HPLC is covered. The content of this chapter is based upon several sources:[104] Snyder, L.R., J.J. Kirkland, and J.W. Dolan, Introduction to modern liquid chromatography. 2011: John Wiley & Sons; [1] Snyder, L.R., J.J. Kirkland, and J.L. Glajch, Practical HPLC method development. 2012: John Wiley & Sons; [105] Cazes, J. and R.P. Scott, Chromatography theory. Vol. 88. 2002: CRC Press; [106] Hanai, T., HPLC: a practical guide. Vol. 6. 1999: Royal Society of Chemistry; [107] Meyer, V.R., Practical high-performance liquid chromatography. 2013: John Wiley & Sons and various journals that are referenced throughout.

2.1 The origin of chromatography

Whilst the studies of Runge [108], Day [109] and Tsweet [110] were not considered significant at the time (1855-1903) their initial ideas would form the basis of the discovery of chromatography in the early 1930s, when the work of Tsweet was finally revisited by Kuhn and Lederer [111, 112], leading to subsequent fast developments in chromatography. A.J.P Martin and his co-workers made major contribution to liquid-liquid chromatography through invention of paper chromatography [113] and development of thin-layer chromatography[114] between the 1930s and mid 1950s. In the late 1950s, the amino-acid analyser was invented, which had the ability to analyse a mixture of amino acids via ion-exchange chromatography [115]. This technique was a fundamental precursor for the development of HPLC. Shortly after, Moore [116] invented gel permeation chromatography followed by a publication of a gel-permeation

chromatography by Waters Associates [117]. Both ion-exchange and gel permeation chromatography techniques were the precursor of HPLC development as they share very similar system set up.

Both techniques involve the pumping of solvents at high pressure through a reusable column; the column eluent is monitored via a selected detector which finally generates a chromatogram. However, each technique was limited to analysing a specific type of samples. The research groups of both Csaba Horváth and Josef Huber investigated the development of a multi-purpose HPLC system. Research groups and other scientists published their findings between 1966 to 1968 [118-121]. In the late 1960s, commercially available HPLC systems were first introduced by Waters Associates and DuPont which initially dominated the market. Consequently, several companies took interest in providing similar equipment and thus HPLC research became of interest. Furthermore, the first HPLC books were published in 1971 [122, 123]. Major developments in HPLC took place between 1960 and 2010. Some of the HPLC development involved drastic reduction of retention time, smaller particle size of the stationary phase and discovery of column materials with different supporting material and ligand groups for selectivity. However, the fundamental theory of HPLC development was proposed by Martin [124] in 1941 by suggesting that enhanced column efficiency can be obtained by using smaller particle size and high pressure across the column [104].

A decade later, Martin invented gas chromatography [125] (GC) which led to several theoretical findings[126, 127] which had a fundamental impact for the underlying theory of HPLC development. In early 1960, Giddings extended these theoretical studies to develop more specified applications of HPLC. This work proved to be crucial for the evolution of column efficiency and HPLC experimental method development which is now heavily used across the globe. Herein, only a very short but concise summary of the history and development in chromatography has been covered. More detailed contributions have been reported in several publications [128, 129].

2.2 HPLC Chromatography Process

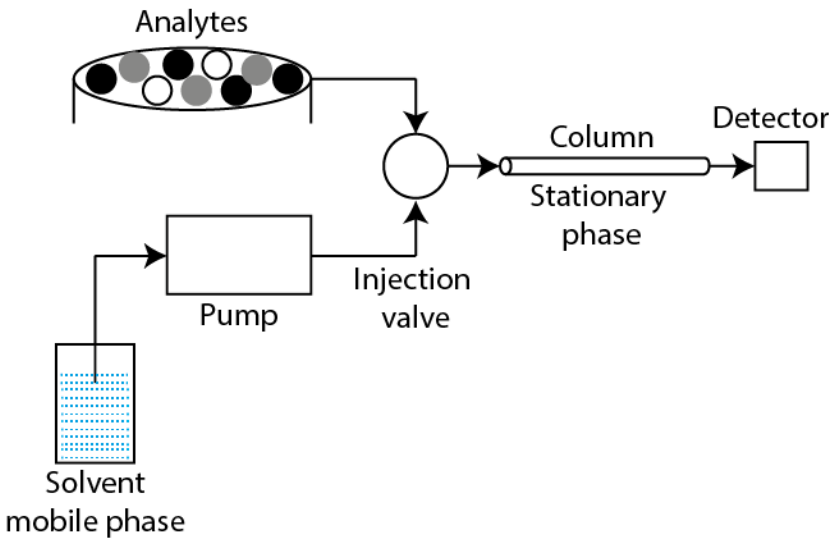

Figure 2.1. Schematic of HPLC system

An illustration of a typical HPLC system is shown in Figure 2.1. The arrows illustrate the flow of the solvent which is stored in the solvent reservoir and migrates to the detector. The solvent in HPLC is referred to as the mobile phase of the system. Once the sample is injected (usually very small amounts 1 to 20 μL), the chromatography process takes place in the column. The column is the stainless steel vessel into which the stationary phase slurry is packed. Once the samples leave the column, they are observed via a detector most frequently ultraviolet absorption (UV) coupled with mass spectrometer (MS). The mode of separation is determined by the column and mobile phase used in the system. Throughout this study, reversed-phase HPLC (RP-HPLC) is used unless stated otherwise. This involves the use of a nonpolar column (e.g. C18) and a polar mobile phase which consist of water and an organic solvent (e.g. acetonitrile). The mobile phase can be pumped through the column in various elution methods depending on the complexity of the sample requiring separation. For example, isocratic elution is a method whereby the composition of the mobile phase is kept constant throughout the run while gradient elution provides a method by which the mobile phase composition can be varied throughout the run and here the aqueous and organic components can be mixed via a mixing and proportionating valve in the pump and programmed to vary across the whole chromatographic analysis in a linear or indeed non-linear fashion. The stationary phase

plays a fundamental role in RP-HPLC as this is predominantly where separation takes place.

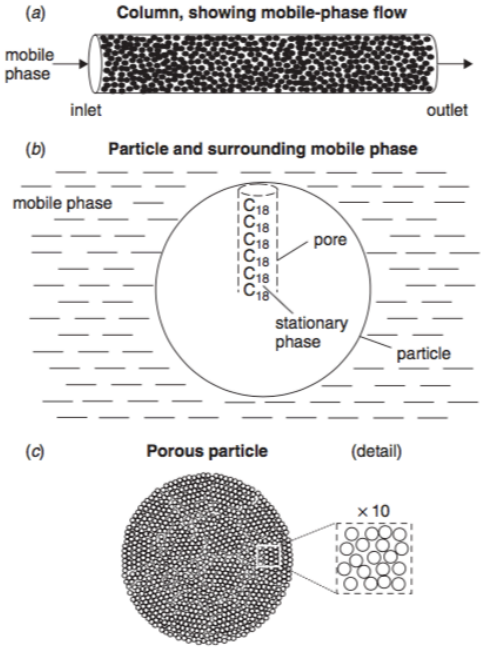

Figure 2.2. HPLC Column packed with porous particles. (a) Column packed with spherical particles, (b) schematic of an individual particle, showing an idealised pore with attached C18 chains, (c) picture of a spherical, porous particle, showing detail (10x expansion). Adapted from [104].

The column is a cylindrical tube typically packed with small particles (usually 1.7 to 5 µm in diameter and typically spherical) (Figure 2.2a and 2.3). These particles are typically made of porous silica (illustrated in Figure 2.2b).

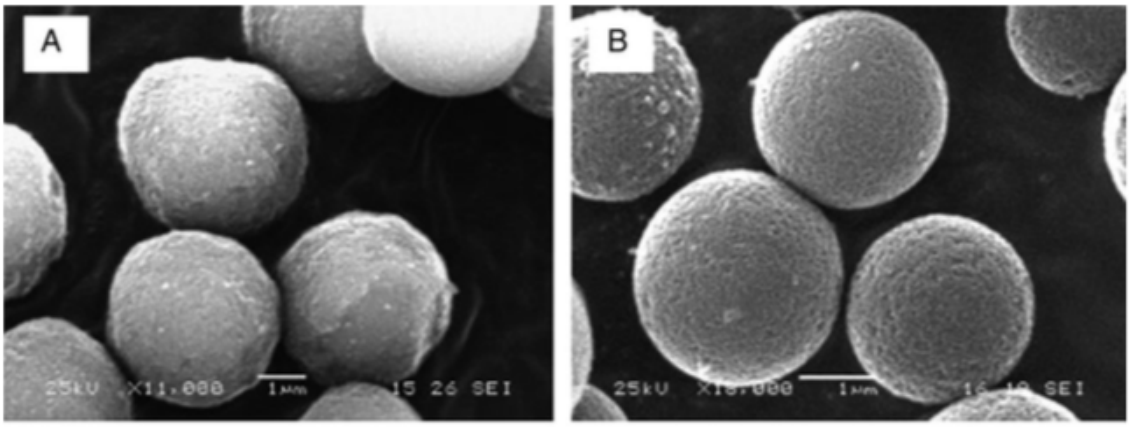

Figure 2.3. SEM images of the 3.6 µm core-shell Aeris WP C18 (A) and 1.7 µm stationary phase BEH300 C18. Adapted from [130, 131].

The inside of each pore is covered with the stationary phase ligand functional groups (in this case C_{18} groups are bounded onto the silica particles) for selectively. Since most of the surface of the particle is contained within these pores, most of the analyte molecules are retained inside the particle rather than its surface. Additionally, the internal surface of the pores forms approximately 99% of the total surface area of the particle. The external surface area (effect on separation) is in most cases considered to be negligible [104].

Even though retention is mainly controlled by the bonded ligand functional group and mobile phase chemistry, the surface area of the packing material also plays a crucial role. The surface area available is dependent on the pore size of the particle packed into the column. The pore size is of the particle is selected so that the analyte molecules can easily access the pores. The surface area of a particle is inversely proportional to the pore diameter [132]. For instance, a 3-µm particle with a 100 Å pore column will have approximately three times the surface area as a 3-µm particle, 300 Å pore column. Typically, particles pores with 100-150 Å are used to analyse small molecules and peptides while ≥300 Å pore size particles are used to separate proteins [133]. The analyte molecules can enter the particle pores via diffusion (there is usually no significant flow of mobile phase through the particle).

The elution order and retention time of a mixture of analytes is determined by the column as illustrated in Figure 2.4. Figure 2.4 shows a modelled separation of three aromatic compounds through a BEH-C18 column. For simplicity, the three analytes are represented as: ⊕ for toluene, ⊡ for naphthalene and • for biphenyl. The molecules of the mobile phase which leaves the column is known as the solvent front and is represented by x. Initially, the mixture is carried through the column by the mobile phase in consecutive steps (see Figure 2.4). Finally, the analyte leaves the column resulting in a change in the plot of the detector response against time. This is known as the chromatogram as shown in Figure 2.4. The intensities on the chromatograph are referred to as peaks. Each peak is characterised by the time each analyte leaves the column which is known as the retention time, t_R. At this point, the mixture has been separated. The different speed at which each analyte migrates through the column defines chromatography. As illustrated in Figure 2.4, toluene ($t_R = 2$) leaves the column followed by naphthalene ($t_R = 4$) and biphenyl ($t_R = 6$). This suggests, toluene moves through column the fastest, which indicates it is the least retained among the three analytes. The

next sections in this chapter cover several components of a HPLC system and the retention mechanisms in RP-HPLC.

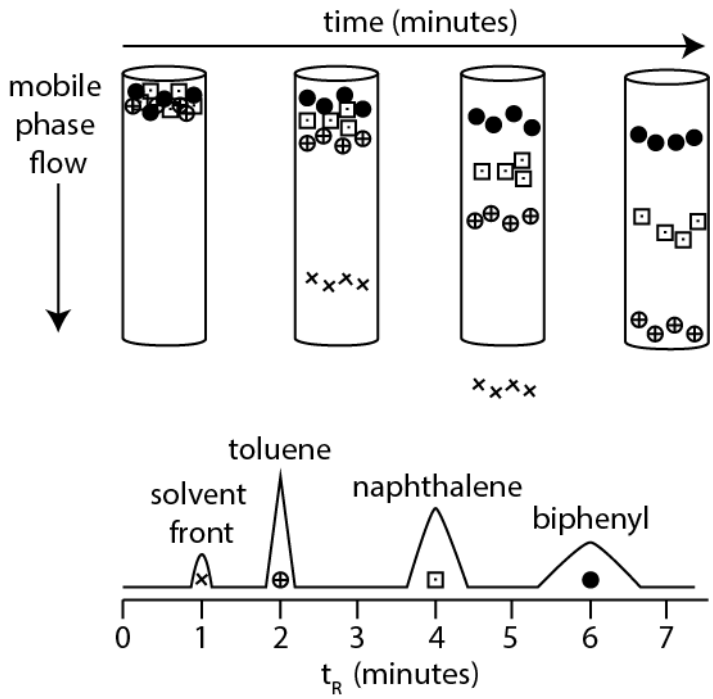

Figure 2.4. Modelled separation process in HPLC of a mobile phase (x), toluene (⊕), naphthalene (⊡) and biphenyl (•) with a corresponding chromatogram.

2.3 RP-HPLC Retention

The time it takes an analyte to travel through the column to the detector is known as the retention time, t_R. As shown in Figure 2.4, the modelled retention time of toluene, naphthalene and biphenyl are 2, 4 and 6 minutes respectively. The retention time of the solvent (solvent front) is 1 minute which is known as the column dead time t_0. This dead time essentially represents the time taken for a molecule which has 'zero' interactions with the stationary or mobile phase to travel from the point of injection to the detector. The velocity u_a at which toluene (a) flows through the column can be expressed as:

$$u_a = Ru \tag{2.1}$$

where u is velocity of solvent molecules and R is the fraction of toluene's molecules in the mobile phase.

Figure 2.5 illustrate the equilibrium distribution of toluene and naphthalene between the stationary phase and mobile phase. From Figure 2.5, R of toluene's molecules in the mobile phase can be determined by the equilibrium process:

$$toluene\ molecules\ in\ MP \Leftrightarrow toluene\ molecules\ in\ SP \tag{2.2}$$

where MP and SP represents mobile and stationary phase respectively. As shown in Figure 2.5, the molecules of toluene have a higher number of molecules in the mobile phase compared to the stationary phase pores, however naphthalene have a larger number of molecules present in the stationary phase compared to mobile which suggest naphthalene is retained longer compared to toluene. Due to the equilibrium process of naphthalene, naphthalene migrates more slowly through the column than toluene, as illustrated in Figure 2.5. However, the migration rate of an analyte is dependent on, the physic-chemical properties of the analyte together with the chemical characteristics of the mobile and stationary phases as well as the temperature of the system.

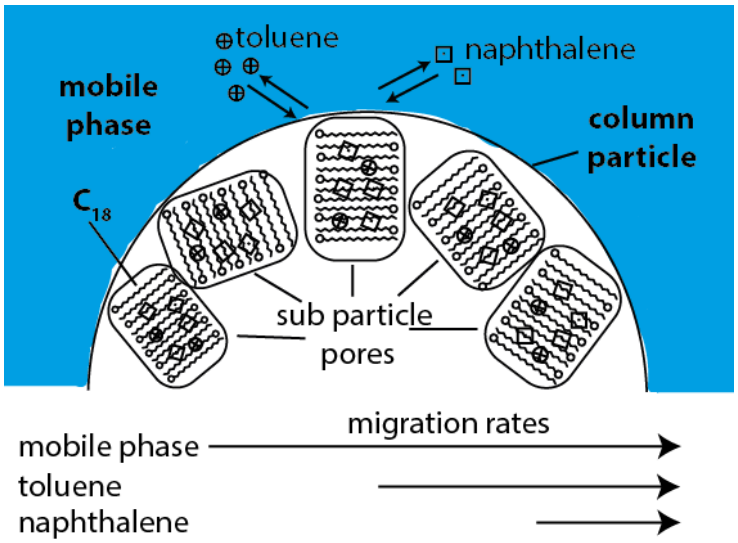

Figure 2.5. Illustration of the equilibrium distribution and migration rates of toluene (⊕), naphthalene (⊡) between a mobile phase and BEH-C18 stationary phase.

2.4 Column dead-time (t_0) and retention factor (k)

The retention factor of an analyte is defined as the amount of solute present in the stationary phase (s), divided by the amount of solute in the mobile phase (m). The quantity of the solute in each environment is equal to its concentration (C_s or C_m respectively) multiplied by the volume of the phase (V_s or V_m respectively) which equates to:

$$k = \frac{C_s V_s}{C_m V_m} = {}^{C_s}/_{C_m} \times {}^{V_s}/_{V_m} \tag{2.3}$$

$$= K\Psi \tag{2.4}$$

where $K = (C_s/C_m)$ is the equilibrium constant which is expressed in terms of the concentration of the analyte in the stationary phase (C_s) and mobile phase (C_m), and $\Psi = (V_s/V_m)$ is known as phase ratio (ratio of SP and MP in the column) [117]. The retention factor plays a major role for each peak observed in chromatography and furthermore enables us to improve the resolution and quality of the separation. Some solute molecules are either present in the MP or SP so that if the quantity of solute molecules in MP is defined R, the quantity of solutes present in the SP = 1 – R. Equation 2.3 can be expressed as:

$$k = \frac{1 - R}{R} \tag{2.5}$$

$$R = \frac{1}{1 + k} \tag{2.6}$$

The retention time of toluene (a) can be expressed as the distance travelled divided by its speed (u_a) such as:

$$t_R = \frac{L}{u_a} \tag{2.7}$$

where L is the column length which varies depending on the dimensions of column used. The solvent front can also be expressed as:

$$t_0 = \frac{L}{u} \tag{2.8}$$

Both equation 2.7 and 2.8 can be combined to give:

$$t_R = \frac{t_0 u}{u_a} \tag{2.9}$$

Recalling equation 2.1 ($R = u_a/u$), equation 2.9 can be rewritten as:

$$t_R = t_0(1 + k) \tag{2.10}$$

Equation 2.10 can be rewritten in terms of the mobile phase flow (F) and retention volume $V_R = t_R F$ such as:

$$V_R = V_m(1 + k) \tag{2.11}$$

where V_m is column dead volume = $t_0 F$. Equation 2.10 can be rearranged as:

$$k = \frac{t_R - t_0}{t_0} \tag{2.12}$$

Equation 2.12 enables us to determine the retention factor of each peak observed in a chromatograph. However, to determine this retention factor of an analyte, the solvent front must be determined which is usually observed in the early parts of the chromatogram.

2.5 RP-HPLC resolution

As previously mentioned, RP-HPLC method development is the process of selecting the optimal separating conditions to achieve the desired goals of separation [134]. The separation of two peaks (e.g. i and j) can be expressed in terms of their resolution (R_s) such as:

$$R_s = \frac{2\left[t_{R(j)} - t_{R(i)}\right]}{W_i + W_j} \tag{2.13}$$

Where $t_{R(i)}$ and $t_{R(j)}$are the retention time of peak i and j respectively. Additionally, W_i and W_j are the baseline width of peak i and j respectively. Better separation (higher resolution) is achieved with larger difference in retention time and narrow peak width. The essential role of HPLC method development is to achieve the best separation and resolution of every compound in a mixture. Generally, if two or more compounds are analysed, a $R_s \geq 2$ is expected. Alternatively, RP-HPLC R_s can be approximately expressed as:

$$R_s = \left(\frac{1}{4}\right) \underbrace{\left[\frac{k}{(1+k)}\right]}_{(a)} \underbrace{(\alpha - 1)}_{(b)} \underbrace{\sqrt{N}}_{(c)} \tag{2.14}$$

where k is the retention factor (term a), α is the separation factor (term b) and N is the column efficiency (term c)[135]. The retention factor is the ratio of the analyte retention time on the column to the retention time of a non-retained compound. The column efficiency also known as the number of theoretical plates is a measure of the dispersion of the analyte band as it goes through the HPLC system and column which indicates the column performance [136-138]. The separation factor is also referred to as the separation selectivity is the ability of the chromatographic system to chemically differentiate between sample components [138, 139] and can be expressed as:

$$\alpha = \frac{k_j}{k_i} \tag{2.15}$$

where k_j and k_i are the retention factor of peak i and j respectively. Each term in equation 2.14 can be varied to improve the final resolution of the chromatogram.

However, the separation factor (term b) by far provides the greatest effect on the final resolution achieved. Furthermore, the Purnell equation [140, 141] is commonly used to determine the R_s between two peaks:

$$R_s = \frac{\sqrt{N}}{4}\left(\frac{\alpha - 1}{\alpha}\right)\left(\frac{k}{(1+k)}\right) \tag{2.16}$$

To achieve the optimal separating RP-HPLC conditions, several experimental parameters must be systematically varied to achieve the separation goals of the method (see Table 2.1). This process can be divided into 4 stages. Initially, a column is carefully selected which is most likely to separate the compounds. Secondly, the organic solvent (%B) percentage is varied to an appropriate range. A flow rate is also chosen according to the column properties (e.g. column length, diameter and stationary particle size). Finally, a running time which is sufficiently long enough to allow all the analytes to elute must be used.

2.5.1 Optimising the retention factor (*k*)

The retention factor (term a of equation 2.14) of analytes in RP-HPLC chromatography can be altered by changing the organic solvent percentage (solvent B%). The first step of achieving a good retention factor is by setting the running times not too long or too short. The overall aim is to set a running time where all the analytes elute with sharp and narrow peaks (good resolution). This step during method development can be challenging when dealing with bulky and ionisable analytes. The running time must be chosen wisely to reduce running time of large set of samples. Additionally, in some cases some analytes do not elute after long running times in isocratic mode. Therefore, steep gradient elution can be used to elute the analytes with shorter running times. As previously mentioned, the effect of the organic solvent percentage in RP-HPLC retention [142-144] can be expressed as:

$$\log k = \log k_w - S\emptyset \tag{2.17}$$

Initially, a high percentage of the organic solvent can be used (90% or 80%) to ensure all the analytes are eluted. This percentage can gradually be reduced until desirable (~50%). As a rule of thumb, it is not suitable to change the organic solvent by more than 30% between different experiments.

2.5.2 Optimising selectivity (α)

When the separation needs additional improvement, the method selectivity (term b of equation 2.14) is adjusted to obtain a better separation. Several experimental conditions proposed in Table 2.1 can be adjusted to optimise the selectivity of the method including the %B, the chosen solvent B (generally acetonitrile or methanol), temperature, column type, mobile phase pH, buffer concentration and additive ion-pair reagents. However, changes to these experimental conditions can also affect the retention factor. Hence, this needs to be taken into consideration. Similarly, to optimise the retention factor, the organic solvent percentage is varied. This is then followed by a change in temperature until good peak shapes and resolution is obtained.

2.5.3 Optimizing the column plate number (*N*)

2.5.3.1 Column properties

Once a good peak separation and resolution is achieved, the method can be optimised further by varying the column properties (e.g. column length, flow rate, particle size). A change in such column properties can either increase or reduce the number of theoretical plates N (equation 2.18).

$$N = 16\left(\frac{tr}{W}\right)^2 \tag{2.18}$$

Where *tr* is the retention time and *W* is the peak width. Under isocratic conditions, a change in column properties will not affect either peak retention or spacing (k and α). Therefore, previous suggested optimised parameter will not be affected by a change in column properties. As a rule of thumb, an increase in N increases the resolution of the chromatogram at the expense of longer running times. Conversely, a reduction in N reduces the running time of the experiments. Since the running time is proportional to the column length/flow rate, running times increases uniformly with increased column length or a reduction in flow rate. However, the column length, flow rate and particle size need to be carefully selected to achieve a reasonable running time. Furthermore, *N* can be increased with larger column particle size. In recent years, small column particle (e.g. 1.7

μm) have been favoured over the commonly used 5 μm column particle size for faster analysis.

2.5.3.2 Fast HPLC

RP-HPLC separation of a series of analytes can be achieved in couple of minutes with an adequate optimised method. Once the k and α are fully optimised, the resolution and running time can then be optimised by N. Additionally reduction of running times can be achieved without affecting the N by using ultra-high pressure RP-HPLC, higher temperature and specially designed column particles.

2.5.3.3 Ultra-high pressure

Conventional HPLC systems run at a maximum of 6000 psi or 400 bar. Ultra-high pressure liquid chromatography or U-HPLC can exceed pressures of 6000 psi which yields shorter running times[145, 146]. U-HPLC can reduce running times by 2 to 6 folds in some cases [119]. Even though U-HPLC enables a reduction to the experimental running time, this comes with a cost; the mobile phase viscosity increases with an increase in pressure. Due to the viscosity of the mobile phase through the packed stationary phase, the internal temperature of the column potentially fluctuates which consequently affects k, α and N [147]. Thus, U-HPLC systems can further complicate the method development.

2.5.3.4 High temperature

RP-HPLC analyses usually operate between room temperature and 50 °C, however some experiments have proven possible at extremely high temperatures above 100 °C. Using extremely high temperatures enables a shortened experimental running time, sometimes improving resolution and therefore increasing the N [148-151]. As far as the optimised column length, particle size and flow are carefully selected, an increase in a temperature will improve N. Furthermore, an increase in temperature reduces the mobile phase viscosity and increases the solute diffusion coefficient (D_m). A lowering of mobile phase viscosity enables higher flow rates for the same pressure [104]. Subsequently, an increase in temperature shortens the running time while keeping N the same and vice versa.

Even though using higher temperatures has proven to be advantageous, this technique can lead to a few complications. Using high temperatures can lead to sample degradation and temperature gradients can be caused by using higher temperatures [152, 153]. Temperature gradients can be minimised by using narrower diameter columns, which enables faster system equilibration to be achieved or by careful use of extra system heating components pre and post column to remove temperature gradients. Additionally, at higher temperatures, columns stability can be affected especially under extreme pH conditions.

2.5.3.5 Specially designed column particles

Several column designs are commercially available including column particles with either pellicular or shell particles design. These particles of special designs have proven useful for selectively separating large or small analytes and which are robust at high flow rates [154].

2.6 HPLC experimental parameters and effect on separation

Table 2.1 shows the effect of varying various conditions to control the retention (k) behaviour of an analyte and more specifically control the separation selectivity (α) or column efficiency (N).

2.6.1 Mobile phase

In RP-HPLC, the mobile phase is made of a mixture of water or aqueous buffer (solvent A) and an organic solvent (solvent B) such as acetonitrile, methanol etc [155]. Other organic solvents such as isopropanol (IPA) and tetrahydrofuran (THF) are less frequently used. Ideally, the organic solvents need to be water-miscible, non-viscous, stable under a range of conditions, transparent and commercially available at reasonable cost.

Table 2.1. Effect of different experimental conditions on the retention (k), selectivity (α) and column efficiency (N)[104].

Condition	k	α	N
Organic solvent (acetonitrile, methanol etc.)	+	++*	-
Organic solvent strength	++*	+*	-
Temperature	+	+*	+
Colum chemistry (C18, phenyl etc.)	+	++*	-
Mobile phase pH[a]	++	++*	+
Buffer concentration[a]	+	+	-
Ion-pair-reagent concentration[a]	++	++*	+
Column length (L)	0	0	++*
Column particle size	0	0	++*
Flow rate	0	0	+*
Pressure	-	-	+*

where; ++ indicates major effect, + minor effect, - relatively small effect and 0 no effect. [a] indicate condition that primarily affects ionisable analytes (acids and bases). * indicates the experimental conditions that predominantly dominates the k, α and N respectively. For example, the organic solvent or column chemistry is varied to control α while pressure is varied to only control N.

2.6.2 Organic solvent strength

The retention in RP-HPLC is dependent on the percentage of organic solvent (solvent B) in the mobile phase as:

$$\log k = \log k_w - S\emptyset \tag{2.19}$$

where k_w is the value of k with 0% of solvent B, S is a constant for a given analyte when only solvent B is varied and $\emptyset$ is the volume ratio of solvent B in the mobile phase. As the ratio of the organic solvent (solvent B) is increased, the analytes retention is reduced

and hence elute faster. A mobile phase which provides small retention times (higher solvent B%) is referred to a strong mobile phase [119, 120]. Furthermore, a mobile phase with higher water percentage is known as a weak mobile phase. An increase of 10% of organic solvent usually reduces the retention times by a factor of 2 to 3 [121, 122]. The final percentage of solvent B must be carefully selected to obtain suitable separation and retention within the series of analytes.

2.6.3 Column chemistry

Typically, a non-polar stationary phase (e.g. BEH-C18) and polar (water containing) mobile phases are used in RP-HPLC. Polar analytes will interact more with polar mobile phases and thus, will be eluted quicker (larger *R* and shorter *k*), while non-polar analytes will interact strongly with the stationary phase and hence will be retained longer (smaller *R* and longer *k*).

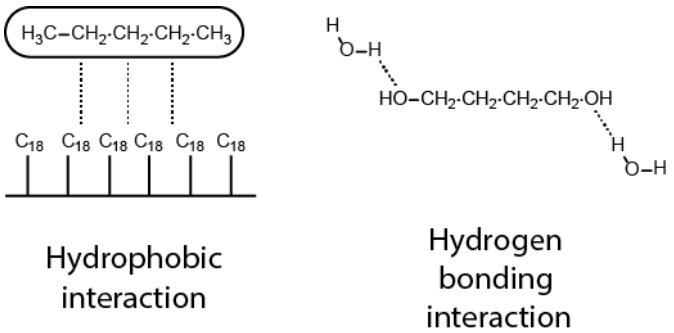

Figure 2.6. Illustration of hydrophobic interactions and hydrogen bonding interactions.

Figure 2.6 illustrates hydrophobic interactions that could occur between a nonpolar analyte and stationary phase and hydrogen bonding within a polar mobile phase and polar analyte. The "column chemistry" plays a fundamental role in RP-HPLC selectivity. Hence, the stationary phase must be carefully selected for the appropriate goal of separation. Several column parameters should be taken into consideration for selecting the optimal column. Table 2.2 illustrates a few reversed phase stationary phases with their hydrophobicity properties. Most of these reversed phase stationary phases can be prepared by anchoring different organic moieties to substrates, generally mono-, di- or trifunctional (see Figure 2.7) silanes to silica, under specific reaction conditions [73, 156-165]. This can lead to a network of structural elements at the surface of the stationary phases which influences the separation process [73, 161, 165, 166].

Table 2.2. Commonly used RP-HPLC stationary phases with hydrophobicity properties.

Stationary Phase		
C18	Decreasing	Non-polar
C8	Hydrophobicity/	Analytes
C4	increasing polarity	are retained
Cyano		
Phenyl		
Amino		

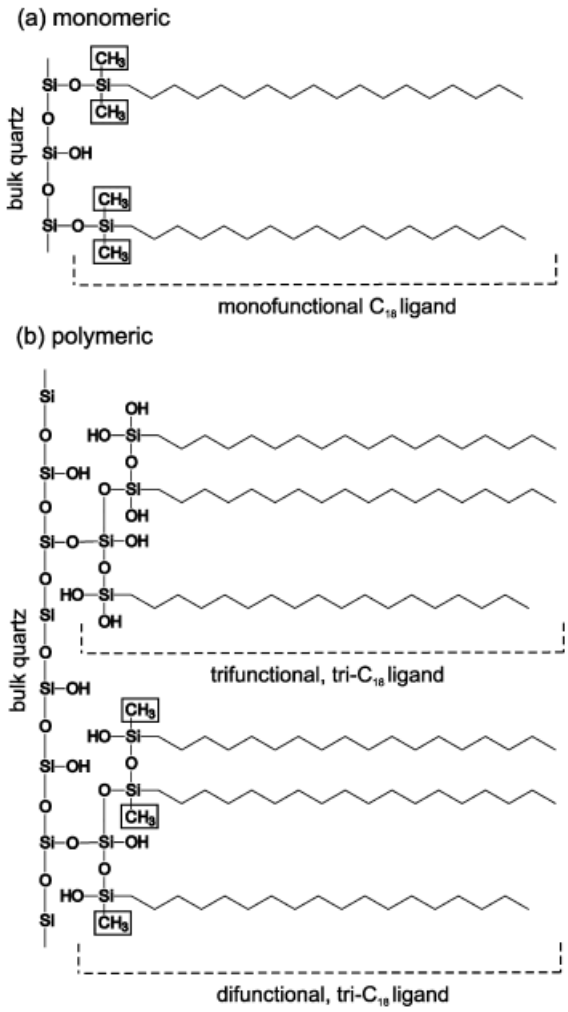

Figure 2.7. Structure illustration of (a) monomeric C18 and (b) polymeric C18 chromatography models illustrating the different ligand types. Adapted from [167].

2.6.4 Particle shape

There are two main types of basic silica particle shapes available; spherical and irregular. Irregular shaped silica is cheaper because of poor column packing which leads to less homogeneity and worsened resolution. Furthermore, the use of high flow and pressure rates can disintegrate the column materials into fine particles which can eventually block the system. Thus, spherical shaped column particles are generally used in RP-HPLC. Typically, the particle shape is determined by scanning electron microscopy. Figure 2.8 demonstrates irregular and spherical shaped silica columns [168, 169].

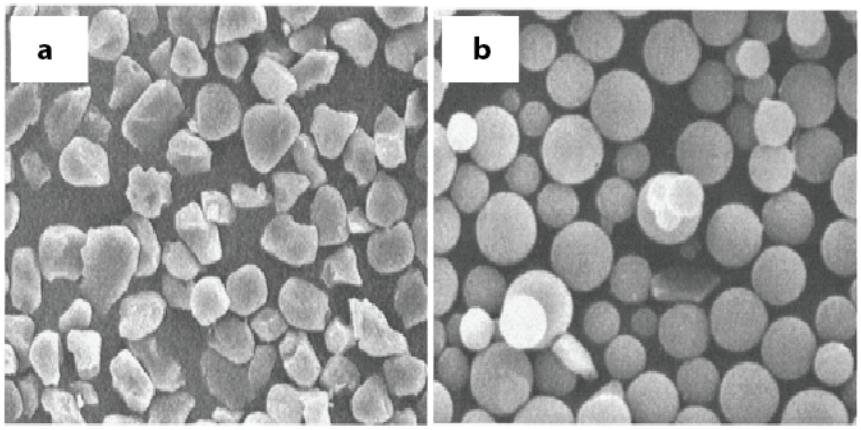

Figure 2.8. SEMs of (a) PXS PAC column and (b) Brownlee RP-18 column. Adapted from [168].

2.6.5 Particle size

Particle size refers to the average diameter of the column packing material. Reducing the particle size's diameter increases the ability for faster analyses. However, using smaller particle size diameter increases the back pressure in the system. However, the particle size cannot be defined as a single value but as a distribution of particles over a wide range sizes [170]. Most HPLC packing materials have a Gaussian particle size distribution where the position of the maximum is the mean particle diameter and the standard deviation represents the distribution width [171-174]. Smaller particle size distribution leads to uniform column packing and therefore better separation efficiency. However, small particles (fines less than 1 μm) leads to the column frit clogging which in turns rises the column back pressure [175-177]. The particle size and distribution can be acquired

using several analytical techniques including electron microscopy [168, 178, 179] and laser diffraction [180]. Figure 2.9 illustrates the particle size distribution of RP18 columns [178, 181].

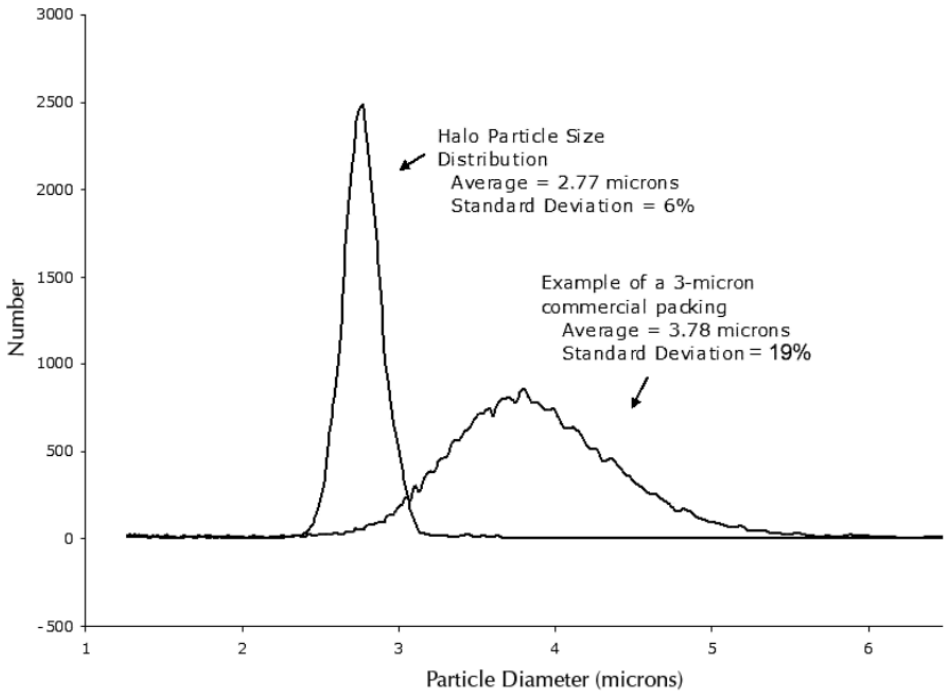

Figure 2.9. Particle size distributions of 2.7 µm particles (very narrow distribution) compared to 3 µm totally porous particle. Adapted from [178, 181].

2.6.6 Pore size

Pore sizes of stationary phases are proportional to the hydrodynamic volume of the analyte molecule. Larger pores enable larger molecules to access the bounded ligand within the pores of the stationary phase where the maximum separation takes place. Pore sizes of 150 Å are used to retain small molecules. 300 Å or larger pore sizes are used to retain larger molecular weight compounds (>2000 Da). Generally, the pore sizes should be three times the hydrodynamic diameter of the molecule to enable easy access to the pores [129]. Additionally, the stationary phase pore sizes provided by the manufacturers is the diameter corresponding to the maximum of the pore size distribution curve, acquired from the adsorption branch of nitrogen isotherm [177]. The pore size distribution of several HPLC stationary phases can vary considerably as illustrated in Figure 2.10.

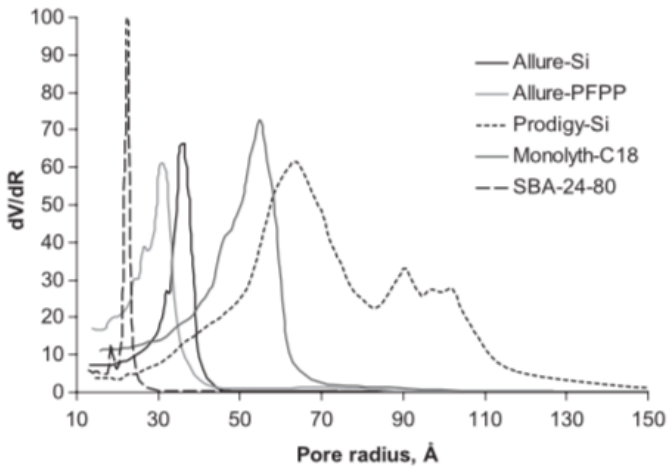

Figure 2.10. Pore size distribution of various HPLC materials. Adapted from [177].

2.6.7 Surface area

The surface area can affect several chromatographic parameters and the efficiency of the column. Columns with higher surface area tend to have better retention, capacity and resolution. In comparison, smaller surface area columns can equilibrate quicker which is very useful for gradient elution experiment.

BET (Brunauer, Emmett and Teller) nitrogen or argon adsorption/desorption measurements [182, 183] are commonly used to determine the surface area of HPLC stationary phases based on the multilayer adsorption of nitrogen at the boiling temperature of liquid nitrogen (77 K). There are several variation of BET theory available and different instrumental approaches to determination of nitrogen isotherms [184]. A typical nitrogen absorption isotherm is displayed in Figure 2.11 [177]. The region between 0.05 and 0.25 of relative pressure is known as the monolayer capacity (n_m) which is the amount of nitrogen molecules absorbed onto the sample surface in a monolayer approach and where the BET theory is valid. The BET equation illustrates the dependence of the amount of absorbed nitrogen as a function of relative equilibrium pressure (p/p_0):

$$\frac{\frac{p}{p_0}}{n\left(1-\frac{p}{p_0}\right)} = \frac{1}{n_m C} + \frac{(C-1)}{n_m C}\frac{p}{p_0} \tag{2.20}$$

where n_m is the monolayer capacity, C is energetic constant of nitrogen interaction with the surface, p/p_0 is the relative equilibrium pressure and n amount of adsorbed [177]. Figure 2.11 demonstrates the dependence of the amount of nitrogen adsorbed onto the

sample surface against the relative pressure. The surface area of the sample is calculated by the product of the total amount of nitrogen in the monolayer and the nitrogen molecular area (16.4 Å^2). This is with the assumption that a nitrogen molecule occupies 16.4 Å^2 [177, 185] on the silica surface.

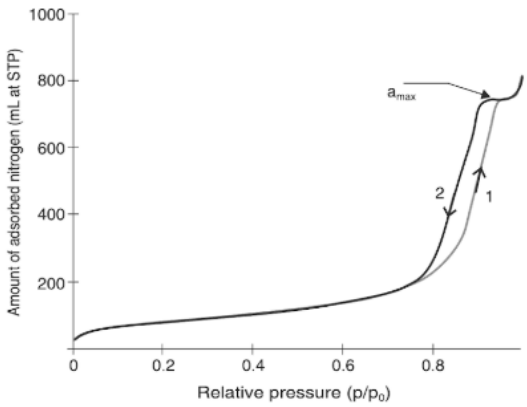

Figure 2.11. Nitrogen adsorption isotherm: 1, adsorption branch: 2, desorption branch. Adapted from [177].

2.6.8 Pore volume

The pore volume of the columns considers the pore size and the number of pores in the stationary phase. The pore volume of different stationary phases is usually similar. From Figure 2.11, above 0.7 there is a fast increase of adsorbed amount of nitrogen. This is due to the capillary condensation of nitrogen inside the adsorbent pores. The amount of adsorbed nitrogen increases until the pore volume is completely filled with liquid nitrogen. The small flat section (a_{max}) indicates all the pores are filled and therefore relative equilibrium pressure approaches the saturation pressure. This flat section can be used to determine the adsorbent pore volume:

$$V_{pore} = V_L \frac{a_{max} P}{RT} \tag{2.21}$$

where V_{pore} is the pore volume, V_L is the molar volume of liquid nitrogen (34.7 mL/mol), $a_{max}$is the maximum amount of nitrogen in the pores expressed in mL at 1 atm and 25 °C, P is the pressure (1 atm), R is the gas constant ($0.082 \frac{L \cdot atm}{K \cdot mol}$) and T is the temperature at 298 K [177]. Furthermore, the desorption branch of Figure 2.11 is generally used to determine the pore size distribution of the adsorbent [177].

2.6.9 pH range

The pH range indicates the pH values at which the column can operate without damaging the stationary phase. The pH range of the columns is crucial for the separation of compounds which can be ionised and needs to be kept under a controlled pH by using buffer solution. Traditional bare silica is robust within pH values of 2.5 to 7.5. More recently, a variety of stationary phases have been manufactured with larger pH ranges.

2.6.10 Mobile phase pH and buffer concentration

The functional groups of analytes are fundamental for the retention properties of RP-HPLC. Polar (less hydrophobic) functional groups such as –NHCHO, CH_2OH or –OH will have shorter retention times in comparison to less polar (more hydrophobic) groups such as methyl and ethyl moieties. Acids and bases can easily be ionized in RP-HPLC and therefore have little or no retention [186, 187]. The pH of the mobile phase can be altered by using additives and buffers to increase the retention properties of such ionised analytes. The Henderson-Hasselbalch [188, 189] equation is generally used to calculate the pH of a system using the pK_a of acidic species in the solution such as:

$$HA \overset{K_a}{\Leftrightarrow} A^- + H_3O^+ \tag{2.22}$$

$$K_a = \frac{[H_3O^+][A^-]}{[HA]} \tag{2.23}$$

$$log_{10}K_a = log_{10}[H_3O^+] + log_{10}\frac{[A^-]}{[HA]} \tag{2.24}$$

$$-pK_a = -pH + log_{10}\frac{[A^-]}{[HA]} \tag{2.25}$$

$$pH = pK_a + log_{10}\frac{[A^-]}{[HA]} \tag{2.26}$$

Buffers in RP-HPLC are generally used for either acids and bases which must maintain a constant pH to achieve reproducible retention times during the separation process. Measuring the pH of a mobile phase with the presence of the organic solvent leads to irreproducible measurements because the electrode response tends to drift for the organic-water mobile phase. Thus, the pH of buffers is generally measured in solvent A only (water content) prior to the addition of the selected organic solvent. Even though the final

pH of the final mobile phase could be slightly different, this small difference in pH is insignificant in RP-HPLC [190]. Several buffer properties need to be taken into consideration in RP-HPLC such as:

- buffer pH range and pK_a
- solubility
- UV absorbance (when UV detector is used)
- volatility (when mass spectrometric detector is used)
- ion-pairing properties
- stability and compatibility with system

For buffers to maintain a controlled and stable pH, this depends on a few factors such as:

- buffer concentration
- pK_a of the buffer
- pH of mobile phase

Buffer capacity can be described as the efficiency of a buffer to resist small changes to pH. The buffer capacity (β) can be expressed in terms of the amount of strong acid and base (in grams) which is required to change 1 litre buffer solution by 1 pH unit [191]:

$$\beta = \frac{\Delta B}{\Delta pH} \tag{2.27}$$

where ΔB is weight of strong acid or base to change the pH of 1 litre of buffer solution by 1 pH unit and ΔpH is the change of pH caused by added strong acid or base. The buffer capacity depends on the ratio of the salt to acid or base and buffer concentration. The Van Slyke equation [130] expressed the relationship between the buffer capacity and buffer concentration such as:

$$\beta = 2.3C\frac{K_a[H_3O^+]}{(K_a + [H_3O^+])_2} \tag{2.28}$$

where C is the buffer concentration. The optimum buffering capacity is achieved when the concentration of the two forms of the buffer (e.g. HA and A^-) are equal, in other words, when the pK_a value is the same as the mobile phase pH. The capacity of the buffer decreases as the pK_a value of the buffer and the pH of the mobile phase become increasingly different. The buffer pK_a needs to be within ±1 of the mobile pH to achieve an acceptable capacity. Typically, a concentration range of 5 to 25 mM is used for buffers

in RP-HPLC. To acquire optimal buffering throughout the system, the analytes are also dissolved in the mobile phase [192]. Table 2.3 proposes a few examples of commonly used buffers in RP-HPLC with properties such as pK_a values, buffer estimated range and UV ranges.

Table 2.3. Commonly used buffers in RP-HPLC. Adapted from [1]

Buffer acid	pK_a (25 °C)	Estimated buffer range	UV range
Trifluoroacetic acid	>2	1.5-2.5	210 nm
Phosphoric acid	2.1	1.5-3.5	< 200 nm
Monophosphate	7.2	6.0-8.5	< 200 nm
Diphosphate	12.3	11.0-13.5	< 200 nm
Citric acid	3.1	2.0-4.5	230 nm
Formic acid	3.8	2.5-5.0	210 nm
Acetic acid	4.8	3.5-6.0	210 nm
Ammonia	9.2	8.0-10.5	200 nm

2.6.11 Endcapping

Endcapping enables the minimisation of unwanted surface silanol groups which can lead to secondary interaction which can reduce the selectivity and resolution of the column. This predominantly affects basic and ionic analytes. Silylating reagents (e.g. trimethylchlorosilane or dichlorodimethylsilane) are used to produce trimethylsilyl (TMS) capped groups. The reaction of these end-capping reagents can reduce the silanol surface concentration by a factor of 2 (from approximately 8 μmol/m^2 to 4 μmol/m^2) [193].

2.6.12 Carbon load

Carbon load signifies the percentage weight of the carbon in the stationary phase. This indicates the amount of organic material present on the surface of the stationary phase. The higher the carbon load, the longer non-polar analyte can be retained. Stationary

phases with different endcapping groups will have different carbon load percentages. More importantly, the carbon load of the stationary phase depends on both the relative surface coverage and the chain length of the bonded function groups [136]. Generally, a CHN (carbon, hydrogen and nitrogen) analyser is used to determine the carbon load of the stationary phase. The carbon load is measured by heating up the stationary phase until the functional ligand (e.g. hydrocarbon chains for BEH-C18) burns off as CO_2 [177, 194-196]. The carbon percentage of carbon quantified by either measuring the released CO_2 or weight difference.

2.6.13 Surface Coverage (ligand density)

The surface coverage of the stationary phase indicates a measure of the retentivity and hydrophobicity of the column. This is the concentration of the stationary phase per unit area which is bonded to the supporting material. The carbon percent [197, 198] of the stationary phase can be used to calculate the ligand surface density (μmol/m^2):

$$surface\ coverage\ \left(\frac{\mu\text{mol}}{m^2}\right) = \frac{\%C\ \times\ 10^6}{1200nA} \tag{2.29}$$

where $\%C$ is expressed as a ratio weights, n is the number of carbons in the bonded phase, A is the surface area of the substrate (m^2/g). Additionally, the surface coverage of HPLC stationary phases has previously been investigated via CP/MAS NMR techniques [69, 92, 199-202].

2.6.14 Temperature effect on retention

Temperature has a substantial effect on retention in RP-HPLC. For most analytes, the effect of varied temperature on the HPLC retention can be expressed in terms of the Van't Hoff equation:

$$\log k = A + \frac{B}{T_K} \tag{2.30}$$

where A and B are the temperature independent constants of an analyte and T_K is the temperature (K). The retention time usually decreases with an increase in temperature per

1-2% per °C [1]. Therefore, a 50 °C increase in temperature will reduce the retention time by 2-fold. Furthermore, an increase in temperature deteriorates the separation as some analyte could coelute.

2.6.15 Temperature Limit

Stationary phase manufacturers such as Waters propose temperature limits at which the columns can operate without any damage taking place. High temperature can potentially lead to basic hydrolysis of the silica support and acidic hydrolysis of the stationary phase.

2.7 Intermolecular interactions

The force of attraction between an analyte, mobile phase and stationary phase could be due a variety of intermolecular interactions. Different types of intermolecular interaction that take places in RP-HPLC are illustrated in Figure 2.12.

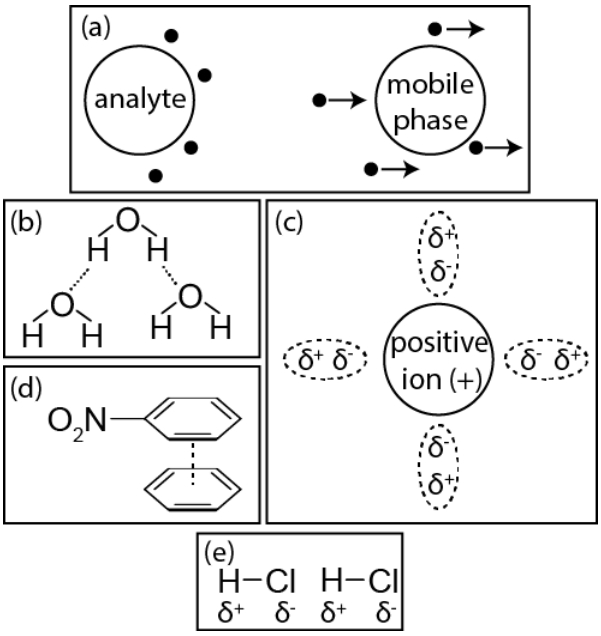

Figure 2.12. Visualisation of HPLC intermolecular interactions such as (a) dispersion interactions, (b) hydrogen bonding, (c) ionic interactions, (d) charge transfer and (e) dipole-dipole interactions.

Three properties are fundamental in any molecular interaction which includes the type of interaction, the strength of interaction and the probability for the interaction to occur. A quantitative atomic scale measurement of these interactions could potentially enable

scientists to predict the retention properties of numerous compounds based on their chemical structures.

2.7.1 Dispersion interactions

Dispersion interaction (or London's dispersive force) were first described by London [203]. One of the best definitions of dispersion interactions was proposed by Glasstone; "Although the physical significance probably cannot be clearly defined, it may be imagined that an instantaneous picture of a molecule would show various arrangements of nuclei and electrons having dipole moments. These rapidly varying dipoles, when averaged over many configurations, would give a resultant of zero. However, at any instant, they would offer electrical interactions with another molecule, resulting in interactive forces" [105, 204]. Dispersion forces are ubiquitous and present in all molecular interactions [105]. These interactions are due to random, instantaneous position of electrons surrounding adjacent atoms of either the solvent or analyte molecules. This type of intermolecular force is responsible for hydrophobic interactions (water-fearing) [205]. This term has arisen because hydrocarbons do not dissolve readily in water. As the strength of dispersion interaction increases for large, less polar analytes, the retention behaviour between the analytes and stationary phases correspondingly increases in RP-HPLC.

2.7.2 Hydrophobic interactions

As previously mentioned, hydrophobic force in simple terms means the "fear of water" force. There is no clear indication of how the term hydrophobic was generated but could be due to the immiscibility property of *n*-heptane with a very polar solvent such as water. Both *n*-heptane and water are immiscible, not because they repel each other but simply because the forces within the *n*-heptane and the force within the water molecule are greater than the force between *n*-heptane and water molecules. Thus, immiscibility occurs between the forces of interaction within each solvent is very much greater compared to force between each other. In RP-HPLC, the stationary phase is hydrophobic (e.g. alkyl chains) which has a strong affinity for hydrophobic compounds. Thus, the hydrophobic

molecules in the system will bind to the column while the hydrophilic molecule will elute with the mobile phase.

2.7.3 Dipole-dipole interactions

Dipole-dipole interactions take place between the negative side of a molecule and an adjacent positive side of another molecule. Dipoles are formed due to a large difference in electronegativity within two covalently bonded atoms. Thus, the electrons are unequally shared because the dominating electronegative atom attracts the shared electrons towards itself. Therefore, this atom has a slightly negative charge while the other has positive charge. Since dipole-dipole interactions predominantly take place in close proximities, the strength of dipole-dipole interaction is dependent on the dipole moments of each interacting environment.

2.7.4 Hydrogen bonding

Hydrogen bonding interactions are formed between a hydrogen atom which is covalently linked to an electronegative atom (e.g. O, N, F) which forms an electrostatic link with neighbouring electronegative atom within the same molecule or adjacent molecules. Hydrogen bond interactions increases with increase in hydrogen-bond acidity and basicity of the species (see Table 2.4).

2.7.5 Ionic interactions

Ionic interactions take place between a positive charged molecule (X+) and a negatively charged stationary phase or mobile phase. The positively charged analyte leads to a displacement of charge in the surrounding molecule (mobile phase) to achieve optimal electrostatic interaction. Table 2.4 lists the relative contributions to solvent polarity from the relative hydrogen-bond acidity (α), hydrogen-bond basicity (β) or dipolarity (π^*), a measure of the overall solvent polarity (P') and values of the dielectric constant (ε) of three solvents [104]. α represents the solvents ability to act as a hydrogen bond donor towards a basic solute, β indicates the solvent's ability to act as a hydrogen bond acceptor towards protic solute, π^* denotes the solvent's ability to interact with the solute by dipolar

and polarization factors [104], P' (polarity index) is a measure of the ability of the solvent to interact with various polar solutes [206] and (ε) is a measure of the solvent's polarity [207]. Solvents with larger dielectric constant (ε) have stronger strength of ionic interaction (see Table 2.4).

Table 2.4. Solvent selectivity characteristics.

	Normalised selectivity				
Solvent	H-B Acidity α/∑	H-B Basicity β/∑	Dipolarity π*/∑	P'	ε
Water	0.43	0.18	0.45	10.2	80
Acetonitrile	0.15	0.25	0.60	5.8	37.5
Methanol	0.43	0.29	0.28	5.1	32.7

where ∑ signifies the sum of α, β and π* for each solvent[1, 106, 208, 209]

2.7.6 Charge transfer

Charge transfer or π-π interaction can take place between a π-acid (electron poor) solute such as 1,3-dinitrobenzene and a π-base (electron rich) solvent such as benzene. This interaction can also take place between any aromatic analytes. The strength of this interaction increases with stronger π-bases (e.g. naphthalene and anthracene) and stronger π-acids (e.g. aromatic substituted by electron withdrawing nitro groups) [1]. Additionally, acetonitrile (π-acid) can also interact with aromatic analytes to form π-π interactions [109].

2.7.7 Polar interactions

Polar interactions take place when a molecule contain one or more dipoles which forms a localised charge situated on different positions of the molecule. Each charge has a corresponding opposite charge in a different part of the molecule; hence the molecule has no net charge associated with it. Interactions takes place between the charges of the different molecules but these interactions are accompanied with dispersive interactions. The strength of the polar interactions depends on the strength of the dipoles.

2.8 RP-HPLC method development

As briefly mentioned in Chapter 1, method development involves the selection of optimal separation conditions in HPLC. Several steps are involved for achieving the separation goals in HPLC method development such as [104]:

- assessment of sample properties and separation goals
- sample pre-treatment and preparation
- selection of chromatographic mode
- detector selection
- separation conditions (primarily stationary phase and mobile phase pH/organic component) followed by temperature and mobile phase gradient characteristics)
- refining of starting conditions – checking most especially pH
- method validation

However, for some complicated analyte mixtures, these steps might be adjusted by the chromatographer to achieve the goals of separation required due to special complications [14, 210].

2.8.1 Assessment of sample properties and separation goals

Initially, the analyte physico-chemical properties are reviewed such as molecular weight, functional groups, pK_a values and many more. However, if the analytes are basic or acidic, buffers might be added to the mobile phase to stabilize the pH of the system at a pH to best exploit ionisation of a particular functional group for example. Once this information has been reviewed, the separation goals and aims can be determined. This also depends on the equipment and system available in the research facilities.

2.8.2 Sample pre-treatment and preparation.

Some complicated mixtures of analytes might require special preparation to avoid column damaging and separation interference. Several procedures can be used to prepare these sort of mixtures [211-213]. Generally, previous pre-treatment methods for similar mixtures of analytes can be reused to save time.

2.8.3 Selection of chromatography mode

Usually, reversed phase HPLC is the first choice of chromatographic mode used in HPLC. However, in some cases, bare silica (unbonded) referred to as Normal phase HPLC (NP-HPLC) is preferred for isomeric analytes.

2.8.4 Detector selection

Many detectors are available in HPLC, but a first to-go choice is generally UV-Vis detection given that the majority of (small) pharmaceutical molecules contain a chromophore. Nevertheless, choosing the adequate detector depends on physical and chemical properties of the analytes being analysed. Mass spectrometric detection (LC-MS) is popularly used to complement UV detectors due to its ability to analyse a variety of analytes.

2.8.5 Method validation

Once the HPLC method development has been achieved, the method is tested on a suitable batch of samples to determine the accuracy, precision, robustness, repeatability and reproducibility of the method. Other properties such as the resolution, peak shape and many more are also determined. Method validation is required by any regulated laboratories to prove that the method developed is fit for its intended purpose. In the pharmaceutical industry the International Conference for Harmonisation (ICH) contains guidelines dictating how analytical methods must be developed [214].

3 NUCLEAR MAGNETIC RESONANCE THEORY

In this chapter, the fundamental theory of NMR magnetisation, nuclear spin interactions, Fourier transform and NMR experimental techniques are covered. The content of this chapter is based upon a number of texts: [215] Keeler, J., Understanding NMR spectroscopy. 2011: John Wiley & Sons; [216] Levitt, M.H., *Spin dynamics: basics of nuclear magnetic resonance*. 2001: John Wiley & Sons; [217] Duer, M.J., *Solid state NMR spectroscopy: principles and applications*. 2008: John Wiley & Sons and various journals that are referenced throughout.

3.1 Nuclei Fundamental Properties

Nuclear Magnetic Resonance (NMR) spectroscopy is a technique known for its ability to determine the molecular structure of a variety of samples. Thus, NMR spectroscopy has a great number of applications such as probing molecular interactions, determination of sample purity and understanding kinetics and molecular motions of various systems including proteins. Furthermore, this technique can be applied to variety of nuclei. As NMR is a type of spectroscopy, atoms in the systems must get excited which leads to a response e.g. emitted signal. Before we proceed any further in understanding NMR spectroscopy, it is crucial to determine what is *really* going on. Atomic nuclei can be characterised by four main physical properties: mass, electric charge, magnetism and spin [216]. The *mass* of the actual matter is mostly dependent on the mass of the nucleus. The

thermal properties of a given matter are dependent on the mass of the atomic nuclei. The nucleus itself is made of protons and neutrons, which are positive and neutral respectively.

More importantly, an element can have the same number of protons, but different number of neutrons. Consequently, the element could have different isotopes. Isotopes play an important role in NMR, since they can be distinguished by two main properties, spin quantum number I and gyromagnetic ratio γ. The allowed values for I are positive integer values (including 0) and positive half integer values. The spin angular moment (along the z-axis traditionally corresponding to the direction of the applied external magnetic field denoted B_0) is characterised by a quantum number known as the azimuthal quantum number m. The quantum number m can only have $2I+1$ values between $+I$ and $-I$ in integer steps such as:

$$I = 0, 1, 2, \ldots \tag{3.1}$$

$$m = -I, -I + 1, -I + 2 \ldots + I \tag{3.2}$$

The operator which corresponds to the total observable energy in the system is known as the Hamiltonian operator. The Hamiltonian $\widehat{H}$ for a nuclear spin in a static magnetic field is represented as:

$$\widehat{H} = -\hat{\mu} \cdot B_0 \tag{3.3}$$

where $\hat{\mu}$ is magnetic moment and B_0 is the strength of the applied magnetic field. This Hamiltonian operator is also known as the Zeeman Hamiltonian. The magnetic moment can be written in terms of the spin quantum number such as:

$$\hat{\mu} = \gamma \cdot \hat{I} \tag{3.4}$$

where γ is the gyromagnetic ratio. With an applied field along the z-axis, equation 3.3 and 3.4 can be combined to form:

$$\widehat{H} = -\gamma \hat{I}_z B_0 = \omega_0 B_0 \tag{3.5}$$

where the Larmor frequency, ω_0, equals to $-\gamma \cdot B_0$. If the nuclei have spin number of $I \geq 1/2$, they will possess both a magnetic moment and angular momentum, hence will precess about the B_0 magnetic field at the Larmor frequency, ω_0.

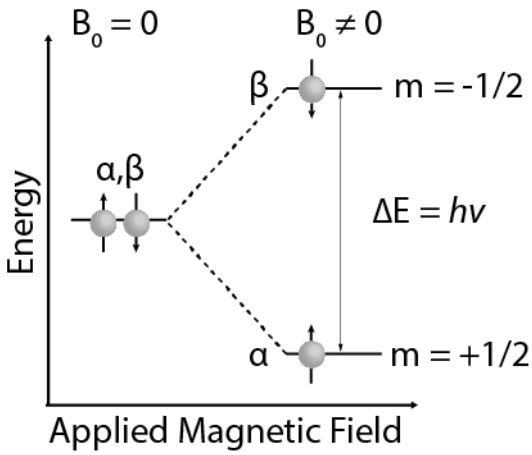

Figure 3.1. Two energy levels of single spin ½ nucleus with and without an applied magnetic field, B_0. The spin up (α) and spin down (β) have an energy gap of $\Delta E = hv$.

For nuclei with spin quantum number I = 1/2, by convention the spin states are represented as α (m = +1/2) and β (m = -1/2) or also described as "spin up" and "spin down" respectively. The Eigenstates can also have two energy levels:

$$E_\alpha = -\frac{1}{2}\hbar\gamma B_0 \qquad E_\beta = +\frac{1}{2}\hbar\gamma B_0 \tag{3.6}$$

where $\hbar$ is the reduced Planck's constant. Whether α or β is in the lower energy level depends on the sign (positive or negative) of the gyromagnetic ratio of the nuclei. These states are known as the *Zeeman states*. In quantum mechanics, the only allowed transitions are when m changes by either +1 or -1. For instance, if we go from β state (m = -1/2), to α state (m = +1/2), the change in m is:

$$\Delta m_{\beta\to\alpha} = +\frac{1}{2} - \left(-\frac{1}{2}\right) = +1 \tag{3.7}$$

Additionally, α to β transition is also allowed, where Δm = -1. These transitions result in *Zeeman splitting* as shown in Figure 3.1. The transition energy gap ΔE between the two spin states corresponds to $\hbar\gamma B_0$ which is the Larmor frequency ω_0 (in Hertz). The transition energy difference can be attained by applying a radio frequency (RF) pulse. However, at equilibrium the population difference between the two Eigenstates is dependent on the Boltzmann distribution of the nuclear spins over these two states.

3.2 Nuclear Spin Interactions

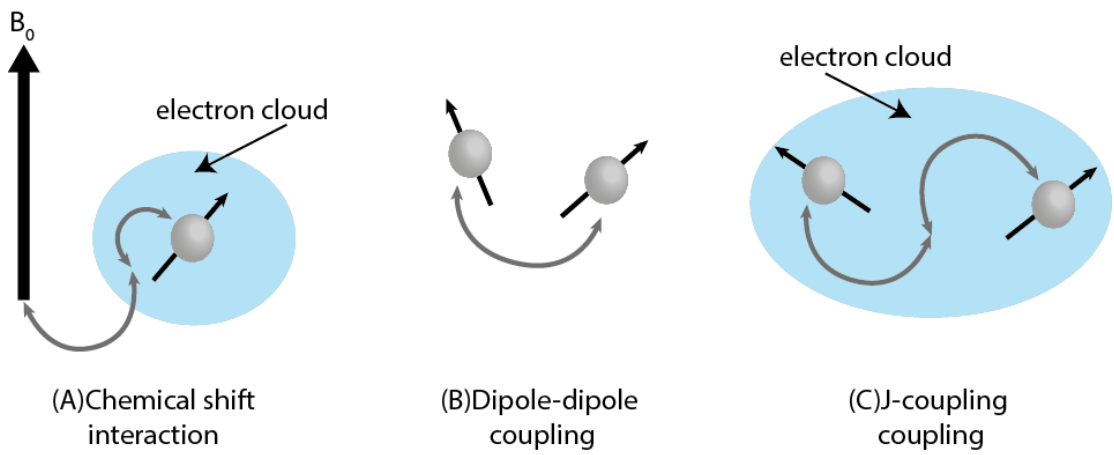

Figure 3.2. Visualisation of (a) chemical shift interaction, (b) direct dipole-dipole coupling and (c) indirect dipole-dipole coupling (J-coupling). The electrons are represented by the blue cloud.

3.2.1 Chemical Shift and chemical shift anisotropy

One form of interaction which enables scientists to obtain such structural information is known as *chemical shift (see Figure 3.2)*. For a nucleus, the effective magnetic field does not only include the applied magnetic field B_0, but also the magnetic field of both nearby electrons and nuclei. This effective magnetic [218] field at the nucleus can mathematically be expressed as:

$$B_{eff} = B_0(1 - \sigma) \tag{3.8}$$

Where σ is known as the shielding factor and here it is relatively small compared to the applied magnetic field varying from 10^{-3} to 10^{-5} depending on the nuclei of interest. Furthermore, the magnetic field experienced by nuclei at different sites of the same molecule could differ if the electronic environments are different. Consequently, this will cause the signal to be absorbed at slightly different frequency. This type of interaction is known as *the chemical shift*. In short, chemical shift is the indirect interaction of the applied external magnetic field and the nuclear spins via electrons. This interaction enables NMR to be a successful method to determine the chemical structure of various compounds.

The chemical shift mechanism can be divided into two steps. Initially, an applied external magnetic field B_0 induces currents in the electron clouds of the molecule. Therefore, the circulating current further generates another magnetic field known as the induced field. Hence, the strength of the induced current (induced field) is directly proportional to the applied field. The induced field interaction is composed of two contributions: (a) the external magnetic field causes the electrons to circulate around it; This leads to a secondary field which opposes the applied field at the centre of motion. This is known as the diamagnetic contribution [216, 219]; (b) the external magnetic field may also mix excited electronic states which possess paramagnetic properties with the ground state which creates a small amount of paramagnetism in the ground state of the molecule while it is in the magnetic field. This creates a field which supports the applied field at the nucleus which in turns deshields the nucleus. This is known as the paramagnetic contribution [216, 219].

Spectroscopy is commonly used to quote the observed absorptions in terms of frequency or wavelength, however in NMR the position or chemical shift (δ) of the peaks are quoted in parts per million (ppm). The main reason for using the chemical shift scale is due to the fact that NMR frequencies are directly proportional to the magnetic field strength. In other words, doubling the magnetic field strength also doubles the frequency separation as illustrated in Figure 3.3.

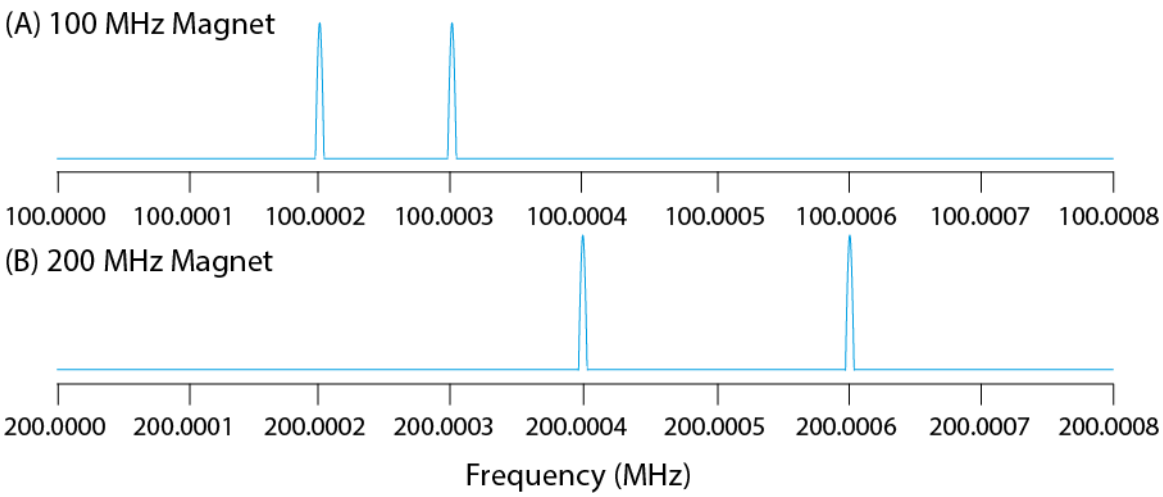

Figure 3.3. Illustration of an NMR spectrum split into two lines. In (a) the magnetic field results in the two lines appearing at 100.0002 and 100.0003 respectively. The separation between the two peaks is 100 Hz. If the applied magnetic field is doubled as shown in (b) the frequency of each peak is doubled and so is the separation between them.

The ppm scale enables the measured frequencies to be independent of the applied magnetic field strength. Thus, this enables the comparison of spectra acquired on different spectrometers. A simple reference compound can be used to calibrate the chemical shift scale. For ^{1}H and ^{13}C spectra tetramethylsilane (TMS) or 4,4-dimethyl-4-silapentane-1-sulfonic acid (DSS) are normally used as reference compounds. Both compounds give rise to a single peak which enables them to be easily identified. The DSS peak is then referenced to 0 ppm. The position of all the other peaks is determined by their frequency separation from the reference peak, and then dividing this difference by the reference peak frequency. Chemical shift is mathematically expressed by:

$$\delta\ (ppm) = 10^{6} \times \frac{v - v_{ref}}{v_{ref}} \tag{3.9}$$

where v is the frequency of the NMR peak of interest and v_{ref} is the frequency of the peak from the reference compound. The ratio is then multiplied by 10^6 to upscale the number into ppm. The reference compound will have a chemical shift of 0 ppm as previously stated. This ratio (δ) specifies the positions of the peaks independently on the applied magnetic field.

The main difference between solution and solid state NMR is that in solid state NMR, the overall molecular motion is restricted. The orientation-dependent component of the chemical shift is known as the *chemical shift anisotropy (CSA).* For example, if a single crystal is analysed, only one peak will be observed because each molecule will be orientated in the same direction. However, a powdered sample (2 or more crystals) will lead to a so called *powder pattern*. In other words, a broad peak is observed due to each chemical shift of each crystallite being orientated different with respect to the applied magnetic field B_0. Figure 3.4 illustrate the powder pattern with the possible orientations and the 3 by 3 matrix that represents the chemical shift tensor.

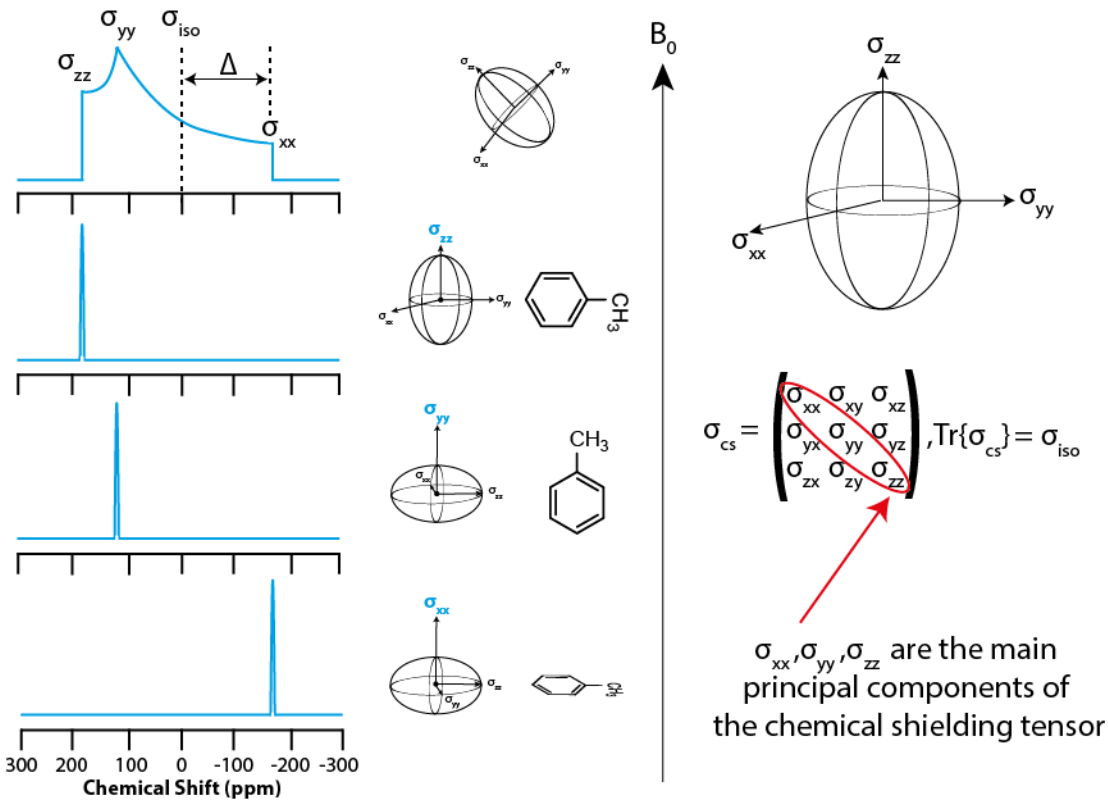

Figure 3.4. Illustration of chemical shift anisotropy powder pattern due to the random orientation of crystallites with respect to the applied field B_0. Where (Δ) is the shielding anisotropy, $\boldsymbol{\sigma_{zz}}$, $\boldsymbol{\sigma_{yy}}$ and $\boldsymbol{\sigma_{xx}}$ are the principal components of the chemical shielding tensor.

3.2.2 Dipole-Dipole Coupling

The magnetic moment of individual nuclear spin can interact through space. This is known as through-space dipole-dipole coupling, or dipole-dipole coupling for short (*see Figure 3.2*). This type of interaction is not mediated by the electrons but rather directly through space.

In solution samples, the dipole-dipole is averaged to its isotropic value (zero), via molecular tumbling. However, this is not the case for solids samples where this interaction is a major contributor of line broadening. Let's take for example two nuclear spins (*I* and *S*) which are separated by a distance ***r*** as shown in Figure 3.5,

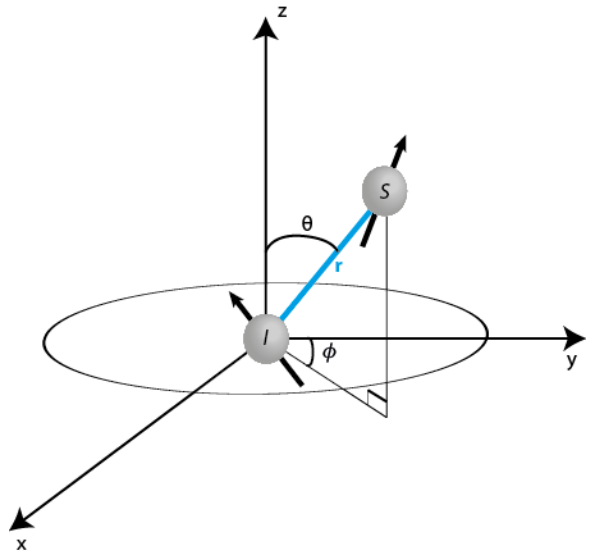

Figure 3.5. An illustration of the polar angles θ and ϕ which denotes the orientation of the I-S internuclear vector with respect to the B_0 field along the z-axis in the laboratory frame.

To obtain the interaction Hamiltonian ($\widehat{H}_{dd}$) for the dipolar coupling between two spins (I and S) is given by:

$$\widehat{H}_{dd} = -\left(\frac{\mu_0}{4\pi}\right)\gamma_I\gamma_S\hbar\left(\frac{I\cdot S}{r^3} - 3\frac{(I\cdot r)(S\cdot r)}{r^5}\right) = d_{IS}\left(I\cdot S - \frac{3(I\cdot r)(S\cdot r)}{r^2}\right) \quad (3.10)$$

Equation 3.13 represents the full dipolar Hamiltonian. Additionally, d_{IS} is known as the homonuclear and heteronuclear dipolar coupling constant (units in rad·s^{-1}):

$$d_{IS=-}\frac{\mu_0\gamma_I\gamma_S\hbar}{4\pi}\frac{1}{r^3} \quad (3.11)$$

The dipolar-coupling constant has a dependence of ($\frac{1}{r^3}$) which represents the distance between two coupled spins.

3.2.3 J-Coupling

J-coupling also known as scalar coupling arises from magnetic moments of the same molecule affecting one another through the electron cloud. This interaction is mediated through the chemical bond (*see Figure 3.2*). The peak multiplicity, the magnitude of coupling and sign of coupling can all be obtained from the J-coupling.[220]

Unlike dipolar interactions, J-coupling is independent of the applied magnetic field. The J-coupling between two spins I_j and I_k can be expressed in terms of a Hamiltonian as:

$$\hat{H}_{jk}^{J,full} = 2\pi \hat{I}_j \cdot J_{jk} \cdot \hat{I}_k \tag{3.12}$$

Where J_{jk} represents the J-coupling tensor and 2π is to enable to convert *J-coupling* into rads^{-1} instead of Hz. In general, J coupling may have both anisotropic and isotropic contributions. However, the anisotropic contribution is typically much smaller than the isotropic part [221, 222].

In solution, there are two types of j-coupling which are homonuclear coupling (e.g. H-H) and heteronuclear coupling (e.g. H-C). The strength of J-coupling is dependent on the molecular structural properties (e.g. bond angle, bond length, heteronuclear and homonuclear coupling).

Both anisotropic liquids and solids experience some J-coupling. However, the J-anisotropy strength of interaction is almost negligible compared to dipole-dipole coupling. In most cases, linewidths obtained in solid state (100 Hz – 10 kHz) are greater compared to J-spitting (10-100's of Hz).

3.2.4 Magic Angle Spinning

For liquid sample in low viscosity solutions, the angular term of the dipolar couplings (*D*) is averaged to zero as the molecule can freely rotate and as a results no dipolar coupling is observed (see equation 3.13). With heterogenous or solid samples where the motion is restricted, the dipolar couplings are not fully averaged to zero, thus are reintroduced which leads to broadening of the NMR peaks. The time-averaged angular dependent of dipolar couplings is expressed as:

$$D \propto r^{-3}(3cos^2\theta - 1) \tag{3.13}$$

Where r is the internuclear separation and θ the angle between the static field and the internuclear vector between the dipolar coupled spins [223]. However, sample heterogeneity can also contribute to line broadening. Heterogenous samples could suffer from local field inhomogeneity due to magnetic susceptibility differences which in turns leads to severe line broadening [223]. Line broadening from both dipolar coupling and susceptibility can be minimised or eliminated by rotating the sample about the so called magic angle (54.74°). As a result, the angular term of equation 3.13 becomes zero and the molecular motion of the sample emulates that of a liquid sample. Magic angle spinning

(MAS) has the ability to average the effect of chemical shift anisotropy [224]. Figure 3.6 shows the experimental setup of MAS.

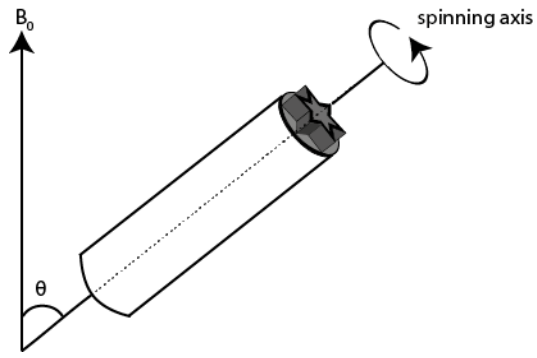

Figure 3.6. The magic angle spinning set up. The sample is packed in a cylindrical rotor which is spun rapidly about the spinning axis oriented at an angle θ with respect to the applied magnetic field B_0. The magic angle (θ = 54.74°) removes both heteronuclear dipolar coupling and chemical shielding anisotropy interactions.

In order to achieve a well resolved spectrum, the MAS needs to be fast enough compared to the size of the anisotropic interactions to average them effectively. This means spinning the rotor by a factor of 3 to 4 times greater than the anisotropic interactions. When the spinning frequency is not fast enough with respect to the size of the anisotropic interaction that is to be averaged *spinning sidebands* are observed. These are lines on both sides of the main peak of interest spaced in the intervals of the spinning frequency. For example, if the spinning speed is 5 kHz, the spinning sidebands will be located in the intervals of 5 kHz on either side of the main peak of interest – the number of the observed side bands depends on the ratio of the magnitude of the anisotropic interaction and the spinning frequency. The intensity of these spinning sidebands can be reduced by an increase in the speed of the spinning frequency. At the time of writing this thesis, the spinning frequency of NMR rotor can vary from anything from 10 Hz to 150 kHz. The maximum frequency with which the rotors can be spun depends on the size of the rotor (typically rotors with diameters from 7 to 0.6 mm are in use these days). However, for some anisotropic interactions such as ^{1}H-^{1}H dipolar couplings even the fastest spinning frequencies currently available are not sufficient for achieving effective averaging. If the presence of spinning side bands is not desired other methods besides faster MAS can be used to remove the spinning sidebands, e.g. special pulse sequences [225, 226]. On the other hand, spinning sidebands can be rather useful, as they can be used to determine the anisotropy and asymmetry properties of nuclear spin interactions, which are in turn linked to important molecular properties [227-229].

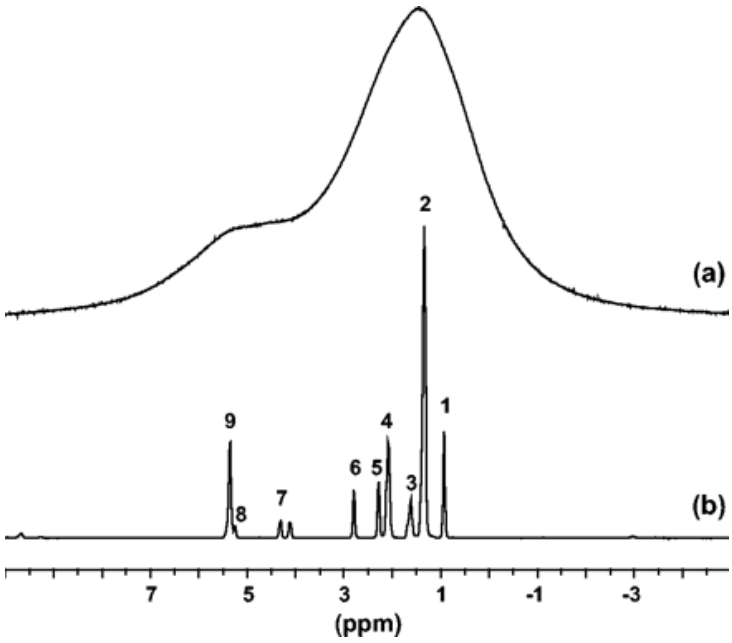

Figure 3.7. ^{1}D ^{1}H spectra of single dry seed of western white pine (a) static and (b) under 3 kHz magic angle spinning. Adapted from [230].

In the context of the work presented in this thesis, an important aspect is the MAS capability of minimizing magnetic susceptibility-induced line broadening [231]. Over the years, magnetic-susceptibility broadening found in heterogeneous systems can be removed by MAS [232, 233]. MAS has proven to be very effective for narrowing both ^{1}H and ^{13}C linewidths. This magnetic susceptibility broadening is not only due to the mismatch within the sample but also the materials used to manufacture the probe which in some cases can only be removed by careful probe design. The so called Nanonmr probe has been used to eliminate the line broadening [234]. In a recent study, Nanoprobe generated the best resolved spectra for both ^{1}H and ^{13}C 1D spectra [235].

Figure 3.7 displays the true power of MAS technique for minimizing both anisotropic and magnetic susceptibility line broadening. This experiment is known as ^{1}H high resolution MAS NMR (^{1}H HR MAS) technique which is heavily used in this project.

3.3 NMR Experiment

3.3.1 The vector model

Before we can move any further we need to understand terms such as the vector model, bulk magnetisation, pulses and many more in order to understand how NMR experiments actually work. The sample has to be packed in either a rotor (solid-state) or into an NMR

tube (solution-state), which is then placed into a probe and finally inserted into a superconducting electromagnet. When the nucleus of interest is placed in a strong magnetic field, there is an interaction taking place between the applied field and magnetic moment of the nucleus. The magnitude of the interaction is dependent on the angle between the applied field and magnetic moment of the nucleus. The highest energy can be observed when the magnetic moment is anti-parallel to the applied field, while the lowest energy arrangement is when the magnetic moment is parallel to the applied field (angle is zero). The energy of interaction is minimised when each individual magnetic moment is aligned to the applied field. However, this alignment is perturbed by random thermal molecular motion of the molecules which leads to random orientation of the magnetic moments. Because the magnitude of the energy of the thermal molecular motion is far greater compared to the energy of interaction between the applied field and magnetic moments, the alignment of the magnetic moments can easily be disordered.

In terms of NMR, we do not look at individual magnetic moments but the sum (as a whole) of all magnetic moments in all nuclei. If a magnetic field B_0 is applied and the system is allowed to reach an equilibrium, each individual magnetic moments will align with the applied field. The sum of these magnetic moments is known as the bulk magnetisation or net magnetisation (M) as shown in Figure 3.8. The term (M) is the sum of each individual magnetic moments (μ_i) of all the nuclei in the substance:

$$M = \sum_i \mu_i \tag{3.14}$$

The term “bulk” reminds us that the magnetisation is a property of the whole sample but not just an individual magnetic moment. Additionally, magnetisation is a vector quantity that possesses both magnitude and direction. The vector model enables us to visualise and determine what happens to the bulk magnetisation without the need for any complicated quantum mechanics. Once the sample is placed in a magnetic field, after a certain amount of time the magnetisation builds up and reaches an equilibrium. The process by which the sample reaches equilibrium is illustrated in Figure 3.8. The process by which the spins reaches equilibrium is called NMR relaxation. NMR relaxation measurements have been used for probing molecular dynamics. In Chapter 4 we will look more into details on how NMR relaxation works and methods by which it can be measured.

As previously mentioned the energy of interaction between the applied field and individual magnetic moment is dependent on the angle between them. However, the energy of interaction is independent of the orientation of the magnetic moments on the

xy-plane. At equilibrium, the components of magnetic moments in the transverse plane (xy-plane) are randomly distributed. As a result, the transverse components of individual magnetic moments will cancel out and hence no bulk magnetisation is formed on the transverse plane. Furthermore, the bulk magnetisation at equilibrium will align on the z-axis. Radio frequency (RF) pulses can be used to transfer the bulk magnetisation from the longitudinal plane to the transverse plane.

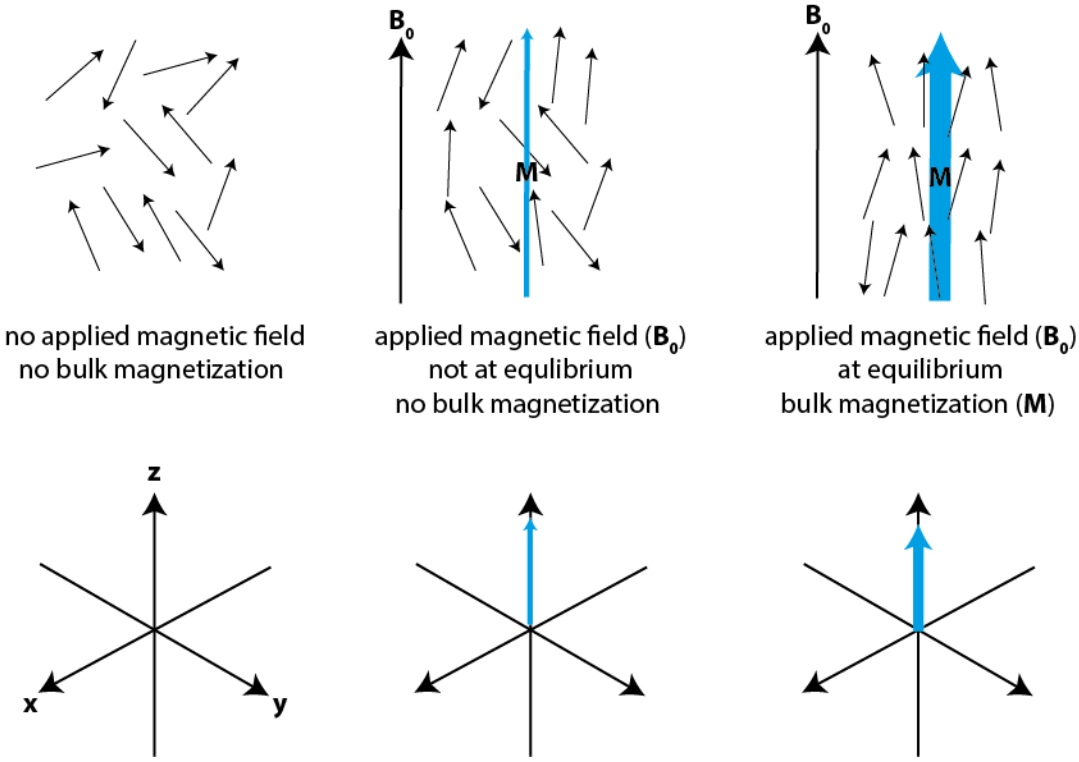

Figure 3.8. Illustration of how bulk magnetisation reaches equilibrium. Initially with no applied magnetic field, each individual magnetic moment is randomly orientated (as shown on the left). At this point, no net magnetisation is formed. Once the magnetic field is applied (B_0), the individual magnetic moments start to align with the field but it requires a certain amount time. When the field is first applied, no net bulk magnetisation is formed. After waiting for an adequate amount of time, more populated magnetic moment align to the applied field as shown on the right. As a result, a bulk magnetisation (M) is formed parallel to the applied field (z-axis).

Once the bulk magnetisation reaches an equilibrium, it is fixed on the z-axis and does not vary over time. However, if the bulk magnetisation is suddenly tipped away from the B_0 field, it will rotate around the applied field in a cone shape with a constant angle at the frequency called the Larmor frequency. This particular type of motion is known as precession. Therefore, the bulk magnetisation precesses about the applied field. The

Larmor frequency can be specified in two ways. The Larmor frequency can be expressed in terms of radians per seconds (in rads^{-1}):

$$\omega_0 = -\gamma B_0 \tag{3.15}$$

it can also be expressed as cycles per second or in Hz:

$$v_0 = -\frac{1}{2\pi}\gamma B_0 \tag{3.16}$$

Looking at the equations 3.15 and 3.16, the Larmor frequency has a defined negative sign. The sign provides fundamental information of the direction of precession of the bulk magnetisation about the applied magnetic field. For instance, most nuclei have a positive gyromagnetic ratio, which means the Larmor frequency calculated will be negative. This means the bulk magnetisation will precess clockwise around the applied field. However, some nuclei such as ^{15}N and ^{29}Si have negative gyromagnetic ratios, which leads to positive Larmor frequency. Thus, in that case the bulk magnetisation of such nuclei will rotate counter clockwise about the applied field. It is important to note that precession of the bulk magnetisation will only take place when it is at an angle with the applied magnetic field. If the bulk magnetisation is not tipped at an angle but parallel to the z-axis, the bulk magnetisation will remain stationary.

The magnetisation can be rotated from the z-axis onto the x-y-plane by applying an on-resonance radiofrequency (RF) pulse. The RF pulses are generated by a coil around the sample: an oscillating current induces the required oscillating magnetic field along the x-axis. This process is how a radiofrequency or RF field is created.

When the RF pulse is applied through the coil along the x-axis, an oscillating magnetic field is generated along the x-axis (perpendicular to the z-axis and B_0 field). The oscillating magnetic field can be thought of as a vector that starts along from the +x and gradually reduces to zero and then increases across the –x direction and finally back to its starting position along the +x. This vector can be separated into two components with frequencies of $\pm\omega_{rf}$, where ω_{rf} is the frequency of the rf pulse. ω_{rf} is called the transmitter frequency simply because a RF transmitter is used to generate the power. Additionally, the only component which precesses in the same direction as the precession of the bulk magnetisation vector (M) about the B_0 will have an effect on M. This

component can be represented as $B_1(t)$. The effect of the $B_1(t)$ can be visualised a lot more easily by transforming the whole system into a rotating frame. The rotating frame of reference which rotates at the Larmor frequency about the B_0 field. Employing this "trick", the B_1 field will appear to be static and hence the time dependence of the B_1 field is also removed. When viewed under the rotating frame, the RF field is not rotating nor oscillating but just stationary.

As a result, the time dependence of the RF field is removed. For instance, if the rotating frame rotates at the same frequency as the Larmor precession, the magnetization will appear to be stationary (the apparent Larmor frequency would be zero. Additionally, if rotating frame has a frequency of ω_{rf}, the Larmor frequency is reduced to ω_0 - ω_{rf} about the B_0 field. The difference between the two frequencies is known as the offset and is represented by Ω,

$$\Omega = \omega_0 - \omega_{rf} \tag{3.17}$$

If the rotating frame precess at the offset frequency Ω, the apparent magnetic field ΔB can be calculated as:

$$\Delta B = -\frac{\Omega}{\gamma} \tag{3.18}$$

where ΔB is known as the reduced field in the rotating frame. If the offset is zero, so would be the reduced field.

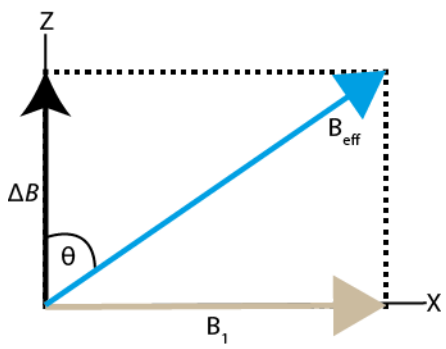

Figure 3.9. Illustration of the effective field (B_{eff}) in the rotating frame. Where B_{eff} is sum of the B_1 and ΔB and θ is the angle between the ΔB and B_{eff}.

Additionally, in the rotating frame, the reduced field is along the z-axis and the B_1 field is along the x-axis which both add vertically to give the so-called effective field B_{eff} as illustrated in Figure 3.9. The size of the effective field B_{eff} can be expressed as:

$$B_{eff} = \sqrt{B_1^2 + (\Delta B)^2} \tag{3.19}$$

The angle between the reduced field ΔB and B_{eff} is known as the tilt angle and is given the symbol θ. From Figure 3.9, the tilt angle can be determined by:

$$sin\,\theta = \frac{B_1}{B_{eff}} \qquad cos\,\theta = \frac{\Delta B}{B_{eff}} \qquad tan\,\theta = \frac{B_1}{\Delta B} \tag{3.20}$$

Furthermore, Equation 3.19 can be expressed in term in frequencies:

$$\omega_{eff} = \sqrt{\omega_1^2 + (\Omega)^2} \tag{3.21}$$

As a result, Equation 3.21 can be rewritten in terms of frequencies and hence also express the tilt angle in terms of frequencies:

$$sin\,\theta = \frac{\omega_1}{\omega_{eff}} \qquad cos\,\theta = \frac{\Omega}{\omega_{eff}} \qquad tan\,\theta = \frac{\omega_1}{\Omega} \tag{3.22}$$

Pulses are radio frequency that matches that of the Larmor frequency (on-resonance). If the time of the RF pulse is applied for is t_p, and the precession frequency as ω_1, we can determine the so-called *flip angle (β) of the pulse* as:

$$\beta = \omega_1 t_p \tag{3.23}$$

The nutation frequency ω_1 plays a crucial role in NMR experiments as it determines the rf field strength, particularly the amount of pulsing power applied to a sample. If $\omega_1 \gg \Omega$, this is known as a hard pulse. In this situation, high power is used for a short duration of time (e.g. few µs). These pulses are non-selective and therefore excite a large range of chemical shifts for a specific nucleus (e.g. ^{1}H). Conversely, soft pulses (when $\omega_1 \ll \Omega$), also known as shaped pulses are long pulse (range of ms) with weak power. Soft pulses excite only a specific region of interest.

The flip angle can be altered by altering the pulse length. Figure 3.10 illustrates the motion of the bulk magnetisation from z-axis to the transverse plane over a period time (t). In the most common NMR experiments, the flip angle is set to 90° $\left(\frac{\pi}{2}\right)$ and 180° (π). As shown in Figure 3.10, a 90° pulse is applied along the x-axis (anti-clockwise).

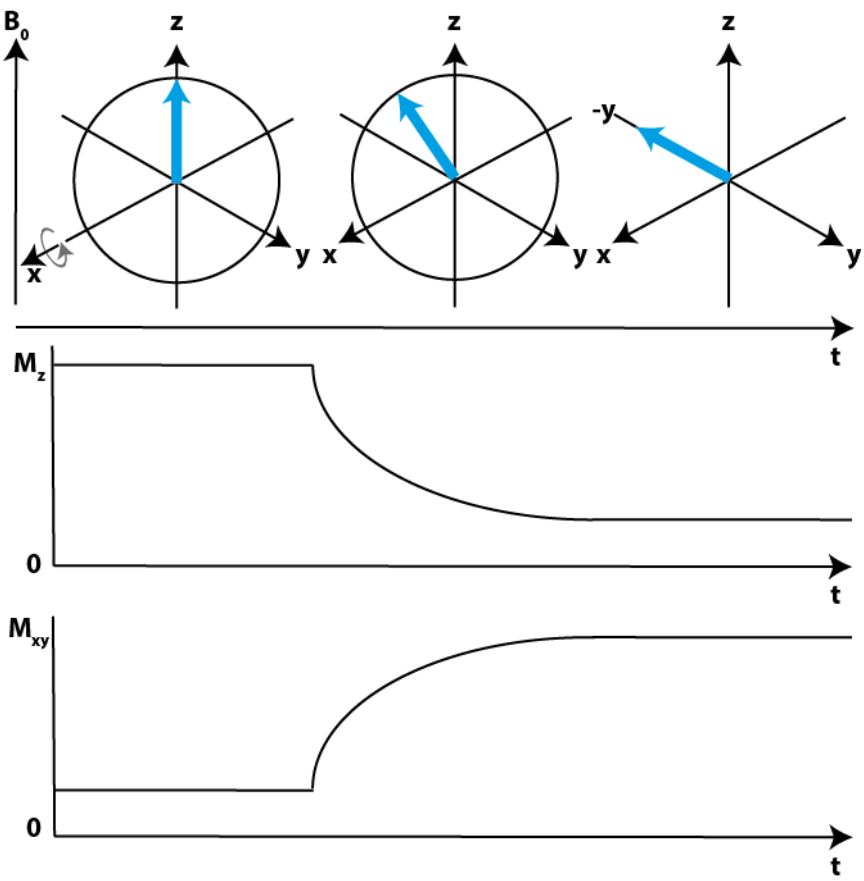

Figure 3.10. Graphical illustration of how the transverse bulk magnetisation is generated with time. Initially (from left to right) the bulk magnetisation is at equilibrium. A 90° anticlockwise pulse is applied about the x-axis (when a maximum measurable signal is obtained), this starts tilting the bulk magnetisation away from the longitudinal plane axis (z-axis) and towards the transverse plane (xy-axis). After a while, the bulk magnetisation is fully transferred onto the transverse plane.

For example, let's take the pulse length of t_{180} for a flip angle of 180° (π). This can be expressed as:

$$\pi = \omega_1 t_{180} \tag{3.24}$$

$$\therefore\ \omega_1 = \frac{\pi}{t_{180}} \text{ (in rad/s)} \tag{3.25}$$

or

$$\frac{\omega_1}{2\pi} = \frac{1}{2t_{180}} \text{ (in Hz)} \tag{3.26}$$

3.3.2 Fourier Transform

In NMR spectroscopy after a pulse or series of pulses are applied, the oscillating decaying signal is recorded as the so-called free induction decay (FID). It is often more convenient to work with NMR signals in frequency domain rather than time domain. To convert the time domain FID into a frequency domain spectrum is accomplished using mathematical Fourier transform (FT). In preparation for FT the analog signal needs to be digitised so that the decaying wave is represented by number of points with increments.

In order to understand what one would expect a spectrum obtained as a result of FT to be it is useful to consider how the observed signal could be expressed mathematically. The bulk magnetisation, M_0, rotated into the transverse plane by a 90° pulse with phase y will precess about z axis with the x and y components expressed as:

$$M_y = M_0 sin\Omega t \qquad M_x = M_0 cos\Omega t \tag{3.27}$$

where Ω is the offset (in rad·s^{-1}). The precession of the bulk magnetisation will generate a current in the RF coil which results in a signal voltage which is then digitized and stored in the computer memory. The signals from both components can be written as:

$$S_x = S_0 cos\Omega t \qquad S_y = S_0 sin\Omega t \tag{3.28}$$

where S_x and S_y are the detected signals and S_0 is proportional to M_0. In the presence of transverse relaxation, the FID decays exponentially such as:

$$\begin{aligned} S_x &= S_0 cos\Omega t\ exp\left(\frac{-t}{T_2}\right) = S_0 cos\Omega t\ exp(-R_2 t) \\ S_y &= S_0 sin\Omega t\ exp\left(\frac{-t}{T_2}\right) = S_0 sin\Omega t\ exp(-R_2 t) \end{aligned} \tag{3.29}$$

where T_2 is a time constant called the transverse relaxation corresponding to the relaxation rate, R_2 (R_2=1/T_2). As R_2 increases (T_2 decreases), the decay becomes more rapid which leads to broader peak widths. Relaxation will be revisited in chapter 4.

Both the x and y components can be combined into a complex (time-domain) signal $S(t)$:

$$S(t) = S_x + iS_y \tag{3.30}$$

$$= S_0 cos\Omega t\ exp\left(\frac{-t}{T_2}\right) + i\left[S_0 sin\Omega t\ exp\left(\frac{-t}{T_2}\right)\right] \tag{3.31}$$

$$= S_0(cos\Omega t + isin\Omega t)\ exp\left(\frac{-t}{T_2}\right) \tag{3.32}$$

$$where\ \ cos\theta + isin\theta\ \equiv \exp\,(i\theta) \tag{3.33}$$

$$\therefore S(t) = S_0\ exp(i\Omega t)exp\left(\frac{-t}{T_2}\right) = S_0\ exp(i\Omega t)\frac{-t}{T_2}exp(-R_2 t) \tag{3.34}$$

where S_x is the x component (real part) and S_y is the y component (imaginary part). After applying the Fourier transform to $S(t)$, a complex (frequency-domain) signal S(ω) is generated:

$$S(t) \overset{FT}{\rightarrow} S(\omega) \tag{3.35}$$

$$S_0\ exp(i\Omega t)exp(-R_2 t) \overset{FT}{\rightarrow} \underbrace{\frac{S_0 R_2}{R_2^2 + (\omega - \Omega)^2}}_{real} + i\underbrace{\frac{-S_0(\omega - \Omega)}{R_2^2 + (\omega - \Omega)^2}}_{imaginary} \tag{3.36}$$

The real part is known as the *absorption mode Lorentzian line shape* while the imaginary part is called the *dispersion mode Lorentzian line shape* as illustrated in Figure 3.11. S_0 = 1.

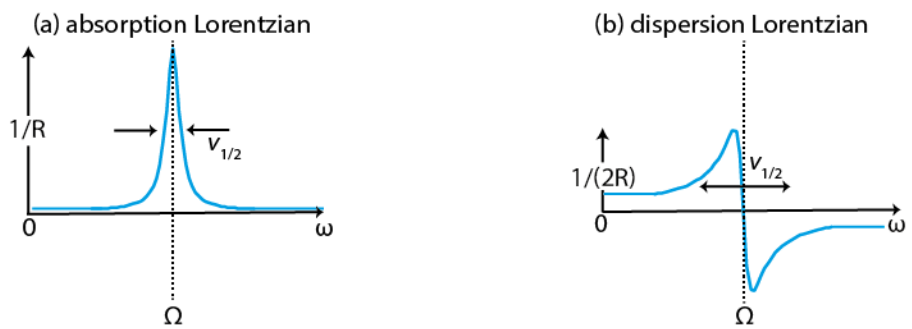

Figure 3.11. Illustration of (a) absorption and (b) dispersion Lorentzian line shapes due to Fourier transform of the decaying FID signal.

On-resonance, where $\omega = \Omega$, S(ω) becomes:

$$S(\omega) = \frac{R_2}{R_2^2 + (\Omega - \Omega)^2} + i\frac{-(\Omega - \Omega)}{R_2^2 + (\Omega - \Omega)^2} \tag{3.37}$$

$$= \frac{R_2}{R_2^2} + 0 \tag{3.38}$$

$$= \frac{1}{R_2} \tag{3.39}$$

Where the real part is $1/R_2$ and the imaginary part becomes zero. As illustrated in Figure 3.11, the absorption line shape has a maximum peak intensity of $1/R_2$ while the dispersion line shape goes through zero at the same point of frequency, Ω. The absorption peak width at half height, $v_{1/2}$ is $2R_2$ (in rad/s) and R_2/π (in Hz). Thus transverse relaxation plays a crucial part in NMR as it determines the peaks width of the NMR signal observed.

3.3.3 Sensitivity in NMR

Although NMR has proven to be a very successful technique over the years, it is considered to be insensitive in comparison to other spectroscopy techniques. This is because the NMR signal intensity is dependant to the population difference between the energy levels. This population difference is described by the Boltzmann distribution:

$$\frac{N_{upper}}{N_{lower}} = e^{\left(\frac{-\Delta E}{kT}\right)} \tag{3.40}$$

where N_{upper} and N_{lower} are the population of the nuclei in upper and lower energy levels respectively, ΔE is the energy difference between the two energy levels (in J), k is the Boltzmann constant (1.3805 x 10^{-23} J/K) and T is the temperature (in K). Because the energy difference between the upper and lower energy states is small the population difference is small, which renders NMR a highly insensitive technique.

Overall, the NMR sensitivity is dependent on a number of factors:

$$\text{NMR Signal} \propto \frac{N\gamma^3 B_0^2}{T} \tag{3.41}$$

where N is the amount of sample in the NMR rotor, γ is the gyromagnetic ratio of the nuclei of interest, B_0 is the applied magnetic field strength and T is the temperature. N does not only depend on the sample volume but also other factors such as the sample concentration and isotopic abundance. For example, ^{1}H proton is typically much more

sensitive than other nuclei. This is because ^{1}H has a high natural abundance of approximately 100% compared to 1.1% for carbon ^{13}C as shown in Table 3.1.

The signal to noise ratio of the NMR signal can be improved by increasing the concentration of the sample (related to N), using higher magnetic field strength to increase the energy difference between the spins or repeating the experiments. When an experiment is repeated the signal is correlated and adds constructively but noise is random and cancels out over time. Consequently, the signal to noise ratio is proportional to number of repetitions as:

$$\frac{\text{Signal}}{\text{Noise}} \propto \sqrt{number\ of\ repetitions} \tag{3.42}$$

Table 3.1. Nuclear properties of nuclei investigated in this study.

Nucleus	Spin, *I*	Natural abundance (%)	Gyromagnetic ratio MHz/T	Larmor frequency, 11.74 T (MHz)
^{1}H	1/2	99.98	42.58	500.00
^{2}H	1	0.015	6.54	76.75
^{13}C	1/2	1.1	10.71	125.72
^{29}Si	1/2	4.70	8.46	99.32

To improve the signal to noise ratio of the spectra, the NMR experiment is repeated over a number of times and added together. The number of times the experiments is repeated is known as *transients* or *number of scans, N.* Due to the random nature of the noise observed in the NMR spectra,

However, the total amount of time it takes to obtain one repetition (single scan) depends on the so called recycle delay required for the excited spins to return back to thermal

equilibrium. The process by which the spins return back to equilibrium is governed by spin-lattice or longitudinal relaxation T_1. T_1 relaxation can range from ms to hours depending on the nucleus of interest. As a rule of thumb, the recycle delay needs to be 5 times greater than the T_1 of the sample relaxation, which can lead to really long experimental times [236]. Paramagnetic additives can be added to the samples to shorten the T_1 times [237].

An common approach for enhancing sensitivity for observation of insensitive nuclei is to transfer polarisation from more sensitive nuclei, typically protons. In the solid state, one of such well-known methods is cross-polarization (CP) as shown in Figure 3.12.

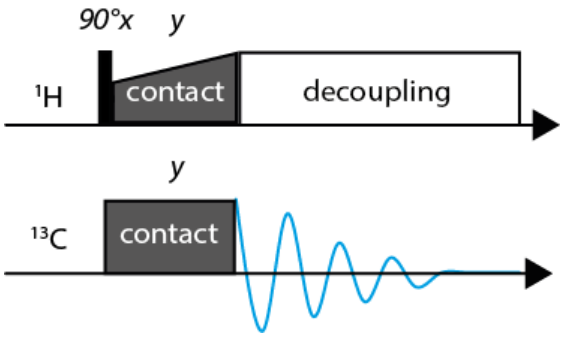

Figure 3.12. A cross polarization pulse sequence scheme.

In order for the polarization transfer to take place, irradiation on both coupled nuclei (e.g. ^{1}H and ^{13}C) need to fulfil the Hartmann-Hahn condition. Under static conditions it means that the nutation frequencies of irradiation on the two channels need to be equal as shown in Figure 3.13. Under MAS this condition is modified so that sum or difference of nutation frequencies on the two channels have to be equal to spinning frequency or twice the spinning frequency.

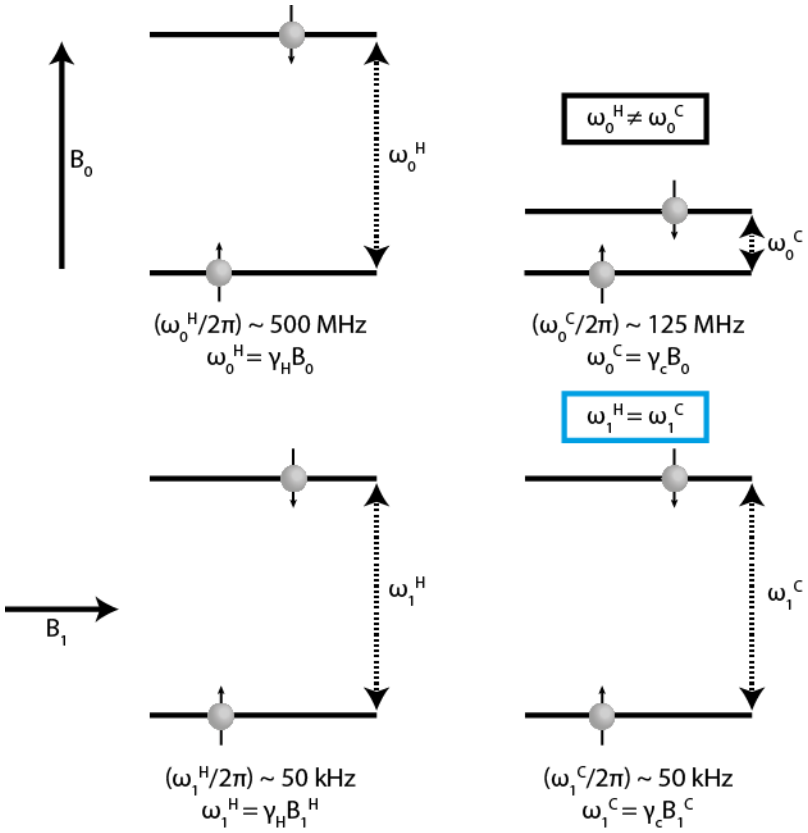

Figure 3.13. Illustration of the energy splitting of ^{1}H and ^{13}C nuclei about the B_0 and B_1 field. Where the Larmor frequencies (energy difference) of both nuclei about the B_0 are not equal. However, the Larmor frequencies of both nuclei about the B_1 field are equal. Hence, Hartmann-Hann matching is achieved.

When low sensitive nuclei are observed by solid-state NMR (e.g. ^{13}C) with neighbouring higher abundant nuclei (e.g. ^{1}H), strong heteronuclear dipolar coupling lead to broadening of spectrum observed. Applying high-power (~70-125 kHz ^{1}H nutation frequency) ^{1}H decoupling during acquisition enables the removal of such line broadening. The decoupling power needs to be calibrated carefully, as an excess of power can lead in extreme cases to sample heating and degradation and/or damage of the probe [238, 239]. In solution much lower power decoupling is used to decouple scalar couplings.

3.3.4 Two-Dimensional NMR

Over the years, two-dimensional NMR has been used in both solution and solid-state NMR to characterise complex biomolecules such as DNA, RNA and proteins. These types of complex molecules before the introduction of 2D NMR would seem impossible to study. After 2D NMR techniques were well established, scientists were able to develop both 3D and 4D for studying even larger biomolecules. These techniques have proven to be very successful over the years. The primary advantage of using 2D NMR techniques is for situations when a 1D NMR spectrum is overloaded with information (e.g. when peaks overlap with one another). Introducing another spectral dimension, first simplifies the 1D spectra and also enables further valuable information to be extracted. 2D NMR is very useful to determine a connectivity between two different sets of nuclei (e.g. proton and carbon). In a typical 1D spectrum, the peak intensity is plotted against the frequency. While in 2D NMR, the peak intensity is plotted against two frequencies. These two frequencies purely depend on the type of experiment that is used and on the information that is required from the sample of interest.

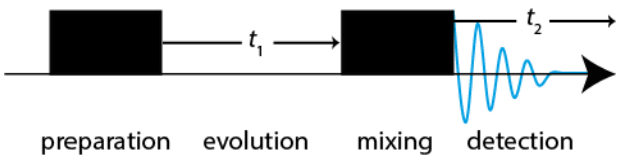

Figure 3.14. Graphical scheme of how 2D NMR data sets are recorded using the pulse sequence shown in Figure 3.16. A graphical scheme of a 2D NMR pulse sequence made up of a preparation, evolution (t_1), mixing and detection time (t_2).

In general, 2D NMR experiments are all composed of 4 simple steps; preparation time, evolution, mixing period and detection (*see Figure 3.14*). The preparation time is made up of either a single pulse or a series of pulses which generates a single-quantum coherence or multiple-quantum coherence. This can be a 90° degree pulse which transfers the bulk magnetisation from the longitudinal axis to the transverse plane or far more complicated pulses with delays.

The evolution period (incremental delay) t_1, is a running time that is not fixed and will be different depending on the type of experiment used. The coherence that is generated from the preparation time is allowed to evolve during t_1. No observations are made during

the t_1 increments. This is then followed by the mixing time. This part of the experiment is fundamental as it enables the magnetisation to be transferred from one nucleus to another. The magnetisation can be transferred via two mechanisms; dipolar or scalar coupling. The mixing time typically involves sequence of pulses that control evolution of the spins under specific couplings. Finally, this is followed by the detection period, t_2 where the signal is recorded in the form of an FID.

In 2D NMR experiments, the data are recorded with regular intervals for both the t_1 and t_2 period. Essentially, the experiment is repeated for different increments of the t_1. Initially, the t_1 is set to zero. As a result, there is no time delay between the preparation and mixing time and the FID is recorded as a function of t_2. After the first experiment, the t_1 is incremented with a fixed amount (Δ_1) and the whole experiment is repeated and the data are stored (see Figure 3.15). The whole experiment is repeated with $t_1 = \Delta_2, t_1 = \Delta_3 \ldots\ldots$ until adequate data is acquired in the t_1 dimension. Every individual value of t_1 requires a separate experiment. Thus, the signal in the t_2 dimension either has amplitude or phase or both modulated according to the evolution in t_1. Consequently, repeating the experiment for successive t_1 incremented delays generates a two-dimensional time domain dataset [219]. This is one of the many reasons why undertaking 2D NMR experiments can become a lengthy process. Hence, the number of t_1 incremented delay has to be chosen wisely for the experiments to be time efficient.

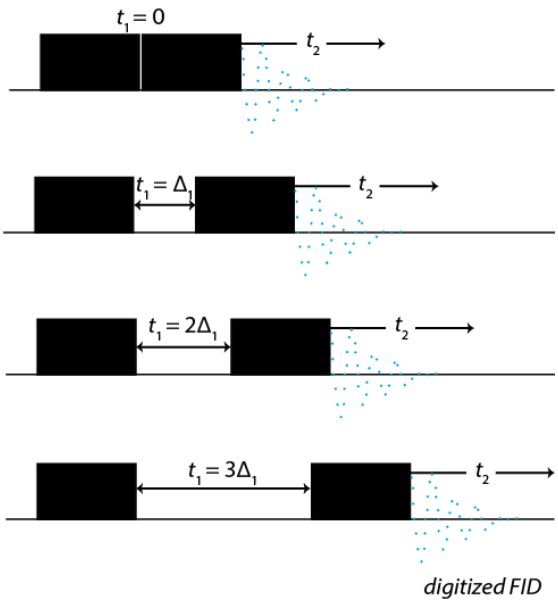

Figure 3.15. Initially, t_1 is set to zero, the sequence is executed and FID is digitized with regular increments as a function of t_2 and then stored. The process is repeated where t_1 is set to $\boldsymbol{\Delta_1}$, $\boldsymbol{2\Delta_1}$, $\boldsymbol{3\Delta_1}$ and so on for as many values of t_1 required.

Once the data are acquired, this is stored as a matrix. This matrix contains rows that are set to fixed values of t_1 but changing value of t_2. Similarly, to 1D experiments, the 2D time domains need to be Fourier transformed into a 2D spectrum. However, because this is a 2D NMR spectrum, the time domain needs to be Fourier transformed twice in order to obtain a spectrum. First of all, the rows (t_1 $converted\ to\ \omega_1$) are Fourier transformed followed by the column (t_2 $converted\ to\ \omega_2$) into a new matrix of the Fourier transformed rows and columns respectively. The final matrix is the 2D NMR spectrum.

Various heteronuclear and homonuclear 2D NMR techniques are used for structural and conformational analysis. For instance, heteronuclear single-quantum coherence (HSQC) or heteronuclear single-quantum correlation experiment is a type of 2D NMR experiment that has proven useful for structural elucidation of both small and large organic molecules. This experiment has also been used to solve biomolecule structures (i.e. proteins). A 2D spectrum is obtained the first axis (f_2 dimension) containing a protons spectrum and the second axis (f_1) contains the heteronuclear nuclei such as ^{15}N or ^{13}C. A cross peak of each individual proton attached to its corresponding hetero nucleus is observed.

Heteronuclear multiple bond correlation (HMBC) similarly to HSQC is also 2D NMR experiment that probes the correlations between proton and a heteronuclear nucleus (mainly for ^{13}C). However, one bond correlation between the protons and carbons are suppressed. As a result, HMBC provides longer range of correlations of two, three and in some cases four bond correlation compared to HSQC.

2D NMR experiments can also be homonuclear, where correlation between the same nuclei is observed (e.g. ^{1}H-^{1}H). Nuclear Overhauser Effect Spectroscopy (NOESY) and Exchange Spectroscopy (EXSY) are identical experiments but provide different fundamental information. NOESY identifies two spins that are close together in space via cross relaxation. EXSY probes chemical exchange processes in a system. EXSY 2D NMR spectrum can also be used to obtain quantitative measure of the rate of exchange. However, this type of quantitative measurements can be very time consuming.

4 NUCLEAR MAGNETIC RESONANCE RELAXATION

The content of this chapter is based upon a number of texts: [215] Keeler, J., Understanding NMR spectroscopy. 2011: John Wiley & Sons; [216] Levitt, M.H., Spin dynamics: basics of nuclear magnetic resonance. 2001: John Wiley & Sons; [217] Duer, M.J., Solid state NMR spectroscopy: principles and applications. 2008: John Wiley & Sons; [240] Rule, G.S. and T.K. Hitchens, Fundamentals of protein NMR spectroscopy. Vol. 5. 2006: Springer Science & Business Media; [223] Claridge, T.D., High-resolution NMR techniques in organic chemistry. Vol. 27. 2016: Elsevier; [236] Apperley, D.C., R.K. Harris, and P. Hodgkinson, Solid-State NMR: Basic Principles and Practice. 2012: Momentum Press; [241] Stejskal, E. and J.D. Memory, High resolution NMR in the solid state: fundamentals of CP/MAS. 1994: Cambridge University Press; [242] Pochapsky, T.C. and S. Pochapsky, NMR for physical and biological scientists. 2008: Garland Science and various journals that are referenced through-out.

As mentioned in Chapter 3, in NMR the process by which the perturbed bulk magnetisation returns to thermal equilibrium is known as relaxation. The basic definitions of T_1 and T_2 relaxation times was introduced in Chapter 3 Section 3.3.3/3.3.2. Since the NMR experiments in this study are heavily dependent on NMR relaxation measurements, in this chapter we outline the general concepts necessary for understanding NMR relaxation.

NMR relaxation is a natural process and is primarily driven by molecular motion. Because of that NMR relaxation can be used as an indirect probe of molecular motion. As mentioned in Chapter 3, each individual spin has a magnetic moment. The sum of each

magnetic moment adds up to the bulk magnetisation. However, each magnetic moment behaves in the same manner of the bulk magnetisation. Relaxation is caused by magnetic fields, which are not applied (e.g. RF pulses) but generated locally within the sample by the thermal motion of the molecules. This is known as local magnetic fields. Each spin experiences different local magnetic fields as illustrated in Figure 4.1.

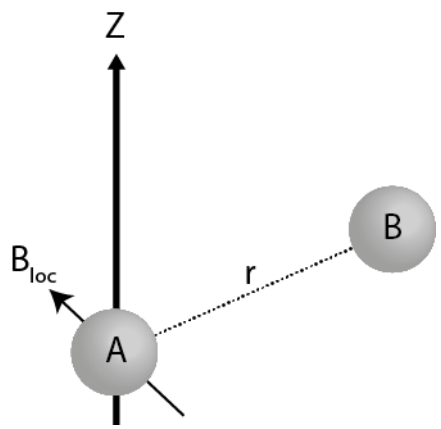

Figure 4.1. Spin A experiencing a local field, B_{loc}, generated from the magnetic moment of neighbouring spin B.

For instance, if we take two spins (A and B), where spin B has a magnetic moment, which generates a small magnetic field that is then experienced by spin A. This is an example of a local magnetic field at A that is generated by B. The orientation and amplitude (size) of the local field is dependent on the orientation and length (r) of spin B with respect to spin A (see Figure 4.1). These local fields are only experienced in very short distances. Spins from different parts of the sample will experience different local magnetic field due to the tumbling motion of the molecules. Thus, local magnetic fields are random and are different for each spin in the sample. This local magnetic field drives NMR relaxation. As shown in Figure 4.2, each spin is representing by a dot, if the spin is aligned along the +z or -z axis, the component takes a value of +1 or -1 respectively.

The local magnetic fields generated in the sample oscillate at random frequency, but in some cases, the oscillating frequency will be identical to the Larmor frequency. Hence, this can change the orientation of the spins.

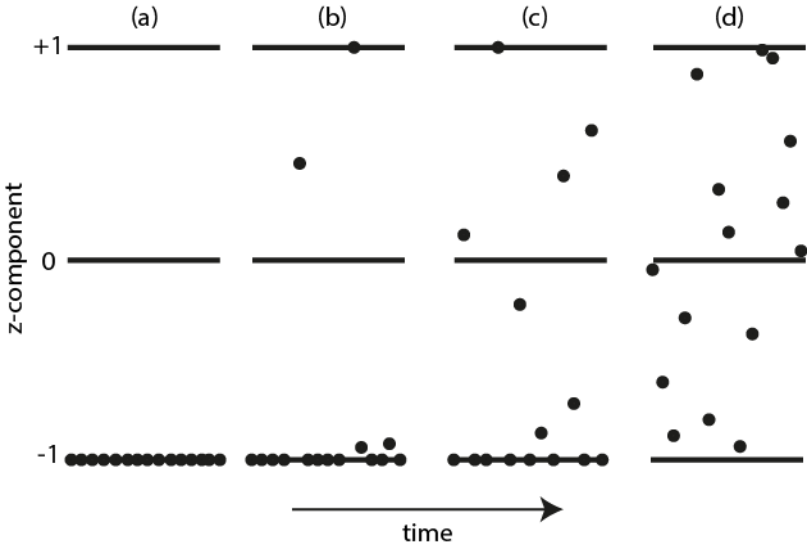

Figure 4.2. Illustration of how the bulk magnetisation (along –z axis) reaches to zero via random changes of the magnetic moment (z-component) of individual spins. Adapted from [215].

As shown in Figure 4.2, with time the spins change orientation at random which affects their z-components. After a while, the z component will become zero. This illustrates how the random field fluctuation close to the Larmor frequency drives relaxation to take place. However, Figure 4.2 (d), suggests there is no overall z-magnetisation at equilibrium, which is not true. As previously mentioned, the z-magnetisation at thermal equilibrium is finite. For a spin to go from a low to high state, some sort of energy is required. This energy is acquired from the "surroundings" of the spin. In contrast, when a spin goes from a high to low state, energy is given out to the surroundings. There is a higher probability for the energy to be added to the surroundings instead of being removed. Due to the disproportionate probability of giving or absorbing energy of the surroundings, it is more probable that the spins are driven towards a low energy state than a high-energy state. Hence, the spins are aligned parallel to the applied magnetic field. Thus, z-magnetisation is finally restored. The process by which the bulk magnetisation is restored to thermal equilibrium (along the longitudinal plane) is known as longitudinal relaxation. The main question that remains unanswered is how these local magnetic fields cause relaxation to take place? This is explained by relaxation mechanisms.

4.1 Relaxation mechanisms

The two main relaxation mechanisms for spins ½ nuclei are; the dipolar coupling and chemical shift anisotropy mechanisms.

4.1.1 Dipolar coupling

As previously mentioned, this mechanism is between two spins (*see Figure 4.1*). Where by one spin generates the local magnetic field and neighbouring spins experience it. This mechanism is dependent on three main properties: (1) the distance between the two spins ($1/r^6$), (2) the gyromagnetic ratio of the spins e.g. larger gyromagnetic ratio leads to larger magnetic moment and hence larger generated local field and (3) the orientation of the vector joining the two spins relative to the applied magnetic field.

4.1.2 Chemical shift anisotropy

Chemical shift of a nucleus in a molecule arises from the nuclear shielding effect of an applied magnetic field, caused by an induced magnetic field resulting from the circulation of surrounding electrons [48, 216, 243-246]. The magnitude of the induced field (size of the chemical shift) depends on the orientation of molecule with respect to the applied magnetic field, B_0. Due to the Brownian motion of molecules in solution, the chemical shift and hence the local magnetic field is constantly changing and pointing in random orientations which causes relaxation of the nucleus.

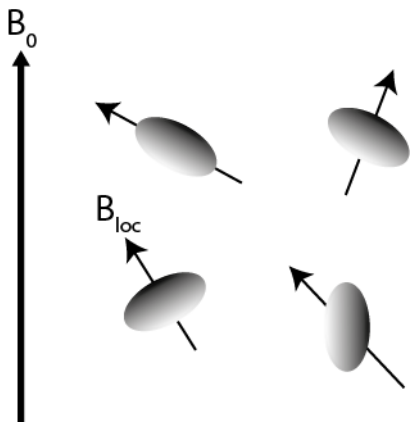

Figure 4.3. Visualisation of how a local field is generated due to the interaction between surrounding electrons and the applied field (B_0)

The generated local field is dependent on the strength of the applied field and the gyromagnetic ratio of the nucleus. These random local magnetic fields drive the system back into thermal equilibrium. The random nature (e.g. motion) of the fields (*see Figure 4.3*) is dependent on time and can be described by the correlation time.

4.2 Describing thermal random motion

4.2.1 Correlation time and correlation function

As previously mentioned, for relaxation to take place, the random motion of the molecules must be close to the Larmor frequency so that they can induce transitions between the spin energy levels.

In solution samples, the molecules undergo Brownian motion. Each collision on a molecule only changes it orientation by a very small amount. Thus, a molecule will rotate with very small steps. Since the collision of the molecules is random, the rotation will therefore be irregular. This motion is known as rotational diffusion. This motion is characterised by correlation time, τ_c. The correlation time is the average amount of time required for a molecule to rotate a full radian. Correlation time describes the timescale of the random motion of the molecules. If the molecule has a short correlation time, this indicates the molecule will rotate quickly as it requires a shorter amount of time to rotate one radian. Conversely, if a molecule has a long correlation time, the molecule will take longer to rotate by one radian. The correlation function $G(t,\tau)$ is used to mathematically express the time dependence of the random motion of a sample:

$$G(t,\tau) = \frac{1}{N}\left[B_{loc,1}(t)B_{loc,1}(t+\tau) + B_{loc,2}(t)B_{loc,2}(t+\tau) + \ldots\right] \tag{4.1}$$

$$= \frac{1}{N}\sum_{i=1}^{N} B_{loc,i}(t)B_{loc,i}(t+\tau) \tag{4.2}$$

$$= \overline{B_{loc}(t)B_{loc}(t+\tau)} \tag{4.3}$$

where N is the number of spins in the sample and the horizontal line in equation 4.3 (known as bar) represents an average. If a spin (i) experiences a local field at time (t) which varies with time so that at a time τ the local field becomes $B_{loc,i}(t+\tau)$. Both $B_{loc}(t)$ and $B_{loc}(t+\tau)$ are multiplied and the process is repeated for all other spins in the sample, which is divided by the number of spins in the sample. The correlation function is the average product of the local field at time (t) with that at time ($t+\tau$). This function is used to probe how rapidly a random field fluctuates. The local field varies over a period due to thermal motions present in the sample as shown in Figure 4.4.

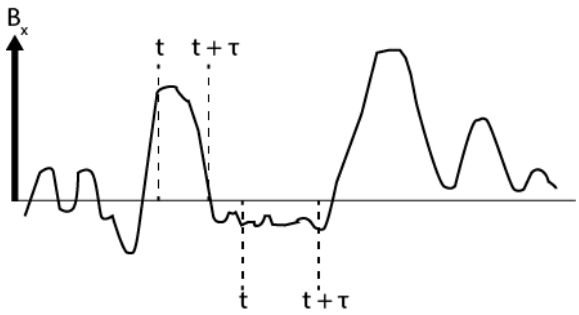

Figure 4.4. Probing of correlation function G(t,τ). This Figure illustrates how the function is independent on time but dependent on the time interval (τ).

Hence, $B_{loc}(t)$ is a random function of time. This function is not dependent on the time at which is measured (t) but only depends on the time interval (τ). The correlation function finally is written as:

$$G(\tau) = \overline{B_{loc}(t)B_{loc}(t+\tau)} \tag{4.4}$$

Slow fluctuations (*see Figure 4.5*) will lead to slower decaying of $G(\tau)$ and faster fluctuations tend to lead to faster decaying of $G(\tau)$ (*see Figure 4.5*).

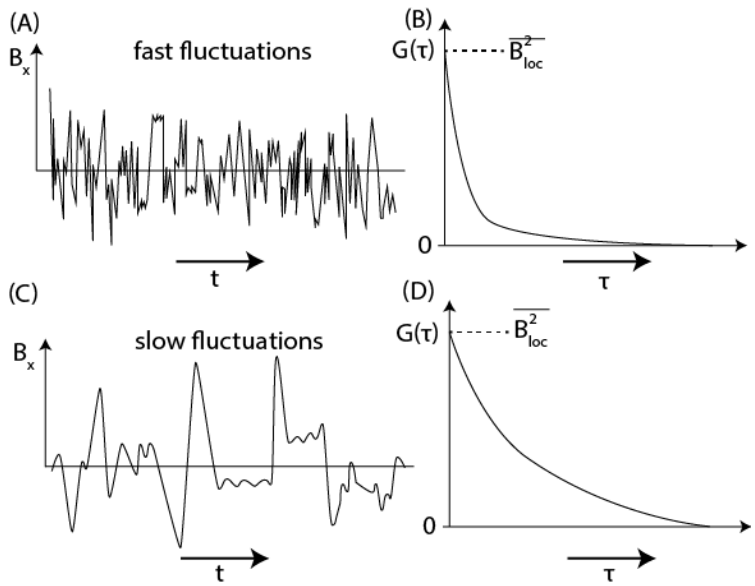

Figure 4.5. (a) Spectral density function of fast fluctuating fields with (b) its corresponding decaying plot and (c) spectral density function of slow fluctuating fields with (d) its corresponding decaying plot. Adapted from [216].

The simplest form of correlation function can be assumed as a simple decaying exponential:

$$G(\tau) = \overline{B_{loc}^2}\ exp^{(-\frac{|\tau|}{\tau_c})} \tag{4.5}$$

Where $\overline{B_{loc}^2}$ is the average of the square of the local field and τ_c is the correlation time. The magnitude of $G(\tau)$ is defined by the $\overline{B_{loc}^2}$ and τ_c signifies how fast is the fluctuation (faster motion will have smaller τ_c).

The exponential decay component of the correlation function is independent on the source of local field. The reduced correlation function $g\ (\tau)$ is independent on the local field:

$$g\ (\tau) = \ exp^{(-\frac{|\tau|}{\tau_c})} \tag{4.6}$$

$$\therefore G(\tau) = \ \overline{B_{loc}^2}\ g\ (\tau) \tag{4.7}$$

4.2.2 <u>The spectral density</u>

The correlation function $G\ (\tau)$ is a function of time. If the correlation function is Fourier transformed a function of frequency is obtained (e.g. like Fourier transforming an FID). The spectral density $J\ (\omega)$ is the Fourier transform of a correlation function:

$$G(\tau) \overset{FT}{\rightarrow} J\ (\omega) \tag{4.8}$$

The spectral density indicates the amount of motion at a specific frequency ω. The amount of motion at the Larmor frequency is simply calculating $J\ (\omega)$ when $\omega = \ \omega_0$.

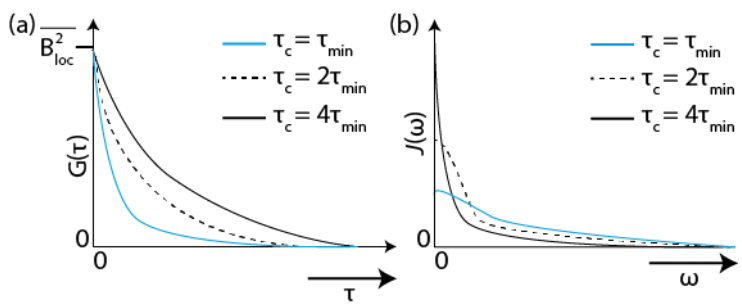

Figure 4.6. (a) Exponential plot of the correlation function, G(τ), and (b) corresponding plots of the spectral density function, J (ω), for three different correlation time, $\boldsymbol{\tau_c}$.

The spectral density of an exponential correlation function is a Lorentzian:

$$\overline{B_{loc}^2}\ exp^{(-\frac{|\tau|}{\tau_c})} \overset{FT}{\rightarrow} \overline{B_{loc}^2}\ \frac{2\tau_c}{1 + \ \omega^2\tau_c^2} \tag{4.9}$$

$$\therefore J\,(\omega) \;=\; \overline{B_{loc}^2}\,\frac{2\tau_c}{1+\;\omega^2\tau_c^2} \tag{4.10}$$

Figure 4.6 illustrates plots of the spectral density function with different correlation time values. The spectral density function has maximum value of $2\overline{B_{loc}^2}\,\tau_c$ when $\omega = 0$. It is clear the amount of motion decreases with an increase in ω. The shorter the correlation time, the spectral density spreads out to higher ω. This indicates that the area under the curves is independent on the correlation time and the spectral density at the Larmor frequency can be expressed as:

$$J\,(\omega_0) \;=\; \overline{B_{loc}^2}\,\frac{2\tau_c}{1+\;\omega^2\tau_c^2} \tag{4.11}$$

Figure 4.7 shows a plot of the spectral density function at the Larmor frequency against the correlation time. At a specific correlation time, the spectral density reaches a maximum. This value is reached when $\omega_0\tau_c = 1, \therefore\; \tau_c = 1/\omega_0$. The longitudinal relaxation rate also has a maximum value when $\tau_c = 1/\omega_0$ which is later discussed further.

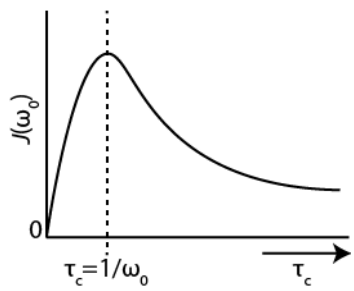

Figure 4.7. A plot of the spectral density at the Larmor Frequency, $\boldsymbol{J\,(\omega_0)}$, against correlation time. A maximum value of the spectral density is reached at $\boldsymbol{\tau_c = 1/\omega_0}$.

Similarly, to the correlation function, the reduced correlation function (equation 4.6) can also be Fourier transformed to generate a reduced spectral density:

$$g\,(\tau) \xrightarrow{FT} j\,(\omega) \tag{4.12}$$

$$exp^{(-\frac{|\tau|}{\tau_c})} \xrightarrow{FT} \frac{2\tau_c}{1+\;\omega^2\tau_c^2} \tag{4.13}$$

$$\therefore \mathrm{J}(\omega) = \;\overline{B_{loc}^2}\;j\,(\omega) \tag{4.14}$$

4.2.3 Motional regimes

It is important to understand the correlation between the spectral density at the Larmor frequency and correlation time as shown in Figure 4.7. This correlation enables us to differentiate between fast and slow motion regimes. As previously mentioned, the reduced spectral density at the Larmor frequency is given as:

$$j\,(\omega_0) = \frac{2\tau_c}{1 + \omega^2\tau_c^2} \tag{4.15}$$

The fast motion regime takes place when $\omega_0\tau_c \ll 1$, so $1 + \omega^2\tau_c^2 \approx 1$. The reduced spectral density in the fast regime is expressed as:

$$j\,(\omega_0) = 2\tau_c \tag{4.16}$$

Fast motion takes place when the correlation time is extremely short and typically involves small molecules. Conversely, the slow-motion regime is when $\omega_0\tau_c \gg 1$. In this regime, the correlation time is significantly larger and typically involves larger molecules (i.e. small proteins).

In this case, $1 + \omega^2\tau_c^2 \approx \omega^2\tau_c^2$, the reduced spectral density in the slow regime is expressed as:

$$j(\omega_0) = \frac{2}{\omega_0^2\tau_c} \tag{4.17}$$

4.3 Populations

4.3.1 Z-magnetisation in terms of populations

Expressing the z-magnetisation[215] in terms of populations of the spin states α (spin up) or β (spin down) simplifies how to determine the bulk z-magnetisation. Such treatment helps us to describe how relaxation takes place. A spin in the α states contributes $+\frac{1}{2}\hbar\gamma$ to magnetisation and another spin in the β states also contributes $-\frac{1}{2}\hbar\gamma$ to the bulk magnetisation. Therefore, the z-magnetisation will depend on the population difference between the two states:

$$M_z = \frac{1}{2}\hbar\gamma(n_\alpha - n_\beta) \tag{4.18}$$

where n_α is the population of the α state and n_β is the population of the β states. If both the α or β states were equal in population, the z-magnetisation would be zero. The population of the states at equilibrium is dependent on the Boltzmann distribution:

$$n_\alpha^0 = \frac{1}{2}\, N \exp\left(-\frac{E_\alpha}{k_B T}\right) \tag{4.19}$$

$$n_\beta^0 = \frac{1}{2}\, N \exp\left(-\frac{E_\beta}{k_B T}\right) \tag{4.20}$$

The energies of E_α and E_β are considerably smaller compared to the $k_\mathrm{B}T$. Hence, $(E_\beta/k_B T)$ is significantly smaller than 1:

$$\exp(-x) \approx 1 - x \tag{4.21}$$

When $x \ll 1$. Equations 4.19 and 4.20 can therefore be rewritten as:

$$n_\alpha^0 = \frac{1}{2}\, N\left(1 - \frac{E_\alpha}{k_B T}\right) \tag{4.22}$$

$$n_\beta^0 = \frac{1}{2}\, N\left(1 - \frac{E_\beta}{k_B T}\right) \tag{4.23}$$

The z-magnetisation at equilibrium, M_z^0 can be expressed in terms of populations:

$$M_z^0 = \frac{1}{2}\hbar\gamma(n_\alpha^0 - n_\beta^0) \tag{4.24}$$

$$M_z^0 = \frac{1}{4}\hbar\gamma N \frac{E_\beta - E_\alpha}{k_B T} \tag{4.25}$$

Recalling from Chapter 3, the energy of both α and β states were expressed as:

$$E_\alpha = -\frac{1}{2}\hbar\gamma B_0 \tag{4.26}$$

$$E_\beta = +\frac{1}{2}\hbar\gamma B_0 \tag{4.27}$$

Therefore, M_z^0 can be written as:

$$M_z^0 = \frac{\gamma^2\hbar^2 N B_0}{4k_B T} \tag{4.28}$$

From equation 4.28, the z-magnetisation at equilibrium is directly proportional to the nuclei's gyromagnetic ratios, strength of the magnetic field and the number of spins. Since

it is not feasible to determine the absolute NMR signal, it is more practical to exclude the constant and express the z-magnetisation in terms of the population difference:

$$M_z = n_\alpha - n_\beta \tag{4.29}$$

$$\therefore M_z^0 = n_\alpha^0 - n_\beta^0 \tag{4.30}$$

4.3.2 Relaxation in terms of populations

As previously mentioned, the z-magnetisation is dependent on the population difference between the α or β energy levels. The longitudinal relaxation is the process that pushes the z-magnetisation back to equilibrium. Therefore, longitudinal relaxation is generated by transitions between these two energy levels. Figure 4.8 illustrates the α or β energy levels and rate of transition.

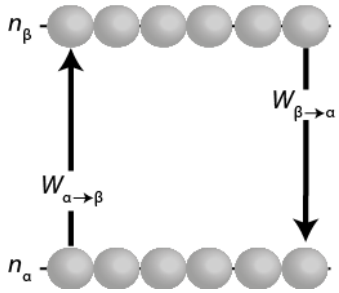

Figure 4.8. Illustration of the population of the energy level associated with a specific spin e.g. α with population $\boldsymbol{n_\alpha}$. $\boldsymbol{n_\alpha}$ will decrease with a transition from α to β state.

For simplicity, we can assume the rate of transition from α to β state is proportional to the population of the α state, n_α:

$$\text{Rate from } \alpha \text{ to } \beta = W_{\alpha\to\beta} n_\alpha \tag{4.31}$$

Where $W_{\alpha\to\beta}$ is the rate constant. Likewise, the rate of transition from β and α state is expressed as:

$$\text{Rate from } \beta \text{ to } \alpha = W_{\beta\to\alpha} n_\beta \tag{4.32}$$

The overall change of the α state includes two terms, a positive (increase term) and negative term (decrease term):

$$\text{Overall rate of chance of } n_\alpha = \underbrace{+W_{\beta\to\alpha} n_\beta}_{increase\ in\ n_\alpha} \underbrace{-W_{\alpha\to\beta} n_\alpha}_{decrease\ in\ n_\alpha} \tag{4.33}$$

Where the plus sign signifies an increase of population of the β state while the negative sign indicates a decrease of population of the α state. Similarly, the overall change of the β state can also be expressed as:

$$\text{Overall rate of change of } n_\beta = \underbrace{+W_{\alpha\to\beta}n_\alpha}_{increase\ in\ n_\beta}\ \underbrace{-W_{\beta\to\alpha}n_\beta}_{decrese\ in\ n_\beta} \tag{4.34}$$

At thermal equilibrium, the changes in populations reach steady state. Therefore, the rate of change will be zero:

$$0 = W_{\beta\to\alpha}n_\beta^0 - W_{\alpha\to\beta}n_\alpha^0 \tag{4.35}$$

$$0 = W_{\alpha\to\beta}n_\alpha^0 - W_{\beta\to\alpha}n_\beta^0 \tag{4.36}$$

$$\therefore\ \frac{n_\alpha^0}{n_\beta^0} = \frac{W_{\beta\to\alpha}}{W_{\alpha\to\beta}} \tag{4.37}$$

The simple theory commonly used would predict that at thermal equilibrium $W_{\beta\to\alpha} = W_{\alpha\to\beta}$ and as a result, $n_\alpha^0 = n_\beta^0$ which is not always true. As previously mentioned, per the Boltzmann distribution, the lower state will have a higher population compared to the higher state. To avoid this issue, the equations 4.33 and 4.34 can be rewritten in terms of the deviation of the population from equilibrium:

$$\text{Rate of change of } n_\alpha = W_{\alpha\beta}\left(n_\beta - n_\beta^0\right) - W_{\alpha\beta}(n_\alpha - n_\alpha^0) \tag{4.38}$$

$$\text{Rate of change of } n_\beta = -W_{\alpha\beta}\left(n_\beta - n_\beta^0\right) + W_{\alpha\beta}(n_\alpha - n_\alpha^0) \tag{4.39}$$

All the rate constants are expressed as $W_{\alpha\beta}$, which is then multiplied by the population deviation from equilibrium $(n_\alpha - n_\alpha^0)$ and $\left(n_\beta - n_\beta^0\right)$ Recalling that equations 4.29:

$$M_z = n_\alpha - n_\beta \tag{4.29}$$

$$\begin{aligned}\therefore\ rate\ of\ change\ of\ M_z \\ = rate\ of\ change\ of n_\alpha - rate\ of\ chance\ of n_\beta\end{aligned} \tag{4.40}$$

$$rate\ of\ change\ of\ M_z = 2W_{\alpha\beta}\left(n_\beta - n_\beta^0\right) - 2W_{\alpha\beta}(n_\alpha - n_\alpha^0) \tag{4.41}$$

$$rate\ of\ change\ of\ M_z = -2W_{\alpha\beta}\left[(n_\alpha - n_\beta) - (n_\alpha^0 - n_\beta^0)\right] \tag{4.42}$$

$$rate\ of\ change\ of\ M_z = -2W_{\alpha\beta}(M_z - M_z^0) \tag{4.43}$$

Equation 4.43 can be written in terms of calculus where the rate of change of M_z is a derivative with respect to time, $dM_z/\mathrm{d}t$:

$$\frac{dM_z(t)}{\mathrm{d}t} = -R_z[M_z(t) - M_z^0] \tag{4.44}$$

where $2W_{\alpha\beta} = R_z$ is the longitudinal relaxation rate constant ($R_z = 1/T_1$). The z-magnetisation is written as $M_z(t)$ to emphasise it is a function of time. T_1 is known as the longitudinal relaxation. Equation 4.44 can be rewritten as:

$$\frac{dM_z(t)}{\mathrm{d}t} = -\frac{1}{T_1}[M_z(t) - M_z^0] \tag{4.45}$$

4.4 Longitudinal (T_1) relaxation

If a 90° RF pulse is applied along the x-axis, the magnetisation will move away from the +z-axis (longitudinal plane) onto the +y axis (transverse plane). The process by which the bulk magnetisation is restored to thermal equilibrium (along the longitudinal plane) is known as longitudinal relaxation (*see Figure 4.9*).

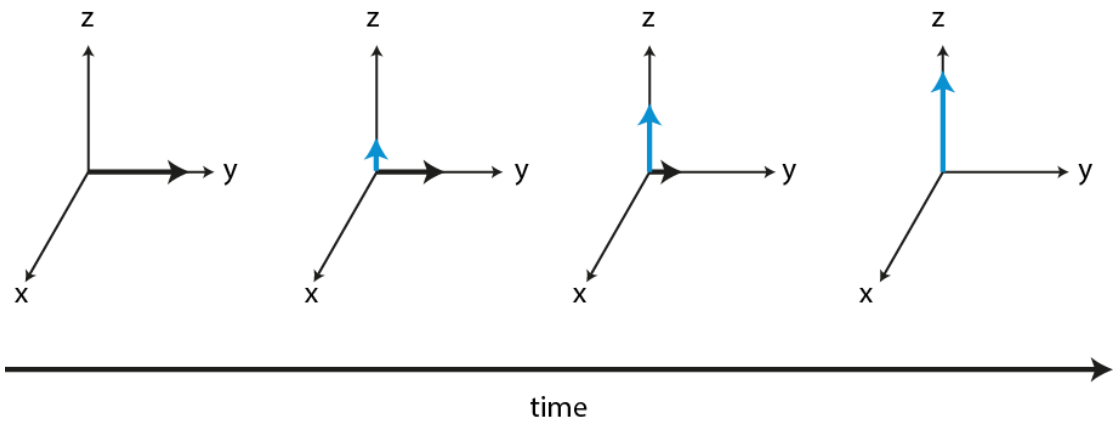

Figure 4.9. Representation of the T_1 relaxation mechanism.

As previously shown, the z magnetisation (M_z) exponentially returns to equilibrium:

$$\frac{dM_z(t)}{\mathrm{d}t} = -R_z[M_z(t) - M_z^0] \tag{4.44}$$

Where R_z is the rate constant for T_1 relaxation (or $1/T_1$), $M_z(t)$ is the z-magnetisation as a function of time and M_z^0 is the equilibrium z-magnetisation. The negative sign indicates with an increase in time, the restoration of the magnetisation also increases. The R_z probes how fast the magnetisation is approaching equilibrium. Each term would be easier to comprehend with an example. If we assume at time zero, the z-magnetisation is $M_z(0)$. Equation 4.44 can be rearranged to have all the M_z components on the left and the time components on the right such as:

$$\frac{1}{\{M_z(t) - M_z^0\}} \, \mathrm{d}M_z(t) = -R_z \mathrm{d}t \tag{4.46}$$

The left-hand side is integrated with respect to $M_z(t)$ and the right-hand side with respect to t:

$$\int \frac{1}{\{M_z(t) - M_z^0\}} \, \mathrm{d}M_z(t) = -R_z \mathrm{d}t \tag{4.47}$$

$$ln\{M_z(t) - M_z^0\} = -R_z t + constant \tag{4.48}$$

At time t = 0, equation 4.48 become;

$$ln\{M_z(0) - M_z^0\} = constant \tag{4.49}$$

Equation 4.49 can be substituted into equation 4.48:

$$ln\{M_z(t) - M_z^0\} = -R_z t + ln\{M_z(0) - M_z^0\} \tag{4.50}$$

$$ln\left\{\frac{M_z(t) - M_z^0}{M_z(0) - M_z^0}\right\} = -R_z t \tag{4.51}$$

Then take exponential on both sides:

$$\frac{M_z(t) - M_z^0}{M_z(0) - M_z^0} = e^{-R_z t} \tag{4.52}$$

$$M_z(t) = \{M_z(0) - M_z^0\} e^{-R_z t} + M_z^0 \tag{4.53}$$

In specific cases, if the bulk magnetisation is tilted onto the transverse plane, then $M_z(0) = 0$. Therefore, equation 4.53 can be simplified into:

$$M_z(t) = M_z^0 (1 - e^{-R_z t}) \tag{4.54}$$

4.4.1 Measuring (T_1) relaxation

4.4.1.1 Inversion recovery

A well-known method used to measure T_1 relaxation is known as inversion-recovery pulse sequence (*see Figure 4.10*). Initially, a $180°_x$ pulse is applied, which transforms the bulk magnetisation from the +z-axis $[M_z(0)]$ onto long the –z-axis $(-M_z^0)$.

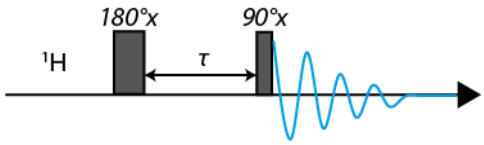

Figure 4.10. Inversion recovery pulse sequence.

This perturbed magnetisation relaxes for a certain time, τ. Finally, a 90°$_x$ pulse is applied which brings the magnetisation onto the transverse plane so that an FID is recorded (see Figure 4.11.a). Knowing t = τ and $M_z(0) = (-M_z^0)$, these values can be substituted into equation 4.53 such as:

$$M_z(\tau) = -2M_z^0 e^{-R_z\tau} + M_z^0 \tag{4.55}$$

$$M_z(\tau) = M_z^0\{1 - 2e^{-R_z\tau}\} \tag{4.56}$$

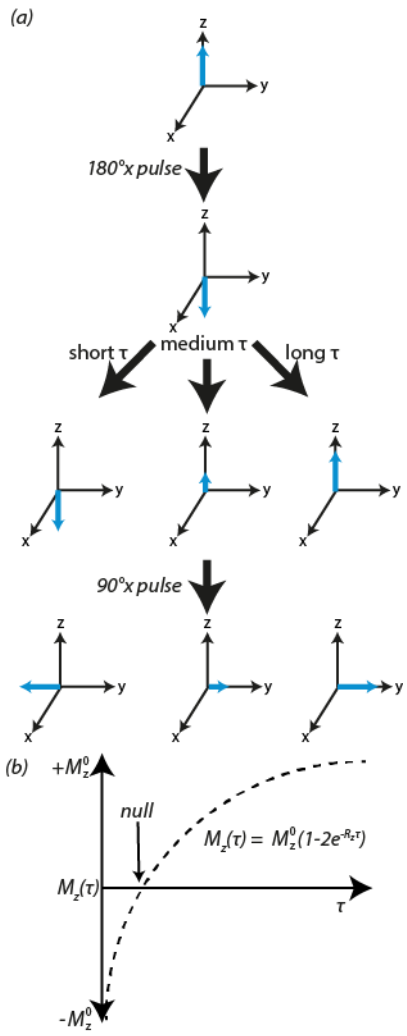

Figure 4.11. (a)Visualisation of the bulk magnetisation during an inversion recovery pulse sequence and (b) an inversion recovery plot.

The experiment is repeated with incremented values of τ to obtain enough points for a fit. The $M_z(\tau)$ is directly proportional to the peaks signal, S(τ), just before the $90°_x$ is applied. Figure 4.11.b illustrates a classic inversion recovery plot. Equation 4.56 can be used to find the R_1 rate of relaxation of a given sample (see Figure 4.11.b).

4.4.1.2 Saturation recovery

A major limitation of using inversion recovery is that the magnetisation must return to thermal equilibrium before recording another experiment. As previously mentioned, a recycle delay of 5xT_1 is required to enable the sample to do so. Saturation recovery (*see Figure 4.12*) is not dependent on this recycle delay [247, 248].

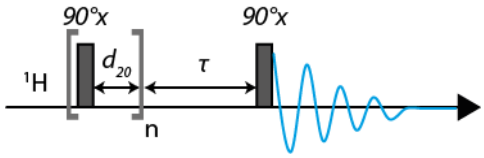

Figure 4.12. Saturation recovery pulse sequence.

Initially, the bulk magnetisation is at equilibrium. Shortly after a train of $90°_x$ pulses are applied which saturates the two energy levels (the two levels are equalized). The system relaxes for a time delay, τ, which enables the magnetisation to return to equilibrium followed by another $90°_x$ to record the FID (*see Figure 4.13a*). The recovery of the bulk magnetisation from the saturated state is expressed as[223]:

$$M_z(\tau) = M_z^0\{1 - e^{-R_z\tau}\} \qquad (4.57)$$

A typical saturation recovery exponential plot is shown in Figure 4.13b. Equation 4.57 can be used to obtain the T_1 relaxation rate. Saturation recovery does not require the magnetisation to fully return to thermal equilibrium enabling the recycle delay to be considerably shorter compared to inversion recovery technique. This is simply because the spin populations of the two energy levels are equalised before each repetition. The two energy levels therefore will no longer give a resonance signal (longitudinal magnetisation is set to zero). This is a major time saving feature compared to inversion recovery pulse sequence [223, 249, 250].

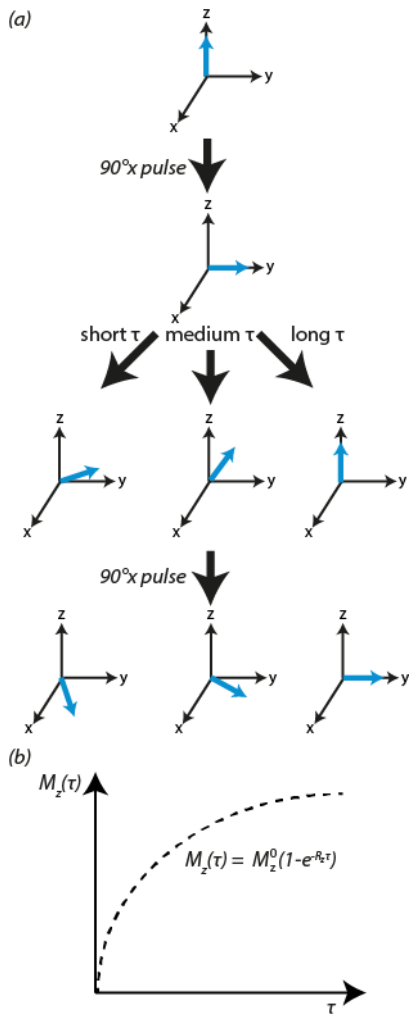

Figure 4.13. (a)Visualization of the bulk magnetisation during a saturation recovery pulse sequence and (b) a saturation recovery plot.

4.5 Transverse (T_2) relaxation

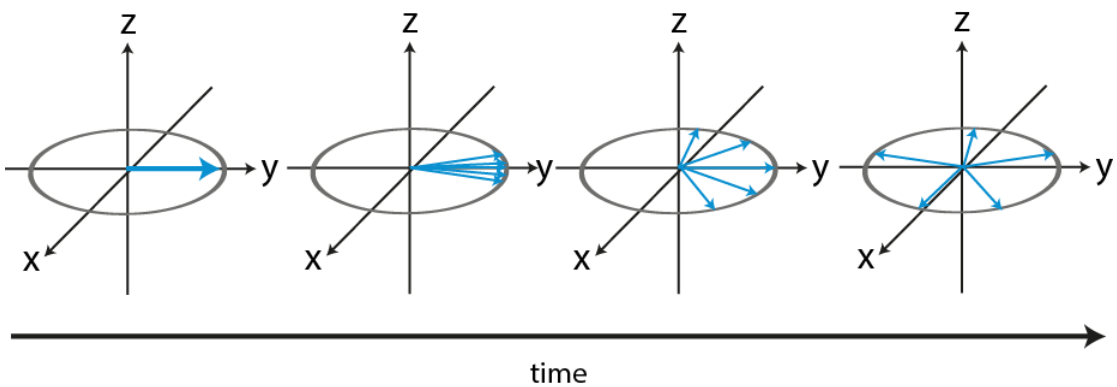

Figure 4.14. Representation of the T_2 relaxation mechanism.

Per the Bloch theory of NMR, the transverse relaxation (e.g. x-magnetisation, M_x) can be expressed as:

$$\frac{\mathrm{d}M_x(t)}{\mathrm{d}t} = -R_{xy}M_x(t) \tag{4.58}$$

where R_{xy} is the rate constant for T_2 relaxation (or $1/T_2$). Similarly, to section 4.4 (T_1 equation), the equation can be simplified to prove the magnetisation exponentially decays to zero:

$$\frac{\mathrm{d}M_x(t)}{M_x(t)} = -R_{xy}\mathrm{d}t \tag{4.59}$$

$$\int \frac{\mathrm{d}M_x(t)}{M_x(t)} = \int -R_{xy}\mathrm{d}t \tag{4.60}$$

$$lnM_x(t) = -R_{xy}t + constant \tag{4.61}$$

At time t = 0, equation 4.61 becomes;

$$lnM_x(0) = const \tag{4.62}$$

Equation 4.62 can be substituted into equation 4.61:

$$lnM_x(t) = -R_{xy}t + lnM_x(0) \tag{4.63}$$

$$lnM_x(t) - lnM_x(0) = -R_{xy}t \tag{4.64}$$

$$ln\frac{M_x(t)}{M_x(0)} = -R_{xy}t \tag{4.65}$$

$$\frac{M_x(t)}{M_x(0)} = e^{-R_{xy}t} \tag{4.66}$$

$$M_x(t) = M_x(0)e^{-R_{xy}t} \tag{4.67}$$

The y-magnetisation also decays in the same manner.

4.5.1 Measuring T_2 relaxation

4.5.1.1 Peak line width at half height

A quick method to determine the T_2 relaxation is by using the peak at half height (equation 4.65). However, this technique can only be used if there is an absence of inhomogeneous broadening. If inhomogeneous broadening is observed, a spin echo pulse sequence can be used to determine accurate T_2 relaxation time (see Figure 4.14 for an illustration of T_2 relaxation mechanism).

$$\Delta v_{1/2} = \frac{1}{\pi T_2} \tag{4.68}$$

4.5.1.2 Spin echo (CPMG pulse sequence).

A spin echo pulse sequence has the ability of refocusing any inhomogeneous broadening contributions at the end of the echo[251, 252]. This pulse sequence is based on the spin-echo pulse sequence (*see Figure 4.15*).

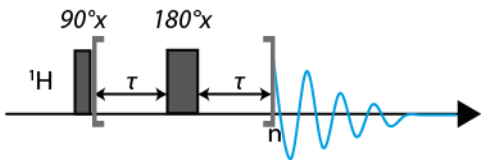

Figure 4.15. CPMG pulse sequence.

Initially, a 90°x pulse is applied to transfer the bulk magnetisation from the z-axis onto the transverse plane. The spin-echo period (τ-180°x-τ) dictates the decay of the transverse magnetisation, M_{xy}, where τ, is an optimised time delay. It is crucial to optimise the τ delay to avoid any J-modulation. Typically, τ is short in comparison to the inverse of any spin-spin couplings [253, 254]. The spin-echo period is known as a loop, which is repeated for a set number of times (n). Finally, the FID is acquired and stored. Figure 4.16, illustrates how the bulk magnetisation is distorted during the CPMG pulse sequence. As shown in Figure 4.16a, the final τ delay, refocuses the spins and hence an echo is formed. The T_2 relaxation is obtained by repeating the CPMG pulse sequence with incremented loop numbers (e.g. 2,4,6….). The height of each echo decreases with an increase in loop number due to T_2 de-phasing.

Equation 4.69 can be used to determine the transverse relaxation. An exponentially decaying plot of transverse relaxation over incremented τ delays is shown in Figure 4.16b

$$M_{xy}(\tau) = M_{xy}(0)e^{-R_{xy}\tau} \tag{4.69}$$

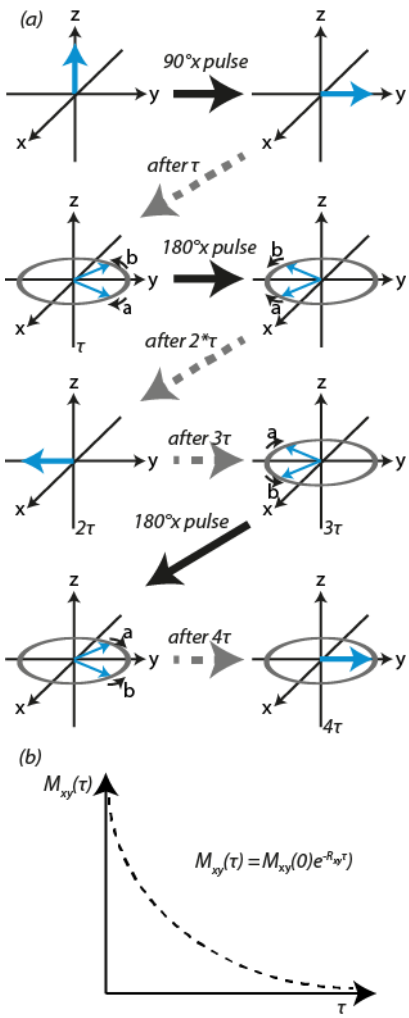

Figure 4.16. (a) Visualization of the bulk magnetisation during a CPMG pulse sequence and (b) a CPMG exponential plot.

4.6 Relaxation rates in the fast and slow motional regime

Nevertheless, it is essential to comprehend how both the longitudinal and transverse relaxation rate constant (R_z and R_{xy}) compare in fast and slow motion regimes. In the fast motion regime, $j(\omega_0) = 2\tau_c$ and independent of motional regime, $j(0) = 2\tau_c$. Both longitudinal and transverse relaxation rates are:

$$\text{In the fast motion regime: } R_z = \gamma^2 \overline{B_{loc}^2}\, j(\omega_0) \tag{4.70}$$

$$= 2\gamma^2 \overline{B_{loc}^2}\, \tau_c \tag{4.71}$$

and

$$\text{In the fast motion regime: } R_{xy} = \frac{1}{2}\gamma^2 \overline{B_{loc}^2}\, j(0) + \frac{1}{2}\gamma^2 \overline{B_{loc}^2}\, j(\omega_0) \tag{4.72}$$

$$= \gamma^2 \overline{B_{loc}^2}\, \tau_c + \gamma^2 \overline{B_{loc}^2}\, \tau_c \tag{4.73}$$

$$= 2\gamma^2\overline{B_{loc}^2}\,\tau_c \tag{4.74}$$

Equations 4.71 and 4.74 illustrate the fast motion regime of both relaxation rate constants are exactly equal. This is because spectral density is independent of frequency. Similarly, in the slow-motion regime, $j(0) = 2\tau_c$ and the reduced spectral density at the Larmor frequency becomes:

$$j\,(\omega_0) = \frac{\tau_c}{\omega^2\tau_c} \tag{4.75}$$

Therefore, the longitudinal rate constant in the slow-motion regime is:

In the slow-motion regime: $R_z = \gamma^2\overline{B_{loc}^2}\,j(\omega_0)$ (4.76)

$$= \frac{2\gamma^2\overline{B_{loc}^2}}{\omega^2\tau_c} \tag{4.77}$$

In the slow-motion regime, the longitudinal rate constant is inversely proportional to correlation time. As the correlation time increases, the rate constant decreases. In comparison, the transverse rate constant goes up with an increase in correlation time:

In the slow-motion regime:

$$R_{xy} = \tfrac{1}{2}\gamma^2\overline{B_{loc}^2}\,j(0) + \tfrac{1}{2}\gamma^2\overline{B_{loc}^2}\,j(\omega_0) \tag{4.78}$$

$$= \gamma^2\overline{B_{loc}^2}\,\tau_c \tag{4.79}$$

where $j(\omega_0) = 0$ as it is negligible in contrast to $j(0)$. This is due to the secular contribution of the transverse rate constant. Additionally, both R_z and R_{xy} can be expressed in terms of dipolar constant (b)[216]:

$$b = \frac{\mu_0}{4\pi}\frac{\hbar\gamma^2}{r^3} \tag{4.80}$$

$$R_z = \frac{1}{T_1} = \frac{3}{10}b^2\{j(\omega_0) + 4j(2\omega_0)\} \tag{4.81}$$

$$R_{xy} = \frac{1}{T_2} = \frac{3}{20}b^2\{3j(0) + 5j(\omega_0) + 2j(2\omega_0)\} \tag{4.82}$$

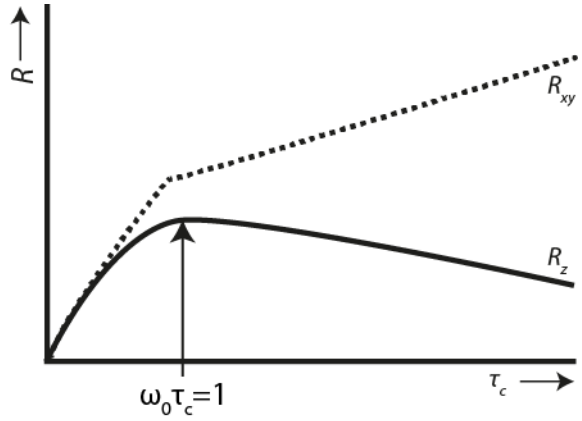

Figure 4.17. Plot of longitudinal ($\boldsymbol{R_z}$) and transverse ($\boldsymbol{R_{xy}}$) relaxation rates against correlation time, $\boldsymbol{\tau_c}$.

Figure 4.17 illustrates the plots of both relaxation rate constants against correlation time. The fast motion regime is observed where the two rate constants are equal. As a correlation time increases, the longitudinal rate constant also increases until it reaches a maximum. Recall that $j(\omega_0)$ is maximum where $\omega_0\tau_c = 1$, at this value R_z reaches its maximum rate. As correlation increases further, R_z gradually reduces. In comparison, R_{xy} steadily rises with the increase in correlation time.

4.7 Longitudinal dipolar relaxation of two spins

4.7.1 Energy levels and transition rates

It is crucial to understand the relaxation mechanism of two coupled spins that are interacting via dipolar coupling. As previously mentioned, two coupled spins are associated with 4 energy levels as shown in Figure 4.18. The main point of interest of this figure is to illustrate whether the relaxation processes can cause transitions between these energy levels. Dipolar interactions can cause relaxation-induced transitions between any two energy levels. Each single transition has a specific rate constant associated with it, which is expressed as $W_{\Delta M}$ where the subscript ΔM indicates the change in total magnetic quantum number that is associated with the transition. Single quantum transition rates also include a superscript that indicates the position of the flipped spin and the spin of interest respectively.

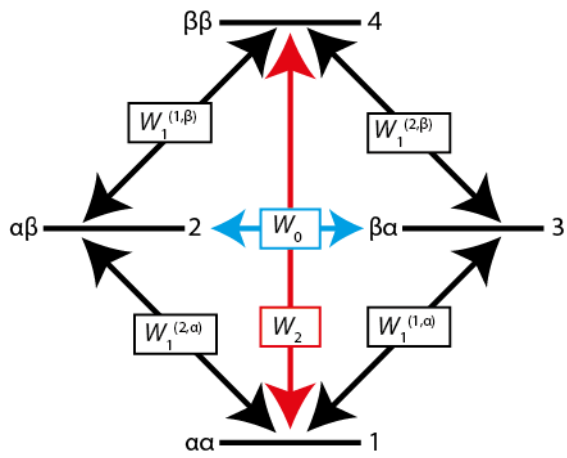

Figure 4.18. Energy levels of a two-spin system with transitions rates, W, caused by dipolar relaxation.

Furthermore, it is possible to describe how the population of the energy levels changes as a function of time. This is achieved by considering both the gain and loss process of energy level. The rate of change of the population of the energy level 1 can be expressed as:

$$\frac{\mathrm{d}n_1}{\mathrm{d}t} = \underbrace{-W_1^{(2,\alpha)}(n_1 - n_1^0) - W_1^{(1,\alpha)}(n_1 - n_1^0) - W_2(n_1 - n_1^0)}_{(loss\ from\ energy\ level\ 1)} + \underbrace{W_1^{(2,\alpha)}(n_2 - n_2^0)}_{gain\ from\ level\ 2} + \underbrace{W_1^{(1,\alpha)}(n_3 - n_3^0)}_{gain\ from\ level\ 3} + \underbrace{W_2(n_4 - n_4^0)}_{gain\ from\ level\ 4} \tag{4.83}$$

where n_i is the population of the ith level and n_i^0 is the equilibrium population of the same level. The negative and positive sign in equation 4.83 indicate a loss and gain in the population of the energy level respectively. This differential equation can be simplified by writing the magnetisation in terms of the populations. The spin 1 total z-magnetisation I_{1z} can be expressed as:

$$I_{1z} = (n_1 - n_3) + (n_2 - n_4) \tag{4.84}$$

The primary reason why equation 4.84 is associated with $(n_1 - n_3)$ and $(n_2 - n_4)$ is because both are transitions associated with spin 1. Similarly, this can also be applied to spin 2 such as:

$$I_{2z} = (n_1 - n_2) + (n_3 - n_4) \tag{4.85}$$

Another magnetisation term also must be taken into consideration, which is dependent on the difference in the population difference across the spin 1 levels:

$$2I_{1z}I_{2z} = (n_1 - n_3) - (n_2 - n_4)\ or\ (n_1 - n_2) - (n_3 - n_4) \tag{4.86}$$

Conversely, the z-magnetisation also has equilibrium values which are defined in terms of equilibrium populations (at equilibrium, $2I_{1z}I_{2z} = 0$):

$$I_{1z}^0 = n_1^0 - n_3^0 + n_2^0 - n_4^0 \tag{4.87}$$

$$I_{2z}^0 = n_1^0 - n_2^0 + n_3^0 - n_4^0 \tag{4.88}$$

After a lot of tedious algebra, the rate equations for the population of the individual spins can be expressed as[255]:

$$\frac{\mathrm{d}I_{1z}}{\mathrm{d}t} = -R_z^{(1)}(I_{1z} - I_{1z}^0) - \sigma_{12}(I_{2z} - I_{2z}^0) \tag{4.89}$$

$$\frac{\mathrm{d}I_{2z}}{\mathrm{d}t} = -\sigma_{12}(I_{1z} - I_{1z}^0) - R_z^{(2)}(I_{2z} - I_{2z}^0) \tag{4.90}$$

$$\frac{\mathrm{d}2I_{1z}I_{2z}}{\mathrm{d}t} = -R_z^{(1,2)}2I_{1z}I_{2z} \tag{4.91}$$

where the rate constants are:

$$R_z^{(1)} = 2W_1^{(1)} + W_2 + W_0 \tag{4.92}$$

$$R_z^{(2)} = 2W_1^{(2)} + W_2 + W_0 \tag{4.93}$$

$$\sigma_{12} = W_2 - W_{0.} \tag{4.94}$$

$$R_z^{(1,2)} = 2W_1^{(1)} + 2W_1^{(2)} \tag{4.95}$$

These equations are known as the Solomon equations for the relaxation of spin α and β. $R_z^{(1)}$ is the self-relaxation rate constant of spin 1. Similarly, $R_z^{(2)}$ is the self-relaxation rate constant for spin 2. The σ_{12} rate constant describes the rate at which the magnetisation is transferred from spin 1 to 2. This is known as cross-relaxation rate constant between spin 1 and 2. This cross-relaxation connects the z-magnetisation of the two spins. The cross-relaxation phenomenon is mainly responsible for the nuclear Overhauser effect (NOE). The NOE effect has been widely used in solution NMR for structural characterization of molecules due to its dependence to dipolar coupling [256, 257].

4.8 Chemical exchange

Transverse local fields which oscillate near the Larmor frequency lead to longitudinal relaxation. These fields can affect both the y- and x-components of the individual magnetic moment and hence also cause transverse relaxation. This is known as the non-secular contribution to transverse relaxation, which the rate depends on $J(\omega_0)$. Therefore, this non-secular contribution was already covered. However, another contribution known as the secular contribution is also present. This contribution is caused by the z-components of the local fields. The secular contribution rate depends on $J(0)$. A way of understanding the origin of this secular contribution is by understanding a process known as chemical exchange. The process where a nucleus exchanges between two or more environments is known as NMR chemical exchange (see Figure 4.19). This process can have a severe effect on the spectra observed (chemical shift) and relaxation properties of a nucleus.

For simplicity, we can consider chemical exchange between two sites (A and B) as shown below:

$$A \underset{k_2}{\overset{k_1}{\rightleftharpoons}} B \tag{4.96}$$

Where k_1 is the forward exchange rate constant of A to B and k_2 is the reverse exchange rate constant. The equilibrium constant (K_{eq}) can be calculated as:

$$\mathrm{K}_{eq} = \frac{k_1}{k_2} \tag{4.97}$$

However, what is observed in Figure 4.19 heavily depends on the comparison between exchange rate constants (k_{ex}) and the separation between the resonances ($\Delta\omega$) of the two sites. $\Delta\omega$ can be expressed as:

$$\Delta\omega = \omega_A - \omega_B \tag{4.98}$$

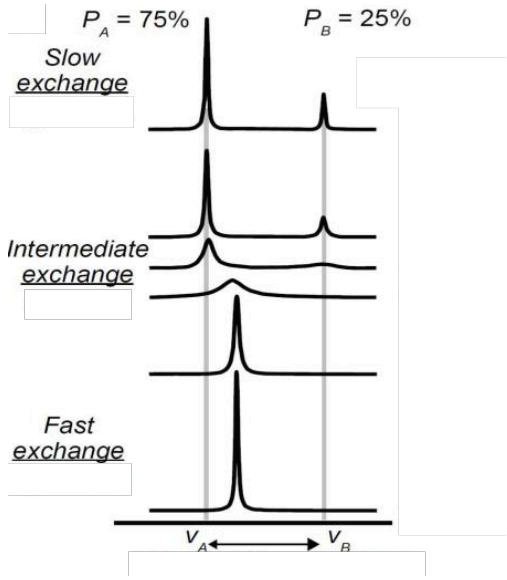

Figure 4.19. Illustrating the effect of chemical exchange on lineshape. The figure shows a simulated 1D NMR spectra for nuclei exchanging between two distinct chemical environments. Adapted from [258, 259].

Table 4.1 shows the relationship between the resonance separation ($\Delta\omega$) and exchange rate constants (k_{ex}). The chemical exchange theory is explained in the following section.

Table 4.1. The effect of chemical exchange (at different regime) on the characteristics of the NMR spectrum observed.

Chemical Exchange Rate	$k_{ex}$and Δv Comparison	Observed Spectrum
Very slow	$k_{ex} \ll \Delta\omega$	Two Resonances
Slow	$k_{ex} < \Delta\omega$	Two Broadened Resonances
Intermediate	$k_{ex} \approx \Delta\omega$	Complex Lineshape
Fast	$k_{ex} > \Delta\omega$	Single Broadened Resonance
Very Fast	$k_{ex} \gg \Delta\omega$	Single Resonance

4.8.1 Slow chemical exchange

If the exchange rate constant is smaller than the resonance separation, two resonances will be observed as shown in Figure 4.19. This is due to the resonances at $\omega_A$and at ω_B. This is known as slow chemical exchange.

4.8.2 Very Slow chemical exchange

When the exchange rate is extremely small compared to the resonance separation of the two resonances, this is known as very slow chemical exchange. The peak intensity of each environment is proportional to the population of each state. Consequently, the equilibrium constant can be calculated from the line intensities:

$$K_{eq} = \frac{I_B}{I_A} \tag{4.99}$$

If the exchange rate is way smaller than transverse relaxation rate R_2, the exchange may have little or no effect on the line width. However, if the exchange rate is faster than R_1, other methods such as exchange spectroscopy (EXSY) can be used to determine rate of exchange[260]. As mentioned in Chapter 3, if the system is going through very slow chemical exchange, a cross peak between the two sites ($\omega_A$and at ω_B) will be observed in the 2D spectra. 2D EXSY experiment can also be used to quantify the rate of exchange in a system by following the signal intensity of the cross peak as a function of the mixing time[261]. Nonetheless, this process can be time consuming.

In this time regime, it is possible to obtain both the equilibrium constant and the rate constants of the system. The equilibrium constant can be obtained from the integrated intensities of each resonance. Thus, the ratio of the forward and reverse rate of exchange can also be used as follows:

$$\mathrm{K}_{eq} = \frac{Intensity_B}{Intensity_A} = \frac{\frac{k_1}{k_1 + k_2}}{\frac{k_2}{k_1 + k_2}} = \frac{k_1}{k_2} \tag{4.100}$$

Moreover, both the forward and reverse rate constants can be determined by measuring the difference in peak line width due to the chemical exchange:

$$\pi \Delta v_{1/2}^{A} = R_2^A + k_1 \tag{4.101}$$

$$\pi\Delta v_{1/2}^{B} = R_2^B + k_1 \tag{4.102}$$

Where Δv is peak at half height and R_2 is transverse relaxation rate. R_2 values can be determined by using a CPMG pulse sequence.

4.8.3 Slow to intermediate exchange:

Once the rate of exchange between the two sites increases, at one point the two resonances merge into one peak and are said to have coalesced. At the so-called coalescence point, the peak flattens out. Once the rate goes above the coalescence point, a single peak is observed. At this point, the system enters the fast-intermediate regime.

4.8.4 Fast Chemical exchange

If the exchange rate is much larger than then resonance separation, only one set of resonance will be observed and this is known as fast chemical exchange. The single resonance observed is dependent on the weighted average of chemical shifts of the two individual environments:

$$\omega = p_A\omega_A + p_B\omega_B \tag{4.103}$$

Where p_A and p_B represents the population of environments A and B respectively. The observed transverse relaxation rate R_2^{obs}can be expressed as[262]:

$$R_2^{obs} = 1/T_2^{obs} \tag{4.104}$$

$$R_2^{obs} = R_2^0 + \frac{p_A p_B (\Delta\omega)^2}{k_{ex}} \tag{4.105}$$

$$R_2^0 = 1/T_2^0 \tag{4.106}$$

Where R_2^0 is the transverse relaxation rate in the absence of exchange. From this equation, it is apparent that the dynamic properties of the system can be difficult to probe via line shape analysis since $\Delta\omega$, p_A and p_B are normally unknown. An increase in the rate constant can further reduce the peak linewidth. This mechanism is known as exchange narrowing.

4.8.5 Differentiating fast and slow chemical exchange

It is apparent that if two separated resonances are observed, the system is going through slow chemical exchange. Nevertheless, if one single resonance is observed, this doesn't necessarily mean the system is going through fast chemical exchange. This could also indicate the system is going through slow chemical exchange where the population of one environment is considerably smaller than the other (e.g. $p_B \ll p_A$) resulting in the second resonance not being observed on the NMR spectra. This mystery can be solved using two methods.

4.8.5.1 Temperature dependence

Change in temperature enables us to probe the timescale of the chemical exchange. Temperature is directly proportional to the chemical exchange rate. Additionally, the chemical exchange rate is also dependent on the activation enthalpy, $\Delta H^{\dagger}$, for exchange:

$$k_{ex} \propto e^{-\frac{\Delta H^{\dagger}}{RT}} \tag{4.107}$$

If the system is in the slow chemical exchange regime, increase in temperature leads to line broadening which indicates the system is transitioning towards the intermediate exchange regime. However, narrowing of the line width does not always indicate the system is going through fast chemical exchange. The narrowing of lines occurs irrespective of the chemical exchange due to the reduction of the correlation time with increase in temperature. Unless the temperature dependence of the activation enthalpy of for exchange is greater than the correlation time, it is extremely difficult to determine whether the system is going through fast chemical exchange.

4.8.5.2 Magnetic field dependence

Another way to differentiate between fast and slow chemical rate regime is by using different magnetic fields. If the system is going through very slow chemical exchange, the resonance line will broaden due to the exchange rate constant, k_1:

$$R_{2,A}^{obs} = R_{2,A}^{0} + k_1 \tag{4.108}$$

Where $R_{2,A}^{obs}$ is the transverse relaxation rate in presence of chemical exchange and $R_{2,A}^{0}$ with absence of chemical exchange for environment A. As clearly shown in equation 4.108, the resonance line width is independent of magnetic field strength. On the other hand, if the system is going through fast chemical exchange, the resonance line width is:

$$R_2^{obs} = R_2^0 + \frac{p_a p_b (\Delta\omega)^2}{k_{ex}} \tag{4.109}$$

In the fast-chemical exchange regime, the line width contribution due to exchange depends on the square of the magnetic field ($\Delta\omega^2$)[263].

5 ^{1}H HIGH RESOLUTION MAGIC ANGLE SPINNING RELAXATION METHOD DEVELOPMENT AND OPTIMISATION

5.1 Abstract

Over the years, ^{1}H high resolution magic angle spinning NMR (^{1}H HR MAS NMR) relaxation techniques have been used to probe the molecular motion of various systems. In this study, we propose a series of systematic steps for achieving the optimum experimental conditions for acquiring reliable, reproducible and robust quantitative ^{1}H HR MAS NMR T_1 and T_2 relaxation measurements for a variety of analytes, mobile phases and RP-HPLC stationary phases (heterogeneous systems). We determined the impact of several factors during our NMR method development such as: (1) rotor sizes, (2) radio frequency (RF) pulse powers, (3) T_1 pulse sequences, (4) spinning frequency, (5) temperature, (6) analyte concentration, (7) mobile phase ratio, (8) organic solvent, (9) buffer, (10) mixtures of analytes, (11) analyte chemical and physical properties and (12) DSS concentration effect on ^{1}H HR MAS NMR spectra and relaxation measurements. The repeatability and robustness of our developed and optimised method was determined via statistical tests. Furthermore, the effect of sample preparation on the method reproducibility was also determined through a linear regression statistical model.

5.2 Introduction

Acquiring an atomic scale resolution measurement of the structural arrangement and molecular motion of a series of compounds in the presence of RP-HPLC mobile phases and stationary phases may provide some insight into the molecular interactions between analytes and stationary phases and thus provide an additional molecular (system) descriptor for a quantitative structure retention relationship (QSRR) in silico model. NMR spectrometry is well known for its utility in structural elucidation and it has also been used to probe the dynamic characteristics of chromatographic separation processes (see Chapter 1). In particular, ^{1}H high resolution magic angle spinning (MAS) NMR has been particularly exploited to achieve insight into chromatographic analyte stationary phase interactions. MAS is essential for minimising any anisotropic interaction including magnetic susceptibility, chemical shift anisotropy and other line-broadening mechanisms within the system [264, 265]. This technique has allowed scientists to determine the chemical structures of a variety of HPLC stationary phases in a non-destructive way [66, 68, 266-269].

Recent advances in ^{1}H HR-MAS NMR longitudinal (T_1)[215] and transverse (T_2) NMR relaxation measurements enable us to probe site specific information about the molecular dynamic properties of chromatographic separation processes.

However, several factors can affect the reliability and sensitivity of NMR relaxation measurements such as long longitudinal relaxation times, heterogeneous systems, temperature, analyte concentration, quality of shimming, rotor spinning frequency and pulse sequences delays. The optimisation of each factor can improve the sensitivity and resolution of our ^{1}H HR-MAS NMR relaxation measurements. For the purposes of the thesis of this body of work, it was important that we systematically optimised an approach for quantitative NMR relaxation measurements on analyte-stationary phase systems which would be robust for all chromatographic systems analysed so relaxation times could be compared without significant error. The primary motivation of this study was therefore to determine the optimal experimental conditions for acquiring reliable and reproducible NMR relaxation measurements between a series of analytes, mobile phases and RP-HPLC stationary phases. Furthermore, the robustness, repeatability and reproducibility of optimised NMR relaxation method and sample preparation was determined via statistical methodologies.

5.3 Experimental

5.3.1 Materials

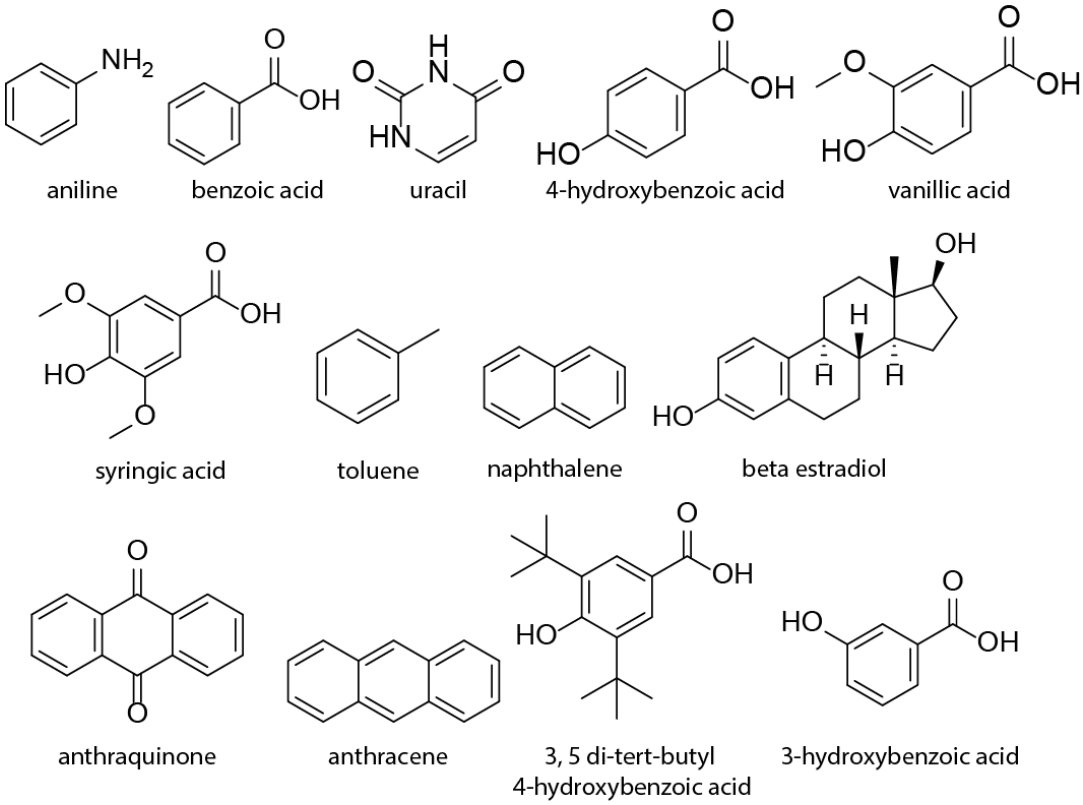

Figure 5.1. Chemical structure of molecules considered in this study.

The analytes considered in this study included: aniline, benzoic acid, uracil, 4-hydroxybenzoic acid, vanillic acid, syringic acid, toluene, naphthalene, beta estradiol, anthraquione, anthracene, 3, 5 di-tert-butyl 4 hydroxybenzoic acid and 3 hydroxybenzoic acid (see Figure 5.1). 4,4-dimethyl-4-silapentane-1-sulfonic acid (DSS) was added to the samples as an internal reference. The considered solvents were deuterium oxide and acetonitrile. All the chemicals were purchased from Sigma Aldrich and used without further purification. The following stationary phase materials were obtained from commercially available XBridge^{TM} columns with particle sizes of 5 µm and average pore diameter of 145 Å: BEH-C18 (~17% w/w carbon loading), BEH-phenyl (~15% w/w carbon loading), BEH-RP18 (~16% w/w carbon loading), CSH hexyl-phenyl (~14% w/w carbon loading) and HSS T3 (~11% w/w carbon loading). Pfizer has an experimental screening method for new compounds which uses the combination of these stationary phases and mobile phases to provide a range of selectivity.

5.3.2 NMR Method

For the samples with analytes in the presence of mobile phase and absence of stationary phase ("solution only"), 80 µL of the analyte was measured using an automated pipette and then placed into a 4 mm rotor. For the analytes with added stationary phase, 10 mg of stationary phase was initially packed into the rotor followed by addition of 60 µL of the dissolved analyte measured using an automated pipette and then additional 10 mg of stationary phase (*see Figure 5.2*).

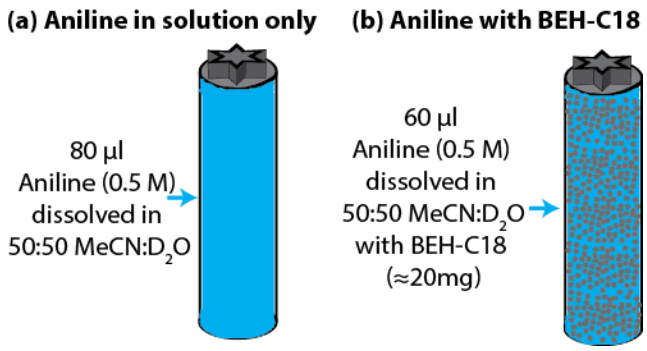

Figure 5.2. Illustration of (a) aniline in solution only and (b) aniline in the presence of BEH C18 stationary phase.

^{1}H HR MAS NMR experiments were conducted on a Bruker UltraShield 500 Spectrometer operating at 500 MHz ^{1}H Larmor frequency. The prepared samples were placed into 4 mm ZrO_2 MAS rotors (Bruker Biospin, Rhein-stetten, Germany) with no spacer. The rotor was spun using high pressure nitrogen at the magic angle ($\theta = 54.4°$) at a spinning speed of 5 kHz at 313 K. The ^{1}H HR MAS NMR experiments were conducted using a 90° one-pulse sequence, where 8 transients were collected into 20 k data points over a spectral width of 20000 Hz (40 ppm) with an acquisition time of 1 second. Exponential line-broadening of 0.5 Hz was applied before FT.

5.3.3 Inversion recovery

^{1}H T_1 was measured by using a standard inversion-recovery pulse sequence (180º – τ – 90º– FID) with pulse nutation frequencies of 25 kHz. 8 transients were collected into 20 k data points over a spectral width of 20000 Hz (40 ppm) with an acquisition time of 1 seconds, relaxation delay of 16 seconds and where τ (the recovery time) was ranged from

0 to 5 seconds with increments of 0.5 seconds. Exponential line-broadening of 2.0 Hz was applied before FT. The ^{1}H T_1 values were calculated by applying an exponential fitting of the peaks integration. Data were plotted and fitted to model equations in TopSpin 3.2

5.3.4 Saturation recovery

^{1}H T_1 was also measured by using a standard saturation-recovery pulse sequence (saturation – τ – 90º– FID) with pulse nutation frequencies of 25 kHz. 8 transients were collected into 20 k data points over a spectral width of 20000 Hz (40 ppm) with an acquisition time of 1 second, relaxation delay of 2 seconds and where the recovery time was ranged from 0 to 30 seconds. Exponential line-broadening of 2.0 Hz was applied before FT. The ^{1}H T_1 values were calculated by applying an exponential fitting of the peaks integration. Data were plotted and fitted to model equations in TopSpin 3.2.

5.3.5 Transverse Relaxation (T_2) Measurements CPMG pulse sequence

^{1}H T_2 relaxation times were measured by using the CPMG pulse sequence (90° - [τ – 180° – τ]n – FID) with a pulse nutation frequency of 25 kHz. 8 transients were collected into 20 k data points over a spectral width of 20000 Hz (40 ppm) with an acquisition time of 1 second, relaxation delay of 16 seconds, spin echo time (ts) of 1.2 ms, loop time was fixed at 2.5 ms and the number of loops (*n*) were varied accordingly to obtain relaxation curves with the peak intensity decaying below 30% of its initial value.

5.4 Results

5.4.1 NMR method compared to HPLC

To achieve an accurate comparison between the HPLC and NMR techniques several experimental parameters were taken into consideration as shown in Table 5.1. Obtaining identical experimental conditions between the techniques is impossible with the equipment available in our facility. However, experimental parameters such as

temperature, mobile phase composition and buffers were kept constant. The ratio mobile phase and stationary phase packed rotor was determined from previous studies [92, 93, 270] and also optimised to determine ratio provided more reproducibility and repeatable results.

The concentration of analytes used in the NMR experiments are considerably higher compared to the HPLC technique in order to obtain sufficient sensitivity for practical applications. The ^{1}H HR MAS experiments could potentially be ran at lower concentrations (50~5 mM) but would potentially take days to weeks compared to 30 minutes for obtaining reliable quantitative relaxation measurements. This is because the NMR peaks intensities are directly proportional to concentration and therefore must be carefully selected. Higher sample concentrations in HPLC analyses do not affect the elution order of the analytes but primarily affect peak shape (height, width and symmetry) which in turn can affect the resolution between closely eluting peaks. Despite a desire to match sample concentration between the two techniques, we were unable to achieve adequate sensitivity in the NMR measurements so needed to increase sample concentration for our NMR experiments.

As shown in section 5.4.7, various concentrations were initially investigated. An appropriate concentration was used throughout this project to improve the robustness, reliability and repeatability of our optimised method which we have achieved and demonstrated in section 5.4.14.

Table 5.1. Comparison of NMR and HPLC experimental conditions

Parameters	NMR	HPLC
Temperature	40 °C	40 °C
Mobile phase	50:50 (% v/v) MeCN:D_2O	50:50 (% v/v) MeCN:H_2O
Stationary phases	20 mg added into rotor	~2.5 g
Flow	No flow (60 μL)	1.0 mL/min
Buffers	No buffer added	No buffer added
Concentration	0.5 M	~5 mM
Data collected	^{1}H spectra, T_1 and T_2 relaxation	Chromatogram and retention times

5.4.2 Rotor sizes

4 mm NMR rotors were used in previous literature studies [91-95, 270] to investigate chromatographic systems under ^{1}H HR MAS NMR. We explored using different rotor sizes for instance 3.2 and 2.5 mm. Analytes dissolved in solution were able to spin (~ 5 kHz spinning frequency), however in the presence of the stationary phases, it was impossible to get the rotors (3.2 and 2.5 mm) to either stabilise or even spin in most cases. This could easily lead to the rotor crashing and potentially destroying the probe's stator. Using a smaller rotor size reduces the amount of analyte, mobile phase and stationary phase investigated in turn the signal to noise whilst simultaneously increasing the run times. Larger rotor sizes (e.g. 7 mm) could potentially be used at the expense of using more stationary phase. After some investigations therefore, the 4 mm rotor size used in previous literature studies was also selected for experiments in this body of work.

5.4.3 Radio frequency (RF) pulse powers

During the early stages of ^{1}H T_1 and T_2 relaxation measurements, 100 kHz nutation frequency was used for ^{1}H 90° pulses. However, in some cases such power led to rf induced sample heating in the NMR rotor. This was observable by a shift of the temperature-sensitive water peak over time of both T_1 and T_2 relaxation measurements. Figure 5.3 illustrates how induced sample heating takes place during long RF pulsing. This induced heating can be minimised by using lower RF powers, E-free probe, lower analyte concentration, smaller NMR rotor and by cooling down the sample [238, 271, 272] (*see Figure A.1 and A.2 in appendix*). To avoid such complication, the nutation frequency was reduced to 25 kHz for both T_1 and T_2 relaxation pulses sequences. Negligible sample heating is observed at 25 kHz nutation frequency.

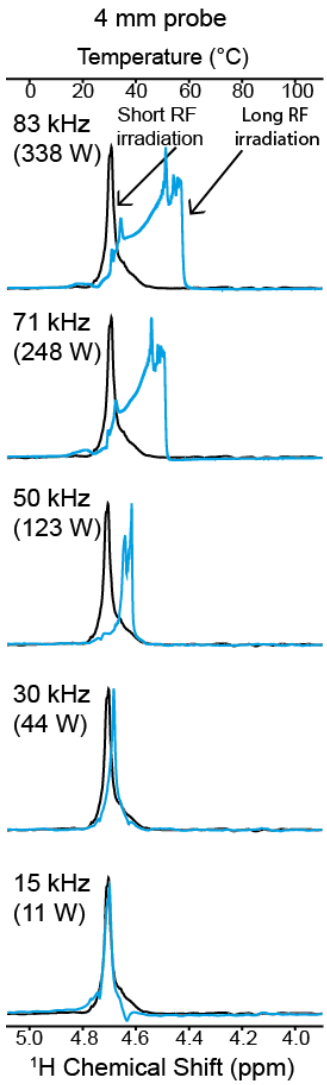

Figure 5.3. ^{1}H 600 MHz NMR spectra of water peaks in 100 mM phosphate buffer (pH 5.5) in 4 mm rotor. From top to bottom, the ^{1}H irradiation nutation frequencies of the RF pulse were 83 kHz, 71 kHz, 50 kHz, 30 kHz and 15 kHz respectively. The black spectra represent the reference with short, 10 µs, pulse only. The blue spectra depict experiments with long, 30 ms, irradiation with nutation frequencies specified in the top left corner of the spectrum. The spectra with the long RF irradiation (blue) were scaled for the intensity to match that of the experiments with short RF irradiation pulse lengths (black). All spectra were acquired at 298 K target temperature at 10 kHz spinning frequency.

5.4.4 T_1 pulse sequence

Throughout the experiments, saturation recovery pulse sequence was used instead of inversion recovery. This was because inversion recovery when used during the

preliminary stages of this study resulted in low reproducibility of T_1 relaxation measurements. This effect may be attributable to insufficiently long recycling delays (recycling delay > $5T_1$) during which, magnetisation had inadequate time to return to equilibrium [273, 274]. As previously mentioned, saturation recovery does not require the magnetisation to return to equilibrium in comparison to inversion recovery [275, 276]. This enabled us to use a shorter recycling delay and therefore reduced the overall running time and cost of our T_1 relaxation experiments [247, 277].

5.4.5 Spinning frequency

The spinning frequency dependence of T_1 and T_2 relaxation was also investigated. If the spinning frequency employed is on the same order or larger than the overall strength of bulk magnetic susceptibility, high resolution spectra of heterogeneous systems can be obtained. Samples containing solid particles usually exhibit broad NMR peaks due to homo- and hetero-nuclear dipolar coupling, chemical shift anisotropy and quadrupolar interactions. The difference of magnetic susceptibility within heterogenous samples tends to reduce the resolution. As previously mentioned, HR-MAS NMR has the ability to produce high resolution NMR spectra. This spectral resolution improvement by MAS is due to the Hamiltonians describing the dipolar, CSA and magnetic susceptibility interactions all containing an orientation component which scales as at $(3\cos^2\theta\text{-}1)$ where θ is the angle between the spinning axis and applied magnetic field [278]. For samples where residual dipolar interactions or difference in magnetic susceptibility are small, MAS can reduce the line width to mimic those observed in solution state HR-NMR spectroscopy. Moderate magic angle spinning frequency is required to average the bulk magnetic susceptibility [278]. However, the spinning frequency must be selected carefully to ensure the residual spinning sidebands fall outside the spectral window. Typically, for heterogeneous samples, MAS speeds between 1 to 2 kHz are sufficient to improve the resolution observed. Several studies have utilised various spinning frequencies to determine the effect on spectra resolution [279-281].

Figures 5.4 and 5.5 illustrate the effect of spinning frequency on the ^{1}H HR MAS NMR spectra of aniline dissolved in 50:50 (% v/v) MeCN:D_2O in the presence of HSS T3 RP-HPLC stationary phase. Under static conditions (0 kHz spinning frequency), broad peaks are observed at approximately 4.2 and 7.0 ppm which corresponds to the water and

aromatic proton peaks of aniline respectively. As illustrated in Figure 5.4, a spinning frequency of 2 kHz is sufficient to improve the resolution of the NMR spectrum. The peak at 0 ppm corresponds to the DSS signal. Low intensity and broad peaks were observed at 0.8 and 1.25 ppm which corresponds to the CH_3 and CH_2 groups of HSS T3 stationary phase. The water peak is observed at approximately 4.2 ppm. The peaks between 6.0 and 8.0 ppm correspond to the aromatic protons of aniline. As demonstrated in Figure 5.5, four well resolved peaks at 7.15 ppm, 7.08 ppm, 6.77 ppm and 6.65 ppm. The two sets of aromatic protons peaks represent aniline, which is "free" in solution and "bound" to the reversed phase stationary phases. Furthermore, the T_1 and T_2 relaxation of the aromatic protons of aniline was obtained as a function of spinning frequency. Figure 5.6 illustrates the average measured T_1 and T_2 relaxation values of aniline against spinning frequency. As illustrated in Figure 5.6, the T_1 and T_2 relaxation slightly changed with an increase in spinning frequency. This likely due to a change in sample temperature due to frictional heating induced by spinning [271], which is not fully compensated by the applied cooling.

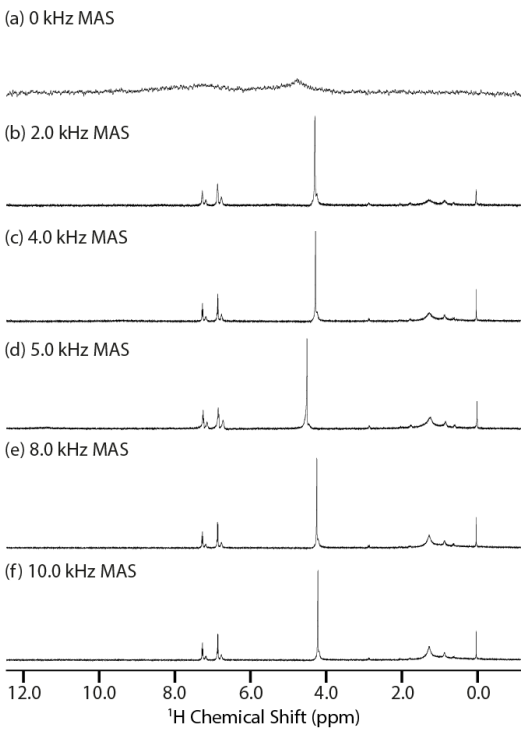

Figure 5.4. 500 MHz ^{1}H HR-MAS NMR spectra of aniline in the presence of HSS T3 stationary phase at 313 K and (a) 0.0, (b) 2.0, (c) 4.0, (d) 5.0, (e) 8.0 and (f) 10.0 kHz spinning frequency.

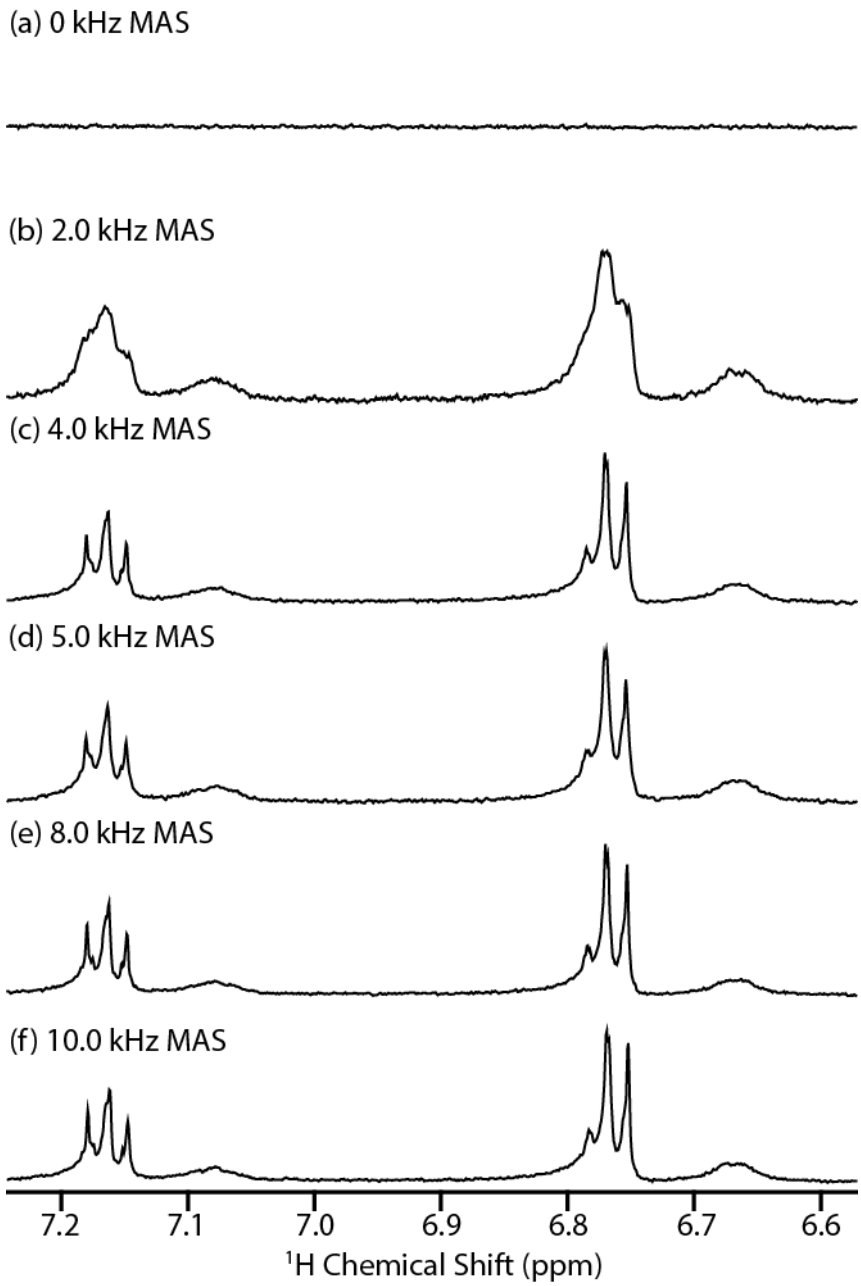

Figure 5.5. 500 MHz ^{1}H HR-MAS NMR spectra (aromatic protons) of aniline in the presence of HSS T3 stationary phase at 313 K and (a) 0.0, (b) 2.0, (c) 4.0, (d) 5.0, (e) 8.0 and (f) 10.0 kHz spinning frequency. Note: no signal is observed in the aromatic region of aniline at 0 kHz.

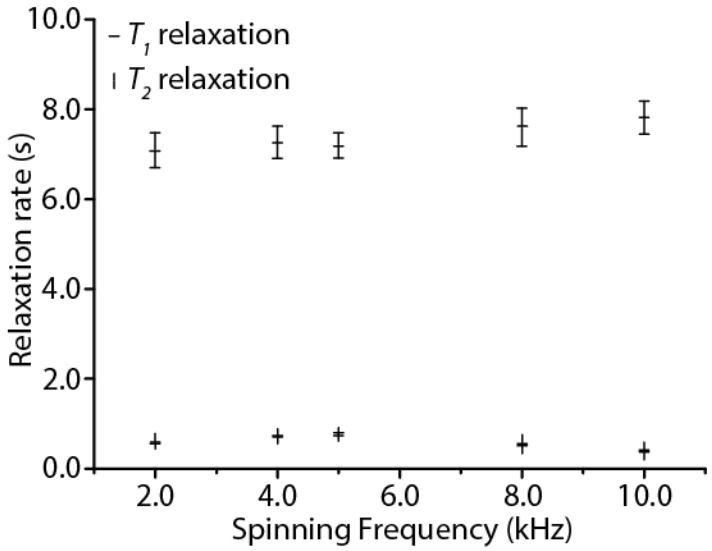

Figure 5.6. 500 MHz ^{1}H HR-MAS weighted average T_1 and T_2 relaxation of aniline in the presence of BEH-C18 against varied spinning frequency (kHz).

During the early stages of NMR method development, T_1 and T_2 relaxation measurements were acquired using a 2 kHz spinning frequency. However, when repeating the experiments, both T_1 and T_2 were significantly different when utilising the same packed rotor. This could be because the spinning frequency fluctuates at low spinning speed. MAS spinning stability is achieved at higher spinning rates. However, induced frictional heating can be introduced by employing high spinning frequencies [271]. Therefore, a 5-kHz spinning frequency with controlled temperatures using a variable temperature unit (VT-unit) was used throughout the study which enabled us to improve the robustness, repeatability and reproducibly of our NMR method as later demonstrated.

5.4.6 Temperature dependence on relaxation

The ^{1}H HR MAS NMR spectra of aniline in solution only and in the presence of RP-HPLC stationary phases were obtained at various temperatures. This was to determine the effect of temperature on the molecular motion of aniline in the presence of five RP-HPLC stationary phases.

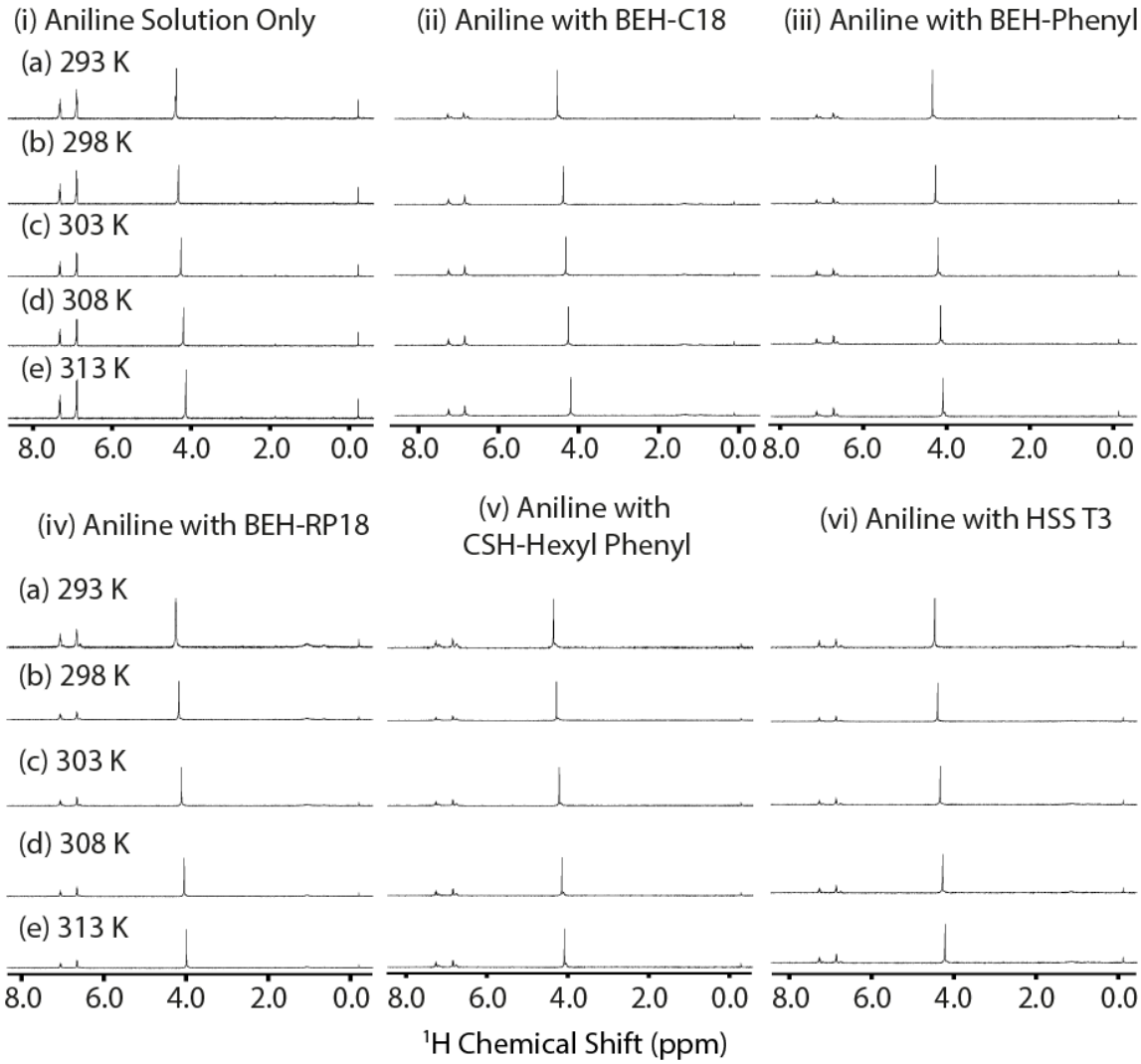

Figure 5.7. 1D ^{1}H HR-MAS NMR spectra of 0.5 M aniline in 50:50 % v/v of MeCN:D_2O mobile phase (i) in the absence of stationary phases (solution only) and in the presence of either (ii) BEH-C18, or (iii) BEH-phenyl, or (iv) BEH-RP18, or (v) CSH hexyl-phenyl or (vi) HSS T3 stationary phases with varied temperature of (a) 293, (b) 298, (c) 303, (d) 308 and (e) 313 K. All spectra were obtained at 500 MHz spectrometer with 5.0 kHz spinning frequency.

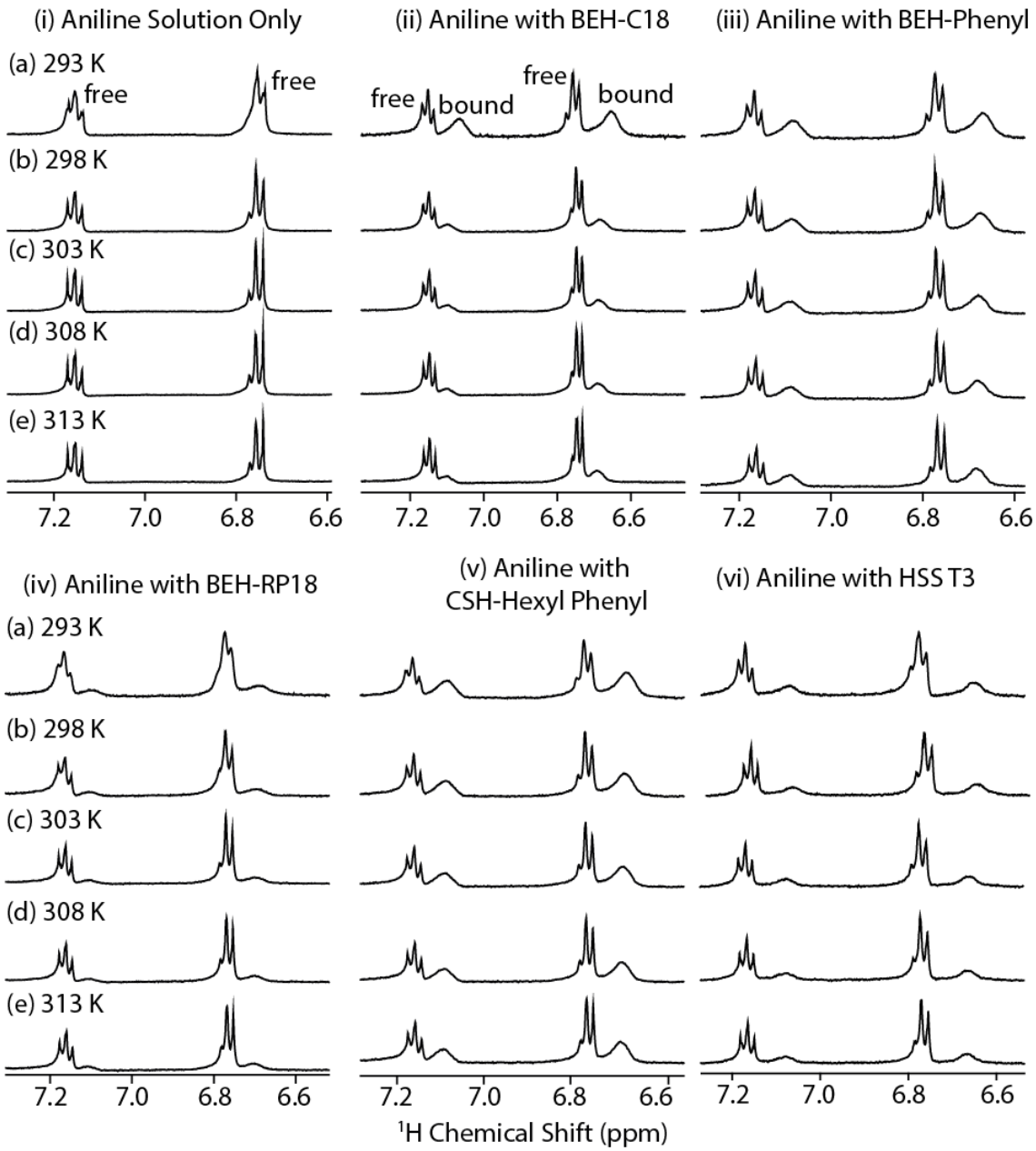

Figure 5.8. 1D ^{1}H HR-MAS NMR spectra of 0.5 M aniline (aromatic region) in 50:50 % v/v of MeCN:D_2O mobile phase (i) in the absence of stationary phases (solution only) and in the presence of either (ii) BEH-C18, or (iii) BEH-phenyl, or (iv) BEH-RP18, or (v) CSH hexyl-phenyl or (vi) HSS T3 stationary phases with varied temperature of (a) 293, (b) 298, (c) 303, (d) 308 and (e) 313 K. All spectra were obtained at 500 MHz spectrometer with 5.0 kHz spinning frequency.

The ^{1}H HR MAS NMR spectra of aniline in solution only and in presence of the five selected RP-HPLC stationary phases are shown in Figure 5.7 and 5.8. Both “free” (free

analyte in solution) and "bound" peaks (analyte bound to the stationary phase) of aniline in the presence of stationary phase were observed. The "free" peaks can be assigned as the free in solution fraction of aniline molecules and the "bound" peaks as aniline bound to the RP-HPLC stationary phases. This indicates aniline is going through a two-site slow chemical exchange. Similar ^{1}H HR MAS NMR spectra were previously published [95, 282]. The spectra of aniline across the 5 different temperatures show negligible differences. In some cases, the chemical shift difference between the 'free" and 'bound' peaks gradually reduced with an increase in temperature (see Figure 5.8). This could suggest aniline is gradually going from slow to intermediate exchange regime.

The spectra of aniline in solution only (50:50 MeCN:D_2O v/v) and in the presence of five different RP-HPLC stationary phases at 313 K is demonstrated in Figure 5.9. As shown in Figure 5.9, the "bound" peaks of aniline across the RP-HPLC stationary phases were dependent upon the stationary phase material used. For instance, the chemical shift difference between the "free" and "bound" peaks, "bound" peak intensities and "bound" peak width all varied across the stationary phases. This suggests, the chemical exchange rates of aniline in the presence of stationary phase is dependent on the RP-HPLC stationary phases (see Figure 5.9).

With an increase in temperature from 293 to 313 K, both the T_1 values of free and bound aromatic protons of aniline increases (*see Figure 5.10 and Table A.1 in appendix*). On the other hand, the T_2 values of free and bound aromatic protons of aniline slightly reduced with the increase in temperature (*see Figure 5.11 and Table A.1 in appendix*).

As illustrated in Figure 5.10, the T_1 relaxation value increases with an increase of temperature. It can be assumed, an increase in temperature reduces the correlation time and therefore increases the T_1 relaxation. However, this trend was not observed with the T_2 relaxation values as demonstrated in Figure 5.11. The primary reason for this observation is because T_2 relaxation is dependent on both molecular tumbling and chemical exchange. The rate of exchange increases with an increase in temperature, with the rate of increase dependent on the activation enthalpy, $\Delta H^{\dagger}$, for exchange [240]:

$$k_{ex} \propto e^{-\Delta H^{\dagger}/RT} \tag{5.2}$$

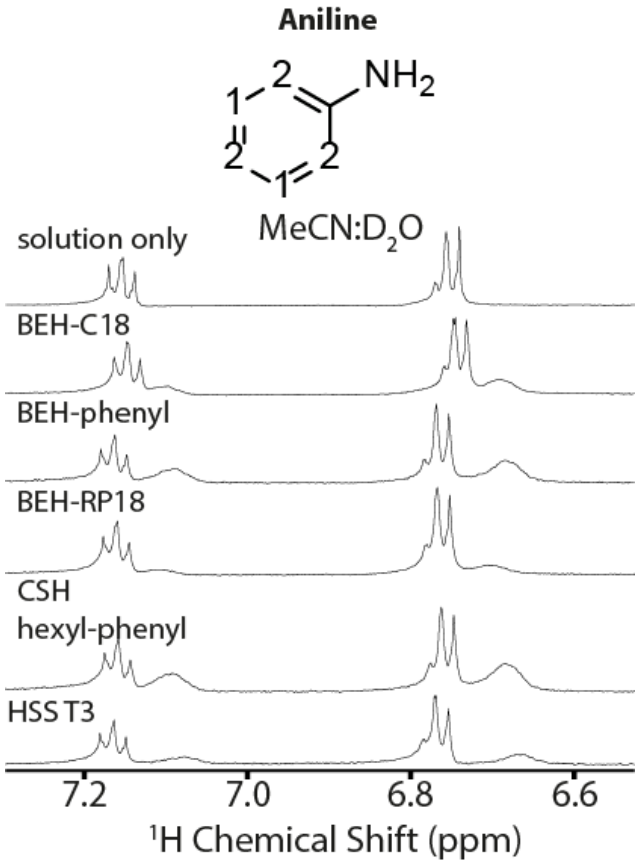

Figure 5.9. 1D ^{1}H HR-MAS NMR spectra of 0.5 M aniline (aromatic region) in 50:50 % v/v of MeCN:D_2O mobile phase (i) in the absence of stationary phases (solution only) and in the presence of either (ii) BEH-C18, or (iii) BEH-phenyl, or (iv) BEH-RP18, or (v) CSH hexyl-phenyl or (vi) HSS T3 stationary phases. All spectra were obtained at 500 MHz spectrometer at 313 K and 5.0 kHz spinning frequency.

As observed in Figure 5.8, the increase in temperature reduced the spacing between the "free" and "bound" peaks of aniline which implies the system is gradually transitioning from slow to intermediate exchange. Knowing the exchange rate is inversely proportional to T_2 relaxation [240], an increase in temperatures increases the exchange rate and therefore will reduce the observed T_2 relaxation values as shown in Figure 5.11. The bound aromatic proton T_1 and T_2 values of aniline were significantly smaller than the free aromatic protons which would indicate slow molecular motion taking place with an increase in temperature.

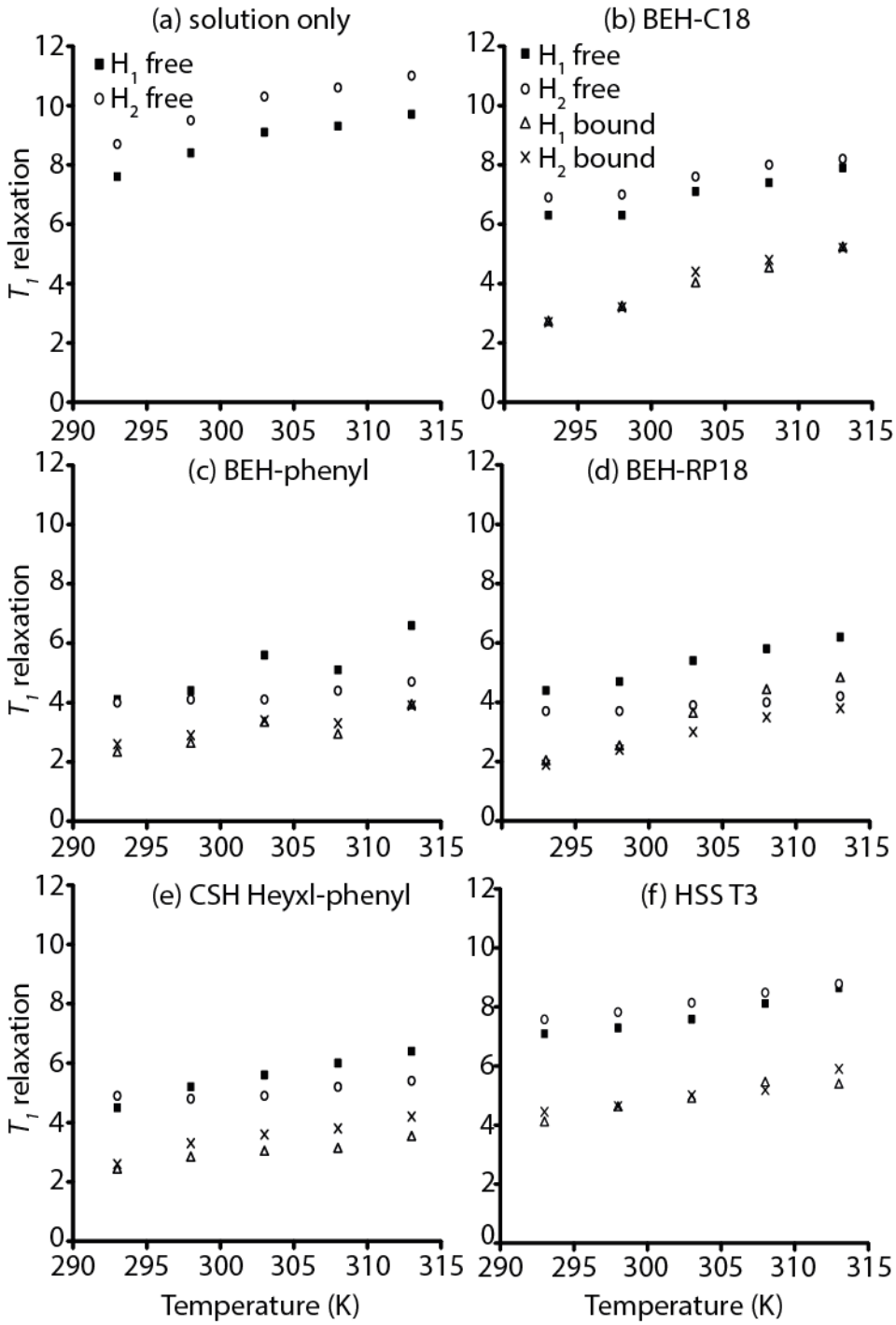

Figure 5.10. 500 MHz ^{1}H HR-MAS T_1 relaxation of aniline in (a) solution only, (b) BEH-C18, (c) BEH-phenyl, (d) BEH-RP18, (e) CSH hexyl-phenyl and (f) HSS T3 against varied temperatures of 293, 298, 303, 308 and 313 K. All spectra were obtained at 500 MHz spectrometer with 5.0 kHz spinning frequency.

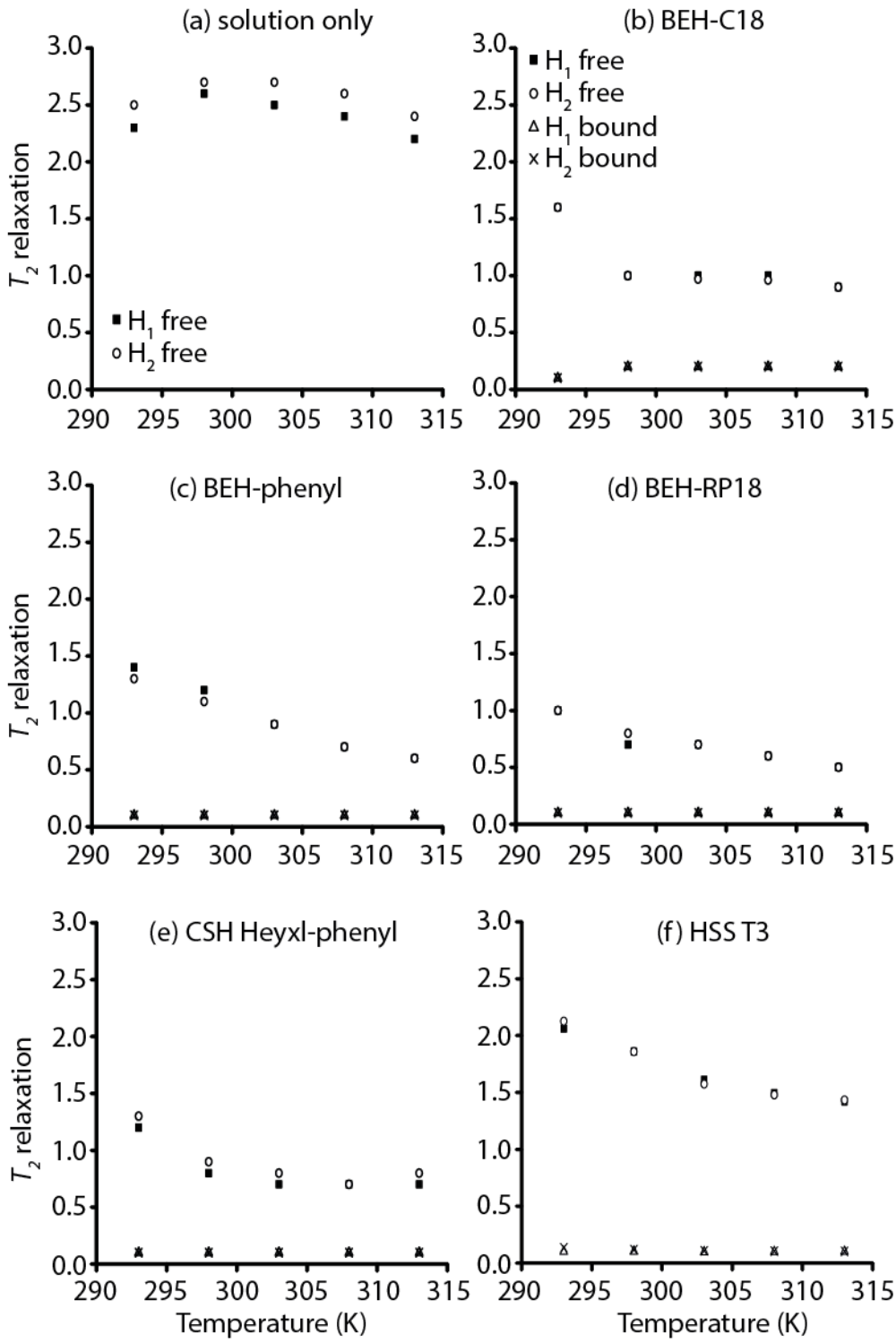

Figure 5.11. 500 MHz ^{1}H HR-MAS T_2 relaxation of aniline in (a) solution only, (b) BEH-C18, (c) BEH-phenyl, (d) BEH-RP18, (e) CSH hexyl-phenyl and (f) HSS T3 against varied temperatures of 293, 298, 303, 308 and 313 K.

5.4.7 Analyte concentration dependence on ^{1}H HR MAS NMR spectra

The next step of this study was determining the optimal analyte concentration to achieve the best signal to noise ratio of the ^{1}H HR MAS NMR spectrum of analytes free in solution and in the presence of RP-HPLC stationary phases. If the analyte concentration is relatively low, this will lead to poor peaks intensities and therefore low reproducibility of T_1 and T_2 measurements. On the other hand, if the analyte concentration is too high, this will lead to higher temperature gradients within the rotor and furthermore both probe tuning and shimming would be harder to achieve. In addition, higher concentrations of analytes also deviate more from the conditions under which HPLC experiments are undertaken.

The ^{1}H HR MAS NMR spectra of aniline at 0.25, 0.50 and 1.00 M concentrations was acquired to determine the dependence of analyte concentration on ^{1}H HR MAS NMR spectra as shown in Figure 5.12 and 5.13. To obtain comparable results, all three concentrations of aniline were run under identical experimental conditions (e.g. number of scans, delays, pulse powers etc.). The highest signal to noise ratio of aniline in solution only was obtained with a concentration of 1.00 M followed by 0.50 and 0.25 M. However, with added RP-HPLC stationary phase, both 1.00 M and 0.50 M concentrations showed similar peaks intensities for the “free” peaks while the “bound” peaks were more resolved and observable with the 0.5 M concentration. On the other hand, aniline with a concentration of 0.25 M showed very low intensity peaks. This would eventually lead to noisy and difficult to reproduce T_1 and T_2 relaxation exponential plots. Smaller peak intensity of the “bound” of aniline with a concentration of 1.0 M was observed compared to 0.25 and 0.5 M. Using the ^{1}H NMR integrals of aniline (unbound aromatic protons) and the CH_2 peaks of BEH-C18 stationary phase, the mole ratio of aniline to RP-HPLC stationary phases at 0.25, 0.5 and 1.0 M were approximately 1:0.51, 1:0.26 and 1:0.17 respectively. Although the amount of stationary phase packed in the NMR rotor was kept constant, the molar ratio of [aniline]/[stationary phases] gets larger with increasing [aniline]. Analyte concentration of 0.25 M led to irreproducible T_1 and T_2 relaxation plots. As a result, analyte concentration of 0.5 M was used during the rest of this study.

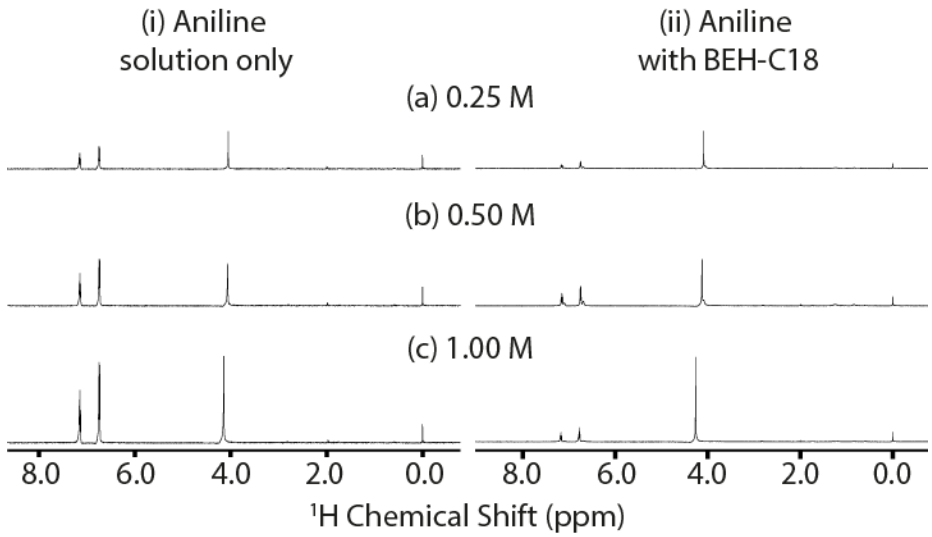

Figure 5.12. 1D ^{1}H HR-MAS NMR spectra of aniline in 50:50 % v/v of MeCN:D_2O mobile phase (i) in the absence of stationary phases (solution only) and in the presence of (ii) BEH-C18 with concentrations of (a) 0.25 M, (b) 0.50 M and (c) 1.00 M. All spectra were obtained at 500 MHz spectrometer at 313 K and 5.0 kHz spinning frequency.

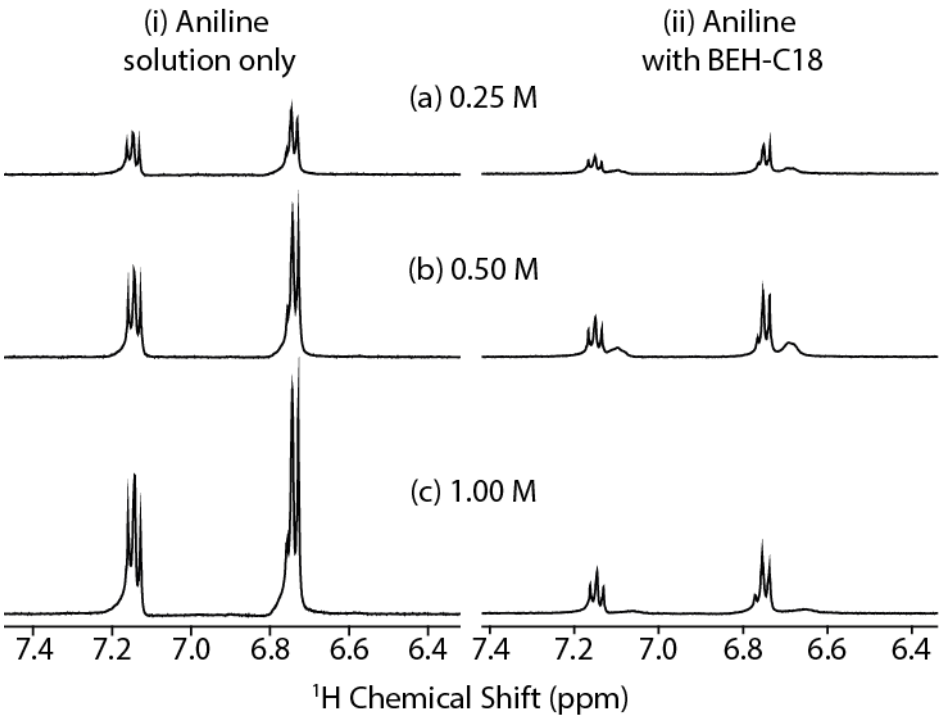

Figure 5.13. 1D ^{1}H HR-MAS NMR spectra of aniline (aromatic region) in 50:50 % v/v of MeCN:D_2O mobile phase (i) in the absence of stationary phases (solution only) and in the presence of (ii) BEH-C18 with concentrations of (a) 0.25 M, (b) 0.50 M and (c) 1.00 M. All spectra were obtained at 500 MHz spectrometer at 313 K and 5.0 kHz spinning frequency.

5.4.8 Dependence of ^{1}H spectra on mobile phase ratio

As a rule of thumb, a higher percentage of organic solvent will elute the analytes faster under similar RP-HPLC experimental conditions. Therefore, we obtained the ^{1}H HR MAS NMR spectra of toluene dissolved in MeCN:D_2O at 50:50, 70:30 and 90:10 (% v/v) as shown in Figure 5.14 and Figure 5.15. The mobile phase ratio was investigated using toluene to determine the effect of organic solvents on analyte with both aromatic and methyl protons.

The peak at 0 ppm corresponds to the DSS signal. Low intensity and broad peaks were observed at 0.8 and 1.25 ppm which corresponds to the CH_3 and CH_2 groups of BEH-C18 stationary phase. The CH_3 groups of toluene were observed at approximately 2.4 ppm. The water peaks were observed at 2.5, 3.7 and 4.2 ppm with 90:10, 70:30 and 50:50 MeCN:D_2O (% v/v) respectively. The peaks between 6.8 and 7.4 ppm correspond to the aromatic protons of toluene. The "bound" and "free" peaks of toluene are clearly assigned as demonstrated in Figure 5.15. Both the aromatic and methyl "bound" peaks of toluene with an increase of acetonitrile shifted closer to the "free" peaks. Additionally, the "bound" peaks signal intensity also reduced with an increase of acetonitrile as shown in Figure 5.15 which suggests toluene is transitioning from slow chemical exchange into intermediate-fast chemical exchange.

Using the ^{1}H NMR integrals of toluene (aromatic protons) and the CH_2 peaks of BEH-C18 stationary phase, the mole ratio of toluene to the RP-HPLC stationary phases with a mobile phase composition of 50:50, 70:30 and 90:10 MeCN:D_2O (% v/v) were approximately 1:0.55, 1:0.27 and 1:0.14 respectively. Even though the amount of stationary phase packed in the rotor was kept constant, the mole ratio of analyte to stationary phase reduced significantly with an increase of organic solvent which supplements why toluene is transition from slow to intermediate-fast exchange regime.

As a rule of thumb, increasing the organic solvent ratio in a mobile phase in RP-HPLC decreases the polarity of the mobile phase and as a result increases the retention time of the analytes [283, 284]. Therefore, the spectra of toluene in Figure 5.15 could suggest the exchange rate between toluene (aromatic and methyl protons) and BEH-C18 phase increases with higher organic solvent content. Thus, the mobile phases used in both NMR and RP-HPLC experiments were kept the same unless stated otherwise (e.g. MeCN:D_2O at 50:50 (% v/v) would be used in both techniques).

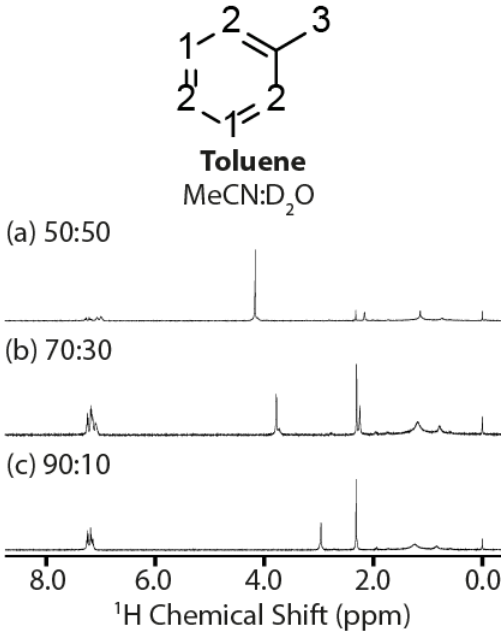

Figure 5.14. 1D ^{1}H HR-MAS NMR spectra of aniline in (a) 50:50, (b) 70:30 and (c) 90:10 % v/v of MeCN:D_2O mobile phase in the presence of BEH-C18 stationary phase. All spectra were obtained at 500 MHz spectrometer at 313 K and 5.0 kHz spinning frequency.

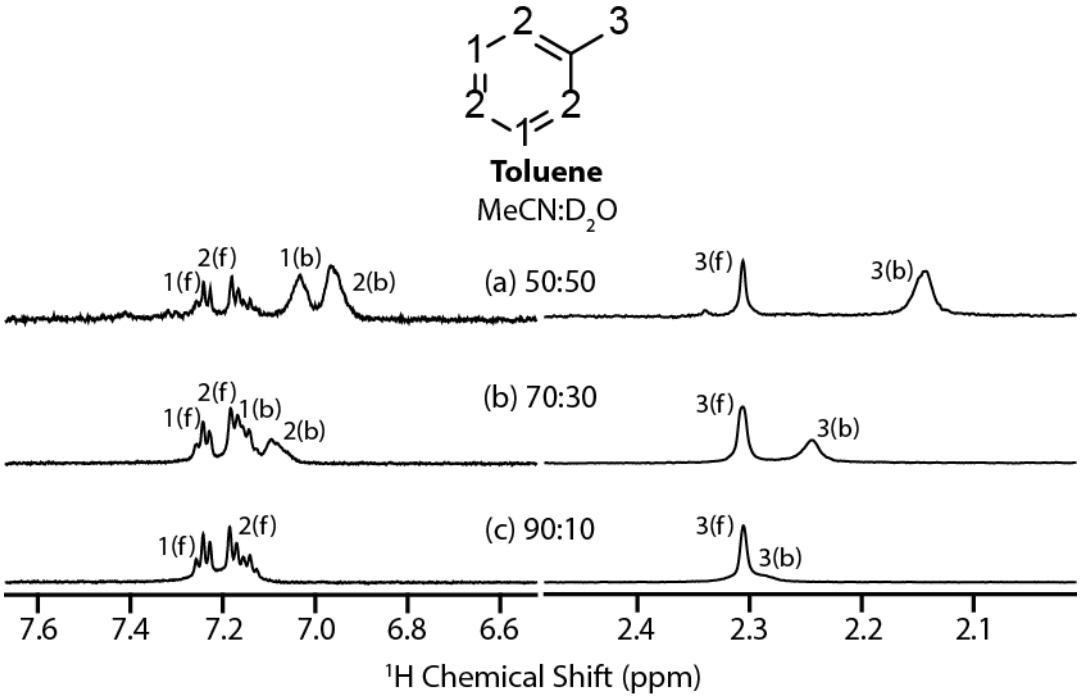

Figure 5.15. 1D ^{1}H HR-MAS NMR spectra of aniline (aromatic and methyl protons) in (a) 50:50, (b) 70:30 and (c) 90:10 % v/v of MeCN:D_2O mobile phase in the presence of BEH-C18 stationary phase. All spectra were obtained at 500 MHz spectrometer at 313 K and 5.0 kHz spinning frequency.

5.4.9 ^{1}H relaxation dependence on organic solvent

To determine the effect of organic solvent on the ^{1}H relaxation measurements, both T_1 and T_2 relaxation of aniline dissolved in 50:50 MeCN:D_2O and MeOH:D_2O were obtained. As illustrated in Figure 5.16 and 5.17, aniline is in slow exchange in both types of mobile phase. The difference between the two mobile phases as illustrated in Figure 5.16 , is the peak observed between 4 to 5 ppm which is due to the different organic solvent used. However, the different mobile phases influence the relaxation to different extent. For example, both the observed line widths and relaxation measurements (see Table A. 2 in the appendix) indicate large difference in of T_2 relaxation of aniline in the presence of stationary phases compared to solution only when dissolved in MeOH:D_2O. As illustrated in Figure 5.17, the "bound" peaks of aniline across the 5 RP-HPLC stationary phase were dependent on the stationary phase and mobile phase used. This suggests, the chemical exchange rates of aniline in the presence of stationary phase is dependent on both the organic solvent and RP-HPLC stationary phases. Therefore, it is important to use similar mobile phases in both NMR and RP-HPLC techniques.

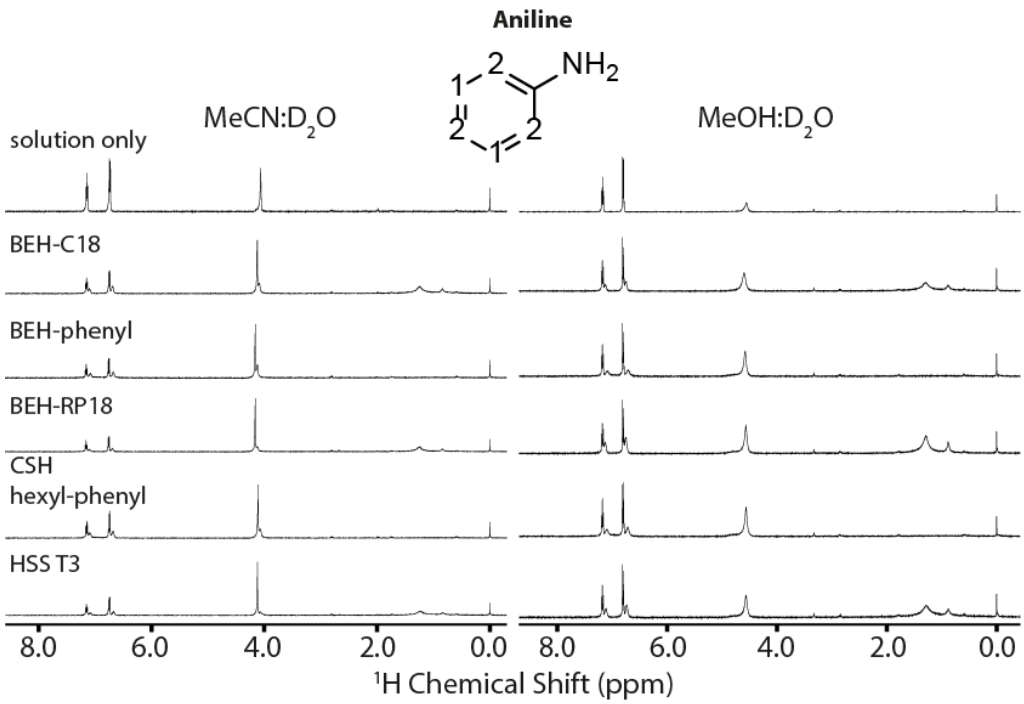

Figure 5.16. 1D ^{1}H HR-MAS NMR spectra of aniline in 50:50 % v/v of MeCN:D_2O (left) and MeOH:D_2O (right) mobile phase (from top to bottom): in the absence of stationary phases (solution only) and in the presence of either BEH-C18, or BEH-phenyl, or BEH-RP18, or CSH hexyl-phenyl or HSS T3 stationary phases as indicated on the left of each spectrum. All spectra were obtained at 500 MHz spectrometer at 313 K and 5.0 kHz spinning frequency.

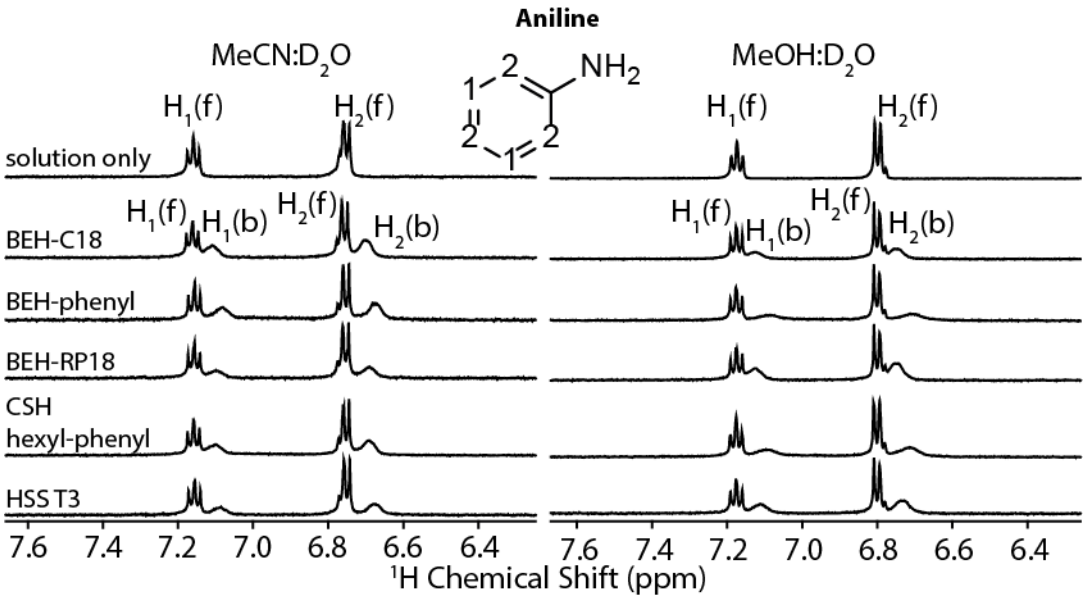

Figure 5.17. 1D ^{1}H HR-MAS NMR spectra of aniline (aromatic region) in 50:50 % v/v of MeCN:D_2O (left) and MeOH:D_2O (right) mobile phase (from top to bottom): in the absence of stationary phases (solution only) and in the presence of either BEH-C18, or BEH-phenyl, or BEH-RP18, or CSH hexyl-phenyl or HSS T3 stationary phases as indicated on the left of each spectrum. All spectra were obtained at 500 MHz spectrometer at 313 K and 5.0 kHz spinning frequency.

5.4.10 Buffer effect on ^{1}H relaxation

During our NMR method development, we used ammonium acetate buffer to control the pH of the mobile phase. The pH was adjusted accordingly using weak acid and bases to match the HPLC mobile phase pH. Due to the high analyte concentration (e.g. 0.5 M) used in the NMR experiments, the ammonium acetate buffer concentration was similarly high to be within its buffering capacity (e.g. 0.25 M). However, we discovered adjusting the pH led to few complications such as: (1) the pH dramatically affected the T_2 relaxation plots (e.g. bi exponential instead of mono exponential plots were observed) and (2) due to the high salt content of the buffer, probe power calibration and power optimisation were nearly impossible. These complications led to irreproducible and inconsistent data obtained. To overcome this issue, both NMR and HPLC measurements were obtained with non-buffered mobile phases.

5.4.11 Analysing mixtures

An alternative approach of stabilising the pH of the analytes, the relaxation measurements were obtained on two mixtures of several analytes. This would enable us to save both experimental time and run the analytes under specific pH conditions. Mixture 1 contained uracil, benzoic acid and aniline while mixture 2 was made up of 4 hydroxybenzoic acid, vanillic acid and syringic acid.

For instance, if mixture 1 dissolved 50:50 (% v/v) has a final pH of approximately 6.4, the HPLC mobile phase can be adjusted to approximately 6.4 to match that of mixture 1. This could potentially enable us to run experiments at various pH. On average, T_1 and T_2 relaxation measurements of an analyte in the presence of stationary phase can approximately take 1 hour 20 minutes. Running the samples as a mixture of 3 analytes saves approximately 2 hours 40 minutes in the presence of one stationary phase or 16 hours in solution only and in the presence of 5 stationary phases.

Well resolved ^{1}H HR MAS NMR spectra of each mixture in solution only and in the presence of BEH-C18, BEH-phenyl, BEH-RP18, CSH hexyl-phenyl and HSS T3 was obtained. All the analytes apart from aniline were going through fast chemical exchange. Aniline was undergoing slow chemical exchange, which suggests aniline is in close contact with the RP-HPLC stationary phases.

To understand the molecular tumbling and interaction of the mixtures in the presence of the stationary phase T_2 relaxation rates were also obtained. However, in some cases, the exponential decaying T_2 plots of the mixtures were not exponential but biexponential and multiexponential which suggests that multiple processes contribute to the observed relaxation rates. Additionally, in some cases the aromatic protons peaks of the analytes overlapped with one another.

Furthermore, some mixtures of analytes can potentially interact with one another which add further complications to the data analysis. Thus, analysing the analytes individually has proven easier to interpret with fewer complications encountered.

5.4.12 Dependence of ^{1}H spectra on analyte chemical and physical properties

The physical and chemical properties of each analyte was taken into consideration during the early phases of this project. Some analytes (e.g. beta estradiol and anthraquinone)

showed poor solubility in the HPLC mobile phases. The resulting dilute solutions led to poor ^{1}H spectra (*see Figure 5.18 and 5.19*) and make it challenging to obtain relaxation measurements of quality required for quantification. Therefore, it is crucial to consider both the chemical and physical properties of the compounds when selecting the series of analytes to be investigated further in this study.

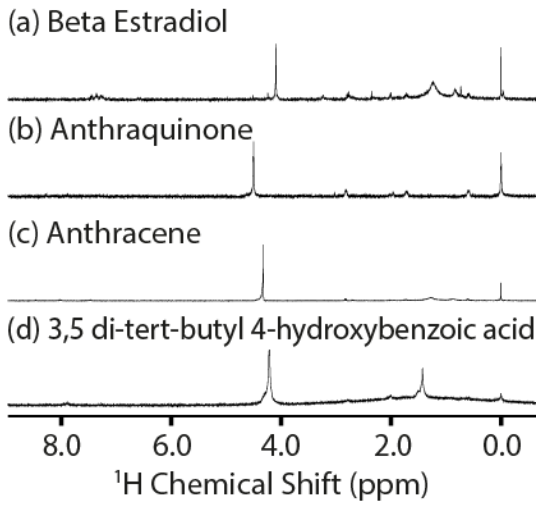

Figure 5.18. 1D ^{1}H HR-MAS NMR spectrum of (a) beta estradiol, (b) anthraquinone, (c) anthracene and (d) 3,5 di-tert-butyl 4-hydroxybenzoic acid in 50:50 % v/v of MeCN:D_2O All spectra were obtained at 500 MHz spectrometer at 313 K and 5.0 kHz spinning frequency.

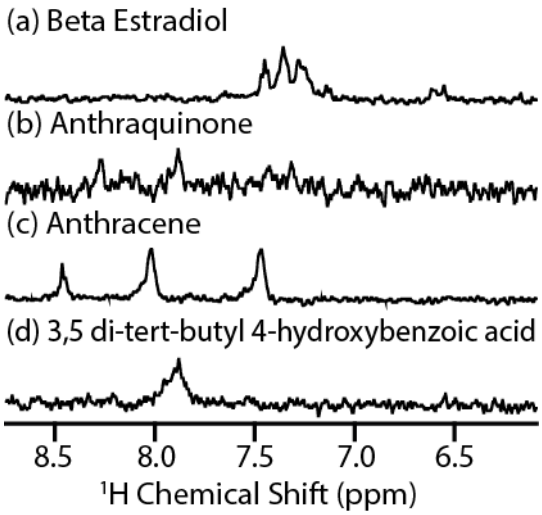

Figure 5.19. 1D ^{1}H HR-MAS NMR spectrum (aromatic protons) of (a) beta estradiol, (b) anthraquinone, (c) anthracene and (d) 3,5 di-tert-butyl 4-hydroxybenzoic acid in 50:50 % v/v of MeCN:D_2O All spectra were obtained at 500 MHz spectrometer at 313 K and 5.0 kHz spinning frequency.

5.4.13 DSS

DSS (4,4-dimethyl-4-silapentane-1-sulfonic acid) is used as a referencing compound in a wide range of ^{1}H NMR spectroscopy experiments [285-287]. During this study, we also used the DSS peak for shimming purposes to obtain the highest peak intensities. Three different DSS concentrations were used to determine the effect of DSS on ^{1}H HR MAS NMR spectra.

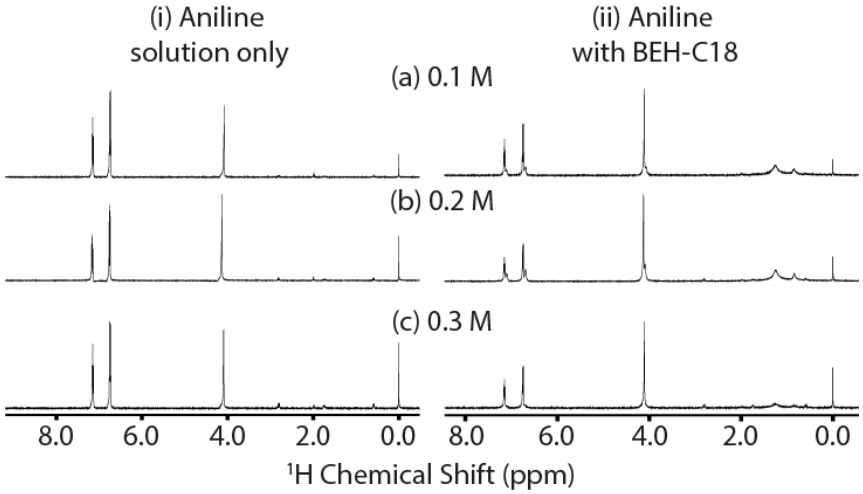

Figure 5.20. 1D ^{1}H HR-MAS NMR spectra of aniline in 50:50 % v/v of MeCN:D_2O mobile phase (i) in the absence of stationary phases (solution only) and in the presence of (ii) BEH-C18 with DSS concentrations of (a) 0.1 M, (b) 0.2 M and (c) 0.3 M. All spectra were obtained at 500 MHz spectrometer at 313 K and 5.0 kHz spinning frequency.

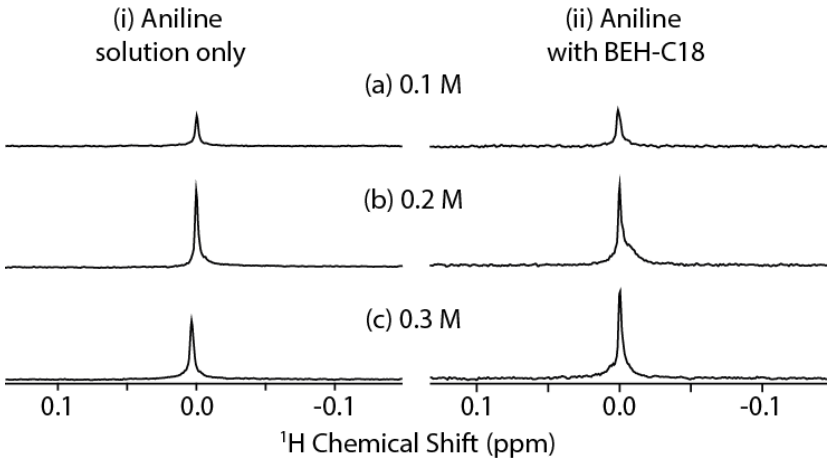

Figure 5.21. 1D ^{1}H HR-MAS NMR spectra of aniline in 50:50 % v/v of MeCN:D_2O mobile phase (i) in the absence of stationary phases (solution only) and in the presence of (ii) BEH-C18 (zoomed on the DSS ^{1}H peak) with DSS concentrations of (a) 0.1 M, (b) 0.2 M and (c) 0.3 M. All spectra were obtained at 500 MHz spectrometer at 313 K and 5.0 kHz spinning frequency.

The spectra of aniline in solution only and in the presence of BEH-C18 at various concentrations is shown in Figure 5.20. The singlet peak of DSS at different concentration is shown in Figure 5.21. The lowest peak intensity was observed with a concentration of 0.1 M. Low peak intensity make it harder to shim the probe as efficiently as possible. Conversely, both DSS at 0.2 and 0.3 M showed higher peaks intensities with little or no significant difference. As a result, DSS concentration of 0.2 M was used during the rest of this study. Additionally, Figure 5.21 suggests the DSS peaks does not bind onto the stationary phase as it is not in the slow exchange regime in comparison to aniline illustrated in Figure 5.22. As illustrated in Figure 5.22, DSS at 0.3 M altered the chemical exchange regime of aniline in the presence of BEH-C18. This could suggest, DSS at 0.3 M concentrations interferes with the analyte to stationary phase interactions. The peak intensity of DSS is relatively low and therefore, reliable and accurate T_1 and T_2 relaxation measurements of DSS were not obtainable.

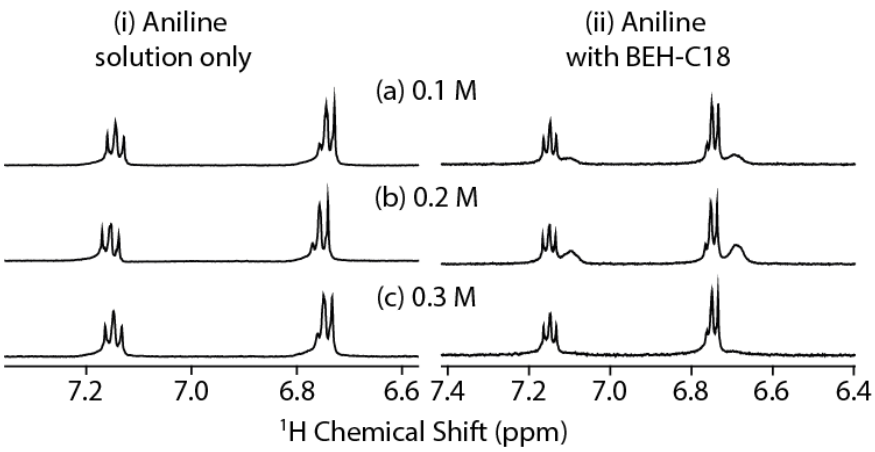

Figure 5.22. 1D ^{1}H HR-MAS NMR spectra (aromatic region) of aniline in 50:50 % v/v of MeCN:D_2O mobile phase (i) in the absence of stationary phases (solution only) and in the presence of (ii) BEH-C18 with DSS concentrations of (a) 0.1 M, (b) 0.2 M and (c) 0.3 M. All spectra were obtained at 500 MHz spectrometer at 313 K and 5.0 kHz spinning frequency.

5.4.14 Statistical analysis

Once the ^{1}H HR MAS NMR relaxation method was finalised, the robustness and repeatability of the developed method was determined. To establish the reliability and reproducibility of the method, both T_1 and T_2 measurements were obtained on the same sample. A two-way paired sample t-test was used to analyse the repeated sample measurements. This paired sample t-test will indicate the method robustness and repeatability. The null and alternative hypotheses are as follows:

- H_o (null) = the mean relaxation values of aniline (with BEH-C18) at different time of the day are both equal.
- H_i (alternative) = the mean relaxation of aniline (with BEH-C18) at different times are greater or lower than one another.

The measurements discussed in this section are of aniline in the presence of BEH-C18 stationary phase. The statistical results are shown in Table 5.2. The p value of the paired sample t-test for both T_1 and T_2 were well above 0.05 (0.45 and 0.25 respectively) which indicates this method has a good repeatability and reproducibility.

Table 5.2. Statistical summary (T_1 and T_2 relaxation) of aniline in the presence of BEH-C18 measured on different times of the day. Where mean: average of the relaxation values, SD: the standard deviation, SEM: standard error of the mean and P Value: the paired t-test score. The SD and SEM was calculated from the aromatic protons of aniline

Relaxation	Sample	Mean	SD	SEM	P value
T_1	1	5.19	1.58	0.79	0.45
	2	5.20	1.48	0.74	
T_2	1	1.67	0.10	0.05	0.25
	2	1.74	0.24	0.12	

To further understand the effect of sample preparation on the method, 2 sets of T_1 and T_2 measurements of aniline in the presence of BEH-C18 stationary phase were obtained. The first set includes 3 measurements obtained on the same packed sample (set 1) while the other was made up of 3 different prepared samples (set 2). A linear regression model can be used to determine the standard error within the measurements:

$$y_i = \beta_1 X_i + \beta_0 + \varepsilon_i \rightarrow lm(measure \sim proton) \tag{5.1}$$

Where y_i is the dependent variable, $\beta_1 X_i$ is the linear component, β_0 is the y intercept, ε_i is the error term, $measure$ represent the individual relaxation measurements and $proton$ the specific assigned proton of aniline in the presence of BEH-C18. The standard error (S) of each set of relaxation measurement can be calculated by using the following equation:

$$S^2 = \frac{1}{8}\sum_{i=1}^{r=4}\sum_{j=1}^{c=3}(y_{ij} - \bar{y}_i)^2 \tag{5.2}$$

A hypothesis test can be used to determine the effect of sample preparation on the robustness and repeatability of the method where the null and alternative hypotheses are as follows (at a 95% level of confidence):

- H_o (null) = the standard error of the two sets of measurements are equal.
- H_i (alternative) = the standard error of the two set of measurements are greater or lower than one another.

This hypothesis can be mathematically expressed as:

$$Proportion\ of\ variation = \frac{\sigma_1^2(set\ 1)}{\sigma_1^2 + \sigma_2^2(set\ 2)} \tag{5.3}$$

where set 1 measurements are primarily dependent on method errors (σ_1^2) while set 2 measurements are dependent on both the method and sample preparation errors ($\sigma_1^2 + \sigma_2^2$). Table 5.3 illustrates the summary of each model obtained. Each model was generated via Rstudio 3.3.3 (see console statistical script 1 in appendix). As illustrated in Table 5.3, there is a significant difference between the standard error of both T_1 and T_2 relaxation measurements of aniline in the presence of BEH-C18 of the repeated packed sample and separately prepared sample. However, since both proportion of variation of T_1 and T_2 were approximately 0.35 and 0.06, we fail to reject the alternative hypothesis. This indicates that sample preparation affects the reproducibility and robustness of the data obtained. However, we must consider the relaxation measurements could potentially be different due to nature of random molecular motion.

Table 5.3. Standard errors of aniline (T_1 and T_2 relaxation) in the presence of BEH-C18 stationary phase.

Relaxation	Sample	Number of measurements	Standard error	Proportion of variance
T_1	Same packed sample	3	0.07	0.35
	Different packed sample	3	0.20	
T_2	Same packed sample	3	0.02	0.06
	Different packed sample	3	0.32	

5.5 Conclusion

The results presented in this study demonstrated that ^{1}H HR MAS NMR spectra, T_1 and T_2 relaxation measurements are dependent on a series of experimental parameters and conditions. Randomly selecting each experimental parameter can lead to several errors in the NMR relaxation measurements. Such errors can be avoided by a systematic method development and optimisation of several experimental parameters as proved in this study. More importantly, the physico-chemical properties of each analyte must be taken into consideration under these experimental conditions. The statistical analysis used in this study confirms that both our method and sample preparation has a good repeatability and reproducibility. It was determined that sample preparation influences the method repeatability but not significantly enough to affect the developed NMR method robustness and reproducibility.

Furthermore, this developed and optimised NMR relaxation method will be used to probe the molecular tumbling of a library of 15 analytes, 2 mobile phases and 5 RP-HPLC stationary phases which is discussed in Chapter 8.

6 STRUCTURAL CHARACTERISATION OF ALIPHATIC CHAIN AND PHENYL BONDED SILICA RP HPLC STATIONARY PHASES

6.1 Abstract

The surface morphology and chemical makeup of BEH-C18, BEH-Phenyl, BEH-RP18, CSH Phenyl-Hexyl and HSS T3 were investigated using atomic force microscopy (AFM), Raman and NMR spectroscopy. AFM was used to determine the surface topography and morphology of the stationary phases. Raman spectroscopy was utilised to characterise the different bonds present across the investigated reversed phase HPLC (RP-HPLC) stationary phases. ^{1}H magic angle spinning (MAS) NMR, ^{13}C and ^{29}Si cross polarisation magic angle spinning (CP/MAS) NMR were also used to characterise the molecular structures of the RP-HPLC stationary phases.

Keywords: surface morphology, structural characteristics, atomic force microscopy, topography, Raman spectroscopy, RP-HPLC stationary phases, ^{1}H HR-MAS NMR, ^{13}C and ^{29}Si CP/MAS NMR.

6.2 Introduction

Over the years, a vast number of chromatographic stationary phases have been developed to increase the range of compounds applicable across a variety of industrial sectors. Furthermore, several improvements have been achieved to increase the robustness and efficiency of stationary phases. The improvement of stationary phase chemistries (e.g. trifunctional or sterically hindered monofunctional silanes) [288-290] has proven successful for improving the column chemical stability at low and high pH. However, the silica supporting material is equally important for separation selectivity. Thus, several innovations have occurred over the years of the silica supporting material in RP-HPLC.

In 2005, Waters released new RP-HPLC columns known as ACQUITY UPLC™ BEH (ethylene-bridged hybrid) technology columns. BEH Technology ™ allowed for an increase in the pH range of experimental conditions whilst offering potential for improved peak symmetry, temperature stability, and column efficiency [291]. The BEH linkage was achieved by embedding bridged ethane in the silica matrix. Furthermore, numerous functionalities in BEH technology columns were manufactured by Waters to extend the selectivity range of different compounds (see Figure 6.1).

For instance, Xbridge™ C18 with chemical stability over a large range of pH (1-12) has a wider range of analyte selectivity. Xbridge™ Phenyl is known a very stable phenyl embedded phase. In contrast, Xbridge™ Shield RP18 has an embedded polar carbamate group which has the ability of retaining phenolic compounds and improving peak shapes of basic analytes [292-299].

Both Xbridge™ C18 and Phenyl phases have embedded trifunctional silanes while a patented monofunctional silane is embedded into the Xbridge™ RP18 [292] (see Figure 6.1). All the stationary phases mentioned are manufactured via a proprietary endcapping method for achieving excellent peak shapes for basic compounds and optimal pH stability.

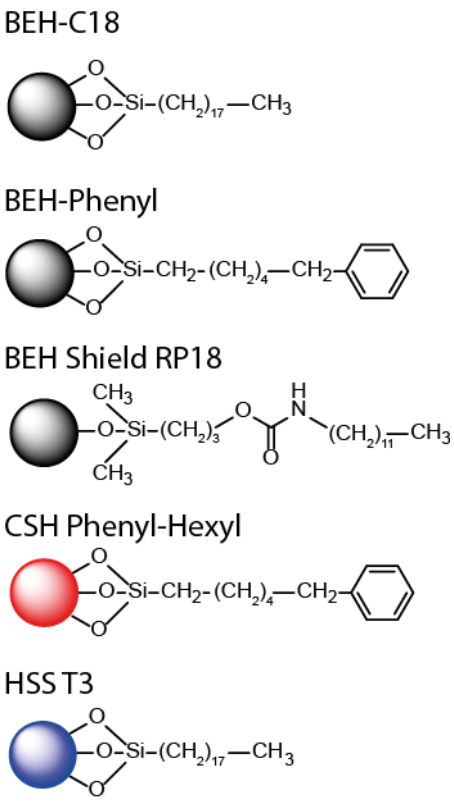

Figure 6.1. Molecular structures of BEH-C18, BEH-Phenyl, BEH shield RP18, CSH Phenyl-Hexyl and HSS T3. The circles represent the silica particles.

Yet, one of the main challenges encountered in RP-HPLC was the ability to obtain excellent efficiency, reproducibility and selectivity. This challenge was solved by the invention of a charged surface hybrid (CSH) column particle [300]. Depending on the mobile phase, the surface charge of the CSH particle varies. For instance, the use of acidic mobile phases leads to a low-level positive surface charge while basic mobile phases ionise the silanol groups which leads to a negative surface charge. This surface charge characteristic of the CSH particle is essential for its selectivity power. More importantly, the surface charge material has a major impact on ionised analytes [301-303]. The bonded ligand groups of the ACQUITY UPLC® CSH particles were carefully selected by Waters to achieve optimal peak shapes, selectivity, pH stability and efficiency. The CSH Phenyl-Hexyl RP-HPLC phases have built-in trifunctional bonding chemistries and end capped via a proprietary process to achieve optimal chemical stability and peak shapes.

Furthermore, a high-strength silica (HSS) particle was developed to improve the stability and lifetime of the stationary phases. Additionally, propriety T3-bonding is attached to the silica particle for enhanced selectivity. This T3 bonding uses a trifunctional C18 alkyl phase which enables superb performance, peak shape and longer retention for polar

compounds. Depending on the system used, different particle sizes are commercially available for each stationary phase shown in Figure 6.1. Typically, 5 and 3.5 μm particle sizes are used for high performance liquid chromatography (HPLC) systems and 1.7 μm particle sizes are used ultra-performance liquid chromatography (UPLC) [304, 305]. Even though several stationary phases are commercially available, BEH-C18, BEH-Phenyl, BEH-RP18, CSH Phenyl-Hexyl and HSS T3 stationary phases were carefully selected based on the orthogonal selectivity offered for the analytes selectivity we were investigating throughout this study and the robustness of the phases with time.

Several spectroscopy methods have previously been reported to characterise the molecular arrangement of many RP-HPLC phases. For instance, atomic force microscopy (AFM) [306, 307] for mapping the surface morphology of the phases and Raman spectroscopy[308] for identify different bonds present in various RP-HPLC stationary phases. Furthermore, ^{1}H HR-MAS, ^{13}C and ^{29}Si CP/MAS NMR [71, 309-314] have been successful over the years for understanding the molecular arrangements and dynamic motion of several stationary phases at an atomic level.

In this study, AFM, Raman and solid-state NMR spectroscopy methods are utilised to determine the atomic scale structural and morphology characteristics of BEH-C18, BEH-Phenyl, BEH-RP18, CSH Phenyl-Hexyl and HSS T3 stationary phases used throughout this study. The latter three phases mentioned have not yet been investigated using these methods at the time of writing this study.

6.3 Experimental:

6.3.1 Samples

Each of the RP-HPLC stationary phase materials are commercially available and were ordered from Waters Corporation Ltd. (Hertfordshire, UK). The RP-HPLC columns were emptied to acquire the stationary phases packing materials. The physical and chemical properties of each stationary phase are shown in Table 6.1. Each property was previously discussed in Chapter 2.

Table 6.1. Physical and chemical properties of commercially available RP-HPLC stationary phases.

	C18	*Phenyl*	*Shield RP_{18}*	*Phenyl-Hexyl*	*HSS T3*
Particle Shape	Spherical	Spherical	Spherical	Spherical	Spherical
Ligand Density µmol/m²	3.1	3.0	3.3	2.3	1.6
Particle Size (µm)	1.7	1.7	1.7	1.7	1.7
Pore Size (Å)	130	130	130	130	100
Surface Area (m^2/g)	185	185	185	185	230
Pore Volume (cc/g)	0.7	0.7	0.7	0.7	0.7
% Carbon Load	18	15	17	14	11
End Capped	Yes	Yes	Yes	Yes	Yes

6.3.2 Atomic force microscopy method

AFM images of BEH-C18, BEH-Phenyl, BEH-RP18, CSH Phenyl-Hexyl and HSS T3 topography were recorded in air, using Bioscope Catalyst microscope with a Nanoscope V controller (Veeco). Images were acquired in tapping mode using silicon-tips on a nitride lever with a spring constant of 0.35 Nm^{-1} according to manufacturer (SNL-10, Bruker).

6.3.3 Raman spectroscopy method

The Raman spectra of the 5 stationary phases were obtained using a Renishaw inVia reflex Raman microscope with a 532-nm laser attached to a CCD detector. Only 10% (1.4 mW) of the optimum laser power was used in these experiments. An exposure time of 10 seconds and 2 accumulations was used. A small amount of each stationary phase was used to obtain the Raman spectra. The Raman spectra were recorded on different spots of each stationary phase for reproducibility and repeatability. All spectra obtained were baseline corrected and extracted using inVia WIRE software.

6.3.4 Solid State NMR method

The NMR experiments were carried out using a 500 MHz Bruker Avance III with a magnetic field of 11.75 T. A 4 mm triple resonance MAS probe was used. The stationary phases were packed into individual 4 mm ZrO_2 rotors. A spinning frequency of 10 kHz was used across all the solid-state MAS NMR experiments. All spectra were obtained at 298 K. The ^{1}H HR-MAS NMR spectra were recorded using a single pulse experiment with a 25-kHz nutation frequency and 2 seconds recycling delay. The ^{13}C CP/MAS NMR spectra were obtained using a proton 90° pulse length of 2.5 µs with a contact time and recycling delay of 0.7 ms and 2 seconds, respectively.

The ^{29}Si CP/MAS NMR spectra were recorded using a proton 90° pulse length of 2.5 µs with a contact time and recycling delay of 8.0 ms and 5 seconds, respectively. The ^{1}H, ^{13}C and ^{29}Si NMR spectra were externally referenced and shimmed to DSS, alanine and kaolinite (relative to TMS) respectively. Furthermore, the three mentioned references were used for pulse optimization and calibration. These referencing compounds were used as they provide good signal to noise ratio, easy to handle and are primarily used in Warwick University NMR group.

6.4 Results and Discussion

6.4.1 Atomic force microscopy

The morphology and topography of the stationary phase surface was investigated by AFM. The atomic force micrographs of the RP-HPLC five stationary phases studied are illustrated in Figure 6.2 and 6.3. The images were obtained on 2 different scan sizes. The largest scale images (5µm x 5µm and 3.1 x 5µm), represented in Figure 6.2, confirm that four of the column materials are spherical in shape. Note importantly, that AFM at this scale was not performed on HSS T3 stationary phase, though, Raman spectroscopy images were used to confirm its spherical shape characteristics (*see Figure A.3 and A.4 in appendix*). The range of particle sizes across the 4 stationary phases as illustrated in Figure 6.2 were expected. As previously established, the particle size cannot be defined as a single value but as a distribution of the particles over a range of sizes [170]. The particle size of HPLC packing material is usually the mean value of all particle diameters [315-317].

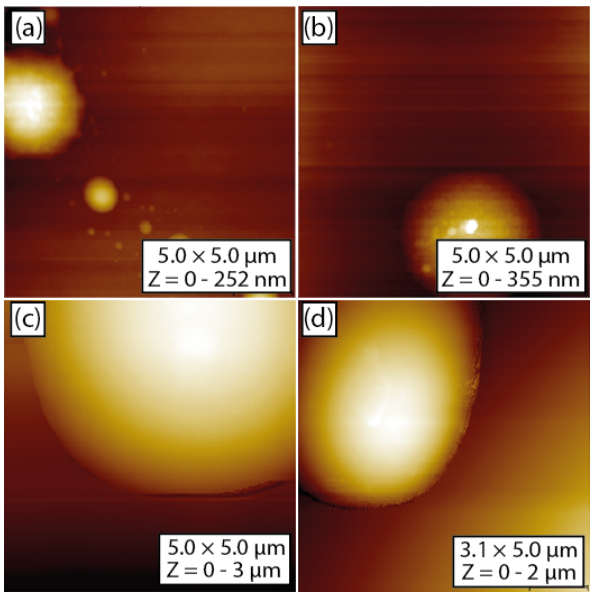

Figure 6.2. AFM images of four RP-HPLC stationary phases: (a) BEH-C18, (b) BEH-Phenyl, (c) BEH-RP18 and (d) CSH Phenyl-Hexyl. Each scanning size and depth (z-range) is indicated on each corresponding image.

However, the smaller scaled images (1µm x 1µm and 0.5 µm x 0.5µm) enable us to gain morphological and topographical information about the column particles as shown in Figure 6.3. The results indicate pores within the particles.

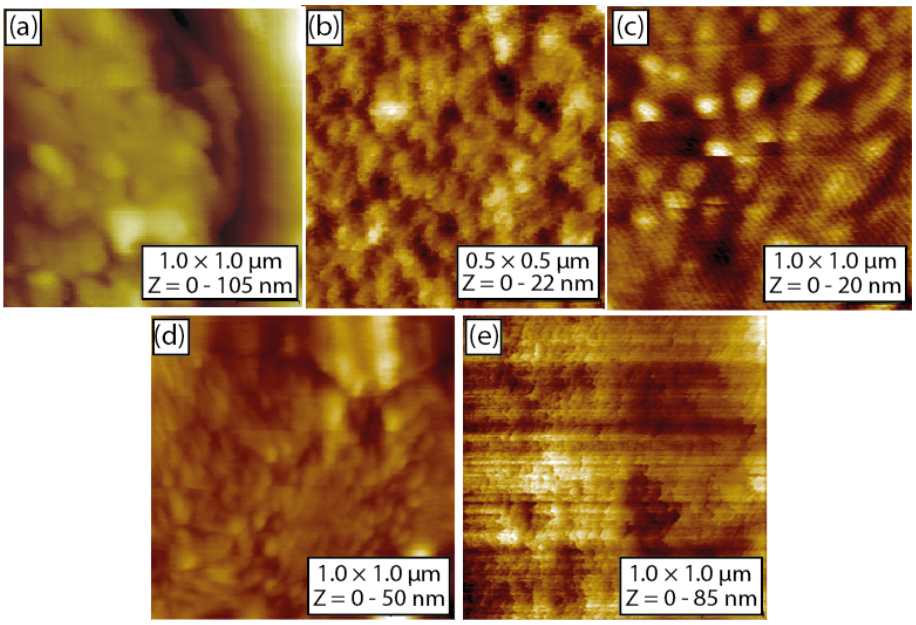

Figure 6.3. AFM images of five RP-HPLC stationary phases: (a) BEH-C18, (b) BEH-Phenyl, (c) BEH-RP18, (d) CSH Phenyl-Hexyl and (e) HSS T3. Each scanning sizes and depth (z-range) is indicated on each corresponding image. The z-axis scale of each image indicates the depth of individual pores in the scanned area of each stationary phase.

Furthermore, the analytes are mainly retained in the particle internal pores rather than on the particle surface. Theses pores form approximately 99% of the total surface area of the particle [104]. AFM images show that BEH-C18 and HSS T3 surfaces have the most heterogeneous topography, ranging from 105 to 85 nm respectively.

6.4.2 Raman spectroscopy

Raman spectroscopy was used to determine the characteristics of the bonds and ligands presents in the 5 RP-HPLC stationary phases. The non-subtracted Raman spectra of the five investigated stationary phases were obtained as illustrated in Figure 6.4 and 6.5 for the C-C stretching and C-H bending regions (low wavenumber region) and C-H stretching region (high wavenumber region) respectively. The spectrum obtained of BEH-C18 indicated that peaks present at ~1200 and ~1400 cm^{-1} are due to the methylene twisting ($_T(CH_2)$) and methyl asymmetric bending and methylene scissoring (δ_a (CH_3) and δ_{sci} (CH_2)) respectively. Similar peaks were also observed with HSS T_3 but with lower signal intensities.

However, significantly different well-resolved peaks were observed with BEH-Phenyl stationary phase. In the low wavenumber region, several peaks were observed at 1000, 1200, 1350 and 1560 cm^{-1} which was due to the in-phase ring stretching 'breathing' (ν(C-C)$_{breath}$), aryl-methine stretching (δ_S(C-C)$_{quad}$), methyl symmetric bending (δ_s (CH_3)), carbon-carbon asymmetric and symmetric 'quadrant' ring stretching (ν_a(C-C)$_{quad}$ and ν_s(C-C)$_{quad}$) of the mono-substituted Phenyl rings were respectively observed.

Similar results and band notations were previously reported by Doyle *et al.* [318]. Both BEH-RP18 and CSH Phenyl-Hexyl show little or no peaks present in the low wavenumber region. In the high wavenumber region, a major band was observed across all five stationary phases as shown in Figure 6.5. This high intensity band at approximately 2890 cm^{-1} is due to the methylene asymmetric stretching ($\nu_a(CH_2)$) and symmetric stretching of the methyl groups [318-320] ($\nu_s(CH_3)$). The low intensity bands at around 2724 cm^{-1} are due to methylene twisting [321] ($_T(CH_2)_{T.G}$). A low intensity band at around 3060 cm^{-1} was observed in the presence of both BEH-Phenyl and CSH Phenyl-Hexyl which exhibit aryl ring C-H stretching[318, 319].

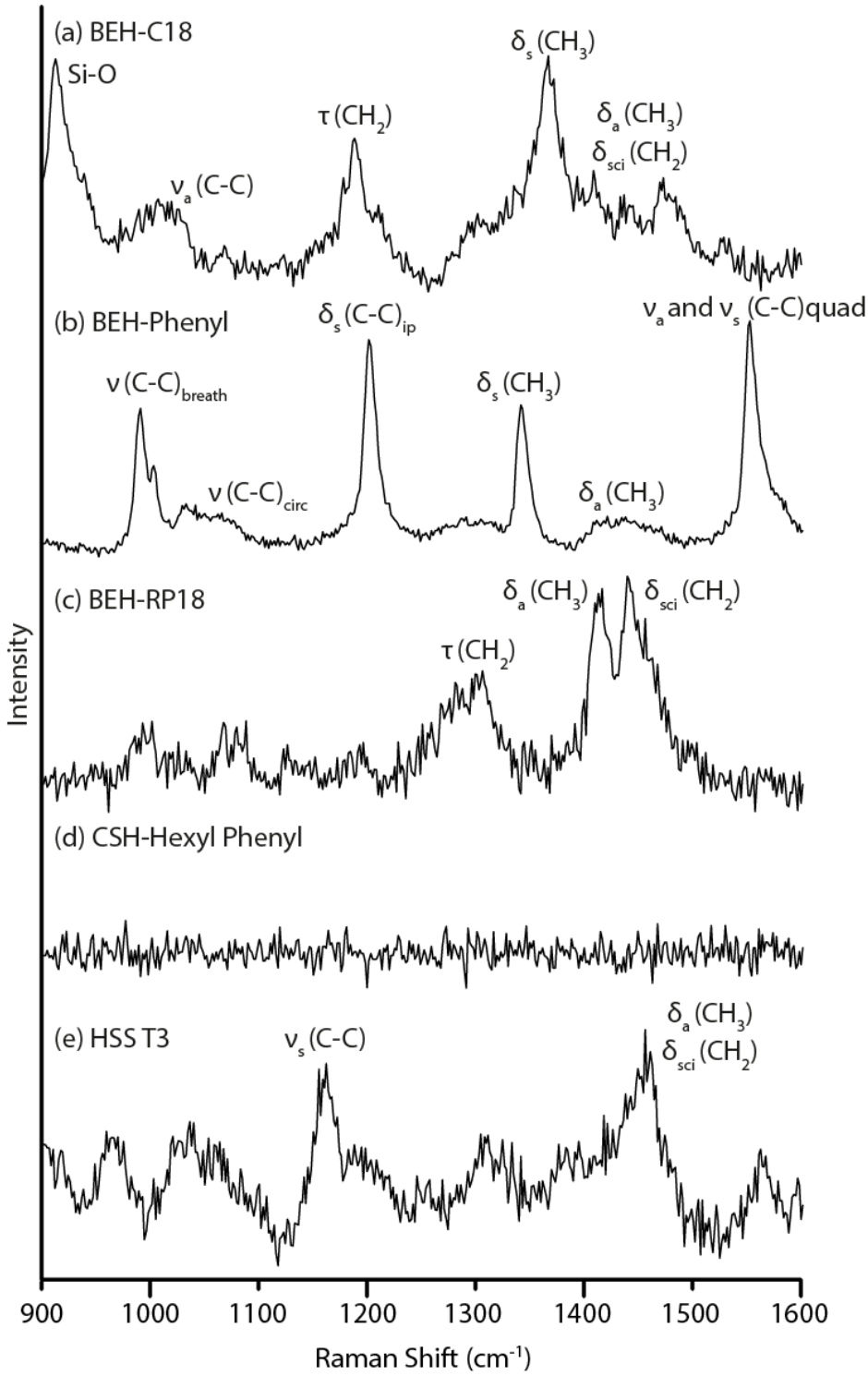

Figure 6.4. Raw, non-subtracted, Raman vibrational spectra in the low wavenumber region for the C-C stretching and C-H bending region of (a) BEH-C18, (b) BEH-Phenyl, (c) BEH-RP18, (d) CSH Phenyl-Hexyl and (e) HSS T3.

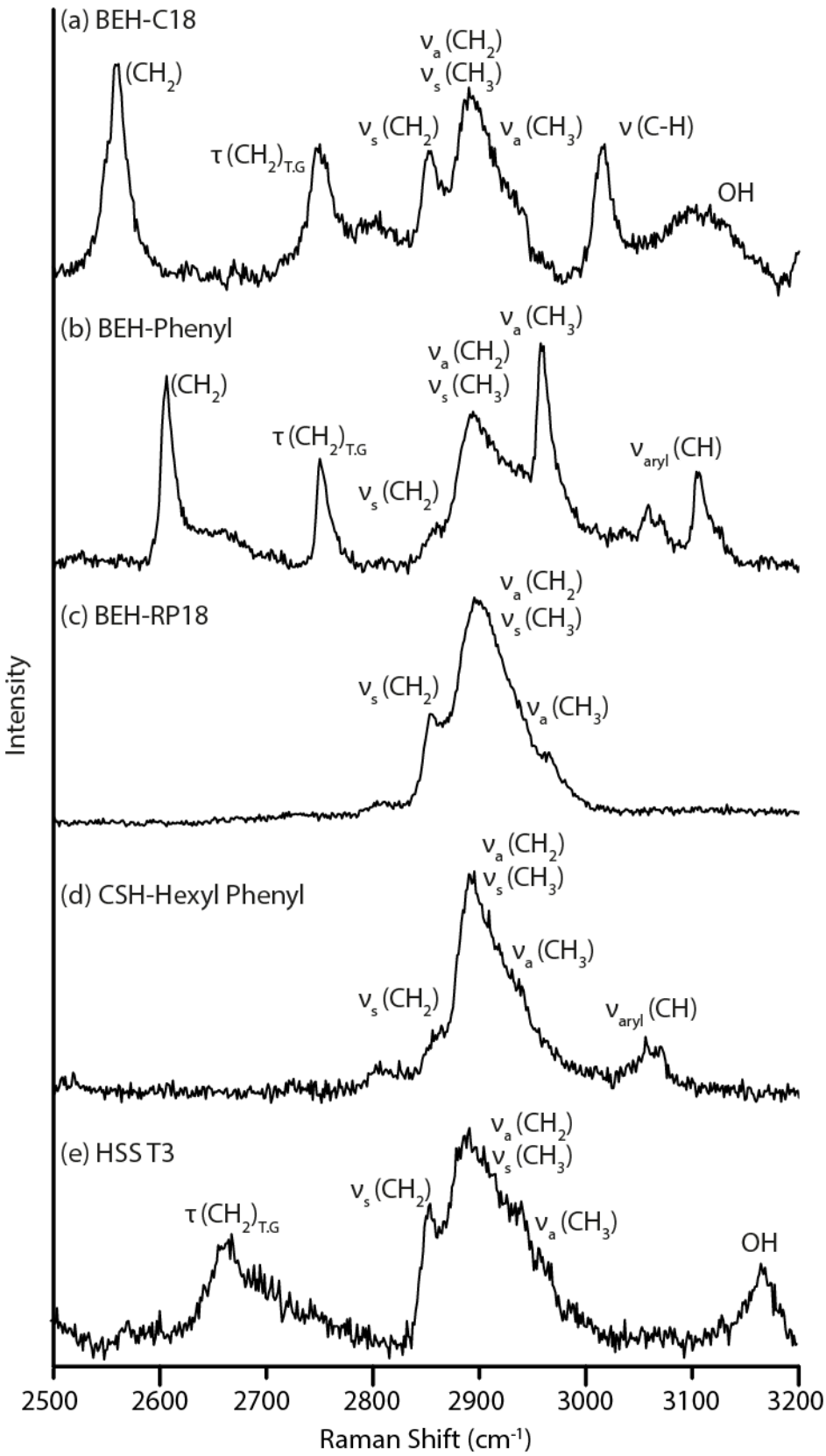

Figure 6.5. Raw, non-subtracted, Raman vibrational spectra in the high wavenumber region for C-H stretching region of (a) BEH-C18, (b) BEH-Phenyl, (c) BEH-RP18, (d) CSH Phenyl-Hexyl and (e) HSS T3.

For simplicity, the typical band assignments for the saturated and mono-substituted hydrocarbons [318-321] of the stationary phases are summarised in Table 6.2 and 6.3.

Table 6.2. Band assignments of C-C stretching, C-H bending and C-H stretching for saturated hydrocarbons[318-321].

Raman shift (cm-1)	*Notation*	*Description*
1040-1100	ν_a (C-C)	carbon-carbon asymmetric stretching
1065	ν_a $(C\text{-}C)_T$	C-C asymmetric stretching ('trans' conformations)
1080	ν $(C\text{-}C)_G$	C-C stretching ('gauche' conformations)
1120-1180	ν_s (C-C)	carbon-carbon symmetric stretching
1124	ν_s $(C\text{-}C)_T$	C-C symmetric stretching ('trans' conformations)
1295-1305	$_T$ (CH_2)	methylene $-(CH_2)_n-$ in-phase twisting
1370-1380	δ_s (CH_3)	methyl symmetric bending
1440-1470	δ_a (CH_3)	methyl asymmetric bending
1445-1475	δ_{sci} (CH_2)	methylene scissoring
2724	$_T$ $(CH_2)_{T.G}$	methylene twisting
2843-2863	ν_s (CH_2)	methylene symmetric stretching
2862-2882	ν_s (CH_3)	methyl symmetric stretching
2890	ν_a (CH_2)	methylene asymmetric stretching
2916-2936	ν_a (CH_2)	methylene asymmetric stretching
2927	ν_s $(CH_2)_{FR}$	methylene free rotation
2952-2972	ν_a (CH_3)	methyl asymmetric stretching
2957	ν_s (CH_3)	methyl symmetric stretching

Table 6.3. Band assignments of C-C stretching, C-H bending and C-H stretching for mono-substituted hydrocarbons[318-321]

Raman shift (cm-1)	*Notation*	*Description*
990-1010	$\nu(C\text{-}C)_{breath}$	mixing of in-phase ring stretching (or 'breathing') and in-plane ring bending
1027	$\nu(C\text{-}C)_{circ}$	mixing of 'semi-circle' stretching and in-plane CH bending
1146-1166	$\delta_a(C\text{-}C)_{ip}$	asymmetric CH in-plane bending
1170-1180	$\delta_s(C\text{-}C)_{ip}$	symmetric CH in-plane bending
1565-1590	ν_a $(C\text{-}C)_{quad}$	carbon-carbon asymmetric 'quadrant' ring stretching
1585-1620	ν_s $(C\text{-}C)_{quad}$	carbon-carbon symmetric 'quadrant' ring stretching
3030-3070	ν_{aryl} (CH)	aromatic (or aryl) C-H stretching

6.4.3 NMR spectroscopy

6.4.3.1 ^{1}H HR MAS NMR spectroscopy

NMR spectroscopy enabled us to determine the structural arrangement of RP-HPLC phases. The five stationary phases investigated in this study can be divided into two groups. The first containing aliphatic chain bonded phase ligands (e.g. BEH-C18, BEH-RP18 and HSS T3) and the second group contains aromatic ring bonded phase ligands (e.g. BEH-Phenyl and CSH Phenyl-Hexyl).

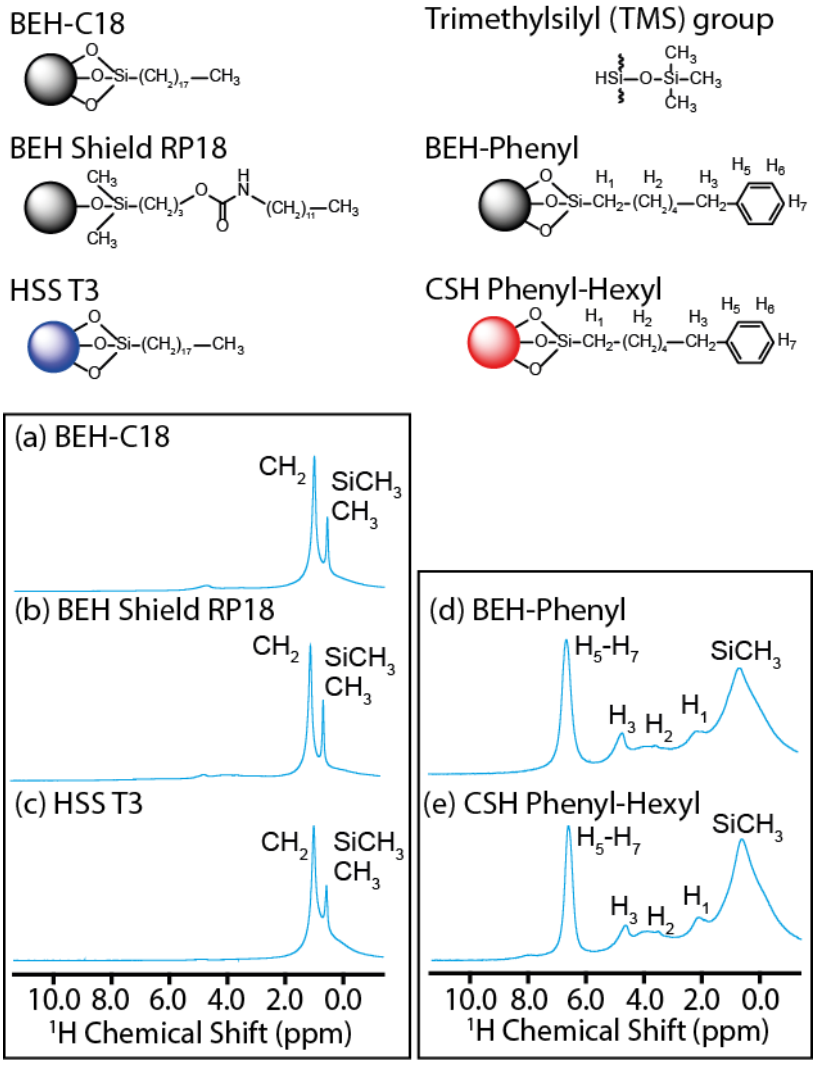

Figure 6.6. 1D ^{1}H HR-MAS NMR spectra of (a) BEH-C18, (b)BEH-RP18, (c) HSS T3 (d) BEH-Phenyl and (e) CSH Phenyl-Hexyl stationary phases in the absences of mobile phase. All spectra were obtained at 500 MHz spectrometer at room temperature and 10.0 kHz spinning frequency.

Figure 6.6 illustrates the corresponding ^{1}H HR-MAS NMR spectra of BEH-C18, BEH-Phenyl, BEH-RP18, CSH Phenyl-Hexyl and HSS T3 phases. The ^{1}H HR-MAS NMR of BEH-C18, BEH-RP18 and HSS T3 (aliphatic phases), as illustrated in Figure 6.6 a-c, showed no significant difference. The two dominating resonances observed across the three stationary phases at approximately 0.6 and 1.0 ppm corresponds to the CH_3 (terminal methyl group) and CH_2 groups of the ligands attached to the phases respectively [202].

In contrast, the ^{1}H MAS NMR of both BEH-Phenyl and CSH Phenyl-Hexyl (aromatic phases) showed additional distinctive peaks in comparison to the other phases. At 0.7 ppm, only one broad peak was observed (*Figure 6.6 d and e*) with BEH-Phenyl and CSH Phenyl-Hexyl which is primarily due to the $Si(CH_3)_3$ group, which is used for endcapping. Three low intensity peaks were also observed at 2.2, 3.9 and 4.8 ppm due to the alkyl spacer between the phenyl group and the silica surface. Additionally, a well resolved peak at approximately 6.7 ppm (*Figure 6.6 d and e*) is due to the phenyl protons (functional ligand) of the phases [322]. Additionally, methylene protons line widths for both BEH Phenyl and CSH Phenyl-Hexyl stationary phases are greater than the remaining stationary phases. This suggests that the aliphatic chain between the aromatic ligand and silica are in a more rigid environment than the chains of BEH C18, BEH RP18 and HSS T3, which leads to stronger dipolar couplings.

At a glance, Figure 6.6 clearly indicates broad peaks obtained from the protons present across the stationary phases. Obtaining ^{13}C and ^{29}Si CP/MAS NMR spectra of RP-HPLC phases will provide additional information for characterising the molecular arrangement of RP-HPLC phases. Similar results were previously reported [202].

As illustrated in various Figures in Chapter 5, the ^{1}H peaks of the stationary phases are generally observed at lower intensity and broader in comparison to the solvent peaks which is primarily due to the lower quantity of stationary phase packed into the rotor. This enabled us to measure ^{1}H T_1 and T_2 relaxation for the protons of the analyte without interference from the peaks from the stationary phases.

6.4.3.2 ^{13}C CP/MAS NMR spectroscopy

Figure 6.7 shows the ^{13}C CP/MAS NMR spectra of the five RP-HPLC phases investigated in this study. ^{13}C CP/MAS NMR spectra provide supplementary information of the structure and arrangement of the alkyl and aromatic ligand groups of the stationary

phases. In this case, the ^{13}C CP/MAS NMR spectra of the five stationary phases can be divided into three groups. The first group contains the aliphatic phases BEH-C18 and HSS T3, where the methyl peaks of BEH-C18 were broader which could indicate inhomogeneous environments within the sample. The second group consist of BEH-RP18 (aliphatic phase) which has an embedded polar group.

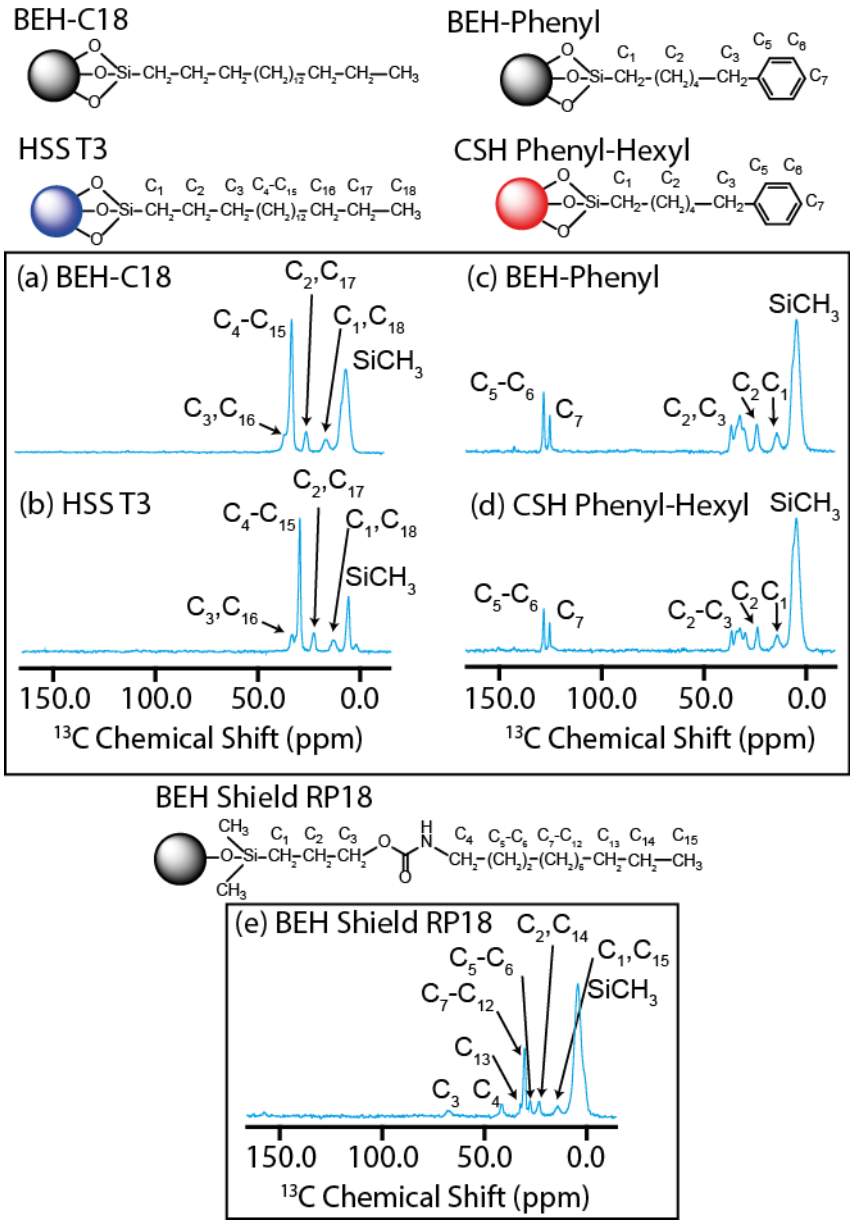

Figure 6.7. 1D ^{13}C CP/MAS NMR spectra of (a) BEH-C18, (b) HSS T3, (c) BEH-Phenyl, (d) CSH Phenyl-Hexyl and (e) BEH-RP18 stationary phases in the absences of mobile phase. All spectra were obtained at 500 MHz spectrometer at room temperature and 10.0 kHz spinning frequency.

Finally, the last group contains aromatic ring bonded phase ligands (e.g. BEH-Phenyl and CSH Phenyl-Hexyl). The peaks observed within 10 to 40 ppm are due to the carbon atoms of the octadecyl attached ligand group of BEH-C18 and HSS T3 (Figure 6.7a and b). The ^{13}C peaks arrangement of the BEH-C18 and HSS T3 from left to right is as follows: C1 and C18 at 13.7 ppm, C2 and C17 at 23.5 ppm, C4 to C15 at 30.3 ppm and C3 and C16 at 34.2 ppm. The C4 to C15 carbons peaks of HSS T3 were sharper and narrower compared to the remaining stationary phases which indicates higher mobility which is consistent with the manufacturers claims that HSS T3 has the lower ligand density. Additionally, across all 5 stationary phases a dominant peak at approximately 6.5 ppm is due to the methyl carbons of the trimethylsilyl group ($Si(CH_3)_3$) used for endcapping the residual silanols.

The ^{13}C spectra of C18, RP18 and Phenyl stationary phases presented in this study have previously been reported [200, 323]. The ^{13}C peaks arrangement of BEH-RP18 (Figure 6.7 e) from left to right is as follows: C1 and C15 at 14.3 ppm, C2 and C14 at 23.5 ppm, C5 and C6 at 27.8 ppm, C7 to C12 at 30.5 ppm, C13 at 32.6 ppm, C4 at 41.7 ppm and C3 at 67.6 ppm. Two very distinct small peaks at 41.7 ppm and 67.6 ppm were only observed with BEH-RP18 and are due to embedded carbamate functional group which is consistent with the claims of the manufacturer. The ^{13}C CP/NMR spectra of BEH-Phenyl and CSH Phenyl-Hexyl (Figure 6.7 c and d) look very similar. The broad peak at approximately 5.1 ppm corresponds to the $Si(CH_3)_3$ group, while the alkyl linkage carbons C1, C2 and C3 are observed at 14.0 ppm, 23.5 ppm and 29.6 ppm respectively. Additionally, two peaks further downfield at about 126 ppm were observed only with BEH-Phenyl and CSH Phenyl-Hexyl phases. The peaks at 124.9 and 127.9 ppm are due to the C7 (p-carbons) and C5-C6 (o and m-carbons) of the phenyl functional group of theses phases. The spectra obtained are very similar to previous spectra reported by Albert *et al.* [324].

6.4.3.3 ^{29}Si CP/MAS NMR spectroscopy

Figure 6.8 illustrates the ^{29}Si CP/MAS NMR spectra of the five RP-HPLC phases investigated and the chemical structures of T^2, T^3, Q^3, Q^4 and M sites. Three distinctive peaks were observed across all five phases around -105, -61 and 10 ppm. The peaks can be assigned using both T^n and Q^n notations. Across all five stationary phases, the peaks at -101.7 ppm and -110.5 pm are due to the silanols (Q^3) and siloxanes (Q^4) respectively [291, 325, 326] which is predominantly found on the silica surface and largely dominated by Q_4 moiety. The peaks observed at -66.2 (T^3) and -57.7 ppm (T^2) are due to the presence

of partially and completely cross-linked silanol groups. The peak at ~65 ppm is due to the presence on the surface of another bonded moiety that is attached directly to the surface by a stable Si-C bond as shown in Figure 6.8 [200, 327]. Similar spectra have been reported by Brindle *et al.* [328]. Furthermore, the peak at approximately 13.4 ppm (M), confirms the presence of endcapping trimethylsilyl groups in each stationary phase. Additionally, even though the packing materials have been endcapped, the spectra obtained across all five stationary phases indicate the presence of residual silanols. The ^{29}Si peak area percentage distributions are illustrated in Table 6.4. As expected, the relative peak area percentages are similar across the stationary phases with the exception of HSS T3.

Table 6.4. ^{29}Si peak identities and area percentage distributions.

Chemical Moiety	Chemical Shift (~ppm)	*Percentage (% by peak area)*				
		BEH C18	BEH-Phenyl	BEH-RP18	CSH Hexyl-Phenyl	HSS T3
Q_4	-112	24.7	26.9	20.7	22.9	29.1
Q_3	-102	14.4	14.0	14.9	12.7	33.9
T_3	-66	44.3	44.2	45.2	40.9	14.6
T_2	-56	13.6	12.6	15.6	21.2	8.9
M	11	3.0	2.2	3.5	2.2	13.6

The ^{29}Si spectra of the HSS T3 stationary phase was significantly different to the remaining stationary phases. For instance, HSS T3 showed a higher peak area percentage at 13.4 ppm which is consistent with the fact that HSS T3 has the lowest ligand density (1.6 $\mu mol/m^2$) in comparison to the other stationary phases and as a result a higher proportion of trimethylsilyl end capping groups. The ligand density of HSS T3 also justifies the low relative intensity of T_2 and T_3 species. Furthermore, higher peak area percentages for both Q_3 and Q_4 moieties were also observed in the presence of HSS T3. This is expected as HSS T3 has a higher silanophilicity (100% silica) and higher surface area of 230 m^2/g compared to 185 m^2/g (see Table 6.1) in comparison to both BEH and CSH technology which corresponds to the claims suggested by the manufacturers [329].

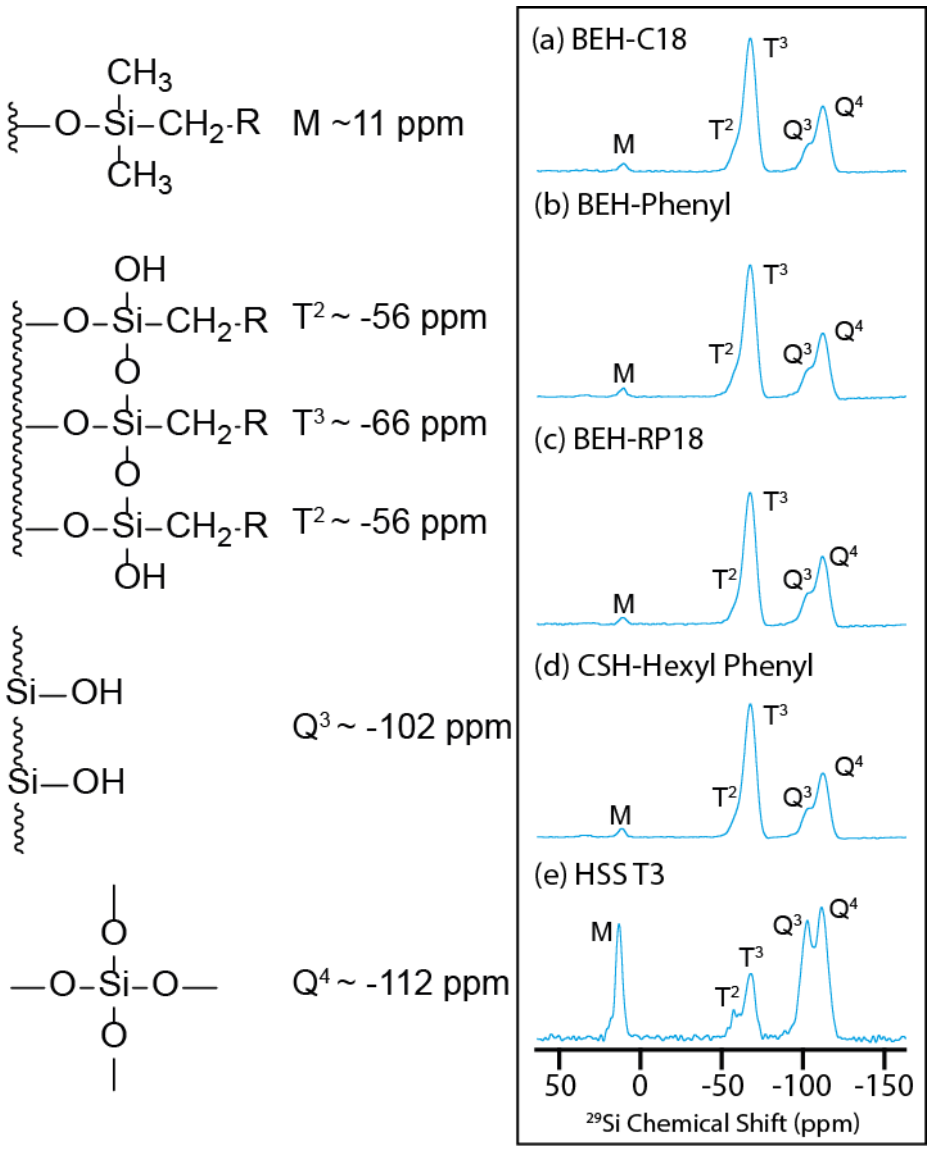

Figure 6.8. 1D ^{29}Si CP/MAS NMR spectra of (a) BEH-C18, (b) BEH-Phenyl, (c) BEH-RP18, (d) CSH Hexyl-Phenyl and (e) HSS T3 stationary phases in the absences of mobile phase. All spectra were obtained at 500 MHz spectrometer at room temperature and 10.0 kHz spinning frequency.

6.5 Conclusion

AFM microscopy enabled us to probe the topography and morphology of the stationary phases investigated in this study. Several spectral features of the five RP-HPLC stationary phase materials were achieved via Raman spectroscopy. Distinctive spectral information was obtained with different ligand functional groups. We used ^{1}H HR-MAS, ^{13}C and ^{29}Si CP/MAS NMR spectroscopy to confirm the chemical composition of RP-HPLC

stationary phases employed in this study. ^{1}H, ^{13}C and ^{29}Si CP-MAS NMR spectroscopy are extremely valuable tools for characterising the structural features of the RP-HPLC phase. These experiments highlighted significant differences between the aliphatic and aromatic ligand grouped stationary phases. Furthermore, 1D ^{29}Si CP/MAS NMR spectra of HSS T3 was different to the remaining phases which is mostly likely due to lower ligand density, higher surface area and particle chemistry of HSS T3. In summary, considering that the 1D ^{1}H peaks of the stationary phases were broad and overlapping, the ^{1}H relaxation time of the analytes was used to characterise the interactions driving the retention mechanism. Additionally, utilising the ^{1}H T_1 and T_2 relaxation of the analytes would enable us to achieve site specific measurements. The stationary phase characteristics could be investigated further. For instance, the dynamic behaviour of attached ligand can be obtained using variable temperature and relaxation experiments. The hydrolytic stability of the packing materials in aqueous conditions could also be developed by ^{29}Si CP-MAS experiments.

7 NMR RELAXATION APPROACHES FOR PROBING RP-HPLC MOLECULAR INTERACTIONS

7.1 Abstract

In this chapter, we explore the use of ^{1}H HRMAS T_1 and T_2 NMR relaxation measurements for probing molecular interactions between analytes and reversed-phase HPLC stationary phases using a variety of mobile phases all used in typical experimental method development screening conditions in Pfizer. We examine several approaches for using T_1 and T_2 relaxation times as descriptors of interactions and suggest that the combined use of both ^{1}H T_1 and T_2 relaxation times provides the most general and robust framework to facilitate our understanding of reversed-phase HPLC retention mechanism discussed in Chapter 8.

7.2 Introduction

A wide selection of NMR techniques has been developed for structural elucidation and probing of molecular motion of HPLC heterogeneous systems. Over the years, ^{1}H HR MAS NMR longitudinal (T_1) and transverse (T_2) relaxation measurements have been applied to provide fundamental insights into dynamics and kinetics of analytes dissolved in a mobile phase and in the presence of a HPLC stationary phase [91, 92, 94, 95, 270]

based on the premise that interactions between molecules lead to changes in their motional behaviour. There are a number of NMR active nuclei that could be employed to characterise such systems but because of their high gyromagnetic ratio and high natural abundance protons provide a particularly sensitive and convenient probe to determine atomic resolution view of interaction within an LC system. Regardless, ^{2}H [330, 331], ^{13}C [332-339], ^{14}N [340] and ^{29}Si [341-351] relaxation techniques have also been previously used for probing the dynamic behaviour and characterising various HPLC stationary phases[332, 333, 337, 338, 350]. However, obtaining, e.g. ^{13}C relaxation rates can be time consuming due to the poor sensitivity of experiments involving detection of ^{13}C nuclei at natural abundance or costly if isotopic labelling is involved.

To provide some context for the current work we first survey briefly published to date studies that exploit relaxation measurements to probe interactions between analytes and stationary phases. We examine the basic assumptions made in the mentioned studies and consider their strengths and weaknesses.

In the first study we consider, Skogsberg *et al.* established correlation between ^{1}H T_1 relaxation and strength of interaction with stationary phases for (*R*)- and (S) 1,1'-binaphthyl-2,2'-diol (binol), (+) and (-)-O,O'-dibenzoyl-tartaric acid and two structurally similarly chiral stationary phases (CSPs) (Kromasil-DMD and TBB) in a study where ^{1}H HR MAS NMR T_1 relaxation measurements were reinforced by transferred Nuclear Overhauser Spectroscopy (trNOESY) measurements [93]. Superior HPLC separation of (*R*)- and (*S*)-binol was observed in the presence of Kromasil-DMB compared to Kromasil-TBB in a cyclohexane mobile phase. Due to the stronger interactions between (*R*)-binol and the CSPs, (*S*)-binol always elutes before (*R*)-binol under this experiment's conditions. Typically a small analyte interacting with a large molecule will have the correlation time of a large molecule and hence negative NOE crosspeaks would be observed. The suspended-state HR/MAS trNOESY spectra of (*S*)-binol dissolved in $CDCl_3$ showed positive cross peaks between the aromatic groups. Negative trNOESY crosspeaks between the aromatic protons of (*S*)-binol in the presence of Kromasil-DMB stationary phase were observed. The change from positive (in the absence of Kromasil-DMB) to negative cross peaks suggest the analyte interacts with the stationary phase. Furthermore, the naphthyl groups in (*S*)-binol have close proximities to the benzoyl groups of Kromasil-DMB which suggests either steric or π-π interactions are taking place between aromatic groups of (*S*)-binol and of Kromasil-DMB

Additionally, HR/MAS trNOESY experiments of (*R*)- and (*S*)-binol dissolved in a mixture of 2-propanol-d_8 (5%) in cyclohexane-d_{12} (C_6D_{12}) in the presence of Kromasil-DMB were obtained. The trNOESY experiment demonstrated stronger trNOESY crosspeaks were observed for (*R*)-binol compared to (*S*)-binol which suggest (*R*)-binol interacts stronger with Kromasil-DMB stationary phase than (*S*)-binol. ^{1}H T_1 measurements of (*R*)- and (*S*)-binol dissolved in C_6D_{12} were also acquired to probe the proximities of the analytes and Kromasil-DMB stationary phases. The T_1 values of (*R*)-binol were significantly shorter compared to (*S*)-binol which could suggest stronger interactions between (*R*)-binol and Kromasil-DMB are taking place.

However, the assumption that ^{1}H T_1 becomes shorter in the presence of interaction is not always valid as T_1 relaxation depends on the correlation time of motion, which goes through a minimum at the correlation time equal to the inverse of proton Larmor frequency (*see Figure 7.1*). This means that, for example, if the interaction with the stationary phase slows down the motion of the molecule sufficiently the T_1 can become longer compared to T_1 in the absence of the interaction. We have observed such effect in some of the cases in the extensive set of measurements performed in this thesis.

Around the same time Skogsberg *et al.* work was reported, Coen *et al*. used both ^{1}H T_1 and T_2 relaxation measurements at variable temperature to probe the molecular interaction between p-xylene and C18 RP-HPLC stationary phase [95]. Both ^{1}H T_1 and T_2 relaxation increased with higher temperature consistent with an increase in the chain flexibility (see Fig. 7.1). Even though Coen *et al*. have recognised the usefulness of considering both T_1 and T_2 as probes of interactions and mobility they have not fully exploited the power of the combined use of these two parameters. For example, the direction of relative changes of T_1 and T_2 relaxation times in the absence and presence of stationary phase can be used to determine the correlation time regime for the interacting molecules. This means that one can in principle tell whether the correlation time for the interacting molecules is on the left or on the right from the T_1 minimum in Fig. 7.1. For example, since increasing of temperature results in shortening of the correlation time, an increase in both T_1 and T_2 relaxation times when temperature increases indicates that the correlation times are faster than the correlation time at T_1 minimum. On the other hand, a decrease in T_1 with simultaneous increase in T_2 with rising temperature suggests that the correlation times are slower than the correlation time at T_1 minimum [91]. As Coen *et al.* measured their parameters at variable temperatures, they could obtain the energy of activation for rotation

of the functional groups by fitting the T_1 trends as function of temperature. The values of activation energy indicated a restriction of motion for bound methyl group of p-xylene.

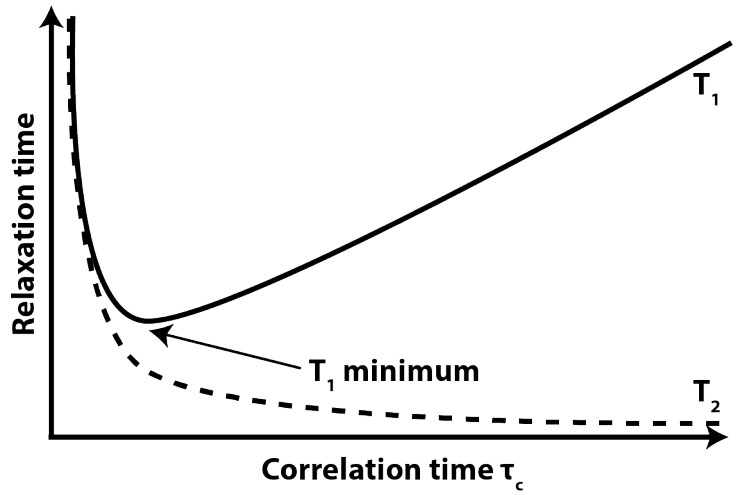

Figure 7.1. A plot of T_1 and T_2 relaxation against correlation time.

In 2009, Albert *et al.* [270] investigated the relationship between separation of (R)- and (S)-benzyl mandelate enantiomers in the presence of polysaccharide-based chiral stationary phase (CSP) and mobile phase consisting of methanol with 0.1% TFA using both HPLC and ^{1}H HRMAS NMR experiments. The HPLC chromatogram revealed the (*R*)-enantiomer elutes prior to the (*S*)-enantiomer indicating that (*S*)-enantiomer interact more with the stationary phase than (*R*). (S)-benzyl mandelate enantiomer, which has the highest binding affinity towards the chiral stationary phase (CSP), appeared to have the shortest ^{1}H T_1 values in the measurement in the presence of CSP compared to measurements performed in solution in the absence of the CSP. The authors interpreted the shorter T_1 relaxation in the presence of stationary phase as an indication of restricted molecular motions due to interaction of the analyte with stationary phases (SP) [352, 353]. The same line of thinking was used as an indication of interaction with the SP for different analytes and a variety of HPLC stationary phases in other studies [69, 89]. In addition to relaxation measurements, NOESY and trNOESY experiments were also performed with (*R*)- and (*S*) enantiomer in presence and absence of CSP to confirm the binding affinity of (*S*) enantiomer towards the CSP. In absence of CSP, weak positive (up) NOE diagonal peaks were observed. The NOESY HR/MAS NMR spectra of (*S*) and (*R*)-enantiomer revealed intense negative (down) diagonal peaks between the aromatic benzyl mandelate protons and aliphatic region of the stationary phase. Additionally, the aromatic benzyl mandelate integral values of (*S*) compared to (*R*)-enantiomer were stronger possibly due

to greater interaction of (S) enantiomer and the CSP which complements the HPLC elution order.

More recently, Yeman *et al.* investigated the interactions of aniline and phenol with monomeric and hydride-modified stationary phases via ^{1}H HR MAS NMR spectroscopy [92]. The ^{1}H HR MAS NMR spectra of the analytes in the presence of C18 stationary phase showed two sets of peaks. One set of peaks were sharp, which suggests the molecules are free to rotate, as is in the case of molecules dissolved in the mobile phase and not involved in interactions with stationary phase. The other set of observed peaks was broad and upfield of the narrow peaks. The broad nature of the peaks indicates presence of interactions between the analyte and C18 stationary phase (the molecules are adsorbed onto the stationary phase). Observation of two distinct sets of peaks for the analytes suggests that they are undergoing slow chemical exchange between the free and adsorbed forms. Similar distinctive spectra were reported in other studies [30,79, 80, 82, 196, 208]. The ^{1}H T_1 relaxation of the peaks for the "adsorbed" fraction of the analyte were considerably shorter than ^{1}H T_1 relaxation of the peaks for the "free" fraction, which could indicate the analytes in the "adsorbed" states undergo restricted motion due to interaction with the C18 chains. This conclusion was made based on the assumption that T_1 relaxation is inversely proportional to correlation time. Additionally, the ^{1}H T_1 relaxation of the analytes in the presence of hydride-modified phases were shorter compared to the monomeric phases due to higher bonded C_{18} ligand on the surface of the hydride-modified phases which increases the overall hydrophobicity. Additionally, higher HPLC retention factor for both aniline and phenol where observed in the presence of hydride-modified phase than monomeric phases which indicates aniline and phenol interact more strongly with hydride-modified phases [92].

The primary aim of this chapter is to investigate several approaches of using ^{1}H relaxation for probing molecular motions in chromatographic systems as reporters of mobility and interactions. Similarly to Coen *et al.* [95], we propose using both ^{1}H T_1 and T_2 relaxation to gain atomic resolution insights into the retention mechanism of analytes across five different RP-HPLC stationary phases. This approach will then be used in Chapter 8 to probe details of interactions behind the retention mechanisms for a series of analytes and RP-HPLC stationary phases.

7.3 Experimental Methods

7.4 Materials

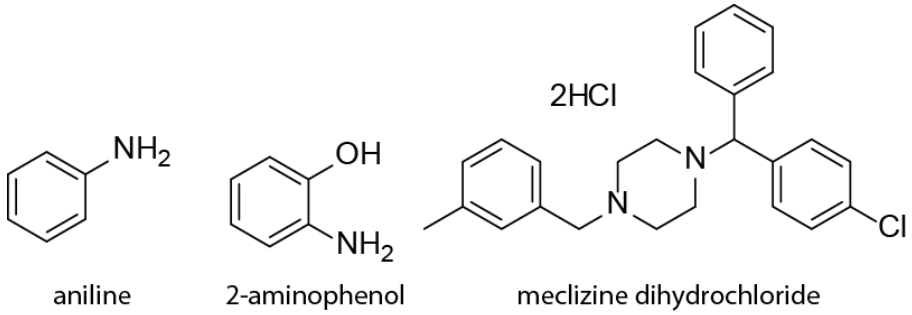

Figure 7.1. Chemical structure of aniline, 2-aminophenol and meclizine dihydrochloride.

To illustrate our discussion we will use throughout this Chapter data measured on aniline, 2-aminophenol, and meclizine dihydrochloride. The analytes were obtained from Sigma Aldrich and used without any further purification. The analytes were dissolved at 0.5 M concentration in mobile phases consisting of various proportions of deuterium oxide, acetonitrile and methanol (see figure captions for details). 4,4-dimethyl-4-silapentane-1-sulfonic acid (DSS) was added to the samples as an internal standard**.** BEH-C_{18} (~17% w/w carbon loading), BEH-phenyl (~15% w/w carbon loading), BEH-RP_{18} (~16% w/w carbon loading), CSH-phenyl (~14% w/w carbon loading) and HSS T3 (~11% w/w carbon loading) stationary phase were extracted from commercially available XBridge™ columns (Waters) with particle size of 1.7 µm and average pore diameter of 145 Å. The physical chemistry properties of the five RP-HPLC stationary phases were previously shown in Chapter 6.

7.5 HPLC Method

The RP-HPLC measurements were carried out at Pfizer on Waters Acquity UPLC with UV (PDA) and MS detectors. Each analyte at the concentration of approximately ~5 mM was individually run through the five studied stationary phases. The mobile phase was either solvent A consisting of acetonitrile (MeCN) and water or solvent B consisting of methanol (MeOH) and water. For both mobile phases the solvents were mixed in a 50:50

(% v/v) ratio under isocratic conditions. The used solvents were HPLC grade. Flow rate of 0.4 mL/min at a temperature of 40 °C was used.

7.6 NMR Method

Deuterium oxide, d_3-MeCN and d_4-methanol purchased from Sigma Aldrich. Stock solutions of 0.5 M aniline, 2-aminophenol and meclizine were prepared in deuterated mobile phase compositions consisting of either 50:50 (% v/v) MeCN:D_2O or 50:50 (% v/v) MeOH:D_2O. The calculated molar ratio of analyte/stationary phase was approximately 1:0.25. For the samples with analytes in the presence of mobile phase and absence of stationary phase ("solution only"), 80 µL of the analyte was measured using an automated pipette and then placed into a 4 mm rotor.

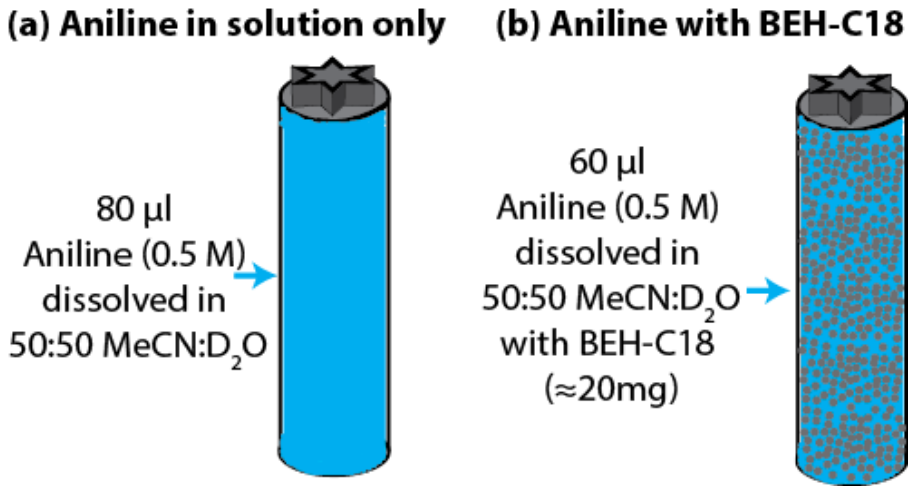

Figure 7.2. Illustration of (a) aniline in solution only and (b) aniline in the presence of BEH C18 stationary phase.

For the analytes with added stationary phase, 10 mg of stationary phase was initially packed into the rotor followed by addition of 60 µL of the dissolved analyte and then additional 10 mg of stationary phase (*see Figure 7.3*). ^{1}H HR MAS NMR experiments were conducted on a Bruker Ultrashield 500 Spectrometer operating at 500 MHz ^{1}H Larmor frequency. The prepared samples were placed into 4 mm ZrO_2 MAS rotors (Bruker Biospin, Rheinstetten, Germany) with no spacer. The rotor was spun using high pressure nitrogen at the magic angle (θ = 54.4°) at a spinning speed of 5 kHz at 313 K. The ^{1}H HR MAS NMR experiments were conducted using a 90° one-pulse sequence, where 8 transients were collected into a 64 k data points over a spectral width of 20000

Hz (40 ppm) with an acquisition time of 1 second. Exponential line-broadening of 0.5 Hz was applied before FT.

7.7 Saturation recovery (T_1) Measurements

^{1}H T_1 was also measured by using a standard saturation-recovery pulse sequence (saturation – τ – 90º– FID) with pulse nutation frequencies of 25 kHz. 8 transients were collected into 20 k data points over a spectral width of 20000 Hz (40 ppm) with an acquisition time of 1 seconds, relaxation delay of 2 seconds and where the recovery time was ranged from 0 to 30 seconds. Exponential line-broadening of 0.5 Hz was applied before FT. The ^{1}H T_1 values were obtained from fitting of the peaks integrals (obtained using Topspin 3.5) as a function of the relaxation delay to equation ($I[\tau] = I[0](1 - \exp(-\tau/T_1))$). The fitting was performed in Origin 9.3.

7.8 CPMG (T_2) Measurements

^{1}H T_2 relaxation times were measured using the CPMG pulse sequence (90° - [τ – 180° – τ]n – FID) with a pulse nutation frequency of 25 kHz. 8 transients were collected into a 20k data points over a spectral width of 20000 Hz (40 ppm) with an acquisition time of 1 second, relaxation delay of 16 seconds, spin echo time (ts) of 1.2 ms, loop time was fixed at 2.5 ms and the number of loops (*n*) were varied accordingly to obtain relaxation curves with the peak intensity decaying below 30% of its initial value. Exponential line-broadening of 0.5 Hz was applied before FT.

The ^{1}H T_2 values were obtained from fitting of the peaks integrals (obtained using Topspin 3.5) as a function of the relaxation delay to equation ($I[\tau] = I[0]\exp(-\tau/T_2)$). The fitting was performed in Origin 9.3.

7.9 Results and discussion

7.10 Chemical exchange regimes for analytes binding transiently to stationary phases

Figure 7.4 shows 1D ^{1}H HRMAS NMR spectra of aniline in 50:50 (% v/v) MeCN:D_2O mobile phase in the absence of any stationary phase, in the presence of BEH-C18, BEH-phenyl, BEH-RP18, CSH hexyl-phenyl and HSS T3 stationary phases obtained at 500 MHz spectrometer. The peak observed at 0 ppm corresponds to the 4,4-dimethyl-4-silapentane-1-sulfonic acid (DSS) signal, which is used as the internal reference. Weak broad peaks observed in three of the spectra at 0.8 and 1.25 ppm correspond to the CH_3 and CH_2 groups of BEH-C18, BEH RP18 and HSS T3 stationary phases. The average peak for amine protons in fast exchange with water is observed at approximately 4.2 ppm. The peaks between 6.75 and 7.14 ppm correspond to the aromatic protons of aniline as indicated in Figure 7.4: the peak at 7.14 ppm corresponds to protons in the *meta* position with respect to NH_2 (labelled "1") and the peak at 6.75 ppm is a result of overlap of signals for protons in *ortho* and *para* positions (labelled "2").

Only one set of sharp aromatic proton peaks was observed in the spectrum of aniline in the 50:50 MeCN:D_2O mobile phase in the absence of stationary phases (see Figure 7.4b). On the other hand, the spectra of aniline in the presence of all the RP-HPLC stationary phases show two sets of aromatic protons with well resolved peaks at 7.15 ppm, 7.10 ppm, 6.75 ppm and 6.70 ppm. In analogy to the Coen *et al.* [95] and Yeman *et al.* [92] studies we could assign one set of the peaks to "free" in solution aniline and aniline "bound" to the reversed phase stationary phases. The "free" peaks at 7.15 ppm and 6.75 ppm have narrow line widths consistent with the molecule undergoing fast overall rotational diffusion. The broad aromatic peaks at ~7.10 ppm and ~6.70 ppm suggests restriction of motion for the molecule consistent with it being adsorbed onto the RP-HPLC stationary phases.

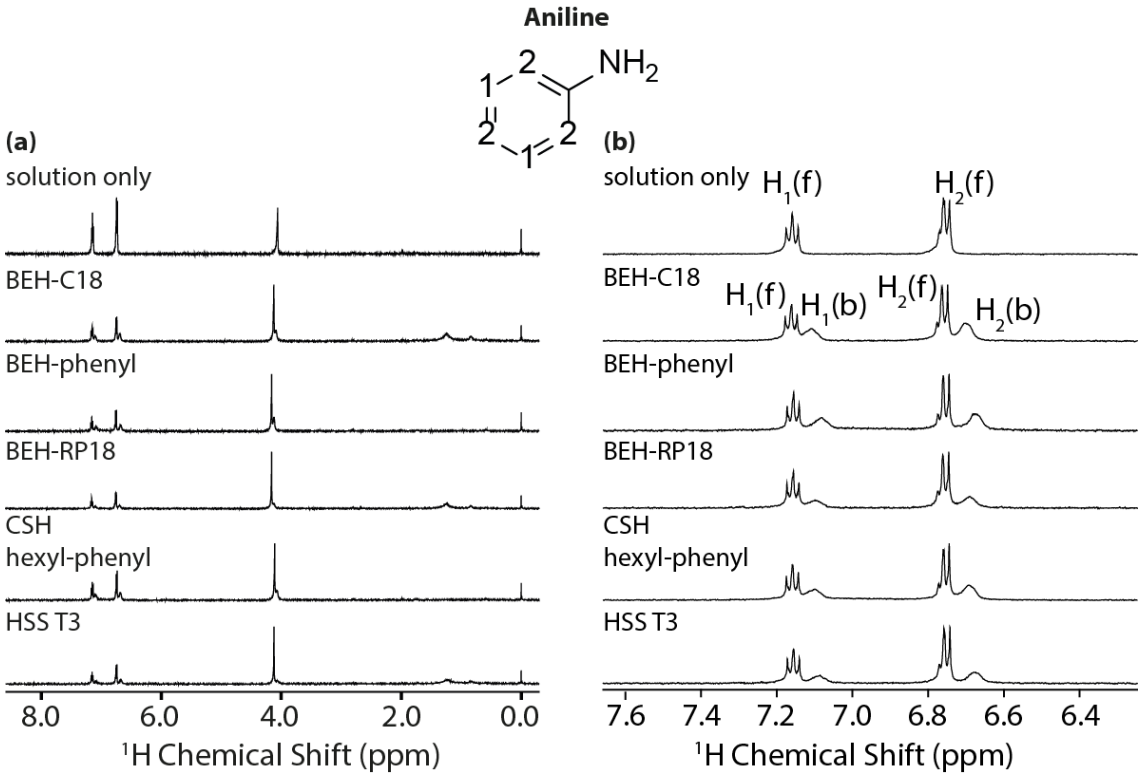

Figure 7.3. 1D ^{1}H HR-MAS NMR spectra of 0.5 M aniline in the 50:50 % v/v of MeCN:D_2O mobile phase (from top to bottom): in the absence of stationary phases and in the presence of either BEH-C18, or BEH-phenyl, or BEH-RP18, or CSH hexyl-phenyl, or HSS T3 stationary phase as indicated on the left hand side of each spectrum. (a) Full spectra. (b) Expansions of the aromatic region. The resonance assignments are indicated with the numbers, e.g. proton labelled as 2 in the molecule is identified with a label H-2 in the spectrum. The letters "f" and "b" in the parenthesis indicate free and bound forms, respectively. All spectra were obtained at 500 MHz spectrometer at 313 K and 5.0 kHz magic angle spinning frequency.

The resonance due to fast exchange between water and NH_2 protons also appears to split into "free" and "bound" components in the presence of stationary phases. The presence of the two sets of peaks suggest that aniline is in the slow exchange regime where the rate of chemical exchange is smaller than the chemical shift difference for the analytes in the two different environments ($k_{ex} < \Delta\omega$).

Table 7.1. Chemical shift difference between "free' and "bound" forms of aniline in the presence of either BEH-C18, or BEH-phenyl, or BEH-RP18, or CSH hexyl-phenyl, or HSS T3 stationary phase.

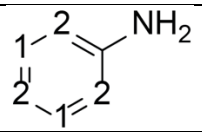

SP	HPLC retention time (mins)	Chemical shift difference (Hz)		
		H-1(f)-H-1(b)	H-2(f) -H-2(b)	NH_2+H_2O (f)-NH_2+H_2O (b)
BEH-C18	3.58	27.1±5.4	30.5±6.1	18.6±3.7
BEH-Phenyl	3.67	36.6±7.3	42.0±8.4	19.7±3.9
BEH-RP18	3.73	29.1±5.8	35.4±7.1	18.2±3.6
CSH hexyl phenyl	3.80	28.3±5.7	34.3±6.9	20.5±4.1
HSS T3	4.22	32.9±6.6	40.8±8.2	20.9±4.2

Interestingly, the chemical shift difference of the "bound" peaks to the "free" peaks changes on different stationary phases. The difference is also site specific, i.e. the magnitude of the shift is not the same for all the sites in the sample. For example, the separation for H-2 proton environments is the largest on BEH phenyl stationary phase and smallest on BEH C18 stationary phase, which would be consistent with the idea that interaction of the aromatic ring with stationary phases with aromatic functional groups leads to largest chemical shift changes.

However, not all the analytes are in the slow exchange regime in the presence of stationary phases. In some cases only one set of sharp peaks were observed for analytes both in the absence and in the presence of the stationary phases. 2-aminophenol in 50:50 (% v/v) MeOH:D_2O mobile phase in BEH-phenyl and CSH hexyl-phenyl stationary phases appears to be in slow exchange for aromatic sites (with populations heavily weighted towards free form; sometimes it might be difficult to distinguish fast exchange from slow exchange where one of the states is lowly populated) and in fast exchange for the water/NH_2 site (see Figure 7.4).

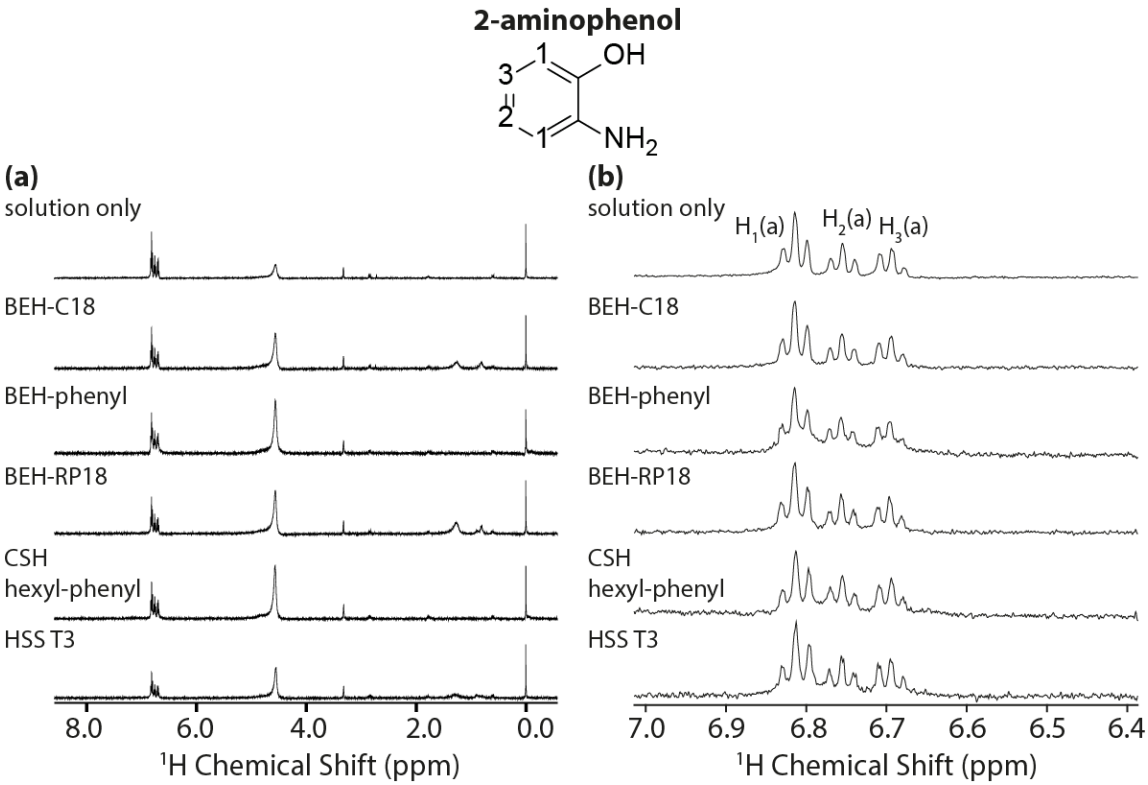

Figure 7.4. 1D ^{1}H HR-MAS NMR spectra of 0.5 M 2-aminophenol in 50:50 % v/v of MeOH:D_2O mobile phase (from top to bottom): in the absence of stationary phases (solution only) and in the presence of either BEH-C18, or BEH-phenyl, or BEH-RP18, or CSH hexyl-phenyl or HSS T3 stationary phases as indicated on the left of each spectrum. (a) Full range spectra. (b) Expansion of the aromatic region. The peak assignments are given in the "solution only" spectrum. The letter "a" in the parenthesis indicate average of the free and bound forms (e.g. fast exchange regime). All spectra were obtained at 500 MHz spectrometer at 313 K and 5.0 kHz spinning frequency.

However, all of the sites in 2-aminophenol are apparently in fast exchange in the presence of BEH-C18, BEH-RP18 and HSS T3 stationary phases. As a consequence of the rate of interconversion between the free and bound state being significantly larger than the chemical shift difference induced by the binding ($k_{ex} > \Delta\omega$) only one set of peaks at the average position is observed.

Since we observed both fast and slow chemical exchange in different cases it is likely that intermediate exchange can also be observed, as previously discussed in Chapter 4. However, under our experimental conditions with the series of analytes investigated we could not identify clear examples where this is the case. Overall, it is clear that because all possible chemical exchange regimes can be observed for analytes interacting with

stationary phases the approaches using ^{1}H relaxation to probe molecular interactions proposed in the existing literature have to be considered with caution and adjusted depending on the exchange regime.

7.11 NMR relaxation as a probing of molecular motions

Several relaxation-related parameters can be utilised for probing the changes in dynamics of analytes in chromatographic systems and hence indirectly the nature of their transient interactions with stationary phases. Here we consider ^{1}H T_1 and T_2 relaxation times as well as various parameters used for characterisation of chemical exchange processes. We outline the assumptions made when using different parameters. We discuss the advantages and limitations of each approach.

7.12 Application of ^{1}H T_1 relaxation times to probe analyte interactions

As we have already discussed above ^{1}H T_1, i.e. longitudinal relaxation, has previously been used to probe the molecular interactions between analytes and various HPLC stationary phases. One of the simplest ways ^{1}H T_1 can be used to monitor interactions of analytes with stationary phases is to take advantage of the fact that transient interactions lead to changes in the effective correlation time for the overall rotational diffusion and hence lead to change in the observed T_1. In a number of studies decrease in ^{1}H T_1 relaxation time for analytes dissolved in the mobile phase in the absence and in the presence of RP-HPLC stationary phase was interpreted as restriction of molecular motion due to interaction with stationary phase [192, 352, 353]. Generally, it is assumed that "free" molecules rotate with correlation times in the fast narrowing regime, which leads to long T_1 times. Hinderance of rotation due to transient interactions results in shorter T_1 times compared to free tumbling molecule. This assumption is correct if the correlation times for overall rotational diffusion of free and interacting analyte are both in the fast motion limit, i.e. on the left hand side of the T_1 minimum in Figure 7.1. Table 7.2 lists the site specific ^{1}H T_1 relaxation times of aniline in 50:50 (% v/v) MeCN:D_2O mobile phase in the absence and in the presence of BEH-C18, BEH-phenyl, BEH-RP18, CSH hexyl-phenyl and HSS T3 stationary phases measured using saturation recovery method. Thanks

to the high resolution of HR-MAS technique, atomic resolution site specific relaxation measurements are achievable (except for the overlap of signals for aromatic protons *ortho* and *para* positions, which are jointly indicated with "2"). Since aniline is in the slow exchange regime with well resolved peaks, the ^{1}H T_1 relaxation values of both "free" (indicated by "f") and "bound" (indicated by "b") peaks were obtained. Note that the exchange process leads to partial "mixing" of the relaxation rates for the molecule in the two states so the measured rates are not the "true" rates for each state: depending on the specific parameters of the exchange process the measured rates either under or overestimate the true relaxation times [354]. In general, this could be considered a disadvantage as complex analysis is required to extract the true relaxation rates for each site but it is actually an advantage for our application because we are interested in the influence of the exchange on the measured parameters. More specifically because of the influence of the exchange on the measured T_1 we can use for our analysis not only the T_1 of the bound analyte but also of the free analyte (in the absence of the exchange the T_1 of the free analyte in the presence of stationary phase should be the same as the one measured in the absence of stationary phase under the same conditions).

Table 7.2. ^{1}H T_1 relaxation of 0.5 M aniline in 50:50 % v/v MeCN:D_2O mobile phase (from top to bottom according to HPLC elution order): in the absence of stationary phase ("solution only"), and in the presence of BEH-C18, BEH-phenyl, BEH-RP18, CSH hexyl-phenyl and HSS T3 stationary phases. Data measured at 500 MHz spectrometer at 313 K and 5.0 kHz magic angle spinning frequency.

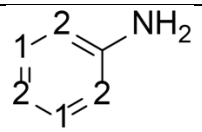

SP	HPLC Retention time (mins)	^{1}H T_1 (s)					
		H-1(f)	H-1(b)	H-2(f)	H-2(b)	NH_2+H_2O (f)	NH_2+H_2O (b)
Solution only		6.4 ± 0.3	n/a	7.0 ± 0.4	n/a	8.6±1.7	n/a
BEH-C18	3.58	7.4 ± 0.4	3.9 ± 0.2	8.0 ± 0.4	3.9 ± 0.2	7.0±1.4	2.8±1.4
BEH-Phenyl	3.67	7.6 ± 0.4	4.1 ± 0.2	8.7± 0.4	4.8 ± 0.2	8.3±1.7	3.4±1.7
BEH-RP18	3.73	7.5 ± 0.4	4.0 ± 0.2	8.1 ± 0.4	3.7 ± 0.2	7.5±1.5	3.5±1.8
CSH hexyl phenyl	3.80	6.7 ± 0.3	3.7 ± 0.2	7.5 ± 0.4	4.3 ± 0.2	6.7±1.3	3.4±1.7
HSS T3	4.22	8.4 ± 0.4	6.1 ± 0.3	7.9 ± 0.4	5.6 ± 0.3	5.3±1.1	2.9±1.4

As shown in Table 7.2, the T_1 values for aniline "free" peaks are considerably longer than those of the "bound" peaks consistent with the fact that the bound molecules undergo restricted motion compared to the free molecules. However, the ^{1}H T_1 relaxation values of the "free" peaks in the presence of stationary phase are generally longer compared to the measurement in the absence of stationary phases (referred to, in the following, as the

"solution only" measurement). As we mentioned above the lengthening of the measured T_1 for free aniline compared to aniline in the absence of any stationary phase is a result of the exchange process taking place during the measurement. Note that even though the peak near 4.2 ppm is likely to be an average peak for water and amine protons that are in fast exchange, it still changes significantly echoing the behaviour of the amine protons with particularly strong effect for aniline on HSS T3 stationary phase, which is designed for enhanced retention of polar compounds.

At this point it is worth to note that even if we neglect the effect of chemical exchange T_1 relaxation times do not always have to be reduced in the presence of a stationary phase. The restriction of motion due to interaction with stationary phase can take the overall motion of the analyte into the correlation time regime beyond the T_1 minimum, where the relaxation times become longer as the motion becomes more restricted. Thus the correlation between the magnitude of T_1 relaxation time and the extent of restriction of motion is simple only in case when the correlation of the free and bound analyte are in the same correlation time regime, e.g. fast motion regime, but becomes more complex and difficult to interpret when the correlation times span a wide range of values on both sides of T_1 minimum. To resolve such ambiguity other measurements might be necessary, e.g. T_2 measurement, which has a different dependence on the correlation time.

Because aniline dissolved in 50:50 (% v/v) MeCN:D_2O mobile phase is in a slow exchange on all the stationary phases it is possible in this case to obtain the apparent relaxation times for the free and adsorbed analyte separately. However, for 2-aminophenol, which is mostly in the fast exchange regime only an average value for the analytes in the two environments is available as shown in Table 7.3. Similarly to aniline, it is nontrivial to interpret the T_1 relaxation times of 2-aminophenol in the context of analyte-stationary phase interactions without any additional information. Sometimes the ^{1}H T_1 of 2-aminophenol in the presence of stationary phases is longer and sometimes shorter compared to the solution only measurement. Such alternation of the pattern of T_1 changes could indicate that 2-aminophenol does not interact strongly with stationary phases as the effect is small and does not have a clear direction but it is difficult to draw a clear conclusion in the absence of any additional data (though in general 2-aminophenol

elutes faster than aniline on all the stationary phases). Joint T_1 and T_2 relaxation analysis could potentially reduce such ambiguity.

Table 7.3. ^{1}H T_1 relaxation times of 0.5 M 2-aminophenol in 50:50 % v/v MeOH:D_2O (from top to bottom according to HPLC elution order): in the absence of stationary phase (solution only) and in the presence of BEH-C18, BEH-phenyl, BEH-RP18, CSH hexyl-phenyl and HSS T3 stationary phases. Measurements were performed at 500 MHz spectrometer at 313 K and 5.0 kHz magic angle spinning frequency.

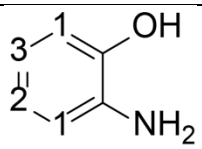

SP	HPLC Retention time (mins)	^{1}H T_1 (s)				
		H-1(a)	H-2(a)	H-3(a)	NH_2+H_2O (a)	MeOH(a)
Solution only		4.3±0.2	3.8±0.2	3.9±0.2	6.4±0.6	7.2±1.8
BEH-C18	3.13	4.5±0.2	4.4±0.2	4.1±0.2	5.6±0.6	5.3±1.3
BEH-RP18	3.34	4.3±0.2	3.9±0.2	3.7±0.2	5.8±0.6	5.4±1.4
HSS T3	3.56	4.0±0.2	3.8±0.2	3.9±0.2	5.9±0.6	5.3±1.3
BEH-Phenyl	3.59	4.2±0.2	3.5±0.2	3.6±0.2	7.5±0.8	7.7±1.9
CSH hexyl phenyl	3.81	4.2±0.2	3.4±0.2	3.9±0.2	6.5±0.7	6.7±1.7

7.13 Application of ^{1}H T_2 relaxation times to probe analyte interactions

Another parameter that could be used for probing the molecular motion of analytes is ^{1}H T_2 relaxation time. Just as in the case of ^{1}H T_1 a comparison of ^{1}H T_2 in the presence and absence of stationary phases could be used to provide insights on the interactions of analytes with stationary phases. Here we consider two approaches for obtaining ^{1}H T_2 relaxation times: extraction of T_2 from peak width at half height and measurement of T_2 using CPMG experiment.

7.14 Estimation of ^{1}H T_2 from peak width at half height

In principle, under ideal conditions the T_2 relaxation time of an analyte is directly related to the peak width at half height (in Hz):

$$v_{1/2} = 1/\pi T_2 \qquad (7.1)$$

The method to estimate the T_2 relaxation times from the peak widths has been used previously in studies of interactions of analytes with stationary phases [94, 95].

Estimating T_2 in this manner is only accurate if relaxation is the only source of broadening. However, often there are additional contribution to the line width due to magnetic field inhomogeneities or unresolved long range ^{1}H-^{1}H scalar couplings.

In general, the overall line width can be split into homogeneous and inhomogeneous contributions:

$$v_{1/2} = v_{1/2,homo} + v_{1/2,inhomo} \tag{7.2}$$

$v_{1/2,homo}$ contains a contribution from the relaxation processes $(1/\pi T_2)$ and any unresolved ^{1}H-^{1}H scalar couplings (this is especially a problem for aromatic protons where the long range couplings in the 1-3 Hz cannot be easily resolved in HRMAS experiments). $v_{1/2,inhomo}$ contains the contributions from the field inhomogeneities or so called inhomogeneous broadening. The inhomogeneities of the magnetic field throughout the volume of the sample due to instrumental imperfection can be minimised by shimming but obtaining perfect shimming is not always easy in heterogeneous samples consisting of mixture of liquid and solid.

Whereas the relaxation-related fraction of the homogenous broadening could be indirectly linked to the interactions between the analytes and stationary phases, the fraction of the homogeneous broadening due to unresolved ^{1}H-^{1}H scalar couplings and $v_{1/2,inhomo}$ are completely independent of them. Thus ultimately one would like to use method for estimating T_2, which is either completely free or at least with minimal contribution from the two latter factors.

First, we consider whether ^{1}H T_2 relaxation of aniline and 2-aminophenol calculated from the peak width at half height is dominated by relaxation. Table 7.4 shows the peak widths and the corresponding ^{1}H T_2 relaxation times of aniline in 50:50 % v/v MeCN:D_2O mobile phase in the absence and in the presence of BEH-C18, BEH-phenyl, BEH-RP18, CSH hexyl-phenyl and HSS T3 stationary phases. Table 7.5 shows analogous data for 2-aminophenol in 50:50 % v/v MeOH:D_2O mobile phase.

Table 7.4.[1]H peak widths and corresponding [1]H T_2 relaxation times of 0.5 M aniline in the 50:50 % v/v MeCN:D_2O (from top to bottom according to HPLC elution order): mobile phase in the absence of stationary phase (solution only) and in the presence of BEH-C18, BEH-phenyl, BEH-RP18, CSH hexyl-phenyl and HSS T3 stationary phases. Data obtained at 500 MHz spectrometer at 313 K and 5.0 kHz spinning frequency. Peak assignments are shown in Figure 7.4.

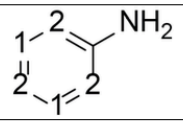

SP	HPLC Rt (mins)	[1]H peak width (Hz)						Estimated [1]H T_2 (s)					
		H_1(f)	H_1(b)	H_2(f)	H_2(b)	H_2O(f)	H_2O(b)	H_1(f)	H_1(b)	H_2(f)	H_2(b)	H_2O(f)	H_2O(b)
Solution only		3.5±0.2	n/a	2.3±0.2	n/a	4.8±0.5	n/a	0.1±0.01	n/a	0.1±0.014	n/a	0.1±0.007	n/a
BEH-C18	3.58	2.9±0.2	18.1±0.9	3.1±0.3	21.5±2.2	5.2±0.5	22.0±2.2	0.1±0.01	0.02±0.002	0.1±0.01	0.01±0.001	0.1±0.006	0.01±0.001
BEH-Phenyl	3.67	2.7±0.1	20.0±1.0	3.0±0.3	18.0±1.8	4.8±0.5	17.0±1.7	0.1±0.01	0.02±0.002	0.1±0.01	0.02±0.002	0.1±0.007	0.02±0.002
BEH-RP18	3.73	3.1±0.2	21.3±1.1	3.1±0.3	22.9±2.3	4.2±0.4	25.8±2.6	0.1±0.01	0.01±0.001	0.1±0.01	0.01±0.001	0.1±0.008	0.01±0.001
CSH hexyl phenyl	3.80	2.9±0.2	22.2±1.1	3.8±0.4	21.3±2.1	5.0±0.5	22.5±2.3	0.1±0.01	0.01±0.001	0.1±0.08	0.01±0.001	0.1±0.006	0.01±0.001
HSS T3	4.22	3.1±0.2	22.0±0.2	3.5±0.4	22.7±2.3	3.8±0.4	47.3±4.7	0.1±0.01	0.01±0.001	0.1±0.09	0.01±0.001	0.1±0.008	0.01±0.001

The [1]H T_2 relaxation times of aniline estimated from the peak widths range from ~0.01 to 0.14 s. These values are much shorter than the [1]H T_1 relaxation times measured on the same sample at the same experimental conditions (typically a few seconds; see Table 7.2 and 7.4). Such results suggest that either overall correlation times for aniline are long in this chromatographic system (i.e. to the right of the T_1 minimum in Figure 7.1) or that the T_2 relaxation times obtained from peaks widths are underestimated, e.g. due to the inhomogeneous broadening contribution. The first of these explanations is unlikely because to obtain such a large difference between [1]H T_1 and T_2 in solution only would mean that aniline would have to be heavily aggregated into rather large particles (the larger the molecule the slower it tumbles). Thus explanation that the T_2 times are underestimated because of additional contributions to the observer line width that are not related to relaxation. On the flipside, even though the absolute values of T_2 appear to be incorrect, they do show some expected qualitative trends. For example, the [1]H T_2 relaxation times measured using the broad peaks of "bound" aniline in the presence of stationary phase (H-1(b) and H-2(b)) range from 0.01 to 0.02 s compared to 0.11 s obtained for the "free" aniline (narrow peaks labelled H-1(f) and H-2(f)). Such a trend would suggest that broad peaks arise from the aromatic protons of aniline that are motionally restricted compared to the "free" aniline.

As in the case of aniline, the ^{1}H T_2 relaxation times estimated from peak widths for 2-aminophenol also appear to be underestimated due to significant contribution of inhomogeneous broadening or scalar coupling to the observed peak widths (see Tables 7.5 and 7.7)

Table 7.5. ^{1}H peak widths and the corresponding T_2 relaxation times for 2-aminophenol in 50:50 % v/v MeOH:D_2O (from top to bottom according to HPLC elution order): mobile phase in the absence of stationary phases (solution only) and in the presence of BEH-C18, BEH-phenyl, BEH-RP18, CSH hexyl-phenyl and HSS T3 stationary phases. HR-MAS data were obtained at 500 MHz spectrometer at 313 K and 5.0 kHz spinning frequency.

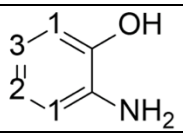

SP	HPLC Rt (mins)	Peak width (Hz)				T_2 from line width (s)			
		H-1(a)	H-2(a)	H-3(a)	MeOH(a)	H-1(a)	H-2(a)	H-3(a)	MeOH(a)
Solution only		4.1±0.8	3.6±0.7	3.3±0.7	6.3±1.2	0.1±0.02	0.1±0.02	0.1±0.02	0.1±0.01
BEH-C18	3.13	4.2±0.9	3.7±0.7	3.8±0.8	5.7±1.1	0.1±0.02	0.1±0.02	0.1±0.02	0.1±0.01
BEH-RP18	3.34	4.0±0.8	3.5±0.7	3.5±0.7	5.3±1.1	0.1±0.02	0.1±0.02	0.1±0.02	0.1±0.01
HSS T3	3.56	4.1±0.8	4.0±0.8	3.4±0.7	5.6±1.1	0.1±0.02	0.1±0.02	0.1±0.02	0.1±0.01
BEH-Phenyl	3.59	4.7±0.9	5.0±1.0	6.2±1.2	7.3±1.5	0.1±0.01	0.1±0.01	0.1±0.01	0.0±0.08
CSH hexyl phenyl	3.81	3.7±0.7	3.9±0.8	3.7±0.8	6.3±1.3	0.1±0.02	0.1±0.02	0.1±0.02	0.1±0.01

7.15 ^{1}H T_2 relaxation measured using CPMG

To test the hypothesis that T_2 times estimated from line width are compromised by broadening not related to motion, we employed CPMG pulse sequence, which refocuses the inhomogeneous broadening and aids suppressing the effect of homonuclear scalar couplings, and thus should provide more accurate T_2 relaxation times. As mentioned before, CMPG pulse sequence accomplishes refocusing of the inhomogeneous broadening through application of a train of π pulses [355, 356]. Table 7.6 compares the ^{1}H T_2 relaxation values of aniline obtained using CPMG pulse sequence and estimated from the peak widths. The ^{1}H T_2 relaxation times measured for "solution only" and "free" aniline using CPMG range between approximately 0.5 ad 2.9s, which is considerably longer than T_2 values obtained from peak widths and more along the values expected for this kind of system. Similarly, the ^{1}H T_2 times measured on the 2-aminophenol using

CPMG are order of magnitude longer than the ones obtained from peak widths and more similar to ^{1}H T_1 as one would expect for small molecules in solution.

The CPMG-derived ^{1}H T_2 times of both "free" and "bound" aniline in the presence of stationary phases are all shorter compared to analogous times measured in the absence of stationary phase, which is not always the case for the T_2 times evaluated from peak widths. Furthermore, the CPMG-derived T_2 values for "bound" aniline are shorter by approximately one order of magnitude compared to the "free" aniline consistent with restriction of rotation induced by the interaction with stationary phase. The CPMG-derived ^{1}H T_2 times for 2-aminophenol in "solution only" are also in general longer than ^{1}H T_2 times for 2-aminophenol in the presence of stationary phases except the CSH hexyl-phenyl phase (we'll discuss this case below).

Our results suggest that the line widths we observe have contribution between 2 to 14 Hz that is either due to inhomogeneous broadening or unresolved scalar couplings. Since using peak widths to estimate T_2 does not appear sufficiently accurate for our purposes, in this project, we only employ CPMG for T_2 relaxation measurements.

Table 7.6. ^{1}H T_2 relaxation measured using CPMG and peak width analysis of 0.5 M aniline in the 50:50 % v/v MeCN:D_2O (from top to bottom according to HPLC elution order): mobile phase in the absence of stationary phases (solution only) and in the presence of BEH-C18, BEH-phenyl, BEH-RP18, CSH hexyl-phenyl and HSS T3 stationary phases. HR-MAS data were obtained at 500 MHz spectrometer at 313 K and 5.0 kHz spinning frequency.

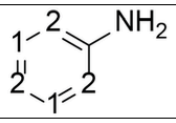

SP	HPLC Rt (mins)	^{1}H T_2 from CPMG (s)						^{1}H T_2 from line width (s)					
		H_1(f)	H_1(b)	H_2(f)	H_2(b)	NH_2+H_2O (f)	NH_2+H_2O (b)	H_1(f)	H_1(b)	H_2(f)	H_2(b)	NH_2+H_2O (f)	NH_2+H_2O (b)
Solution only		2.8±0.4	n/a	2.9±0.4	n/a	0.6±0.11	n/a	0.1±0.02	n/a	0.1±0.02	n/a	0.1±0.01	n/a
BEH-C18	3.58	1.6±0.2	0.1±0.02	1.6±0.2	0.1±0.02	0.7±0.13	0.1±0.04	0.1±0.02	0.02±0.003	0.1±0.02	0.02±0.003	0.1±0.01	0.01±0.01
BEH-Phenyl	3.67	1.5±0.2	0.1±0.02	1.6±0.2	0.1±0.01	1.0±0.21	0.1±0.1	0.1±0.02	0.02±0.003	0.1±0.02	0.02±0.003	0.1±0.01	0.02±0.001
BEH-RP18	3.73	1.3±0.2	0.1±0.02	1.3±0.2	0.1±0.02	0.8±0.15	0.1±0.1	0.1±0.02	0.02±0.003	0.1±0.02	0.01±0.002	0.1±0.02	0.01±0.01
CSH hexyl phenyl	3.80	1.5±0.2	0.1±0.02	1.6±0.2	0.1±0.02	0.6±0.11	0.1±0.1	0.1±0.02	0.01±0.002	0.1±0.01	0.02±0.003	0.1±0.01	0.01±0.01
HSS T3	4.22	1.2±0.2	0.2±0.02	1.2±0.2	0.1±0.2	0.5±0.10	0.1±0.04	0.1±0.02	0.01±0.002	0.1±0.01	0.01±0.02	0.1±0.02	0.02±0.01

Because in our experiments we observe analytes in different chemical exchange regimes, we need to consider how this affects the measured relaxation rates.

In the slow exchange regime, T_2 for both bound and free analyte can be obtained provided the peaks are well resolved. The CPMG-derived T_2 times of aniline in the absence of stationary phases given in Table 7.6 can be used as a reference relaxation time where no exchange process with stationary phase is possible. The data in Table 7.6 show that for both the "free" and "bound" aniline the CPMG-derived T_2 relaxation times in the presence of stationary phase are shorter compared to aniline in solution only due to exchange contribution to the rate induced by transient interaction. Shorter T_2 indicates longer correlation time for the overall tumbling and/or presence of exchange process. The relaxation times for "bound" aniline are consistent with them representing molecules adsorbed on the stationary phase are shorter by an order of magnitude compared to "free" peaks.

Table 7.7. ^{1}H T_2 relaxation times for 0.5 M 2-aminophenol in 50:50 % v/v MeOH:D_2O (from top to bottom according to HPLC elution order): mobile phase measured using CPMG and estimated from peak widths in the absence of stationary phases (solution only) and in the presence of BEH-C18, BEH-phenyl, BEH-RP18, CSH hexyl-phenyl and HSS T3 stationary phases. HR-MAS data were obtained at 500 MHz spectrometer at 313 K and 5.0 kHz spinning frequency.

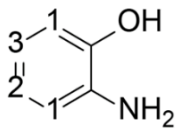

SP	HPLC Rt (mins)	^{1}H T_2 from CPMG (s)				^{1}H T_2 from line width (s)			
		H_1(a)	H_2(a)	H_3(a)	MeOH(a)	H_1(a)	H_2(a)	H_3(a)	MeOH(a)
Solution only		2.5±0.3	2.4±0.2	2.3±0.2	4.4±0.4	0.1±0.01	0.1±0.01	0.1±0.01	0.1±0.01
BEH-C18	3.13	1.6±0.2	1.5±0.2	1.6±0.2	2.4±0.2	0.1±0.01	0.1±0.01	0.1±0.01	0.1±0.01
BEH-RP18	3.34	1.6±0.2	1.7±0.2	1.5±0.2	2.8±0.3	0.1±0.01	0.1±0.01	0.1±0.01	0.1±0.01
HSS T3	3.56	1.5±0.2	1.5±0.2	1.4±0.1	2.6±0.3	0.1±0.01	0.1±0.01	0.1±0.01	0.1±0.01
BEH-Phenyl	3.59	1.7±0.2	1.7±0.2	1.7±0.2	2.6±0.3	0.1±0.01	0.1±0.01	0.1±0.01	0.1±0.004
CSH hexyl phenyl	3.81	2.2±0.2	2.3±0.2	2.2±0.2	3.0±0.3	0.1±0.01	0.1±0.01	0.1±0.01	0.1±0.01

In the fast exchange regime where only one resonance is observed at the average position for the chemical shifts in the bound and free form, the measured T_2 reflects the population weighted average of relaxation times in the two environments [240]:

$$\frac{1}{T_2^{avg}} = \frac{p_F}{T_2^F} + \frac{p_B}{T_2^B} \tag{7.3}$$

where p_F and p_B are the populations of the molecules in, respectively, free and bound state, T_2^F is the T_2 for free analyte and T_2^B is the T_2 for the bound analyte.

For 2-aminophenol, which is mostly in the fast exchange regime, the CPMG-derived ^{1}H T_2 relaxations times measured in solution only are longer than those measured in the presence of stationary phases. The shortest ^{1}H T_2 relaxation times were observed for 2-aminophenol in the presence of HSS-T3 stationary phase and the longest in the presence of CSH hexyl phenyl stationary phase (see Table 7.7). Interestingly, 2-aminophenol has the longest retention time on CSH hexyl phenyl SP but the retention time on HSS-T3 SP is in the "middle of the pack" (see Table 7.7).

However, there is one observation that does not seem to make much physical sense: some of the T_2 times measured for 2-aminophenol in the presence of CSH-hexyl-phenyl SP appear longer than T_2 times measured in the absence of any stationary phase. As we will see below this can be explained and points us towards limitations of the approach proposed so far.

In general, relaxation measurements are dependent on the time scale and amplitude of motion. For a molecule tumbling freely in solution the overall motion will dominate the measured relaxation rate and the molecule will sample all possible orientations with respect to the direction of the magnetic field in a very short amount of time [357]. The so far unspoken in our discussion and, in fact, most related studies in the literature is the assumption that because of the transient nature of the interactions between analytes and stationary phases, as a result of the interaction, only the effective correlation time will be affected and not really the amplitude – it is expected that the molecules will still sample all possible orientation just like the free molecules in solution. However, if sufficiently strong interactions are present the amplitude of the motion may be also affected with at least some of the interactions (we have to remember that typically multiple interaction contribute to retention mechanism) preventing the adsorbed molecule from sampling all possible orientations. We propose this to be the case for 2-aminophenol interacting with CSH-hexyl-phenyl SP. However, we have observed an even clearer case of such phenomenon for some bulky analytes employed in our study. Table 7.8 lists the ^{1}H T_2 relaxation times of meclizine in 50:50 % v/v MeOH:D_2O mobile phase in the absence of any stationary phase (solution only) and in the presence of our five stationary phases. For some protons in meclizine in the presence of stationary phases the measured T_2 is longer compared to the T_2 measured in the absence of any stationary phase, which is not physically possible in case where only effective correlation time is affected by the interaction. The only physically plausible explanation of this observation is that strong interaction of the analyte with stationary phase leads to partial immobilisation of the

molecule, which causes decrease of the amplitude of motion. This interpretation is consistent with the fact that meclizine sticks to the stationary phases in HPLC under employed conditions and does not elute (see Chapter 8).

To quantify generalised amplitude of motion one can use so called order parameter, S^2, which takes values between 0 and 1 with 0 indicating unrestricted motion and 1 indicating complete rigidity [355, 357-359]. Meclizine tumbling freely in solution will sample all possible orientations with the order parameter for this motion being equal to 0. If meclizine interact transiently with a stationary phase then it can still sample all possible orientations with the amplitude of the motions being characterised by $S^2 = 0$ but will have longer effective correlation time. In such a case, in the presence of stationary phase, the measured T_2 would decrease [240]. However, if meclizine is arrested for longer periods of time in specific orientations the effective S^2 will become greater than 0. In that case we will have two competing effects: increase in S^2 will result in increase of T_2 but the increase in the effective correlation time will result in decrease of T_2. In cases, where the effect of the changing amplitude of motion becomes dominant the T_2 measured in the presence of stationary phase will be longer than T_2 measured in the absence of stationary phase. Such ambiguity means that under some conditions and without sufficient data constructing a complete picture of the internal dynamics from T_1 and T_2 relaxation may be challenging or even impossible [357].

Table 7.8. ^{1}H T_2 relaxation of meclizine in 50:50 % v/v MeOH:D_2O (from top to bottom according to HPLC elution order): mobile phase in the absence of stationary phase (solution only) and in the presence of BEH-C18, BEH-phenyl, BEH-RP18, CSH hexyl-phenyl and HSS T3 stationary phases. HR-MAS data were obtained at 500 MHz spectrometer at 313 K and 5.0 kHz spinning frequency.

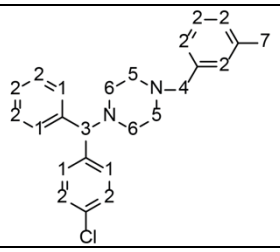

	T_2 (s)					
Peak assignment	Solution only	BEH-C18	BEH-Phenyl	BEH-RP18	CSH-Phenyl	HSS T3
H-1 (average)	0.7±0.07	1.0±0.1	0.8±0.08	0.8±0.08	0.7±0.07	0.7±0.2
H-2 (average)	0.9±0.09	0.9±0.09	0.8±0.08	0.7±0.07	0.7±0.07	0.3±0.3
H-3 (average)	0.4±0.04	0.5±0.05	0.4±0.04	0.4±0.04	0.7±0.2	0.4±0.05
H-4 (average)	0.3±0.03	0.3±0.03	0.3±0.02	0.3±0.03	0.3±0.03	0.3±0.03
H-5 (average)	0.2±0.02	0.2±0.02	0.2±0.02	0.2±0.02	0.2±0.02	0.2±0.02
H-6 (average)	0.2±0.02	0.1±0.01	0.2±0.02	0.1±0.01	0.2±0.02	0.2±0.02
H-7 (average)	0.7±0.07	0.9±0.09	0.7±0.07	0.7±0.07	0.7±0.07	0.7±0.07

7.16 Chemical exchange

As we have mentioned above binding of analyte to stationary phase can be considered at least a two-site exchange process between free (F) and bound (B) forms:

$$F \underset{k_2}{\overset{k_1}{\rightleftharpoons}} B \tag{7.4}$$

where k_1 is the rate constant of analyte adsorption onto the stationary phase and k_2 is the rate constant of analyte desorption from the stationary phase. In such case, the equilibrium constant for the process can be expressed as:

$$K_{eq} = \frac{k_1}{k_2} = \frac{I_B}{I_F} \tag{7.5}$$

where I_F and I_B are the integrated intensities of peak for the free and bound analyte, which are proportional to the populations of molecules in these states [240]. Consequently, for an analyte in the slow exchange regime, when peaks in different environments are well resolved, it should be possible, in principle, to obtain K_{eq} for the process. For instance, the relative integrals of peaks for "free" and "bound" forms (normalised to the "free" form integrals) and K_{eq} rate constant for aniline in the 50:50 (% v/v) MeCN:D_2O mobile phase in presence of BEH-C18, BEH-phenyl, BEH-RP18, CSH hexyl-phenyl and HSS T3 stationary phases is listed in Table 7.9. Overall, the equilibrium constants estimated from H-2 protons integrals are larger compared to the equilibrium constants estimated from H-1 integrals. This would suggest that the population of molecules interacting through H-2 protons is larger than the population of molecules interacting through H-1 protons, i.e. the probability of interaction through H-2 protons is higher than interaction through H-1 protons. In turn, this could indicate that the H-2 protons dominate the retention mechanism of aniline across all considered stationary phases.

Table 7.9. Relative integrals and equilibrium constants for aniline in 50:50 % v/v MeCN:D_2O (from top to bottom according to HPLC elution order): mobile phase in the presence of BEH-C18, BEH-phenyl, BEH-RP18, CSH hexyl-phenyl and HSS T3 stationary phases. HR-MAS data were obtained at 500 MHz spectrometer at 313 K and 5.0 kHz spinning frequency.

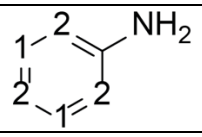

SP	HPLC Retention time (mins)	I_F		I_B		K_{eq}	
		H-1(f)	H-2(f)	H-1(b)	H-2(b)	H-1	H-2
BEH-C18	3.58	1.00	1.00	0.38	0.50	0.38	0.50
BEH-Phenyl	3.67	1.00	1.00	0.50	0.54	0.50	0.54
BEH-RP18	3.73	1.00	1.00	0.26	0.31	0.26	0.31
CSH hexyl phenyl	3.80	1.00	1.00	0.47	0.62	0.47	0.62
HSS T3	4.22	1.00	1.00	0.30	0.37	0.30	0.37

Even though this way to gain insights into the interactions between analytes and stationary phases is relatively quick and simple, it also comes with several limitations. To calculate the equilibrium constants we assumed a two site exchange model, but often multiple site exchange needs to be considered [95]. Also overlapping peaks complicate the estimation of equilibrium constant. However, such information may be useful in specific cases where it is available.

In principle, in the slow exchange it could be also possible to extract the rates for adsorption and desorption of the analyte as the transverse relaxation rates are expressed as:

$$\frac{1}{T_{2,F}^{obs}} = R_{2,F}^{obs} = R_{2,F}^{0} + k_1 \text{ and } \frac{1}{T_{2,B}^{obs}} = R_{2,B}^{obs} = R_{2,B}^{0} + k_2 \qquad (7.6)$$

where $R_{2,F}^{0}$ and $R_{2,B}^{0}$ are contribution to transverse relaxation from the overall tumbling in the absence of exchange process, and k_1 and k_2 are respectively rates of adsorption and desorption of the analyte onto the stationary phase. However, even though $R_{2,F}^{0}$ could be, to a good approximation, estimated from T_2 measured in the absence of stationary phases, it is difficult to obtain a similar estimate for $R_{2,B}^{0}$. Thus rates of adsorption of analyte onto stationary phases could be estimated in a straightforward manner but rates of desorption are far more challenging to obtain.

Obviously, if the analyte is in the fast exchange regime as, e.g., 2-aminophenol, equilibrium constant cannot be estimated from peak integrals as only a single peak is observed at a frequency corresponding to the population weighted average of the chemical shift in the two environments:

$$\omega = p_F\omega_F + p_B\omega_B \tag{7.7}$$

where p_F and p_B are the populations of the molecule in the free and bound states, ω_F and ω_B are the chemical shift of the molecule in free and bound state.

For the analyte in fast exchange it is not easy to extract the rates for adsorption and desorption because the observed relaxation rate $R_2^{obs}(1/T_2^{obs})$ is expressed as:

$$R_2^{obs} = R_2^0 + \frac{p_F p_B(\Delta\omega)^2}{k_{ex}} \tag{7.8}$$

where R_2^0 $(1/T_2^0)$ is transverse relaxation in the absence of exchange, p_F and p_B are the populations of molecule in the free and bound state, $\Delta\omega$ is the chemical shift difference for the molecule in the free and bound states, k_{ex} is the exchange rate ($k_{ex} = k_1 + k_2$). Typically, the number of the correlated unknown variables is too large to obtain the relative populations in the different states.

7.17 Combined application of ^{1}H T_1 and T_2 to probe analyte interactions

As it can be seen from the discussion so far because of the various factors contributing to relaxation rates as well as averaging effects it might not be easy to understand what is happening when using a single relaxation probe. Because ^{1}H T_1 and T_2 depend differently on the time scale of motion and are differently affected by the presence of chemical exchange their combined application may increase our chances of understanding the processes occurring in the chromatographic system. For example, because T_2 decreases monotonically with the increasing correlation time when paired with T_1 it can aid resolving ambiguity of whether the correlation time is below or above the T_1 minimum (see Figure 7.1). In addition, by examining both T_1 and T_2 one might have an easier time to identify the cases where changes in amplitude of motion play a significant role in

addition to the changes in the effective correlation time as a result of interaction. Finally, the combination of the two parameters may help to interpret the behaviour of the molecules in the different exchange regimes observed in the RP HPLC systems.

Table 7.10 lists together ^{1}H T_1 and T_2 relaxation times for aniline in 50:50 % v/v MeCN:D_2O mobile phase in the absence of stationary phases and in the presence of BEH-C18, BEH-phenyl, BEH-RP18, CSH hexyl-phenyl and HSS T3 stationary phases. More than two times shorter ^{1}H T_2 compared to T_1 in the absence of stationary phase suggest that the correlation time for overall tumbling of aniline is longer than the T_1 minimum, which in turn means that under the considered conditions aniline exists in oligomeric rather than monomeric state (i.e. the correlation time is more consistent with tumbling species with the molecular weight/size larger than monomer of aniline). The apparent ^{1}H T_1 times for "free" aniline in the presence of all stationary phases appear to be generally longer than "solution only" values and the ^{1}H T_2 times for "free" aniline in the presence of all stationary phases appear to be generally 2-fold shorter than "solution only" values which is either due to longer tumbling correlation time or exchange processes. As illustrated in Table 7.10, the ^{1}H T_2 of the bound aniline molecules are approximately 10-fold shorter than free aniline in the presence of stationary phases which suggest restricted motion of aniline molecules onto the stationary phases due to transient interactions.

In general, there is no easy link between the ^{1}H T_1 or T_2 relaxation measurements and HPLC retention times of aniline across the five stationary phases. However, the largest change of ^{1}H T_2 was observed between the free aniline in solution only and in the presence of HSS T3 across both H-1 and H-2 protons. Likewise, the longest HPLC retention time of aniline was also observed in the presence of HSS T3. This is unsurprising as HSS T3 is known to provide superior polar compound retention due to its T3 endcapping process which has proven more effective than trimethylsilane (TMS) endcapping [329, 360-362]. Additionally, the HSS T3 stationary phase used in this study is reported to have a higher surface area compared to the remaining stationary phases (230 m^2/g compared to 185 m^2/g) which can yield higher ligand density and thus higher retention [177, 363-365]. Furthermore, the ^{1}H T_2 relaxation times of free aniline in the presence of BEH-RP18 stationary phase are slightly shorter compared to BEH-C18, BEH-Phenyl and CSH hexyl-phenyl stationary phases. This difference in the presence of BEH-RP18 could potentially be attributed to Van der Waals and hydrogen bonding interactions from the polar embedded polar embedded groups [292, 366-369]. Generally,

the ^{1}H NMR data of aniline suggests hydrophobic, Van der Waals and hydrogen bonding interactions dictates the retention mechanism of aniline across all five stationary phases.

The ^{1}H T_1 and T_2 relaxation times for 2-aminophenol in 50:50 % v/v MeOH:D_2O mobile phase, where is in the fast exchange regime, and in the presence of different stationary phase is presented in Table 7.11. The ^{1}H T_1 relaxation times for 2-aminophenol in solution only and in the presence of stationary phase are similar and generally shorter except for the case of BEH-C18 SP where they are longer (2-aminophenol is the least retained on BEH-C18 SP under these conditions – see Chapter 8).

Table 7.10. ^{1}H T_1 and T_2 relaxation times for aniline in 50:50 % v/v MeCN:D_2O (from top to bottom according to HPLC elution order): mobile phase in the absence of stationary phase (solution only) and in the presence of BEH-C18, BEH-phenyl, BEH-RP18, CSH hexyl-phenyl and HSS T3 stationary phases. Data were obtained at 500 MHz spectrometer at 313 K and 5.0 kHz spinning frequency.

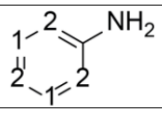

SP	HPLC Rt (mins)	^{1}H T_1 (s)*						^{1}H T_2 (s)					
		H_1(f)	H_1(b)	H_2(f)	H_2(b)	NH_2+H_2O (f)	NH_2+H_2O (b)	H_1(f)	H_1(b)	H_2(f)	H_2(b)	NH_2+H_2O (f)	NH_2+H_2O (b)
Solution only		6.4 ± 0.3	n/a	7.0 ± 0.4	n/a	8.6±1.7	n/a	2.8±0.4	n/a	2.9±0.4	n/a	0.6±0.1	n/a
BEH-C18	3.58	7.4 ± 0.4	3.9 ± 0.2	8.0 ± 0.4	3.9 ± 0.2	7.0±1.4	2.8±1.4	1.6±0.2	0.1±0.02	1.6±0.2	0.1±0.02	0.7±0.1	0.07±0.04
BEH-Phenyl	3.67	7.6 ± 0.4	4.1 ± 0.2	8.7 ± 0.4	4.8 ± 0.2	8.3±1.7	3.4±1.7	1.5±0.2	0.1±0.02	1.6±0.2	0.1±0.01	1.0±0.2	0.11±0.06
BEH-RP18	3.73	7.5 ± 0.4	4.0 ± 0.2	8.1 ± 0.4	3.7 ± 0.2	7.5±1.5	3.5±1.8	1.3±0.2	0.1±0.02	1.3±0.2	0.1±0.02	0.8±0.2	0.12±0.06
CSH hexyl phenyl	3.80	6.7 ± 0.3	3.7 ± 0.2	7.5 ± 0.4	4.3 ± 0.2	6.7±1.3	3.4±1.7	1.5±0.2	0.1±0.02	1.6±0.2	0.1±0.02	0.6±0.1	0.10±0.05
HSS T3	4.22	8.4 ± 0.4	6.1 ± 0.3	7.9 ± 0.4	5.6 ± 0.3	5.3±1.1	2.9±1.4	1.2±0.2	0.2±0.02	1.2±0.2	0.1±0.02	0.5±0.1	0.08±0.04

Overall, the largest changes in ^{1}H T_1 are observed for the H-2, which also follow the elution order observed in HPLC experiments (see Table 7.11), which could suggest that H-2 reports on the interaction that is mainly responsible for the different retention on the considered set of stationary phases. The correlation of the ^{1}H T_2 to HPLC retention data is less clear. Overall, there are no strong systematic differences between 2-aminophenol on different stationary phases. The most distinct is the set of T_2 times on CSH-hexyl-phenyl SP, which are the closest to the "solution only" values with H-3 being slightly larger potentially pointing to slightly preferred orientation for the interacting analyte. Again, 2-aminophenol is the most retained on CSH-hexyl-phenyl SP. Another aspect to point out is that the aromatic protons are in a slow exchange on BEH-phenyl and CSH-hexyl-phenyl SPs, which are also characterised by the longest retention times of 2-aminophenol. Overall, the data suggest that one of the main factors for this molecule that determines the elution order is the polarity (i.e. the compound is more retained on

stationary phases according to their selectivity for polar interactions) with extra contribution from π-π stacking on stationary phases with aromatic functional groups.

Table 7.11. ^{1}H T_1 and T_2 relaxation for 2-aminophenol in 50:50 % v/v MeOH:D_2O (from top to bottom according to HPLC elution order): mobile phase in the absence of stationary phases (solution only) and in the presence of BEH-C18, BEH-phenyl, BEH-RP18, CSH hexyl-phenyl and HSS T3 stationary phases. Data were obtained at 500 MHz spectrometer at 313 K and 5.0 kHz spinning frequency.

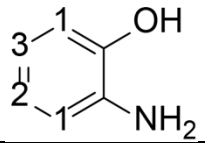

SP	HPLC Rt (mins)	^{1}H T_1 (s)					^{1}H T_2 (s)			
		H-1(a)	H-2(a)	H-3(a)	NH_2+H_2O (a)	MeOH (a)	H-1(a)	H-2(a)	H-3(a)	MeOH (a)
Solution only		4.3±0.2	3.8±0.2	3.9±0.2	6.4±0.6	7.2±1.8	2.5±0.3	2.4±0.2	2.3±0.2	4.4±0.4
BEH-C18	3.13	4.5±0.2	4.4±0.2	4.1±0.2	5.6±0.6	5.3±1.3	1.6±0.2	1.5±0.2	1.5±0.2	2.4±0.2
BEH-RP18	3.34	4.3±0.2	3.9±0.2	3.7±0.2	5.8±0.6	5.4±1.4	1.6±0.2	1.7±0.2	1.5±0.2	2.8±0.3
HSS T3	3.56	4.0±0.2	3.8±0.2	3.9±0.2	5.9±0.6	5.3±1.3	1.5±0.2	1.5±0.2	1.4±0.1	2.6±0.3
BEH-Phenyl	3.59	4.2±0.2	3.5±0.2	3.6±0.2	7.5±0.8	7.7±1.9	1.7±0.2	1.7±0.2	1.7±0.2	2.6±0.3
CSH hexyl phenyl	3.81	4.2±0.2	3.4±0.2	3.9±0.2	6.5±0.7	6.7±1.7	2.2±0.2	2.3±0.2	2.2±0.2	3.0±0.3

7.18 Conclusion

In this Chapter we have explored the use of ^{1}H T_1 and T_2 relaxation times for probing the nature of interactions between analytes and stationary phases. We have critically evaluated the basic premise of our approach that changes in molecular motions of analytes due to interactions with stationary phases can be used to indirectly report on the interactions. We have shown that a whole range of chemical exchange regimes, from slow to fast exchange, can be observed for analytes interacting with stationary phases. We have also demonstrated that different sites in molecules can exhibit exchange in different regime at the same time. We have shown that the chemical exchange regime and strength of the interaction can lead to different effects on the measured relaxation rates.

T_1 relaxation was investigated to probe the molecular interactions between aniline, 2-aminophenol and various HPLC stationary phases. We have established, hinderance of rotation due to transient interactions leads to shorter T_1 times only if the correlation times

for overall rotational diffusion of free and interacting analyte are in the fast motion limit. However, interpreting T_1 times can be complex when the correlation time is over a range of values.

Two approaches of estimating T_2 relaxation times were investigated. Due to additional contributions from magnetic field inhomogeneities and unresolved long range ^{1}H-^{1}H scalar couplings, the T_2 relaxation times obtained using peak widths based method were generally underestimated. The T_2 relaxation values using CPMG pulses sequence were more representative of what we would expect for this kind of chromatographic system. To obtain accurate, reliable and reproducible ^{1}H T_2 relaxations measurements, data throughout this project were acquired using CPMG pulse sequence.

We established that the challenging nature of the problem where the changes in time scale and amplitude of motion as a result of interaction have complex effects on the measured rates and contribute in a different way in different exchange regimes, often requires that we consider both T_1 and T_2 in order to get insights into the complex interdependencies for different interactions between analytes and stationary phase.

At the same time we learned that, in spite of this complexity, we can gain considerable understanding of the retention mechanisms for different analytes provided that we are aware of the basic assumptions and limitations of the proposed approach. For example, we can discover which parts of molecules are most affected on different stationary phases and thus potentially link that insight to specific types of interactions. In addition, in favourable cases we can get an idea if adsorption or if favourable orientations takes place on stationary phases.

Finally, we established the equilibrium constants are obtainable for an analyte in the slow exchange regime with well resolved peaks. Although this approach is quick and simple for probing the interactions between analytes and stationary phases, it does come with several limitations. For instance, overlapping peaks complicates the estimations of the equilibrium constants and if the analyte is in the fast exchange regime the equilibrium constants are not obtainable.

In the absence of simple “one fits all” approach we established that analysis combining both ^{1}H T_1 and T_2 relaxation times is the most robust and informative from all the considered approaches. This best approach will be used to study interactions of the analytes with stationary phases for the remainder of discussions.

8 PROBING THE INTERMOLECULAR INTERACTIONS IN RP-HPLC BY NMR RELAXATION

8.1 Abstract

Following the investigation of relaxation approaches (Chapter 7) for utility in gaining insights of molecular interactions between analytes and stationary phases in RP-HPLC, in the work presented here, the ^{1}H HR MAS NMR relaxation measurement approach was used. 15 analytes, 2 mobile phases and 5 RP-HPLC stationary phase combinations were examined and comparisons of the relaxation measurement data with HPLC were made.

8.2 Introduction

For years, it was assumed that hydrophobic interactions were responsible for the only retention mechanisms, where the stationary phase plays a passive role and the mobile phase controls the separation [370]. However, it was discovered that several additional interactions could take place on the stationary phase [371-379]. For instance, residual ionised silanols (-SiO^{-}) can retain protonated bases via cation-exchange, and neutral silanols (-SiOH) can interact with proton-acceptor solutions by hydrogen bonding interactions [380]. Furthermore, several additional interactions can contribute to the RP-HPLC retention mechanism such as hydrogen bonding between basic (acceptor) analytes and acidic (donor) column groups, hydrogen bonding between acidic analytes and basic

column groups, column shape selectivity [381], cation-exchange, ionic interactions and π-π stacking. Many of these interactions are not incorporated into the solvation equation model [382]. However, a more advanced model known as the Hydrophobic Subtraction Model (HSM) of selectivity reflects these several interactions [371, 375]:

$$\log \alpha = \log\left(\frac{k}{k_{EB}}\right) = \eta'\boldsymbol{H} - \sigma'\boldsymbol{S}^* * + \beta'\boldsymbol{A} + \alpha'\boldsymbol{B} + \kappa'\boldsymbol{C} \qquad (8.1)$$

where k is the retention factor of an analyte, k_{EB} is the k value of a non-polar reference (e.g. ethylbenzene) under identical experimental conditions, the rest of the equation symbols represent either empirical, eluent and temperature-dependent properties of the analytes (η',σ', β', α', κ') or eluent and temperature independent properties of the stationary phase (H, S*, A, B, C) [370]. These parameters measure the physico-chemical nature of numerous stationary phases: H for hydrophobicity, S* represents the steric hindrance of bulky analyte molecules, A stationary phase hydrogen-bond acidity, B stationary phase hydrogen-bond basicity, C cation-exchange activity. The other parameters represent chemical properties of analyte; η' analyte hydrophobicity, σ'analyte bulkiness, β' hydrogen-bond basicity, α' hydrogen-bond acidity and κ' overall charge of the analyte. The parameters of these analytes are relative to the values of ethylbenzene (non-polar reference). The five terms (a to e) of Equation 8.1 represent five interactions which take place between an analyte and stationary phase (*see Figure 8.1*). Terms a and c - e are attractive interactions and therefore positive. However, term b is repulsive interaction and thus is negative [375].

In recent years, our understanding of such interactions has evolved by characterising and probing the molecular dynamics of various HPLC stationary phases via several NMR spectroscopy techniques. Both solution and solid-state NMR (^{1}H HRMAS, ^{13}C and ^{29}Si MAS CP NMR) were previously used to characterise the chemical arrangement of a variety of stationary phases. ^{1}H HRMAS NMR T_1 and T_2 relaxation techniques have been developed and were used successfully for probing such RP-HPLC interactions. One major advantage of HRMAS NMR technique is that the measurements can be obtained both on the analyte with mobile phase only (homogenous system) and analyte with mobile and stationary phase (heterogeneous system) to probe the strength of molecular dynamics (interaction) in different environments. However, a logical and in-depth understanding

between a variety of analytes, mobile and stationary phases remains a mystery. The primary aim of this study was to obtain an atomic scale measure of the type of interactions which take place between a series of analytes and RP-HPLC stationary phase. This data would either complement or improve our understanding of RP-HPLC experimental data obtained under similar conditions.

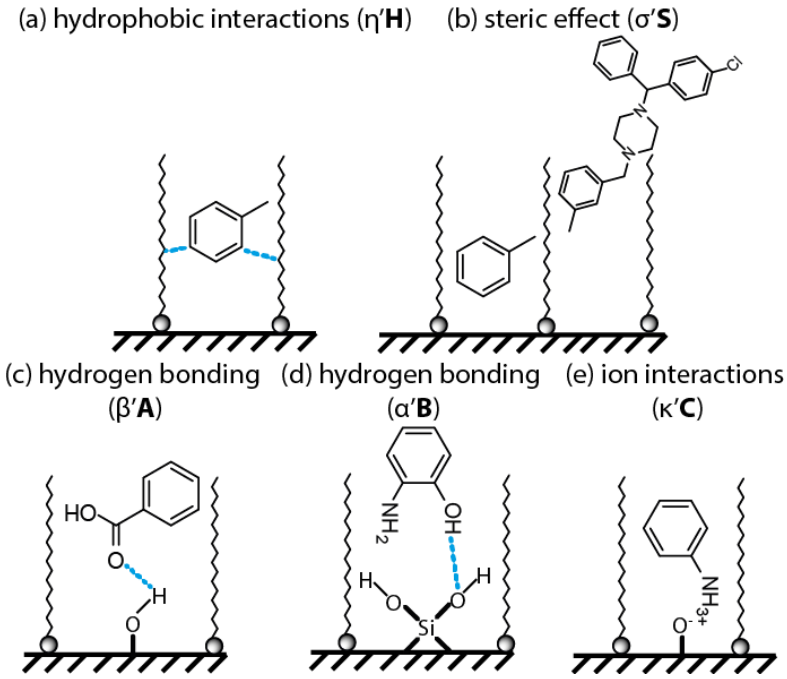

Figure 8.1. Visual representation of the analyte-stationary phase interactions of Equation 8.1.

The ^{1}H HRMAS NMR relaxation measurements obtained in this study were compared to HPLC retention times. This approach could theoretically provide further information about the contributions to the RP-HPLC retention.

8.3 Experimental Methods

A series of 15 analytes were investigated as shown in Figure 8.2 includes: (i) toluene, (ii) naphthalene, (iii) acenaphthylene, (iv) benzophenone, (v) biphenyl, (vi) propranolol, (vii) 2-aminophenol, (viii) aniline, (ix) 3-hydroxybenzoic acid, (x) dipropyl phthalate, (xi) butyl 4-hydroxybenzoate, (xii) benzoic acid, (xiii) amitriptyline hydrochloride, (xiv) hydroxyzine dihydrochloride, (xv) meclizine dihydrochloride. DSS (4,4-dimethyl-4-silapentane-1-sulfonic acid) was added to the samples as an internal reference. The solvents used were deuterium oxide, acetonitrile and methanol. BEH-C_{18} (~17% w/w carbon loading), BEH-phenyl (~15% w/w carbon loading), BEH-RP_{18} (~16% w/w carbon

loading), CSH-phenyl (~14% w/w carbon loading) and HSS T_3 (~11% w/w carbon loading) stationary phases were taken from commercially available XBridge™ columns with particle size of 5 µm and average pore diameter of 145 Å. The molecular weight, pKa, molar volume, logP, logD, number of hydrogen bond donors and acceptors (data obtained from ACD labs) of all 15 analytes are listed in Table 8.1.

Table 8.1. Chemical and physical properties of 15 analytes investigated in this study.

Analytes	Molecular weight (g/mol)	pKa	Molar Volume (cm^3)	LogP	LogD	No. of *H* Bond Donors	No. of *H* Bond Acceptors
toluene	92.14	n/a	105.7 ± 3.0	2.68 ± 0.17	2.61	0	0
aniline	93.13	4.6 ± 0.4	91.7 ± 3.0	0.94 ± 0.19	1.13	2	1
2-aminophenol	109.13	4.6 ± 0.4 10.3 ± 0.4	90.1 ± 3.0	0.44 ± 0.21	0.59	3	2
Benzoic acid	122.12	4.1 ± 0.4	101.9 ± 3.0	1.89 ± 0.21	-0.63	1	2
naphthalene	128.17	n/a	123.5 ± 3.0	3.45 ± 0.16	3.37	0	0
3-hydroxybenzoic acid	138.12	4.0 ± 0.4 10.5 ± 0.5	100.3 ± 3.0	1.5 ± 0.22	-1.03	2	3
acenaphthene	154.21	n/a	134.9 ± 3.0	4.19 ± 0.2	4.01	0	0
biphenyl	154.21	n/a	154.7 ± 3.0	3.98 ± 0.23	3.76	0	0
benzophenone	182.22	n/a	167.5 ± 3.0	3.18 ± 0.29	2.98	0	1
Butyl 4-hydroxybenzoate	194.23	8.5 ± 0.4	175.2 ± 3.0	3.46 ± 0.22	3.21	1	3
Dipropyl phthalate	250.29	n/a	231.2 ± 3.0	3.76 ± 0.25	4.07	0	4
propranolol	259.34	13.9 ± 0.4 9.5 ± 0.4	237.1 ± 3.0	3.1 ± 0.25	0.18	2	3
amitriptyline	277.4	9.2 ± 0.28	257.7 ± 3.0	4.92 ± 0.64	2.55	0	1
hydroxyzine	374.9	14.8 ± 0.5 7.0 ± 0.5	317.1 ± 3.0	2.03 ± 0.84	2.61	1	4
Meclizine	390.95	5.9 ± 0.5	337.2 ± 3.0	4.99 ± 0.85	5.55	0	2

The column selectivity (hydrophobicity, steric selectivity, acidic, basic and cation exchange parameters) of the 5 RP-HPLC stationary phases used in this study are given in Table 8.2. The columns parameters (*H*, *S**, *A*, *B*, *C*)[370] were obtained from a column selectivity database available on www.hlpccolumns.org.

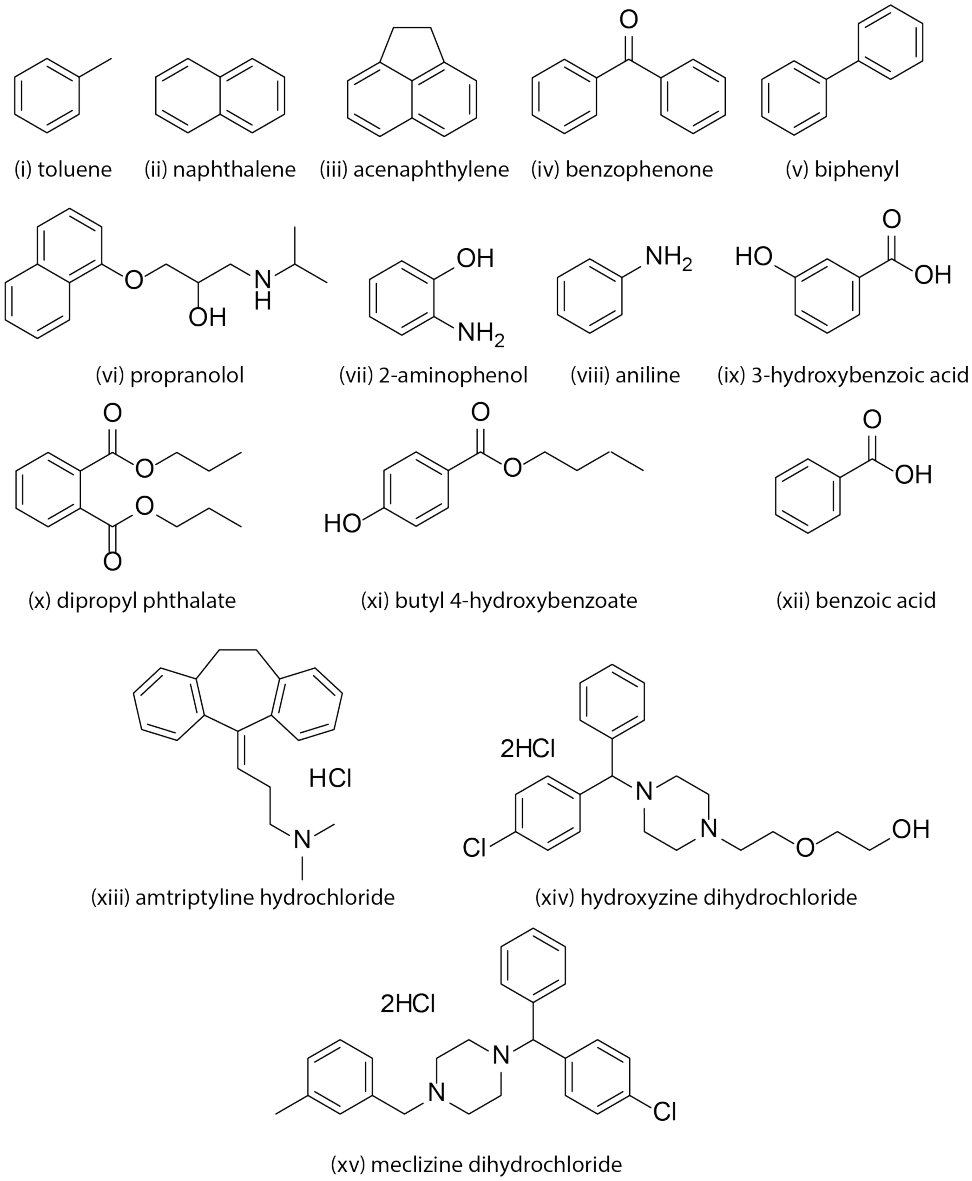

Figure 8.2. Chemical structures of all 15 analytes investigated in this study.

Table 8.2. RP-HPLC stationary phase selectivity parameters[370]

Column	*H*[1]	*S**[2]	*A*[3]	*B*[4]	*C(pH 2.8)*[5]	*C(pH 7.0)*[6]
BEH-C18	1.000	0.020	-0.090	0.000	0.170	0.130
BEH-phenyl	0.730	-0.070	-0.350	0.030	0.190	0.200
BEH-RP18	0.830	-0.020	-0.370	0.090	-0.120	-0.050
CSH hexyl-phenyl	0.708	-0.059	-0.435	0.129	-0.068	0.223
HSS T3	0.940	-0.020	-0.170	0.000	0.030	0.180

[1]*H,* column hydrophobicity, [2]*S*,* steric hindrance of bulky analyte molecules,[3]*A* stationary phase hydrogen-bond acidity,[4]*B* stationary phase hydrogen-bond basicity,[5]*C (pH 2.8)* cation-exchange activity and [6]*C (pH 7.0)* cation-exchange activity

8.3.1 HPLC Methods

The RP-HPLC experiments were carried out at Pfizer laboratories using a Waters Acquity UPLC equipped with both UV (PDA) and MS detectors. Each analyte was individually run through the five studied stationary phases. The mobile phase was either solvent A (acetonitrile:water) (HPLC grade) or solvent B (methanol:water) both with a volume ratio of 50:50 (% v/v). The chromatographic system A flow rate of 0.4 mL/min at a temperature of 40 °C was used. The concentrations of the analytes were 0.25 mg/mL.

8.3.2 NMR Methods

Stock solution of solvent "A" contained deuterium oxide (D_2O) and acetonitrile (MeCN) with a volume ratio of 50:50 was made. Solvent "B" was made of deuterium oxide (D_2O) and methanol (MeOH) with a ratio of 50:50. The analytes were dissolved in either solvent "A" or "B" to a concentration of 0.5 M. ^{1}H HRMAS NMR spectra of each analyte was obtained with the analyte in solution only and with the five stationary phases. For the analytes in solution only, 80 µL of the analyte was measured using an automated pipette and then placed into a 4-mm rotor (*see Figure 8.3*). For the analytes with added stationary phase, 10 mg of stationary phase is initially packed into the rotor followed by 60 µL of the dissolved analyte measured using an automated pipette which is then topped up with a further 10 mg of stationary phase (*see Figure 8.3*).

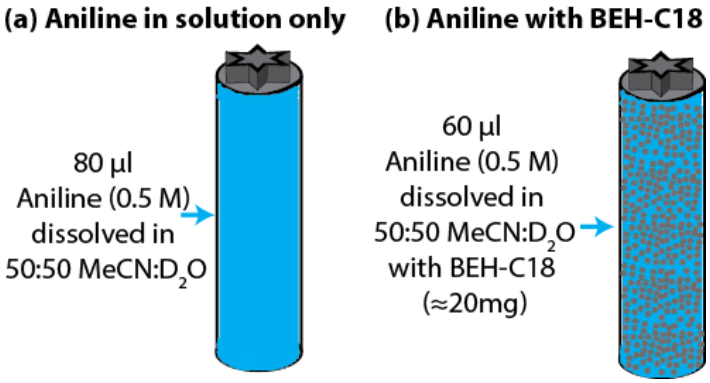

Figure 8.3. Illustration of (a) aniline in solution only and (b) aniline in the presence of BEH C18 stationary phase.

^{1}H MAS NMR experiments were conducted at a ^{1}H frequency of 500 MHz on a Bruker Avance II+ 500 spectrometer. The prepared samples were placed into 4 mm ZrO_2 MAS

rotors (Bruker Biospin, Rheinstetten, Germany) with no spacer. The rotor was spun using air at the magic angle (θ = 54.4°) at a spinning speed of 5 kHz and at a controlled temperature of 313 K. As a standard, 1D ^{1}H MAS NMR experiments were conducted using a 90° one-pulse sequence, where 8 transients were collected into a 20 k data points over a spectral width of 20000 Hz (40 ppm) with an acquisition time of 1 second. Exponential line-broadening of 0.5 Hz was applied before FT. All spectra were referenced to water peak at 313.15 K.

8.3.2.1 Longitudinal Relaxation (T_1) Measurements

^{1}H T_1 was also measured by using a saturation-recovery pulse sequence (saturation – τ – 90º– FID) with pulse nutation frequencies of 25 kHz. 8 transients were collected into 20 k data points over a spectral width of 20000 Hz (40 ppm) with an acquisition time of 1 seconds, relaxation delay of 2 seconds and with the recovery time ranging from 0 to 30 seconds. Exponential line-broadening of 2.0 Hz was applied before FT. The ^{1}H T_1 values were obtained by fitting the peak integrals as a function of recovery time to an exponential. Plots and calculations were performed using TopSpin 3.2 and Origin 9.3.

8.3.2.2 Transverse Relaxation (T_2) Measurements

^{1}H T_2 relaxation times were measured by using the CPMG pulse sequence (90° - [τ_1 – 180° – τ_1]n – FID) with a pulse nutation frequency of 25 kHz. 8 transients were collected into a 20 k data points over a spectral width of 20000 Hz (40 ppm) with an acquisition time of 1 second, relaxation delay of 16 seconds, τ_1 of 1.2 ms and the number of loops (n) were varied accordingly to obtain 100% to 30% of initial intensity. The ^{1}H T_2 values were obtained by fitting the peak integrals as a function of recovery time to an exponential. Plots and calculations were performed using TopSpin 3.2 and Origin 9.3.

8.4 Results and Discussion

The following data can be found in appendix of this chapter: ^{1}H HRMAS NMR spectra (*Figure A.5-A.19 in appendix*), ^{1}H-^{13}C HSQC, ^{1}H-^{13}C HMBC spectra (*Figure A.20-A.26*), RP-HPLC retention times (*Table A.3-A.4 in appendix*), T_1, T_2 relaxation values, (*Tables*

A.5-A.33 in appendix) of all 15 analytes in solution only and the presence of BEH-C18, BEH-phenyl, BEH-RP18, CSH hexyl-phenyl and HSS T3 RP-HPLC stationary phases.

8.4.1 T_1, T_2 weighted average against retention time

To investigate whether there is any simple correlation between the measured relaxation times and the retention times, which would allow grouping of the analytes into subcategories, we plotted the proton number weighted average ratio T_1 and T_2 against retention time in Figure 8.4.

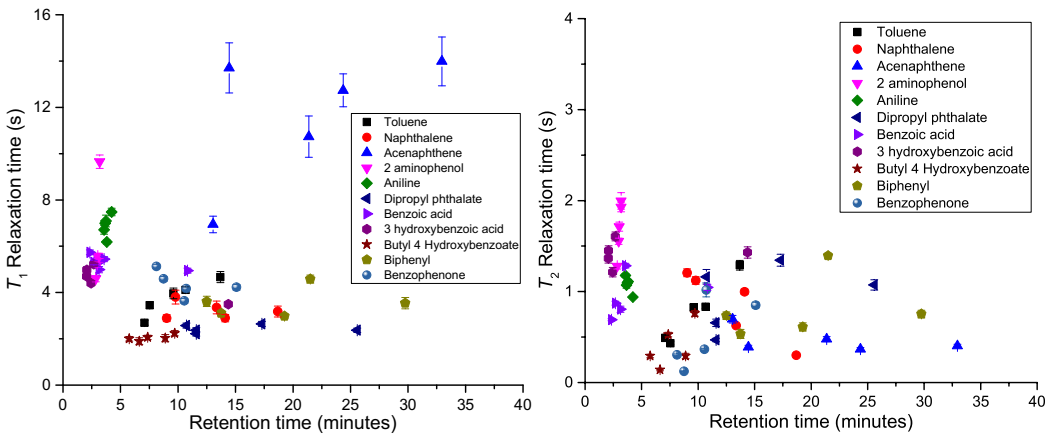

Figure 8.4. Plot of proton number weighted average of ^{1}H T_1 (left) and T_2 (right) against retention time of 11 analytes dissolved in 50:50 (% v/v) MeCN:D_2O in the presence of 5 RP-HPLC stationary phases. HR-MAS data were obtained at 500 MHz spectrometer at 313 K and 5.0 kHz spinning frequency.

Amitriptyline, hydroxyzine, meclizine and propranolol were strongly retained on the 5 stationary phases and if eluted, they could not be detected and thus could not be included onto the plots. Based on Figure 8.4 there is no strong clear correlation between the average of ^{1}H NMR relaxation data and HPLC retention time. As a result, the NMR and HPLC data of each analyte are considered on individual site-specific basis (i.e. comparing the relative effect on different sites of the molecule in the absence of an absolute scale).

8.4.2 Toluene

The measured ^{1}H T_1 and T_2 relaxation times of toluene are given in Table 8.3 and 8.4. Toluene is least and most retained in the presence of BEH-Phenyl and HSS T3 stationary phase, respectively. This elution order was observed across both 50:50 (% v/v) MeCN:H_2O and MeOH:H_2O mobile phases (see Table 8.3 and 8.4 respectively). With an increase in carbon chain, the retention time of toluene increases which could suggest the retention mechanism is driven by hydrophobic interactions. A majority of the analytes also follow the same HPLC elution orders of toluene. Additionally, most of the analyte have longer retention times in the presence of MeOH:H_2O mobile phase compared to MeCN:H_2O. Methanol is more polar compared to acetonitrile which explains the longer retention times. It is worth mentioning, the separation selectivity differs for acetonitrile and methanol. This is because methanol is a polar protic solvent capable of hydrogen bonding while acetonitrile a polar aprotic solvent not capable of forming hydrogen bond.

To supplement this assumption, the hydrophobicity subtraction model selectivity parameters of both and BEH-Phenyl (H = 0.730) and HSS T3 (H = 0.940) are compared in Table 8.5. Since toluene is a neutral analyte and cannot undergo ionic exchange, the retention mechanism of toluene is driven by hydrophobic interactions as illustrated in Table 8.5.

Table 8.3. ^{1}H T_1 and T_2 relaxation times for toluene in 50:50 % v/v MeCN:D_2O (from top to bottom according to HPLC elution order): mobile phase in the absence of stationary phase (solution only) and in the presence of BEH-C18, BEH-phenyl, BEH-RP18, CSH hexyl-phenyl and HSS T3 stationary phases. Data were obtained at 500 MHz spectrometer at 313 K and 5.0 kHz spinning frequency.

MeCN:D_2O 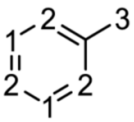 Toluene	SP	HPLC Rt (mins)	T_1(s)					
			H-1(f)	H-2(f)	H-3(f)	H-1(b)	H-2(b)	H-3(b)
	Solution only	n/a	6.4±0.1	6.5±0.1	6.4±0.1		n/a	
	BEH-Phenyl	7.08	3.5±0.3	2.6±0.2	3.8±0.3	2.6±0.1	2.4±0.1	2.8±0.1
	CSH Hexyl-phenyl	7.55	5.7±0.5	4.3±0.1	3.9±0.2	3.1±0.1	2.8±0.1	3.1±0.1
	BEH-RP18	9.61	6.8±0.5	6.2±0.5	4.8±0.2	3.3±0.2	3.1±0.2	2.5±0.1
	BEH-C18	10.66	5.6±0.1	5.1±0.1	4.6±0.1	3.6±0.2	3.4±0.2	3.0±0.1
	HSS T3	13.69	8.5±0.9	6.8±0.5	5.4±0.2	3.5±0.1	3.5±0.1	2.9±0.1
			T_2(s)					
			H-1(f)	H-2(f)	H-3(f)	H-1(b)	H-2(b)	H-3(b)
	Solution only	n/a	3.5±0.1	3.5±0.1	3.5±0.1		n/a	
	BEH-Phenyl	7.08	2.0±0.2	1.8±0.1	1.6±0.01	0.1±0.003	0.1±0.002	0.1±0.002
	CSH Hexyl-phenyl	7.55	1.3±0.1	1.0±0.04	1.1±0.1	0.1±0.003	0.1±0.002	0.1±0.002
	BEH-RP18	9.61	2.2±0.1	2.0±0.1	1.9±0.1	0.2±0.004	0.2±0.003	0.2±0.005
	BEH-C18	10.66	1.8±0.1	1.6±0.1	1.6±0.02	0.1±0.001	0.1±0.002	0.2±0.001
	HSS T3	13.69	2.4±0.1	2.7±0.2	2.5±0.1	0.3±0.002	0.3±0.005	0.5±0.003

The largest changes in ^{1}H T_1 of toluene dissolved in 50:50 (% v/v) MeCN:D_2O are observed for the H-1(f) and H-2(f) protons (see Table 8.3). Additionally, the largest

change in ^{1}H T_1 of toluene dissolved in 50:50 (% v/v) MeOH:D_2O is observed for the H-2(f) and H-2(b), which correlates to the elution order observed in HPLC experiments (see Table 8.4). Overall, the ^{1}H T_1 data could suggest that H-1 and H-2 dictates the interaction that is responsible for the different retention across the stationary phases. The correlation of the ^{1}H T_2 to HPLC retention data is less clear. Overall, there are no strong systematic differences between toluene dissolved in both mobile phase across the different stationary phases. The largest change in ^{1}H T_2 of toluene dissolved in 50:50 (% v/v) MeCN:D_2O and MeOH:D_2O compared to "solution only" was observed in the presence of CSH-hexyl-phenyl and BEH-RP18 respectively.

Table 8.4. ^{1}H T_1 and T_2 relaxation times for toluene in 50:50 % v/v MeOH:D_2O (from top to bottom according to HPLC elution order): mobile phase in the absence of stationary phase (solution only) and in the presence of BEH-C18, BEH-phenyl, BEH-RP18, CSH hexyl-phenyl and HSS T3 stationary phases. Data were obtained at 500 MHz spectrometer at 313 K and 5.0 kHz spinning frequency.

MeOH/D_2O

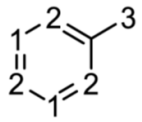

Toluene

SP	HPLC Rt (mins)	T_1(s)					
		H-1(f)	H-2(f)	H-3(f)	H-1(b)	H-2(b)	H-3(b)
Solution only	n/a	6.6±0.3	7.2±0.4	6.6±0.3		n/a	
BEH-Phenyl	12.24	2.9±0.2	2.2±0.1	3.8±02	1.6±0.1	1.6±0.03	2.0±0.1
CSH Hexyl-phenyl	13.32	3.2±0.3	2.5±0.1	3.6±0.4	1.7±0.1	1.9±0.1	2.1±0.1
BEH-RP18	17.55	5.6±0.7	3.9±0.2	4.3±0.3	1.7±0.1	1.7±0.03	1.6±0.1
BEH-C18	21.57	4.8±0.6	4.7±0.5	3.3±0.1	1.5±0.1	1.5±0.1	1.5±0.1
HSS T3	27.73	6.2±0.6	5.2±0.4	3.6±0.1	3.0±0.2	3.0±0.2	1.9±0.2
		T_2(s)					
		H-1(f)	H-2(f)	H-3(f)	H-1(b)	H-2(b)	H-3(b)
Solution only	n/a	3.1±0.2	3.2±0.2	3.1±0.2		n/a	
BEH-Phenyl	12.24	2.5±0.2	2.1±0.1	2.0±0.1	0.05±0.002	0.1±0.003	0.1±0.002
CSH Hexyl-phenyl	13.32	2.5±0.2	2.0±0.2	1.9±0.1	0.1±0.03	0.1±0.004	0.1±0.003
BEH-RP18	17.55	1.9±0.1	1.8±0.04	1.7±0.03	0.1±0.02	0.1±0.002	0.1±0.002
BEH-C18	21.57	2.0±0.2	1.9±0.1	1.8±0.1	0.04±0.03	0.04±0.001	0.1±0.002
HSS T3	27.73	2.7±0.2	2.3±0.1	2.3±0.1	0.2±0.01	0.2±0.02	0.3±0.02

Table 8.5.RP-HPLC stationary phase selectivity parameters of BEH-phenyl and HSS T3[370]

Column	*H*[1]	*S**[2]	*A*[3]	*B*[4]	*C(pH 2.8)*[5]	*C(pH 7.0)*[6]
BEH-phenyl	0.730	-0.070	-0.350	0.030	0.190	0.200
HSS T3	0.940	-0.020	-0.170	0.000	0.030	0.180

[1]*H,* column hydrophobicity, [2]*S*,* steric hindrance of bulky analyte molecules,[3]*A* stationary phase hydrogen-bond acidity,[4]*B* stationary phase hydrogen-bond basicity,[5]*C (pH 2.8)* cation-exchange activity and [6]*C (pH 7.0)* cation-exchange activity

8.4.3 Naphthalene

The ^{1}H T_1 & T_2 relaxation and HPLC elution orders of naphthalene is illustrated in Tables 8.6 and 8.7. The HPLC elution orders of both naphthalene and toluene are identical and thus we can assume hydrophobic interactions drive the retention mechanism. Both free and bound peaks were observed in the ^{1}H NMR spectra of naphthalene dissolved in both the mobile and across all five stationary phases which suggests that naphthalene is in the slow exchange regime. There was no clear correlation between the NMR relaxation and HPLC retentions of naphthalene. However, the largest change in T_1 relaxation in the presence of stationary phase compared to solution only is observed in the presence of HSS T3. The HPLC results also indicated naphthalene is also most retained in the presence of HSS T3.

Table 8.6. ^{1}H T_1 and T_2 relaxation times for naphthalene in 50:50 % v/v MeCN:D_2O (from top to bottom according to HPLC elution order): mobile phase in the absence of stationary phase (solution only) and in the presence of BEH-C18, BEH-phenyl, BEH-RP18, CSH hexyl-phenyl and HSS T3 stationary phases. Data were obtained at 500 MHz spectrometer at 313 K and 5.0 kHz spinning frequency.

MeCN/D_2O

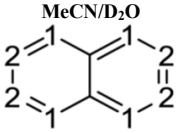

Naphthalene

SP	HPLC Rt (mins)	T_1(s) H-1(f)	H-2(f)	H-1(b)	H-2(b)
Solution only	n/a	5.6±0.1	6.0±0.1	n/a	
BEH-Phenyl	9.02	7.7±0.4	7.8±0.5	4.5±0.1	4.4±0.1
CSH Hexyl-phenyl	9.79	8.3±0.6	7.7±0.5	4.1±0.2	3.8±0.2
BEH-RP18	13.36	7.5±1.2	6.8±0.4	2.8±0.1	3.1±0.1
BEH-C18	14.10	7.1±0.2	7.7±0.5	3.5±0.1	3.5±0.1
HSS T3	18.68	7.1±0.3	9.9±0.4	3.7±0.1	3.8±0.1
		T_2(s) H-1(f)	H-2(f)	H-1(b)	H-2(b)
Solution only	n/a	2.8±0.1	2.9±0.03	n/a	
BEH-Phenyl	9.02	2.0±0.1	2.0±0.1	0.1±0.002	0.1±0.002
CSH Hexyl-phenyl	9.79	2.5±0.1	2.5±0.1	0.1±0.003	0.1±0.007
BEH-RP18	13.36	2.0±0.1	2.2±0.1	0.1±0.002	0.1±0.004
BEH-C18	14.10	2.2±0.03	2.3±0.04	0.1±0.002	0.1±0.001
HSS T3	18.68	1.2±0.1	1.2±0.1	0.2±0.003	0.2±0.001

The largest and smallest changes in T_2 NMR relaxation in the presence of stationary phase compared to solution only were observed for H-1(f) and H-2(f) protons of naphthalene in 50:50 MeCN:D_2O in the presence of HSS T3 (H = 0.940) and CSH Hexyl-phenyl (H = 0.708) respectively (see Table 8.6). To understand this difference in retention time, the hydrophobicity subtraction model selectivity parameters of both and CSH hexyl-phenyl and HSS T3 are compared in Table 8.8. Looking at Table 8.8, it is apparent that HSS T3 has a higher column hydrophobicity compared CSH hexyl-phenyl. Thus, taking into consideration the HPLC retention time and HSM selectivity parameters, the T_2 relaxation

of naphthene in 50:50 MeCN:D_2O could indicate that strong hydrophobic interactions are taking place between naphthalene and HSS T3. Furthermore, for 50:50 MeOH:D_2O mobile phase the largest change in T_2 NMR relaxation of naphthalene in the presence and absence of stationary phase was observed for H-1(f) and H-2(f) protons in the case of BEH-phenyl (see Table 8.7). The origin of this observation is not clear.

Table 8.7. ^{1}H T_1 and T_2 relaxation times for naphthalene in 50:50 % v/v MeOH:D_2O (from top to bottom according to HPLC elution order): mobile phase in the absence of stationary phase (solution only) and in the presence of BEH-C18, BEH-phenyl, BEH-RP18, CSH hexyl-phenyl and HSS T3 stationary phases. Data were obtained at 500 MHz spectrometer at 313 K and 5.0 kHz spinning frequency.

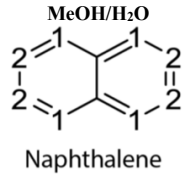

SP	HPLC Rt (mins)	T_1(s) H-1(f)	H-2(f)	H-1(b)	H-2(b)
Solution only	n/a	6.4±0.1	6.7±0.2	n/a	
BEH-Phenyl	20.79	5.1±0.9	4.7±0.5	1.9±0.2	1.7±0.1
CSH Hexyl-phenyl	23.06	5.9±0.7	4.1±0.8	2.1±0.2	1.5±0.1
BEH-RP18	34.17	5.2±0.5	6.0±1.0	1.8±0.3	1.4±0.2
BEH-C18	37.60	5.0±0.3	5.2±0.4	1.4±0.1	1.2±0.1
HSS T3	49.11	8.6±1.8	7.6±1.5	1.9±0.1	2.3±0.1
		T_2(s) H-1(f)	H-2(f)	H-1(b)	H-2(b)
Solution only	n/a	2.4±0.05	2.5±0.1	n/a	
BEH-Phenyl	20.79	1.2±0.05	1.4±0.1	0.1±0.007	0.1±0.004
CSH Hexyl-phenyl	23.06	1.8±0.3	1.7±0.2	0.1±0.05	0.1±0.005
BEH-RP18	34.17	1.9±0.1	1.8±0.1	0.05±±0.003	0.05±0.003
BEH-C18	37.60	1.7±0.1	1.6±0.1	0.04±0.004	0.04±0.002
HSS T3	49.11	1.3±0.2	1.7±0.3	0.1±0.005	0.1±0.007

Table 8.8. RP-HPLC stationary phase selectivity parameters[370]

Column	*H*[1]	*S**[2]	*A*[3]	*B*[4]	*C(pH 2.8)*[5]	*C(pH 7.0)*[6]
CSH hexyl-phenyl	0.708	-0.059	-0.435	0.129	-0.068	0.223
HSS T3	0.940	-0.020	-0.170	0.000	0.030	0.180

[1]*H,* column hydrophobicity, [2]*S*,* steric hindrance of bulky analyte molecules,[3]*A* stationary phase hydrogen-bond acidity,[4]*B* stationary phase hydrogen-bond basicity,[5]*C (pH 2.8)* cation-exchange activity and [6]*C (pH 7.0)* cation-exchange activity.

8.4.4 Acenaphthene

Another analyte which follows the same elution order of toluene and also undergoes slow chemical exchange is acenaphthene. We discovered that acenaphthene is poorly soluble in 50:50 (% v/v) MeOH:D_2O and therefore no NMR and HPLC data were obtained.

Conversely, the T_1 & T_2 relaxation and HPLC data of acenaphthene dissolved in 50:50 (% v/v) MeCN:D_2O is displayed in Table 8.9. Similarly, to naphthalene, no clear agreement between the ^{1}H T_1 or T_2 relaxation measurements and HPLC retention times of acenaphthene across the five stationary phases. Conversely, the largest change of ^{1}H T_1 was observed between the free acenaphthene in solution only and in the presence of HSS T3 across both H_1 and H_4 protons. Similarly, the longest HPLC retention time of acenaphthene was also observed in the presence of HSS T3. This could potentially suggest that both H-1 and H-4 dictate the retention of acenaphthene in the presence of HSS T3.

Additionally, the smallest change in both ^{1}H T_1 and T_2 was observed between free acenaphthene in solution only and presence of BEH-phenyl stationary phase. Likewise, acenaphthene was least retained in the presence of BEH-phenyl. The largest change in ^{1}H T_2 relaxation was observed in the presence of BEH-C18. Keeping in mind both BEH-C18 (H = 1.000) and HSS T3 (H = 0.940) have similar hydrophobicity selectivity parameters (see Table 8.1), we can conclude hydrophobic interactions dictates the retention order of acenaphthene across all five stationary phases.

Table 8.9. ^{1}H T_1 and T_2 relaxation times for acenaphthene in 50:50 % v/v MeCN:D_2O (from top to bottom according to HPLC elution order): mobile phase in the absence of stationary phase (solution only) and in the presence of BEH-C18, BEH-phenyl, BEH-RP18, CSH hexyl-phenyl and HSS T3 stationary phases. Data were obtained at 500 MHz spectrometer at 313 K and 5.0 kHz spinning frequency.

MeCN/D₂O

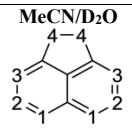

Acenaphthene

SP	HPLC Rt (mins)	T_1(s) H-1(f)	H-2(f)	H-3(f)	H-4(f)	H-1(b)	H-2(b)	H-3(b)	H-4(b)
Solution only	n/a	5.9±0.2	6.1±0.4	5.8±0.3	2.7±0.1		n/a		
BEH-Phenyl	13.05	5.0±0.4	4.5±0.2	4.6±0.3	2.6±0.1	3.2±0.1	2.8±0.1	2.1±0.1	1.4±0.1
CSH Hexyl-phenyl	14.46	9.7±1.2	12.2±2.6	6.4±0.3	3.4±0.1	3.7±0.1	3.4±0.1	2.4±0.1	1.7±0.1
BEH-RP18	21.37	7.5±1.1	7.5±1.2	7.1±0/6	3.4±0.2	2.8±0.1	2.9±0.1	2.7±0.1	1.4±0.1
BEH-C18	24.37	7.4±0.8	7.7±1.1	5.7±0.4	2.7±0.1	2.9±0.1	2.9±0.1	2.9±0.1	1.3±0.04
HSS T3	32.95	10.2±1.9	8.5±1.6	3.8±0.1	3.9±0.2	3.8±0.1	3.2±0.1	3.3±0.1	1.2±0.1
		T_2(s) H-1(f)	H-2(f)	H-3(f)	H-4(f)	H-1(b)	H-2(b)	H-3(b)	H-4(b)
Solution only	n/a	1.8±0.1	2.2±0.1	2.2±0.1	1.8±0.05		n/a		
BEH-Phenyl	13.05	1.8±0.1	1.9±0.1	1.7±0.1	1.2±0.07	0.1±0.004	0.1±0.004	0.1±0.004	0.1±0.003
CSH Hexyl-phenyl	14.46	1.6±0.1	1.6±0.1	0.2±0.005	1.2±0.07	0.1±0.005	0.1±0.002	0.1±0.003	0.1±0.002
BEH-RP18	21.37	1.5±0.1	1.3±0.1	1.2±0.1	1.2±0.1	0.2±0.004	0.1±0.006	0.1±0.007	0.1±0.002
BEH-C18	24.37	1.4±0.1	1.2±0.1	1.3±0.1	1.2±0.03	0.1±0.02	0.1±0.03	0.1±0.003	0.1±0.003
HSS T3	32.95	1.7±0.1	1.7±0.1	0.3±0.004	1.4±0.07	0.3±0.04	0.2±0.003	0.2±0.004	0.1±0.002

8.4.5 Benzophenone

Even though the HPLC elution order of benzophenone is similar to that of toluene, the T_1 and T_2 relaxation of benzophenone dissolved in MeCN:D_2O had no clear agreement with the HPLC elution orders (see Table 8.10). Therefore, correlating the NMR and HPLC retention of benzophenone across the five stationary phases is challenging.

For instance, the largest change of T_2 relaxation was observed between the free benzophenone in solution only and in the presence of CSH hexyl-phenyl and BEH-phenyl. Conversely, the smallest change was in T_2 relaxation observed in the presence of HSS T3. The HPLC retention indicates that benzophenone is most retained on HSS T3 and least retained on the BEH-phenyl stationary phases which opposes the NMR data.

On the other hand, the largest change in T_2 relaxation of benzophenone dissolved in 50:50 MeOH:D_2O was observed in the presence of HSS T3 (H = 0.940) stationary phase (see Table 8.11) which suggest hydrophobic interactions are taking place.

Table 8.10. ^{1}H T_1 and T_2 relaxation times for benzophenone in 50:50 % v/v MeCN:D_2O (from top to bottom according to HPLC elution order): mobile phase in the absence of stationary phase (solution only) and in the presence of BEH-C18, BEH-phenyl, BEH-RP18, CSH hexyl-phenyl and HSS T3 stationary phases. Data were obtained at 500 MHz spectrometer at 313 K and 5.0 kHz spinning frequency.

MeCN:D₂O

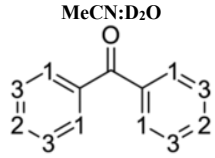

Benzophenone

SP	HPLC Rt (mins)	T_1(s) H-1(f)	H-2(f)	H-3(f)	H-1(b)	H-2(b)	H-3(b)
Solution only	n/a	4.5±0.1	5.1±0.2	4.5±0.1		n/a	
BEH-Phenyl	8.12	6.1±0.1	6.1±0.4	5.5±0.2	4.3±0.1	4.3±0.1	3.9±0.1
CSH Hexyl-phenyl	8.74	7.8±0.6	14.7±1.1	7.7±0.6	4.7±0.1	4.6±0.1	4.2±0.1
BEH-RP18	10.55	5.8±0.3	7.1±0.7	6.0±0.3	3.3±0.1	3.3±0.1	3.2±0.1
BEH-C18	10.71	5.8±0.2	6.2±0.3	5.1±0.1	3.9±0.1	3.9±0.1	3.7±0.04
HSS T3	15.09	6.0±0.3	6.3±0.3	5.2±0.2	3.7±0.1	3.7±0.1	3.5±0.1
		T_2(s) H-1(f)	H-2(f)	H-3(f)	H-1(b)	H-2(b)	H-3(b)
Solution only	n/a	2.8±0.05	3.0±0.1	2.8±0.04		n/a	
BEH-Phenyl	8.12	1.5±0.1	1.5±0.1	1.4±0.05	0.2±0.004	0.1±0.003	0.1±0.003
CSH Hexyl-phenyl	8.74	1.1±0.1	0.4±0.1	0.5±0.1	0.1±0.002	0.1±0.001	0.1±0.002
BEH-RP18	10.55	1.9±0.02	1.9±0.1	1.8±0.02	0.2±0.07	0.1±0.005	0.1±0.04
BEH-C18	10.71	2.1±0.03	2.1±0.1	1.9±0.1	0.8±0.1	0.8±0.1	0.7±0.1
HSS T3	15.09	2.2±0.02	2.2±0.04	2.1±0.04	0.4±0.04	0.3±0.04	0.3±0.03

Table 8.11. ^{1}H T_1 and T_2 relaxation times for benzophenone in 50:50 % v/v MeOH:D_2O (from top to bottom according to HPLC elution order): mobile phase in the absence of stationary phase (solution only) and in the presence of BEH-C18, BEH-phenyl, BEH-RP18, CSH hexyl-phenyl and HSS T3 stationary phases. Data were obtained at 500 MHz spectrometer at 313 K and 5.0 kHz spinning frequency.

MeOH/D$_2$O

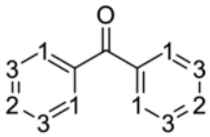

Benzophenone

SP	HPLC Rt (mins)	H-1(f)	H-2(f)	H-3(f)	H-1(b)	H-2(b)	H-3(b)
				T_1(s)			
Solution only	n/a	3.8±0.5	3.4±0.6	3.5±0.2		n/a	
BEH-Phenyl	21.46	1.5±0.1	1.2±0.1	1.3±0.1	1.5±0.1	1.2±0.1	1.3±0.1
BEH-RP18	22.54	2.3±0.1	1.3±0.1	2.2±0.3	1.3±0.1	1.1±0.1	1.2±0.03
CSH Hexyl-phenyl	23.01	1.5±0.1	1.4±0.1	1.4±0.1	1.5±0.1	1.4±0.1	1.4±0.1
BEH-C18	24.70	3.5±0.2	4.4±1.0	2.4±0.1	1.3±0.1	1.2±0.1	1.2±0.1
HSS T3	37.33	1.3±0.1	0.7±0.2	1.1±0.1	1.3±0.1	0.7±0.2	1.1±0.1
				T_2(s)			
		H-1(f)	H-2(f)	H-3(f)	H-1(b)	H-2(b)	H-3(b)
Solution only	n/a	2.5±0.1	2.2±0.2	2.4±0.1		n/a	
BEH-Phenyl	21.46	0.1±0.004	0.1±0.004	0.08±0.004	0.1±0.004	0.1±0.004	0.08±0.004
BEH-RP18	22.54	1.9±0.2	0.03±0.003	2.1±0.2	0.03±0.003	0.02±0.001	0.02±0.001
CSH Hexyl-phenyl	23.01	0.1±0.003	0.05±0.004	0.05±0.004	0.09±0.003	0.05±0.004	0.05±0.004
BEH-C18	24.70	1.5±0.1	1.5±0.1	1.7±0.1	0.03±0.002	0.02±0.001	0.02±0.001
HSS T3	37.33	0.04±0.002	0.03±0.001	0.02±0.002	0.04±0.002	0.03±0.009	0.02±0.002

8.4.6 Biphenyl

^{1}H T_1 & T_2 relaxation and HPLC elution orders of biphenyl is illustrated in Tables 8.12 and 8.13. The 1D ^{1}H NMR spectra of biphenyl indicates it is undergoing slow exchange across all 5 stationary phases. However, both the H-1 (bound) and H-2 (free) peaks overlapped and hence were not reported. Biphenyl also followed the HPLC elution order of toluene which suggests an increase in retention with an increase of stationary phase hydrophobicity. However, no clear correlation was identified between the NMR data and HPLC retention times. The ^{1}H T_1 relaxation of biphenyl (H_3 free peak) dissolved in 50:50 MeCN:D_2O followed the HPLC elution order with the largest change in the presence of stationary phase and solution only was observed in the presence of HSS T3. Additionally, the ^{1}H T_1 relaxation of biphenyl (H-2 bound peak) dissolved in 50:50 MeOH:D_2O also followed the HPLC elution order. The ^{1}H T_1 data suggest, H-3 and H-2 potentially dominate the retention mechanism of biphenyl dissolved in MeCN:D_2O and MeOH:D_2O respectively. On the other hand, the ^{1}H T_2 relaxation data of biphenyl showed no agreement with the HPLC elution order in both mobile phases which remains unclear.

Table 8.12. ^{1}H T_1 and T_2 relaxation times for biphenyl in 50:50 % v/v MeCN:D_2O (from top to bottom according to HPLC elution order): mobile phase in the absence of stationary phase (solution only) and in the presence of BEH-C18, BEH-phenyl, BEH-RP18, CSH hexyl-phenyl and HSS T3 stationary phases. Data were obtained at 500 MHz spectrometer at 313 K and 5.0 kHz spinning frequency.

MeCN/D₂O

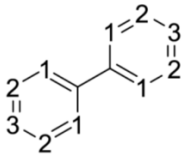

Biphenyl

SP	HPLC Rt (mins)	T_1(s) H-1(f)	H-3(f)	H-2(b)	H-3(b)
Solution only	n/a	4.2±0.1	4.7±0.1	n/a	
BEH-Phenyl	12.51	6.1±0.5	3.5±0.2	2.9±0.1	2.7±0.1
CSH Hexyl-phenyl	13.76	4.5±0.2	3.3±0.4	2.9±0.1	2.8±0.1
BEH-RP18	19.26	5.1±0.1	4.1±0.1	2.4±0.1	2.6±0.1
BEH-C18	21.51	5.8±0.2	6.0±0.2	3.3±0.1	3.4±0.2
HSS T3	29.76	5.1±0.3	8.0±0.4	2.7±0.2	2.8±0.2
		T_2(s) H-1(f)	H-3(f)	H-2(b)	H-3(b)
Solution only	n/a	2.8±0.03	2.9±0.04	n/a	
BEH-Phenyl	12.51	2.1±0.1	2.0±0.2	0.1±0.002	0.1±0.006
CSH Hexyl-phenyl	13.76	2.1±0.1	2.2±0.4	0.1±0.002	0.1±0.002
BEH-RP18	19.26	2.1±0.2	1.5±0.2	0.2±0.003	0.2±0.005
BEH-C18	21.51	2.6±0.04	2.7±0.1	0.2±0.004	0.1±0.005
HSS T3	29.76	2.3±0.1	2.2±0.3	0.3±0.006	0.3±0.007

Table 8.13. ^{1}H T_1 and T_2 relaxation times for biphenyl in 50:50 % v/v MeOH:D_2O (from top to bottom according to HPLC elution order): mobile phase in the absence of stationary phase (solution only) and in the presence of BEH-C18, BEH-phenyl, BEH-RP18, CSH hexyl-phenyl and HSS T3 stationary phases. Data were obtained at 500 MHz spectrometer at 313 K and 5.0 kHz spinning frequency.

MeOH/D₂O

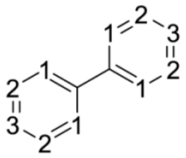

Biphenyl

SP	HPLC Rt (mins)	T_1(s) H-1(f)	H-3(f)	H-2(b)	H-3(b)
Solution only	n/a	2.4±0.3	4.2±0.2	n/a	
BEH-Phenyl	40.45	1.3±0.05	1.3±0.04	1.2±0.02	1.2±0.01
CSH Hexyl-phenyl	46.31	1.2±0.2	1.2±0.1	1.3±0.1	1.2±0.1
BEH-RP18	66.41	1.4±0.03	1.2±0.1	1.3±0.1	1.2±0.1
BEH-C18	79.98	3.5±0.4	1.6±0.05	1.5±0.03	1.6±0.1
HSS T3	88.10	1.4±0.1	1.4±0.1	1.9±0.2	1.4±0.1
		T_2(s) H-1(f)	H-3(f)	H-2(b)	H-3(b)
Solution only	n/a	2.2±0.2	2.1±0.1	n/a	
BEH-Phenyl	40.45	0.6±0.1	0.1±0.02	0.1±0.001	0.1±0.003
CSH Hexyl-phenyl	46.31	0.1±0.005	0.1±0.01	0.1±0.004	0.1±0.009
BEH-RP18	66.41	0.1±0.004	0.1±0.04	0.1±0.002	0.1±0.004
BEH-C18	79.98	1.4±0.1	0.1±0.003	0.1±0.001	0.1±0.002
HSS T3	88.10	0.1±0.003	0.1±0.002	0.2±0.001	0.1±0.002

8.4.7 Butyl 4-Hydroxybenzoate

^{1}H NMR relaxation and HPLC retention times of butyl 4-hydroxybenzoate is illustrated in Tables 8.14 and 8.15. Butyl 4-hydroxybenzoate acid HPLC elution order is slightly

different to the analytes previously discussed. Butyl 4-hydroxybenzoate is least retained in presence of BEH-Phenyl (H = 0.730 and B = 0.030) and most retained with BEH-RP18 (H = 0.830 and B = 0.090) and HSS T3 (H = 0.940 and B = 0.000) respectively. Based on the HPLC elution order and HSM selectivity parameters (see Table 8.2) of all 5 stationary phases, it can be assumed that hydrophobic and hydrogen-bond basicity interactions drive the retention mechanism of butyl 4-hydroxybenzoate. The NMR relaxation of butyl 4-hydroxybenzoate which undergoes slow exchange regime is illustrated in both Tables 8.14 and 8.15. Overall, the largest change in ^{1}H T_1 and T_2 relaxation of butyl 4-hydrobenzoate dissolved in MeCN:D_2O was observed in the presence of BEH-RP18.

Table 8.14. ^{1}H T_1 and T_2 relaxation times for butyl 4-hydroxybenzoate in 50:50 % v/v MeCN:D_2O (from top to bottom according to HPLC elution order): mobile phase in the absence of stationary phase (solution only) and in the presence of BEH-C18, BEH-phenyl, BEH-RP18, CSH hexyl-phenyl and HSS T3 stationary phases. Data were obtained at 500 MHz spectrometer at 313 K and 5.0 kHz spinning frequency.

MeCN/D$_2$O

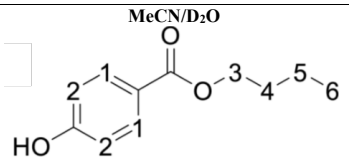

Butyl 4-hydroxybenzoate

SP	HPLC Rt (mins)	T_1(s)											
		H-1(f)	H-2(f)	H-3(f)	H-4(f)	H-5(f)	H-6(f)	H-1(b)	H-2(b)	H-3(b)	H-4(b)	H-5(b)	H-6(b)
Solution only	n/a	2.8±0.002	3.0±0.002	1.6±0.0001	1.6±0.0001	1.9±0.0001	2.1±0.0001	n/a					
BEH-Phenyl	5.75	4.1±0.3	2.1±0.1	4.9±0.04	1.7±0.1	1.7±0.1	2.2±0.2	2.8±0.05	2.6±0.02	3.3±0.1	1.3±0.1	1.7±0.2	1.9±0.1
CSH Hexyl-phenyl	6.64	4.2±0.5	1.7±0.1	3.5±0.05	2.0±0.2	1.7±0.2	2.0±0.1	2.2±0.1	1.9±0.1	2.6±0.1	1.3±0.2	1.5±0.2	1.7±0.1
BEH-C18	7.36	4.1±0.1	4.6±0.2	5.7±0.1	1.7±0.1	1.8±0.1	1.8±0.1	2.9±0.1	2.8±0.1	2.4±0.2	1.4±0.1	1.5±0.1	1.5±0.1
BEH-RP18	8.90	4.5±0.3	4.2±0.6	6.6±0.1	2.9±0.2	2.2±0.2	1.7±0.1	1.8±0.1	1.7±0.1	4.4±0.2	1.4±0.1	1.3±0.1	1.5±0.1
HSS T3	9.72	3.5±0.1	4.0±0.1	2.2±0.1	1.6±0.2	1.8±0.1	1.8±0.1	3.0±0.1	3.2±0.1	1.7±0.1	1.4±0.1	1.6±0.1	1.8±0.1
		T_2(s)											
		H-1(f)	H-2(f)	H-3(f)	H-4(f)	H-5(f)	H-6(f)	H-1(b)	H-2(b)	H-3(b)	H-4(b)	H-5(b)	H-6(b)
Solution only	n/a	1.7±0.1	1.7±0.1	0.9±0.02	1.0±0.02	1.3±0.02	1.4±0.02	n/a					
BEH-Phenyl	5.75	0.4±0.1	0.5±0.05	0.1±0.004	0.5±0.04	0.5±0.04	0.6±0.03	0.3±0.02	0.3±0.02	0.1±0.01	0.1±0.01	0.2±0.01	0.2±0.003
CSH Hexyl-phenyl	6.64	0.1±0.001	0.5±0.04	0.1±0.02	0.1±0.03	0.2±0.03	0.7±0.05	0.1±0.01	0.1±0.01	0.05±0.01	0.04±0.003	0.1±0.01	0.1±0.03
BEH-C18	7.36	0.8±0.04	0.9±0.03	0.1±0.004	0.7±0.05	1.1±0.04	1.2±0.03	0.4±0.03	0.3±0.04	0.2±0.1	0.2±0.02	0.3±0.01	0.3±0.02
BEH-RP18	8.90	0.4±0.04	0.5±0.1	0.8±0.02	0.4±0.04	0.6±0.06	0.8±0.05	0.1±0.01	0.1±0.02	0.6±0.1	0.1±0.03	0.1±0.01	0.2±0.01
HSS T3	9.72	0.8±0.02	0.8±0.05	0.1±0.01	0.7±0.03	0.9±0.03	1.1±0.02	0.8±0.05	0.8±0.04	0.5±0.03	0.5±0.03	0.5±0.04	0.8±0.03

Table 8.15. ^{1}H T_1 and T_2 relaxation times for butyl 4-hydroxybenzoate in 50:50 % v/v MeOH:D_2O (from top to bottom according to HPLC elution order): mobile phase in the absence of stationary phase (solution only) and in the presence of BEH-C18, BEH-phenyl, BEH-RP18, CSH hexyl-phenyl and HSS T3 stationary phases. Data were obtained at 500 MHz spectrometer at 313 K and 5.0 kHz spinning frequency.

MeOH/D_2O

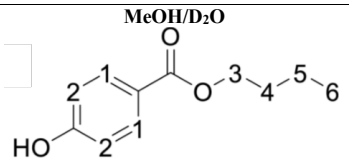

Butyl 4-hydroxybenzoate

SP	HPLC Rt (mins)	T_1(s) H-1(f)	H-2(f)	H-3(f)	H-4(f)	H-5(f)	H-6(f)	H-1(b)	H-2(b)	H-3(b)	H-4(b)	H-5(b)	H-6(b)
Solution only	n/a	1.8±0.02	1.9±0.04	1.1±0.02	1.0±0.07	1.3±0.07	1.7±0.07	n/a					
BEH-Phenyl	10.12	2.7±0.1	2.4±0.04	1.4±0.03	1.2±0.1	1.3±0.1	1.9±0.1	1.8±0.1	1.7±0.1	0.9±0.05	N/A	1.1±0.1	1.4±0.1
CSH Hexyl-phenyl	21.63	2.6±0.05	2.2±0.04	1.5±0.02	1.3±0.1	1.3±0.05	2.0±0.1	1.7±0.1	1.6±0.1	1.0±0.1	N/A	1.1±0.04	1.4±0.1
BEH-C18	26.79	2.8±0.1	2.9±0.1	1.5±0.1	1.1±0.1	1.2±0.05	1.4±0.1	1.8±0.1	1.8±0.1	1.0±0.1	1.0±0.04	1.0±0.02	1.1±0.04
BEH-RP18	29.18	2.4±0.1	2.7±0.1	1.5±0.1	1.4±0.1	1.4±0.1	1.6±0.1	1.2±0.04	1.3±0.1	1.1±0.04	1.0±0.06	1.1±0.1	1.1±0.1
HSS T3	38.00	2.4±0.1	2.9±0.1	1.4±0.04	1.1±0.1	1.1±0.04	1.4±0.05	1.5±0.1	1.5±0.1	0.8±0.04	0.8±0.03	0.8±0.03	0.9±0.04
		T_2(s) H-1(f)	H-2(f)	H-3(f)	H-4(f)	H-5(f)	H-6(f)	H-1(b)	H-2(b)	H-3(b)	H-4(b)	H-5(b)	H-6(b)
Solution only	n/a	1.2±0.03	1.2±0.1	0.6±0.01	0.7±0.02	1.0±0.01	1.1±0.01	n/a					
BEH-Phenyl	10.12	0.9±0.04	0.8±0.1	0.6±0.03	0.7±0.04	1.0±0.04	1.1±0.04	0.1±0.01	0.2±0.01	0.02±0.01	N/A	0.1±0.01	0.1±0.01
CSH Hexyl-phenyl	21.63	1.0±0.1	1.1±0.1	0.8±0.05	0.8±0.04	1.1±0.05	1.2±0.04	0.05±0.01	0.01±0.01	0.02±0.01	N/A	0.06±0.01	0.06±0.01
BEH-C18	26.79	0.6±0.03	0.6±0.04	0.6±0.04	0.6±0.04	0.9±0.03	1.0±0.02	0.1±0.01	0.1±0.01	0.04±0.01	0.04±0.01	0.04±0.01	0.1±0.01
BEH-RP18	29.18	0.7±0.1	0.8±0.1	0.6±0.04	0.5±0.04	0.7±0.03	0.9±0.05	0.02±0.01	0.04±0.01	0.02±0.01	0.04±0.01	0.03±0.01	0.06±0.01
HSS T3	38.00	0.7±0.05	0.8±0.1	0.8±0.04	0.6±0.03	0.8±0.04	1.0±0.04	0.06±0.01	0.05±0.01	0.03±0.01	0.06±0.01	0.04±0.01	0.1±0.01

Similarly, the largest change in ^{1}H T_1 of butyl 4-hydrobenzoate dissolved in MeOH:D_2O was observed in the presence of BEH-RP18 and HSS T3. The ^{1}H T_1 relaxation of H-1 (free) and H-6 (bound) followed the HPLC elution order which could suggest they both drive the elution of butyl 4-hydroxybenzoate across all 5 stationary phases. The most remarkable difference in ^{1}H T_1 relaxation was observed for the H-3 (free) proton of butyl 4-hydrobenzoate in the presence of BEH-RP18. Knowing that BEH-RP18 has an embedded polar group, butyl 4-hydroxybenzoate has a hydroxy group and looking at the HSM selectivity parameters of BEH-RP18, this could suggest hydrogen bonding basicity interactions are taking place between butyl 4-hydrobenzoate and the polar embedded group of BEH-R18. Additionally, largest difference in ^{1}H T_2 when dissolved in butyl 4-hydroxybenzoate was also observed in the presence of BEH-RP18. The NMR results indicate a higher tendency of probing the hydrogen bonding basicity interactions followed by hydrophobic interactions between butyl 4-hydroxybenzoate and the 5 stationary phases. Keeping in mind this analyte is most retained in the presence of BEH-RP18 and HSS T3 respectively, taking both the NMR and HPLC data acquired we can conclude

that 4-butyl hydroxybenzoate is retained by hydrophobic interaction followed by hydrogen bonding acidity interactions.

8.4.8 Dipropyl phthalate

Dipropyl phthalate and many other analytes have the same elution order as toluene. The ^{1}H NMR spectra of dipropyl phthalate in presence of the stationary phases indicates that this analyte is in the fast chemical exchange regime. ^{1}H T_1 & T_2 and HPLC retention times are compared in Tables 8.16 and 8.17. Similar to previously discussed analytes, the ^{1}H NMR relaxation data did not match the HPLC elution orders. However, across both mobile phases the largest difference in T_1 relaxation measurements between solution only and in the presence of stationary phase was observed with BEH-C18. In contrast, dipropyl phthalate in the presence of BEH-RP18 when dissolved in MeCN:D_2O has the largest perturbation on the ^{1}H T_2 relaxation. The ^{1}H T_2 relaxation of dipropyl phthalate dissolved in MeOH:D_2O was harder to interpret across the stationary phases.

Table 8.16. ^{1}H T_1 and T_2 relaxation times for dipropyl phthalate in 50:50 (% v/v) MeCN:D_2O (from top to bottom according to HPLC elution order): mobile phase in the absence of stationary phase (solution only) and in the presence of BEH-C18, BEH-phenyl, BEH-RP18, CSH hexyl-phenyl and HSS T3 stationary phases. Data were obtained at 500 MHz spectrometer at 313 K and 5.0 kHz spinning frequency.

MeCN/D₂O

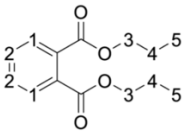

Dipropyl phthalate

SP	HPLC Rt (mins)	T_1(s) H-1(a)	H-2(a)	H-3(a)	H-4(a)	H-5(a)
Solution only	n/a	2.4±0.04	2.1±0.03	1.9±0.04	1.6±0.1	1.6±0.1
BEH-Phenyl	10.73	3.6±0.1	3.0±0.1	2.4±0.1	2.0±0.1	2.1±0.2
CSH Hexyl-phenyl	11.59	3.2±0.1	2.7±0.1	2.2±0.1	1.9±0.1	2.0±0.1
BEH-RP18	11.59	3.1±0.1	2.6±0.1	2.1±0.1	1.9±0.1	1.7±0.1
BEH-C18	17.30	3.9±0.1	3.2±0.04	2.6±0.1	1.9±0.2	2.0±0.2
HSS T3	25.59	3.4±0.1	2.8±0.1	2.3±0.1	1.8±0.1	1.8±0.1
		T_2(s) H-1(a)	H-2(a)	H-3(a)	H-4(a)	H-5(a)
Solution only	n/a	2.0±0.08	1.9±0.05	1.3±0.04	0.8±0.03	1.3±0.02
BEH-Phenyl	10.73	1.7±0.1	1.8±0.2	1.0±0.1	0.5±0.01	0.9±0.05
CSH Hexyl-phenyl	11.59	0.8±0.04	0.7±0.1	0.7±0.05	0.5±0.06	0.6±0.02
BEH-RP18	11.59	0.5±0.02	0.4±0.01	0.5±0.01	0.4±0.04	0.5±0.02
BEH-C18	17.30	2.2±0.1	2.1±0.1	1.0±0.05	0.5±0.05	1.1±0.1
HSS T3	25.59	1.4±0.1	1.4±0.1	0.9±0.1	0.7±0.03	0.9±3

Table 8.17. ^{1}H T_1 and T_2 relaxation times for dipropyl phthalate in 50:50 (% v/v) MeOH:D_2O (from top to bottom according to HPLC elution order): mobile phase in the absence of stationary phase (solution only) and in the presence of BEH-C18, BEH-phenyl, BEH-RP18, CSH hexyl-phenyl and HSS T3 stationary phases. Data were obtained at 500 MHz spectrometer at 313 K and 5.0 kHz spinning frequency.

MeOH/D₂O

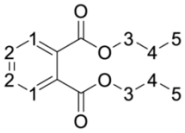

Dipropyl phthalate

SP	HPLC Rt (mins)	T_1(s) H-1(a)	H-2(a)	H-3(a)	H-4(a)	H-5(a)
Solution only	n/a	0.9±0.05	0.8±0.05	0.9±0.03	1.8±0.05	1.8±0.1
BEH-RP18	34.80	1.2±0.1	1.0±0.1	0.9±0.1	1.8±0.1	1.4±0.1
BEH-Phenyl	37.76	1.3±0.1	1.0±0.1	0.8±0.1	1.9±0.1	2.0±0.1
CSH Hexyl-phenyl	40.16	1.4±0.1	1.2±0.1	0.9±0.1	1.4±0.1	1.7±0.1
BEH-C18	52.04	1.5±0.05	1.1±0.04	1.0±0.04	1.5±0.1	1.4±0.1
HSS T3	90.00	1.3±0.1	1.0±0.1	0.8±0.1	1.3±0.1	1.2±0.1
		T_2(s) H-1(a)	H-2(a)	H-3(a)	H-4(a)	H-5(a)
Solution only	n/a	0.6±0.01	0.6±0.01	0.5±0.02	0.2±0.05	1.2±0.05
BEH-RP18	34.80	0.2±0.002	0.1±0.003	0.2±0.05	0.3±0.2	0.8±0.1
BEH-Phenyl	37.76	0.2±0.004	0.1±0.003	0.2±0.04	0.4±0.3	0.7±0.1
CSH Hexyl-phenyl	40.16	0.1±0.01	0.1±0.005	0.2±0.05	0.3±0.05	1.1±0.1
BEH-C18	52.04	0.2±0.002	0.1±0.002	0.2±0.02	0.3±0.003	0.9±0.04
HSS T3	90.00	0.2±0.004	0.1±0.003	0.2±0.008	0.2±0.03	1.1±0.1

8.4.9 Benzoic acid and 3-hydroxybenzoic acid.

Specific protons of both benzoic acid and 3-hydroxybenzoic acid were in the slow or fast exchange regime. This could indicate both weak and strong interactions are taking place between these acids and the 5 RP-HPLC stationary phases. This assumption correlates with the HPLC results as both analytes are the fastest eluting out of the whole series. However, very long HPLC retention times (see Figure 8.4) were observed for both analytes in the presence of BEH-RP18 which suggest either hydrogen bonding or ionic interactions taking place between 3-hydroxybenzoic acid, benzoic acid and the polar embedded group of BEH-RP18 [376].

As both benzoic acid and 3-hydroxybenzoic acid were least retained in the presence of BEH-phenyl, the hydrophobicity subtraction model selectivity parameters of both and BEH-Phenyl (B = 0.030) and BEH-RP18 (B = 0.090) are compared in Table 8.18. The HSM selectivity parameters of BEH-RP18 suggest strong stationary phase hydrogen-bond basicity interactions are taking place between benzoic acid, 3-hydroxybenzoic acid and the polar embedded group of BEH-RP18 [138, 353, 383]. Thus, we can assume, both benzoic acid and 3-hydroxybenzoic act as hydrogen bond donors while the carbamate group of BEH-RP18 stationary phase acts as hydrogen bond acceptor (ester group).

The ^{1}H T_1 of benzoic acid dissolved in MeOH:H_2O correlated with the elution order across all 5 stationary phases (see Table 8.19). However, there is no clear agreement between remaining NMR relaxation data of both benzoic acid and 3-hydroxybenzoic

compared to the HPLC retention times. This is not surprising as both acids can be considered to be unretained against the stationary phases (except BEH-RP18) due to their low logP, logD and retention times.

Table 8.18. RP-HPLC stationary phase selectivity parameters of BEH-phenyl and HSS T3[370]

Column	*H*[1]	*S**[2]	*A*[3]	*B*[4]	*C(pH 2.8)*[5]	*C(pH 7.0)*[6]
BEH-phenyl	0.730	-0.070	-0.350	0.030	0.190	0.200
BEH-RP18	0.830	-0.020	-0.370	0.090	-0.120	-0.050

[1]*H,* column hydrophobicity, [2]*S*,* steric hindrance of bulky analyte molecules,[3]*A* stationary phase hydrogen-bond acidity,[4]*B* stationary phase hydrogen-bond basicity,[5]*C (pH 2.8)* cation-exchange activity and [6]*C (pH 7.0)* cation-exchange activity

Table 8.19.[1]H T_1 and T_2 relaxation times for benzoic acid in 50:50 (% v/v) MeOH:D_2O (from top to bottom according to HPLC elution order): mobile phase in the absence of stationary phase (solution only) and in the presence of BEH-C18, BEH-phenyl, BEH-RP18, CSH hexyl-phenyl and HSS T3 stationary phases. Data were obtained at 500 MHz spectrometer at 313 K and 5.0 kHz spinning frequency.

	SP	HPLC Rt (mins)	T_1(s)				
			H-1(f)	H-2(f)	H-3(f)	H-1(b)	H-3(b)
MeOH/D_2O 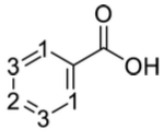 Benzoic acid	Solution only	n/a	4.0±0.1	4.4±0.1	3.7±0.1	n/a	
	BEH-Phenyl	3.02	4.6±0.1	5.3±0.1	4.1±0.1	3.0±0.1	2.9±0.1
	CSH Hexyl-phenyl	4.00	4.6±0.1	5.2±0.1	4.1±0.04	3.0±0.1	2.8±0.1
	BEH-C18	4.30	3.7±0.1	5.0±0.1	3.9±0.1	2.7±0.1	2.5±0.1
	HSS T3	6.80	3.8±0.1	5.1±0.2	3.6±0.1	2.6±0.1	2.4±0.1
	BEH-RP18	19.00	3.2±0.04	4.6±0.1	3.4±0.05	n/a	2.0±0.1
			T_2(s)				
			H-1(f)	H-2(f)	H-3(f)	H-1(b)	H-3(b)
	Solution only	n/a	1.6±0.1	2.2±0.03	1.6±0.1	n/a	
	BEH-Phenyl	3.02	0.5±0.02	0.8±0.02	0.6±0.03	0.1±0.01	0.2±0.05
	CSH Hexyl-phenyl	4.00	0.7±0.03	1.0±0.02	0.8±0.03	0.2±0.03	0.6±0.1
	BEH-C18	4.30	0.6±0.01	0.8±0.02	0.7±0.01	0.2±0.01	0.1±0.01
	HSS T3	6.80	0.5±0.03	0.9±0.02	0.6±0.03	0.2±0.02	0.1±0.01
	BEH-RP18	19.00	0.4±0.03	0.9±0.02	0.6±0.03	n/a	0.1±0.02

8.4.10 Meclizine, hydroxyzine, propranolol and amitriptyline

The ^{1}H spectra of Meclizine, hydroxyzine, propranolol and amitriptyline suggests all the analytes are in the fast exchange regime. The HPLC chromatograms of all four compounds indicate that they are all strongly retained onto the column and thus no retention time was acquirable. However, as discussed in Chapter 4, if one single resonance is observed, this doesn't necessarily mean the system is going through fast

chemical exchange. This could also indicate the system is going through slow chemical exchange where the population of one environment is considerably smaller than the other resulting in the second resonance not being observed on the NMR spectra.

Generally, the ^{1}H T_2 of the four analytes in the presence of any stationary phase was either close or longer compared to the T_2 measured in the absence of any stationary phases. As previously discussed in Chapter 7, this suggest interactions between the analyte and stationary phases potentially leads to the strong retention of the molecule which in turns decreases the amplitude of motion. This is consistent with the HPLC chromatograms acquired of all four analytes. This is likely as all four analytes have the highest molecular volume, logD and logP (see Table 8.2). Generally, as a rule of thumb, the retention times of analytes increases with larger logD or logP values [384-388]. Therefore, we can assume hydrophobic interactions dominate the retention mechanism since higher logP values indicate more hydrophobic characteristics of analyte [389]. The strength of these interactions can be minimised by optimising the HPLC method which we discuss further in Chapter 9.

8.4.11 Aniline and 2-aminophenol

Please refer to Chapter 7 for the data analysis of both aniline and 2-aminophenol.

8.5 Conclusion

^{1}H HR MAS NMR relaxation measurements have offered supplementary information for probing molecular interactions of several analytes with different functional groups, mobile phases and RP-HPLC stationary phases. It was important to consider several parameters (e.g. chemical structure, functional group, stationary phases selectivity parameters and exchange processes etc.) to understand the type of interaction dominating the retention mechanism of an analyte and RP-HPLC stationary phase.

Based on the HSM selectivity parameters, HPLC and NMR relaxation measurements obtained we can conclude the following: (1) Hydrophobic interactions drive the retention mechanism of most analytes in the presence of BEH C18 (H = 1.000) and HSS T3 (H = 0.940) stationary phase (aliphatic chain phases) as they both have the highest hydrophobicity selectivity, (2) π-π stacking interactions take place in the presence of

BEH-phenyl (S^* = -0.070) and CSH hexyl-phenyl (S^* = -0.059) (e.g. 2-aminophenol dissolved in 50:50 MeOH:D_2O) as both phases have the lowest steric hindrance selectivity, (3) hydrogen bonding basicity interactions drives the retention mechanism between hydrogen donor functional groups (e.g. hydroxy group of benzoic acid) and the hydrogen acceptor groups from the polar embedded carbamate group of BEH-RP18 (ester group) and (4) analytes with large molecular volume, logD and logP values (e.g. meclizine and amitriptyline) are strongly retained across the 5 stationary phases.

As discussed in this chapter, the HPLC chromatograms of some analytes (e.g. amitriptyline, hydroxyzine and meclizine) and ^{1}H NMR relaxation data suggest they were strongly retained onto the column. This work can be taken further by optimising a RP-HPLC method to enable all the analytes to elute, therefore allowing us to compare both NMR relaxation and HPLC elution orders. Another avenue to explore further would be comparing RP-HPLC elution orders, RP-HPLC predicted (via Pfizer's QSRR predicted model) elution orders and NMR relaxation data.

9 ^{1}H HR MAS NMR RELAXATION TO FACILITATE SOFTWARE-ASSISTED RP-HPLC METHOD DEVELOPMENT

9.1 Abstract

^{1}H HR MAS NMR relaxation techniques are well known for probing the change in molecular motion and type of interactions between an analyte, mobile phase and RP-HPLC stationary phase. However, these NMR techniques have never been used to further our understanding of the retention mechanism and predictive power of a quantitative structure-retention relationship model (QSRR). In this study, NMR T_1 and T_2 relaxation, experimental and predicted HPLC retention times were compared to determine the type of interactions dominating the retention mechanism of a RP-HPLC heterogeneous system generated by an algorithm RP-HPLC predictive model tool developed by Pfizer.

9.2 Introduction

As previously mentioned, HPLC method development can be a time-consuming process of experimental trial and error. Changing a specific experimental parameter at a time (e.g. stationary phase, mobile phase content, organic solvent, pH etc.) can be both labour

intensive and repetitive. As a result, this is no longer an effective procedure used in the pharmaceutical industry [390].

In recent years, a so called "computed simulation" strategy [16, 391-398] has been used to optimise HPLC method development. Several predictive software have been developed including ChromSword [17], ChromGenius [18], OSIRIS [399], ACD/LC simulator[11, 400, 401] and Drylab[395, 397]. Pfizer uses Drylab predictive software during HPLC method development to acquire the optimal separating conditions with minimum labour. Drylab has been employed several times to facilitate HPLC method development with success [393, 397, 402, 403]. Drylab can simulate the effect of several separation conditions on the retention time (e.g. column properties, gradient conditions, pH, temperature etc.) with few experimental runs.

Method development software Drylab is based upon the following relationships: (1) dependence of retention on mobile phase proportion (see Equation 9.1), (2) dependence of column plate number on experimental conditions, (3) correlation between isocratic and gradient elution and (4) predictability of gradient retention as a function of gradient conditions [398].

The prediction of retention times using computer simulation are based on the dependence of analyte retention time on the mobile phase composition. There is no perfect theory which enables us to predict HPLC retention as a function of mobile proportion. However, several studies [161] have established a formula for such correlation [393, 398]:

$$\log k' = \log k_w - S\varphi \tag{9.1}$$

Where k' is the capacity factor of an analyte, φ is the percentage of ratio of the strong solvent, k_w and S are characteristic constants of the solute and solvent.

The robustness and repeatability of computer simulated retention times has been reported to be accurate (±1-3% prediction accuracy) [283, 393, 404-409] but requires attention to the experimental setup and equipment used. The experimental conditions used for the predictive model tool must be carefully selected to obtain reliable predictions. Furthermore, several factors can affect the predictive power of the computer simulations such as [16]: (1) equipment problems and errors, (2) column processes [406, 409], (3) column degradation [406, 410], (4) co-eluting peaks [406], (5) extrapolated predictions and (6) non-linear relationship between $\log k'$ and φ.

Although several predictive software are commercially available, the research and development team at Pfizer over the years has developed a quantitative structure-retention relationships (QSRRs) model to facilitate their RP-HPLC method development [21]. QSRR models can be used on a wide range applications such as understanding retention mechanisms, characterising stationary phases and generating predictive HPLC retention times [411, 412]. The primary aim of QSRR models is to determine a trend in the descriptors with comparable trends to the retention parameters. However, to obtain accurate and repeatable predictive HPLC retention times, the model requires several descriptors to increase the robustness and reliability of the model. Typically, QSRR models can be developed from a library of molecular descriptors with a solid understanding of their physiochemical properties [413-416]. Therefore, the robustness of the QSRR models heavily depends on the prior theoretical knowledge of the retention mechanisms and molecular descriptors [21, 417]. However, the number of descriptors incorporated into a model must be chosen wisely as increasing the number of descriptors typically improves the model predictive power, but also decreasing the number of uninformative variables also tends to improve the predictive effectiveness of the model [418-420].

Even though several computed simulated and QSRR models have heavily been used to facilitate HPLC method development, to date, no spectroscopy atomic level quantitative measurements of the molecular interactions within a RP-HPLC heterogeneous system has been used to improve our understanding of the predictive power of such prediction software.

The aim of this study was to determine how ^{1}H NMR relaxation measurements could help us understand further the predictive power of Pfizer's algorithm predictive model tool across BEH-C18, BEH-phenyl and BEH-RP18 RP-HPLC stationary phases. In particular, we wanted to investigate whether NMR relaxation measurements can aid us to identify factors that need to be considered to improve predictions in cases where they diverge from experimentally observed elution orders.

As mentioned in Chapter 8, the large bulky analytes (e.g. meclizine, hydroxyzine, propranolol and amitriptyline) were strongly retained onto the RP-HPLC stationary under unbuffered mobile phase with an isocratic elution. Thus, to ensure all the analytes eluted,

all 15 analytes were run under gradient elution with a buffered mobile phase to enable all the analytes to elute under RP-HPLC conditions.

It has previously been reported that gradient elution [143, 421] reduces the retention times of the analytes and buffered mobile phases [422-427] improve the peak shape and chromatogram resolution but does not affect the elution order of the compounds in a mixture. On this basis, due to the limitation that NMR experiments cannot be run under gradient elution, the relaxation measurements were obtained under isocratic conditions with a non-buffered mobile phase. The NMR relaxation, experimental and predicted RP-HPLC retention times were all correlated.

9.3 Experimental Methods

The analytes, sample preparation and NMR method can be found in Chapter 8.

9.3.1 HPLC method

To use the QSRR model, the retention times of all 15 analytes across 3 RP-HPLC stationary phases were experimentally obtained to enable the chromatographic simulations to be calculated. The RP-HPLC experiments were carried out at Pfizer. Each analyte was individually run through BEH-C18, BEH-phenyl and BEH-RP18 RP-HPLC stationary phases. BEH-C18, BEH-phenyl and BEH-PR18 were selected as these three stationary phases are primarily used in the HPLC method development screening conditions in Pfizer due to their retention selectivity properties. Due to the retention characteristics of meclizine, hydroxyzine, propranolol and amitriptyline (e.g. sticking to the column), a gradient elution and buffered mobile phase was used to elute these analytes from the columns. The gradient mobile phase was made of solvent A and B where solvent A was made of MeCN:H_2O (95:5 % v/v) at a pH of 2.6 and solvent B was 0.1% formic acid at a pH of 2.6.

To obtain the gradient retention time measurements, the following gradient program was applied (% v/v): 0-1.7 min,0-0% A and 100-100% B; 1.7-8.7 min,0-100% A and 100-0% B; 8.7-10.4 min, 100-100%A and 0-0% B;10.4-10.5 min, 100-0% A and 0%-100% B; 10.5-13.0 min, 0-0% A and 100-100% B. The chromatography system used was a Waters Acquity UPLC with UV (PDA) and MS detectors. A flow rate of 0.4 mL/min at a temperature of 303.15 K was used. The concentrations of the analytes were 0.25 mg/mL.

The HPLC computer simulations were carried out with QSRR model using a Windows computer.

9.4 Results

The ^{1}H HRMAS NMR spectra (*Figure A.5-A.19 in appendix*), ^{1}H-^{13}C HSQC, ^{1}H-^{13}C HMBC spectra (*Figure A.20-A.26*), RP-HPLC experimental retention times (*Table A.34 in appendix*), RP-HPLC predicted retention times (*Table A.35 in appendix*), ^{1}H T_1 & T_2 relaxation times, (*Tables A.36-A.50 in appendix*) of all 15 analytes in solution only and the presence of BEH-C18, BEH-phenyl and BEH-RP18 stationary phases can be found in appendix of this chapter. The NMR relaxation data presented in this Chapter are reproduced from the respective tables in Chapter 8. To determine whether there is an agreement between the experimental and predicted retentions, we plotted the experimental and predicted retention times of the series of analytes in the presence of BEH-C18, BEH-phenyl and BEH-RP18 as illustrated in Figure 9.1. As shown in Figure 9.1 a good agreement between the two sets of HPLC data were obtained. Keeping in mind that only 15 analytes were used to generate the predicted retention times, increasing the data set could potentially improve the predicting power of the QSRR model.

Similarly to the discussion in Chapter 8, the NMR and HPLC data of each analyte are considered on individual basis unless strong correlations between parameters were observed. To understand the type of interactions taking place within a system, the stationary phase selectivity parameters were also taken into consideration when interpreting the data.

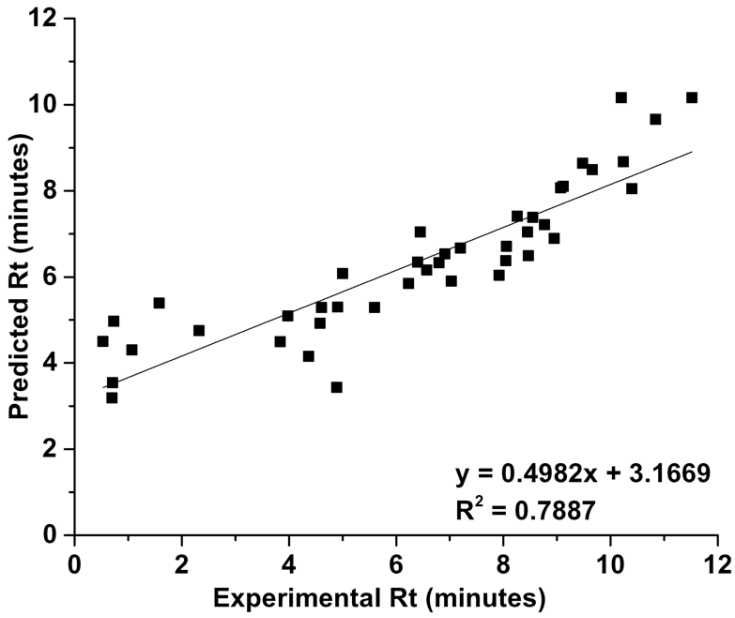

Figure 9.1. Correlation between experimental and predicted retention times in minutes.

9.4.1 Toluene

The ^{1}H relaxation times, experimental and predicted HPLC retention times of toluene are shown in Table 9.1. Toluene is least and most retained in the presence of BEH-RP18 and BEH-Phenyl stationary phase respectively. The majority of the analytes also follow the same HPLC elution orders of toluene.

Table 9.1. ^{1}H T_1 and T_2 relaxation times for toluene in 50:50 % v/v MeCN:D_2O (from top to bottom according to HPLC experimental elution order): mobile phase in the absence of stationary phase (solution only) and in the presence of BEH-RP18, BEH-C18 and BEH-Phenyl stationary phases. Data were obtained at 500 MHz spectrometer at 313 K and 5.0 kHz spinning frequency. Where I: experimental HPLC data and **II**: predicted HPLC data.

	SP	HPLC Rt (mins) I/**II**	T_1(s)					
			H-1(f)	H-2(f)	H-3(f)	H-1(b)	H-2(b)	H-3(b)
MeCN/D_2O	Solution only	n/a	6.4±0.1	6.5±0.1	6.4±0.1	n/a		
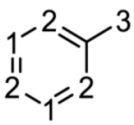	BEH-RP18	6.23/**5.85**	6.8±0.5	6.2±0.5	4.8±0.2	3.3±0.2	3.1±0.2	2.5±0.1
	BEH-C18	7.92/**6.04**	5.6±0.1	5.1±0.1	4.6±0.1	3.6±0.2	3.4±0.2	3.0±0.1
	BEH-Phenyl	8.26/**7.41**	3.5±0.3	2.6±0.2	3.8±0.3	2.6±0.1	2.4±0.1	2.8±0.1
			T_2(s)					
			H-1(f)	H-2(f)	H-3(f)	H-1(b)	H-2(b)	H-3(b)
Toluene	Solution only	n/a	3.5±0.1	3.5±0.1	3.5±0.1	n/a		
	BEH-RP18	6.23/**5.85**	2.2±0.1	2.0±0.1	1.9±0.1	0.2±0.004	0.2±0.003	0.2±0.005
	BEH-C18	7.92/**6.04**	1.8±0.1	1.6±0.1	1.6±0.02	0.1±0.001	0.1±0.002	0.2±0.001
	BEH-Phenyl	8.26/**7.41**	2.0±0.2	1.8±0.1	1.6±0.05	0.1±0.003	0.1±0.002	0.1±0.002

The predicted elution order was the same as the experimentally determined elution order. To understand the elution order of toluene, the HSM selectivity parameters of BEH-C18, BEH-phenyl and BEH-RP18 stationary phase are given in Table 9.2. As toluene is a neutral analyte and cannot undergo ionic exchange, based on the HSM selectivity parameters, the retention mechanism of toluene is driven by π-π interactions followed by hydrophobic interactions.

The 1D ^{1}H NMR spectra of toluene in the presence of the stationary phases indicate it is undergoing slow chemical exchange. The largest changes in ^{1}H T_1 of toluene in the presence of stationary phase compared to solution only are observed in the presence of BEH-phenyl across all the free peaks. The ^{1}H T_1 relaxation of H-1(f), H-2(f) and H-3(f) all follow the elution order observed in HPLC experiments (see Table 9.1).

The correlation of the ^{1}H T_2 to HPLC retention data is less clear. Generally, the largest change in ^{1}H T_2 of toluene in the presence of stationary phase compared to "solution only" was observed in the presence of BEH-C18 and BEH-phenyl. As listed in Table 9.2, BEH-phenyl stationary phase has the lowest steric hindrance resistance selectivity and

BEH-C18 has the highest column hydrophobicity. As π-π interactions have been reported to take place between aromatic compounds and phenyl phases [428, 429], the results could suggest the difference in retention of toluene on BEH-phenyl (*S** = -0.070 and *H* = 0.730*)* and BEH-C18 (*S** = 0.020 and *H* = 1.000*)* is due to π-π interactions rather than hydrophobic interactions.

Table 9.2. RP-HPLC stationary phase selectivity parameters [370]

Column	*H*[1]	*S**[2]	*A*[3]	*B*[4]	*C(pH 2.8)*[5]	*C(pH 7.0)*[6]
BEH-C18	1.000	0.020	-0.090	0.000	0.170	0.130
BEH-phenyl	0.730	-0.070	-0.350	0.030	0.190	0.200
BEH-RP18	0.830	-0.020	-0.370	0.090	-0.120	-0.050

[1]*H,* column hydrophobicity*,* [2]*S**, steric hindrance resistance of bulky analyte molecules,[3]*A* stationary phase hydrogen-bond acidity,[4]*B* stationary phase hydrogen-bond basicity,[5]*C (pH 2.8)* cation-exchange activity and [6]*C (pH 7.0)* cation-exchange activity.

9.4.2 Naphthalene

The HPLC elution orders of both naphthalene and toluene are identical and thus we can assume π-π interactions followed by hydrophobic interactions drives the retention mechanism. ^{1}H T_1 & T_2 relaxation and HPLC elution orders of naphthalene are listed in Table 9.3. Both free and bound peaks were observed in the ^{1}H NMR spectra of naphthalene in the presence of all three stationary phase which suggest that naphthalene is in the slow exchange regime. The largest change in T_1 relaxation in the presence of stationary phase compared to "solution only" was observed in the presence of BEH-phenyl. In parallel, the experimental and predicted HPLC data indicate naphthalene is most retained in the presence of BEH-phenyl. Additionally, the ^{1}H T_1 relaxation of H-2(f), H-1(b) and H-2(b) all follow the HPLC elution orders.

On the other hand, no clear correlation was observed between the ^{1}H T_2 NMR relaxation and HPLC retentions of naphthalene. Similarly to ^{1}H T_1 relaxation, slightly shorter T_2 relaxation of H-2(f) in the presence of BEH-phenyl stationary phase compared to "solution only" is observed. Taking into consideration the HSM selectivity parameters (see Table 9.2), it is apparent that BEH-phenyl has the least steric hindrance compared to BEH-C18 and BEH-RP18. Similarly to toluene, the results could suggest the difference

in experimental and predicted HPLC retention times of naphthalene on BEH-phenyl (S^* = -0.070 and H = 0.730*)* and BEH-C18 (S^* = 0.020 and H = 1.000*)* is due to π-π interactions rather than hydrophobic interactions.

Table 9.3. ^{1}H T_1 and T_2 relaxation times for naphthalene in 50:50 % v/v MeCN:D_2O (from top to bottom according to HPLC experimental elution order): mobile phase in the absence of stationary phase (solution only) and in the presence of BEH-RP18, BEH-C18 and BEH-Phenyl stationary phases. Data were obtained at 500 MHz spectrometer at 313 K and 5.0 kHz spinning frequency. Where I: experimental HPLC data and **II**: predicted HPLC data.

	SP	HPLC Rt (mins) I/**II**	T_1(s)			
			H-1(f)	H-2(f)	H-1(b)	H-2(b)
	Solution only	n/a	5.6±0.1	6.0±0.1	n/a	
MeCN/D_2O	BEH-RP18	6.80/**6.33**	7.5±1.2	6.8±0.4	2.8±0.1	3.1±0.1
	BEH-C18	8.47/**6.49**	7.1±0.2	7.7±0.5	3.5±0.1	3.5±0.1
	BEH-Phenyl	9.07/**8.07**	7.7±0.4	7.8±0.5	4.5±0.1	4.4±0.1
			T_2(s)			
			H-1(f)	H-2(f)	H-1(b)	H-2(b)
Naphthalene	Solution only	n/a	2.8±0.1	2.9±0.03	n/a	
	BEH-RP18	6.80/**6.33**	2.0±0.1	2.2±0.1	0.1±0.002	0.1±0.004
	BEH-C18	8.47/**6.49**	2.2±3.0E-2	2.3±0.04	0.1±0.002	0.1±0.001
	BEH-Phenyl	9.07/**8.07**	2.0±0.1	2.0±0.1	0.1±0.002	0.1±0.002

9.4.3 Acenaphthene

The HPLC and NMR data of acenaphthene across BEH-C18, BEH-phenyl and BEH-RP18 is illustrated in Table 9.4. The QSRR predicting model tool was not able to generate HPLC retention times. Acenaphthene and amitriptyline are the only two analytes containing an ethylene bridge between two aromatic rings. However, the QSRR model was able to generate a predictive retention time of Amitriptyline. It must be considered that amitriptyline is a large bulky molecule which also contains an aliphatic chain and amine group. Thus, acenaphthene is structurally different compared to the remaining analytes, which could explain why the QSRR model was not able to generate accurate predictions of retention times. Acquiring the experimental retention time of acenaphthene derivatives (e.g. acenaphthylene, benz(a)anthracene and fluoranthene) could improve the predictive power of the model and thus generate retention times of acenaphthene. On the hand, acenaphthene similarly to toluene, was most and least retained in the presence of BEH-phenyl and BEH-RP18 respectively.

The 1D ^{1}H NMR spectra of acenaphthene in the presence of the stationary phases indicates it is undergoing slow chemical exchange. The ^{1}H T_1 relaxation of H-1(f), H-3(f)

and H-4(f) protons in the presence of the stationary phases followed the HPLC elution order. Additionally, the largest changes in ^{1}H T_1 relaxation of H-2(f) and H-3(f) protons in the presence of stationary phase compared to "solution only" was observed in the presence of BEH-Phenyl.

Table 9.4. ^{1}H T_1 and T_2 relaxation times for acenaphthene in 50:50 % v/v MeCN:D_2O (from top to bottom according to HPLC experimental elution order): mobile phase in the absence of stationary phase (solution only) and in the presence of BEH-RP18, BEH-C18 and BEH-Phenyl stationary phases. Data were obtained at 500 MHz spectrometer at 313 K and 5.0 kHz spinning frequency. Where I: experimental HPLC data and **II**: predicted HPLC data

	SP	HPLC Rt (mins) I/**II**	T_1(s)							
			H-1(f)	H-2(f)	H-3(f)	H-4(f)	H-1(b)	H-2(b)	H-3(b)	H-4(b)
MeCN/D_2O 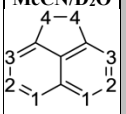 Acenaphthene	Solution only	n/a	5.9±0.2	6.1±0.4	5.8±0.3	2.7±0.1	n/a			
	BEH-RP18	7.33/**n.a**	7.5±1.1	7.5±1.2	7.1±0/6	3.4±0.2	2.8±0.1	2.9±0.1	2.7±0.1	1.4±0.1
	BEH-C18	9.18/**n.a**	7.4±0.8	7.7±1.1	5.7±0.4	2.7±0.1	2.9±0.1	2.9±0.1	2.9±0.1	1.3±0.04
	BEH-Phenyl	9.83/**n.a**	5.0±0.4	4.5±0.2	4.6±0.3	2.6±0.1	3.2±0.1	2.8±0.1	2.1±0.1	1.4±0.1
			T_2(s)							
			H-1(f)	H-2(f)	H-3(f)	H-4(f)	H-1(b)	H-2(b)	H-3(b)	H-4(b)
	Solution only	n/a	1.8±0.1	2.2±0.1	2.2±0.1	1.8±0.05	n/a			
	BEH-RP18	7.33/**n.a**	1.5±0.1	1.3±0.1	1.2±0.1	1.2±0.1	0.2±0.004	0.1±0.006	0.1±0.007	0.1±0.02
	BEH-C18	9.18/**n.a**	1.4±0.1	1.2±0.1	1.3±0.1	1.2±0.03	0.1±0.02	0.1±0.03	0.1±0.003	0.1±0.03
	BEH-Phenyl	9.83/**n.a**	1.8±0.1	1.9±0.1	1.7±0.1	1.2±0.07	0.1±0.004	0.1±0.004	0.1±0.004	0.1±0.003

Similarly to the previously discussed analytes, no clear correlation was observed between the ^{1}H T_2 relaxation data and HPLC elution orders. However, the largest change in ^{1}H T_2 relaxation of the H-1(f) and H-2(f) protons of acenaphthene in the presence of stationary phase compared to "solution only" measurements was observed in the presence of BEH-C18. As acenaphthene was most retained in the presence of BEH-phenyl and closely followed by BEH-C18, the results could suggest the slight difference in retention of acenaphthene on BEH-phenyl (S^* = -0.070 and H = 0.730*)* and BEH-C18 (S^* = 0.020 and H = 1.000*)* is due to π-π interactions rather than hydrophobic interactions.

9.4.4 Benzophenone

Another analyte which also goes through slow chemical exchange and has the same HPLC elution order of toluene is benzophenone. Both the HPLC and NMR data are summarised in Table 9.5. As illustrated from Table 9.5, the ^{1}H T_1 relaxation time of both

H-1(b) and H-2(b) protons of benzophenone follow the HPLC elution orders which could suggest both protons contribute towards the elution order observed.

Even though, the relative values of ^{1}H T_2 relaxation times of the free form of benzophenone do not correlate with the HPLC elution orders, the largest change in ^{1}H T_2 relaxation of the H-1(f)-H-3(f) protons of benzophenone in the presence of stationary phase compared to "solution only" measurements was observed in the presence of BEH-phenyl which is consistent with the strongest overall interaction with BEH-phenyl stationary phase (Rt = 9.12 mins).

Similarly to the previous analytes, the results indicate the difference in experimental and predicted retention times of benzophenone on BEH-phenyl and BEH-C18 phase is due to π-π interactions rather than hydrophobic interactions whilst also taking into consideration both the steric hindrance and hydrophobicity of both stationary phases.

Table 9.5. ^{1}H T_1 and T_2 relaxation times for benzophenone in 50:50 % v/v MeCN:D_2O (from top to bottom according to HPLC experimental elution order): mobile phase in the absence of stationary phase (solution only) and in the presence of BEH-RP18, BEH-C18 and BEH-Phenyl stationary phases. Data were obtained at 500 MHz spectrometer at 313 K and 5.0 kHz spinning frequency. Where I: experimental HPLC data and **II**: predicted HPLC data

	SP	HPLC Rt (mins) I/**II**	T_1(s)					
			H-1(f)	H-2(f)	H-3(f)	H-1(b)	H-2(b)	H-3(b)
MeCN/D_2O 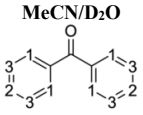 Benzophenone	Solution only	n/a	4.5±0.1	5.1±0.2	4.5±0.1	n/a		
	BEH-RP18	6.57/**6.16**	5.8±0.3	7.1±0.7	6.0±0.3	3.3±0.1	3.3±0.1	3.2±0.05
	BEH-C18	8.06/**6.71**	5.8±0.2	6.2±0.3	5.1±0.1	3.9±0.1	3.9±0.1	3.7±0.04
	BEH-Phenyl	9.12/**8.10**	6.1±0.1	6.1±0.4	5.5±0.2	4.3±0.1	4.3±0.1	3.9±0.1
			T_2(s)					
			H-1(f)	H-2(f)	H-3(f)	H-1(b)	H-2(b)	H-3(b)
	Solution only	n/a	2.8±0.04	3.0±0.1	2.8±0.04	n/a		
	BEH-RP18	6.57/**6.16**	1.9±0.02	1.9±0.1	1.8±0.02	0.2±0.01	0.1±0.01	0.1±0.004
	BEH-C18	8.06/**6.71**	2.1±0.03	2.1±0.1	1.9±0.1	0.8±0.1	0.8±0.1	0.7±0.1
	BEH-Phenyl	9.12/**8.10**	1.5±0.1	1.5±0.1	1.4±0.05	0.2±0.004	0.1±0.01	0.1±0.03

9.4.5 Biphenyl

The ^{1}H 1D spectra of biphenyl in the presence of the stationary phases indicate it is in the slow exchange regime. Similarly the previously discussed analytes, biphenyl is also most and least retained in the presence of BEH-phenyl and BEH-RP18 stationary phase respectively.

^{1}H T_1 & T_2 relaxation and HPLC elution orders of biphenyl is illustrated in Table 9.6. A strong correlation between experimental and predicted HPLC elution order of biphenyl

across the 3 stationary phases was obtained. The ^{1}H T_1 relaxation of biphenyl (H-1 free peak) followed the HPLC elution order and had the largest change in T_1 relaxation in the presence of stationary phase compared to "solution only" measurements in the presence of BEH-phenyl.

Even though no clear correlation between the ^{1}H T_2 relaxation data and HPLC retention times was observed, slightly shorter T_2 relaxation was induced in the presence of BEH-Phenyl stationary phase compared to the "solution only" measurements. More precisely, this marginal difference in T_2 relaxation was observed for the H-1(f), H-2(b) and H-3(b) protons of biphenyl. Based upon the previous analyte discussed, overall the results indicate the selectivity in retention of biphenyl on BEH-phenyl and BEH-C18 phase is due to π-π interactions rather than hydrophobic interactions. This assumption is justified by taking into consideration both the steric hindrance and hydrophobicity of both stationary phases. As BEH-RP18 has lower column hydrophobicity (H = 0.830*)* compared to BEH-C18 (H = 1.000*)*, which possibly explains why biphenyl is least retained in the presence of BEH-RP18.

Table 9.6. ^{1}H T_1 and T_2 relaxation times for biphenyl in 50:50 % v/v MeCN:D_2O (from top to bottom according to HPLC experimental elution order): mobile phase in the absence of stationary phase (solution only) and in the presence of BEH-RP18, BEH-C18 and BEH-Phenyl stationary phases. Data were obtained at 500 MHz spectrometer at 313 K and 5.0 kHz spinning frequency. Where I: experimental HPLC data and **II**: predicted HPLC data

MeCN/D_2O 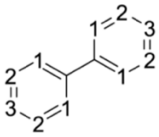 Biphenyl	SP	HPLC Rt (mins) I/**II**	T_1(s)			
			H-1(f)	H-3(f)	H-2(b)	H-3(b)
	Solution only	n/a	4.2±0.1	4.7±0.1	n/a	
	BEH-RP18	7.20/**6.67**	5.1±0.1	4.1±0.1	2.4±0.1	2.6±0.1
	BEH-C18	8.95/**6.89**	5.8±0.2	6.0±0.2	3.3±0.1	3.4±0.2
	BEH-Phenyl	9.66/**8.49**	6.1±0.5	3.5±0.2	2.9±0.1	2.7±0.1
			T_2(s)			
			H-1(f)	H-3(f)	H-2(b)	H-3(b)
	Solution only	n/a	2.8±0.03	2.9±0.04	n/a	
	BEH-RP18	7.20/**6.67**	2.1±0.2	1.5±0.2	0.2±0.003	0.2±0.005
	BEH-C18	8.95/**6.89**	2.6±0.04	2.7±0.1	0.2±0.004	0.1±0.005
	BEH-Phenyl	9.66/**8.49**	2.1±0.1	2.0±0.2	0.1±0.002	0.1±0.006

9.4.6 Butyl 4-Hydroxybenzoate

The elution order for butyl 4-hydrobenzoate is different to most of the analytes discussed so far. As listed in Table 9.7, the experimental HPLC data indicate butyl 4-hydroxybenzoate is most retained in the presence of BEH-C18. The HPLC experimental retention time of butyl 4-hydroxybenzoate in the presence of both BEH-Phenyl (Rt = 6.45 mins) and BEH-RP18 (Rt = 6.40 mins) were very similar to each other but shorter in comparison to BEH-C18 (Rt = 8.05 mins). As BEH-C18 has the highest hydrogen bonding acidity selectivity (A= -0.090) and both BEH-phenyl and BEH-RP18 (A= -0.350 and -0.370 respectively) have lower hydrogen bonding acidity selectivity, we can assume the retention mechanism of butyl 4-hydroxybenzoate is driven by the hydrogen bonding acidity interactions. Hydrogen bonding interactions could potentially be taking place either the ester or hydroxy group of butyl 4-hydroxybenzoate and the stationary phases. However, no direct agreement between the predicted and experimental HPLC results was obtained. This could be due to the different functional groups present within butyl 4-hydroxybenzoate (e.g. hydroxy group) and could indicate additionally phenol derivatives (e.g. phenol and cresol), are required to improve the predictive power of the model.

The 1D ^{1}H NMR spectra of butyl 4-hydroxybenzoate across the 3 stationary phases indicated it is undergoing slow chemical exchange as two sets of peaks were observed. No clear correlation was observed between the NMR and HPLC data. This is not surprising as both the experimental and predicted HPLC data did not correlate. However, analysing the ^{1}H T_1 relaxation times of both H-2 (b) and H-3(b) protons followed the experimental HPLC elution orders. Additionally, the largest change in ^{1}H T_1 and T_2 relaxation of butyl 4-hydroxybenzoate in the presence of stationary phase compared to "solution only" measurements was observed in the presence of BEH-RP18 stationary phase.

This could suggest the ^{1}H NMR relaxation is mostly perturbed by hydrogen bonding basicity interactions. Even though, the relative values of ^{1}H T_2 relaxation times of the free form of butyl 4-hydroxybenzoate do not correlate with the HPLC elution orders, the largest change in ^{1}H T_2 relaxation of the H-3(f) proton was observed in the presence of BEH-C18 and BEH-phenyl. This could suggest the hydrogen bonding interactions are taking place between the carbonyl group of butyl 4-hydroxybenzoate which is adjacent to H-3 protons and the stationary phases.

Table 9.7. ^{1}H T_1 and T_2 relaxation times for butyl 4-hydroxybenzoate in 50:50 % v/v MeCN:D_2O (from top to bottom according to HPLC experimental elution order): mobile phase in the absence of stationary phase (solution only) and in the presence of BEH-RP18, BEH-phenyl and BEH-C18 stationary phases. Data were obtained at 500 MHz spectrometer at 313 K and 5.0 kHz spinning frequency. Where I: experimental HPLC data and **II**: predicted HPLC data

MeCN/D_2O

Butyl 4-hydroxybenzoate

SP	HPLC Rt (mins)	T_1(s)											
		H-1(f)	H-2(f)	H-3(f)	H-4(f)	H-5(f)	H-6(f)	H-1(b)	H-2(b)	H-3(b)	H-4(b)	H-5(b)	H-6(b)
Solution only	n/a	2.8±0.01	3.0±0.01	1.6±0.01	1.6±0.01	1.9±0.01	2.1±0.01	n/a					
BEH-RP18	6.40/**6.34**	4.5±0.3	4.2±0.6	6.6±0.1	2.9±0.2	2.2±0.2	1.7±0.1	1.8±0.1	1.7±0.1	4.4±0.2	1.4±0.1	1.3±0.1	1.5±0.1
BEH-Phenyl	6.45/**7.04**	4.1±0.3	2.1±0.1	4.9±0.04	1.7±0.1	1.7±0.1	2.2±0.2	2.8±0.05	2.6±0.02	3.3±0.1	1.3±0.1	1.7±0.2	1.9±0.1
BEH-C18	8.05/**6.38**	4.1±0.1	4.6±0.2	5.7±0.1	1.7±0.1	1.8±0.1	1.8±0.1	2.9±0.1	2.8±0.1	2.4±0.2	1.4±0.1	1.5±0.1	1.5±0.1
		T_2(s)											
		H-1(f)	H-2(f)	H-3(f)	H-4(f)	H-5(f)	H-6(f)	H-1(b)	H-2(b)	H-3(b)	H-4(b)	H-5(b)	H-6(b)
Solution only	n/a	1.7±0.1	1.7±0.1	0.9±0.02	1.0±0.02	1.3±0.02	1.4±0.02	n/a					
BEH-RP18	6.40/**6.34**	0.4±0.04	0.5±0.1	0.8±0.02	0.4±0.04	0.6±0.06	0.8±0.05	0.1±0.01	0.1±0.02	0.6±0.1	0.1±0.03	0.1±0.01	0.2±0.01
BEH-Phenyl	6.45/**7.04**	0.4±0.1	0.5±0.05	0.1±0.01	0.5±0.04	0.5±0.04	0.6±0.03	0.3±0.02	0.3±0.02	0.1±0.01	0.1±0.01	0.2±0.01	0.2±0.01
BEH-C18	8.05/**6.38**	0.8±0.04	0.9±0.03	0.1±0.01	0.7±0.05	1.1±0.04	1.2±0.03	0.4±0.03	0.3±0.04	0.2±0.1	0.2±0.02	0.3±0.01	0.3±0.02

9.4.7 Dipropyl phthalate

The ^{1}H NMR relaxation and HPLC elution orders of dipropyl phthalate is illustrated in Table 9.8. Both the experimental and predicted HPLC elution orders had a good agreement. Similarly to previous analytes discussed, dipropyl phthalate is most and least retained in the presence of BEH-phenyl and BEH-RP18 which enables to assume that π-π and hydrophobic interactions drive the retention of dipropyl phthalate across the 3 stationary phases. The ^{1}H NMR spectra of dipropyl phthalate in presence of the stationary phases indicates that this analyte is in the fast chemical exchange regime. It is apparent that there was no strong correlation between the NMR and HPLC data obtained. However, the ^{1}H T_1 relaxation of H-4(a) and H-5(a) followed the HPLC elution order. Additionally, the largest change in T_1 relaxation of H-3(a) in the presence of stationary phase in comparison to solution only was observed in the presence of BEH-C18.

Table 9.8. ^{1}H T_1 and T_2 relaxation times for dipropyl phthalate in 50:50 % v/v MeCN:D_2O (from top to bottom according to HPLC experimental elution order): mobile phase in the absence of stationary phase (solution only) and in the presence of BEH-RP18, BEH-C18 and BEH-Phenyl stationary phases. Data were obtained at 500 MHz spectrometer at 313 K and 5.0 kHz spinning frequency. Where I: experimental HPLC data and **II**: predicted HPLC data

MeCN/D_2O 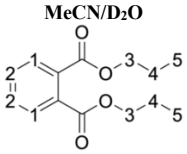 Dipropyl phthalate	SP	HPLC Rt (mins)	T_1(s)				
			H-1(a)	H-2(a)	H-3(a)	H-4(a)	H-5(a)
	Solution only	n/a	2.4±0.04	2.1±0.03	1.9±0.04	1.6±0.1	1.6±0.1
	BEH-RP18	6.91/**6.53**	3.1±0.1	2.6±0.1	2.1±0.1	1.9±0.1	1.7±0.1
	BEH-C18	8.45/**7.04**	3.9±0.1	3.2±0.04	2.6±0.1	1.9±0.2	2.0±0.2
	BEH-Phenyl	9.48/**8.64**	3.6±0.1	3.0±0.1	2.4±0.1	2.0±0.1	2.1±0.2
			T_2(s)				
			H-1(a)	H-2(a)	H-3(a)	H-4(a)	H-5(a)
	Solution only	n/a	2.0±0.09	1.9±0.05	1.3±0.04	0.8±0.03	1.3±0.02
	BEH-RP18	6.91/**6.53**	0.5±0.02	0.4±0.01	0.5±0.01	0.4±0.04	0.5±0.02
	BEH-C18	8.45/**7.04**	2.2±0.1	2.1±0.1	1.0±0.05	0.5±0.05	1.1±0.1
	BEH-Phenyl	9.48/**8.64**	1.7±0.1	1.8±0.2	1.0±0.1	0.5±0.08	0.9±0.05

On the other hand, the largest change in T_2 relaxation of all protons in the presence of stationary phase compared to "solution only" was observed in the presence of BEH-RP18. This could suggest the ^{1}H NMR relaxation measurements reports mostly on hydrophobic interaction, which makes sense if one considers that all the observed protons are located in parts of the molecule involved in hydrophobic interactions.

9.4.8 Benzoic acid and 3-hydroxybenzoic acid.

The HPLC experimental retention times of both benzoic acid and 3-hydroxybenzoic acid in the presence of both BEH-C18 and BEH-phenyl were short compared to other analytes in this study. This is not surprising as both analytes have low molecular volumes, logP and logD values (see Table 8.1 in Chapter 8). The experimental HPLC retention time of both benzoic acid and 3-hydroxybenzoic acid (Rt = 0.73 and 0.53 mins respectively) in the presence BEH-phenyl is so short it could be assumed to be unretained which could also explain why the experimental and predicted HPLC elution order did not correlate (see Tables 9.9 and 9.10).

Similarly to butyl 4-hydroxybenzoate, both analytes contain a hydroxy group which could be another reason why the QSRR model is not able to generate accurate predictive retention times. The predictive HPLC data of both analytes could suggest additionally

benzoic acid derivatives (e.g. 2-hydroxybenzoic and 4-hydroxybenzoic acid) are required to improve the accuracy of the model.

However, a significant increase in the experimental retention time for both analytes was observed in the presence of BEH-RP18. As BEH-RP18 (B = 0.090) has the highest hydrogen bonding basicity compared to both BEH-phenyl and BEH-C18 stationary phases (B = 0.030 and 0.000 respectively), the experimental HPLC data could suggest hydrogen bonding basicity interactions (see Figure 8.1) are taking place between 3-hydroxybenzoic acid, benzoic acid and the polar embedded group of BEH-RP18. Even though the experimental and predictive retention time did not correlate, the HPLC predictive data also indicate both analytes are most retained in the presence of BEH-RP18.

The ^{1}H T_1 H-1(f), H-1(b), H-2(b) and H-3(b) protons of benzoic acid followed the experimental HPLC elution order. The largest change in ^{1}H T_1 relaxation of benzoic acid in the presence of stationary phase compared to solution only was observed in the presence of BEH-RP18 across H-1-H-3(b) protons. However, no clear correlation was observed between the ^{1}H T_2 relaxation and the HPLC elution orders.

On the other hand, the ^{1}H T_1 H-1(f) and H-2(f) protons of 3-hydroxybenzoic acid followed the experimental HPLC elution order. The largest change in ^{1}H T_1 relaxation of 3-hydrobenzoic acid in the presence of stationary phase compared to "solution only" was also observed in the presence of BEH-RP18 across H-1*(f), H-2(b) and H-3(b) protons. Even though no clear correlation was as observed between the ^{1}H T_2 relaxation of 3-hydroxybenzoic acid and the HPLC data, the largest change in ^{1}H T_2 relaxation of 3-hydroxybenzoic acid in the presence of stationary phase compared to "solution only" was observed in the presence of BEH-RP18 across H-2(b) and H-3(b) protons. This could suggest hydrogen bonding interactions are taking place between the hydroxy group of 3-hydroxybenzoic acid which is adjacent to H-2 and H-3 protons and the carbamate group of BEH-RP18 which is consistent with the strongest overall interaction with BEH-RP18 stationary phase (Rt = 3.89 mins). This is a good example of how the ^{1}H NMR relaxation data supplements the HPLC experimental retention time which could potentially improve the reliability of the predictive model tool by providing atomic level information.

Table 9.9. ^{1}H T_1 and T_2 relaxation times for benzoic acid in 50:50 % v/v MeCN:D_2O (from top to bottom according to HPLC experimental elution order): mobile phase in the absence of stationary phase (solution only) and in the presence of BEH-phenyl, BEH-C18 and BEH-RP18 stationary phases. Data were obtained at 500 MHz spectrometer at 313 K and 5.0 kHz spinning frequency. Where I: experimental HPLC data and **II**: predicted HPLC data

	SP	HPLC Rt (mins)	T_1(s)					
			H-1(f)	H-2(f)	H-3(f)	H-1(b)	H-2(b)	H-3(b)
MeCN/D_2O	Solution only	n/a	4.4±0.1	4.6±0.1	4.1±0.1	n/a		
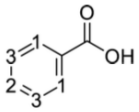	BEH-Phenyl	0.73/**4.97**	5.9±0.1	6.8±0.1	5.5±0.1	5.0±0.2	5.8±0.3	4.7±0.1
	BEH-C18	2.32/**4.75**	5.5±0.1	6.3±0.1	5.1±0.1	4.6±0.1	4.4±0.1	4.2±0.1
	BEH-RP18	4.61/**5.29**	5.0±0.1	6.7±0.2	5.2±0.1	3.8±0.1	3.1±0.2	3.3±0.1
			T_2(s)					
			H-1(f)	H-2(f)	H-3(f)	H-1(b)	H-2(b)	H-3(b)
Benzoic acid	Solution only	n/a	2.0±0.05	2.3±0.05	1.9±0.05	n/a		
	BEH-Phenyl	0.73/**4.97**	0.7±0.01	1.0±0.02	0.8±0.01	0.4±0.01	0.3±0.02	0.3±0.03
	BEH-C18	2.32/**4.75**	0.9±0.02	1.1±0.01	1.0±0.02	0.5±0.04	0.3±0.05	0.3±0.04
	BEH-RP18	4.61/**5.29**	1.1±0.03	1.5±0.04	1.2±0.02	0.7±0.07	0.3±0.04	0.3±0.05

As a whole, taking into consideration the HSM selectivity parameters, HPLC and NMR data we can assume, both benzoic acid and 3-hydroxybenzoic acts as hydrogen bond donors (hydroxy group) while the carbamate group of BEH-RP18 stationary phase acts as hydrogen bond acceptor (ester group).

Table 9.10. ^{1}H T_1 and T_2 relaxation times for 3-hydroxybenzoic acid in 50:50 % v/v MeCN:D_2O (from top to bottom according to HPLC experimental elution order): mobile phase in the absence of stationary phase (solution only) and in the presence of BEH-phenyl, BEH-C18 and BEH-RP18 stationary phases. Data were obtained at 500 MHz spectrometer at 313 K and 5.0 kHz spinning frequency. Where I: experimental HPLC data and **II**: predicted HPLC data

	SP	HPLC Rt (mins)	T_1(s)					
			H-1(f)	H-1*(f)	H-2(f)	H-3(f)	H-2(b)	H-3(b)
MECN/D_2O	Solution only	n/a	3.8±0.1	6.4±0.05	3.2±0.03	4.7±0.05	n/a	
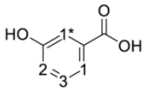	BEH-Phenyl	0.53/**4.50**	4.3±0.1	7.1±0.1	3.7±0.03	5.1±0.1	3.5±0.1	4.6±0.1
	BEH-C18	1.07/**4.30**	4.2±0.1	7.3±0.1	3.6±0.1	5.6±0.2	3.7±0.1	5.5±0.2
	BEH-RP18	3.98/**5.09**	3.4±0.1	4.6±0.1	3.1±0.04	4.3±0.1	2.4±0.1	3.1±0.1
			T_2(s)					
			H-1(f)	H-1*(f)	H-2(f)	H-3(f)	H-2(b)	H-3(b)
3-hydroxybenzoic acid	Solution only	n/a	2.6±0.04	3.4±0.04	2.4±0.03	2.6±0.03	n/a	
	BEH-Phenyl	0.53/**4.50**	1.5±0.05	1.7±0.04	1.5±0.1	1.5±0.06	0.7±0.04	1.3±0.1
	BEH-C18	1.07/**4.30**	1.7±0.04	1.8±0.04	1.6±0.05	1.7±0.05	0.9±0.07	1.0±0.1
	BEH-RP18	3.98/**5.09**	2.0±0.1	2.1±0.1	2.0±0.1	2.1±0.05	0.2±0.01	0.3±0.03

9.4.9 Aniline and 2-aminophenol.

Similarly to benzoic acid and 3-hydroxybenzoic acid, aniline and 2-aminophenol also have small molecular volumes, logD and logP values which correlates with the short HPLC retention time obtained (see Tables 9.11 and 9.12).

The ^{1}H NMR relaxation and HPLC elution orders of aniline is illustrated in Table 9.11. Both the experimental and predicted HPLC elution orders had a good correlation. Similarly to previous analytes discussed, aniline is most and least retained in the presence of BEH-phenyl and BEH-RP18. Overall, the results indicate the selectivity in retention of aniline on BEH-phenyl and BEH-C18 phase is due to π-π interactions rather than hydrophobic interactions. As BEH-RP18 has lower column hydrophobicity (see Table 9.2) compared to BEH-C18, which possibly explains why aniline is least retained in the presence of BEH-RP18.

The 1D ^{1}H NMR spectra of aniline in the presence of the stationary phases indicate aniline is undergoing slow chemical exchange. The ^{1}H T_1 NMR of H_2(b) proton of aniline followed the HPLC elution orders across the stationary phases. Additionally, the largest change in ^{1}H T_1 NMR relaxation in the presence of stationary phase compared to "solution only" measurements was observed for H-2(f) proton of aniline in the presence of BEH-phenyl. On the other hand, the ^{1}H T_2 NMR relaxation of aniline has proven harder to interpret as little difference was observed across the 3 stationary phases. Furthermore, the largest change in T_2 NMR relaxation in the presence of stationary phase compared to "solution only" measurements was observed for H-1(f) and H-2(f) protons of aniline in the presence of BEH-RP18 which still remains unclear.

On the other hand, no direct agreement between the predicted and experimental HPLC results of 2-aminophenol was obtained. The experimental HPLC retention time of 2-aminophenol (Rt = 0.70 mins) in the presence BEH-RP18 is so short it could be assumed to be unretained which could affect the accuracy of the predictive model (see Table 9.12). Additionally, 2-aminophenol also contains a hydroxy group which could be another reason why the QSRR model is not able to generate accurate predictive retention times. The predictive HPLC data of 2-aminophenol could suggest additionally derivatives (e.g. 3-aminophneol and 4-aminophenol) are required to improve the accuracy of the model.

The HPLC experimental retention time of 2-aminophenol indicates it is most and least retained in the presence of BEH-C18 and BEH-RP18 respectively. As BEH-C18 has the highest hydrogen bonding acidity selectivity (A = -0.090) and both BEH-phenyl and BEH-RP18 (A = -0.350 and -0.370 respectively) have lower hydrogen bonding acidity selectivity (see Table 9.2), we can assume the retention mechanism of 2-aminophenol is driven by the hydrogen bonding acidity interactions. Hydrogen bonding interactions could potentially be taking place either the amine or hydroxy group of 2-aminophenol and the stationary phases.

The ^{1}D ^{1}H NMR spectra of 2-aminophenol suggest it is in the fast exchange regime in the presence of the 3 stationary phases. No direct correlation was observed between the NMR relaxation measurements and the HPLC elution orders which could be due to the short retention times acquired across both BEH-RP18 and BEH-phenyl stationary phase. However, the largest change in both T_1 and T_2 relaxation measurements was observed in the presence of BEH-C18 compared to "solution only" measurements which also complements the HPLC retention of 2-aminophenol in the presence of BEH-C18. This is another great example of how the ^{1}H NMR relaxation measurements could benefit the predictive power of the QSRR model.

Table 9.11. ^{1}H T_1 and T_2 relaxation times for aniline in 50:50 % v/v MeCN:D_2O (from top to bottom according to HPLC experimental elution order): mobile phase in the absence of stationary phase (solution only) and in the presence of BEH-RP18, BEH-C18 and BEH-phenyl stationary phases. Data were obtained at 500 MHz spectrometer at 313 K and 5.0 kHz spinning frequency. Where I: experimental HPLC data and **II**: predicted HPLC data

	SP	HPLC Rt (mins)	T_1(s)			
			H-1(f)	H-2(f)	H-1(b)	H-2(b)
	Solution only	n/a	6.4 ± 0.3	7.0 ± 0.4	n/a	
MECN/D$_2$O	BEH-RP18	0.71/**3.54**	7.5 ± 0.4	8.1 ± 0.4	4.0 ± 0.2	3.7 ± 0.2
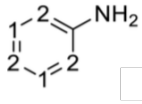	BEH-C18	4.58/**4.92**	7.4 ± 0.4	8.0 ± 0.4	3.9 ± 0.2	3.9 ± 0.2
	BEH-Phenyl	5.00/**6.08**	7.6 ± 0.4	8.7 ± 0.4	4.1 ± 0.2	4.8 ± 0.2
			T_2(s)			
			H-1(f)	H-2(f)	H-1(b)	H-2(b)
Aniline	Solution only	n/a	2.8±0.4	2.9±0.4	n/a	
	BEH-RP18	0.71/**3.54**	1.3±0.2	1.3±0.2	0.1±0.02	0.1±0.02
	BEH-C18	4.58/**4.92**	1.6±0.2	1.6±0.2	0.1±0.02	0.1±0.02
	BEH-Phenyl	5.00/**6.08**	1.5±0.2	1.6±0.2	0.1±0.02	0.1±0.01

Table 9.12. ^{1}H T_1 and T_2 relaxation times for 2-aminophenol in 50:50 % v/v MeCN:D_2O (from top to bottom according to HPLC experimental elution order): mobile phase in the absence of stationary phase (solution only) and in the presence of BEH-RP18, BEH-phenyl and BEH-C18 stationary phases. Data were obtained at 500 MHz spectrometer at 313 K and 5.0 kHz spinning frequency. Where I: experimental HPLC data and **II**: predicted HPLC data

	SP	HPLC Rt (mins)	T_1(s)		
			H-1(a)	H-2(a)	H-3(a)
MECN/ D_2O	Solution only	n/a	9.2±0.1	9.4±0.1	9.0±0.2
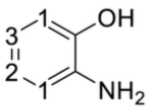	BEH-RP18	0.70/**3.19**	5.0±0.1	5.5±0.2	5.3±0.1
	BEH-Phenyl	1.58/**5.39**	5.1±0.1	6.2±0.1	6.0±0.2
	BEH-C18	3.84/**4.49**	3.7±0.1	5.4±0.2	5.6±0.1
			T_2(s)		
			H-1(a)	H-2(a)	H-3(a)
2-aminophenol	Solution only	n/a	1.8±0.02	1.8±0.02	1.7±0.02
	BEH-RP18	0.70/**3.19**	1.6±0.03	1.5±0.04	1.5±0.04
	BEH-Phenyl	1.58/**5.39**	1.8±0.03	1.6±0.1	1.6±0.1
	BEH-C18	3.84/**4.49**	1.3±0.02	1.2±0.05	1.3±0.04

9.4.10 Meclizine, hydroxyzine, propranolol and amitriptyline

Using buffered mobile phase enabled us to improve the peak shapes and obtain HPLC retention times of meclizine, hydroxyzine, propranolol and amitriptyline across the 3 stationary phase used in this study. The HPLC elution order of all 4 analytes were all the same with the longest and shortest retention time observed in the presence of BEH-phenyl and BEH-RP18 respectively. As these analytes followed the same elution order as toluene, based on the HSM selectivity parameters, the retention mechanism of these analytes is driven by π-π interactions followed by hydrophobic interactions.

The ^{1}H T_1 NMR relaxation of the all 4 analytes in the presence of the stationary phases compared to solution only were very similar. Additionally, in some cases the ^{1}H T_2 of particular protons across the 4 analytes in the presence of stationary phases were longer compared to the T_2 measured in the absence of any stationary phase (as illustrated in Table 9.13). As we previously established in Chapter 7, this could suggest strong interactions between the analyte and stationary phase leads to strong retention of the molecule which leads to a decrease of the amplitude of motion. This is plausible as all 4 analytes have the longest retention times with large molecular volumes, logP and logD values. However, T_1 and T_2 relaxation is not sufficient to fully comprehend the internal dynamics of theses analytes [357].

Table 9.13. ^{1}H T_1 and T_2 relaxation times for meclizine in 50:50 % v/v MeCN:D_2O (from top to bottom according to HPLC experimental elution order): mobile phase in the absence of stationary phase (solution only) and in the presence of BEH-RP18, BEH-C18 and BEH-phenyl stationary phases. Data were obtained at 500 MHz spectrometer at 313 K and 5.0 kHz spinning frequency. Where I: experimental HPLC data and **II**: predicted HPLC data

MECN/D_2O 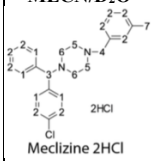 Meclizine 2HCl	SP	HPLC Rt (mins)	T_1(s)						
			H-1(a)	H-2(a)	H-3(a)	H-4(a)	H-5(a)	H-6(a)	H-7(a)
	Solution only	n/a	1.2±0.03	1.8±0.03	0.6±0.03	0.4±0.05	0.4±0.03	0.4±0.02	1.1±0.02
	BEH-RP18	5.60/**5.29**	1.2±0.02	1.7±0.03	0.5±0.04	0.4±0.04	0.3±0.04	0.3±0.05	0.9±0.1
	BEH-C18	10.24/**8.67**	1.2±0.1	1.7±0.1	0.5±0.1	0.4±0.1	0.3±0.1	0.3±0.1	0.9±0.1
	BEH-Phenyl	11.52/**10.16**	1.1±0.04	1.5±0.1	0.5±0.1	0.4±0.1	0.3±0.05	0.3±0.1	0.9±0.1
			T_2(s)						
			H-1(a)	H-2(a)	H-3(a)	H-4(a)	H-5(a)	H-6(a)	H-7(a)
	Solution only	n/a	0.6±0.03	1.0±0.02	0.5±0.01	0.3±0.01	0.2±0.002	0.2±0.002	0.8±0.01
	BEH-RP18	5.60/**5.29**	0.6±0.02	0.7±0.02	0.3±0.01	0.3±0.004	0.2±0.002	0.2±0.004	0.7±0.01
	BEH-C18	10.24/**8.67**	0.8±0.02	1.0±0.02	0.4±0.01	0.3±0.02	0.2±0.005	0.2±0.004	0.8±0.02
	BEH-Phenyl	11.52/**10.16**	0.6±0.02	0.7±0.03	0.4±0.01	0.3±0.01	0.2±0.003	0.2±0.004	0.7±0.01

9.5 Conclusion

In this chapter we investigated the predictive power of QSRR model tool of 15 analytes across BEH-C18, BEH-phenyl and BEH-RP18 HPLC stationary phases. We have shown a that a good agreement between the experiment and predicted HPLC elution order were obtained.

However, the QSRR model was not able to generate predictive retention time for acenaphthene. Apart from amitriptyline, acenaphthene is the only aromatic analyte with a bridge ethylene group between two aromatic rings. As acenaphthene is structurally different to the remaining analytes, this outcome could suggest additionally experimental HPLC retention time of acenaphthene derivatives (e.g. acenaphthylene and fluoranthene) is required to improve the predictive power of the QSRR model.

We have also compared the ^{1}H T_1 and T_2 relaxation to both the predicted and experimental HPLC data. Even though no quick and simple correlation was established between the NMR relaxation and HPLC data, some correlation between T_1 relaxation and HPLC data of specific protons was observed. Furthermore, the largest change in T_1 or T_2 relaxation (proton specific) in the presence of stationary phases compared to solution only measurements was observed with the stationary phases which the analytes were most retained.

Based on the HSM selectivity parameters, HPLC data and NMR data the following observations were made: (1) Generally most analytes were most retained in the presence of BEH-phenyl followed by BEH-C18 and BEH-RP18 where the difference in retention of these analytes on BEH-phenyl (S^* = -0.070 and H = 0.730*)* and BEH-C18 (S^* = 0.020 and H = 1.000*)* is due to π-π interactions rather than hydrophobic interactions, (2) both 2-aminophenol and butyl 4-hydroxybenzoate were most and least retained in the presence of BEH-C18 (A = -0.090) and BEH-RP18 (A = -0.370) respectively which could indicate the difference in retention of both analytes on BEH-C18 and BEH-RP18 is due to hydrogen bonding acidity rather than hydrophobic interactions, (3) benzoic acid and 3-hydroxybenzoic acid both have small molecular volumes, logP and logD values but were significantly retained in the presence of BEH-RP18 (B = 0.090) and least retained in the presence of BEH-phenyl (B = 0.030) which suggests this distinguishable difference in retention times on BEH-RP18 and BEH-phenyl is due to hydrogen bonding basicity interactions potentially taking place between the analyte hydroxy group and carbamate embedded group of BEH-RP18, (4) the QSRR model was not able to accurately predict the elution order of butyl 4-hydroxybenzoate, benzoic acid, 3-hydroxybenzoic acid and 2-aminophenol. Some of these analytes have low molecular volumes, logP, logD and in some cases very short experimental retention time was obtained (e.g. 0.53 and 0.73 minutes) which could be assumed to be unretained in the presence of certain stationary phases. However, one important factor to take into consideration is the fact that all four analytes have a hydroxy group. In some cases, the NMR results have indicated large changes in ^{1}H T_2 relaxation with protons adjacent to the hydroxy group (e.g. 3-hydroxybenzoic acid in the presence of BEH-RP18). This could suggest additional experimental HPLC data of phenol derivatives is required to improve the predictive power of the QSRR Model and (5) in contrast, meclizine, hydroxyzine, propranolol and amitriptyline which are bulky molecules with large molecular volumes, high logP and logD had the longest retention time which was expected. However both T_1 and T_2 relaxation is not sufficient enough to fully understand the internal dynamics of these analytes.

This study can be taken further by increasing the number of analytes (e.g. more functional groups), mobile phases and stationary phases. Due to the limited library of HPLC data acquired by Pfizer, the algorithm software was only able to predict data across BEH-C18, BEH-phenyl and BEH-RP18 stationary phases. This study can be taken further by obtaining retention times of the analytes in the presence of CSH hexyl-phenyl and HSS

T3 stationary phase. Moreover, the ^{1}H NMR relaxation measurements could be incorporated as quantitative descriptors into the algorithm model to determine whether our NMR measurements improves the overall predictive performance of the algorithm model. Additionally, NMR relaxation measurements could be used to facilitate our understanding of the effect of temperature, organic solvent, buffer and pH on the predictive power of the algorithm model. Furthermore, the robustness and repeatability of algorithm model could be investigated by obtaining repeated experiment HPLC, predictive HPLC and NMR measurement through a linear regression model.

10 SUMMARY

Both suspended and solid state NMR spectroscopy techniques have previously been used to characterise the chemical structures of various HPLC stationary phase and to probe the molecular motion within a HPLC system. The development of MAS has enabled us to investigate RP-HPLC heterogeneous systems by averaging dipolar coupling, anisotropic interactions and susceptibility variation in heterogenous samples. Several studies have used ^{1}H, ^{2}H, ^{13}C, ^{14}N and ^{29}Si NMR techniques to determine the chemical structures of various stationary phases. Additionally, ^{1}H and ^{13}C T_1 and T_2 relaxation measurements are well known for probing the molecular motion within a heterogeneous HPLC system. However, a major advantage of ^{1}H HR MAS NMR relaxation compared to ^{13}C relaxation is the ability to obtain both qualitative and quantitative information at an atomic level reasonably quickly.

In this thesis, a range of NMR techniques were used to improve our understanding of the molecular structures and dynamics of several RP-HPLC heterogeneous system.

Developing a robust, reliable and reproducible method is essential in analytical chemistry. Therefore, in chapter 5 we proposed logical step by step method development to optimise both T_1 and T_2 NMR relaxation measurements. We discovered several factors such as (1) rotor sizes, (2) radio frequency (RF) pulse powers, (3) T_1 pulse sequences, (4) spinning frequency, (5) temperature, (6) analyte concentration, (7) mobile phase ratio, (8) organic solvent, (9) buffer, (10) mixtures of analytes, (11) analyte chemical and physical properties and (12) DSS concentration influences the ^{1}H HR MAS NMR spectra and relaxation measurements within a system. A paired sample t-test showed our developed NMR technique to be robust and reliable. Additionally, a linear regression model was

used to determine the effect of sample preparation on reliability of the NMR method. Our model illustrated sample preparation has an effect on the NMR method but not significant enough to affect the method's reproducibility and repeatability.

Elucidating the chemical structures of the RP-HPLC stationary phases investigated in this study is crucial for probing potential molecular interactions. In Chapter 6, we used AFM to probe the topography and morphology of the BEH-C18, BEH-phenyl, BEH-RP18, CSH hexyl-phenyl and HSS T3 RP-HPLC stationary phases. Furthermore, both Raman and NMR spectroscopy was used to determine the atomic bonds and chemical structures of the 5 RP-stationary phases respectively. ^{1}H, ^{13}C and ^{29}Si NMR techniques have proven extremely reliable to confirm the chemical arrangement and functional groups embedded in each RP-HPLC stationary phase. Furthermore, there was a significant difference between the aliphatic and aromatic ligand grouped stationary phases via NMR spectroscopy. This study could be taken further by obtaining ^{1}H, ^{13}C and ^{29}Si spectra of the stationary phases at varied temperature and in the presence of mobile phase to determine the molecular motion and dynamics of the RP-HPLC stationary phases. Furthermore, the hydrolytic stability of the packing materials in aqueous conditions could also be developed by ^{29}Si CP-MAS experiments.

The true power of ^{1}H HR MAS NMR is its ability to probe the dynamic processes within a system. In Chapter 7 we demonstrated several approaches of interpreting and expressing both T_1 and T_2 for probing the molecular interactions within a system. We have critically evaluated the basic premise of our approach that changes in molecular motions of analytes due to interactions with stationary phases can be used to indirectly report on the interactions.

We have illustrated how a whole range of chemical exchange regimes, from slow to fast exchange, can be observed for analytes interacting with the stationary phase. We have also shown that different sites in molecules can exhibit exchange in different regimes at the same time. We have demonstrated the measured relaxation rates depend upon the chemical regime and strength of interaction. The T_1 relaxation was investigated to probe the molecular interactions between aniline, 2-aminophenol and various HPLC stationary phases. We have discovered, hinderance of rotation due to transient interactions leads to shorter T_1 times only if the correlation times for overall rotational diffusion of free and interacting analytes are in the fast motion limit. However, interpreting T_1 times can be complex when the correlation time is over a range of values.

We have investigated two approaches of estimating T_2 relaxation times. Due to the additional contributions from magnetic field inhomogeneities and unresolved long range ^{1}H-^{1}H scalar couplings, the T_2 relaxation times obtained using peak widths based method were generally underestimated. The T_2 relaxation values acquired via CPMG pulses sequence were more representative of what we would expect. To acquire accurate, reliable and reproducible ^{1}H T_2 relaxation measurements, the data discussed throughout this project was obtained using CPMG pulse sequence.

We demonstrated that the challenging nature of the problem where the changes in time scale and amplitude of motion as a result of interaction have complex effects on the measured rates and contribute in a different way in different exchange regimes, often requires that we consider both T_1 and T_2 in order to get insights into the complex interdependencies for different interactions between analytes and stationary phase.

In spite of this challenge, we can gain considerable understanding of the retention mechanisms for different analytes provided that we are aware of the basic assumptions and limitations of the proposed approach. For instance, we can determine which parts of the molecules are the most affected on different stationary phases and thus potentially link it to specific types of interactions.

Finally, we demonstrated the equilibrium constants are obtainable for an analyte in the slow exchange regime with well resolved peaks. Although this approach is rapid and simple for probing the interactions between analytes and stationary phases, it does come with several constraints. For example, overlapping peaks complicates the estimations of the equilibrium constants and the equilibrium constants are not obtainable if an analyte is in the fast exchange regime.

In the absence of simple “one fits all” approach we shown that analysis combining both ^{1}H T_1 and T_2 relaxation times is the most robust and informative from all the considered approaches. This best approach was used to study interactions of the analytes with stationary phases in the remainder of this thesis.

In Chapter 8, we have demonstrated ^{1}H NMR relaxation measurements have offered supplementary information for probing molecular interactions of several analytes with different functional groups, mobile phases and RP-HPLC stationary phases. It is crucial to consider several parameters such as chemical structure, functional group, stationary phases selectivity parameters and exchange processes to comprehend the type of

interaction which drives the retention mechanism of analyte and RP-HPLC stationary phase.

From both the NMR and HPLC results obtained, we discovered, (1) As expected, hydrophobic interactions drive the retention mechanism of most analytes in the presence of BEH-C18 (H = 1.000) and HSS T3 (H = 0.940) stationary phases (aliphatic chain phases) as they both have the highest hydrophobicity selectivity, (2) as expected, pi-pi stacking interactions takes place in the presence of BEH-phenyl (S^* = -0.070) and CSH hexyl-phenyl (S^* = -0.059) (i.e. 2-aminophenol dissolved in 50:50 MeOH:D_2O) as both phases have the lowest steric hindrance selectivity, (3) hydrogen bonding basicity interactions again as expected - drive retention between hydrogen donor functional groups (e.g. hydroxy group of benzoic acid) and the hydrogen acceptor groups from the polar embedded carbamate group of BEH-RP18 (ester group) and (4) analytes with large molecular volume, logD and logP values (e.g. meclizine and amitriptyline) are more strongly retained relative to the other analytes studies across the 5 stationary phases.

Finally, Chapter 9 focused on using ^{1}H HR MAS NMR T_1 and T_2 relaxation measurements to provide new insights on the predictive power and varieties of RP-HPLC interactions generated by QSRR predictive model tool. Since not all the analytes eluted under isocratic conditions as discussed in Chapter 8, both buffered mobile phase and gradient elution was used during the RP-HPLC experiments to ensure all the analytes are eluted in a shorter experimental time to enable reduced band broadening and thus detection of the eluting peaks. Retention times of individual peaks from experimental runs were used as input data for the QSRR model tool. Additionally, the QSRR model tool was used to predict the retention of all 15 analytes with one mobile phase and with the presence of BEH-C18, BEH-phenyl and BEH-RP18 stationary phases.

Similarly to Chapter 8, all measurements across all 3 techniques (NMR relaxation, HPLC experimental and predictive retention time) were compared. The experimental and predictive HPLC data indicated a majority of the analytes were most retained in the presence of BEH-Phenyl followed by BEH-C18 and BEH-RP18 where the difference in retention of these analytes on BEH-phenyl (S^* = -0.070 and H = 0.730) and BEH-C18 (S^* = 0.020 and H = 1.000) is due to π-π interactions rather than hydrophobic interactions. Even though no quick and simple correlation was established between the NMR relaxation and HPLC data, some correlation between proton specific T_1 relaxation of most analytes was obtained. Additionally, in some cases the largest change in T_2 relaxation (proton specific) in the presence of stationary phase compared to solution only

measurements was observed in the presence of BEH-phenyl (H-1(f) and H-2(f) protons of benzophenone) consistent with the strongest overall interactions with stationary phase.

Both 2-aminophenol and butyl 4-hydroxybenzaote were most and least retained in the presence of BEH-C18 (A = -0.090) and BEH-RP18 (A = -0.370) respectively which could indicate the difference in retention of both analytes on BEH-C18 and BEH-RP18 is due to hydrogen bonding acidity interactions rather than hydrophobic interactions. Even though no clear correlation between the NMR relaxation and HPLC elution orders (predicted and experimental) of 2-aminphenol was observed, the largest change in both T_1 and T_2 (H-1(f) and H-2(f) protons) in the presence of stationary phase compared to solution only was observed in the presence of BEH-C18 which consistent with the strongest overall interactions with BEH-C18 stationary phase.

Benzoic acid and 3-hydroxybenzoic acid both have small molecular volumes, logP and logD values but were significantly retained in the presence of BEH-RP18 (B = 0.090) and least retained in the presence of BEH-phenyl (B = 0.030) which suggest this distinguishable difference in retention times on BEH-RP18 and BEH-phenyl is due to hydrogen bonding basicity interactions potentially taking place between the analyte hydroxy group and carbamate embedded group of BEH-RP18. For instance, the largest change in ^{1}H T_2 relaxation of 3-hydroxybenzoic acid in the presence of stationary phase compared to solution only was observed in the presence of BEH-RP18 across H-2(b) and H-3(b) protons. This could suggest the hydrogen bonding interactions are taking place between the hydroxy group of 3-hydroxybenzoic acid which is adjacent to H-2 and H-3 protons and the carbamate group of BEH-RP18 consistent with the strongest overall interaction with stationary phase.

However, the QSRR model was not able to generate predictive retention time of acenaphthene. Considering acenaphthene is structurally different to the remaining analytes (e.g. contains a bridged ethylene group between the two aromatic rings), this could suggest further experimental HPLC retention time of acenaphthene derivatives (e.g. acenaphthylene and fluoranthene) is required to improve the predictive power of the QSRR model.

Furthermore, the QSRR model was not able to accurately predict the elution order of butyl 4-hydroxybenzoate, benzoic acid, 3-hydroxybenzoic acid and 2-aminophenol. Some of these analytes have low molecular volumes, logP, logD and in some cases very short experimental retention time was obtained (e.g. 0.53 and 0.73 minutes) which could be

assumed to be unretained in the presence of certain stationary phases. However, one important factor to take into consideration is the fact that all four analytes have a hydroxy group. In some cases, the NMR results has indicated large changes in ^{1}H T_2 relaxation with protons adjacent to the hydroxy group (e.g. 3-hydroxybenzoic acid in the presence of BEH-RP18). Similarly to acenaphthene, this could suggest additionally experimental HPLC data of phenol derivatives is required to improve the predictive power of the QSRR Model.

Finally, meclizine, hydroxyzine, propranolol and amitriptyline which are bulky molecules with large molecular volumes and high logP and logD had the longest retention times which was expected. However, as we have established in both Chapter 7 and 8, both T_1 and T_2 relaxation is not sufficient to fully understand the internal dynamics of these analytes.

In summary, the ^{1}H HR MAS NMR relaxation measurements have provided an insight of the chemical structures and molecular dynamics of RP-HPLC heterogeneous systems. As mentioned throughout this thesis, NMR relaxation measurements can be used to uncover various interactions between many analytes, mobile phases and RP-HPLC stationary phases.

The NMR techniques used in this study have several potential future applications such as temperature-dependent solid-state NMR experiments could probe the mobility of HPLC bonded stationary phases functional ligands. Both ^{1}H MAS NMR and ^{13}C CP/MAS NMR spectra can be used to determine the bonding densities and surface modification chemistry of HPLC stationary phases. Furthermore, the influence of solvents on bonded-phase structures can be examined via NMR relaxation measurements.

Since our developed and optimised method has proven robust, this preliminary study is currently applied in a variety of projects. For instance, one project aims to gain a further insight into the molecular behaviour of bare silica (un-bonded) and amide functionalised stationary phases in HILIC by NMR techniques. Both ^{1}H and ^{13}C MAS solid state NMR are used to investigate HILIC amide stationary phase as a function of the mobile phase and additives.

In another project, our developed and optimised ^{1}H HR MAS NMR T_1 and T_2 relaxation techniques will be used to characterise the interactions between six analytes, two buffered mobile phases, bare silica and amide functionalised stationary phase in RP-HPLC

heterogeneous systems. Furthermore, measurements of solvent relaxation will also be used to determine the role of solvent in the retention mechanism.

11 REFERENCES

1. Snyder, L.R., J.J. Kirkland, and J.L. Glajch, *Practical HPLC method development*. 2012: John Wiley & Sons.
2. Singh, R., *HPLC method development and validation-an overview.* Journal of Pharmaceutical Education and Research, 2013. **4**(1): p. 26.
3. Watanabe, N. and E. NIKI, *Direct-coupling of FT-NMR to high performance liquid chromatography.* Proceedings of the Japan Academy, Series B, 1978. **54**(4): p. 194-199.
4. Lindon, J.C., J.K. Nicholson, and I.D. Wilson, *Direct coupling of chromatographic separations to NMR spectroscopy.* Progress in Nuclear Magnetic Resonance Spectroscopy, 1996. **29**(1-2): p. 1-49.
5. Albert, K., *On-line use of NMR detection in separation chemistry.* Journal of Chromatography A, 1995. **703**(1-2): p. 123-147.
6. Swartz, M., *HPLC Detectors: A Brief Review.* Journal of Liquid Chromatography & Related Technologies, 2010. **33**(9-12): p. 1130-1150.
7. Arayne, M.S., N. Sultana, and M.H. Zuberi, *Development and validation of RP-HPLC method for the analysis of metformin.* Pakistan Journal of Pharmaceutical Sciences, 2006. **19**(3): p. 231-5.
8. Shanker, K., A. Fatima, A. Negi, V. Gupta, M. Darokar, M. Gupta, and S. Khanuja, *RP-HPLC method for the quantitation of glabridin in Yashti-madhu (Glycyrrhiza glabra).* Chromatographia, 2007. **65**(11-12): p. 771-774.
9. Dumarey, M., R. Sneyers, W. Janssens, I. Somers, and Y. Vander Heyden, *Drug impurity profiling: Method optimization on dissimilar chromatographic systems: Part I: pH optimization of the aqueous phase.* Analytica Chimica Acta, 2009. **656**(1-2): p. 85-92.
10. Fanali, S., P.R. Haddad, C. Poole, and M.-L. Riekkola, *Liquid chromatography: fundamentals and instrumentation*. 2017: Elsevier.
11. Tyrkkö, E., A. Pelander, and I. Ojanperä, *Prediction of liquid chromatographic retention for differentiation of structural isomers.* Analytica Chimica Acta, 2012. **720**: p. 142-148.
12. Hoang, T., D. Cuerrier, S. McClintock, and M. Di Maso, *Computer-assisted method development and optimization in high-performance liquid chromatography.* Journal of Chromatography A, 2003. **991**(2): p. 281-287.
13. Hewitt, E.F., P. Lukulay, and S. Galushko, *Implementation of a rapid and automated high performance liquid chromatography method development strategy for pharmaceutical drug candidates.* Journal of Chromatography A, 2006. **1107**(1-2): p. 79-87.
14. Xiao, K.P., Y. Xiong, F.Z. Liu, and A.M. Rustum, *Efficient method development strategy for challenging separation of pharmaceutical molecules using*

advanced chromatographic technologies. Journal of Chromatography A, 2007. **1163**(1-2): p. 145-56.

15. Djurdjevic, P., A. Ciric, A. Djurdjevic, and M.J. Stankov, *Optimization of separation and determination of moxifloxacin and its related substances by RP-HPLC.* Journal of Pharmaceutical and Biomedical Analysis, 2009. **50**(2): p. 117-26.
16. Dolan, J., D. Lommen, and L. Snyder, *Drylab® computer simulation for high-performance liquid chromatographic method development: II. Gradient elution.* Journal of Chromatography A, 1989. **485**: p. 91-112.
17. Boswell, P.G., D.R. Stoll, P.W. Carr, M.L. Nagel, M.F. Vitha, and G.A. Mabbott, *An advanced, interactive, high-performance liquid chromatography simulator and instructor resources.* Journal of Chemical Education, 2013. **90**(2): p. 198-202.
18. Tyteca, E., J.-L. Veuthey, G. Desmet, D. Guillarme, and S. Fekete, *Computer assisted liquid chromatographic method development for the separation of therapeutic proteins.* Analyst, 2016. **141**(19): p. 5488-5501.
19. Borman, P., J. Roberts, C. Jones, M. Hanna-Brown, R. Szucs, and S. Bale, *The development phase of an LC method using QbD principles.* Separation Sciences, 2010. **2**: p. 2-8.
20. Hanna-Brown, M., P. Borman, S. Bale, R. Szucs, J. Roberts, and C. Jones, *Development of chromatographic methods using QbD principles.* Separation Sciences, 2010. **2**: p. 12-20.
21. Talebi, M., G. Schuster, R.A. Shellie, R. Szucs, and P.R. Haddad, *Performance comparison of partial least squares-related variable selection methods for quantitative structure retention relationships modelling of retention times in reversed-phase liquid chromatography.* Journal of Chromatography A, 2015. **1424**: p. 69-76.
22. Tyteca, E., M. Talebi, R. Amos, S.H. Park, M. Taraji, Y. Wen, R. Szucs, C.A. Pohl, J.W. Dolan, and P.R. Haddad, *Towards a chromatographic similarity index to establish localized quantitative structure-retention models for retention prediction: use of retention factor ratio.* Journal of Chromatography A, 2017. **1486**: p. 50-58.
23. Talebi, M., S.H. Park, M. Taraji, Y. Wen, R.I. Amos, P.R. Haddad, R.A. Shellie, R. Szucs, C.A. Pohl, and J.W. Dolan, *Retention time prediction based on molecular structure in pharmaceutical method development: a perspective.* LCGC North America, 2016. **34**(8): p. 550-558.
24. Amos, R.I., E. Tyteca, M. Talebi, P.R. Haddad, R. Szucs, J.W. Dolan, and C.A. Pohl, *Benchmarking of Computational Methods for Creation of Retention Models in Quantitative Structure–Retention Relationships Studies.* Journal of Chemical Information and Modeling, 2017. **57**(11): p. 2754-2762.
25. Taraji, M., P.R. Haddad, R.I. Amos, M. Talebi, R. Szucs, J.W. Dolan, and C.A. Pohl, *Error measures in quantitative structure-retention relationships studies.* Journal of Chromatography A, 2017. **1524**: p. 298-302.
26. Wen, Y., M. Talebi, R.I. Amos, R. Szucs, J.W. Dolan, C.A. Pohl, and P.R. Haddad, *Retention prediction in reversed phase high performance liquid chromatography using quantitative structure-retention relationships applied to the Hydrophobic Subtraction Model.* Journal of Chromatography A, 2018. **1541**: p. 1-11.
27. Amos, R.I., P.R. Haddad, R. Szucs, J.W. Dolan, and C.A. Pohl, *Molecular Modelling and Prediction Accuracy in Quantitative Structure-Retention Relationship Calculations for Chromatography.* TrAC Trends in Analytical Chemistry, 2018.

28. Kaliszan, R., *QSRR: quantitative structure-(chromatographic) retention relationships.* Chemical Reviews, 2007. **107**(7): p. 3212-3246.
29. Dander, A., L.A. Mueller, R. Gallasch, S. Pabinger, F. Emmert-Streib, A. Graber, and M. Dehmer, *[COMMODE] a large-scale database of molecular descriptors using compounds from PubChem.* Source Code for Biology and Medicine, 2013. **8**(1): p. 22.
30. Becker, E.D., *Magnetic resonance: An account of some key discoveries and their consequences.* Applied spectroscopy, 1996. **50**(11): p. 16A-28A.
31. Gorter, C. and L. Broer, *Negative result of an attempt to observe nuclear magnetic resonance in solids.* Physica, 1942. **9**(6): p. 591-596.
32. Ramsey, N.F., *Early history of magnetic resonance.* Physics in perspective, 1999. **1**(2): p. 123-135.
33. Rabi, I.I., S. Millman, P. Kusch, and J.R. Zacharias, *The Molecular Beam Resonance Method for Measuring Nuclear Magnetic Moments. The Magnetic Moments of Li 6 3, Li 7 3 and F 19 9.* Physical Review, 1939. **55**(6): p. 526.
34. Braak, D., Q.-H. Chen, M.T. Batchelor, and E. Solano, *Semi-classical and quantum Rabi models: in celebration of 80 years.* Journal of Physics A: Mathematical and Theoretical, 2016. **49**(30): p. 300301.
35. Pfeifer, H., *A short history of nuclear magnetic resonance spectroscopy and of its early years in Germany.* Magnetic Resonance in Chemistry, 1999. **37**(13).
36. Rigden, J.S., *Quantum states and precession: The two discoveries of NMR.* Reviews of Modern Physics, 1986. **58**(2): p. 433.
37. Bloch, F. and I.I. Rabi, *Atoms in variable magnetic fields.* Reviews of Modern Physics, 1945. **17**(2-3): p. 237.
38. Purcell, E.M., H. Torrey, and R.V. Pound, *Resonance absorption by nuclear magnetic moments in a solid.* Physical Review, 1946. **69**(1-2): p. 37.
39. Bloch, F., *Nuclear induction.* Physical review, 1946. **70**(7-8): p. 460.
40. Manoharan, P. and G. Chandramouli, *Evolution of Magnetic Resonance Spectroscopy.* ChemInform, 2000. **31**(43).
41. Proctor, W. and F. Yu, *The dependence of a nuclear magnetic resonance frequency upon chemical compound.* Physical Review, 1950. **77**(5): p. 717.
42. Dickinson, W., *Dependence of the F 19 nuclear resonance position on chemical compound.* Physical Review, 1950. **77**(5): p. 736.
43. Ramsey, N.F., *Magnetic shielding of nuclei in molecules.* Physical Review, 1950. **78**(6): p. 699.
44. Gutowsky, H. and C. Hoffman, *Chemical Shifts in the Magnetic Resonance of F 19.* Physical Review, 1950. **80**(1): p. 110.
45. Meyer, L., A. Saika, and H. Gutowsky, *Electron Distribution in Molecules. III. The Proton Magnetic Spectra of Simple Organic Groups1.* Journal of the American Chemical Society, 1953. **75**(18): p. 4567-4573.
46. Rabi, I.I., N. Ramsey, and J. Schwinger, *Use of rotating coordinates in magnetic resonance problems.* Reviews of Modern Physics, 1954. **26**(2): p. 167.
47. Ernst, R.R. and W.A. Anderson, *Application of Fourier Transform Spectroscopy to Magnetic Resonance.* Review of Scientific Instruments, 1966. **37**(1): p. 93-102.
48. Ernst, R.R., G. Bodenhausen, and A. Wokaun, *Principles of nuclear magnetic resonance in one and two dimensions*. Vol. 14. 1987: Clarendon Press Oxford.
49. Ernst, R.R., *Nuclear Magnetic Resonance Fourier Transform Spectroscopy (Nobel lecture).* Angewandte Chemie International Edition in English, 1992. **31**(7): p. 805-823.
50. Andrew, E., A. Bradbury, and R. Eades, *Nuclear magnetic resonance spectra from a crystal rotated at high speed.* Nature, 1958. **182**(4650): p. 1659.

51. Andrew, E., A. Bradbury, and R. Eades, *Removal of dipolar broadening of nuclear magnetic resonance spectra of solids by specimen rotation.* Nature, 1959. **183**(4678): p. 1802-1803.
52. Lowe, I., *Free induction decays of rotating solids.* Physical Review Letters, 1959. **2**(7): p. 285.
53. Agarwal, V., S. Penzel, K. Szekely, R. Cadalbert, E. Testori, A. Oss, J. Past, A. Samoson, M. Ernst, and A. Böckmann, *De Novo 3D Structure Determination from Sub-milligram Protein Samples by Solid-State 100 kHz MAS NMR Spectroscopy.* Angewandte Chemie International Edition, 2014. **53**(45): p. 12253-12256.
54. Kobayashi, T., K. Mao, P. Paluch, A. Nowak-Król, J. Sniechowska, Y. Nishiyama, D.T. Gryko, M.J. Potrzebowski, and M. Pruski, *Study of Intermolecular Interactions in the Corrole Matrix by Solid-State NMR under 100 kHz MAS and Theoretical Calculations.* Angewandte Chemie International Edition, 2013. **52**(52): p. 14108-14111.
55. Hartmann, S. and E. Hahn, *Nuclear double resonance in the rotating frame.* Physical Review, 1962. **128**(5): p. 2042.
56. Pines, A., M. Gibby, and J. Waugh, *Proton-Enhanced Nuclear Induction Spectroscopy. A Method for High-Resolution NMR of Dilute Spins in Solids*. 1972, Massachusetts Inst. of Tech., Cambridge.
57. Sarkar, S.K., R.S. Garigipati, J.L. Adams, and P.A. Keifer, *An NMR method to identify nondestructively chemical compounds bound to a single solid-phase-synthesis bead for combinatorial chemistry applications.* Journal of the American Chemical Society, 1996. **118**(9): p. 2305-2306.
58. Stover, H. and J. Fréchet, *NMR characterization of crosslinked polystyrene gels.* Macromolecules, 1991. **24**(4): p. 883-888.
59. Gross, J., P. Costa, J. Dubacq, D. Warschawski, P. Lirsac, P. Devaux, and R. Griffin, *Multidimensional NMR in lipid systems. Coherence transfer through J couplings under MAS.* Journal of Magnetic Resonance, Series B, 1995. **106**(2): p. 187-190.
60. Maas, W., F. Laukien, and D. Cory, *Gradient, high resolution, magic angle sample spinning NMR.* Journal of the American Chemical Society, 1996. **118**(51): p. 13085-13086.
61. Alam, T.M. and J.E. Jenkins, *HR-MAS NMR spectroscopy in material science*. 2012.
62. Wong, A., B. Jiménez, X. Li, E. Holmes, J.K. Nicholson, J.C. Lindon, and D. Sakellariou, *Evaluation of high resolution magic-angle coil spinning NMR spectroscopy for metabolic profiling of nanoliter tissue biopsies.* Analytical Chemistry, 2012. **84**(8): p. 3843-3848.
63. Beckonert, O., M. Coen, H.C. Keun, Y. Wang, T.M. Ebbels, E. Holmes, J.C. Lindon, and J.K. Nicholson, *High-resolution magic-angle-spinning NMR spectroscopy for metabolic profiling of intact tissues.* Nature Protocol, 2010. **5**(6): p. 1019-32.
64. Lakshmi, L.J., P.K. Rao, V.M. Mastikhin, and A.V. Nosov, *Characterization of tungsten trioxide/aluminum phosphate hydrotreating catalysts by proton magic angle spinning [MAS] NMR spectroscopy and low-temperature oxygen chemisorption.* The Journal of Physical Chemistry, 1993. **97**(44): p. 11373-11375.
65. Anderson, M.W., J. Klinowski, and P.J. Barrie, *Proton magic-angle-spinning NMR studies of the adsorption of alcohols on molecular sieve catalysts.* The Journal of Physical Chemistry, 1991. **95**(1): p. 235-239.

66. Fitch, W.L., G. Detre, C.P. Holmes, J.N. Shoolery, and P.A. Keifer, *High-resolution 1H NMR in solid-phase organic synthesis.* The Journal of Organic Chemistry, 1994. **59**(26): p. 7955-7956.
67. Pursch, M., G. Schlotterbeck, L.H. Tseng, K. Albert, and W. Rapp, *Monitoring the reaction progress in combinatorial chemistry: 1H MAS NMR investigations on single macro beads in the suspended state.* Angewandte Chemie International Edition in English, 1996. **35**(23-24): p. 2867-2869.
68. Keifer, P.A., *Influence of resin structure, tether length, and solvent upon the high-resolution 1H NMR spectra of solid-phase-synthesis resins.* The Journal of Organic Chemistry, 1996. **61**(5): p. 1558-1559.
69. Pursch, M., L.C. Sander, and K. Albert, *Peer reviewed: understanding reversed-phase LC with solid-state NMR.* Analytical Chemistry, 1999. **71**(21): p. 733A-741A.
70. Sentell, K.B., *Nuclear magnetic resonance and electron spin resonance spectroscopic investigations of reversed-phase liquid chromatographic retention mechanisms: stationary phase structure.* Journal of Chromatography A, 1993. **656**(1-2): p. 231-263.
71. Maciel, G.E. and D.W. Sindorf, *Silicon-29 NMR study of the surface of silica gel by cross polarization and magic-angle spinning.* Journal of the American Chemical Society, 1980. **102**(25): p. 7606-7607.
72. Sindorf, D.W. and G.E. Maciel, *Carbon-13 CP/MAS NMR study of molecular motion in n-alkylsilane bonded to the silica surface.* Journal of the American Chemical Society, 1983. **105**(7): p. 1848-1851.
73. Bayer, E., K. Albert, J. Reiners, M. Nieder, and D. Müller, *Characterization of chemically modified silica gels by 29Si and 13C cross-polarization and magic angle spinning nuclear magnetic resonance.* Journal of Chromatography A, 1983. **264**: p. 197-213.
74. Hetem, M.J., J.W. De Haan, H.A. Claessens, L.J. Van de Ven, C.A. Cramers, P.W. Wijnen, and J.N. Kinkel, *Influence of alkyl chain length on the stability of n-alkyl-modified reversed phases. 2. Model dissolution study.* Analytical Chemistry, 1990. **62**(21): p. 2296-2300.
75. Scholten, A.B., J.W. De Haan, H.A. Claessens, L.J. Van de Ven, and C.A. Cramers, *29-Silicon NMR evidence for the improved chromatographic siloxane bond stability of bulky alkylsilane ligands on a silica surface.* Journal of Chromatography A, 1994. **688**(1): p. 25-29.
76. Jinno, K., T. Ibuki, N. Tanaka, M. Okamoto, J. Fetzer, W. Biggs, P. Griffiths, and J. Olinger, *Retention behaviour of large polycyclic aromatic hydrocarbons in reversed-phase liquid chromatography on a polymeric octadecylsilica stationary phase.* Journal of Chromatography A, 1989. **461**: p. 209-227.
77. Pursch, M., S. Strohschein, H. Haendel, and K. Albert, *Temperature-Dependent Behavior of C30 Interphases. A Solid-State NMR and LC− NMR Study.* Analytical Chemistry, 1996. **68**(2): p. 386-393.
78. Earl, W.L. and D. VanderHart, *Observations in solid polyethylenes by carbon-13 nuclear magnetic resonance with magic angle sample spinning.* Macromolecules, 1979. **12**(4): p. 762-767.
79. Gao, W. and L. Reven, *Solid-state NMR studies of self-assembled monolayers.* Langmuir, 1995. **11**(6): p. 1860-1863.
80. Albert, K., J. Schmid, B. Pfleiderer, and E. Bayer, *Chemically Modified Surfaces*. 1992, Elsevier Science Publishers: Amsterdam.
81. Ohta, H., K. Jinno, Y. Saito, J. Fetzer, W. Biggs, J.J. Pesek, M. Matyska, and Y.-L. Chen, *Effect of temperature on the mechanism of retention of fullerenes in*

liquid chromatography using various alkyl bonded stationary phases. Chromatographia, 1996. **42**(1-2): p. 56-62.

82. Gilpin, R. and M. Gangoda, *Effect of solvent viscosity and polarity on reversed-phase chromatographic surfaces. 13C spin-lattice relaxation of labeled immobilized alkyl ligands.* Journal of Magnetic Resonance (1969), 1985. **64**(3): p. 408-413.
83. Shah, P., L. Rogers, and J.C. Fetzer, *Differences in carbon 13 nuclear magnetic resonance spectra for monomeric and polymeric octadecyl derivatized silica column packings for liquid chromatography.* Journal of Chromatography A, 1987. **388**: p. 411-419.
84. Gilpin, R. and M. Gangoda, *Nuclear magnetic resonance spectrometry of alkyl ligands immobilized on reversed-phase liquid chromatographic surfaces.* Analytical Chemistry, 1984. **56**(8): p. 1470-1473.
85. Bliesner, D.M. and K.B. Sentell, *Deuterium nuclear magnetic resonance spectroscopy as a probe for reversed-phase liquid chromatographic bonded phase solvation: methanol and acetonitrile mobile phase components.* Journal of Chromatography A, 1993. **631**(1-2): p. 23-35.
86. Albert, K., B. Evers, and E. Bayer, *NMR investigation of the dynamic behavior of alkyl-modified silica.* Journal of Magnetic Resonance (1969), 1985. **62**(3): p. 428-436.
87. Gangoda, M., R. Gilpin, and B. Ung, *Effect of temperature on reversed-phase chromatographic surfaces studied by 13C NMR.* Journal of Magnetic Resonance (1969), 1987. **74**(1): p. 134-138.
88. Zeigler, R.C. and G.E. Maciel, *A study of the structure and dynamics of dimethyloctadecylsilyl-modified silica using wide-line 2H NMR techniques.* Journal of the American Chemical Society, 1991. **113**(17): p. 6349-6358.
89. Pfleiderer, B., K. Albert, E. Bayer, K.D. Lork, K.K. Unger, and H. Brückner, *Correlation of the Dynamic Behavior of n-Alkyl Ligands of the Stationary Phase with the Retention Times of Paracelsin Peptides in Reversed Phase HPLC.* Angewandte Chemie International Edition in English, 1989. **28**(3): p. 327-329.
90. Stejskal, E., J. Schaefer, M. Sefcik, and R. McKay, *Magic-angle carbon-13 nuclear magnetic resonance study of the compatibility of solid polymeric blends.* Macromolecules, 1981. **14**(2): p. 275-279.
91. Bachmann, S., C. Hellriegel, J. Wegmann, H. Händel, and K. Albert, *Characterization of polyalkylvinyl ether phases by solid-state and suspended-state nuclear magnetic resonance investigations.* Solid State Nuclear Magnetic Resonance, 2000. **17**(1-4): p. 39-51.
92. Yeman, H., T. Nicholson, M.T. Matyska, J.J. Pesek, and K. Albert, *Simulation of the chromatographic separation process in HPLC employing suspended-state NMR spectroscopy–comparison of interaction behavior for monomeric and hydride-modified C18 stationary phases.* Journal of separation science, 2013. **36**(1): p. 173-181.
93. Skogsberg, U., H. Händel, D. Sanchez, and K. Albert, *Comparisons of the interactions between two analytes and two structurally similar chiral stationary phases using high-performance liquid chromatography, suspended-state high-resolution magic angle spinning nuclear magnetic resonance and solid-state nuclear magnetic resonance spectroscopy.* Journal of Chromatography A, 2004. **1023**(2): p. 215-223.
94. Coen, M., J.C. Lindon, C. Gavaghan, E. Holmes, E. Humpfer, I.D. Wilson, P.D. Stanley, and J.K. Nicholson, *Investigation of water environments in a C18 bonded silica phase using 1H magic angle spinning (MAS) nuclear magnetic resonance (NMR) spectroscopy.* Analyst, 2001. **126**(5): p. 548-550.

95. Coen, M., I.D. Wilson, J.K. Nicholson, H. Tang, and J.C. Lindon, *Probing molecular dynamics in chromatographic systems using high-resolution 1H magic-angle-spinning NMR spectroscopy: interaction between p-xylene and C18-bonded silica.* Analytical Chemistry, 2004. **76**(11): p. 3023-3028.
96. Viel, S., F. Ziarelli, and S. Caldarelli, *Enhanced diffusion-edited NMR spectroscopy of mixtures using chromatographic stationary phases.* Proceedings of the National Academy of Sciences of the United States of America, 2003. **100**(17): p. 9696-8.
97. Delaurent, C. and S. Caldarelli, *Simplified analysis of mixtures of small molecules by chromatographic NMR spectroscopy.* Angewandte Chemie International Edition, 2006. **45**(36): p. 5950-5953.
98. Caldarelli, S., *Chromatographic NMR: a tool for the analysis of mixtures of small molecules.* Magnetic Resonance in Chemistry, 2007. **45(S1)**: p. S48-55.
99. Carrara, C., S. Viel, C. Delaurent, F. Ziarelli, G. Excoffier, and S. Caldarelli, *Chromatographic NMR in NMR solvents.* Journal of Magnetic Resonance, 2008. **194**(2): p. 303-6.
100. Reddy, G.N.M., R. Ballesteros-Garrido, J. Lacour, and S. Caldarelli, *Determination of labile chiral supramolecular ion pairs by chromatographic NMR spectroscopy.* Angewandte Chemie International Edition in English, 2013. **52**(11): p. 3255-8.
101. Laverde, A., G.J.A. da Conceição, S.C.N. Queiroz, F.Y. Fujiwara, and A.J. Marsaioli, *An NMR tool for cyclodextrin selection in enantiomeric resolution by high-performance liquid chromatography.* Magnetic Resonance in Chemistry, 2002. **40**(7): p. 433-442.
102. Hoffman, R.E., H. Arzuan, C. Pemberton, A. Aserin, and N. Garti, *High-resolution NMR "chromatography" using a liquids spectrometer.* Journal of Magnetic Resonance, 2008. **194**(2): p. 295-9.
103. Kavakka, J.S., I. Kilpeläinen, and S. Heikkinen, *General chromatographic NMR method in liquid state for synthetic chemistry: polyvinylpyrrolidone assisted DOSY experiments.* Organic Letters, 2009. **11**(6): p. 1349-1352.
104. Snyder, L.R., J.J. Kirkland, and J.W. Dolan, *Introduction to modern liquid chromatography*. 2011: John Wiley & Sons.
105. Cazes, J. and R.P. Scott, *Chromatography theory*. Vol. 88. 2002: CRC Press.
106. Hanai, T., *HPLC: a practical guide*. Vol. 6. 1999: Royal Society of Chemistry.
107. Meyer, V.R., *Practical high-performance liquid chromatography*. 2013: John Wiley & Sons.
108. Bussemas, H., G. Harsch, and L. Ettre, *Friedlieb Ferdinand Runge (1794–1867):"self-grown pictures" as precursors of paper chromatography.* Chromatographia, 1994. **38**(3): p. 243-254.
109. Croes, K., A. Steffens, D. Marchand, and L. Snyder, *Relevance of π–π and dipole–dipole interactions for retention on cyano and phenyl columns in reversed-phase liquid chromatography.* Journal of Chromatography A, 2005. **1098**(1): p. 123-130.
110. Snyder, L., P. Carr, and S. Rutan, *Solvatochromically based solvent-selectivity triangle.* Journal of Chromatography A, 1993. **656**(1-2): p. 537-547.
111. Kuhn, R. and E. Lederer, *Fractionation and isomerization of Carotene.* Naturwissenschaften, 1931. **14**.
112. Riddick, J., W. Bunger, J. Riddick, W. Bunger, J. Riddick, and W.B.O. Solvents, *Wiley-Interscience, New York (1970).* Organic Solvents, Wiley-Interscience, New York, 1970: p. 803.

113. Vitha, M. and P.W. Carr, *The chemical interpretation and practice of linear solvation energy relationships in chromatography.* Journal of Chromatography A, 2006. **1126**(1): p. 143-194.
114. Melander, W.R., B.-K. Chen, and C. Horvàth, *Mobile phase effects in reversed-phase chromatography: I. Concomitant dependence of retention on column temperature eluent composition.* Journal of Chromatography A, 1979. **185**: p. 99-109.
115. Buckenmaier, S.M., D.V. McCalley, and M.R. Euerby, *Rationalisation of unusual changes in efficiency and retention with temperature shown for bases in reversed-phase high-performance liquid chromatography at intermediate pH.* Journal of Chromatography A, 2004. **1060**(1): p. 117-126.
116. Moore, J., *Gel permeation chromatography. I. A new method for molecular weight distribution of high polymers.* Journal of Polymer Science Part A: General Papers, 1964. **2**(2): p. 835-843.
117. Heinisch, S., G. Puy, M.-P. Barrioulet, and J.-L. Rocca, *Effect of temperature on the retention of ionizable compounds in reversed-phase liquid chromatography: Application to method development.* Journal of Chromatography A, 2006. **1118**(2): p. 234-243.
118. Rimmer, C.A., C.R. Simmons, and J.G. Dorsey, *The measurement and meaning of void volumes in reversed-phase liquid chromatography.* Journal of Chromatography A, 2002. **965**(1): p. 219-232.
119. Wren, S.A. and P. Tchelitcheff, *Use of ultra-performance liquid chromatography in pharmaceutical development.* Journal of Chromatography A, 2006. **1119**(1): p. 140-146.
120. Wicke, E., *JC Giddings: Dynamics of Chromatography. Part. I: Principles and Theory. Marcel Dekker, New York, 1965. XII und 323 Seiten. 39 Abb. Preis: $11.50.* Berichte der Bunsengesellschaft für physikalische Chemie, 1967. **71**(2): p. 236-236.
121. Melander, W., C. Horvath, and C. Horvath, *High Performance Liquid Chromatography–Advances and Perspectives.* Academic Press, New York, 1980. **2**: p. 176.
122. Hadden, N., F. Baumann, F. MacDonald, M. Munk, R. Stevenson, D. Gere, F. Zamaroni, and R. Majors, *Basic liquid chromatography*. Vol. 110. 1971: Varian Aerograph Palo Alto, CA.
123. Kirkland, J.J., *Modern practice of liquid chromatography.* 1971.
124. Knox, J.H., *Band dispersion in chromatography—a universal expression for the contribution from the mobile zone.* Journal of Chromatography A, 2002. **960**(1): p. 7-18.
125. Kirkup, L., M. Foot, and M. Mulholland, *Comparison of equations describing band broadening in high-performance liquid chromatography.* Journal of Chromatography A, 2004. **1030**(1): p. 25-31.
126. Gritti, F. and G. Guiochon, *General HETP equation for the study of mass-transfer mechanisms in RPLC.* Analytical Chemistry, 2006. **78**(15): p. 5329-5347.
127. Usher, K.M., C.R. Simmons, and J.G. Dorsey, *Modeling chromatographic dispersion: A comparison of popular equations.* Journal of Chromatography A, 2008. **1200**(2): p. 122-128.
128. Touchstone, J.C., *History of chromatography.* Journal of Liquid Chromatography & Related Technologies, 1993. **16**(8): p. 1647-1665.
129. Unger, K.K., R. Ditz, E. Machtejevas, and R. Skudas, *Liquid chromatography—its development and key role in life science applications.* Angewandte Chemie International Edition, 2010. **49**(13): p. 2300-2312.

130. Borges, E.M., *Silica, hybrid silica, hydride silica and non-silica stationary phases for liquid chromatography.* Journal of Chromatographic Science, 2014. **53**(4): p. 580-597.
131. Fekete, S., R. Berky, J. Fekete, J.-L. Veuthey, and D. Guillarme, *Evaluation of recent very efficient wide-pore stationary phases for the reversed-phase separation of proteins.* Journal of Chromatography A, 2012. **1252**: p. 90-103.
132. Mirzaei, H. and M. Carrasco, *Modern Proteomics-Sample Preparation, Analysis and Practical Applications*. Vol. 919. 2016: Springer.
133. Ahmed, K.N., *HPLC of peptides and proteins: methods and protocols, edited by Marie-Isabel Aguilar (methods in molecular biology, volume 251, series editor J. M. Walker). Humana Press, Totowa, NJ, 2003, US$99.50, 413 pp, ISBN: 0-86903-977-3.* Biomedical Chromatography, 2004. **18**(7): p. 475-475.
134. Kirkland, J., *practical HPLC method development.* 1997.
135. Dolan, J.W., *Temperature selectivity in reversed-phase high performance liquid chromatography.* Journal of Chromatography A, 2002. **965**(1): p. 195-205.
136. Lough, W.J. and I.W. Wainer, *High performance liquid chromatography: fundamental principles and practice*. 1995: CRC Press.
137. Poole, C.F., *The essence of chromatography*. 2003: Elsevier.
138. Corradini, D., *Handbook of HPLC*. 2016: CRC Press.
139. Kromidas, S., *More practical problem solving in HPLC*. 2008: John Wiley & Sons.
140. Miller, J.M., *Chromatography: concepts and contrasts*. 2005: John Wiley & Sons.
141. Dean, J.R., *Practical skills in chemistry*. 2002: Pearson Education.
142. Valkó, K., L.R. Snyder, and J.L. Glajch, *Retention in reversed-phase liquid chromatography as a function of mobile-phase composition.* Journal of Chromatography A, 1993. **656**(1-2): p. 501-520.
143. Snyder, L., J. Dolan, and J. Gant, *Gradient elution in high-performance liquid chromatography: I. Theoretical basis for reversed-phase systems.* Journal of Chromatography A, 1979. **165**(1): p. 3-30.
144. Snyder, L. and J. Dolan, *Initial experiments in high-performance liquid chromatographic method development I. Use of a starting gradient run.* Journal of Chromatography A, 1996. **721**(1): p. 3-14.
145. Bidlingmeyer, B., R. Hooker, C. Lochmuller, and L. Rogers, *Improved chromatographic resolution from pressure-induced changes in liquid—solid distribution ratios.* Separation Science and Technology, 1969. **4**(6): p. 439-446.
146. MacNair, J.E., K.C. Lewis, and J.W. Jorgenson, *Ultrahigh-pressure reversed-phase liquid chromatography in packed capillary columns.* Analytical Chemistry, 1997. **69**(6): p. 983-989.
147. Wolcott, R., J. Dolan, and L. Snyder, *Computer simulation for the convenient optimization of isocratic reversed-phase liquid chromatographic separations by varying temperature and mobile phase strength.* Journal of Chromatography A, 2000. **869**(1): p. 3-25.
148. Greibrokk, T. and T. Andersen, *High-temperature liquid chromatography.* Journal of Chromatography A, 2003. **1000**(1): p. 743-755.
149. Yang, X., L. Ma, and P.W. Carr, *High temperature fast chromatography of proteins using a silica-based stationary phase with greatly enhanced low pH stability.* Journal of Chromatography A, 2005. **1079**(1): p. 213-220.
150. Lestremau, F., A. Cooper, R. Szucs, F. David, and P. Sandra, *High-efficiency liquid chromatography on conventional columns and instrumentation by using temperature as a variable: I. Experiments with 25cm× 4.6 mm ID, 5μm ODS columns.* Journal of Chromatography A, 2006. **1109**(2): p. 191-196.

151. Vanhoenacker, G. and P. Sandra, *Elevated temperature and temperature programming in conventional liquid chromatography–fundamentals and applications* Journal of Separation Science, 2006. **29**(12): p. 1822-1835.
152. Antia, F.D. and C. Horváth, *High-performance liquid chromatography at elevated temperatures: examination of conditions for the rapid separation of large molecules.* Journal of Chromatography A, 1988. **435**: p. 1-15.
153. Thompson, J.D. and P.W. Carr, *A study of the critical criteria for analyte stability in high-temperature liquid chromatography.* Analytical Chemistry,, 2002. **74**(5): p. 1017-1023.
154. Tsimidou, M. and R. Macrae, *Influence of injection solvent on the reversed-phase chromatography of triglycerides.* Journal of Chromatography A, 1984. **285**: p. 178-181.
155. Zapala, W., *Influence of mobile phase composition on retention factors in different HPLC systems with chemically bonded stationary phases.* Journal of Chromatographic Science, 2003. **41**(6): p. 289-294.
156. Anderson, D., *LR Snyder and JJ Kirkland, introduction to modern liquid chromatography: Wiley, New York, 1974. XV+ 534 pp., price£ 9.00*. 1975, Elsevier.
157. Halasz, I. and I. Sebestian, *New stationary phase for chromatography.* Angewandte Chemie International Edition in English, 1969. **8**(6): p. 453-454.
158. Abel, E., F. Pollard, P. Uden, and G. Nickless, *A new gas-liquid chromatographic phase.* Journal of Chromatography A, 1966. **22**: p. 23-28.
159. Stewart, H. and S. Perry, *A new approach to liquid partition chromatography.* Journal of Chromatography A, 1968. **37**: p. 97-98.
160. Krstulovic, A.M. and P.R. Brown, *Reversed-phase high-performance liquid chromatograph y: theory, practice, and biomedical applications*. 1982: Wiley.
161. Horváth, C., *High-performance liquid chromatography: advances and perspectives*. 2013: Elsevier.
162. Colin, H. and G. Guiochon, *Introduction to reversed-phase high-performance liquid chromatography.* Journal of Chromatography A, 1977. **141**(3): p. 289-312.
163. Van de Venne, J., J. Rindt, G. Coenen, and C. Cramers, *Synthesis of a nonpolar, chemically bonded stationary phase with low residual hydroxyl group content.* Chromatographia, 1980. **13**(1): p. 11-17.
164. Sander, L.C. and S.A. Wise, *Synthesis and characterization of polymeric C18 stationary phases for liquid chromatography.* Analytical Chemistry, 1984. **56**(3): p. 504-510.
165. Majors, R.E., *Recent advances in HPLC packings and columns.* Journal of Chromatographic Science, 1980. **18**(10): p. 488-511.
166. Claessens, H., C. Cramers, J. De Haan, F. den Otter, L. van de Ven, P. Andree, G. de Jong, N. Lammers, J. Wijma, and J. Zeeman, *Ageing processes of alkyl bonded phases in HPLC; a chromatographic and spectroscopic approach.* Chromatographia, 1985. **20**(10): p. 582-586.
167. Lippa, K.A., L.C. Sander, and R.D. Mountain, *Molecular dynamics simulations of alkylsilane stationary-phase order and disorder. 1. Effects of surface coverage and bonding chemistry.* Analytical Chemistry, 2005. **77**(24): p. 7852-7861.
168. Wilson, T. and D. Simmons, *A particle size distribution analysis of used HPLC column packing material.* Chromatographia, 1993. **35**(5-6): p. 295-301.
169. Ellingsen, T., O. Aune, J. Ugelstad, and S. Hagen, *Monosized stationary phases for chromatography.* Journal of Chromatography A, 1990. **535**: p. 147-161.

170. Gritti, F., I. Leonardis, J. Abia, and G. Guiochon, *Physical properties and structure of fine core–shell particles used as packing materials for chromatography: relationships between particle characteristics and column performance.* Journal of Chromatography A, 2010. **1217**(24): p. 3819-3843.
171. Schmidt-Traub, H., *Preparative chromatography: of fine chemicals and pharmaceutical agents*. 2006: John Wiley & Sons.
172. Cazes, J., *Encyclopedia of Chromatography 2004 Update Supplement*. 2004: CRC press.
173. G., L., *K. K. Unger: Porous Silica — its properties and use as support in column liquid chromatography. Elsevier Scientific Publishing Co., Amsterdam, Oxford, New York 1979. 226 Seiten, Preis: $ 46.25.* Berichte der Bunsengesellschaft für physikalische Chemie, 1980. **84**(1): p. 111-111.
174. Daneyko, A., A. Höltzel, S. Khirevich, and U. Tallarek, *Influence of the particle size distribution on hydraulic permeability and eddy dispersion in bulk packings.* Analytical Chemistry, 2011. **83**(10): p. 3903-3910.
175. Poole, C.F., *Mark F. Vitha: Chromatography: Principles and Instrumentation*. 2017, Springer.
176. Albericio, F., *Solid-phase synthesis: a practical guide*. 2000: CRC Press.
177. Kazakevich, Y.V. and R. Lobrutto, *HPLC for pharmaceutical scientists*. 2007: John Wiley & Sons.
178. DeStefano, J., T. Langlois, and J. Kirkland, *Characteristics of superficially-porous silica particles for fast HPLC: some performance comparisons with sub-2-µm particles.* Journal of Chromatographic Science, 2008. **46**(3): p. 254-260.
179. Unger, K.K., R. Skudas, and M.M. Schulte, *Particle packed columns and monolithic columns in high-performance liquid chromatography-comparison and critical appraisal.* Journal of Chromatography A, 2008. **1184**(1-2): p. 393-415.
180. Kromidas, S., *The HPLC Expert: Possibilities and Limitations of Modern High Performance Liquid Chromatography*. 2016: John Wiley & Sons.
181. Kamour, R., A. Ammar, M. El-Attug, and T. Almog, *Development of fused-core silica HPLC columns and their recent pharmaceutical and biological applications: A review.* International Journal of Pharmacy and Pharmaceutical Sciences, 2013. **5**(3): p. 926-930.
182. Brunauer, S., P. Emmett, and E. Teller, *Absorption of gases in multimolecular layers J Am Chem Soc 60: 309–319.* Find this article online, 1938.
183. Berendsen, G.E., K.A. Pikaart, and L.d. Galan, *Preparation of various bonded phases for HPLC using monochlorosilanes.* Journal of Liquid Chromatography, 1980. **3**(10): p. 1437-1464.
184. Harkins, W.D. and G. Jura, *Surfaces of solids. XII. An absolute method for the determination of the area of a finely divided crystalline solid.* Journal of the American Chemical Society, 1944. **66**(8): p. 1362-1366.
185. Fink, J.K., *Reactive polymers: Fundamentals and applications: A concise guide to industrial polymers*. 2017: William Andrew.
186. Bosch, E., P. Bou, H. Allemann, and M. Rosés, *Retention of Ionizable Compounds on HPLC. pH Scale in Methanol− Water and the p K and pH Values of Buffers.* Analytical Chemistry, 1996. **68**(20): p. 3651-3657.
187. Gennaro, M., D. Giacosa, and C. Abrigo, *The role of pH of the mobile-phase in ion-interaction RP-HPLC.* Journal of Liquid Chromatography & Related Technologies, 1994. **17**(20): p. 4365-4380.
188. Henderson, L.J., *Concerning the relationship between the strength of acids and their capacity to preserve neutrality.* American Journal of Physiology--Legacy Content, 1908. **21**(2): p. 173-179.

189. Po, H.N. and N. Senozan, *The Henderson-Hasselbalch equation: its history and limitations.* Journal of Chemical Education, 2001. **78**(11): p. 1499.
190. Snyder, L., A. Maule, A. Heebsh, R. Cuellar, S. Paulson, J. Carrano, L. Wrisley, C. Chan, N. Pearson, and J. Dolan, *A fast, convenient and rugged procedure for characterizing the selectivity of alkyl-silica columns.* Journal of Chromatography A, 2004. **1057**(1): p. 49-57.
191. Hulanicki, A. and M.R. Masson, *Reactions of acids and bases in analytical chemistry*. 1987: Halsted Press.
192. Juza, M. and S. Kromidas, *HPLC Made to Measure—A Practical Handbook for Optimization*. 2006, Wiley-VCH, Weinheim.
193. Pesek, J.J. and M.T. Matyska, *Hydride-based silica stationary phases for HPLC: Fundamental properties and applications.* Journal of Separation Science, 2005. **28**(15): p. 1845-1854.
194. Hammond, E.W., *Chromatography for the Analysis of Lipids*. 1993: CRC press.
195. Moldoveanu, S.C. and V. David, *Essentials in modern HPLC separations*. 2012: Newnes.
196. Kazakevich, Y. and R. Lobrutto, *Stationary phases.* HPLC for Pharmaceutical Scientists, 2007: p. 75-138.
197. Barrett, D.A., V.A. Brown, P.N. Shaw, M.C. Davies, H. Ritchie, and P. Ross, *Characterization of a range of alkyl-bonded silica HPLC stationary phases: chromatographic behavior of neutral, acidic, and basic test solutes.* Journal of Chromatographic Science, 1996. **34**(3): p. 146-156.
198. Hemetsberger, H., M. Kellermann, and H. Ricken, *Behaviour of chemically bonded alkylmethyldichlorosilanes to silica gel in reversed-phase high-performance liquid chromatography.* Chromatographia, 1977. **10**(12): p. 726-730.
199. Egelhaaf, H.-J., D. Oelkrug, M. Pursch, and K. Albert, *Combined Fluorescence and NMR Studies of Reversed HPLC Stationary Phases with Different Ligand Chain Lengths.* Journal of Fluorescence, 1997. **7**(4): p. 311-315.
200. Abia, J., *Surface Characterization of Some Novel Bonded Phase Packing Materials for HPLC Columns Using MAS-NMR Spectroscopy.* Chromatography, 2015. **2**(2): p. 141-155.
201. Strohschein, S., M. Pursch, H. Händel, and K. Albert, *Structure elucidation of β-carotene isomers by HPLC-NMR coupling using a C30 bonded phase.* Journal of Analytical Chemistry, 1997. **357**(5): p. 498-502.
202. Pursch, M., L.C. Sander, and K. Albert, *Chain order and mobility of high-density C18 phases by solid-state NMR spectroscopy and liquid chromatography.* Analytical Chemistry, 1996. **68**(23): p. 4107-4113.
203. London, F., *The general theory of molecular forces.* Transactions of the Faraday Society, 1937. **33**: p. 8b-26.
204. Glasstone, S., *Textbook of Physical Chemistry. D. Van Norstrand Co.* Inc., 1946. **20**.
205. Wang, P.G. and W. He, *Hydrophilic interaction liquid chromatography (HILIC) and advanced applications*. 2011: CRC press.
206. Snyder, L.R., *Classification of the solvent properties of common liquids.* Journal of Chromatography A, 1974. **92**(2): p. 223-230.
207. Riddick, J. and W. Bunger, *Organic Solvents, Vol. II of Techniques of Chemistry; Weissberger, A., Ed*. 1970, Wiley Interscience: New York.
208. Dean, J., *Lange's Handbook of Chemistry. No. Bd. 15 in LANGE'S HANDBOOK OF CHEMISTRY*. 1999, McGraw-Hill.
209. Lide, D., *Standard Thermodynamic Properties of Chemical Substances, CRC Handbook of Chemistry and Physics*. 2005, CRC Press, Boca Raton, FL.

210. Deng, L., H. Nakano, and Y. Iwasaki, *Direct separation of regioisomers and enantiomers of monoacylglycerols by tandem column high-performance liquid chromatography.* Journal of Chromatography A, 2007. **1165**(1): p. 93-99.
211. Walker, J.M. and R. Rapley, *Medical biomethods handbook*. 2005: Springer.
212. Nugent, K., W. Burton, T. Slattery, B. Johnson, and L. Snyder, *Separation of proteins by reversed-phase high-performance liquid chromatography: II. Optimizing sample pretreatment and mobile phase conditions.* Journal of Chromatography A, 1988. **443**: p. 381-397.
213. Baker, J., *Practical HPLC Methodology and Applications, Brian A. Bidlingmeyer, Wiley, New York, 1992. 452 pp. $54.95*. 1994, Academic Press.
214. Guideline, I.H.T. *Validation of analytical procedures: text and methodology Q2 (R1)*. in *International Conference on Harmonization, Geneva, Switzerland*. 2005.
215. Keeler, J., *Understanding NMR spectroscopy*. 2011: John Wiley & Sons.
216. Levitt, M.H., *Spin dynamics: basics of nuclear magnetic resonance*. 2001: John Wiley & Sons.
217. Duer, M.J., *Solid state NMR spectroscopy: principles and applications*. 2008: John Wiley & Sons.
218. Saitô, H., I. Ando, and A. Ramamoorthy, *Chemical Shift Tensor – the Heart of NMR: Insights into Biological Aspects of Proteins.* Progress in Nuclear Magnetic Resonance Spectroscopy, 2010. **57**(2): p. 181-228.
219. Duer, M.J., *Introduction to solid-state NMR spectroscopy*. 2005: Wiley-Blackwell.
220. Jameson, C.J., H. Fukui, K. Kamienska-Trela, A. Aliev, M.J. Prior, J. Wojcik, T. Watanabe, W. Schilf, R. Ludwig, and H. Kurosu, *Nuclear magnetic resonance*. Vol. 36. 2007: Royal Society of Chemistry.
221. Bloembergen, N., *N. Bloembergen and TJ Rowland, Phys. Rev. 97, 1679 (1955).* Phys. Rev., 1955. **97**: p. 1679.
222. Ito, T., N. Tanaka, I. Hanazaki, and S. Nagakura, *Absolute configuration and polarization of the ligand $\pi^* \leftarrow \pi$ transition of the tris (tropolonato) silicon (IV) ion.* Inorganic and Nuclear Chemistry Letters, 1969. **5**(10): p. 781-784.
223. Claridge, T.D., *High-resolution NMR techniques in organic chemistry*. Vol. 27. 2016: Elsevier.
224. Andrew, E.R., *Magic angle spinning in solid state nmr spectroscopy.* Phil. Trans. R. Soc. Lond. A, 1981. **299**(1452): p. 505-520.
225. Dixon, W.T., *Spinning-sideband-free and spinning-sideband-only NMR spectra in spinning samples.* The Journal of Chemical Physics, 1982. **77**(4): p. 1800-1809.
226. Antzutkin, O.N., Z. Song, X. Feng, and M.H. Levitt, *Suppression of sidebands in magic-angle-spinning nuclear magnetic resonance: General principles and analytical solutions.* The Journal of Chemical Physics, 1994. **100**(1): p. 130-140.
227. Gan, Z., D.M. Grant, and R. Ernst, *NMR chemical shift anisotropy measurements by RF driven rotary resonance.* Chemical Physics Letters, 1996. **254**(5-6): p. 349-357.
228. Maricq, M.M. and J. Waugh, *NMR in rotating solids.* The Journal of Chemical Physics, 1979. **70**(7): p. 3300-3316.
229. Herzfeld, J. and A.E. Berger, *Sideband intensities in NMR spectra of samples spinning at the magic angle.* The Journal of Chemical Physics, 1980. **73**(12): p. 6021-6030.
230. Terskikh, V.V., J.A. Feurtado, S. Borchardt, M. Giblin, S.R. Abrams, and A.R. Kermode, *In vivo 13C NMR metabolite profiling: potential for understanding*

and assessing conifer seed quality. Journal of Experimental Botany, 2005. **56**(418): p. 2253-2265.
231. Yan, B., *Analytical methods in combinatorial chemistry*. Vol. 6. 2000: St. Martin's Press.
232. Drain, L., *The broadening of magnetic resonance lines due to field inhomogeneities in powdered samples.* Proceedings of the Physical Society, 1962. **80**(6): p. 1380.
233. Samoson, A., T. Tuherm, and Z. Gan, *High-field high-speed MAS resolution enhancement in 1 H NMR spectroscopy of solids.* Solid state nuclear magnetic resonance, 2001. **20**(3): p. 130-136.
234. Delepierre, M., *High resolution liquid NMR and magic angle spinning.* Journal de Chimie Physique et de Physico-Chimie Biologique, 1998. **95**(2): p. 235-240.
235. Keifer, P.A., L. Baltusis, D.M. Rice, A.A. Tymiak, and J.N. Shoolery, *A comparison of NMR spectra obtained for solid-phase-synthesis resins using conventional high-resolution, magic-angle-spinning, and high-resolution magic-angle-spinning probes.* Journal of Magnetic Resonance, Series A, 1996. **119**(1): p. 65-75.
236. Apperley, D.C., R.K. Harris, and P. Hodgkinson, *Solid-State NMR: Basic Principles and Practice*. 2012: Momentum Press.
237. Linser, R., V. Chevelkov, A. Diehl, and B. Reif, *Sensitivity enhancement using paramagnetic relaxation in MAS solid-state NMR of perdeuterated proteins.* Journal of Magnetic Resonance, 2007. **189**(2): p. 209-216.
238. De Lacaillerie, J.-B.d.E., B. Jarry, O. Pascui, and D. Reichert, *"Cooking the sample": Radiofrequency induced heating during solid-state NMR experiments.* Solid State Nuclear Magnetic Resonance, 2005. **28**(2): p. 225-232.
239. Wang, J., Z. Zhang, W. Zhao, L. Wang, and J. Yang, *Heating and temperature gradients of lipid bilayer samples induced by RF irradiation in MAS solid-state NMR experiments.* Magnetic Resonance in Chemistry, 2016.
240. Rule, G.S. and T.K. Hitchens, *Fundamentals of protein NMR spectroscopy*. Vol. 5. 2006: Springer Science & Business Media.
241. Stejskal, E. and J.D. Memory, *High resolution NMR in the solid state: fundamentals of CP/MAS.* 1994: Cambridge University Press.
242. Pochapsky, T.C. and S. Pochapsky, *NMR for physical and biological scientists*. 2008: Garland Science.
243. Pople, J.A., W.G. Schneider, and H.J. Bernstein, *High-resolution nuclear magnetic resonance.* 1959.
244. Slichter, C.P., *Principles of magnetic resonance*. Vol. 1. 2013: Springer Science & Business Media.
245. Cambridge, J.K., *RK Harris. Nuclear Magnetic Resonance Spectroscopy. Longman, London, 1986,£ 12.95 (paperback only). ISBN 0 582 44653 8.* Magnetic Resonance in Chemistry, 1987. **25**(3): p. 280-280.
246. Becker, E.D., *High resolution NMR: theory and chemical applications*. 1999: Elsevier.
247. McDonald, G.G. and J.S. Leigh, *A new method for measuring longitudinal relaxation times.* Journal of Magnetic Resonance (1969), 1973. **9**(3): p. 358-362.
248. Vold, R., J. Waugh, M. Klein, and D. Phelps, *Measurement of spin relaxation in complex systems.* The Journal of Chemical Physics, 1968. **48**(8): p. 3831-3832.
249. Hsu, J.J., G.H. Glover, and G. Zaharchuk, *Optimizing saturation–recovery measurements of the longitudinal relaxation rate under time constraints.* Magnetic Resonance in Medicine: An Official Journal of the International Society for Magnetic Resonance in Medicine, 2009. **62**(5): p. 1202-1210.
250. Breitmaier, E. and W. Voelter, *Carbon-13 NMR spectroscopy.* 1987.

251. Carr, H.Y. and E.M. Purcell, *Effects of diffusion on free precession in nuclear magnetic resonance experiments.* Physical Review, 1954. **94**(3): p. 630.
252. Meiboom, S. and D. Gill, *Modified spin-echo method for measuring nuclear relaxation times.* Review of Scientific Instruments 1958. **29**(8): p. 688-691.
253. Tang, H., Y. Wang, J.K. Nicholson, and J.C. Lindon, *Use of relaxation-edited one-dimensional and two dimensional nuclear magnetic resonance spectroscopy to improve detection of small metabolites in blood plasma.* Analytical Biochemistry, 2004. **325**(2): p. 260-272.
254. Aguilar, J.A., M. Nilsson, G. Bodenhausen, and G.A. Morris, *Spin echo NMR spectra without J modulation.* Chemical Communications, 2012. **48**(6): p. 811-813.
255. Solomon, I., *Relaxation processes in a system of two spins.* Physical Review, 1955. **99**(2): p. 559.
256. Bax, A. and D.G. Davis, *Practical aspects of two-dimensional transverse NOE spectroscopy.* Journal of Magnetic Resonance (1969), 1985. **63**(1): p. 207-213.
257. Neuhaus, D. and M.P. Williamson, *The nuclear Overhauser effect in structural and conformational analysis*. 1989: VCH New York.
258. Kleckner, I.R. and M.P. Foster, *An introduction to NMR-based approaches for measuring protein dynamics.* Biochimica et Biophysica Acta (BBA)-Proteins and Proteomics, 2011. **1814**(8): p. 942-968.
259. Mittermaier, A.K. and L.E. Kay, *Observing biological dynamics at atomic resolution using NMR.* Trends in Biochemical Sciences, 2009. **34**(12): p. 601-611.
260. Palmer 3rd, A., C.D. Kroenke, and J.P. Loria, *Nuclear magnetic resonance methods for quantifying microsecond-to-millisecond motions in biological macromolecules.* Methods in Enzymology, 2001. **339**: p. 204.
261. Gennari, M., M. Tegoni, M. Lanfranchi, M.A. Pellinghelli, and L. Marchiò, *A New Chiral N, N ', O-Donor Heteroscorpionate Ligand. Structures of Ni2+, Cu2+, Zn2+ Complexes and Study of Solution Equilibria by Means of 1H NMR/UV− Vis Titrations and EXSY NMR Spectroscopy.* Inorganic chemistry, 2007. **46**(8): p. 3367-3377.
262. Swift, T.J. and R.E. Connick, *NMR-Relaxation Mechanisms of O17 in Aqueous Solutions of Paramagnetic Cations and the Lifetime of Water Molecules in the First Coordination Sphere.* The Journal of Chemical Physics, 1962. **37**(2): p. 307-320.
263. Millet, O., J.P. Loria, C.D. Kroenke, M. Pons, and A.G. Palmer, *The static magnetic field dependence of chemical exchange linebroadening defines the NMR chemical shift time scale.* Journal of the American Chemical Society, 2000. **122**(12): p. 2867-2877.
264. Harris, R.K. and A. Sebald, *Experimental methodology for high-resolution solid-state NMR of heavy-metal spin-1½ nuclei.* Magnetic resonance in chemistry, 1987. **25**(12): p. 1058-1062.
265. Duncan, T.M., *A compilation of chemical shift anisotropies*. 1990: Farragut Press.
266. Wehler, T. and J. Westman, *Magic angle spinning NMR: A valuable tool for monitoring the progress of reactions in solid phase synthesis.* Tetrahedron Letters, 1996. **37**(27): p. 4771-4774.
267. Bachmann, S., C. Hellriegel, J. Wegmann, H. Handel, and K. Albert, *Characterization of polyalkylvinyl ether phases by solid-state and suspended-state nuclear magnetic resonance investigations.* Solid State Nuclear Magnetic Resonance, 2000. **17**(1-4): p. 39-51.

268. Albert, K., *Correlation between chromatographic and physicochemical properties of stationary phases in HPLC: C 30 bonded reversed-phase silica.* TrAC Trends in Analytical Chemistry, 1998. **17**(10): p. 648-658.
269. Albert, K., T. Lacker, M. Raitza, M. Pursch, H.J. Egelhaaf, and D. Oelkrug, *Investigating the selectivity of triacontyl interphases.* Angewandte Chemie International Edition, 1998. **37**(6): p. 777-780.
270. Friebolin, V., S. Marten, and K. Albert, *Characterization of binding affinities in a chromatographic system by suspended state HR/MAS NMR spectroscopy.* Magnetic Resonance in Chemistry, 2010. **48**(2): p. 111-116.
271. Brus, J., *Heating of samples induced by fast magic-angle spinning.* Solid State Nuclear Magnetic Resonance, 2000. **16**(3): p. 151-160.
272. Stringer, J.A., C.E. Bronnimann, C.G. Mullen, D.H. Zhou, S.A. Stellfox, Y. Li, E.H. Williams, and C.M. Rienstra, *Reduction of RF-induced sample heating with a scroll coil resonator structure for solid-state NMR probes.* Journal of Magnetic Resonance, 2005. **173**(1): p. 40-48.
273. Sass, M. and D. Ziessow, *Error analysis for optimized inversion recovery spin-lattice relaxation measurements.* Journal of Magnetic Resonance (1969), 1977. **25**(2): p. 263-276.
274. Scheffler, K. and J. Hennig, *T1 quantification with inversion recovery TrueFISP.* Magnetic Resonance in Medicine, 2001. **45**(4): p. 720-723.
275. Becker, E.D., J.A. Ferretti, R.K. Gupta, and G.H. Weiss, *The choice of optimal parameters for measurement of spin-lattice relaxation times. II. Comparison of saturation recovery, inversion recovery, and fast inversion recovery experiments.* Journal of Magnetic Resonance (1969), 1980. **37**(3): p. 381-394.
276. Freeman, R. and H. Hill, *Fourier transform study of NMR spin–lattice relaxation by "progressive saturation".* The Journal of Chemical Physics, 1971. **54**(8): p. 3367-3377.
277. Vold, R., J. Waugh, M.P. Klein, and D. Phelps, *Measurement of spin relaxation in complex systems.* The Journal of Chemical Physics, 1968. **48**(8): p. 3831-3832.
278. Alam, T.M. and J.E. Jenkins, *HR-MAS NMR spectroscopy in material science*, in *Advanced Aspects of Spectroscopy*. 2012, InTech.
279. Elwinger, F. and I. Furó, *High-resolution magic angle spinning 1H NMR measurement of ligand concentration in solvent-saturated chromatographic beads.* Magnetic Resonance in Chemistry, 2016. **54**(4): p. 291-297.
280. Simpson, A.J., W.L. Kingery, D.R. Shaw, M. Spraul, E. Humpfer, and P. Dvortsak, *The application of 1H HR-MAS NMR spectroscopy for the study of structures and associations of organic components at the solid− aqueous interface of a whole soil.* Environmental Science & Technology, 2001. **35**(16): p. 3321-3325.
281. Pursch, M., D.L. Vanderhart, L.C. Sander, X. Gu, T. Nguyen, S.A. Wise, and D.A. Gajewski, *C30 self-assembled monolayers on silica, titania, and zirconia: HPLC performance, atomic force microscopy, ellipsometry, and NMR studies of molecular dynamics and uniformity of coverage.* Journal of the American Chemical Society, 2000. **122**(29): p. 6997-7011.
282. Coen, M., J.C. Lindon, C. Gavaghan, E. Holmes, J.K. Nicholson, E. Humpfer, I.D. Wilson, and P.D. Stanley, *Investigation of water environments in a C18 bonded silica phase using 1H magic angle spinning (MAS) nuclear magnetic resonance (NMR) spectroscopy.* The Analyst, 2001. **126**(5): p. 548-550.
283. Snyder, L., M. Quarry, and J. Glajch, *Solvent-strength selectivity in reversed-phase HPLC.* Chromatographia, 1987. **24**(1): p. 33-44.

284. Bakalyar, S.R., R. McIlwrick, and E. Roggendorf, *Solvent selectivity in reversed-phase high-pressure liquid chromatography.* Journal of Chromatography A, 1977. **142**: p. 353-365.
285. Wishart, D.S., C.G. Bigam, J. Yao, F. Abildgaard, H.J. Dyson, E. Oldfield, J.L. Markley, and B.D. Sykes, *1 H, 13 C and 15 N chemical shift referencing in biomolecular NMR.* Journal of Biomolecular NMR, 1995. **6**(2): p. 135-140.
286. Morcombe, C.R. and K.W. Zilm, *Chemical shift referencing in MAS solid state NMR.* Journal of Magnetic Resonance, 2003. **162**(2): p. 479-486.
287. Live, D. and S.I. Chan, *The use of DSS as an internal standard in PMR studies of nucleic acid interactions.* Magnetic Resonance in Chemistry, 1973. **5**(6): p. 275-276.
288. Borges, E.M. and M.R. Euerby, *An appraisal of the chemical and thermal stability of silica based reversed-phase liquid chromatographic stationary phases employed within the pharmaceutical environment.* Journal of Pharmaceutical and Biomedical Analysis, 2013. **77**: p. 100-115.
289. Sagliano, N., T. Floyd, R. Hartwick, J. Dibussolo, and N. Miller, *Studies on the stabilization of reversed phases for liquid chromatography.* Journal of Chromatography A, 1988. **443**: p. 155-172.
290. Kirkland, J., J. Glajch, and R. Farlee, *Synthesis and characterization of highly stable bonded phases for high-performance liquid chromatography column packings.* Analytical Chemistry, 1989. **61**(1): p. 2-11.
291. Wyndham, K.D., J.E. O'Gara, T.H. Walter, K.H. Glose, N.L. Lawrence, B.A. Alden, G.S. Izzo, C.J. Hudalla, and P.C. Iraneta, *Characterization and evaluation of C18 HPLC stationary phases based on ethyl-bridged hybrid organic/inorganic particles.* Analytical Chemistry, 2003. **75**(24): p. 6781-6788.
292. O'Gara, J.E., D.P. Walsh, C.H. Phoebe Jr, B.A. Alden, E.S. Bouvier, P.C. Iraneta, M. Capparella, and T.H. Walter, *Embedded-polar-group bonded phases for high performance liquid chromatography.* Lc Gc North America, 2001. **19**(6): p. 632-642.
293. O'GARA, J.E., B.A. Alden, T.H. Walter, J.S. Petersen, C.L. Niederlaender, and U.D. Neue, *Simple preparation of a C8 HPLC stationary phase with an internal polar functional group.* Analytical Chemistry, 1995. **67**(20): p. 3809-3813.
294. Czajkowska, T., M. Jaroniec, and B. Buszewski, *Retention of pyridinecarboxylic acids on monomeric and polymeric alkylamide phases.* Journal of Chromatography A, 1996. **728**(1-2): p. 213-224.
295. Czajkowska, T., I. Hrabovsky, B. Buszewski, R. Gilpin, and M. Jaroniec, *Comparison of the retention of organic acids on alkyl and alkylamide chemically bonded phases.* Journal of Chromatography A, 1995. **691**(1-2): p. 217-224.
296. Czajkowska, T. and M. Jaroniec, *Application of alkylamide phases to separate compounds of different polarity under reversed phase conditions.* Journal of Liquid Chromatography & Related Technologies, 1996. **19**(17-18): p. 2829-2841.
297. Czajkowska, T. and M. Jaroniec, *Selectivity of alkylamide bonded-phases with respect to organic acids under reversed-phase conditions.* Journal of Chromatography A, 1997. **762**(1-2): p. 147-158.
298. McDonald, P.D., *Improving our understanding of reversed-phase separations for the 21st century*, in *Advances in Chromatography: Volume 42*. 2003, CRC Press.
299. Neue, U., Y.-F. Cheng, Z. Lu, B. Alden, P. Iraneta, C. Khoebe, and K. Van Tran, *Properties of reversed phase packings with an embedded polar group.* Chromatographia, 2001. **54**(3-4): p. 169-177.

300. Fountain, K.J., H.B. Hewitson, P.C. Iraneta, and D. Morrison, *Practical applications of charged surface hybrid (CSH) technology.* Waters Application Note 720003720EN, 2010.
301. Méndez, A., E. Bosch, M. Rosés, and U.D. Neue, *Comparison of the acidity of residual silanol groups in several liquid chromatography columns.* Journal of Chromatography A, 2003. **986**(1): p. 33-44.
302. McCalley, D.V., *Selection of suitable stationary phases and optimum conditions for their application in the separation of basic compounds by reversed-phase HPLC.* Journal of Separation Science, 2003. **26**(3-4): p. 187-200.
303. Loeser, E. and P. Drumm, *Investigation of anion retention and cation exclusion effects for several C18 stationary phases.* Analytical Chemistry, 2007. **79**(14): p. 5382-5391.
304. Zoffoli, H.J.O., N.M.B. do Amaral-Sobrinho, E. Zonta, M.V. Luisi, G. Marcon, and A. Tolón-Becerra, *Inputs of heavy metals due to agrochemical use in tobacco fields in Brazil's Southern Region.* Environmental Monitoring and Assessment, 2013. **185**(3): p. 2423-2437.
305. Swartz, M.E., *UPLC™: an introduction and review.* Journal of Liquid Chromatography & Related Technologies, 2005. **28**(7-8): p. 1253-1263.
306. Giessibl, F.J., *Advances in atomic force microscopy.* Reviews of Modern Physics, 2003. **75**(3): p. 949.
307. Seo, Y. and W. Jhe, *Atomic force microscopy and spectroscopy.* Reports on Progress in Physics, 2007. **71**(1): p. 016101.
308. Efremov, E.V., F. Ariese, and C. Gooijer, *Achievements in resonance Raman spectroscopy: Review of a technique with a distinct analytical chemistry potential.* Analytica Chimica Acta, 2008. **606**(2): p. 119-134.
309. Buszewski, B., M. Jezierska, M. Wełniak, and R. Kaliszan, *Cholesteryl-silica stationary phase for liquid chromatography: Comparative study of retention behavior and selectivity.* Journal of Chromatography A, 1999. **845**(1): p. 433-445.
310. Albert, K., *NMR investigations of stationary phases.* Journal of Separation Science, 2003. **26**(3-4): p. 215-224.
311. Thakur, K.A., M. McCormick, W.L. Thompson, C. Cao, and W.J. Schultz, *Proton MAS NMR Analysis of Phenyl Silane Functionalized Silica Nanoparticles*, in *NMR Spectroscopy of Polymers: Innovative Strategies for Complex Macromolecules*. 2011, ACS Publications. p. 495-508.
312. Albert, K., R. Brindle, J. Schmid, B. Buszewski, and E. Bayer, *CP/MAS NMR investigations of silica gel surfaces modified with aminopropylsilane.* Chromatographia, 1994. **38**(5-6): p. 283-290.
313. Pesek, J.J., M. Matyska, E. Soczewiński, and P. Christensen, *Spectroscopic studies of butylphenyl, mono-ol and perfluorinated bonded phases.* Chromatographia, 1994. **39**(9-10): p. 520-528.
314. Chuang, I.-S. and G.E. Maciel, *Probing hydrogen bonding and the local environment of silanols on silica surfaces via nuclear spin cross polarization dynamics.* Journal of the American Chemical Society, 1996. **118**(2): p. 401-406.
315. Ali, F., W.J. Cheong, Z.A. ALOthman, and A.M. ALMajid, *Polystyrene bound stationary phase of excellent separation efficiency based on partially sub-2 μm silica monolith particles.* Journal of Chromatography A, 2013. **1303**: p. 9-17.
316. Nesterenko, E.P., P.N. Nesterenko, D. Connolly, X. He, P. Floris, E. Duffy, and B. Paull, *Nano-particle modified stationary phases for high-performance liquid chromatography.* Analyst, 2013. **138**(15): p. 4229-4254.

317. Henry, R.A., P. Ross, W.R. Betz, G. Parmar, and W.K. Way, *The Importance of Monodisperse Silica in the Evolution of UHPLC and HPLC Column Performance.* American Laboratory, 2015. **47**(6): p. 8-+.
318. Doyle, C.A., T.J. Vickers, C.K. Mann, and J.G. Dorsey, *Characterization of liquid chromatographic stationary phases by Raman spectroscopy Effect of ligand type.* Journal of Chromatography A, 1997. **779**(1-2): p. 91-112.
319. Lin-Vien, D., N.B. Colthup, W.G. Fateley, and J.G. Grasselli, *The handbook of infrared and Raman characteristic frequencies of organic molecules*. 1991: Elsevier.
320. Silverstein, R.M., G.C. Bassler, and T.C. Morrill, *Spectroscopic identification of organic compounds.* Wiley, New York, 1981: p. 196.
321. Thompson, W.R. and J.E. Pemberton, *Raman spectroscopy of covalently bonded alkylsilane layers on thin silica films immobilized on silver substrates.* Analytical Chemistry, 1994. **66**(20): p. 3367-3370.
322. Brindle, R., M. Pursch, and K. Albert, *1H MAS NMR spectroscopy of chemically modified silica gels: a fast method to characterize stationary interphases for chromatography.* Solid State Nuclear Magnetic Resonance, 1996. **6**(3): p. 251-266.
323. Albert, K., R. Brindle, P. Martin, and I.D. Wilson, *Characterisation of C18-bonded silicas for solid-phase extraction by solid-state NMR spectroscopy.* Journal of Chromatography A, 1994. **665**(2): p. 253-258.
324. Ashu-Arrah, B.A., J.D. Glennon, and K. Albert, *Synthesis, characterisation and chromatographic evaluation of pentafluorophenyl and phenyl bonded silica phases prepared using supercritical carbon dioxide as a reaction solvent.* Journal of Chromatography A, 2013. **1273**: p. 34-43.
325. Albert, K. and E. Bayer, *Characterization of bonded phases by solid-state NMR spectroscopy.* Journal of Chromatography A, 1991. **544**: p. 345-370.
326. Bocian, S., G. Rychlicki, M. Matyska, J. Pesek, and B. Buszewski, *Study of hydration process on silica hydride surfaces by microcalorimetry and water adsorption.* Journal of Colloid and Interface Science, 2014. **416**: p. 161-166.
327. PESEKJosephJ, M., *Hydride-Based Separation Materials for High Performance Liquid Chromatography and Open Tubular Capillary Electrochromatography.* 色谱, 2005. **23**(6): p. 595-608.
328. Brindle, R., K. Albert, E. Morgan, P. Martin, and I. Wilson, *Solid state NMR and extraction studies on "phenyl"-bonded stationary phases used for solid phase extraction.* Journal of Pharmaceutical and Biomedical Analysis, 1995. **13**(11): p. 1305-1312.
329. New, L.-S. and E.C. Chan, *Evaluation of BEH C18, BEH HILIC, and HSS T3 (C18) column chemistries for the UPLC-MS-MS analysis of glutathione, glutathione disulfide, and ophthalmic acid in mouse liver and human plasma.* Journal of Chromatographic Science, 2008. **46**(3): p. 209-214.
330. Bliesner, D.M. and K.B. Sentell, *Deuterium nuclear magnetic resonance spectroscopy as a probe for reversed-phase liquid chromatographic bonded phase solvation. 2. Aqueous solvation in methanol and acetonitrile binary mobile phases.* Analytical Chemistry, 1993. **65**(14): p. 1819-1826.
331. Glasel, J.A. and K. Lee, *Interpretation of water nuclear magnetic resonance relaxation times in heterogeneous systems.* Journal of the American Chemical Society, 1974. **96**(4): p. 970-978.
332. Ellwanger, A., R. Brindle, M. Kaiser, W. Wielandt, E. Lindner, and K. Albert, *n-Alkyl fluorenyl phases in chromatography: II. Dynamic behavior and high-*

performance liquid chromatography applications. Journal of Chromatography A, 1999. **858**(2): p. 133-153.
333. Gangoda, M., R. Gilpin, and J. Figueirinhas, *Deuterium nuclear magnetic resonance studies of alkyl-modified silica.* The Journal of Physical Chemistry, 1989. **93**(12): p. 4815-4818.
334. Maciel, G.E., M.J. Sullivan, and D.W. Sindorf, *Carbon-13 and silicon-29 nuclear magnetic resonance spectra of solid poly (methylsiloxane) polymers.* Macromolecules, 1981. **14**(5): p. 1607-1608.
335. Gilpin, R. and M. Gangoda, *Nuclear magnetic resonance spectrometry of chemically and physically altered porous silica surfaces under gas chromatographic conditions.* Talanta, 1986. **33**(2): p. 176-178.
336. Palmer, A.R. and G.E. Maciel, *Relaxation behavior in the carbon-13 nuclear magnetic resonance spectrometric analysis of kerogen with cross polarization and magic-angle spinning.* Analytical Chemistry, 1982. **54**(13): p. 2194-2198.
337. Bayer, E., A. Paulus, B. Peters, G. Laupp, J. Reiners, and K. Albert, *Conformational behaviour of alkyl chains of reversed phases in high-performance liquid chromatography.* Journal of Chromatography A, 1986. **364**: p. 25-37.
338. McNally, M. and L. Rogers, *Examination of the effect of solvent composition on bonded phase liquid chromatography packings by 13C Fourier transform nuclear magnetic resonance spectroscopy.* Journal of Chromatography A, 1985. **331**: p. 23-32.
339. Zeigler, R.C. and G.E. Maciel, *Study of dimethyloctadecylsilyl-modified silica using solid-state carbon-13 lineshapes and relaxation techniques.* The Journal of Physical Chemistry, 1991. **95**(19): p. 7345-7353.
340. Ellison, E.H. and D.B. Marshall, *NMR longitudinal relaxation study of the fluidity at octadecylsilica surfaces: acetonitrile as a probe of surface viscosity.* The Journal of Physical Chemistry, 1991. **95**(2): p. 808-813.
341. Linton, R., M. Miller, G. Maciel, and B. Hawkins, *Surface characterization of chemically modified (trimethylsily) silicas by 29Si solid state NMR, XPS, and IR photoacoustic spectroscopy.* Surface and Interface Analysis, 1985. **7**(4): p. 196-203.
342. De Haan, J., H. Van Den Bogaert, J. Ponjee, and L. Van De Ven, *Characterization of modified silica powders by Fourier transform infrared spectroscopy and cross-polarization magic angle spinning NMR.* Journal of Colloid and Interface Science, 1986. **110**(2): p. 591-600.
343. Köhler, J., D. Chase, R. Farlee, A. Vega, and J. Kirkland, *Comprehensive characterization of some silica-based stationary phase for high-performance liquid chromatography.* Journal of Chromatography A, 1986. **352**: p. 275-305.
344. Pfleiderer, B., K. Albert, E. Bayer, L. Van de Ven, J. De Haan, and C. Cramers, *A new approach to the silica gel surface: characterization of different surface regions by silicon-29 magic angle spinning NMR relaxation parameters and consequences for quantification of silica gels by NMR.* Journal of Physical Chemistry, 1990. **94**(10): p. 4189-4194.
345. Pfleiderer, B., K. Albert, and E. Bayer, *Investigations by 29Si cross-polarization magic angle spinning NMR spectroscopy of reaction pathways of silica gel polyfunctional modification.* Journal of Chromatography A, 1990. **506**: p. 343-355.
346. Sindorf, D.W. and G.E. Maciel, *Silicon-29 CP/MAS NMR studies of methylchlorosilane reactions on silica gel.* Journal of the American Chemical Society, 1981. **103**(14): p. 4263-4265.

347. Sindorf, D.W. and G.E. Maciel, *Silicon-29 NMR study of dehydrated/rehydrated silica gel using cross polarization and magic-angle spinning.* Journal of the American Chemical Society, 1983. **105**(6): p. 1487-1493.
348. Sindorf, D.W. and G.E. Maciel, *Silicon-29 nuclear magnetic resonance study of hydroxyl sites on dehydrated silica gel surfaces, using silylation as a probe.* The Journal of Physical Chemistry, 1983. **87**(26): p. 5516-5521.
349. Sindorf, D.W. and G.E. Maciel, *Solid-state NMR studies of the reactions of silica surfaces with polyfunctional chloromethylsilanes and ethoxymethylsilanes.* Journal of the American Chemical Society, 1983. **105**(12): p. 3767-3776.
350. Claessens, H., J. De Haan, L. Van de Ven, P. De Bruyn, and C. Cramers, *Chromatographic and solid state nuclear magnetic resonance study of the changes in reversed-phase packings for high-performance liquid chromatography at different eluent compositions.* Journal of Chromatography A, 1988. **436**: p. 345-365.
351. Hetem, M., L. Van de Ven, J. De Haan, C. Cramers, K. Albert, and E. Bayer, *Study of the changes in mono-, di-and trifunctional octadecyl-modified packings for reversed-phase high-performance liquid chromatography with different eluent compositions.* Journal of Chromatography A, 1989. **479**: p. 269-295.
352. Diercks, T., M. Coles, and H. Kessler, *Applications of NMR in drug discovery.* Current Opinion in Chemical Biology, 2001. **5**(3): p. 285-291.
353. Kromidas, S., *HPLC made to measure: a practical handbook for optimization*. 2008: John Wiley & Sons.
354. Spencer, R.G. and K.W. Fishbein, *Measurement of spin–lattice relaxation times and concentrations in systems with chemical exchange using the one-pulse sequence: breakdown of the Ernst model for partial saturation in nuclear magnetic resonance spectroscopy.* Journal of Magnetic Resonance, 2000. **142**(1): p. 120-135.
355. Wolfowicz, G., P.-A. Mortemousque, R. Guichard, S. Simmons, M.L. Thewalt, K.M. Itoh, and J.J. Morton, *29Si nuclear spins as a resource for donor spin qubits in silicon.* New Journal of Physics, 2016. **18**(2): p. 023021.
356. Ladd, T., D. Maryenko, Y. Yamamoto, E. Abe, and K. Itoh, *Coherence time of decoupled nuclear spins in silicon.* Physical Review B, 2005. **71**(1): p. 014401.
357. Lipari, G. and A. Szabo, *Model-free approach to the interpretation of nuclear magnetic resonance relaxation in macromolecules. 1. Theory and range of validity.* Journal of the American Chemical Society, 1982. **104**(17): p. 4546-4559.
358. Cheng, J.-W., C.A. Lepre, and J.M. Moore, *15N NMR relaxation studies of the FK506 binding protein: dynamic effects of ligand binding and implications for calcineurin recognition.* Biochemistry, 1994. **33**(14): p. 4093-4100.
359. Kai, L., D. Torchia, and A. Bax, *Backbone dynamics of proteins as studied by 15N inverse detected heteronuclear NMR spectroscopy: application to staphyloccal nuclase.* Biochemistry, 1989. **28**: p. 8972.
360. Bijttebier, S., E. D'Hondt, B. Noten, N. Hermans, S. Apers, and S. Voorspoels, *Ultra high performance liquid chromatography versus high performance liquid chromatography: stationary phase selectivity for generic carotenoid screening.* Journal of Chromatography A, 2014. **1332**: p. 46-56.
361. Gosetti, F., U. Chiuminatto, E. Mazzucco, E. Robotti, G. Calabrese, M.C. Gennaro, and E. Marengo, *Simultaneous determination of thirteen polycyclic aromatic hydrocarbons and twelve aldehydes in cooked food by an automated on-line solid phase extraction ultra high performance liquid chromatography tandem mass spectrometry.* Journal of Chromatography A, 2011. **1218**(37): p. 6308-6318.

362. Serrano, A., M. van Bommel, and J. Hallett, *Evaluation between ultrahigh pressure liquid chromatography and high-performance liquid chromatography analytical methods for characterizing natural dyestuffs.* Journal of Chromatography A, 2013. **1318**: p. 102-111.
363. Dong, M.W., *Modern HPLC for practicing scientists*. 2006: John Wiley & Sons.
364. Ahuja, S. and H. Rasmussen, *HPLC method development for pharmaceuticals*. Vol. 8. 2011: Elsevier.
365. Ahuja, S. and P.S. Ahuja, *Selectivity and detectability optimizations in HPLC*. Vol. 104. 1989: John Wiley & Sons.
366. Grumbach, E.S., T.E. Wheat, M. Kele, and J.R. Mazzeo, *Developing columns for UPLC: design considerations and recent developments.* LC GC Magazine-North America-Solutions for Separation Scientists, 2005. **22**: p. 40-44.
367. Lee, C., J. Zang, J. Cuff, N. McGachy, T.K. Natishan, C.J. Welch, R. Helmy, and F. Bernardoni, *Application of heart-cutting 2D-LC for the determination of peak purity for a chiral pharmaceutical compound by HPLC.* Chromatographia, 2013. **76**(1-2): p. 5-11.
368. Kiridena, W., C.F. Poole, S.N. Atapattu, J. Qian, and W.W. Koziol, *Comparison of the Separation Characteristics of the Organic–Inorganic Hybrid Octadecyl Stationary Phases XTerra MS C 18 and XBridge C 18 and Shield RP 18 in RPLC.* Chromatographia, 2007. **66**(7-8): p. 453-460.
369. Tate, P.A. and J.G. Dorsey, *Column selection for liquid chromatographic estimation of the kw' hydrophobicity parameter.* Journal of Chromatography A, 2004. **1042**(1-2): p. 37-48.
370. Snyder, L., J. Dolan, and P. Carr, *The hydrophobic-subtraction model of reversed-phase column selectivity.* Journal of Chromatography A, 2004. **1060**(1): p. 77-116.
371. Wilson, N., M. Nelson, J. Dolan, L. Snyder, R. Wolcott, and P. Carr, *Column selectivity in reversed-phase liquid chromatography: I. A general quantitative relationship.* Journal of Chromatography A, 2002. **961**(2): p. 171-193.
372. Wilson, N., M. Nelson, J. Dolan, L. Snyder, and P. Carr, *Column selectivity in reversed-phase liquid chromatography: II. Effect of a change in conditions.* Journal of Chromatography A, 2002. **961**(2): p. 195-215.
373. Wilson, N., J. Dolan, L. Snyder, P. Carr, and L.C. Sander, *Column selectivity in reversed-phase liquid chromatography: III. The physico-chemical basis of selectivity.* Journal of Chromatography A, 2002. **961**(2): p. 217-236.
374. Gilroy, J.J., J.W. Dolan, and L.R. Snyder, *Column selectivity in reversed-phase liquid chromatography: IV. Type-B alkyl-silica columns.* Journal of Chromatography A, 2003. **1000**(1): p. 757-778.
375. Gilroy, J.J., J.W. Dolan, P. Carr, and L.R. Snyder, *Column selectivity in reversed-phase liquid chromatography: V. Higher metal content (type-A) alkyl-silica columns.* Journal of Chromatography A, 2004. **1026**(1): p. 77-89.
376. Wilson, N., J. Gilroy, J. Dolan, and L. Snyder, *Column selectivity in reversed-phase liquid chromatography: VI. Columns with embedded or end-capping polar groups.* Journal of Chromatography A, 2004. **1026**(1): p. 91-100.
377. Marchand, D., K. Croes, J. Dolan, and L. Snyder, *Column selectivity in reversed-phase liquid chromatography: VII. Cyanopropyl columns.* Journal of Chromatography A, 2005. **1062**(1): p. 57-64.
378. Marchand, D., K. Croes, J. Dolan, L. Snyder, R. Henry, K. Kallury, S. Waite, and P. Carr, *Column selectivity in reversed-phase liquid chromatography: VIII. Phenylalkyl and fluoro-substituted columns.* Journal of Chromatography A, 2005. **1062**(1): p. 65-78.

379. Dzido, T. and H. Engelhardt, *Retention parameters of aromatic hydrocarbons with mono-substituted polar groups in binary RP-HPLC systems.* Chromatographia, 1994. **39**(1): p. 51-61.
380. Kimata, K., K. Iwaguchi, S. Onishi, K. Jinno, R. Eksteen, K. Hosoya, M. Araki, and N. Tanaka, *Chromatographic characterization of silica C18 packing materials. Correlation between a preparation method and retention behavior of stationary phase.* Journal of Chromatographic Science, 1989. **27**(12): p. 721-728.
381. Sander, L.C. and S.A. Wise, *Shape selectivity in reversed-phase liquid chromatography for the separation of planar and non-planar solutes.* Journal of Chromatography A, 1993. **656**(1-2): p. 335-351.
382. Poole, C.F. and S.K. Poole, *Column selectivity from the perspective of the solvation parameter model.* Journal of Chromatography A, 2002. **965**(1): p. 263-299.
383. Ahuja, S. and M. Dong, *Handbook of pharmaceutical analysis by HPLC*. Vol. 6. 2005: Elsevier.
384. Bodoprost, J. and H. Rosemeyer, *Analysis of phenacylester derivatives of fatty acids from human skin surface sebum by reversed-phase HPLC: chromatographic mobility as a function of physico-chemical properties.* International Journal of Molecular Sciences, 2007. **8**(11): p. 1111-1124.
385. Donovan, S.F. and M.C. Pescatore, *Method for measuring the logarithm of the octanol–water partition coefficient by using short octadecyl–poly (vinyl alcohol) high-performance liquid chromatography columns.* Journal of Chromatography A, 2002. **952**(1-2): p. 47-61.
386. Romieu, A., C. Massif, S. Rihn, G. Ulrich, R. Ziessel, and P.-Y. Renard, *The first comparative study of the ability of different hydrophilic groups to water-solubilise fluorescent BODIPY dyes.* New Journal of Chemistry, 2013. **37**(4): p. 1016-1027.
387. Selby-Pham, S., F. Dunshea, K. Howell, R. Miller, K. Bitter, and L. Bennett. *Modelling passive absorption properties of phytochemicals using physicochemical properties*. in *XXIX International Horticultural Congress on Horticulture: Sustaining Lives, Livelihoods and Landscapes (IHC2014): VI 1106*. 2014.
388. Wilkinson, S.M., H. Gunosewoyo, M.L. Barron, A. Boucher, M. McDonnell, P. Turner, D.E. Morrison, M.R. Bennett, I.S. McGregor, and L.M. Rendina, *The first CNS-active carborane: a novel P2X7 receptor antagonist with antidepressant activity.* ACS Chemical Neuroscience, 2014. **5**(5): p. 335-339.
389. Bhatia, M., *Understanding toxicology: mechanisms and applications.* Cell Biology and Toxicology, 2017. **33**(1): p. 1-4.
390. Baczek, T., *Computer-assisted optimization of liquid chromatography separations of drugs and related substances.* Current Pharmaceutical Analysis, 2008. **4**(3): p. 151-161.
391. Snyder, L., J. Dolan, and M. Quarry, *High-performance liquid chromatographic method-development using computer simulation.* TrAC Trends in Analytical Chemistry, 1987. **6**(5): p. 106-111.
392. Quarry, M., R. Grob, L. Snyder, J. Dolan, and M. Rigney, *Band-spacing in reversed-phase high-performance liquid chromatography as a function of solvent strength: A simple and fast alternative to solvent optimization for method development.* Journal of Chromatography A, 1987. **384**: p. 163-180.
393. Snyder, L. and M. Quarry, *Computer simulation in HPLC method development. Reducing the error of predicted retention times.* Journal of Liquid Chromatography, 1987. **10**(8-9): p. 1789-1820.

394. Zhang, Y.-P., K.-P. Lee, H.-J. Noh, A.M. Showkat, and S.-H. Choi, *Computer-assisted optimization of reversed-phase HPLC isocratic separation of neutral compounds.* Microchemical Journal, 2004. **78**(2): p. 99-106.
395. Baczek, T., R. Kaliszan, H.A. Claessens, and M.A. van Straten, *Computer-assisted optimization of reversed-phase HPLC isocratic separations of neutral compounds.* LC GC EUROPE, 2001. **14**(6): p. 304-313.
396. Li, W. and H.T. Rasmussen, *Strategy for developing and optimizing liquid chromatography methods in pharmaceutical development using computer-assisted screening and Plackett–Burman experimental design.* Journal of Chromatography A, 2003. **1016**(2): p. 165-180.
397. Molnar, I., *Computerized design of separation strategies by reversed-phase liquid chromatography: development of DryLab software.* Journal of Chromatography A, 2002. **965**(1): p. 175-194.
398. Snyder, L., J. Dolan, and D. Lommen, *Drylab® computer simulation for high-performance liquid chromatographic method development: I. Isocratic elution.* Journal of Chromatography A, 1989. **485**: p. 65-89.
399. Heinisch, S., E. Lesellier, C. Podevin, J. Rocca, and A. Tchapla, *Computerized optimization of RP-HPLC separation with nonaqueous or partially aqueous mobile phases.* Chromatographia, 1997. **44**(9): p. 529-537.
400. Jeong, L.N., R. Sajulga, S.G. Forte, D.R. Stoll, and S.C. Rutan, *Simulation of elution profiles in liquid chromatography□ I: Gradient elution conditions, and with mismatched injection and mobile phase solvents.* Journal of Chromatography A, 2016. **1457**: p. 41-49.
401. Reid, G.L., G. Cheng, D.T. Fortin, J.W. Harwood, J.E. Morgado, J. Wang, and G. Xue, *Reversed-phase liquid chromatographic method development in an analytical quality by design framework.* Journal of Liquid Chromatography & Related Technologies, 2013. **36**(18): p. 2612-2638.
402. Sasagawa, T., Y. Sakamoto, T. Hirose, T. Yoshida, Y. Kobayashi, Y. Sato, and K. Koizumi, *Prediction of retention times in ion-exchange chromatography.* Journal of Chromatography A, 1989. **485**: p. 533-540.
403. Jayaraman, K., A. Alexander, Y. Hu, and F. Tomasella, *A stepwise strategy employing automated screening and DryLab modeling for the development of robust methods for challenging high performance liquid chromatography separations: a case study.* Analytica Chimica Acta, 2011. **696**(1): p. 116-124.
404. Quarry, M., R. Grob, and L. Snyder, *Prediction of precise isocratic retention data from two or more gradient elution runs. Analysis of some associated errors.* Analytical Chemistry, 1986. **58**(4): p. 907-917.
405. Dolan, J., L. Snyder, and M. Quarry, *Computer simulation as a means of developing an optimized reversed-phase gradient-elution separation.* Chromatographia, 1987. **24**(1): p. 261-276.
406. Ghrist, B., B. Cooperman, and L. Snyder, *Design of optimized high-performance liquid chromatographic gradients for the separation of either small or large molecules: I. Minimizing errors in computer simulations.* Journal of Chromatography A, 1988. **459**: p. 1-23.
407. Ghrist, B. and L. Snyder, *Design of optimized high-performance liquid chromatographic gradients for the separation of either small or large molecules: II. Background and theory.* Journal of Chromatography A, 1988. **459**: p. 25-41.
408. Ghrist, B. and L. Snyder, *Design of optimized high-performance liquid chromatographic gradients for the separation of either small or large*

molecules: III. An overall strategy and its application to several examples. Journal of Chromatography A, 1988. **459**: p. 43-63.

409. Quarry, M., R. Grob, and L. Snyder, *Measurement and use of retention data from high-performance gradient elution: Contributions from "non-ideal" gradient equipment.* Journal of Chromatography A, 1984. **285**: p. 1-18.
410. Dolan, J.W. and L.R. Snyder, *Troubleshooting LC systems: a comprehensive approach to troubleshooting LC equipment and separations*. 1989: Springer Science & Business Media.
411. D'Archivio, A.A., M.A. Maggi, and F. Ruggieri, *Modelling of UPLC behaviour of acylcarnitines by quantitative structure–retention relationships.* Journal of Pharmaceutical and Biomedical Analysis, 2014. **96**: p. 224-230.
412. Jalali-Heravi, M. and H. Ebrahimi-Najafabadi, *Modeling of retention behaviors of most frequent components of essential oils in polar and non-polar stationary phases.* Journal of Separation Science, 2011. **34**(13): p. 1538-1546.
413. Ledesma, E.B. and M.J. Wornat, *QSRR prediction of chromatographic retention of ethynyl-substituted PAH from semiempirically computed solute descriptors.* Analytical Chemistry, 2000. **72**(21): p. 5437-5443.
414. Wang, C., M.J. Skibic, R.E. Higgs, I.A. Watson, H. Bui, J. Wang, and J.M. Cintron, *Evaluating the performances of quantitative structure-retention relationship models with different sets of molecular descriptors and databases for high-performance liquid chromatography predictions.* Journal of Chromatography A, 2009. **1216**(25): p. 5030-5038.
415. Miller, T.H., A. Musenga, D.A. Cowan, and L.P. Barron, *Prediction of chromatographic retention time in high-resolution anti-doping screening data using artificial neural networks.* Analytical Chemistry, 2013. **85**(21): p. 10330-10337.
416. Muteki, K., J.E. Morgado, G.L. Reid, J. Wang, G. Xue, F.W. Riley, J.W. Harwood, D.T. Fortin, and I.J. Miller, *Quantitative structure retention relationship models in an analytical Quality by Design framework: simultaneously accounting for compound properties, mobile-phase conditions, and stationary-phase properties.* Industrial & Engineering Chemistry Research, 2013. **52**(35): p. 12269-12284.
417. Put, R., M. Daszykowski, T. Baczek, and Y. Vander Heyden, *Retention prediction of peptides based on uninformative variable elimination by partial least squares.* Journal of Proteome Research, 2006. **5**(7): p. 1618-1625.
418. Ghafourian, T. and M.T. Cronin, *The impact of variable selection on the modelling of oestrogenicity.* SAR and QSAR in Environmental Research, 2005. **16**(1-2): p. 171-190.
419. Varmuza, K., P. Filzmoser, and M. Dehmer, *Multivariate linear QSPR/QSAR models: Rigorous evaluation of variable selection for PLS.* Computational and Structural Biotechnology Journal, 2013. **5**(6): p. 1-10.
420. Yasri, A. and D. Hartsough, *Toward an optimal procedure for variable selection and QSAR model building.* Journal of Chemical Information and Computer Sciences, 2001. **41**(5): p. 1218-1227.
421. Schoenmakers, P.J., H.A. Billiet, and L. De Galan, *Use of gradient elution for rapid selection of isocratic conditions in reversed-phase high-performance liquid chormatography.* Journal of Chromatography A, 1981. **205**(1): p. 13-30.
422. Bielejewska, A. and B.K. Głód, *RP-HPLC separation of acetic and trifluoroacetic acids using mobile phase with ion interaction reagent and without buffer.* Chemia analityczna, 2005. **50**(2): p. 387-395.

423. Wells, M.J. and C.R. Clark, *Liquid chromatographic elution characteristics of some solutes used to measure column void volume on C18 bonded phases.* Analytical Chemistry, 1981. **53**(9): p. 1341-1345.
424. Yuan, H. and S.V. Olesik, *Comparison of reversed-phase HPLC separation using carbon dioxide and fluoroform for enhanced-fluidity liquid mobile phases.* Analytical Chemistry, 1998. **70**(8): p. 1595-1603.
425. Engelhardt, H. and T. Lobert, *Chromatographic determination of metallic impurities in reversed-phase HPLC columns.* Analytical Chemistry, 1999. **71**(9): p. 1885-1892.
426. Heyrman, A.N. and R.A. Henry, *Importance of controlling mobile phase pH in reversed phase HPLC.* Keystone Tech Bull, 1999. **99**: p. 1-7.
427. Hashem, H. and T. Jira, *The effect of the process variables on the HPLC separation of tricyclic neuroleptics on a calixarene-bonded stationary phase.* Die Pharmazie-An International Journal of Pharmaceutical Sciences, 2005. **60**(3): p. 186-192.
428. Yang, M., S. Fazio, D. Munch, and P. Drumm, *Impact of methanol and acetonitrile on separations based on π–π interactions with a reversed-phase phenyl column.* Journal of Chromatography A, 2005. **1097**(1-2): p. 124-129.
429. Long, W. and A. Mack, *Comparison of selectivity differences among different Agilent zorbax phenyl columns using acetonitrile or methanol.* Agilent Technologies Application Note, 2009.

12 APPENDICES: TABLES

Table A. 1 T_1 and T_2 relaxation of aniline in solution only and presence of RP-HPLC stationary phases at varied temperatures.

	T_1 293K	T_1 298K	T_1 303K	T_1 308K	T_1 313K	T_2 293K	T_2 298K	T_2 303K	T_2 308K	T_2 313K
Solution Only										
H_1 free	7.6	8.4	9.1	9.3	9.7	2.3	2.6	2.5	2.4	2.2
H_2 free	8.7	9.5	10.3	10.6	11.0	2.5	2.7	2.7	2.6	2.4
BEH-C18										
H_1 free	6.3	6.3	7.1	7.4	7.9	1.6	1.0	1.0	1.0	0.9
H_2 free	6.9	7.0	7.6	8.0	8.2	1.6	1.0	0.97	0.96	0.9
H_1 bound	2.7	3.2	4.0	4.5	5.2	0.1	0.2	0.2	0.2	0.2
H_2 bound	2.7	3.2	4.4	4.8	5.2	0.1	0.2	0.2	0.2	0.2
BEH-Phenyl										
H_1 free	4.1	4.4	5.6	5.1	6.6	1.4	1.2	0.9	0.7	0.6
H_2 free	4.0	4.1	4.1	4.4	4.7	1.3	1.1	0.9	0.7	0.6
H_1 bound	2.3	2.6	3.3	2.9	3.9	0.1	0.1	0.1	0.1	0.1
H_2 bound	2.6	2.9	3.4	3.3	3.9	0.1	0.1	0.1	0.1	0.1
BEH-RP18										
H_1 free	4.4	4.7	5.4	5.8	6.2	1.0	0.7	0.7	0.6	0.5
H_2 free	3.7	3.7	3.9	4.0	4.2	1.0	0.8	0.7	0.6	0.5
H_1 bound	2.0	2.5	3.6	4.4	4.8	0.1	0.1	0.1	0.1	0.1
H_2 bound	1.9	2.4	3.0	3.5	3.8	0.1	0.1	0.1	0.1	0.1
CSH Hexyl-Phenyl										
H_1 free	4.5	5.2	5.6	6.0	6.4	1.2	0.8	0.7	0.7	0.7
H_2 free	4.9	4.8	4.9	5.2	5.4	1.3	0.9	0.8	0.7	0.8
H_1 bound	2.4	2.8	3.0	3.1	3.5	0.1	0.1	0.1	0.1	0.1
H_2 bound	2.6	3.3	3.6	3.8	4.2	0.1	0.1	0.1	0.1	0.1
HSS T3										
H_1 free	7.1	7.3	7.6	8.1	8.6	2.1	1.9	1.6	1.5	1.4
H_2 free	7.6	7.8	8.1	8.5	8.8	2.1	1.9	1.6	1.5	1.4
H_1 bound	4.1	4.6	4.9	5.4	5.4	0.1	0.1	0.1	0.1	0.1
H_2 bound	4.4	4.6	5.0	5.2	5.9	0.1	0.1	0.1	0.1	0.1

Table A. 2 T_1 and T_2 relaxation of aniline in solution only and presence of RP-HPLC stationary phases.

	50:50 MeCN:D_2O		**50:50 MeOH:D_2O**	
	T_1	T_2	T_1	T_2
	Solution Only			
H_1 free	6.4	2.8	4.8	2.6
H_2 free	7.0	2.9	5.4	2.6
	BEH-C18			
H_1 free	7.4	1.6	5.7	1.3
H_2 free	8.0	1.6	6.2	1.3
H_1 bound	3.9	0.1	2.4	0.1
H_2 bound	3.9	0.1	2.5	0.1
	BEH-Phenyl			
H_1 free	7.6	1.5	6.0	1.3
H_2 free	8.7	1.6	6.6	1.3
H_1 bound	4.1	0.1	2.6	0.1
H_2 bound	4.8	0.1	3.1	0.1
	BEH-RP18			
H_1 free	7.5	1.3	5.5	1.4
H_2 free	8.1	1.3	5.9	1.3
H_1 bound	4.0	0.1	2.3	0.1
H_2 bound	3.7	0.1	2.4	0.1
	CSH Hexyl-Phenyl			
H_1 free	6.7	1.5	5.8	2.3
H_2 free	7.5	1.6	6.5	2.4
H_1 bound	3.7	0.1	2.4	0.1
H_2 bound	4.3	0.1	2.9	0.1
	HSS T3			
H_1 free	8.4	1.2	6.4	1.7
H_2 free	7.9	1.2	7.0	1.6
H_1 bound	6.1	0.2	3.4	0.1
H_2 bound	5.5	0.1	3.4	0.1

Table A. 3 Retention times (minutes) of all 15 analytes dissolved in 50:50 MeCN:D_2O across BEH-C18, BEH-phenyl, BEH-RP18, CSH hexyl-phenyl and HSS T3 stationary phases.

Analytes	BEH C18	BEH phenyl	BEH RP18	CSH hexyl-phenyl	HSS T3
			R_t		
i. toluene	10.66	7.08	9.61	7.55	13.69
ii. naphthalene	14.10	9.02	13.36	9.79	18.68
iii. acenaphthylene	24.37	13.05	21.37	14.46	32.95
iv. benzophenone	10.71	8.12	10.55	8.74	15.09
v. biphenyl	21.51	12.51	19.26	13.76	29.76
vi. propranolol	Strongly retained onto column				
vii.2-aminophenol	2.84	3.03	2.97	3.19	3.18
viii. aniline	3.58	3.67	3.73	3.80	4.22
ix.3-hydroxybenzoic acid	2.07	2.06	14.38	2.44	2.67
x. dipropyl phthalate	17.30	10.73	14.59	11.59	25.59
xi. butyl 4-hydroxybenzoate	7.36	5.75	8.90	6.64	9.72
xii. benzoic acid	2.67	2.34	10.82	3.13	3.58
xiii. amitriptyline hydrochloride	Strongly retained onto column				
xiv. hydroxyzine	Strongly retained onto column				
xv. meclizine	Strongly retained onto column				

Table A. 4 Retention times (minutes) of all 15 analytes dissolved in 50:50 (% v/v) MeOH:D_2O across BEH-C18, BEH-phenyl, BEH-RP18, CSH hexyl-phenyl and HSS T3 stationary phases.

Analytes	BEH C18	BEH phenyl	BEH RP18	CSH hexyl-phenyl	HSS T3
			R_t		
i. toluene	21.57	12.24	17.55	13.32	27.73
ii. naphthalene	37.60	20.79	34.17	23.06	49.11
iii. benzophenone	24.70	21.46	22.54	23.01	37.33
iv. biphenyl	79.98	40.45	66.41	46.31	88.10
v. propranolol	Strongly retained onto column				
vi.2-aminophenol	3.13	3.59	3.34	3.81	3.56
vii. aniline	3.86	4.22	4.06	4.39	4.56
viii.3-hydroxybenzoic acid	2.29	2.55	10.30	3.14	2.70
ix. dipropyl phthalate	52.04	37.76	34.80	40.16	90.00
x. butyl 4-hydroxybenzoate	26.79	10.12	29.18	21.63	38.00
xi. benzoic acid	4.30	3.02	19.00	4.00	6.80
xii. amitriptyline hydrochloride	Strongly retained onto column				
xiii. hydroxyzine	Strongly retained onto column				
xiv. meclizine	Strongly retained onto column				

Table A. 5 ^{1}H T_1 and T_2 relaxation times for toluene in 50:50 % v/v MeCN:D_2O (from top to bottom according to HPLC elution order): mobile phase in the absence of stationary phase (solution only) and in the presence of BEH-C18, BEH-phenyl, BEH-RP18, CSH hexyl-phenyl and HSS T3 stationary phases. Data were obtained at 500 MHz spectrometer at 313 K and 5.0 kHz spinning frequency.

	SP	HPLC Rt (mins)	T_1(s)					
			H-1(f)	H-2(f)	H-3(f)	H-1(b)	H-2(b)	H-3(b)
MeCN:D_2O 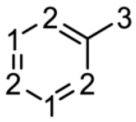 Toluene	Solution only	n/a	6.4±0.1	6.5±0.1	6.4±0.1		n/a	
	BEH-Phenyl	7.08	3.5±0.3	2.6±0.2	3.8±0.3	2.6±0.1	2.4±0.1	2.8±0.1
	CSH Hexyl-phenyl	7.55	5.7±0.5	4.3±0.1	3.9±0.2	3.1±0.1	2.8±0.1	3.1±0.1
	BEH-RP18	9.61	6.8±0.5	6.2±0.5	4.8±0.2	3.3±0.2	3.1±0.2	2.5±0.1
	BEH-C18	10.66	5.6±0.1	5.1±0.1	4.6±0.1	3.6±0.2	3.4±0.2	3.0±0.1
	HSS T3	13.69	8.5±0.9	6.8±0.5	5.4±0.2	3.5±0.1	3.5±0.1	2.9±0.1
			T_2(s)					
			H-1(f)	H-2(f)	H-3(f)	H-1(b)	H-2(b)	H-3(b)
	Solution only	n/a	3.5±0.1	3.5±0.1	3.5±0.1		n/a	
	BEH-Phenyl	7.08	2.0±0.2	1.8±0.1	1.6±0.05	0.1±0.003	0.1±0.002	0.1±0.002
	CSH Hexyl-phenyl	7.55	1.3±0.1	1.0±0.04	1.1±0.1	0.1±0.003	0.1±0.002	0.1±0.002
	BEH-RP18	9.61	2.2±0.1	2.0±0.1	1.9±0.1	0.2±0.004	0.2±0.003	0.2±0.005
	BEH-C18	10.66	1.8±0.1	1.6±0.1	1.6±0.02	0.1±0.001	0.1±0.002	0.2±0.001
	HSS T3	13.69	2.4±0.1	2.7±0.2	2.5±0.1	0.3±0.002	0.3±0.005	0.5±0.003

Table A. 6 ^{1}H T_1 and T_2 relaxation times for toluene in 50:50 % v/v MeOH:D_2O (from top to bottom according to HPLC elution order): mobile phase in the absence of stationary phase (solution only) and in the presence of BEH-C18, BEH-phenyl, BEH-RP18, CSH hexyl-phenyl and HSS T3 stationary phases. Data were obtained at 500 MHz spectrometer at 313 K and 5.0 kHz spinning frequency.

MeOH/D_2O

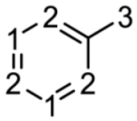

Toluene

SP	HPLC Rt (mins)	T_1(s)					
		H-1(f)	H-2(f)	H-3(f)	H-1(b)	H-2(b)	H-3(b)
Solution only	n/a	6.6±0.3	7.2±0.4	6.6±0.3		n/a	
BEH-Phenyl	12.24	2.9±0.2	2.2±0.1	3.8±02	1.6±0.1	1.6±0.03	2.0±0.1
CSH Hexyl-phenyl	13.32	3.2±0.3	2.5±0.1	3.6±0.4	1.7±0.1	1.9±0.1	2.1±0.1
BEH-RP18	17.55	5.6±0.7	3.9±0.2	4.3±0.3	1.7±0.1	1.7±0.03	1.6±0.1
BEH-C18	21.57	4.8±0.6	4.7±0.5	3.3±0.1	1.5±0.1	1.5±0.1	1.5±0.1
HSS T3	27.73	6.2±0.6	5.2±0.4	3.6±0.1	3.0±0.2	3.0±0.2	1.9±0.2
		T_2(s)					
		H-1(f)	H-2(f)	H-3(f)	H-1(b)	H-2(b)	H-3(b)
Solution only	n/a	3.1±0.2	3.2±0.2	3.1±0.2		n/a	
BEH-Phenyl	12.24	2.5±0.2	2.1±0.1	2.0±0.1	0.05±0.002	0.05±0.003	0.1±0.002
CSH Hexyl-phenyl	13.32	2.5±0.2	2.0±0.2	1.9±0.09	0.1±0.003	0.1±0.004	0.1±0.003
BEH-RP18	17.55	1.9±0.1	1.8±0.04	1.7±0.03	0.1±0.002	0.1±0.002	0.1±0.002
BEH-C18	21.57	2.0±0.2	1.9±0.1	1.8±0.1	0.04±0.003	0.04±0.001	0.05±0.002
HSS T3	27.73	2.7±0.2	2.3±0.1	2.3±0.1	0.2±0.01	0.2±0.02	0.3±0.02

Table A. 7 ^{1}H T_1 and T_2 relaxation times for naphthalene in 50:50 % v/v MeCN:D_2O (from top to bottom according to HPLC elution order): mobile phase in the absence of stationary phase (solution only) and in the presence of BEH-C18, BEH-phenyl, BEH-RP18, CSH hexyl-phenyl and HSS T3 stationary phases. Data were obtained at 500 MHz spectrometer at 313 K and 5.0 kHz spinning frequency.

	SP	HPLC Rt (mins)	T_1(s) H-1(f)	H-2(f)	H-1(b)	H-2(b)
MeCN/D_2O 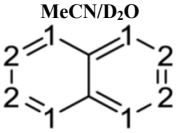 Naphthalene	Solution only	n/a	5.6±0.1	6.0±0.1	n/a	
	BEH-Phenyl	9.02	7.7±0.4	7.8±0.5	4.5±0.1	4.4±0.1
	CSH Hexyl-phenyl	9.79	8.3±0.6	7.7±0.5	4.1±0.2	3.8±0.2
	BEH-RP18	13.36	7.5±1.2	6.8±0.4	2.8±0.1	3.1±0.1
	BEH-C18	14.10	7.1±0.2	7.7±0.5	3.5±0.1	3.5±0.1
	HSS T3	18.68	7.1±0.3	9.9±0.4	3.7±0.1	3.8±0.1
			T_2(s) H-1(f)	H-2(f)	H-1(b)	H-2(b)
	Solution only	n/a	2.8±0.1	2.9±0.03	n/a	
	BEH-Phenyl	9.02	2.0±0.1	2.0±0.1	0.1±0.002	0.1±0002
	CSH Hexyl-phenyl	9.79	2.5±0.1	2.5±0.1	0.1±0.003	0.1±0.007
	BEH-RP18	13.36	2.0±0.1	2.2±0.1	0.1±0.002	0.1±0.004
	BEH-C18	14.10	2.2±0.03	2.3±0.04	0.1±0.002	0.1±0.001
	HSS T3	18.68	1.2±0.1	1.2±0.1	0.2±0.003	0.2±0.001

Table A. 8 ^{1}H T_1 and T_2 relaxation times for naphthalene in 50:50 % v/v MeOH:D_2O (from top to bottom according to HPLC elution order): mobile phase in the absence of stationary phase (solution only) and in the presence of BEH-C18, BEH-phenyl, BEH-RP18, CSH hexyl-phenyl and HSS T3 stationary phases. Data were obtained at 500 MHz spectrometer at 313 K and 5.0 kHz spinning frequency.

	SP	HPLC Rt (mins)	T_1(s) H-1(f)	H-2(f)	H-1(b)	H-2(b)
MeOH/H_2O 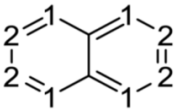 Naphthalene	Solution only	n/a	6.4±0.1	6.7±0.2	n/a	
	BEH-Phenyl	20.79	5.1±0.9	4.7±0.5	1.9±0.2	1.7±0.1
	CSH Hexyl-phenyl	23.06	5.9±0.7	4.1±0.8	2.1±0.2	1.5±0.1
	BEH-RP18	34.17	5.2±0.5	6.0±1.0	1.8±0.3	1.4±0.2
	BEH-C18	37.60	5.0±0.3	5.2±0.4	1.4±0.1	1.2±0.1
	HSS T3	49.11	8.6±1.8	7.6±1.5	1.9±0.1	2.3±0.1
			T_2(s) H-1(f)	H-2(f)	H-1(b)	H-2(b)
	Solution only	n/a	2.4±0.05	2.5±0.1	n/a	
	BEH-Phenyl	20.79	1.2±0.05	1.4±0.1	0.1±0.007	0.1±0.004
	CSH Hexyl-phenyl	23.06	1.8±0.3	1.7±0.2	0.1±0.005	0.1±0.005
	BEH-RP18	34.17	1.9±0.1	1.8±0.1	0.05±0.003	0.05±0.003
	BEH-C18	37.60	1.7±0.1	1.6±0.1	0.04±0.004	0.04±0.002
	HSS T3	49.11	1.3±0.2	1.7±0.3	0.1±0.005	0.1±0.007

Table A. 9 ^{1}H T_1 and T_2 relaxation times for acenaphthene in 50:50 % v/v MeCN:D_2O (from top to bottom according to HPLC elution order): mobile phase in the absence of stationary phase (solution only) and in the presence of BEH-C18, BEH-phenyl, BEH-RP18, CSH hexyl-phenyl and HSS T3 stationary phases. Data were obtained at 500 MHz spectrometer at 313 K and 5.0 kHz spinning frequency.

MeCN/D_2O

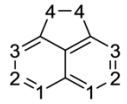

Acenaphthene

SP	HPLC Rt (mins)	T_1(s) H-1(f)	H-2(f)	H-3(f)	H-4(f)	H-1(b)	H-2(b)	H-3(b)	H-4(b)
Solution only	n/a	5.9±0.2	6.1±0.4	5.8±0.3	2.7±0.1		n/a		
BEH-Phenyl	13.05	5.0±0.4	4.5±0.2	4.6±0.3	2.6±0.1	3.2±0.1	2.8±0.1	2.1±0.1	1.4±0.1
CSH Hexyl-phenyl	14.46	9.7±1.2	12.2±2.6	6.4±0.3	3.4±0.1	3.7±0.1	3.4±0.1	2.4±0.1	1.7±0.1
BEH-RP18	21.37	7.5±1.1	7.5±1.2	7.1±0/6	3.4±0.2	2.8±0.1	2.9±0.1	2.7±0.1	1.4±0.1
BEH-C18	24.37	7.4±0.8	7.7±1.1	5.7±0.4	2.7±0.1	2.9±0.1	2.9±0.1	2.9±0.1	1.3±0.04
HSS T3	32.95	10.2±1.9	8.5±1.6	3.8±0.1	3.9±0.2	3.8±0.1	3.2±0.1	3.3±0.1	1.2±0.1
		T_2(s) H-1(f)	H-2(f)	H-3(f)	H-4(f)	H-1(b)	H-2(b)	H-3(b)	H-4(b)
Solution only	n/a	1.8±0.1	2.2±0.1	2.2±0.1	1.8±0.05		n/a		
BEH-Phenyl	13.05	1.8±0.1	1.9±0.1	1.7±0.1	1.2±0.07	0.1±0.004	0.1±0.004	0.1±0.004	0.1±0.003
CSH Hexyl-phenyl	14.46	1.6±0.1	1.6±0.1	0.2±0.005	1.2±0.07	0.1±0.005	0.1±0.002	0.1±0.003	0.1±0.002
BEH-RP18	21.37	1.5±0.1	1.3±0.1	1.2±0.1	1.2±0.1	0.2±0.004	0.1±0.006	0.1±0.07	0.1±0.002
BEH-C18	24.37	1.4±0.1	1.2±0.1	1.3±0.1	1.2±0.03	0.1±0.02	0.1±0.03	0.1±0.003	0.1±0.003
HSS T3	32.95	1.7±0.1	1.7±0.1	0.3±0.004	1.4±0.07	0.3±0.04	0.2±0.003	0.2±0.004	0.1±0.002

Table A. 10 ^{1}H T_1 and T_2 relaxation times for benzophenone in 50:50 % v/v MeCN:D_2O (from top to bottom according to HPLC elution order): mobile phase in the absence of stationary phase (solution only) and in the presence of BEH-C18, BEH-phenyl, BEH-RP18, CSH hexyl-phenyl and HSS T3 stationary phases. Data were obtained at 500 MHz spectrometer at 313 K and 5.0 kHz spinning frequency.

MeCN:D_2O

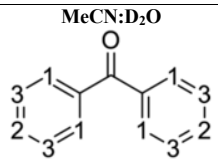

Benzophenone

SP	HPLC Rt (mins)	T_1(s) H-1(f)	H-2(f)	H-3(f)	H-1(b)	H-2(b)	H-3(b)
Solution only	n/a	4.5±0.1	5.1±0.2	4.5±0.1		n/a	
BEH-Phenyl	8.12	6.1±0.1	6.1±0.4	5.5±0.2	4.3±0.1	4.3±0.1	3.9±0.1
CSH Hexyl-phenyl	8.74	7.8±0.6	14.7±1.1	7.7±0.6	4.7±0.1	4.6±0.1	4.2±0.1
BEH-RP18	10.55	5.8±0.3	7.1±0.7	6.0±0.3	3.3±0.1	3.3±0.1	3.2±0.05
BEH-C18	10.71	5.8±0.2	6.2±0.3	5.1±0.1	3.9±0.1	3.9±0.1	3.7±0.04
HSS T3	15.09	6.0±0.3	6.3±0.3	5.2±0.2	3.7±0.1	3.7±0.1	3.5±0.1
		T_2(s) H-1(f)	H-2(f)	H-3(f)	H-1(b)	H-2(b)	H-3(b)
Solution only	n/a	2.8±0.04	3.0±0.1	2.8±0.04		n/a	
BEH-Phenyl	8.12	1.5±0.1	1.5±0.1	1.4±0.05	0.2±0.004	0.1±0.005	0.1±0.003
CSH Hexyl-phenyl	8.74	1.1±0.1	0.4±0.1	0.5±0.1	0.1±0.002	0.1±0.001	0.1±0.002
BEH-RP18	10.55	1.9±0.02	1.9±0.1	1.8±0.02	0.2±0.007	0.1±0.005	0.1±0.004
BEH-C18	10.71	2.1±0.03	2.1±0.1	1.9±0.1	0.8±0.1	0.8±0.1	0.7±0.1
HSS T3	15.09	2.2±0.02	2.2±0.04	2.1±0.04	0.4±0.04	0.3±0.04	0.3±0.03

Table A. 11 ^{1}H T_1 and T_2 relaxation times for benzophenone in 50:50 % v/v MeOH:D_2O (from top to bottom according to HPLC elution order): mobile phase in the absence of stationary phase (solution only) and in the presence of BEH-C18, BEH-phenyl, BEH-RP18, CSH hexyl-phenyl and HSS T3 stationary phases. Data were obtained at 500 MHz spectrometer at 313 K and 5.0 kHz spinning frequency.

MeOH/D_2O

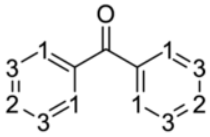

Benzophenone

SP	HPLC Rt (mins)	T_1(s) H-1(f)	H-2(f)	H-3(f)	H-1(b)	H-2(b)	H-3(b)
Solution only	n/a	3.8±0.5	3.4±0.6	3.5±0.2		n/a	
BEH-Phenyl	21.46	1.5±0.1	1.2±0.1	1.3±0.1	1.5±0.1	1.2±0.1	1.3±0.1
BEH-RP18	22.54	2.3±0.1	1.3±0.1	2.2±0.3	1.3±0.1	1.1±0.1	1.2±0.03
CSH Hexyl-phenyl	23.01	1.5±0.1	1.4±0.1	1.4±0.1	1.5±0.1	1.4±0.1	1.4±0.1
BEH-C18	24.70	3.5±0.2	4.4±1.0	2.4±0.1	1.3±0.1	1.2±0.1	1.2±0.1
HSS T3	37.33	1.3±0.1	0.7±0.2	1.1±0.1	1.3±0.1	0.7±0.2	1.1±0.1
		T_2(s) H-1(f)	H-2(f)	H-3(f)	H-1(b)	H-2(b)	H-3(b)
Solution only	n/a	2.5±0.1	2.2±0.2	2.4±0.1		n/a	
BEH-Phenyl	21.46	0.1±0.004	0.1±0.004	0.08±0.004	0.1±0.04	0.1±0.004	0.08±0.004
BEH-RP18	22.54	1.9±0.2	0.03±0.03	2.1±0.2	0.03±0.03	0.02±0.001	0.02±0.001
CSH Hexyl-phenyl	23.01	0.09±0.003	0.05±0.004	0.05±0.04	0.09±0.003	0.05±0.004	0.05±0.004
BEH-C18	24.70	1.5±0.1	1.5±0.1	1.7±0.1	0.03±0.002	0.02±0.001	0.02±0.001
HSS T3	37.33	0.04±0.002	0.03±0.009	0.02±0.002	0.04±0.002	0.03±0.009	0.02±0.002

Table A. 12 ^{1}H T_1 and T_2 relaxation times for biphenyl in 50:50 % v/v MeCN:D_2O (from top to bottom according to HPLC elution order): mobile phase in the absence of stationary phase (solution only) and in the presence of BEH-C18, BEH-phenyl, BEH-RP18, CSH hexyl-phenyl and HSS T3 stationary phases. Data were obtained at 500 MHz spectrometer at 313 K and 5.0 kHz spinning frequency.

MeCN/D_2O

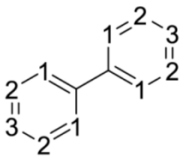

Biphenyl

SP	HPLC Rt (mins)	T_1(s) H-1(f)	H-3(f)	H-2(b)	H-3(b)
Solution only	n/a	4.2±0.1	4.7±0.1	n/a	
BEH-Phenyl	12.51	6.1±0.5	3.5±0.2	2.9±0.1	2.7±0.1
CSH Hexyl-phenyl	13.76	4.5±0.2	3.3±0.4	2.9±0.1	2.8±0.1
BEH-RP18	19.26	5.1±0.1	4.1±0.1	2.4±0.1	2.6±0.1
BEH-C18	21.51	5.8±0.2	6.0±0.2	3.3±0.1	3.4±0.2
HSS T3	29.76	5.1±0.3	8.0±0.4	2.7±0.2	2.8±0.2
		T_2(s) H-1(f)	H-3(f)	H-2(b)	H-3(b)
Solution only	n/a	2.8±0.03	2.9±0.04	n/a	
BEH-Phenyl	12.51	2.1±0.1	2.0±0.2	0.1±0.002	0.1±0.006
CSH Hexyl-phenyl	13.76	2.1±0.1	2.2±0.4	0.1±0.002	0.1±0.002
BEH-RP18	19.26	2.1±0.2	1.5±0.2	0.2±0.003	0.2±0.005
BEH-C18	21.51	2.6±0.04	2.7±0.1	0.2±0.004	0.1±0.005
HSS T3	29.76	2.3±0.1	2.2±0.3	0.3±0.006	0.3±0.007

Table A. 13 ^{1}H T_1 and T_2 relaxation times for biphenyl in 50:50 % v/v MeOH:D_2O (from top to bottom according to HPLC elution order): mobile phase in the absence of stationary phase (solution only) and in the presence of BEH-C18, BEH-phenyl, BEH-RP18, CSH hexyl-phenyl and HSS T3 stationary phases. Data were obtained at 500 MHz spectrometer at 313 K and 5.0 kHz spinning frequency.

MeOH/D_2O

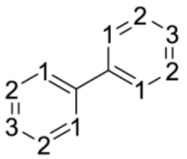

Biphenyl

SP	HPLC Rt (mins)	T_1(s) H-1(f)	H-3(f)	H-2(b)	H-3(b)
Solution only	n/a	2.4±0.3	4.2±0.2	n/a	
BEH-Phenyl	40.45	1.3±0.05	1.3±0.04	1.2±0.02	1.2±0.01
CSH Hexyl-phenyl	46.31	1.2±0.2	1.2±0.1	1.3±0.1	1.2±0.1
BEH-RP18	66.41	1.4±0.03	1.2±0.1	1.3±0.1	1.2±0.1
BEH-C18	79.98	3.5±0.4	1.6±0.05	1.5±0.03	1.6±0.1
HSS T3	88.10	1.4±0.1	1.4±0.1	1.9±0.2	1.4±0.1
		T_2(s) H-1(f)	H-3(f)	H-2(b)	H-3(b)
Solution only	n/a	2.2±0.2	2.1±0.1	n/a	
BEH-Phenyl	40.45	0.6±0.1	0.1±0.02	0.1±0.001	0.1±0.003
CSH Hexyl-phenyl	46.31	0.1±0.005	0.1±0.009	0.1±0.004	0.1±0.01
BEH-RP18	66.41	0.1±0.004	0.1±0.004	0.1±0.002	0.1±0.004
BEH-C18	79.98	1.4±0.1	0.1±0.003	0.1±0.001	0.1±0.002
HSS T3	88.10	0.1±0.003	0.1±0.002	0.2±0.01	0.1±0.002

Table A. 14 ^{1}H T_1 and T_2 relaxation times for butyl 4-hydroxybenzoate in 50:50 % v/v MeCN:D_2O (from top to bottom according to HPLC elution order): mobile phase in the absence of stationary phase (solution only) and in the presence of BEH-C18, BEH-phenyl, BEH-RP18, CSH hexyl-phenyl and HSS T3 stationary phases. Data were obtained at 500 MHz spectrometer at 313 K and 5.0 kHz spinning frequency.

MeCN/D_2O

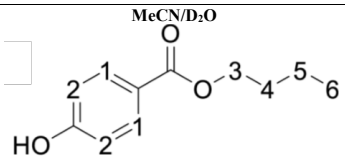

Butyl 4-hydroxybenzoate

SP	HPLC Rt (mins)	T_1(s) H-1(f)	H-2(f)	H-3(f)	H-4(f)	H-5(f)	H-6(f)	H-1(b)	H-2(b)	H-3(b)	H-4(b)	H-5(b)	H-6(b)
Solution only	n/a	2.8±0.0002	3.0±0.0002	1.6±0.0001	1.6±0.0001	1.9±0.0001	2.1±0.0001	n/a					
BEH-Phenyl	5.75	4.1±0.3	2.1±0.1	4.9±0.04	1.7±0.1	1.7±0.1	2.2±0.2	2.8±0.05	2.6±0.02	3.3±0.1	1.3±0.1	1.7±0.2	1.9±0.1
CSH Hexyl-phenyl	6.64	4.2±0.5	1.7±0.1	3.5±0.05	2.0±0.2	1.7±0.2	2.0±0.1	2.2±0.1	1.9±0.1	2.6±0.1	1.3±0.2	1.5±0.2	1.7±0.1
BEH-C18	7.36	4.1±0.1	4.6±0.2	5.7±0.1	1.7±0.1	1.8±0.1	1.8±0.1	2.9±0.1	2.8±0.1	2.4±0.2	1.4±0.1	1.5±0.1	1.5±0.1
BEH-RP18	8.90	4.5±0.3	4.2±0.6	6.6±0.1	2.9±0.2	2.2±0.2	1.7±0.1	1.8±0.1	1.7±0.1	4.4±0.2	1.4±0.1	1.3±0.1	1.5±0.1
HSS T3	9.72	3.5±0.1	4.0±0.1	2.2±0.1	1.6±0.2	1.8±0.1	1.8±0.1	3.0±0.1	3.2±0.1	1.7±0.1	1.4±0.1	1.6±0.1	1.8±0.1
		T_2(s) H-1(f)	H-2(f)	H-3(f)	H-4(f)	H-5(f)	H-6(f)	H-1(b)	H-2(b)	H-3(b)	H-4(b)	H-5(b)	H-6(b)
Solution only	n/a	1.7±0.1	1.7±0.1	0.9±0.02	1.0±0.02	1.3±0.02	1.4±0.02	n/a					
BEH-Phenyl	5.75	0.4±0.1	0.5±0.05	0.1±0.004	0.5±0.04	0.5±0.04	0.6±0.03	0.3±0.02	0.3±0.02	0.1±0.01	0.1±0.01	0.±0.01	0.2±0.003
CSH Hexyl-phenyl	6.64	0.1±0.01	0.5±0.04	0.1±0.02	0.1±0.03	0.2±0.03	0.7±0.05	0.1±0.01	0.1±0.01	0.05±0.01	0.04±0.003	0.1±0.01	0.1±0.003
BEH-C18	7.36	0.8±0.04	0.9±0.03	0.1±0.004	0.7±0.05	1.1±0.04	1.2±0.03	0.4±0.03	0.3±0.04	0.2±0.1	0.2±0.02	0.3±0.01	0.3±0.02
BEH-RP18	8.90	0.4±0.04	0.5±0.1	0.8±0.02	0.4±0.04	0.6±0.01	0.8±0.05	0.1±0.01	0.1±0.02	0.6±0.1	0.1±0.03	0.1±0.01	0.2±0.01
HSS T3	9.72	0.8±0.02	0.8±0.05	0.1±0.01	0.7±0.03	0.9±0.03	1.1±0.02	0.8±0.05	0.8±0.04	0.5±0.03	0.5±0.03	0.5±0.04	0.8±0.03

Table A. 15 ^{1}H T_1 and T_2 relaxation times for butyl 4-hydroxybenzoate in 50:50 % v/v MeOH:D_2O (from top to bottom according to HPLC elution order): mobile phase in the absence of stationary phase (solution only) and in the presence of BEH-C18, BEH-phenyl, BEH-RP18, CSH hexyl-phenyl and HSS T3 stationary phases. Data were obtained at 500 MHz spectrometer at 313 K and 5.0 kHz spinning frequency.

MeOH/D₂O

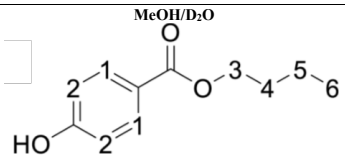

Butyl 4-hydroxybenzoate

SP	HPLC Rt (mins)	T_1(s) H-1(f)	H-2(f)	H-3(f)	H-4(f)	H-5(f)	H-6(f)	H-1(b)	H-2(b)	H-3(b)	H-4(b)	H-5(b)	H-6(b)
Solution only	n/a	1.8±0.02	1.9±0.04	1.1±0.02	1.0±0.07	1.3±0.07	1.7±0.07	n/a					
BEH-Phenyl	10.12	2.7±0.1	2.4±0.04	1.4±0.03	1.2±0.1	1.3±0.1	1.9±0.1	1.8±0.1	1.7±0.1	0.9±0.1	N/A	1.1±0.1	1.4±0.1
CSH Hexyl-phenyl	21.63	2.6±0.05	2.2±0.04	1.5±0.02	1.3±0.1	1.3±0.1	2.0±0.1	1.7±0.1	1.6±0.1	1.0±0.1	N/A	1.1±0.04	1.4±0.1
BEH-C18	26.79	2.8±0.1	2.9±0.1	1.5±0.1	1.1±0.1	1.2±0.05	1.4±0.1	1.8±0.1	1.8±0.1	1.0±0.1	1.0±0.04	1.0±0.04	1.1±0.04
BEH-RP18	29.18	2.4±0.1	2.7±0.1	1.5±0.1	1.4±0.1	1.4±0.1	1.6±0.1	1.2±0.04	1.3±0.1	1.1±0.04	1.0±0.06	1.1±0.1	1.1±0.1
HSS T3	38.00	2.4±0.1	2.9±0.1	1.4±0.04	1.1±0.1	1.1±0.04	1.4±0.05	1.5±0.1	1.5±0.1	0.8±0.04	0.8±0.03	0.8±0.03	0.9±0.04
		T_2(s) H-1(f)	H-2(f)	H-3(f)	H-4(f)	H-5(f)	H-6(f)	H-1(b)	H-2(b)	H-3(b)	H-4(b)	H-5(b)	H-6(b)
Solution only	n/a	1.2±0.03	1.2±0.1	0.6±0.01	0.7±0.02	1.0±0.01	1.1±0.01	n/a					
BEH-Phenyl	10.12	0.9±0.04	0.8±0.1	0.6±0.03	0.7±0.04	1.0 ±0.04	1.1±0.04	0.1±0.01	0.2±0.02	0.02±0.03	N/A	0.1 ±0.004	0.1±0.03
CSH Hexyl-phenyl	21.63	1.0±0.1	1.1±0.1	0.8±0.05	0.8±0.04	1.1±0.05	1.2±0.04	0.01±0.02	0.4±0.02	0.02±0.001	N/A	0.1±0.02	0.1±0.004
BEH-C18	26.79	0.6±0.03	0.6±0.04	0.6±0.04	0.6±0.04	0.9±0.03	1.0±0.02	0.1±0.01	0.1±0.01	0.04±0.02	0.04±0.003	0.04±0.01	0.1±0.01
BEH-RP18	29.18	0.7±0.1	0.8±0.1	0.6±0.04	0.5±0.04	0.7±0.03	0.9±0.05	0.04±0.01	0.04±0.02	0.02±0.001	0.03±0.02	0.03±0.002	0.1±0.003
HSS T3	38.00	0.7±0.05	0.8±0.1	0.8±0.04	0.6±0.03	0.8±0.04	1.0±0.04	0.1±0.03	0.1±0.01	0.03±0.01	0.01±0.01	0.04±0.04	0.1±0.01

Table A. 16 ^{1}H T_1 and T_2 relaxation times for dipropyl phthalate in 50:50 % v/v MeCN:D_2O (from top to bottom according to HPLC elution order): mobile phase in the absence of stationary phase (solution only) and in the presence of BEH-C18, BEH-phenyl, BEH-RP18, CSH hexyl-phenyl and HSS T3 stationary phases. Data were obtained at 500 MHz spectrometer at 313 K and 5.0 kHz spinning frequency.

MeCN/D₂O

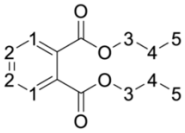

Dipropyl phthalate

SP	HPLC Rt (mins)	T_1(s) H-1(a)	H-2(a)	H-3(a)	H-4(a)	H-5(a)
Solution only	n/a	2.4±0.04	2.1±0.03	1.9±0.04	1.6±0.1	1.6±0.1
BEH-Phenyl	10.73	3.6±0.1	3.0±0.1	2.4±0.1	2.0±0.1	2.1±0.2
CSH Hexyl-phenyl	11.59	3.2±0.1	2.7±0.1	2.2±0.1	1.9±0.1	2.0±0.1
BEH-RP18	11.59	3.1±0.1	2.6±0.1	2.1±0.1	1.9±0.1	1.7±0.1
BEH-C18	17.30	3.9±0.1	3.2±0.04	2.6±0.1	1.9±0.2	2.0±0.2
HSS T3	25.59	3.4±0.1	2.8±0.1	2.3±0.1	1.8±0.1	1.8±0.1
		T_2(s) H-1(a)	H-2(a)	H-3(a)	H-4(a)	H-5(a)
Solution only	n/a	2.0±0.1	1.9±0.05	1.3±0.04	0.8±0.03	1.3±0.02
BEH-Phenyl	10.73	1.7±0.1	1.8±0.2	1.0±0.1	0.5±0.01	0.9±0.05
CSH Hexyl-phenyl	11.59	0.8±0.04	0.7±0.1	0.7±0.05	0.5±0.06	0.6±0.02
BEH-RP18	11.59	0.5±0.02	0.4±0.01	0.5±0.01	0.4±0.04	0.5±0.02
BEH-C18	17.30	2.2±0.1	2.1±0.1	1.0±0.05	0.5±0.05	1.1±0.1
HSS T3	25.59	1.4±0.1	1.4±0.1	0.9±0.1	0.7±0.03	0.9±0.03

Table A. 17 ^{1}H T_1 and T_2 relaxation times for dipropyl phthalate in 50:50 % v/v MeOH:D_2O (from top to bottom according to HPLC elution order): mobile phase in the absence of stationary phase (solution only) and in the presence of BEH-C18, BEH-phenyl, BEH-RP18, CSH hexyl-phenyl and HSS T3 stationary phases. Data were obtained at 500 MHz spectrometer at 313 K and 5.0 kHz spinning frequency.

	SP	HPLC Rt (mins)	T_1(s)				
			H-1(a)	H-2(a)	H-3(a)	H-4(a)	H-5(a)
MeOH/D_2O 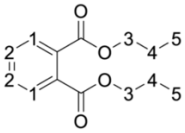 Dipropyl phthalate	Solution only	n/a	0.9±0.05	0.8±0.05	0.9±0.03	1.8±0.05	1.8±0.1
	BEH-RP18	34.80	1.2±0.1	1.0±0.1	0.9±0.1	1.8±0.1	1.4±0.1
	BEH-Phenyl	37.76	1.3±0.1	1.0±0.1	0.8±0.1	1.9±0.1	2.0±0.1
	CSH Hexyl-phenyl	40.16	1.4±0.1	1.2±0.1	0.9±0.1	1.4±0.1	1.7±0.1
	BEH-C18	52.04	1.5±0.05	1.1±0.04	1.0±0.04	1.5±0.1	1.4±0.1
	HSS T3	90.00	1.3±0.1	1.0±0.1	0.8±0.1	1.3±0.1	1.2±0.1
			T_2(s)				
			H-1(a)	H-2(a)	H-3(a)	H-4(a)	H-5(a)
	Solution only	n/a	0.6±0.05	0.6±0.01	0.5±0.002	0.2±0.05	1.2±0.05
	BEH-RP18	34.80	0.2±0.002	0.1±0.003	0.2±0.05	0.3±0.2	0.8±0.1
	BEH-Phenyl	37.76	0.2±0.004	0.1±0.003	0.2±0.04	0.4±0.3	0.7±0.1
	CSH Hexyl-phenyl	40.16	0.1±0.005	0.1±0.005	0.2±0.05	0.3±0.05	1.1±0.1
	BEH-C18	52.04	0.2±0.002	0.1±0.002	0.2±0.02	0.5±0.003	0.9±0.04
	HSS T3	90.00	0.2±0.004	0.1±0.003	0.2±0.08	0.2±0.03	1.1±0.1

Table A. 18 ^{1}H T_1 and T_2 relaxation times for benzoic acid in 50:50 % v/v MeCN:D_2O (from top to bottom according to HPLC elution order): mobile phase in the absence of stationary phase (solution only) and in the presence of BEH-C18, BEH-phenyl, BEH-RP18, CSH hexyl-phenyl and HSS T3 stationary phases. Data were obtained at 500 MHz spectrometer at 313 K and 5.0 kHz spinning frequency.

	SP	HPLC Rt (mins)	T_1(s)					
			H-1(f)	H-2(f)	H-3(f)	H-1(b)	H-2(b)	H-3(b)
MeCN:D_2O 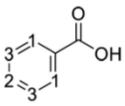 Benzoic acid	Solution only	n/a	4.4±0.1	4.6±0.1	4.1±0.1		n/a	
	BEH-Phenyl	2.34	5.9±0.1	6.8±0.1	5.5±0.1	5.0±0.2	5.8±0.3	4.7±0.1
	BEH-C18	2.67	5.5±0.1	6.3±0.1	5.1±0.1	4.6±0.1	4.4±0.1	4.2±0.1
	CSH Hexyl-phenyl	3.13	5.1±0.1	7.0±0.3	5.1±0.1	4.1±0.1	4.3±0.2	4.1±0.1
	HSS T3	3.58	5.4±0.1	6.3±0.1	5.3±0.1	5.0±0.3	5.2±0.3	4.5±0.1
	BEH-RP18	10.82	5.0±0.1	6.7±0.2	5.2±0.1	3.8±0.1	3.1±0.2	3.3±0.1
			T_2(s)					
			H-1(f)	H-2(f)	H-3(f)	H-1(b)	H-2(b)	H-3(b)
	Solution only	n/a	2.0±0.05	2.3±0.05	1.9±0.05		n/a	
	BEH-Phenyl	2.34	0.7±0.01	1.0±0.02	0.8±0.07	0.4±0.01	0.3±0.02	0.3±0.03
	BEH-C18	2.67	0.9±0.02	1.1±0.01	1.0±0.02	0.5±0.04	0.3±0.05	0.3±0.04
	CSH Hexyl-phenyl	3.13	1.1±0.05	1.4±0.04	1.2±0.05	0.3±0.01	0.2±0.02	0.2±0.01
	HSS T3	3.58	1.3±0.02	1.6±0.02	1.3±0.02	1.0±0.04	0.6±0.1	0.2±0.02
	BEH-RP18	10.82	1.1±0.03	1.5±0.04	1.2±0.02	0.7±0.07	0.3±0.04	0.3±0.05

Table A. 19 ^{1}H T_1 and T_2 relaxation times for benzoic acid in 50:50 % v/v MeOH:D_2O (from top to bottom according to HPLC elution order): mobile phase in the absence of stationary phase (solution only) and in the presence of BEH-C18, BEH-phenyl, BEH-RP18, CSH hexyl-phenyl and HSS T3 stationary phases. Data were obtained at 500 MHz spectrometer at 313 K and 5.0 kHz spinning frequency.

MeOH/D_2O 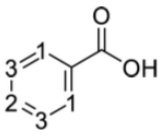 Benzoic acid	SP	HPLC Rt (mins)	T_1(s)				
			H-1(f)	H-2(f)	H-3(f)	H-1(b)	H3-(b)
	Solution only	n/a	4.0±0.1	4.4±0.1	3.7±0.1	n/a	
	BEH-Phenyl	3.02	4.6±0.1	5.3±0.1	4.1±0.1	3.0±0.1	2.9±0.1
	CSH Hexyl-phenyl	4.00	4.6±0.1	5.2±0.1	4.1±0.04	3.0±0.1	2.8±0.1
	BEH-C18	4.30	3.7±0.1	5.0±0.1	3.9±0.1	2.7±0.1	2.5±0.1
	HSS T3	6.80	3.8±0.1	5.1±0.2	3.6±0.1	2.6±0.1	2.4±0.1
	BEH-RP18	19.00	3.2±0.04	4.6±0.1	3.4±0.05	n/a	2.0±0.1
			T_2(s)				
			H-1(f)	H-2(f)	H-3(f)	H-1(b)	H3-(b)
	Solution only	n/a	1.6±0.1	2.2±0.03	1.6±0.1	n/a	
	BEH-Phenyl	3.02	0.5±0.02	0.8±0.02	0.6±0.03	0.1±0.01	0.2±0.05
	CSH Hexyl-phenyl	4.00	0.7±0.03	1.0±0.02	0.8±0.03	0.2±0.03	0.6±0.1
	BEH-C18	4.30	0.6±0.01	0.8±0.02	0.7±0.01	0.2±0.01	0.1±0.01
	HSS T3	6.80	0.5±0.03	0.9±0.02	0.6±0.03	0.2±0.02	0.1±0.01
	BEH-RP18	19.00	0.4±0.03	0.9±0.2	0.6±0.03	n/a	0.1±0.02

Table A. 20 ^{1}H T_1 and T_2 relaxation times for 3-hydroxybenzoic acid in 50:50 % v/v MeCN:D_2O (from top to bottom according to HPLC elution order): mobile phase in the absence of stationary phase (solution only) and in the presence of BEH-C18, BEH-phenyl, BEH-RP18, CSH hexyl-phenyl and HSS T3 stationary phases. Data were obtained at 500 MHz spectrometer at 313 K and 5.0 kHz spinning frequency.

MeCN/D_2O 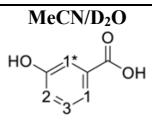 3-hydroxybenzoic acid

SP	HPLC Rt (mins)	T_1(s)						
		H-1(f)	H-1*(f)	H-2(f)	H-3(f)	H-1(b)	H-2(b)	H-3(b)
Solution only	n/a	3.8±0.1	6.4±0.05	3.2±0.03	4.7±0.05	n/a		
BEH-Phenyl	2.06	4.3±0.1	7.1±0.1	3.7±0.03	5.1±0.1	n/a	3.5±0.1	4.6±0.1
BEH-C18	2.07	4.2±0.1	7.3±0.1	3.6±0.1	5.6±0.2	n/a	3.7±0.1	5.5±0.2
CSH Hexyl-phenyl	2.44	4.2±0.1	6.9±0.1	3.6±0.1	4.7±0.1	3.9±0.1	3.5±0.1	3.9±0.1
HSS T3	2.67	4.4±0.05	7.7±0.1	3.8±0.03	5.6±0.05	n/a	3.9±0.1	6.0±0.2
BEH-RP18	14.38	3.4±0.1	4.6±0.1	3.1±0.04	4.3±0.1	n/a	2.4±0.1	3.1±0.1
		T_2(s)						
		H-1(f)	H-1*(f)	H-2(f)	H-3(f)	H-1(b)	H-2(b)	H-3(b)
Solution only	n/a	2.6±0.04	3.4±0.04	2.4±0.03	2.6±0.03	n/a		
BEH-Phenyl	2.06	1.5±0.05	1.7±0.04	1.5±0.1	1.5±0.06	n/a	0.7±0.04	1.3±0.1
BEH-C18	2.07	1.7±0.04	1.8±0.04	1.6±0.05	1.7±0.05	n/a	0.9±0.07	1.0±0.1
CSH Hexyl-phenyl	2.44	1.8±0.1	1.8±0.1	1.8±0.1	1.8±0.1	0.6±0.1	0.4±0.03	0.4±0.02
HSS T3	2.67	2.0±0.04	2.3±0.05	2.0±0.05	2.0±0.04	n/a	0.7±0.1	0.7±0.05
BEH-RP18	14.38	2.0±0.1	2.1±0.1	2.0±0.1	2.1±0.05	n/a	0.2±0.01	0.3±0.03

Table A. 21 ^{1}H T_1 and T_2 relaxation times for 3-hydroxybenzoic acid in 50:50 % v/v MeOH:D_2O (from top to bottom according to HPLC elution order): mobile phase in the absence of stationary phase (solution only) and in the presence of BEH-C18, BEH-phenyl, BEH-RP18, CSH hexyl-phenyl and HSS T3 stationary phases. Data were obtained at 500 MHz spectrometer at 313 K and 5.0 kHz spinning frequency.

MeOH:D_2O

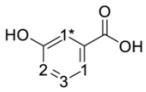

3-hydroxybenzoic acid

SP	HPLC Rt (mins)	T_1(s)						
		H-1(f)	H-1*(f)	H-2(f)	H-3(f)	H-1(b)	H-2(b)	H-3(b)
Solution only	n/a	2.7±0.1	4.3±0.1	2.3±0.1	3.3±0.1		n/a	
BEH-C18	2.29	3.4±0.05	6.0±0.05	2.7±0.04	4.3±0.07	n/a	n/a	n/a
BEH-Phenyl	2.55	3.2±0.04	5.2±0.1	2.7±0.05	3.9±0.1	2.9±0.1	2.5±0.1	3.2±0.1
HSS T3	2.70	2.9±0.05	5.4±0.1	2.5±0.1	3.8±0.1	3.0±0.1	2.2±0.1	3.3±0.1
CSH Hexyl-phenyl	3.14	3.1±0.05	5.3±0.1	2.4±0.03	3.7±0.1	3.3±0.1	1.7±0.1	2.0±0.1
BEH-RP18	10.30	2.7±0.05	4.8±0.1	2.6±0.1	3.6±0.1	2.0±0.1	2.0±0.04	2.6±0.1
		T_2(s)						
		H-1(f)	H-1*(f)	H-2(f)	H-3(f)	H-1(b)	H-2(b)	H-3(b)
Solution only	n/a	1.9±0.01	2.4±0.02	1.8±2.2	2.0±0.02		n/a	
BEH-C18	2.29	1.6±0.05	1.8±0.06	1.5±0.1	1.6±0.06	n/a	n/a	n/a
BEH-Phenyl	2.55	1.8±0.02	1.7±0.03	1.7±0.02	1.8±0.02	1.4±0.1	1.1±0.2	0.5±0.1
HSS T3	2.70	1.8±0.05	2.1±0.03	1.8±0.03	1.9±0.03	0.8±0.1	0.6±0.04	0.8±0.1
CSH Hexyl-phenyl	3.14	2.0±0.03	2.4±0.04	1.9±0.03	2.1±0.03	0.7±0.1	0.3±0.04	0.6±0.1
BEH-RP18	10.30	1.8±0.03	1.9±0.02	1.7±0.02	1.8±0.03	0.2±0.01	0.2±0.01	0.5±0.1

Table A. 22 ^{1}H T_1 and T_2 relaxation times for meclizine in 50:50 % v/v MeCN:D_2O mobile phase in the absence of stationary phase (solution only) and in the presence of BEH-C18, BEH-phenyl, BEH-RP18, CSH hexyl-phenyl and HSS T3 stationary phases. Data were obtained at 500 MHz spectrometer at 313 K and 5.0 kHz spinning frequency.

MeCN:D_2O

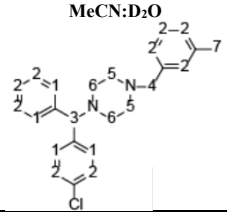

SP	HPLC Rt (mins)	T_1(s)						
		H-1(a)	H-2(a)	H-3(a)	H-4(a)	H-5(a)	H-6(a)	H-7(a)
Solution only	n/a	1.2±0.03	1.8±0.03	0.6±0.03	0.4±0.05	0.4±0.03	0.4±0.02	1.1±0.02
BEH-C18		1.2±0.1	1.7±0.1	0.5±0.1	0.4±0.1	0.3±0.1	0.3±0.1	0.9±0.1
BEH-Phenyl	Strongly	1.1±0.04	1.5±0.1	0.5±0.1	0.4±0.1	0.3±0.05	0.3±0.1	0.9±0.1
BEH-RP18	retained onto	1.2±0.02	1.7±0.03	0.5±0.04	0.4±0.04	0.3±0.04	0.3±0.05	0.9±0.1
CSH Hexyl-phenyl	column	1.3±0.03	1.8±0.02	0.6±0.06	0.4±0.02	0.3±0.04	0.3±0.05	1.0±0.1
HSS T3		1.2±0.01	1.5±0.03	0.6±0.03	0.4±0.03	0.3±0.04	0.3±0.06	1.0±0.1
		T_2(s)						
		H-1(a)	H-2(a)	H-3(a)	H-4(a)	H-5(a)	H-6(a)	H-7(a)
Solution only	n/a	0.6±0.03	1.0±0.02	0.5±0.07	0.3±0.01	0.2±0.02	0.2±0.02	0.8±0.01
BEH-C18		0.8±0.02	1.0±0.02	0.4±0.02	0.3±0.02	0.2±0.05	0.2±0.004	0.8±0.02
BEH-Phenyl	Strongly	0.6±0.02	0.7±0.03	0.4±0.01	0.3±0.01	0.2±0.003	0.2±0.004	0.7±0.01
BEH-RP18	retained onto	0.6±0.02	0.7±0.02	0.3±0.01	0.3±0.01	0.2±0.002	0.2±0.004	0.7±0.01
CSH Hexyl-phenyl	column	0.6±0.02	0.6±0.03	0.5±0.01	0.3±0.01	0.2±0.003	0.2±0.01	0.7±0.01
HSS T3		0.6±0.02	0.6±0.03	0.4±0.02	0.3±0.01	0.2±0.004	0.2±0.01	0.7±0.01

Table A. 23 ^{1}H T_1 and T_2 relaxation times for meclizine in 50:50 % v/v MeOH:D_2O mobile phase in the absence of stationary phase (solution only) and in the presence of BEH-C18, BEH-phenyl, BEH-RP18, CSH hexyl-phenyl and HSS T3 stationary phases. Data were obtained at 500 MHz spectrometer at 313 K and 5.0 kHz spinning frequency.

MeOH:D_2O

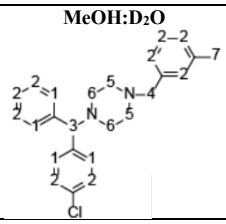

SP	HPLC Rt (mins)	T_1(s)						
		H-1(a)	H-2(a)	H-3(a)	H-4(a)	H-5(a)	H-6(a)	H-7(a)
Solution only	n/a	1.0±0.03	1.5±0.03	0.6±0.03	0.4±0.01	0.3±1	0.4±0.02	0.9±0.05
BEH-C18		1.2±0.04	1.5±0.01	0.5±0.1	0.3±0.03	0.3±0.03	0.4±0.03	1.0±0.04
BEH-Phenyl	Strongly	1.1±0.04	1.5±0.04	0.4±0.1	0.5±0.1	0.3±0.02	0.4±0.02	1.0±0.1
BEH-RP18	retained	1.1±0.02	1.5±0.03	0.5±0.1	0.5±0.02	0.3±0.01	0.4±0.03	0.9±0.1
CSH Hexyl-phenyl	onto column	1.1±0.04	1.4±0.02	0.6±0.1	0.8±0.1	0.4±0.03	0.4±0.03	1.0±0.1
HSS T3		1.2±0.1	1.2±0.03	0.6±0.1	0.5±3.7E-2	0.3±0.02	0.4±0.02	0.9±0.1
		T_2(s)						
		H-1(a)	H-2(a)	H-3(a)	H-4(a)	H-5(a)	H-6(a)	H-7(a)
Solution only	n/a	0.7±0.1	0.9±0.1	0.4±0.04	0.3±0.03	0.2±0.02	0.2±0.02	0.7±0.07
BEH-C18		1.0±0.1	0.9±0.1	0.5±0.1	0.3±0.03	0.2±0.02	0.1±0.01	0.9±0.07
BEH-Phenyl	Strongly	0.8±0.1	0.8±0.1	0.4±0.04	0.3±0.03	0.2±0.02	0.2±0.02	0.7±0.07
BEH-RP18	retained	0.8±0.1	0.7±0.1	0.4±0.04	0.3±0.03	0.2±0.02	0.1±0.01	0.7±0.07
CSH Hexyl-phenyl	onto column	0.7±0.1	0.7±0.1	0.7±0.2	0.3±0.03	0.2±0.02	0.2±0.02	0.7±0.07
HSS T3		0.7±0.2	0.3±0.3	0.4±0.1	0.3±0.03	0.2±0.02	0.2±0.02	0.7±0.07

Table A. 24 ^{1}H T_1 and T_2 relaxation times for hydroxyzine in 50:50 % v/v MeCN:D_2O mobile phase in the absence of stationary phase (solution only) and in the presence of BEH-C18, BEH-phenyl, BEH-RP18, CSH hexyl-phenyl and HSS T3 stationary phases. Data were obtained at 500 MHz spectrometer at 313 K and 5.0 kHz spinning frequency.

MeCN:D_2O

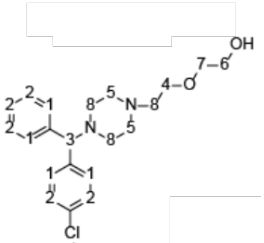

SP	HPLC Rt (mins)	T_1(s)							
		H-1(a)	H-2(a)	H-3(a)	H-4(a)	H-5(a)	H-6(a)	H-7(a)	H-8(a)
Solution only	n/a	1.1±0.02	1.6±0.03	0.5±0.01	0.4±0.02	0.3±0.02	0.9±0.04	0.8±0.04	0.3±0.02
BEH-C18		1.1±0.04	1.7±0.04	0.5±0.04	0.4±0.04	0.3±0.02	0.9±0.04	0.7±0.04	0.3±0.06
BEH-Phenyl	Strongly	1.1±0.01	1.7±0.01	0.5±0.02	0.4±0.04	0.3±0.03	0.9±0.1	0.7±0.1	0.3±0.1
BEH-RP18	retained	1.2±0.02	1.8±0.02	0.5±0.04	0.4±0.05	0.3±0.05	0.8±0.1	0.6±0.05	0.3±0.1
CSH Hexyl-phenyl	onto	1.1±0.04	1.7±0.05	0.5±0.03	0.4±0.05	0.3±0.05	0.9±0.1	0.6±0.1	0.3±0.1
HSS T3	column	1.3±0.03	2.0±0.03	0.6±0.02	0.4±0.02	0.3±0.02	1.0±0.04	0.7±0.04	0.3±0.03
		T_2(s)							
		H-1(a)	H-2(a)	H-3(a)	H-4(a)	H-5(a)	H-6(a)	H-7(a)	H-8(a)
Solution only	n/a	0.7±0.004	0.9±0.02	0.4±0.01	0.3±0.002	0.1±0.002	0.7±0.01	0.7±0.01	0.2±0.003
BEH-C18		0.6±0.005	0.8±0.05	0.3±0.01	0.3±0.01	0.1±0.01	0.7±0.02	0.6±0.01	0.2±0.004
BEH-Phenyl	Strongly	0.6±0.008	0.7±0.01	0.3±0.01	0.3±0.01	0.1±0.004	0.6±0.004	0.6±0.01	0.2±0.002
BEH-RP18	retained	0.6±0.007	0.7±0.01	0.3±0.01	0.3±0.01	0.1±0.004	0.6±0.01	0.5±0.01	0.2±0.004
CSH Hexyl-phenyl	onto	0.6±0.005	0.7±0.01	0.3±0.01	0.3±0.004	0.1±0.003	0.7±0.003	0.6±0.01	0.2±0.003
HSS T3	column	0.7±0.005	0.8±0.004	0.4±0.01	0.3±0.01	0.1±20.003	0.7±0.004	0.6±0.01	0.2±0.001

Table A. 25 ^{1}H T_1 and T_2 relaxation times for hydroxyzine in 50:50 % v/v MeOH:D_2O mobile phase in the absence of stationary phase (solution only) and in the presence of BEH-C18, BEH-phenyl, BEH-RP18, CSH hexyl-phenyl and HSS T3 stationary phases. Data were obtained at 500 MHz spectrometer at 313 K and 5.0 kHz spinning frequency.

MeOH:D₂O

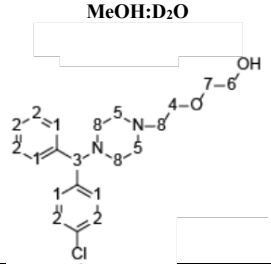

SP	HPLC Rt (mins)	T_1(s)							
		H-1(a)	H-2(a)	H-3(a)	H-4(a)	H-5(a)	H-6(a)	H-7(a)	H-8(a)
Solution only	n/a	0.9±0.03	1.2±0.03	0.5±0.02	0.4±0.006	0.3±0.007	0.8±0.01	0.6±0.01	0.3±0.009
BEH-C18	Strongly retained onto column	1.0±0.03	1.5±0.03	0.5±0.02	0.4±0.004	0.4±0.006	0.8±0.008	0.6±0.02	0.3±0.01
BEH-Phenyl		0.9±0.04	1.3±0.1	0.5±0.05	0.3±0.05	0.3±0.1	0.6±0.1	0.4±0.1	0.2±0.1
BEH-RP18		0.9±0.04	1.2±0.1	0.5±0.1	0.5±0.1	0.3±0.1	0.6±0.1	0.4±0.04	0.3±0.1
CSH Hexyl-phenyl		1.0±0.03	1.4±0.03	0.5±0.04	0.4±0.01	0.4±0.01	0.8±0.01	0.6±0.01	0.3±0.01
HSS T3		0.9±0.1	1.3±0.1	0.4±0.1	0.4±0.1	0.3±0.1	0.6±0.1	0.5±0.1	0.3±0.1
		T_2(s)							
		H-1(a)	H-2(a)	H-3(a)	H-4(a)	H-5(a)	H-6(a)	H-7(a)	H-8(a)
Solution only	n/a	0.5±0.002	0.7±0.003	0.3±0.005	0.2±0.004	0.1±0.004	0.5±0.005	0.4±0.009	0.2±0.002
BEH-C18	Strongly retained onto column	0.5±0.007	0.7±0.006	0.3±0.006	0.2±0.006	0.1±0.006	0.5±0.005	0.4±0.01	0.2±0.002
BEH-Phenyl		0.3±0.005	0.3±0.009	0.2±0.006	0.2±0.007	0.1±0.01	0.4±0.004	0.3±0.008	0.05±0.01
BEH-RP18		0.4±0.007	0.5±0.007	0.2±0.006	0.2±0.007	0.1±0.007	0.4±0.003	0.3±0.01	0.1±0.003
CSH Hexyl-phenyl		0.5±0.006	0.5±0.01	0.2±0.007	0.2±0.005	0.1±0.005	0.5±0.006	0.4±0.008	0.1±0.002
HSS T3		0.4±0.01	0.5±0.008	0.2±0.009	0.2±0.009	0.1±0.008	0.4±0.005	0.3±0.01	0.1±0.002

Table A. 26 ^{1}H T_1 and T_2 relaxation times for propranolol in 50:50 % v/v MeCN:D_2O mobile phase in the absence of stationary phase (solution only) and in the presence of BEH-C18, BEH-phenyl, BEH-RP18, CSH hexyl-phenyl and HSS T3 stationary phases. Data were obtained at 500 MHz spectrometer at 313 K and 5.0 kHz spinning frequency.

MeCN:D₂O

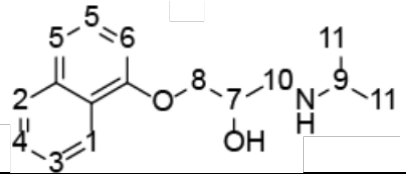

SP	HPLC Rt (mins)	T_1(s)										
		H-1(a)	H-2(a)	H-3(a)	H-4(a)	H-5(a)	H-6(a)	H-7(a)	H-8(a)	H-9(a)	H-10(a)	H-11(a)
Solution only	n/a	2.5±0.04	2.1±0.02	1.9±0.02	1.9±0.02	1.8±0.04	1.3±0.03	1.7±0.04	0.9±0.03	0.7±0.02	0.8±0.1	0.9±0.1
BEH-Phenyl	Strongly retained onto column	2.6±0.1	2.2±0.1	2.2±0.02	2.2±0.03	0.3±0.1	1.1±0.03	1.6±0.1	1.4±0.1	0.5±0.1	0.4±0.1	1.1±0.02
CSH Hexyl-phenyl		2.5±0.1	2.2±0.04	2.1±0.04	2.2±0.05	1.1±0.1	1.3±0.03	1.6±0.1	1.5±0.1	0.5±0.05	0.5±0.05	1.0±0.1
BEH-RP18		2.4±0.04	2.1±0.1	2.0±0.1	2.0±0.1	1.6±0.1	1.0±0.1	1.4±0.04	1.1±0.03	0.6±0.03	0.6±0.1	0.9±0.1
BEH-C18		2.8±0.1	2.4±0.1	2.3±0.04	2.4±0.03	1.4±0.1	1.3±0.03	1.7±0.1	1.2±0.1	0.5±0.05	0.5±0.1	1.0±0.1
HSS T3		2.5±0.1	2.0±0.04	2.1±0.03	2.1±0.04	1.1±0.1	1.1±0.1	1.4±0.1	1.1±0.1	0.5±0.1	0.5±0.1	0.9±0.1
		T_2(s)										
		H-1(a)	H-2(a)	H-3(a)	H-4(a)	H-5(a)	H-6(a)	H-7(a)	H-8(a)	H-9(a)	H-10(a)	H-11(a)
Solution only	n/a	0.4±0.1	1.0±0.03	1.0±0.1	1.0±0.01	1.1±0.02	1.0±0.02	0.7±0.01	0.5±0.01	0.5±0.01	0.5±0.01	0.8±0.003
BEH-Phenyl	Strongly retained onto column	0.1±0.004	0.7±0.1	0.8±0.05	1.0±0.05	0.6±0.04	0.8±0.05	0.6±0.02	0.4±0.02	0.4±0.02	0.4±0.02	0.6±0.01
CSH Hexyl-phenyl		0.3±0.04	0.6±0.04	0.6±0.1	0.8±0.05	0.6±0.04	0.7±0.03	0.5±0.02	0.4±0.02	0.4±0.01	0.4±0.02	0.6±0.01
BEH-RP18		0.1±0.04	0.8±0.04	0.8±0.05	1.0±0.04	0.7±0.03	0.9±0.02	0.5±0.01	0.4±0.01	0.4±0.02	0.4±0.02	0.6±0.01
BEH-C18		0.3±0.1	1.0±0.03	0.5±0.1	1.1±0.03	0.8±0.03	0.9±0.03	0.7±0.02	0.5±0.01	0.5±0.01	0.5±0.02	0.7±0.01
HSS T3		0.04±0.003	0.7±0.03	0.8±0.1	0.9±0.03	0.6±0.04	0.7±0.03	0.5±0.03	0.4±0.01	0.4±0.01	0.4±0.02	0.6±0.01

Table A. 27 ^{1}H T_1 and T_2 relaxation times for propranolol in 50:50 % v/v MeOH:D_2O mobile phase in the absence of stationary phase (solution only) and in the presence of BEH-C18, BEH-phenyl, BEH-RP18, CSH hexyl-phenyl and HSS T3 stationary phases. Data were obtained at 500 MHz spectrometer at 313 K and 5.0 kHz spinning frequency.

MeOH:D_2O

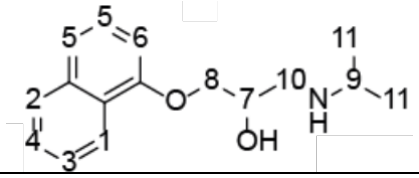

SP	HPLC Rt (mins)	T_1(s) H-1(a)	H-2(a)	H-3(a)	H-4&5(a)	H-5(a)	H-6(a)	H-7(a)	H-8(a)	H-9(a)	H-10(a)
Solution only	n/a	1.9±0.03	1.6±0.03	1.5±0.02	1.5±0.02	1.0±0.02	1.2±0.05	0.5±0.02	1.3±0.02	0.6±0.02	0.8±0.05
BEH-Phenyl		2.3±0.1	2.0±0.05	1.8±0.02	1.7±0.02	1.1±0.02	1.5±0.05	0.5±0.01	1.4±0.05	0.6±0.03	0.8±0.1
CSH Hexyl-phenyl	Strongly	2.2±0.04	1.9±0.04	1.8±0.02	1.8±0.02	1.2±0.03	1.6±0.06	0.6±0.02	1.4±0.07	0.6±0.05	0.8±0.06
BEH-RP18	retained onto	2.2±0.04	1.9±0.03	1.8±0.03	1.8±0.02	1.1±0.03	1.4±0.05	0.5±0.02	1.3±0.1	0.6±0.04	0.9±0.1
BEH-C18	column	2.1±0.1	1.9±0.1	1.7±0.04	1.6±0.04	1.0±0.03	1.6±0.1	0.5±0.03	1.3±0.1	0.6±0.05	0.8±0.05
HSS T3		2.1±0.04	1.9±0.04	1.8±0.02	1.7±0.01	1.1±0.03	1.2±0.03	0.5±0.02	1.3±0.1	0.6±0.05	0.8±0.1
		T_2(s) H-1(a)	H-2(a)	H-3(a)	H-4&5(a)	H-5(a)	H-6(a)	H-7(a)	H-8(a)	H-9(a)	H-10(a)
Solution only	n/a	0.1±0.004	0.9±0.03	0.8±0.1	0.8±0.01	0.8±0.01	0.6±0.01	0.4±0.01	0.7±0.02	0.5±0.02	0.7±0.01
BEH-Phenyl		0.1±0.004	0.8±0.02	0.8±0.1	0.8±0.02	0.7±0.02	0.4±0.02	0.3±0.01	0.4±0.02	0.4±0.02	0.6±0.02
CSH Hexyl-phenyl	Strongly	0.1±0.004	0.7±0.05	0.7±0.1	0.7±0.05	0.7±0.03	0.3±0.02	0.3±0.01	0.3±0.01	0.3±0.02	0.5±0.03
BEH-RP18	retained onto	0.1±0.004	0.6±0.03	0.6±0.06	0.6±0.03	0.6±0.02	0.4±0.01	0.3±0.01	0.4±0.01	0.3±0.02	0.5±0.01
BEH-C18	column	0.1±0.003	0.6±0.02	0.8±0.04	0.6±0.02	0.6±0.03	0.4±0.01	0.3±0.01	0.4±0.01	0.3±0.01	0.5±0.01
HSS T3		0.1±0.002	0.6±0.04	0.6±0.1	0.7±0.02	0.7±0.02	0.4±0.02	0.3±0.01	0.3±0.01	0.3±0.02	0.5±0.01

Table A. 28 ^{1}H T_1 and T_2 relaxation times for amitriptyline in 50:50 % v/v MeCN:D_2O mobile phase in the absence of stationary phase (solution only) and in the presence of BEH-C18, BEH-phenyl, BEH-RP18, CSH hexyl-phenyl and HSS T3 stationary phases. Data were obtained at 500 MHz spectrometer at 313 K and 5.0 kHz spinning frequency.

MeCN:D_2O

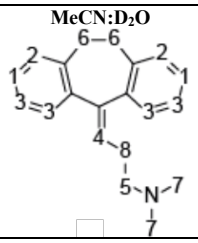

SP	HPLC Rt (mins)	T_1(s) H-1(a)	H-2(a)	H-3(a)	H-4(a)	H-5(a)	H-6(a)	H-7(a)	H-8(a)
Solution only	n/a	1.8±0.1	2.2±0.05	2.1±0.05	1.9±0.04	1.6±0.1	0.7±0.1	1.0±0.1	0.8±0.1
BEH-C18		2.0±0.04	2.4±0.03	2.2±0.03	1.9±0.1	1.5±0.04	0.7±0.1	0.9±0.1	0.7±0.1
BEH-Phenyl	Strongly	2.0±0.03	2.3±0.03	2.1±0.03	1.7±0.05	1.5±0.04	0.7±0.1	0.9±0.1	0.7±0.1
BEH-RP18	retained	2.1±0.03	2.5±0.01	2.4±0.02	2.1±0.04	1.7±0.1	0.7±0.1	0.9±0.1	0.7±0.1
CSH Hexyl-phenyl	onto column	2.1±0.04	2.6±0.02	2.5±0.03	2.2±0.03	1.8±0.03	0.7±0.05	1.0±0.1	0.8±0.1
HSS T3		2.1±0.05	2.5±0.03	2.4±0.02	2.1±0.05	1.6±0.03	0.7±0.1	1.0±0.1	0.7±0.1
		T_2(s) H-1(a)	H-2(a)	H-3(a)	H-4(a)	H-5(a)	H-6(a)	H-7(a)	H-8(a)
Solution only	n/a	1.3±0.02	1.4±0.01	1.4±0.01	1.3±0.01	0.6±0.04	0.1±0.02	0.8±0.02	0.4±0.02
BEH-C18		0.9±0.04	1.0±0.03	1.0±0.04	1.0±0.04	0.3±0.02	0.1±0.01	0.8±0.03	0.2±0.02
BEH-Phenyl	Strongly	1.0±0.04	1.0±0.03	1.0±0.04	1.0±0.03	0.3±0.03	0.1±0.01	0.7±0.03	0.3±0.03
BEH-RP18	retained	1.1±0.04	1.2±0.02	1.2±0.02	1.1±0.02	0.3±0.02	0.1±0.01	0.8±0.03	0.3±0.02
CSH Hexyl-phenyl	onto column	1.3±0.02	1.5±0.01	1.4±0.01	1.4±0.02	0.5±0.02	0.1±0.01	1.0±0.02	0.3±0.03
HSS T3		1.1±0.03	1.2±0.02	1.2±0.02	1.2±0.02	0.4±0.02	0.1±0.01	0.8±0.03	0.3±0.02

Table A. 29 ^{1}H T_1 and T_2 relaxation times for amitriptyline in 50:50 % v/v MeOH:D_2O mobile phase in the absence of stationary phase (solution only) and in the presence of BEH-C18, BEH-phenyl, BEH-RP18, CSH hexyl-phenyl and HSS T3 stationary phases. Data were obtained at 500 MHz spectrometer at 313 K and 5.0 kHz spinning frequency.

MeOH:D₂O

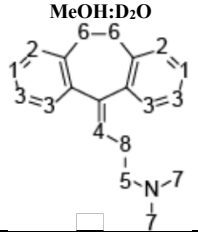

SP	HPLC Rt (mins)	T_1(s)							
		H-1(a)	H-2(a)	H-3(a)	H-4(a)	H-5(a)	H-6(a)	H-7(a)	H-8(a)
Solution only	n/a	1.2±0.02	1.3±0.02	1.3±0.03	1.1±0.03	1.1±0.03	0.6±0.01	0.8±0.02	0.6±0.02
BEH-C18		1.4±0.03	1.6±0.03	1.4±0.04	1.2±0.03	1.1±0.04	0.5±0.04	0.7±0.05	0.4±0.05
BEH-Phenyl	Strongly	1.4±0.01	1.6±0.01	1.4±0.02	1.2±0.02	1.1±0.03	0.5±0.05	0.7±0.06	0.5±0.05
BEH-RP18	retained	1.4±0.02	1.6±0.02	1.6±0.02	1.3±0.02	1.1±0.03	0.5±0.03	0.8±0.03	0.6±0.02
CSH Hexyl-phenyl	onto column	1.3±0.03	1.6±0.03	1.6±0.04	1.4±0.04	1.1±0.04	0.5±0.05	0.7±0.1	0.6±0.1
HSS T3		1.3±0.05	1.5±0.05	1.4±0.1	1.1±0.1	1.1±0.1	0.5±0.1	0.7±0.1	0.5±0.1
		T_2(s)							
		H-1(a)	H-2(a)	H-3(a)	H-4(a)	H-5(a)	H-6(a)	H-7(a)	H-8(a)
Solution only	n/a	1.0±0.01	1.0±0.01	0.9±0.01	0.9±0.01	0.4±0.02	0.1±0.02	0.5±0.03	0.3±0.02
BEH-C18		0.7±0.02	0.8±0.02	0.6±0.03	0.8±0.03	0.2±0.01	0.1±0.01	0.5±0.02	0.1±0.02
BEH-Phenyl	Strongly	0.7±0.02	0.8±0.02	0.6±0.03	0.6±0.03	0.2±0.01	0.1±0.01	0.4±0.02	0.2±0.01
BEH-RP18	retained	0.8±0.01	0.9±0.02	0.9±0.01	0.8±0.01	0.2±0.02	0.1±0.01	0.5±0.01	0.2±0.02
CSH Hexyl-phenyl	onto column	0.8±0.01	0.9±0.02	0.8±0.01	0.8±0.03	0.2±0.01	0.2±0.02	0.5±0.02	0.1±0.01
HSS T3		0.9±0.02	0.9±0.03	0.9±0.03	0.9±0.04	0.2±0.02	0.1±0.01	0.4±0.02	0.2±0.009

Table A. 30 ^{1}H T_1 and T_2 relaxation times for aniline in 50:50 % v/v MeCN:D_2O (from top to bottom according to HPLC elution order): mobile phase in the absence of stationary phase (solution only) and in the presence of BEH-C18, BEH-phenyl, BEH-RP18, CSH hexyl-phenyl and HSS T3 stationary phases. Data were obtained at 500 MHz spectrometer at 313 K and 5.0 kHz spinning frequency.

MeCN/D₂O

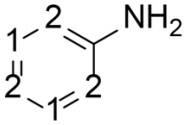

SP	HPLC Rt (mins)	T_1(s)			
		H-1(f)	H-2(f)	H-1(b)	H-2(b)
Solution only	n/a	6.4 ± 0.3	7.0 ± 0.4	n/a	
BEH-C18	3.58	7.4 ± 0.4	8.0 ± 0.4	3.9 ± 0.2	3.58
BEH-Phenyl	3.67	7.6 ± 0.4	8.7 ± 0.4	4.1 ± 0.2	3.67
BEH-RP18	3.73	7.5 ± 0.4	8.1 ± 0.4	4.0 ± 0.2	3.73
CSH hexyl phenyl	3.80	6.7 ± 0.3	7.5 ± 0.4	3.7 ± 0.2	3.80
HSS T3	4.22	8.4 ± 0.4	7.9 ± 0.4	6.1 ± 0.3	4.22
		T_2(s)			
		H-1(f)	H-2(f)	H-1(b)	H-2(b)
Solution only	n/a	2.8±0.4	2.9±0.4	n/a	
BEH-C18	3.58	1.6±0.2	1.6±0.2	0.1±0.02	0.1±0.02
BEH-Phenyl	3.67	1.5±0.2	1.6±0.2	0.1±0.02	0.1±0.02
BEH-RP18	3.73	1.3±0.2	1.3±0.2	0.1±0.02	0.1±0.02
CSH hexyl phenyl	3.80	1.5±0.2	1.6±0.2	0.1±0.02	0.1±0.02
HSS T3	4.22	1.2±0.2	1.2±0.2	0.2±0.02	0.1±0.02

Table A. 31 ^{1}H T_1 and T_2 relaxation times for aniline in 50:50 % v/v MeOH:D_2O (from top to bottom according to HPLC elution order): mobile phase in the absence of stationary phase (solution only) and in the presence of BEH-C18, BEH-phenyl, BEH-RP18, CSH hexyl-phenyl and HSS T3 stationary phases. Data were obtained at 500 MHz spectrometer at 313 K and 5.0 kHz spinning frequency.

MeOH/D_2O

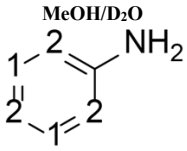

SP	HPLC Rt (mins)	T_1(s) H-1(f)	H-2(f)	H-1(b)	H-2(b)
Solution only	n/a	4.8±0.1	5.4±0.1	n/a	
BEH-C18	3.86	6.0±0.1	6.7±0.1	2.6±0.1	3.1±0.1
BEH-RP18	4.06	5.8±0.1	6.5±0.1	2.4±0.05	2.9±0.1
BEH-Phenyl	4.22	5.5±0.1	5.9±0.1	2.3±0.1	2.4±0.1
CSH hexyl phenyl	4.39	5.7±0.1	6.3±0.1	2.4±0.1	2.5±0.1
HSS T3	4.56	6.4±0.1	7.0±0.1	3.4±0.1	3.4±0.1
		T_2(s) H-1(f)	H-2(f)	H-1(b)	H-2(b)
Solution only	n/a	2.6±0.1	2.6±0.1	n/a	
BEH-C18	3.86	1.3±0.01	1.3±0.01	0.1±0.003	0.03±0.004
BEH-RP18	4.06	2.3±0.04	2.4±0.05	0.1±0.002	0.04±0.003
BEH-Phenyl	4.22	1.4±0.04	1.3±0.03	0.1±0.002	0.1±0.001
CSH hexyl phenyl	4.39	1.3±0.04	1.3±0.04	0.1±0.003	0.1±0.003
HSS T3	4.56	1.7±0.05	1.6±0.04	0.1±0.004	0.1±0.002

Table A. 32 ^{1}H T_1 and T_2 relaxation times for 2-aminophenol in 50:50 % v/v MeCN:D_2O (from top to bottom according to HPLC elution order): mobile phase in the absence of stationary phase (solution only) and in the presence of BEH-C18, BEH-phenyl, BEH-RP18, CSH hexyl-phenyl and HSS T3 stationary phases. Data were obtained at 500 MHz spectrometer at 313 K and 5.0 kHz spinning frequency.

MeCN/D_2O

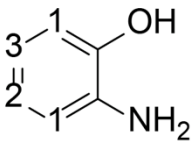

SP	HPLC Rt (mins)	T_1(s) H-1(a)	H-2(a)	H-3(a)
Solution only	n/a	9.2±0.1	9.4±0.1	9.0±0.2
BEH-C18	2.84	3.7±0.1	5.4±0.2	5.6±0.1
BEH-RP18	2.97	5.0±0.1	5.5±0.2	5.3±0.1
BEH-Phenyl	3.03	5.1±0.1	6.2±0.1	6.0±0.2
HSS T3	3.18	9.9±0.2	9.5±0.4	9.3±0.4
CSH hexyl phenyl	3.19	5.6±0.1	5.2±0.1	5.1±0.1
		T_2(s) H-1(a)	H-2(a)	H-3(a)
Solution only	n/a	1.8±0.02	1.8±0.02	1.7±0.02
BEH-C18	2.84	1.3±0.02	1.2±0.05	1.3±0.04
BEH-RP18	2.97	1.6±0.03	1.5±0.04	1.5±0.04
BEH-Phenyl	3.03	1.8±0.03	1.6±0.1	1.6±0.1
HSS T3	3.18	2.0±0.03	1.8±0.1	1.8±0.1
CSH hexyl phenyl	3.19	2.1±0.1	1.8±0.1	2.0±0.2

Table A. 33 ^{1}H T_1 and T_2 relaxation times for 2-aminophenol in 50:50 % v/v MeCN:D_2O (from top to bottom according to HPLC elution order): mobile phase in the absence of stationary phase (solution only) and in the presence of BEH-C18, BEH-phenyl, BEH-RP18, CSH hexyl-phenyl and HSS T3 stationary phases. Data were obtained at 500 MHz spectrometer at 313 K and 5.0 kHz spinning frequency.

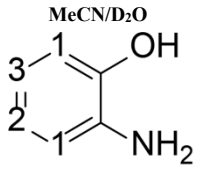

SP	HPLC Rt (mins)	T_1(s) H-1(a)	H-2(a)	H-3(a)
Solution only	n/a	4.3±0.2	3.8±0.2	3.9±0.2
BEH-C18	3.13	4.5±0.2	4.4±0.2	4.1±0.2
BEH-RP18	3.34	4.3±0.2	3.9±0.2	3.7±0.2
BEH-Phenyl	3.56	4.0±0.2	3.8±0.2	3.9±0.2
HSS T3	3.59	4.2±0.2	3.5±0.2	3.6±0.2
CSH hexyl phenyl	3.81	4.2±0.2	3.4±0.2	3.9±0.2
		T_2(s) H-1(a)	H-2(a)	H-3(a)
Solution only	n/a	2.5±0.3	2.4±0.2	2.3±0.2
BEH-C18	3.13	1.6±0.2	1.5±0.2	1.5±0.2
BEH-RP18	3.34	1.6±0.2	1.7±0.2	1.5±0.2
BEH-Phenyl	3.56	1.5±0.2	1.5±0.2	1.4±0.1
HSS T3	3.59	1.7±0.2	1.7±0.2	1.7±0.2
CSH hexyl phenyl	3.81	2.2±0.2	2.3±0.2	2.2±0.2

Table A. 34 Experimental retention times (minutes) of all 15 analytes under gradient elution method across BEH-C18, BEH-phenyl and BEH-RP18 stationary phases.

Analytes	BEH C18	BEH phenyl	BEH RP18
i. toluene	7.92	8.26	6.23
ii. naphthalene	8.47	9.07	6.80
iii. acenaphthylene	9.18	9.83	7.33
iv. benzophenone	8.06	9.12	6.57
v. biphenyl	8.95	9.66	7.2
vi. propranolol	7.03	10.04	4.37
vii.2-aminophenol	3.84	1.58	0.70
viii. aniline	4.58	5.00	0.71
ix.3-hydroxybenzoic acid	1.07	0.53	3.98
x. dipropyl phthalate	8.45	9.48	6.91
xi. butyl 4-hydroxybenzoate	8.05	6.45	6.40
xii. benzoic acid	2.32	0.73	4.61
xiii. amitriptyline hydrochloride	8.55	10.84	4.91
xiv. hydroxyzine	8.77	10.20	4.89
xv. meclizine	10.24	11.52	5.6

Table A. 35 Predicted retention times (minutes) of all 15 analytes under gradient elution method across BEH-C18, BEH-phenyl and BEH-RP18 stationary phases.

Analytes	BEH C18	BEH phenyl	BEH RP18
i. toluene	6.04	7.41	5.85
ii. naphthalene	6.49	8.07	6.33
iii. acenaphthylene		N/A	
iv. benzophenone	6.71	8.10	6.16
v. biphenyl	6.89	8.49	6.67
vi. propranolol	5.90	8.05	4.15
vii.2-aminophenol	4.49	5.39	3.19
viii. aniline	4.92	6.08	3.54
ix.3-hydroxybenzoic acid	4.30	4.50	5.09
x. dipropyl phthalate	7.04	8.64	6.53
xi. butyl 4-hydroxybenzoate	6.38	7.04	6.34
xii. benzoic acid	4.75	4.97	5.34
xiii. amitriptyline hydrochloride	7.38	9.66	5.30
xiv. hydroxyzine	7.21	8.07	3.43
xv. meclizine	8.67	10.16	5.29

Table A. 36 ^{1}H T_1 and T_2 relaxation times for toluene in 50:50 % v/v MeCN:D_2O (from top to bottom according to HPLC experimental elution order): mobile phase in the absence of stationary phase (solution only) and in the presence of BEH-RP18, BEH-C18 and BEH-Phenyl stationary phases. Data were obtained at 500 MHz spectrometer at 313 K and 5.0 kHz spinning frequency. Where I: experimental HPLC data and **II**: predicted HPLC data.

	SP	HPLC Rt (mins) I/**II**	T_1(s)					
			H-1(f)	H-2(f)	H-3(f)	H-1(b)	H-2(b)	H-3(b)
MeCN/D_2O	Solution only	n/a	6.4±0.1	6.5±0.1	6.4±0.1	n/a		
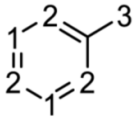	BEH-RP18	6.23/**5.85**	6.8±0.5	6.2±0.5	4.8±0.2	3.3±0.2	3.1±0.2	2.5±0.1
	BEH-C18	7.92/**6.04**	5.6±0.1	5.1±0.1	4.6±0.1	3.6±0.2	3.4±0.2	3.0±0.1
	BEH-Phenyl	8.26/**7.41**	3.5±0.3	2.6±0.2	3.8±0.3	2.6±0.1	2.4±0.1	2.8±0.1
			T_2(s)					
			H-1(f)	H-2(f)	H-3(f)	H-1(b)	H-2(b)	H-3(b)
Toluene	Solution only	n/a	3.5±0.1	3.5±0.1	3.5±0.1	n/a		
	BEH-RP18	6.23/**5.85**	2.2±0.1	2.0±0.1	1.9±0.1	0.2±0.004	0.2±0.003	0.2±0.005
	BEH-C18	7.92/**6.04**	1.8±0.1	1.6±0.1	1.6±0.02	0.1±0.001	0.1±0.002	0.2±0.001
	BEH-Phenyl	8.26/**7.41**	2.0±0.2	1.8±0.1	1.6±0.05	0.1±0.003	0.1±0.003	0.1±0.002

Table A. 37 ^{1}H T_1 and T_2 relaxation times for naphthalene in 50:50 % v/v MeCN:D_2O (from top to bottom according to HPLC experimental elution order): mobile phase in the absence of stationary phase (solution only) and in the presence of BEH-RP18, BEH-C18 and BEH-Phenyl stationary phases. Data were obtained at 500 MHz spectrometer at 313 K and 5.0 kHz spinning frequency. Where I: experimental HPLC data and **II**: predicted HPLC data.

	SP	HPLC Rt (mins) I/**II**	T_1(s)			
			H-1(f)	H-2(f)	H-1(b)	H-2(b)
MeCN/D_2O	Solution only	n/a	5.6±0.1	6.0±0.1	n/a	
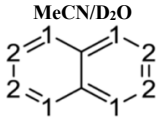	BEH-RP18	6.80/**6.33**	7.5±1.2	6.8±0.4	2.8±0.1	3.1±0.1
	BEH-C18	8.47/**6.49**	7.1±0.2	7.7±0.5	3.5±0.1	3.5±0.1
	BEH-Phenyl	9.07/**8.07**	7.7±0.4	7.8±0.5	4.5±0.1	4.4±0.1
			T_2(s)			
			H-1(f)	H-2(f)	H-1(b)	H-2(b)
Naphthalene	Solution only	n/a	2.8±0.1	2.9±0.03	n/a	
	BEH-RP18	6.80/**6.33**	2.0±0.1	2.2±0.1	0.1±0.002	0.1±0.004
	BEH-C18	8.47/**6.49**	2.2±0.03	2.3±0.04	0.1±0.002	0.1±0.001
	BEH-Phenyl	9.07/**8.07**	2.0±0.1	2.0±0.1	0.1±0.002	0.1±0.002

Table A. 38 ^{1}H T_1 and T_2 relaxation times for acenaphthene in 50:50 % v/v MeCN:D_2O (from top to bottom according to HPLC experimental elution order): mobile phase in the absence of stationary phase (solution only) and in the presence of BEH-RP18, BEH-C18 and BEH-Phenyl stationary phases. Data were obtained at 500 MHz spectrometer at 313 K and 5.0 kHz spinning frequency. Where I: experimental HPLC data and **II**: predicted HPLC data

	SP	HPLC Rt (mins) I/**II**	T_1(s)							
			H-1(f)	H-2(f)	H-3(f)	H-4(f)	H-1(b)	H-2(b)	H-3(b)	H-4(b)
MeCN/D_2O 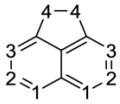 Acenaphthene	Solution only	n/a	5.9±0.2	6.1±0.4	5.8±0.3	2.7±0.1	n/a			
	BEH-RP18	7.33/**n.a**	7.5±1.1	7.5±1.2	7.1±0/6	3.4±0.2	2.8±0.1	2.9±0.1	2.7±0.1	1.4±0.1
	BEH-C18	9.18/**n.a**	7.4±0.8	7.7±1.1	5.7±0.4	2.7±0.1	2.9±0.1	2.9±0.1	2.9±0.1	1.3±0.04
	BEH-Phenyl	9.83/**n.a**	5.0±0.4	4.5±0.2	4.6±0.3	2.6±0.1	3.2±0.1	2.8±0.1	2.1±0.1	1.4±0.1
			T_2(s)							
			H-1(f)	H-2(f)	H-3(f)	H-4(f)	H-1(b)	H-2(b)	H-3(b)	H-4(b)
	Solution only	n/a	1.8±0.1	2.2±0.1	2.2±0.1	1.8±0.05	n/a			
	BEH-RP18	7.33/**n.a**	1.5±0.1	1.3±0.1	1.2±0.1	1.2±0.1	0.2±0.004	0.1±0.006	0.1±0.007	0.1±0.002
	BEH-C18	9.18/**n.a**	1.4±0.1	1.2±0.1	1.3±0.1	1.2±0.03	0.1±0.02	0.1±0.02	0.1±0.003	0.1±0.003
	BEH-Phenyl	9.83/**n.a**	1.8±0.1	1.9±0.1	1.7±0.1	1.2±0.01	0.1±0.004	0.1±0.004	0.1±0.004	0.1±0.003

Table A. 39 ^{1}H T_1 and T_2 relaxation times for benzophenone in 50:50 % v/v MeCN:D_2O (from top to bottom according to HPLC experimental elution order): mobile phase in the absence of stationary phase (solution only) and in the presence of BEH-RP18, BEH-C18 and BEH-Phenyl stationary phases. Data were obtained at 500 MHz spectrometer at 313 K and 5.0 kHz spinning frequency. Where I: experimental HPLC data and **II**: predicted HPLC data

	SP	HPLC Rt (mins) I/**II**	T_1(s)					
			H-1(f)	H-2(f)	H-3(f)	H-1(b)	H-2(b)	H-3(b)
MeCN/D_2O 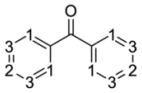 Benzophenone	Solution only	n/a	4.5±0.1	5.1±0.2	4.5±0.1	n/a		
	BEH-RP18	6.57/**6.16**	5.8±0.3	7.1±0.7	6.0±0.3	3.3±0.1	3.3±0.1	3.2±0.05
	BEH-C18	8.06/**6.71**	5.8±0.2	6.2±0.3	5.1±0.1	3.9±0.1	3.9±0.1	3.7±0.04
	BEH-Phenyl	9.12/**8.10**	6.1±0.1	6.1±0.4	5.5±0.2	4.3±0.1	4.3±0.1	3.9±0.1
			T_2(s)					
			H-1(f)	H-2(f)	H-3(f)	H-1(b)	H-2(b)	H-3(b)
	Solution only	n/a	2.8±0.04	3.0±0.1	2.8±0.04	n/a		
	BEH-RP18	6.57/**6.16**	1.9±0.02	1.9±0.1	1.8±0.02	0.2±0.01	0.1±0.01	0.1±0.004
	BEH-C18	8.06/**6.71**	2.1±0.03	2.1±0.1	1.9±0.1	0.8±0.1	0.8±0.1	0.7±0.1
	BEH-Phenyl	9.12/**8.10**	1.5±0.1	1.5±0.1	1.4±0.05	0.2±0.004	0.1±0.005	0.1±0.003

Table A. 40 ^{1}H T_1 and T_2 relaxation times for biphenyl in 50:50 % v/v MeCN:D_2O (from top to bottom according to HPLC experimental elution order): mobile phase in the absence of stationary phase (solution only) and in the presence of BEH-RP18, BEH-C18 and BEH-Phenyl stationary phases. Data were obtained at 500 MHz spectrometer at 313 K and 5.0 kHz spinning frequency. Where I: experimental HPLC data and **II**: predicted HPLC data

MeCN/D_2O	SP	HPLC Rt (mins) I/**II**	T_1(s)			
			H-1(f)	H-3(f)	H-2(b)	H-3(b)
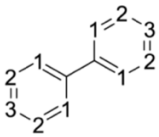	Solution only	n/a	4.2±0.1	4.7±0.1	n/a	
	BEH-RP18	7.20/**6.67**	5.1±0.1	4.1±0.1	2.4±0.1	2.6±0.1
	BEH-C18	8.95/**6.89**	5.8±0.2	6.0±0.2	3.3±0.1	3.4±0.2
	BEH-Phenyl	9.66/**8.49**	6.1±0.5	3.5±0.2	2.9±0.1	2.7±0.1
			T_2(s)			
			H-1(f)	H-3(f)	H-2(b)	H-3(b)
Biphenyl	Solution only	n/a	2.8±0.03	2.9±0.04	n/a	
	BEH-RP18	7.20/**6.67**	2.1±0.2	1.5±0.2	0.2±0.003	0.2±0.01
	BEH-C18	8.95/**6.89**	2.6±0.04	2.7±0.1	0.2±0.04	0.1±0.01
	BEH-Phenyl	9.66/**8.49**	2.1±0.1	2.0±0.2	0.1±0.002	0.1±0.01

Table A. 41 ^{1}H T_1 and T_2 relaxation times for butyl 4-hydroxybenzoate in 50:50 % v/v MeCN:D_2O (from top to bottom according to HPLC experimental elution order): mobile phase in the absence of stationary phase (solution only) and in the presence of BEH-RP18, BEH-phenyl and BEH-C18 stationary phases. Data were obtained at 500 MHz spectrometer at 313 K and 5.0 kHz spinning frequency. Where I: experimental HPLC data and **II**: predicted HPLC data

MeCN/D_2O

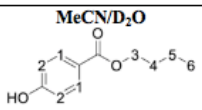

Butyl 4-hydroxybenzoate

SP	HPLC Rt (mins)	T_1(s)											
		H-1(f)	H-2(f)	H-3(f)	H-4(f)	H-5(f)	H-6(f)	H-1(b)	H-2(b)	H-3(b)	H-4(b)	H-5(b)	H-6(b)
Solution only	n/a	2.8±0.002	3.0±0.0003	1.6±0.0001	1.6±0.0001	1.9±0.0001	2.1±0.0001	n/a					
BEH-RP18	6.40/**6.34**	4.5±0.3	4.2±0.6	6.6±0.1	2.9±0.2	2.2±0.2	1.7±0.1	1.8±0.1	1.7±0.1	4.4±0.2	1.4±0.1	1.3±0.1	1.5±0.1
BEH-Phenyl	6.45/**7.04**	4.1±0.3	2.1±0.1	4.9±0.04	1.7±0.1	1.7±0.1	2.2±0.2	2.8±0.05	2.6±0.02	3.3±0.1	1.3±0.1	1.7±0.2	1.9±0.1
BEH-C18	8.05/**6.38**	4.1±0.1	4.6±0.2	5.7±0.1	1.7±0.1	1.8±0.1	1.8±0.1	2.9±0.1	2.8±0.1	2.4±0.2	1.4±0.1	1.5±0.1	1.5±0.1
		T_2(s)											
		H-1(f)	H-2(f)	H-3(f)	H-4(f)	H-5(f)	H-6(f)	H-1(b)	H-2(b)	H-3(b)	H-4(b)	H-5(b)	H-6(b)
Solution only	n/a	1.7±0.1	1.7±0.1	0.9±0.02	1.0±0.02	1.3±0.02	1.4±0.02	n/a					
BEH-RP18	6.40/**6.34**	0.4±0.04	0.5±0.1	0.8±0.02	0.4±0.04	0.6±0.06	0.8±0.05	0.1±0.01	0.1±0.02	0.6±0.1	0.1±0.03	0.1±0.01	0.2±0.01
BEH-Phenyl	6.45/**7.04**	0.4±0.1	0.5±0.05	0.1±0.004	0.5±0.04	0.5±0.04	0.6±0.03	0.3±0.02	0.3±0.02	0.1±0.01	0.1±0.01	0.2±0.01	0.2±0.003
BEH-C18	8.05/**6.38**	0.8±0.04	0.9±0.03	0.1±0.004	0.7±0.05	1.1±0.04	1.2±0.03	0.4±0.03	0.3±0.04	0.2±0.1	0.2±0.02	0.3±0.01	0.3±0.02

Table A. 42 ^{1}H T_1 and T_2 relaxation times for dipropyl phthalate in 50:50 % v/v MeCN:D_2O (from top to bottom according to HPLC experimental elution order): mobile phase in the absence of stationary phase (solution only) and in the presence of BEH-RP18, BEH-C18 and BEH-Phenyl stationary phases. Data were obtained at 500 MHz spectrometer at 313 K and 5.0 kHz spinning frequency. Where I: experimental HPLC data and **II**: predicted HPLC data

	SP	HPLC Rt (mins)	T_1(s)				
			H-1(a)	H-2(a)	H-3(a)	H-4(a)	H-5(a)
MeCN/D₂O 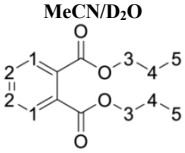 Dipropyl phthalate	Solution only	n/a	2.4±0.04	2.1±0.03	1.9±0.04	1.6±0.1	1.6±0.1
	BEH-RP18	6.91/**6.53**	3.1±0.1	2.6±0.1	2.1±0.1	1.9±0.1	1.7±0.1
	BEH-C18	8.45/**7.04**	3.9±0.1	3.2±0.04	2.6±0.1	1.9±0.2	2.0±0.2
	BEH-Phenyl	9.48/**8.64**	3.6±0.1	3.0±0.1	2.4±0.1	2.0±0.1	2.1±0.2
			T_2(s)				
			H-1(a)	H-2(a)	H-3(a)	H-4(a)	H-5(a)
	Solution only	n/a	2.0±0.09	1.9±0.05	1.3±0.04	0.8±0.03	1.3±0.02
	BEH-RP18	6.91/**6.53**	0.5±0.02	0.4±0.01	0.5±0.01	0.4±0.01	0.5±0.02
	BEH-C18	8.45/**7.04**	2.2±0.1	2.1±0.1	1.0±0.05	0.5±0.05	1.1±0.1
	BEH-Phenyl	9.48/**8.64**	1.7±0.1	1.8±0.2	1.0±0.1	0.5±0.01	0.9±0.05

Table A. 43 ^{1}H T_1 and T_2 relaxation times for benzoic acid in 50:50 % v/v MeCN:D_2O (from top to bottom according to HPLC experimental elution order): mobile phase in the absence of stationary phase (solution only) and in the presence of BEH-phenyl, BEH-C18 and BEH-RP18 stationary phases. Data were obtained at 500 MHz spectrometer at 313 K and 5.0 kHz spinning frequency. Where I: experimental HPLC data and **II**: predicted HPLC data

	SP	HPLC Rt (mins)	T_1(s)					
			H-1(f)	H-2(f)	H-3(f)	H-1(b)	H-2(b)	H-3(b)
MeCN/D₂O 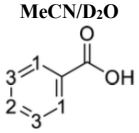 Benzoic acid	Solution only	n/a	4.4±0.1	4.6±0.1	4.1±0.1	n/a		
	BEH-Phenyl	0.73/**4.97**	5.9±0.1	6.8±0.1	5.5±0.1	5.0±0.2	5.8±0.3	4.7±0.1
	BEH-C18	2.32/**4.75**	5.5±0.1	6.3±0.1	5.1±0.1	4.6±0.1	4.4±0.1	4.2±0.1
	BEH-RP18	4.61/**5.29**	5.0±0.1	6.7±0.2	5.2±0.1	3.8±0.1	3.1±0.2	3.3±0.1
			T_2(s)					
			H-1(f)	H-2(f)	H-3(f)	H-1(b)	H-2(b)	H-3(b)
	Solution only	n/a	2.0±0.05	2.3±0.05	1.9±0.04	n/a		
	BEH-Phenyl	0.73/**4.97**	0.7±0.01	1.0±0.02	0.8±0.01	0.4±0.01	0.3±0.02	0.3±0.03
	BEH-C18	2.32/**4.75**	0.9±0.01	1.1±0.01	1.0±0.02	0.5±0.04	0.3±0.05	0.3±0.04
	BEH-RP18	4.61/**5.29**	1.1±0.03	1.5±0.04	1.2±0.02	0.7±0.07	0.3±0.04	0.3±0.05

Table A. 44 ^{1}H T_1 and T_2 relaxation times for 3-hydroxybenzoic acid in 50:50 % v/v MeCN:D_2O (from top to bottom according to HPLC experimental elution order): mobile phase in the absence of stationary phase (solution only) and in the presence of BEH-phenyl, BEH-C18 and BEH-RP18 stationary phases. Data were obtained at 500 MHz spectrometer at 313 K and 5.0 kHz spinning frequency. Where I: experimental HPLC data and **II**: predicted HPLC data

	SP	HPLC Rt (mins)	T_1(s)					
			H-1(f)	H-1*(f)	H-2(f)	H-3(f)	H-2(b)	H-3(b)
	Solution only	n/a	3.8±0.1	6.4±0.05	3.2±0.03	4.7±0.05	n/a	
MeCN/D_2O	BEH-Phenyl	0.53/**4.50**	4.3±0.1	7.1±0.1	3.7±0.03	5.1±0.1	3.5±0.1	4.6±0.1
	BEH-C18	1.07/**4.30**	4.2±0.1	7.3±0.1	3.6±0.1	5.6±0.2	3.7±0.1	5.5±0.2
	BEH-RP18	3.98/**5.09**	3.4±0.1	4.6±0.1	3.1±0.04	4.3±0.1	2.4±0.1	3.1±0.1
			T_2(s)					
			H-1(f)	H-1*(f)	H-2(f)	H-3(f)	H-2(b)	H-3(b)
3-hydroxybenzoic acid	Solution only	n/a	2.6±0.04	3.4±0.04	2.4±0.03	2.6±0.03	n/a	
	BEH-Phenyl	0.53/**4.50**	1.5±0.05	1.7±0.04	1.5±0.1	1.5±0.06	0.7±0.04	1.3±0.1
	BEH-C18	1.07/**4.30**	1.7±0.04	1.8±0.04	1.6±0.05	1.7±0.05	0.9±0.07	1.0±0.1
	BEH-RP18	3.98/**5.09**	2.0±0.1	2.1±0.1	2.0±0.1	2.1±0.05	0.2±0.01	0.3±0.03

Table A. 45 ^{1}H T_1 and T_2 relaxation times for aniline in 50:50 % v/v MeCN:D_2O (from top to bottom according to HPLC experimental elution order): mobile phase in the absence of stationary phase (solution only) and in the presence of BEH-RP18, BEH-C18 and BEH-phenyl stationary phases. Data were obtained at 500 MHz spectrometer at 313 K and 5.0 kHz spinning frequency. Where I: experimental HPLC data and **II**: predicted HPLC data

	SP	HPLC Rt (mins)	T_1(s)			
			H-1(f)	H-2(f)	H-1(b)	H-2(b)
	Solution only	n/a	6.4 ± 0.3	7.0 ± 0.4	n/a	
MeCN/D_2O	BEH-RP18	0.71/**3.54**	7.5 ± 0.4	8.1 ± 0.4	4.0 ± 0.2	3.7 ± 0.2
	BEH-C18	4.58/**4.92**	7.4 ± 0.4	8.0 ± 0.4	3.9 ± 0.2	3.9 ± 0.2
	BEH-Phenyl	5.00/**6.08**	7.6 ± 0.4	8.7 ± 0.4	4.1 ± 0.2	4.8 ± 0.2
			T_2(s)			
			H-1(f)	H-2(f)	H-1(b)	H-2(b)
Aniline	Solution only	n/a	2.8±0.4	2.9±0.4	n/a	
	BEH-RP18	0.71/**3.54**	1.3±0.2	1.3±0.2	0.1±0.02	0.1±0.02
	BEH-C18	4.58/**4.92**	1.6±0.2	1.6±0.2	0.1±0.02	0.1±0.02
	BEH-Phenyl	5.00/**6.08**	1.5±0.2	1.6±0.2	0.1±0.02	0.1±0.01

Table A. 46 ^{1}H T_1 and T_2 relaxation times for 2-aminophenol in 50:50 % v/v MeCN:D_2O (from top to bottom according to HPLC experimental elution order): mobile phase in the absence of stationary phase (solution only) and in the presence of BEH-RP18, BEH-phenyl and BEH-C18 stationary phases. Data were obtained at 500 MHz spectrometer at 313 K and 5.0 kHz spinning frequency. Where I: experimental HPLC data and **II**: predicted HPLC data

	SP	HPLC Rt (mins)	T_1(s)		
			H-1(a)	H-2(a)	H-3(a)
MeCN/ D$_2$O 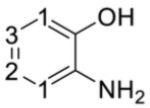 2-aminophenol	Solution only	n/a	9.2±0.1	9.4±0.1	9.0±0.2
	BEH-RP18	0.70/**3.19**	5.0±0.1	5.5±0.2	5.3±0.1
	BEH-Phenyl	1.58/**5.39**	5.1±0.1	6.2±0.1	6.0±0.2
	BEH-C18	3.84/**4.49**	3.7±0.1	5.4±0.2	5.6±0.1
			T_2(s)		
			H-1(a)	H-2(a)	H-3(a)
	Solution only	n/a	1.8±0.02	1.8±0.02	1.7±0.02
	BEH-RP18	0.70/**3.19**	1.6±0.03	1.5±0.04	1.5±0.04
	BEH-Phenyl	1.58/**5.39**	1.8±0.03	1.6±0.1	1.6±0.1
	BEH-C18	3.84/**4.49**	1.3±0.02	1.2±0.05	1.3±0.04

Table A. 47 ^{1}H T_1 and T_2 relaxation times for meclizine in 50:50 % v/v MeCN:D_2O (from top to bottom according to HPLC experimental elution order): mobile phase in the absence of stationary phase (solution only) and in the presence of BEH-RP18, BEH-C18 and BEH-phenyl stationary phases. Data were obtained at 500 MHz spectrometer at 313 K and 5.0 kHz spinning frequency. Where I: experimental HPLC data and **II**: predicted HPLC data

	SP	HPLC Rt (mins)	T_1(s)						
			H-1(a)	H-2(a)	H-3(a)	H-4(a)	H-5(a)	H-6(a)	H-7(a)
MeCN/D$_2$O 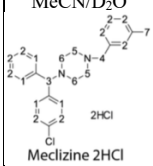 Meclizine 2HCl	Solution only	n/a	1.2±0.03	1.8±0.03	0.6±0.03	0.4±0.05	0.4±0.03	0.4±0.02	1.1±0.02
	BEH-RP18	5.60/**5.29**	1.2±0.02	1.7±0.03	0.5±0.04	0.4±0.04	0.3±0.04	0.3±0.05	0.9±0.1
	BEH-C18	10.24/**8.67**	1.2±0.1	1.7±0.1	0.5±0.1	0.4±0.1	0.3±0.1	0.3±0.1	0.9±0.1
	BEH-Phenyl	11.52/**10.16**	1.1±0.04	1.5±0.1	0.5±0.1	0.4±0.1	0.3±0.05	0.3±0.1	0.9±0.1
			T_2(s)						
			H-1(a)	H-2(a)	H-3(a)	H-4(a)	H-5(a)	H-6(a)	H-7(a)
	Solution only	n/a	0.6±0.03	1.0±0.02	0.5±0.01	0.3±0.01	0.2±0.002	0.2±0.002	0.8±0.01
	BEH-RP18	5.60/**5.29**	0.6±0.02	0.7±0.02	0.3±0.01	0.3±0.01	0.2±0.002	0.2±0.004	0.7±0.01
	BEH-C18	10.24/**8.67**	0.8±0.02	1.0±0.02	0.4±0.01	0.3±0.02	0.2±0.005	0.2±0.004	0.8±0.02
	BEH-Phenyl	11.52/**10.16**	0.6±0.02	0.7±0.03	0.4±0.01	0.3±0.01	0.2±0.003	0.2±0.004	0.7±0.01

Table A. 48 ^{1}H T_1 and T_2 relaxation times for hydroxyzine in 50:50 % v/v MeCN:D_2O (from top to bottom according to HPLC experimental elution order): mobile phase in the absence of stationary phase (solution only) and in the presence of BEH-RP18, BEH-C18 and BEH-phenyl stationary phases. Data were obtained at 500 MHz spectrometer at 313 K and 5.0 kHz spinning frequency. Where I: experimental HPLC data and **II**: predicted HPLC data

MeCN:D₂O

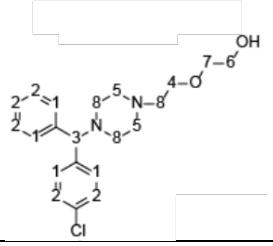

SP	HPLC Rt (mins)	H-1(a)	H-2(a)	H-3(a)	H-4(a)	H-5(a)	H-6(a)	H-7(a)	H-8(a)
						T_1(s)			
Solution only	n/a	1.1±0.02	1.6±0.03	0.5±0.01	0.4±0.02	0.3±0.02	0.9±0.04	0.8±0.04	0.3±0.02
BEH-RP18	4.89/**3.43**	1.2±0.02	1.8±0.02	0.5±0.04	0.4±0.05	0.3±0.05	0.8±0.1	0.6±0.05	0.3±0.1
BEH-C18	8.77/**7.21**	1.1±0.004	1.7±0.04	0.5±0.04	0.4±0.04	0.3±0.03	0.9±0.04	0.7±0.04	0.3±0.06
BEH-Phenyl	10.20/**10.16**	1.1±0.006	1.7±0.01	0.5±0.02	0.4±0.04	0.3±0.03	0.9±0.1	0.7±0.1	0.3±0.1
						T_2(s)			
		H-1(a)	H-2(a)	H-3(a)	H-4(a)	H-5(a)	H-6(a)	H-7(a)	H-8(a)
Solution only	n/a	0.7±0.004	0.9±0.002	0.4±0.006	0.3±0.002	0.1±0.002	0.7±0.005	0.7±0.007	0.2±0.003
BEH-RP18	4.89/**3.43**	0.6±0.007	0.7±0.008	0.3±0.006	0.3±0.005	0.1±0.004	0.6±0.005	0.5±0.009	0.2±0.004
BEH-C18	8.77/**7.21**	0.6±0.005	0.8±0.005	0.3±0.005	0.3±0.005	0.1±0.005	0.7±0.002	0.6±0.009	0.2±0.004
BEH-Phenyl	10.20/**10.16**	0.6±0.008	0.7±0.01	0.3±0.009	0.3±0.005	0.1±0.004	0.6±0.004	0.6±0.01	0.2±0.002

Table A. 49 ^{1}H T_1 and T_2 relaxation times for amitriptyline in 50:50 % v/v MeCN:D_2O (from top to bottom according to HPLC experimental elution order): mobile phase in the absence of stationary phase (solution only) and in the presence of BEH-RP18, BEH-C18 and BEH-phenyl stationary phases. Data were obtained at 500 MHz spectrometer at 313 K and 5.0 kHz spinning frequency. Where I: experimental HPLC data and **II**: predicted HPLC data

MeCN:D₂O

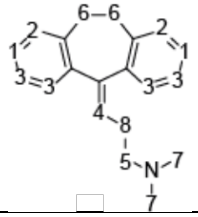

SP	HPLC Rt (mins)	H-1(a)	H-2(a)	H-3(a)	H-4(a)	H-5(a)	H-6(a)	H-7(a)	H-8(a)
						T_1(s)			
Solution only	n/a	1.1±0.02	1.6±0.03	0.5±0.01	0.4±0.02	0.3±0.02	0.9±0.04	0.8±0.04	0.3±0.02
BEH-RP18	4.89/**3.43**	1.2±0.02	1.8±0.02	0.5±0.04	0.4±0.05	0.3±0.05	0.8±0.1	0.6±0.05	0.3±0.1
BEH-C18	8.77/**7.21**	1.1±0.04	1.7±0.04	0.5±0.04	0.4±0.04	0.3±0.03	0.9±0.04	0.7±0.04	0.3±0.06
BEH-Phenyl	10.20/**10.16**	1.1±0.006	1.7±0.02	0.5±0.02	0.4±0.04	0.3±0.03	0.9±0.1	0.7±0.1	0.3±0.1
						T_2(s)			
		H-1(a)	H-2(a)	H-3(a)	H-4(a)	H-5(a)	H-6(a)	H-7(a)	H-8(a)
Solution only	n/a	0.7±0.004	0.9±0.002	0.4±0.01	0.3±0.002	0.1±0.002	0.7±0.01	0.7±0.01	0.2±0.003
BEH-RP18	4.89/**3.43**	0.6±0.01	0.7±0.01	0.3±0.01	0.3±0.01	0.1±0.004	0.6±0.01	0.5±0.01	0.2±0.004
BEH-C18	8.77/**7.21**	0.6±0.005	0.8±0.005	0.3±0.005	0.3±0.005	0.1±0.005	0.7±0.002	0.6±0.009	0.2±0.004
BEH-Phenyl	10.20/**10.16**	0.6±0.008	0.7±0.01	0.3±0.009	0.3±0.005	0.1±0.004	0.6±0.004	0.6±0.001	0.2±0.02

Table A. 50 ^{1}H T_1 and T_2 relaxation times for propranolol in 50:50 % v/v MeCN:D_2O (from top to bottom according to HPLC experimental elution order): mobile phase in the absence of stationary phase (solution only) and in the presence of BEH-RP18, BEH-C18 and BEH-phenyl stationary phases. Data were obtained at 500 MHz spectrometer at 313 K and 5.0 kHz spinning frequency. Where I: experimental HPLC data and **II**: predicted HPLC data.

MeCN:D₂O

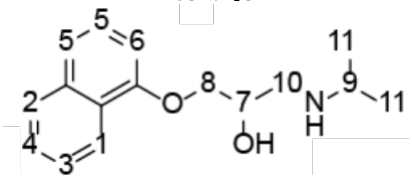

SP	HPLC Rt (mins) I/**II**	T_1(s)										
		H-1(a)	H-2(a)	H-3(a)	H-4(a)	H-5(a)	H-6(a)	H-7(a)	H-8(a)	H-9(a)	H-10(a)	H-11(a)
Solution only	n/a	2.5±0.04	2.1±0.02	1.9±0.02	1.9±0.02	1.8±0.04	1.3±0.03	1.7±0.04	0.9±0.03	0.7±0.02	0.8±0.01	0.9±0.1
BEH-RP18	4.37/**4.15**	2.4±0.04	2.1±0.1	2.0±0.1	2.0±0.1	1.6±0.1	1.0±0.1	1.4±0.04	1.1±0.03	0.6±0.03	0.6±0.1	0.9±0.1
BEH-C18	7.03/**5.90**	2.8±0.1	2.4±0.1	2.3±0.04	2.4±0.03	1.4±0.1	1.3±0.03	1.7±0.1	1.2±0.1	0.5±0.05	0.5±0.1	1.0±0.1
BEH-Phenyl	10.4/**8.05**	2.6±0.1	2.2±0.1	2.2±0.02	2.2±0.03	0.3±0.1	1.1±0.03	1.6±0.1	1.4±0.1	0.5±0.1	0.4±0.1	1.1±0.02
		T_2(s)										
		H-1(a)	H-2(a)	H-3(a)	H-4(a)	H-5(a)	H-6(a)	H-7(a)	H-8(a)	H-9(a)	H-10(a)	H-11(a)
Solution only	n/a	0.4±0.1	1.0±0.03	1.0±0.1	1.0±0.01	1.1±0.02	1.0±0.02	0.7±0.01	0.5±0.01	0.5±0.01	0.5±0.01	0.8±0.004
BEH-RP18	4.37/**4.15**	0.1±0.04	0.8±0.04	0.8±0.05	1.0±0.04	0.7±0.03	0.9±0.02	0.5±0.01	0.4±0.01	0.4±0.02	0.4±0.02	0.6±0.01
BEH-C18	7.03/**5.90**	0.3±0.1	1.0±0.03	0.5±0.1	1.1±0.03	0.8±0.03	0.9±0.03	0.7±0.02	0.5±0.01	0.5±0.01	0.5±0.02	0.7±0.01
BEH-Phenyl	10.4/**8.05**	0.1±0.004	0.7±0.1	0.8±0.05	1.0±0.05	0.6±0.04	0.8±0.05	0.6±0.02	0.4±0.02	0.4±0.02	0.4±0.02	0.6±0.01

13 APPENDICES: FIGURES

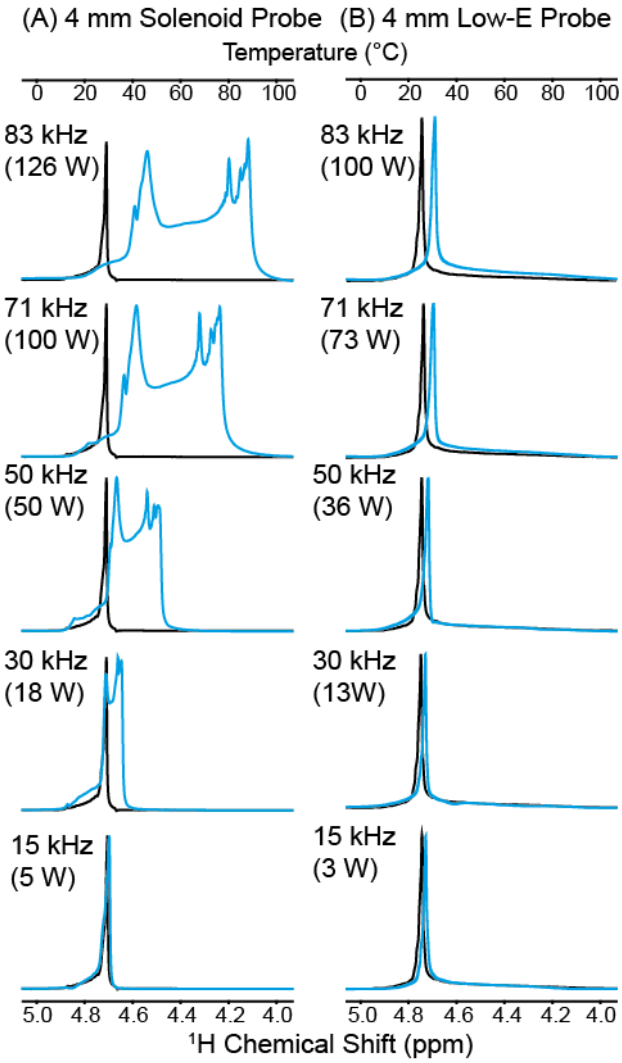

Figure A. 1. ^{1}H 500 MHz NMR spectra of water peaks (in presence of phosphate buffer) using a (a) 4 mm solenoid probe and (b) 4 mm Low-E probes. From top to bottom, the nutation frequencies of the RF pulse were 83 kHz, 71 kHz, 50 kHz, 30 kHz and 15 kHz respectively. The spectra with short irradiation (black) had fixed pulse length of (10 µs), while the long RF irradiation (blue) were varied but kept constant across the different rotors (30 ms). The spectra of the long RF irradiation (blue) were scaled to match that of the short RF irradiation pulse lengths (black). All spectra were acquired at 298 K with 10 kHz MAS spinning frequency.

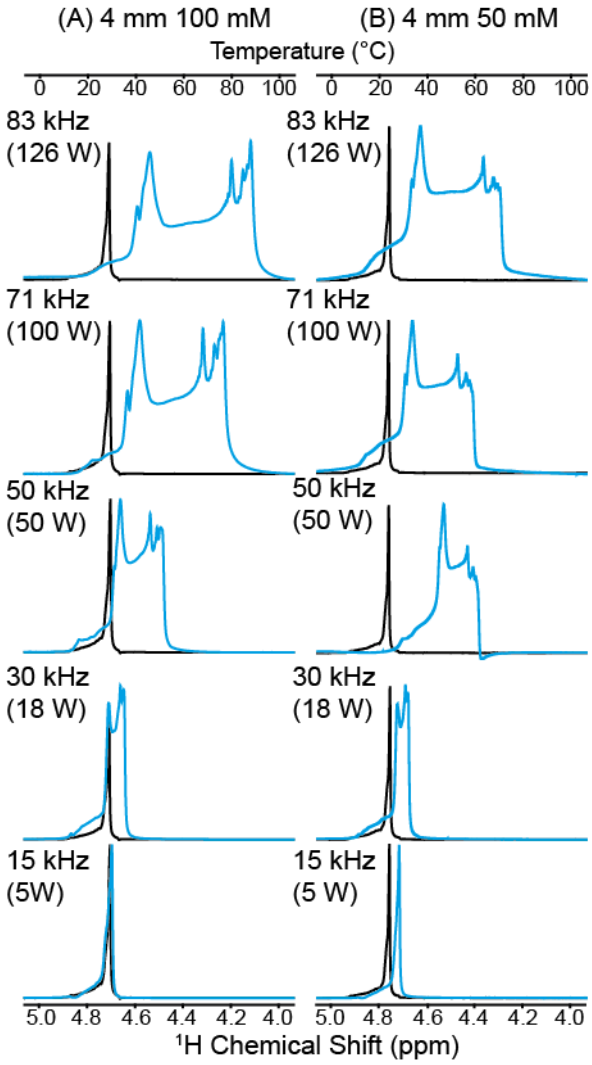

Figure A. 2. ^{1}H 500 MHz NMR spectra of water peaks with (a) 100 mM and (b) 50 mM phosphate buffer concentrations packed into a 4 mm rotor. From top to bottom, the nutation frequencies of the RF pulse were 83 kHz, 71 kHz, 50 kHz, 30 kHz and 15 kHz respectively. The spectra with short irradiation (black) had fixed pulse length of (10 µs), while the long RF irradiation (blue) were varied but kept constant across the different rotors (30 ms). The spectra of the long RF irradiation (blue) were scaled to match that of the short RF irradiation pulse lengths (black). All spectra were acquired at 298 K with 10 kHz MAS spinning frequency.

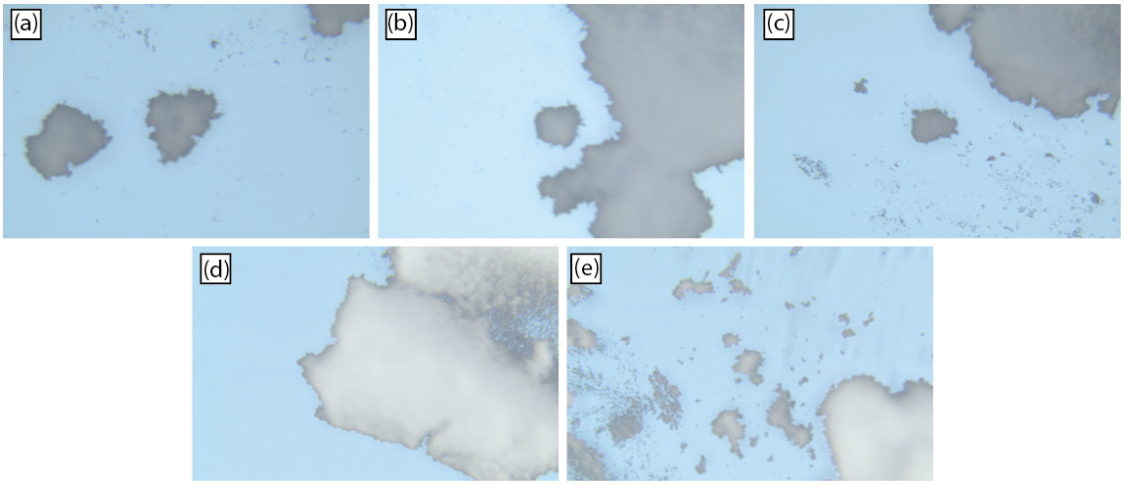

Figure A. 3. Images of samples used for Raman spectroscopy (a) BEH-C18, (b) BEH-Phenyl, (c) BEH-RP18, (d) CSH Hexyl-Phenyl and (e) HSS T3 (5× magnification)

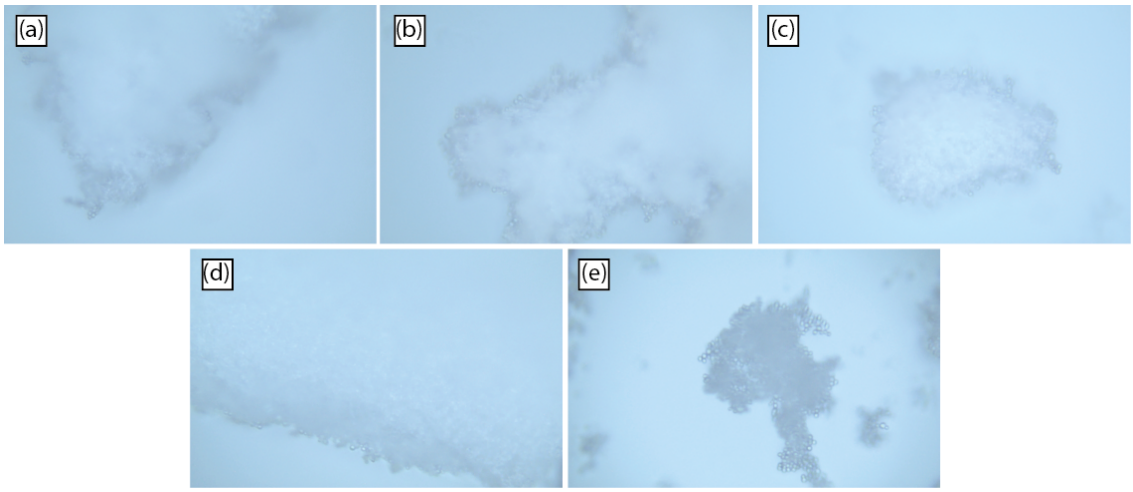

Figure A. 4. Images of samples used for Raman spectroscopy (a) BEH-C18, (b) BEH-Phenyl, (c) BEH-RP18, (d) CSH Phenyl-Hexyl and (e) HSS T3 (20× magnification)

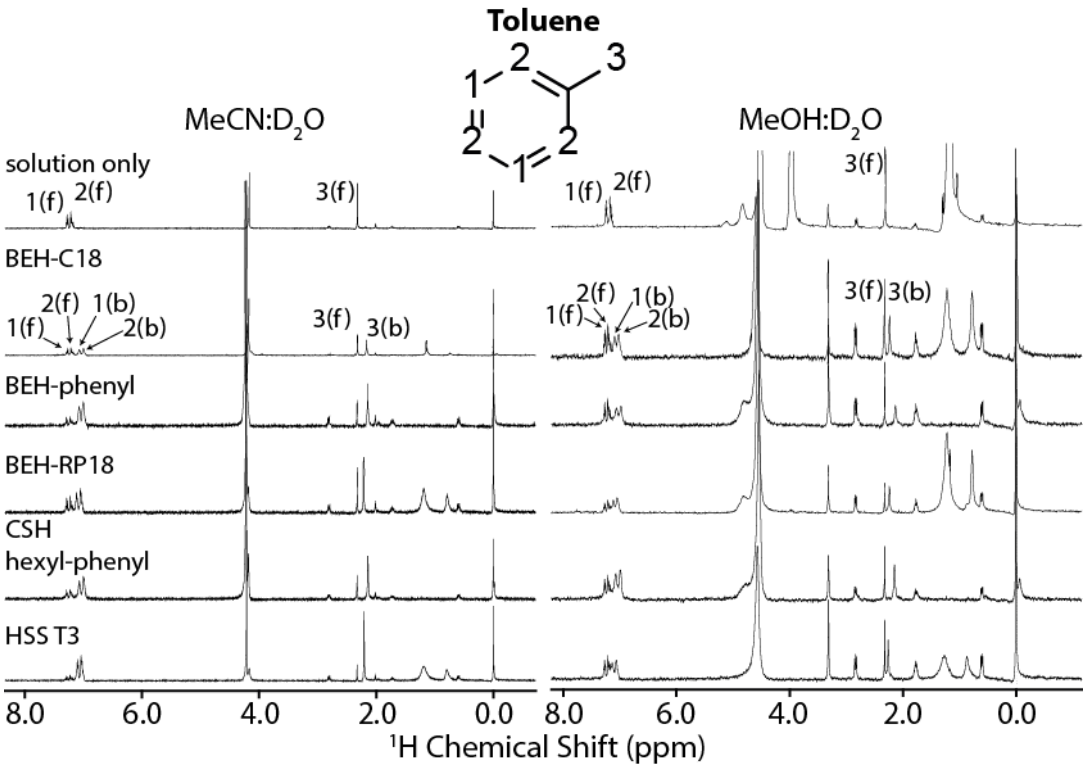

Figure A. 5. 500 MHz ^{1}H HR-MAS NMR spectra of toluene in (from top to bottom) in solution only (50:50 % v/v of MeCN:D_2O and MeOH:D_2O) and in the presence of BEH-C18, BEH-phenyl, BEH-RP18, CSH hexyl-phenyl and HSS T3 stationary phases. All spectra were obtained at 313 K and 5.0 kHz spinning frequency.

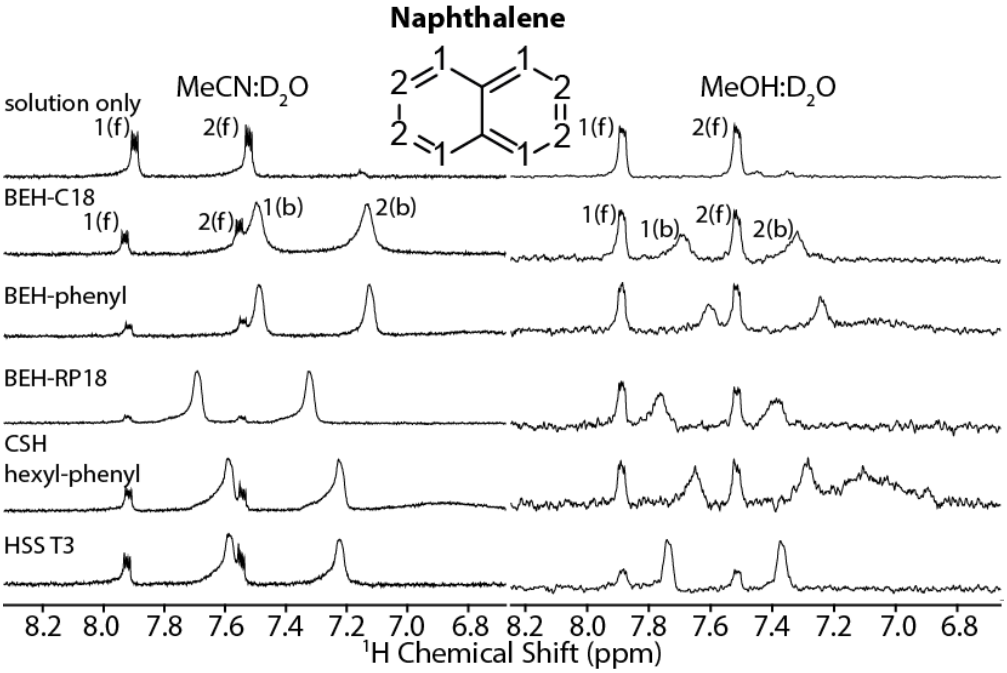

Figure A. 6. 500 MHz ^{1}H HR-MAS NMR spectra (aromatic protons) of naphthalene in (from top to bottom) in solution only (50:50 % v/v of MeCN:D_2O and MeOH:D_2O) and in the presence of BEH-C18, BEH-phenyl, BEH-RP18, CSH hexyl-phenyl and HSS T3 stationary phases. All spectra were obtained at 313 K and 5.0 kHz spinning frequency.

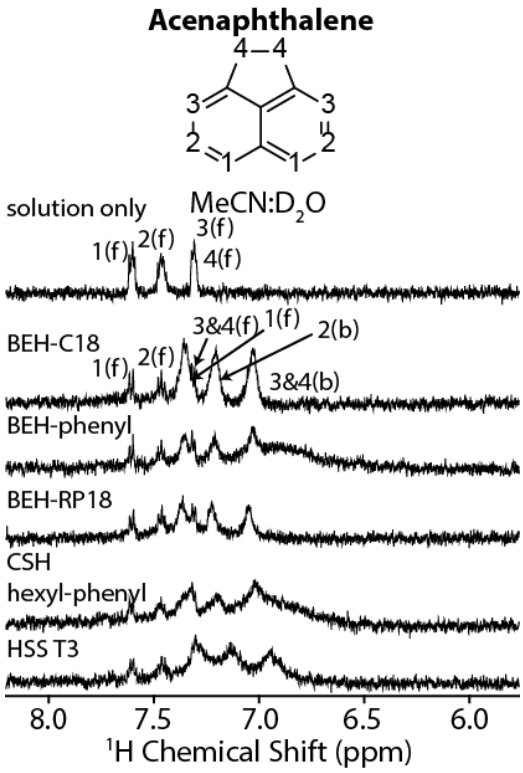

Figure A. 7 500 MHz ^{1}H HR-MAS NMR spectra (aromatic protons) of acenaphthylene in (from top to bottom) in solution only (50:50 % v/v of MeCN:D_2O) and in the presence of BEH-C18, BEH-phenyl, BEH-RP18, CSH hexyl-phenyl and HSS T3 stationary phases. All spectra were obtained at 313 K and 5.0 kHz spinning frequency.

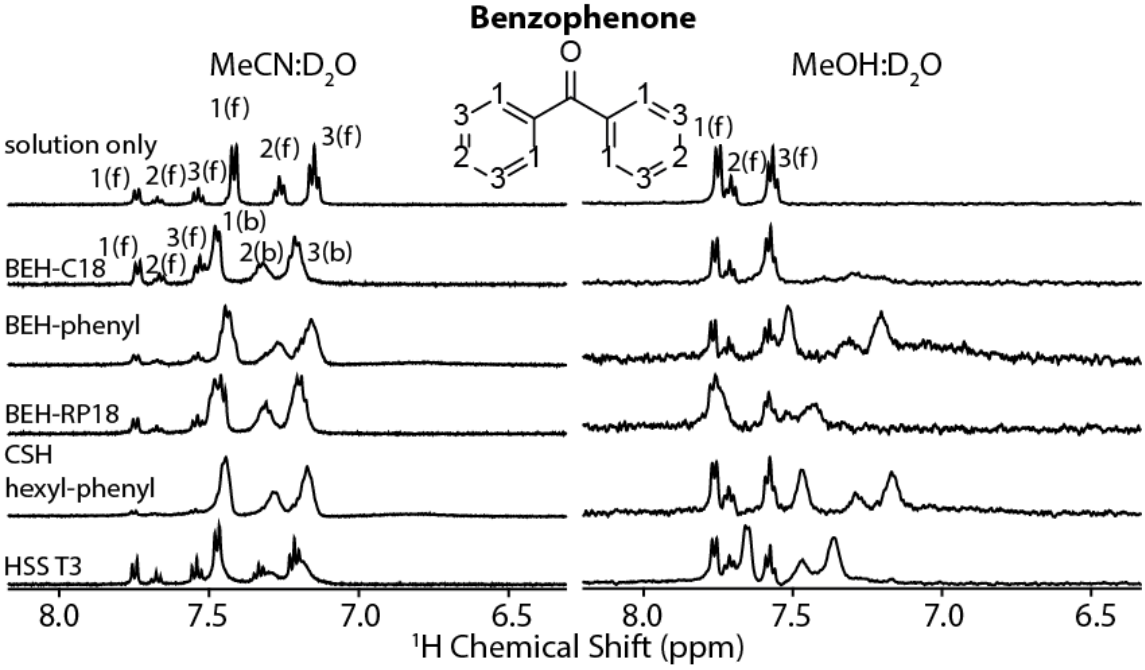

Figure A. 8. 500 MHz ^{1}H HR-MAS NMR spectra (aromatic protons) of benzophenone in (from top to bottom) in solution only (50:50 % v/v of MeCN:D_2O and MeOH:D_2O) and in the presence of BEH-C18, BEH-phenyl, BEH-RP18, CSH hexyl-phenyl and HSS T3 stationary phases. All spectra were obtained at 313 K and 5.0 kHz spinning frequency.

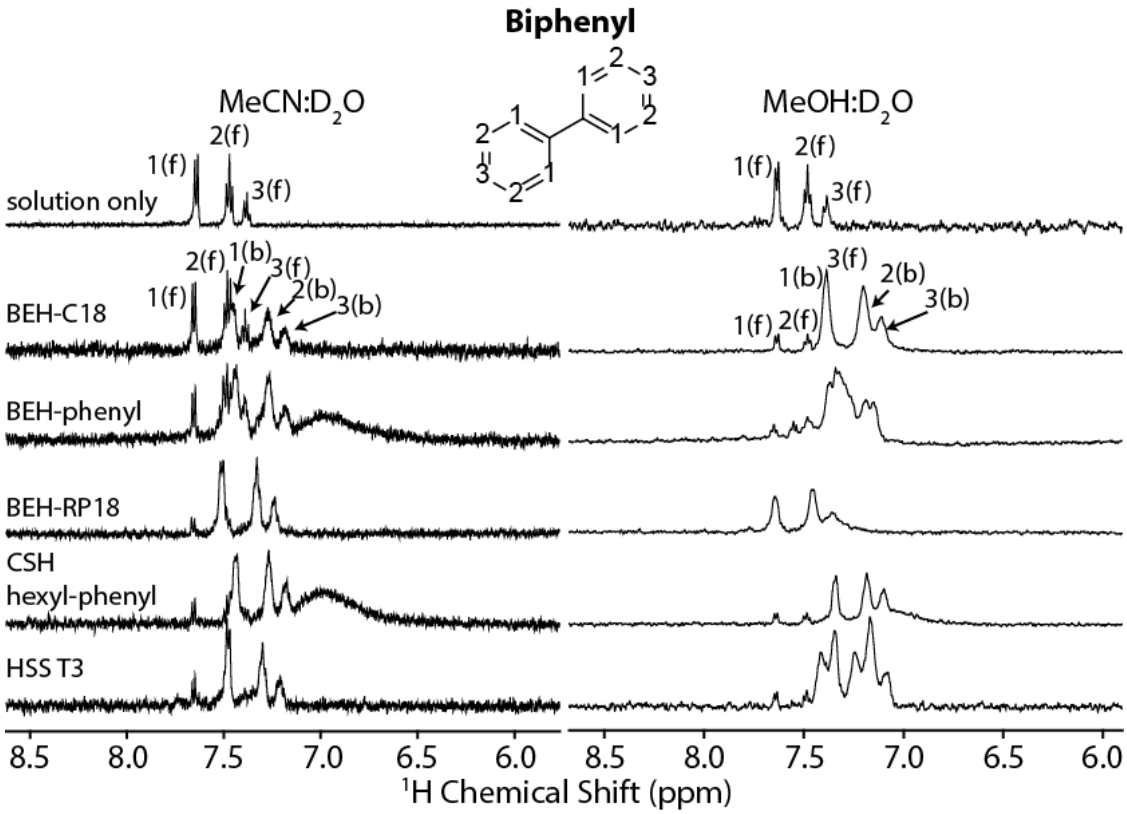

Figure A. 9. 500 MHz ^{1}H HR-MAS NMR spectra (aromatic protons) of biphenyl in (from top to bottom) in solution only (50:50 % v/v of MeCN:D_2O and MeOH:D_2O) and in the presence of BEH-C18, BEH-phenyl, BEH-RP18, CSH hexyl-phenyl and HSS T3 stationary phases. All spectra were obtained at 313 K and 5.0 kHz spinning frequency.

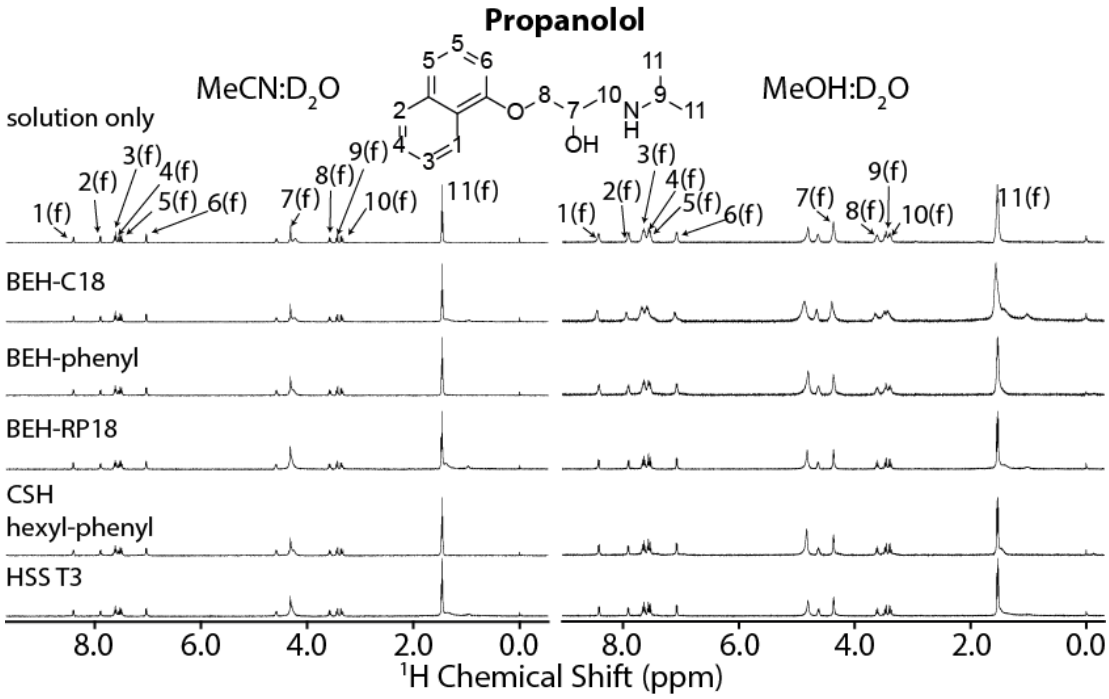

Figure A. 10. 500 MHz ^{1}H HR-MAS NMR spectra of propranolol in (from top to bottom) in solution only (50:50 % v/v of MeCN:D_2O and MeOH:D_2O) and in the presence of BEH-C18, BEH-phenyl, BEH-RP18, CSH hexyl-phenyl and HSS T3 stationary phases. All spectra were obtained at 313 K and 5.0 kHz spinning frequency.

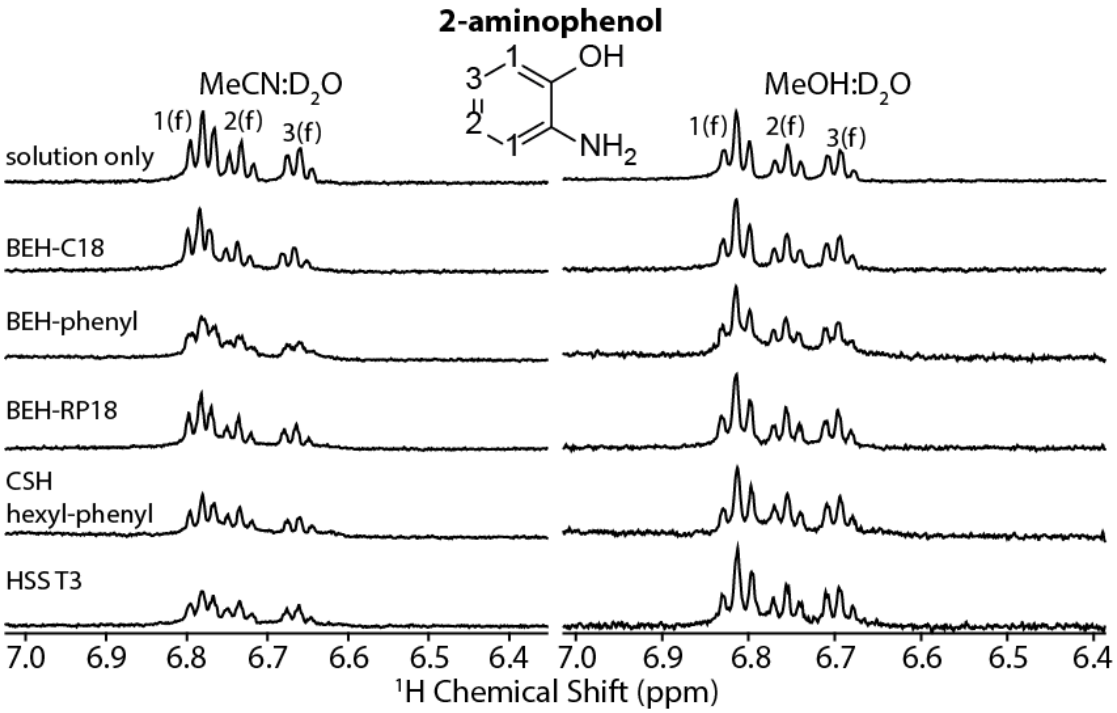

Figure A. 11. 500 MHz ^{1}H HR-MAS NMR spectra (aromatic protons) of 2-aminophenol in (from top to bottom) in solution only (50:50 % v/v of MeCN:D_2O and MeOH:D_2O) and in the presence of BEH-C18, BEH-phenyl, BEH-RP18, CSH hexyl-phenyl and HSS T3 stationary phases. All spectra were obtained at 313 K and 5.0 kHz spinning frequency.

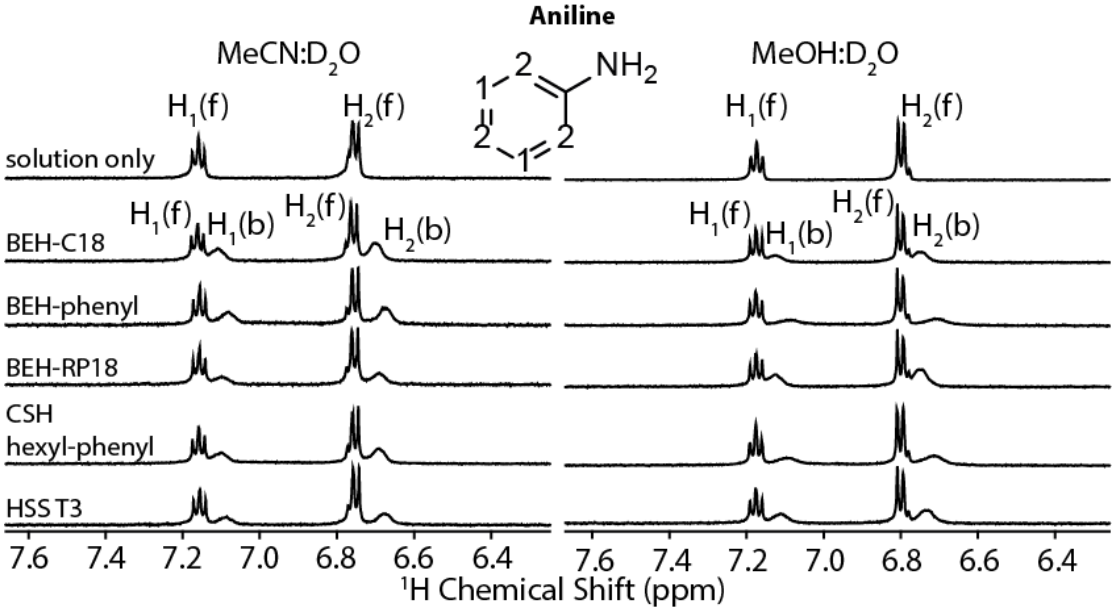

Figure A. 12. 500 MHz ^{1}H HR-MAS NMR spectra (aromatic protons) of aniline in (from top to bottom) in solution only (50:50 % v/v of MeCN:D_2O and MeOH:D_2O) and in the presence of BEH-C18, BEH-phenyl, BEH-RP18, CSH hexyl-phenyl and HSS T3 stationary phases. All spectra were obtained at 313 K and 5.0 kHz spinning frequency.

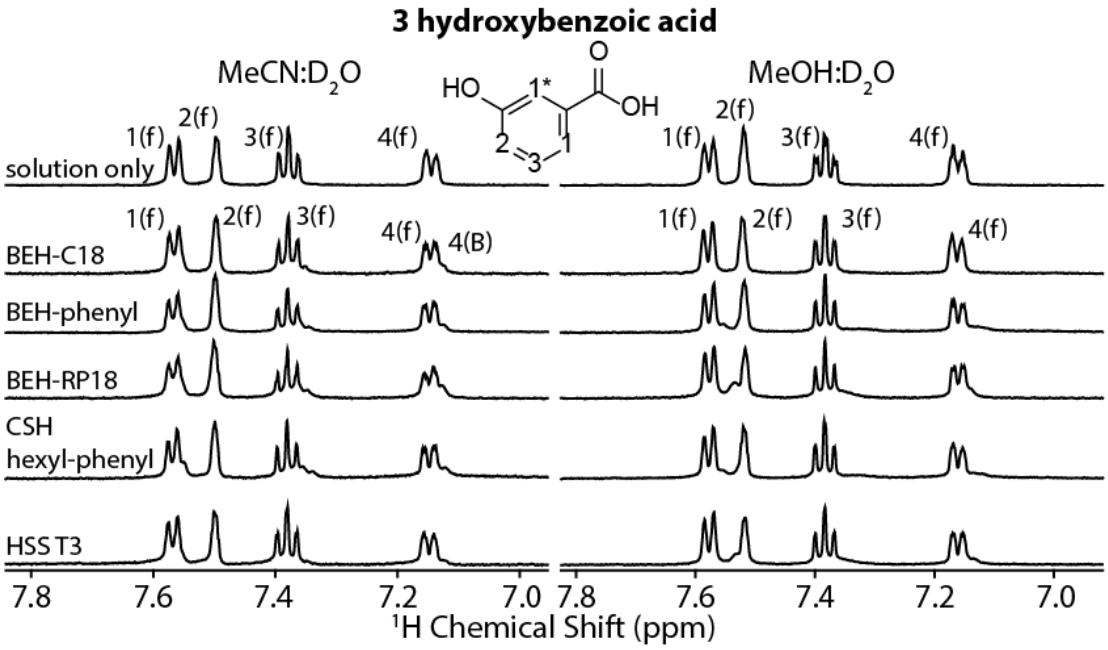

Figure A. 13. 500 MHz ^{1}H HR-MAS NMR spectra (aromatic protons) of 3-hydroxybenzoic acid in (from top to bottom) in solution only (50:50 % v/v of MeCN:D_2O and MeOH:D_2O) and in the presence of BEH-C18, BEH-phenyl, BEH-RP18, CSH hexyl-phenyl and HSS T3 stationary phases. All spectra were obtained at 313 K and 5.0 kHz spinning frequency.

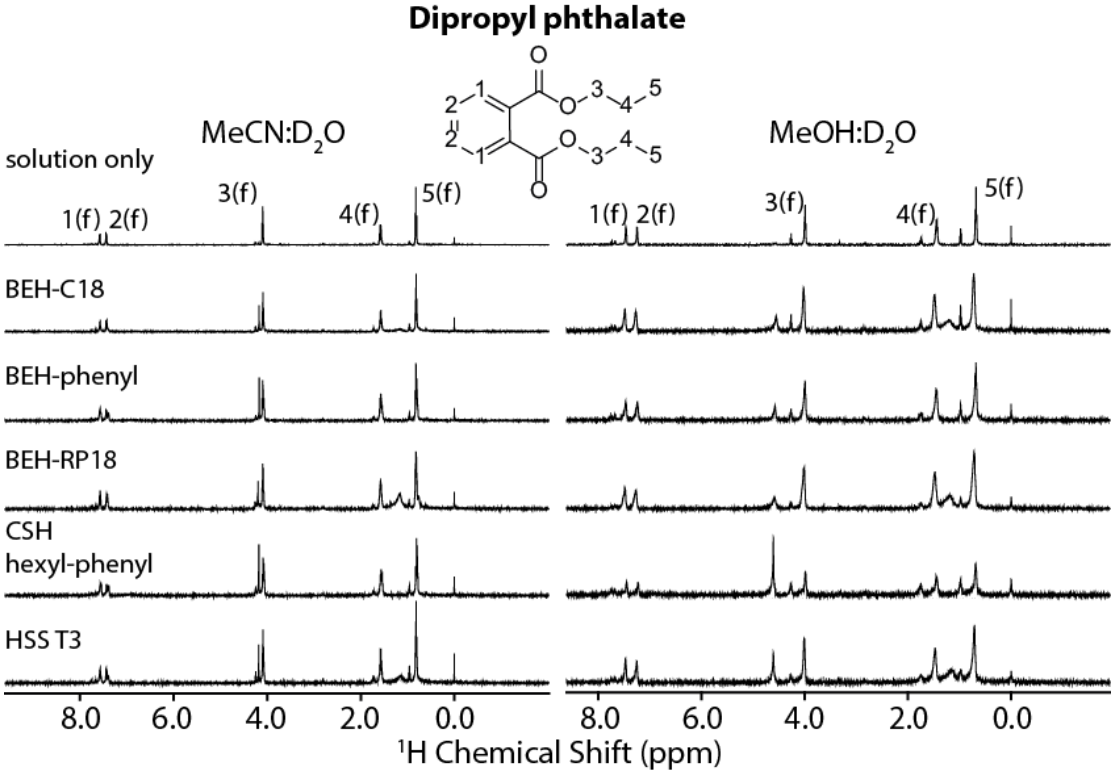

Figure A. 14. 500 MHz ^{1}H HR-MAS NMR spectra of dipropyl phthalate in (from top to bottom) in solution only (50:50 % v/v of MeCN:D_2O and MeOH:D_2O) and in the presence of BEH-C18, BEH-phenyl, BEH-RP18, CSH hexyl-phenyl and HSS T3 stationary phases. All spectra were obtained at 313 K and 5.0 kHz spinning frequency.

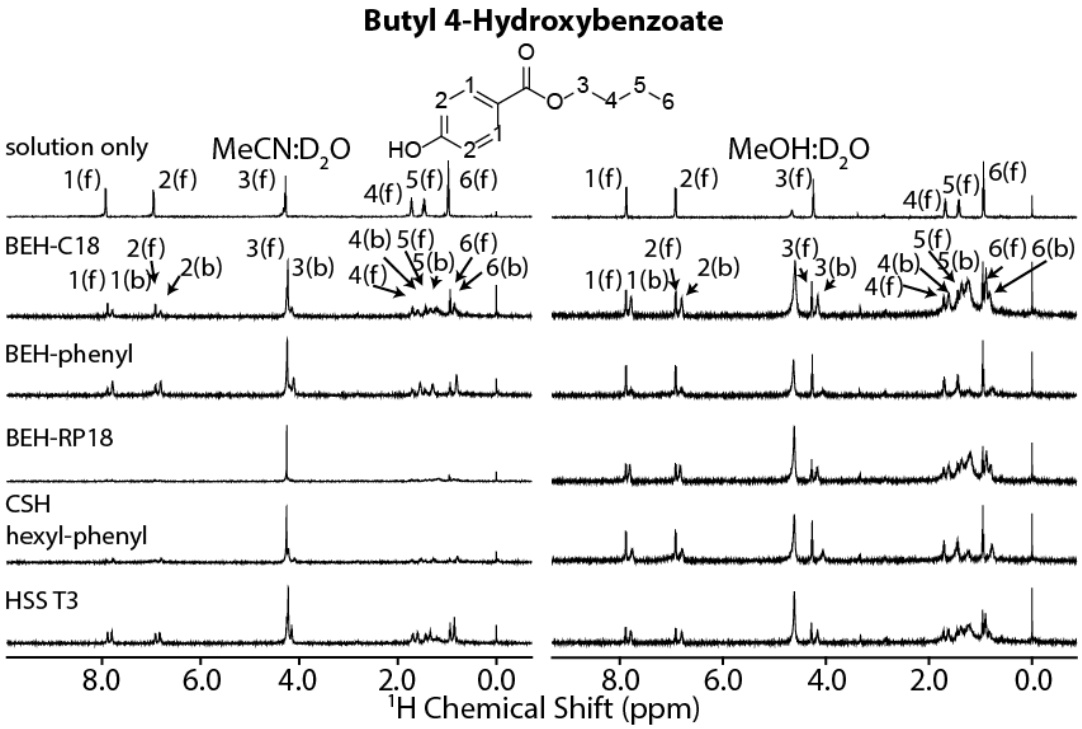

Figure A. 15. 500 MHz ^{1}H HR-MAS NMR spectra of butyl 4-hydroxybenzoate in (from top to bottom) in solution only (50:50 % v/v of MeCN:D_2O and MeOH:D_2O) and in the presence of BEH-C18, BEH-phenyl, BEH-RP18, CSH hexyl-phenyl and HSS T3 stationary phases. All spectra were obtained at 313 K and 5.0 kHz spinning frequency.

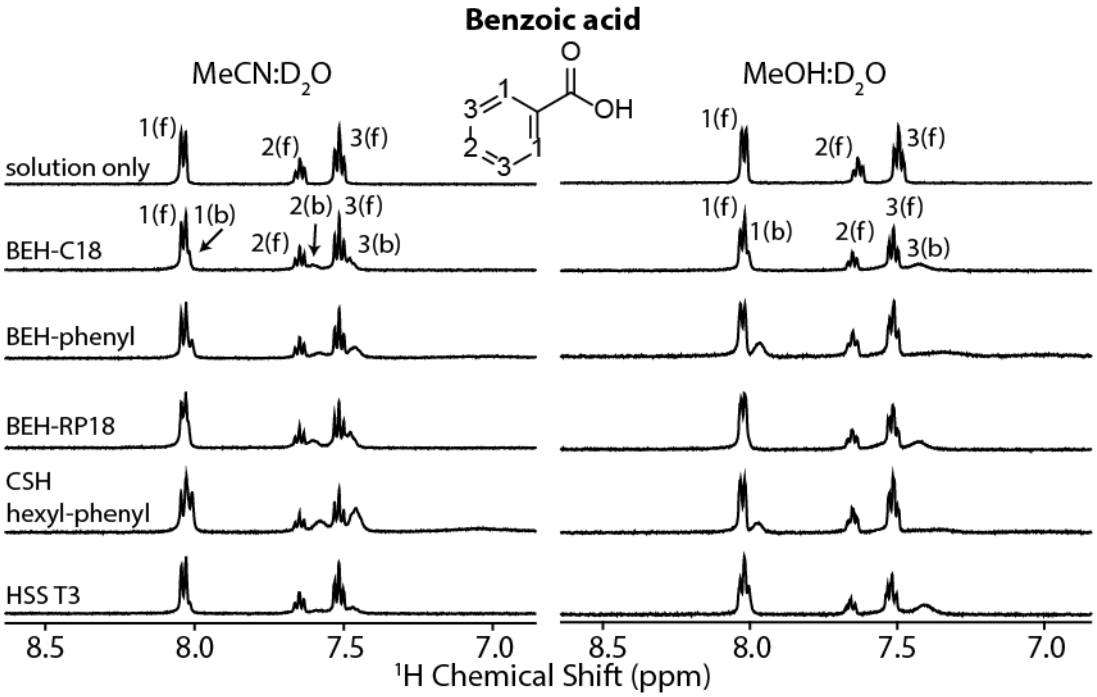

Figure A. 16. 500 MHz ^{1}H HR-MAS NMR spectra (aromatic protons) of benzoic acid in (from top to bottom) in solution only (50:50 % v/v of MeCN:D_2O and MeOH:D_2O) and in the presence of BEH-C18, BEH-phenyl, BEH-RP18, CSH hexyl-phenyl and HSS T3 stationary phases. All spectra were obtained at 313 K and 5.0 kHz spinning frequency.

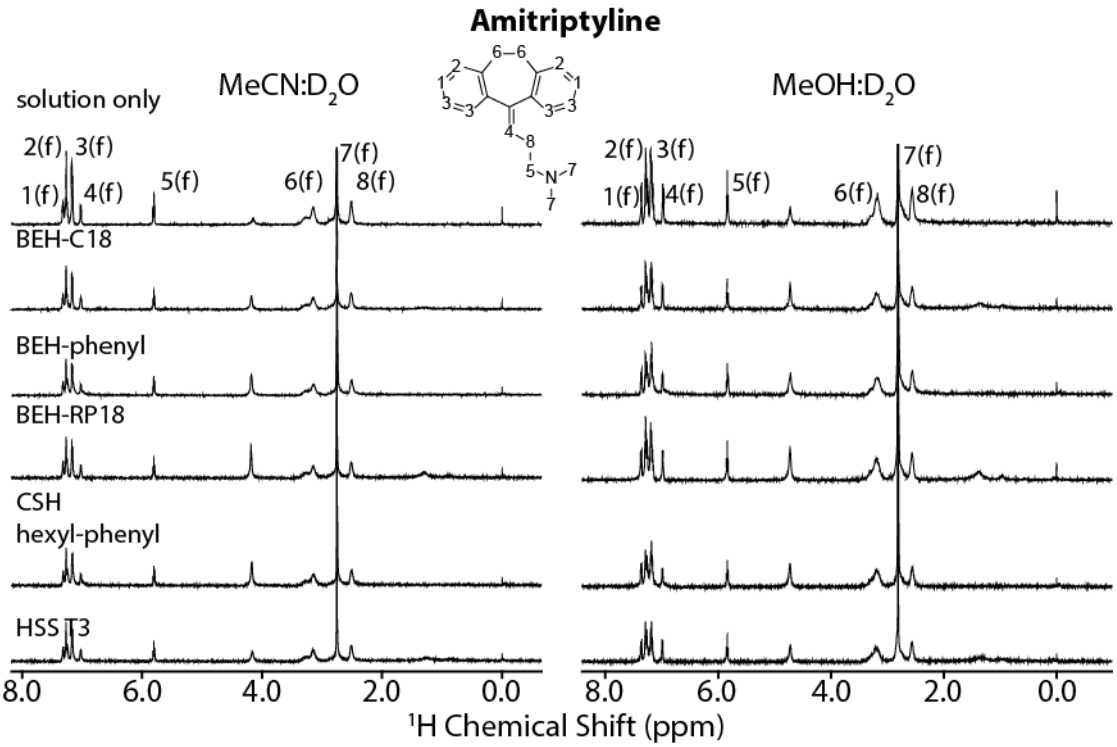

Figure A. 17. 500 MHz ^{1}H HR-MAS NMR spectra of amitriptyline in (from top to bottom) in solution only (50:50 % v/v of MeCN:D_2O and MeOH:D_2O) and in the presence of BEH-C18, BEH-phenyl, BEH-RP18, CSH hexyl-phenyl and HSS T3 stationary phases. All spectra were obtained at 313 K and 5.0 kHz spinning frequency.

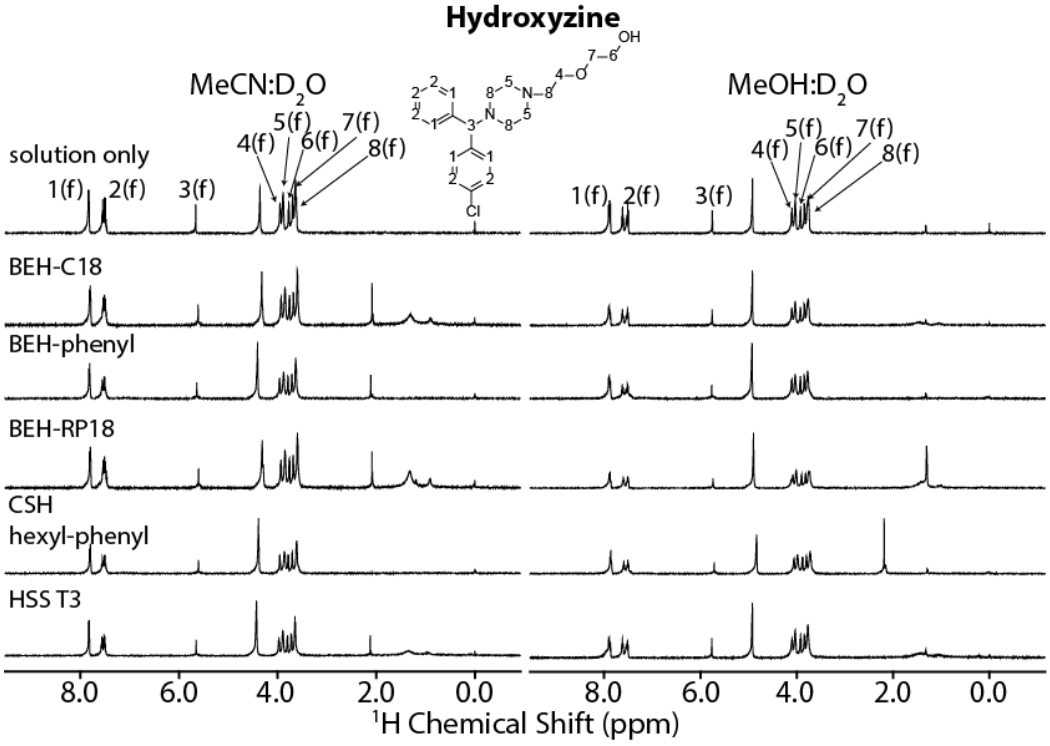

Figure A. 18. 500 MHz ^{1}H HR-MAS NMR spectra of hydroxyzine in (from top to bottom) in solution only (50:50 % v/v of MeCN:D_2O and MeOH:D_2O) and in the presence of BEH-C18, BEH-phenyl, BEH-RP18, CSH hexyl-phenyl and HSS T3 stationary phases. All spectra were obtained at 313 K and 5.0 kHz spinning frequency.

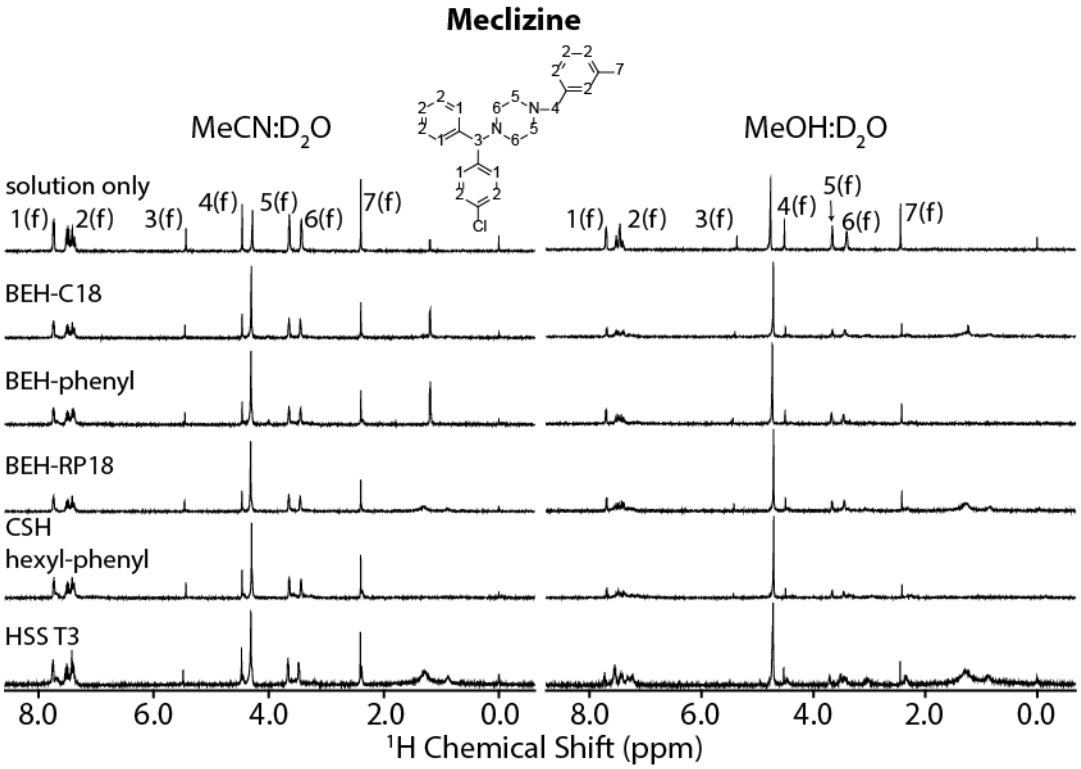

Figure A. 19. 500 MHz ^{1}H HR-MAS NMR spectra of meclizine in (from top to bottom) in solution only (50:50 % v/v of MeCN:D_2O and MeOH:D_2O) and in the presence of BEH-C18, BEH-phenyl, BEH-RP18, CSH hexyl-phenyl and HSS T3 stationary phases. All spectra were obtained at 313 K and 5.0 kHz spinning frequency.

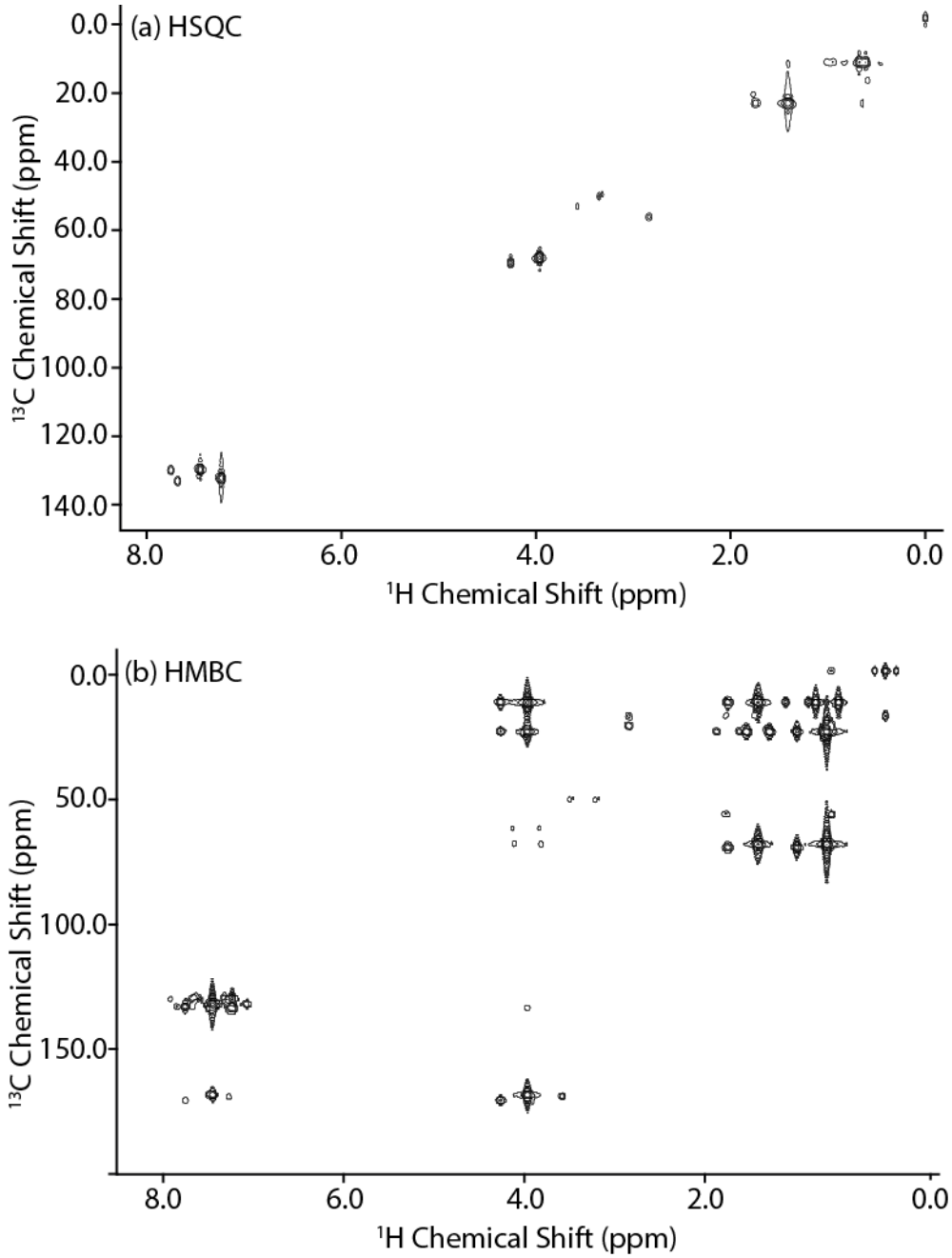

Figure A. 20. 500 MHz ^{1}H-^{13}C (a) HSQC and (b) HMBC spectra of dipropyl phthalate (dissolved in 50:50 % v/v MeCN:D_2O) acquired at 313 K.

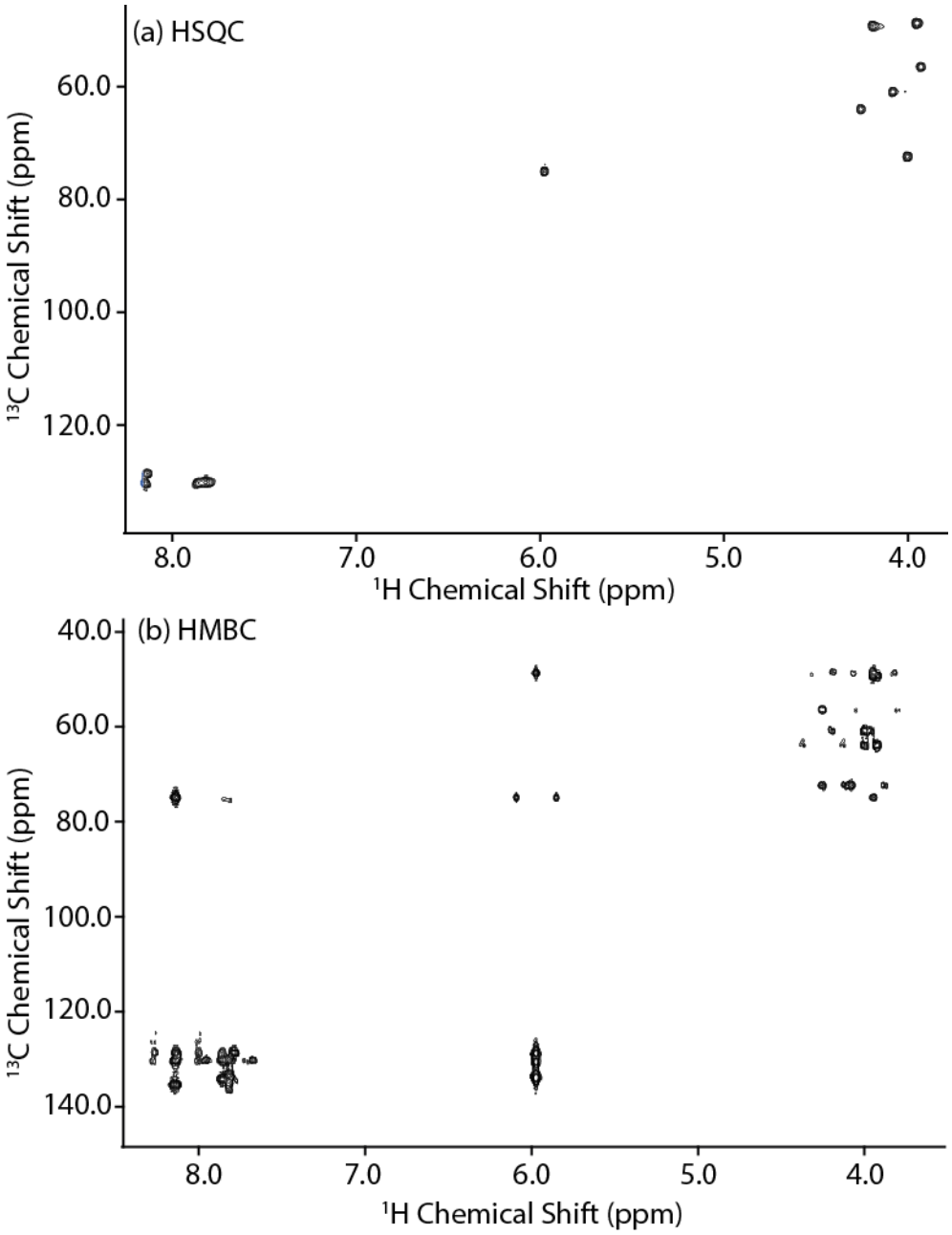

Figure A. 21. 500 MHz 1H-13C (a) HSQC and (b) HMBC spectra of hydroxyzine Acquired (dissolved in 50:50 % v/v MeCN:D_2O) at 313 K.

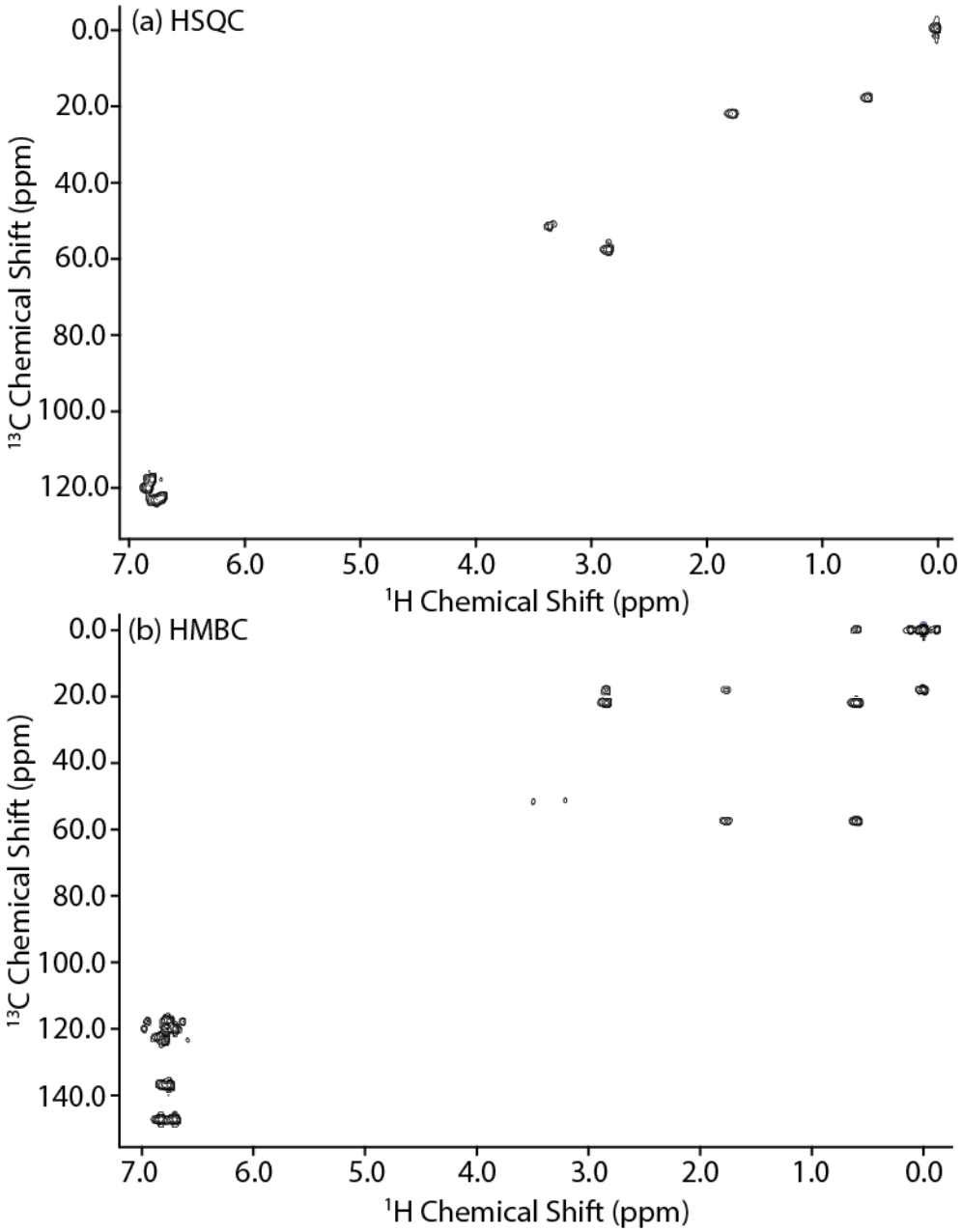

Figure A. 22. 500 MHz 1H-13C (a) HSQC and (b) HMBC spectra of 2-aminophenol (dissolved in 50:50 % v/v MeCN:D_2O) acquired at 313 K.

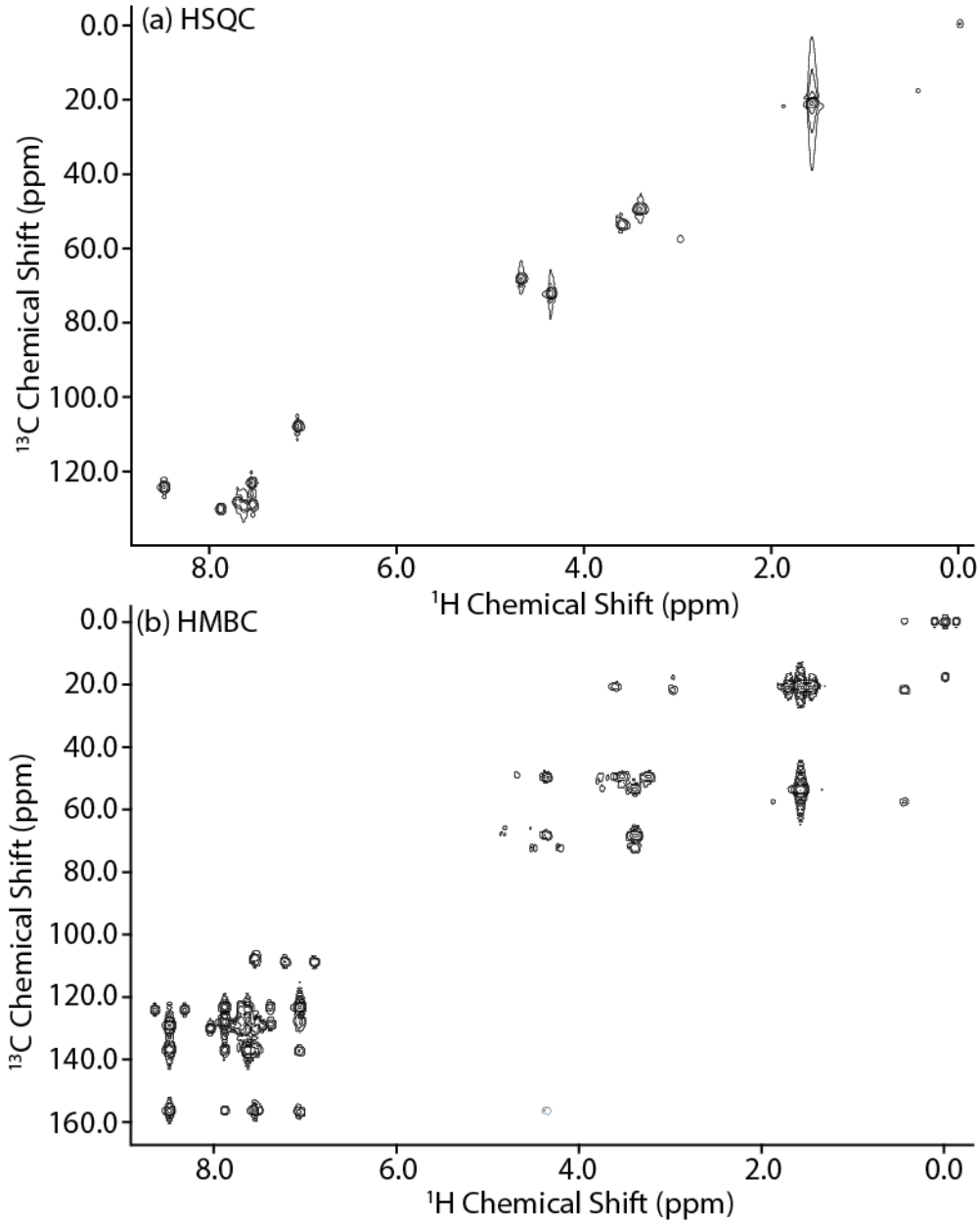

Figure A. 23. 500 MHz 1H-13C (a) HSQC and (b) HMBC spectra of propranolol (dissolved in 50:50 % v/v MeCN:D_2O) acquired at 313 K.

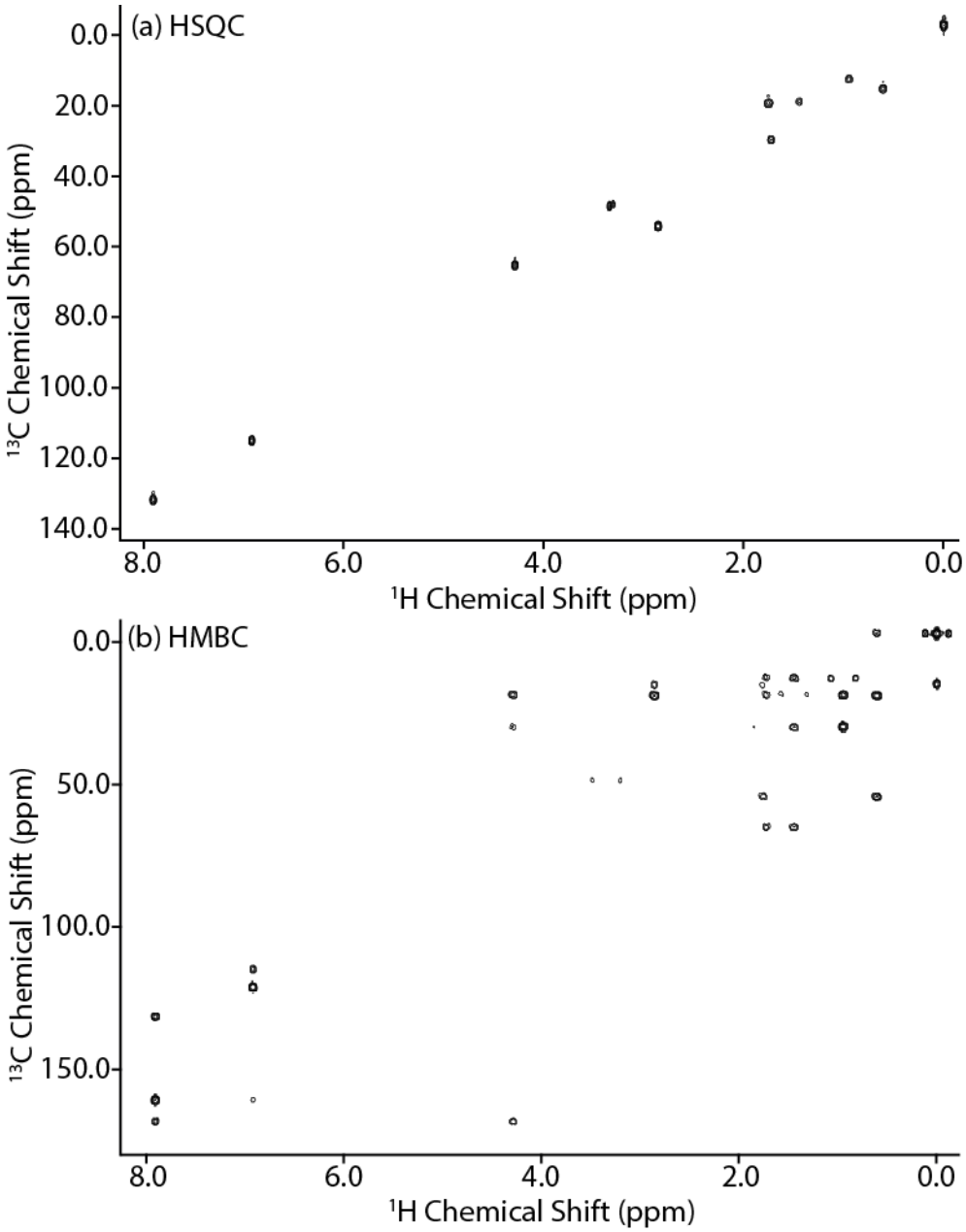

Figure A. 24. 500 MHz 1H-13C (a) HSQC and (b) HMBC spectra of butyl 4-hydroxybenzoate (dissolved in 50:50 % v/v MeCN:D_2O) acquired at 313 K.

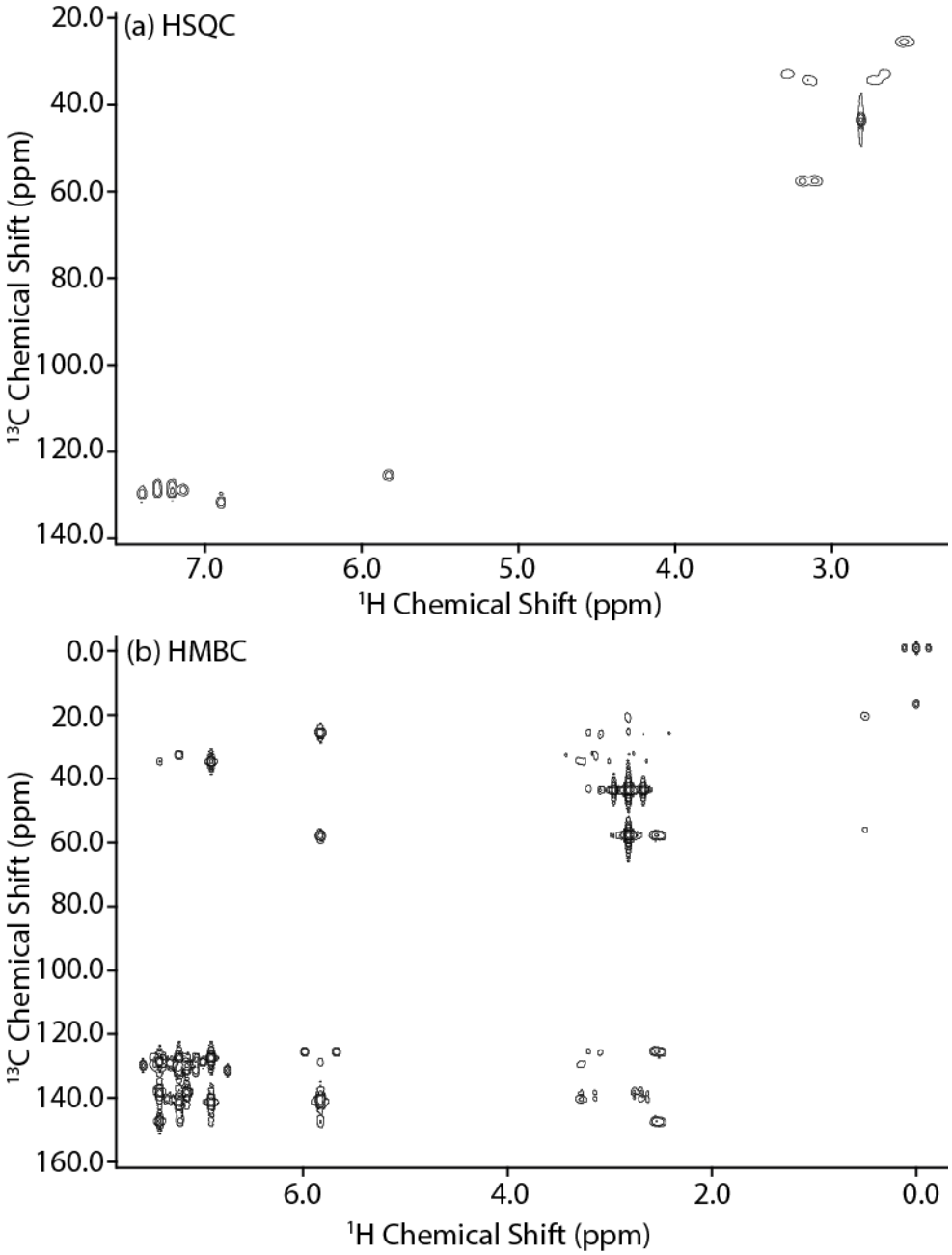

Figure A. 25. 500 MHz 1H-13C (a) HSQC and (b) HMBC spectra of amitriptyline (dissolved in 50:50 % v/v MeCN:D_2O) acquired at 313 K.

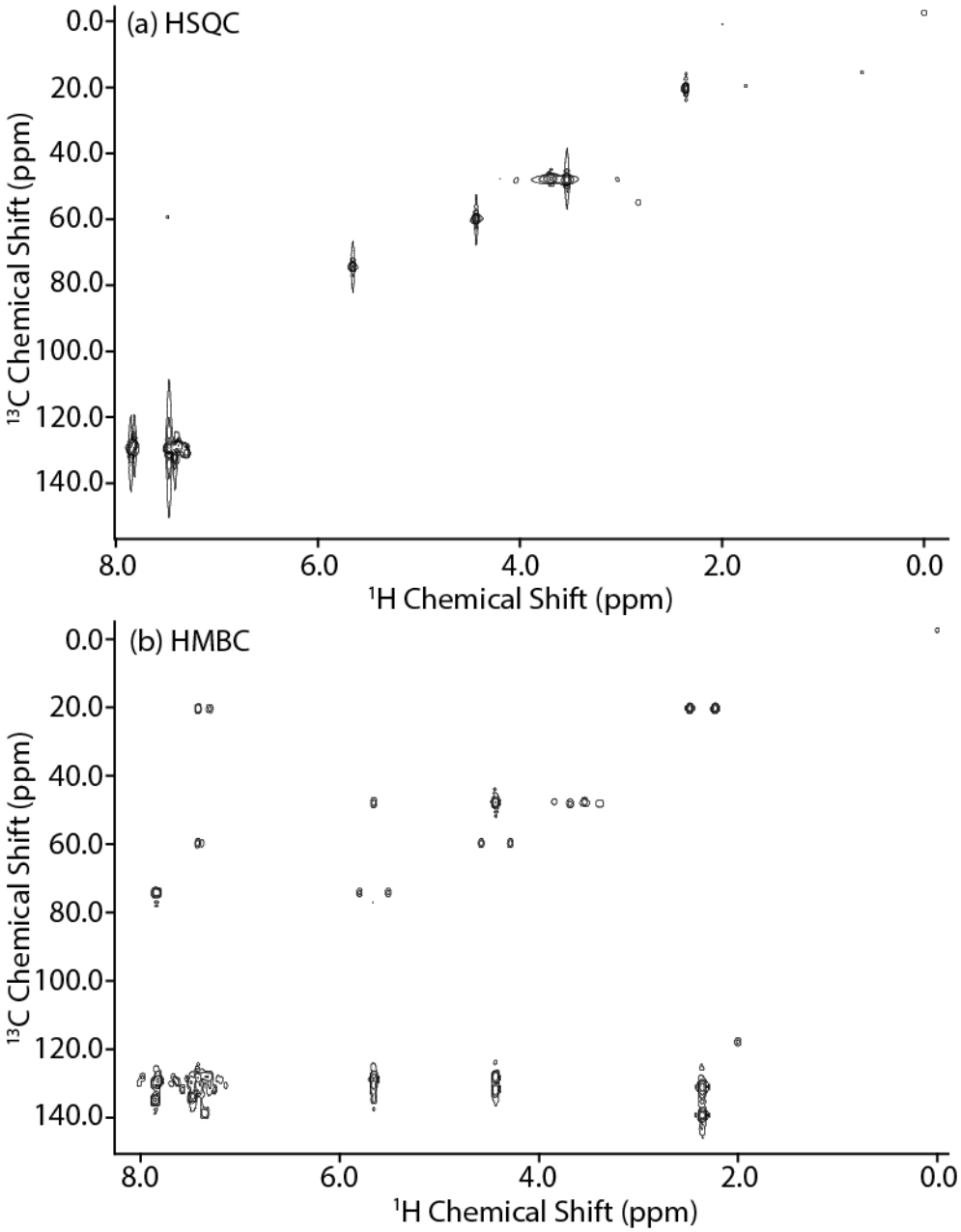

Figure A. 26. 500 MHz 1H-13C (a) HSQC and (b) HMBC spectra of meclizine (dissolved in 50:50 % v/v MeCN:D_2O) acquired at 313 K.

14 APPENDICES: STATISTICAL SCRIP

Statistical Script 1

T1 same measurements

```
> View(t1same)
> attach(t1same)
> mod <- lm(measure ~ proton)
> summary(mod)

Call:
lm(formula = measure ~ proton)

Residuals:
     Min       1Q   Median       3Q      Max 
-0.122773 -0.017544  0.006955  0.031787  0.092157 

Coefficients:
            Estimate Std. Error t value Pr(>|t|)    
(Intercept)  4.53962    0.04293  105.75 7.14e-14 ***
protonH2     2.57078    0.06071   42.35 1.07e-10 ***
protonH3    -1.00940    0.06071  -16.63 1.73e-07 ***
protonH4     1.07972    0.06071   17.79 1.02e-07 ***
---
Signif. codes:  
0 ‘***’ 0.001 ‘**’ 0.01 ‘*’ 0.05 ‘.’ 0.1 ‘ ’ 1

Residual standard error: 0.07435 on 8 degrees of freedom
Multiple R-squared:  0.9979,	Adjusted R-squared:  0.9971 
F-statistic:  1275 on 3 and 8 DF,  p-value: 4.662e-11

> qt(0.975,8)
[1] 2.306004
```

T1 different measurements

```
> View(t1different)
```

```
> attach(t1different)
> mod <- lm(measure ~ proton)
> summary(mod)

Call:
lm(formula = measure ~ proton)

Residuals:
    Min      1Q   Median      3Q     Max
-0.33158 -0.10447 -0.00180  0.09887  0.28740

Coefficients:
            Estimate Std. Error t value Pr(>|t|)
(Intercept)   4.4596     0.1167  38.224 2.41e-10 ***
protonH2      2.3940     0.1650  14.510 4.98e-07 ***
protonH3     -1.1432     0.1650  -6.928 0.000121 ***
protonH4      1.0421     0.1650   6.316 0.000229 ***
---
Signif. codes:  0 ‘***’ 0.001 ‘**’ 0.01 ‘*’ 0.05 ‘.’ 0.1 ‘ ’ 1

Residual standard error: 0.2021 on 8 degrees of freedom
Multiple R-squared:  0.9843,  Adjusted R-squared:  0.9784
F-statistic: 166.8 on 3 and 8 DF,  p-value: 1.501e-07

> qt(0.975,8)
[1] 2.306004
```

T2 same measurements

```
> View(t2same)
> attach(t2same)
> mod <- lm(measure ~ proton)
> summary(mod)

Call:
lm(formula = measure ~ proton)

Residuals:
     Min       1Q    Median       3Q       Max
-0.037963 -0.008080  0.002618  0.008552  0.025017

Coefficients:
            Estimate Std. Error t value Pr(>|t|)
(Intercept)  1.64459    0.01117 147.224 5.07e-15 ***
protonH2     0.13602    0.01580   8.610 2.56e-05 ***
protonH3    -0.08600    0.01580  -5.444 0.000613 ***
protonH4     0.05683    0.01580   3.598 0.007007 **
---
Signif. codes:  0 ‘***’ 0.001 ‘**’ 0.01 ‘*’ 0.05 ‘.’ 0.1 ‘ ’ 1

Residual standard error: 0.01935 on 8 degrees of freedom
Multiple R-squared:  0.9634,  Adjusted R-squared:  0.9497
F-statistic: 70.18 on 3 and 8 DF,  p-value: 4.353e-06
```

```
> qt(0.975,8)
[1] 2.306004
T2 different measurements
> View(t2different)
> attach(t2different)
> mod <- lm(measure ~ proton)
> summary(mod)

Call:
lm(formula = measure ~ proton)

Residuals:
   Min      1Q  Median      3Q     Max 
-0.3498 -0.2446 -0.0419  0.3138  0.3825 

Coefficients:
            Estimate Std. Error t value Pr(>|t|)    
(Intercept)  1.98849    0.18566  10.710 5.07e-06 ***
protonH2     0.13520    0.26256   0.515    0.621    
protonH3    -0.16613    0.26256  -0.633    0.545    
protonH4    -0.02196    0.26256  -0.084    0.935    
---
Signif. codes:  0 ‘***’ 0.001 ‘**’ 0.01 ‘*’ 0.05 ‘.’ 0.1 ‘ ’ 1

Residual standard error: 0.3216 on 8 degrees of freedom
Multiple R-squared:  0.1421,	Adjusted R-squared:  -0.1797 
F-statistic: 0.4416 on 3 and 8 DF,  p-value: 0.7297

> qt(0.975,8)
[1] 2.306004
```